

**ADSORPTION ISOTHERM STUDIES OF GRANULAR ACTIVATED  
CARBONS: ACTIVATION WITH  $Zr^{4+}$  / NANO  $ZrO_2$ , POROSITY,  
SURFACE AREA, KINETICS AND THERMODYNAMICS**

*Thesis submitted to the  
Cochin University of Science and Technology  
In partial fulfillment of the requirements for the degree of  
Doctor of Philosophy  
in  
Chemistry  
Under the Faculty of Environmental Studies*

*By*

**RAJALAKSHMI A. S.  
(Register No.4085)**

*Under the Supervision and Guidance of*

**DR. V. SIVANANDAN ACHARI  
Associate Professor**



**SCHOOL OF ENVIRONMENTAL STUDIES  
COCHIN UNIVERSITY OF SCIENCE AND TECHNOLOGY  
COCHIN-682 022, KERALA, INDIA.**

**November 2017**

**Adsorption Isotherm Studies of Granular Activated Carbons:  
Activation with Zr<sup>4+</sup>/Nano ZrO<sub>2</sub>, Porosity, Surface area, Kinetics  
and Thermodynamics**

*Ph.D. Thesis in Chemistry under the Faculty of Environmental Studies*

*Submitted by*

**Rajalakshmi A. S.**

Research Scholar

School of Environmental Studies

Cochin University of Science and Technology

Kochi – 682 022

Kerala, India

Email: [srajaleshmi@gmail.com](mailto:srajaleshmi@gmail.com)

*Supervising Guide*

**Dr. V. Sivanandan Achari**

Associate Professor

Co-ordinator, UGC-SAP DRS (II) Programme

School of Environmental Studies,

Cochin University of Science and Technology

Kochi – 682 022

Kerala, India

Email: [vsachari@gmail.com](mailto:vsachari@gmail.com)

Phone: 0091-09495383342/0091-0484-2577311

School of Environmental Studies

Cochin University of Science and Technology

Kochi, Kerala, India 682 022

*November 2017*



## **SCHOOL OF ENVIRONMENTAL STUDIES**

**COCHIN UNIVERSITY OF SCIENCE AND TECHNOLOGY**

**Cochin University P.O., Kochi - 682 022, Kerala, India**

**Tel: 91-484-2577311, Fax: 91 - 484-2577311**

**DR. V. SIVANANDAN ACHARI**

Associate Professor in Environmental Chemistry/ Modeling/ Management

(M) : 9495383342 / 0484 282548 / 0484 2577311

(R) : 0484 2306133

E-mail: vsachari@gmail.com, vsachari@cusat.ac.in

**Date: 30-11-2017**

### **Certificate**

Certified that the work presented in the thesis entitled “**Adsorption Isotherm Studies of Granular Activated Carbons: Activation with  $Zr^{4+}$  / Nano  $ZrO_2$ , Porosity, Surface area, Kinetics and Thermodynamics**” is a bonafide work done by Ms. Rajalakshmi A. S. under my supervision and guidance in the School of Environmental Studies, Cochin University of Science and Technology, Kochi-682022 and that this work has not been included in any other thesis submitted previously for the award of any degree. All the relevant corrections and modifications suggested by the audience during the pre-synopsis seminar and recommended by the Doctoral Committee have been incorporated in the thesis.

**Dr. V. Sivanandan Achari**

**Supervising Guide**

**Associate Professor**

Co-ordinator, UGC-SAP DRS (II) Programme

School of Environmental Studies

Cochin University of Science and Technology

Kochi – 682 022

Kerala, India



## *Declaration*

I hereby declare that the work presented in this thesis entitled “**Adsorption Isotherm Studies of Granular Activated Carbons: Activation with  $Zr^{4+}$ / Nano  $ZrO_2$ , Porosity, Surface area, Kinetics and Thermodynamics**” is based on the original work done by me under the supervision of **Dr. V. Sivanandan Achari**, Associate Professor, Co-ordinator, UGC-SAP-DRS (II) Programme [2015 -2020], School of Environmental Studies, Cochin University of Science and Technology, Kochi-682 022 and has not been included in any other thesis submitted previously for the award of any degree.

**Rajalakshmi A. S.**

Kochi-682 022  
30<sup>th</sup> november, 2017



---

## Acknowledgements

First and foremost, I express my profound thanks and indebtedness to my Supervising Teacher and Guide, Dr. V. Sivanandan Achari, Associate Professor, Co-ordinator, UGC-SAP DRS (II) Programme, School of Environmental Studies, Cochin University of Science and Technology, Cochin, India for originating and materialising this doctoral research study. This thesis would not have been possible without his highly focused guidance and active involvement in all aspects and I owe them with the greatest degree of dedication,. His encouragement, tremendous support, finely advice, innovative mind and enthusiasm has allowed me to try and succeed, but, most importantly, to keep trying new ideas without setting boundaries.

I am deeply thankful to Dr. A Mohandas, Emeritus Professor, National Centre for aquatic animal health, Cochin University of Science and Technology, who placed opportunities in front of me and showed me the doors to open. His love and support helped me gracefully during my research days.

I extend my sincere thanks to Dr. Rajathy Sivalingam, The Director, School of Environmental Studies, Cochin University of Science and Technology for all help received during this study.

I am thankful to former Directors Prof. I. S. Bright Singh, Dr. Suguna Yesodharan, Dr. Ammini Joseph, and Dr. Harindranathan Nair for providing all the facilities of the school for the smooth conduct of the study. I also thankful to Professor E. P. Yesodharan, Emeritus Professor and Dr. Anand Madhavan, Assistant Professor of the School of Environmental Studies for their help.

I am grateful to Dr. K. Girishkumar, Professor, Department of Applied Chemistry, Cochin University of Science and Technology for all the help and support received during my study.

I sincerely thank to Mr. O. M. Shibin, Research Scholar, School of Environmental Studies, from the bottom of my heart for all the sincere and dedicated helps and valuable analytical supports received throughout this research study.

I am very much thankful to my colleague Ms. S Jayasree, Research Scholar, School of Environmental Studies, for caring, helping and supporting me to make my day of research a pleasant one. I also like to deliver my thanks to Mr. Prageesh, Husband of Jaysree for his selfless support.

I am grateful to Dr. V. R. Bindumol, wife of my Guide, Dr. V. Sivanandan Achari, Civil Surgeon - Senior Consultant, and Head, Department of Anaesthesiology, Government General Hospital, Ernakulam and children V. S. Adithyasree Harikesav Achari and V. S. Adithyasreeram Sivadev Achari for permit my guide to work continuously for my thesis.

I thank all my lab mates and fellow research scholars of our laboratory, Dr. Bindia Ravindran, Dr. Mercy Thomas, Ms. Regi George, Ms. P Deepa, Ms. M S Ambili and Ms. Raichel Mary Lopez, Ms. Monisha Mohanadas and Mr. Balamuralikrishna for all their

love and support which made my stay in the laboratory a pleasant one. Also, I express my sincere thanks to Ms. Laya Micheal, Project fellow, School of Environmental Studies for extending her selfless service at the time of my thesis writing.

I would like to thank my colleagues in school, Mr Hariprasad Narayanan, Mr Maneesh Kumar, Mr. A Amarnath, Mr. V B Rakesh, Ms K.P Jyothi, Ms Sindhu Joseph, Ms. Gayathri, Ms. Vidyalekshmi, Ms. Anjana, Ms. Samitha, Ms. Chandini for their help and support.

I wish to deliver my sincere thanks to Ms. Jaseela. O, Section Officer and other administrative staffs of the School of Environmental Studies for all helps received.

Also, I express my sincere thanks to my hostel roommates Ms Nayana, Ms Ninya and Ms A. Annapoorneswari for all their love and support received during my study.

I thank Sri. H. Krishnanyyer, Principal Scientist, Central Institute of Fisheries Technology (CIFT), Kochi for most valuable statistical analysis. I greatly acknowledge the support received from Sophisticated Test and Instrumentation Centre (STIC), Cochin University of Science and Technology, Cochin, Amritha Institute of Nano Technology, Cochin and Sophisticated Instrumentation and Computation Centre, University of Kerala, Kariavattom, Thiruvananthapuram for their helps in analysis work. I am grateful to Mr. Binoop Kumar, Indu Photos, University Road, Kochi 682022 for helping in my thesis work.

Last but not least, I am thankful to my father late Mr. A.C Somasekharan and mother K.N Lalitha for showing faith in me and giving liberty to choose what I desired. All the support and love they have provided me over the years was the greatest gift anyone has ever given me. I also thankful to my brother Mr. A.S Rajasekharan, Grand parents Karthyayani Amma, Ammukutti Amma, aunty Ms. Nandini Jayarajan and her husband Late Mr. Jayarajan for their encouragement, love, and support throughout my journey. I would like to thank other family members and friends who have supported me along the way.

A very special gratitude goes out to Cochin University of Science and Technology and UGC-BSR (Order No. AC. C2/ 018862/ 2012 (BSR), Kochi-22, dated 01/02/ 2014 for funding the PhD research.

I would like to thank UGC-SAP- DRS- PHASE- I [F.3-10/ 2009 (SAP-II) for the period 2009- 2014 - Dr. V. Sivanandan Achari, Deputy Co-ordinator] and UGC-SAP- DRS- PHASE- II (SAP - II) [F.4-14/ 2015/DRS-II (SAP-II) for the period 2015- 2020 - Dr. V. Sivanandan Achari, Co-ordinator] sanctioned to the School of Environmental Studies, Cochin University of Science and Technology, being some of the results presented in the thesis are the outcome of this research program implemented.

I thank the one above all, omnipresent God, for giving me the strength during each and every phase of my life.

**Rajalakshmi A.S.**

Research Scholar  
School of Environmental Studies  
Cochin University of Science and Technology  
Kochi – 682 022  
Kerala, India



## ||||| Preface |||||

This research work mainly discuss the preparation, characterisation and adsorption isotherm studies (solid-gas /solid-liquid) of  $Zr^{4+}$  / nano  $ZrO_2$  modified carbons based on coconut shells to study surface area and porosity development under a set of conditions and steam activation. There are four different series of granular activated carbons (GAZR, GACOZR, GACNZR and GACONZR) prepared by chemical activation at temperature ranges 383-1273K. The study is presented in seven chapters with well defined hypothesis and objectives.

Activated carbons produced from organic parent sources (coal, coconut shells, wood, peat and petroleum based residues) by different carbonization and activation conditions have unique properties. Complex pore structure, high surface area and catalytic activity of activated carbon make them an essential material for many applications such as adsorbents, catalyst support and energy related applications, etc. Modification / incorporation of activated carbon using metal, metal oxides, nano particles, and chemical reagents greatly affect the development of surface porosity, surface area and adsorption affinity. In this regard zirconium as zirconyl chloride and  $ZrO_2$  is being identified as new activation agent to improve porosity of coconut shell based GAC. Zirconium ( $Zr^{4+}/ZrO_2$ ) is an important material because of its use in different fields of chemistry (ceramics, fuel cells, biomaterials, thermal barrier coatings and catalysis).

The change in the chemical composition of activated carbon brought by chemical/thermal treatment has been assessed by elemental analysis, Boehm titration, fourier transform infrared spectroscopy, x-ray photoelectron spectroscopy, x-ray diffraction analysis, scanning electron microscopy and transmission electron microscopy. The  $N_2$  adsorption-desorption isotherm data at a temperature of 77 K is subjected to BET,  $I$  plot, Langmuir, Freundlich, Dubinin – Radushkevich (D-R), Alphas S ( $\alpha_s$ ), John isotherm,  $t$ -plot and Baret-Joyner-Halenda (BJH) methods for measuring surface area and pore size distribution. Equilibrium isotherm data obtained from batch experiments using phenol,  $p$ -nitrophenol and methylene blue were subjected to different isotherm models of Langmuir, Freundlich, Dubinin - Radushkevich and John –Sivanandan Achari isotherm equations to optimize the design of specific adsorbent/adsorbate system. Adsorption process is explained by kinetic models; pseudo first order, pseudo second order and intra particle diffusion models. Thermodynamic parameters such as change in free energy ( $\Delta G$ ), enthalpy ( $\Delta H$ ), and entropy ( $\Delta S$ ) based on isotherm studies conducted at 283 K – 323 K for every 10  $^0C$  step wise rise. Ground water collected from a contaminated site, whose initial parameters are known is also used to test the adsorption efficiency of new carbons towards trace metal ions. Concentration in the treated water samples was measured by inductively coupled plasma-mass spectroscopy. Adsorption data were subjected to statistical analysis by two way/ three way ANOVA and Pearsons correlation coefficient to come out with final inferences.



# Contents

## Chapter 1

<b>INTRODUCTION.....</b>	<b>01 - 30</b>
1.1 Introduction .....	01
1.2 Activated Carbon .....	01
1.2.1 Preparation of Granular Activated Carbon .....	03
1.2.2 Physical Activation and Chemical Activation .....	03
1.3 Literature Review .....	04
1.3.1 Activated Carbon Surface Chemistry .....	04
1.3.2 Application of Activated Carbon .....	06
1.3.3 Catalyst Supported Activated Carbon .....	07
1.3.4 Zirconium Based Carbon Materials .....	08
1.3.5 Structural Characterization of Activated Carbons .....	09
1.4 Adsorption Isotherms .....	11
1.5 Porosity Study and Surface Area Determinations.....	12
1.6 Adsorption Isotherm Models .....	13
1.6.1 Brunauer, Emmett and Teller (BET) Isotherm .....	13
1.6.2 <i>I</i> Plot Method .....	14
1.6.3 Langmuir Isotherm .....	14
1.6.4 Freundlich Isotherm .....	15
1.6.5 Dubinin-Radushkevich Isotherm .....	15
1.6.6 <i>t</i> -Plot Method .....	16
1.6.7 Alpha S ( $\alpha_s$ ) Plots .....	16
1.6.8 Barrett Joyner and Halenda (BJH) Method .....	17
1.6.9 John Isotherm Model .....	17
1.6.10 John-Sivanandan Achari Isotherm Plots .....	17
1.7 Aim and Scope of The Study .....	18
1.8 Objective of The Research Study .....	18
1.9 Hypothesis .....	20
1.10 Structure of The Thesis .....	21
Reference .....	26

## Chapter 2

<b>MATERIALS AND METHODS.....</b>	<b>31 - 63</b>
2.1 Introduction .....	31
2.2 Materials .....	32
2.2.1 Preparation of GAC Series .....	32
2.2.2 Preparation of GACO Series .....	32
2.2.3 Preparation of ZrO <sub>2</sub> .....	33

2.2.4	Preparation of GACZR Carbons.....	33
2.2.5	Preparation of GACOZR Carbons .....	34
2.2.6	Preparation of GACNZR Carbons .....	34
2.2.7	Preparation of GACONZR Carbons.....	35
2.3	Carbonisation Procedure .....	35
2.4	Methods.....	37
2.4.1	Carbon Yield and Burn Off.....	37
2.4.2	Elemental Analysis.....	37
2.4.3	Boehm Titration .....	37
2.4.4	Fourier Transform Infrared Spectroscopy (FTIR).....	38
2.4.5	X-ray Photoelectron Spectroscopy (XPS) .....	38
2.4.6	X-ray Powder Diffractometry (XRD) .....	38
2.4.7	Scanning Electron Microscopy (SEM) and Energy Dispersive Spectroscopy (EDS).....	39
2.4.8	High Resolution Transmission Electron Microscopy (HRTEM).....	39
2.4.9	UV-Visible Spectrophotometry.....	39
2.4.10	Inductively Coupled Plasma–Mass Spectrometry (ICP-MS) .....	39
2.5	Other Instruments .....	39
2.5.1	Water Bath .....	39
2.5.2	Water Bath Shaker .....	39
2.5.3	Air Oven.....	40
2.5.4	Autoclave .....	40
2.5.5	Muffle Furnace.....	40
2.5.6	Weighing Balance .....	40
2.5.7	pH .....	40
2.6	Glass Wares .....	40
2.7	Chemicals.....	40
2.8	Solid –Gas Equilibria: Adsorption Studies .....	40
2.9	Solid – Liquid Equilibria: Batch Adsorption Studies .....	41
2.10	Adsorption – Desorption Isotherm Procedure .....	41
2.10.1	Type of Adsorption Isotherm .....	41
2.10.2	Determination of Porosity and Surface area.....	43
2.10.2.1	Brunauer-Emmett-Teller (BET) Model .....	43
2.10.2.2	<i>I</i> Plot Method .....	44
2.10.2.3	Langmuir Isotherm Model .....	45
2.10.2.4	Freundlich Isotherm Model.....	46
2.10.2.5	Dubinin- Radushkevich (D-R) Isotherm Model.....	46
2.10.2.6	Alpha S ( $\alpha_s$ ) Method .....	48
2.10.2.7	John Isotherm Model .....	48
2.10.2.8	<i>t</i> -Plot Method .....	49

2.10.2.9	Barrett Joyner and Halenda (BJH) Method.....	50
2.11	Solid-Liquid Equilibrium.....	51
2.11.1	Phenol (P) and <i>P</i> -Nitrophenol (PNP).....	51
2.11.2	Methylene Blue (MB).....	51
2.11.3	Equilibrium Batch Tests.....	51
2.11.3.1	Langmuir Isotherm.....	52
2.11.3.2	Freundlich Isotherm.....	53
2.11.3.3	Dubinin-Radushkevich (D-R) Isotherm.....	53
2.11.3.4	John – Sivanandan Achari Isotherm.....	54
2.11.4	Kinetic Studies.....	54
2.11.4.1	Lagergren Pseudo-First Order Kinetics.....	54
2.11.4.2	Ho Pseudo-Second Order Kinetics.....	55
2.11.4.3	Intraparticle Diffusion Model.....	56
2.11.5	Diffusion Coefficient.....	56
2.11.6	Thermodynamic Studies.....	57
2.11.7	Activation Energy.....	58
2.12	Design of Batch Adsorption from Isotherm Data.....	58
2.13	Trace Elements Removal by Activated Carbon.....	59
2.14	Statistical Analysis.....	60
	Reference.....	61

### *Chapter 3*

	<b>GRANULAR ACTIVATED CARBON PREPARED BY ACTIVATION WITH ZIRCONYL CHLORIDE (GACZR): PREPARATION, CHARACTERIZATION AND ADSORPTION ISOTHERM STUDIES .....</b>	<b>65 - 181</b>
3.1	Introduction.....	65
3.2	Granular Activated Carbons – GACZR Series.....	66
3.2.1	Effect of Zr <sup>4+</sup> / GAC Impregnation Ratio.....	66
3.3	Characterization Studies.....	68
3.3.1	Carbon Yield and Burn Off.....	68
3.3.2	Elemental Analysis.....	68
3.3.3	Boehm Surface Analysis.....	69
3.3.4	Fourier Transform Infrared Spectroscopy (FTIR) Analysis.....	70
3.3.5	X- ray Photoelectron Spectroscopy (XPS) Analysis.....	73
3.3.6	X-ray Diffraction (XRD) Analysis.....	76
3.3.7	Scanning Electron Microscopy (SEM) Analysis.....	78
3.3.8	Transmission Electron Microscopy (TEM) Analysis.....	80
3.4	Solid-Gas Adsorption Equilibria.....	83
3.4.1	Adsorption Isotherm Analysis.....	84

3.4.1.1	Brunauer-Emmett-Teller (BET) Isotherm Analysis .....	85
3.4.1.2	The BET-Scatchard (B-S) Plots ( <i>I</i> Point Analysis).....	87
3.4.1.3	Langmuir Isotherm Analysis .....	90
3.4.1.4	Freundlich Isotherm Analysis .....	92
3.4.1.5	Dubinin - Radushkevich (D-R) Isotherm Analysis .....	93
3.4.1.6	Alpha S ( $\alpha_s$ ) Method.....	95
3.4.1.7	John Isotherm Analysis .....	97
3.4.1.8	<i>t</i> - Plot Method .....	100
3.4.1.9	Barrett-Joyner-Halenda (BJH) Method.....	102
3.5	Solid – Liquid Equilibria: Adsorption Studies .....	106
3.5.1	Effect of Adsorbent Dose .....	106
3.5.2	Effect of Contact Time .....	107
3.5.3	Selection of Carbon in GACZR Series for Solid-Liquid Equilibria .....	107
3.5.4	Adsorption Studies of Phenol, <i>P</i> -Nitrophenol and Methylene Blue .....	108
3.5.5	Equilibrium Adsorption Isotherm .....	109
3.5.5.1	Langmuir Isotherm for Solid – Liquid Equilibria .....	111
3.5.5.2	Freundlich Isotherm for Solid – Liquid Equilibria.....	111
3.5.5.3	Dubinin-Radushkevich Isotherm for Solid-Liquid Equilibria.....	112
3.5.6	Adsorption of Phenol on GACZR 1273, GAC 383 and GACO 383 at Temperatures .....	112
3.5.7	Adsorption of <i>P</i> -Nitrophenol on GACZR 1273, GAC 383 and GACO 383 at Temperatures.....	117
3.5.8	Adsorption of Methylene Blue (MB) on GACZR 1273, GAC 383 and GACO 383 at Temperatures .....	121
3.5.9	John-Sivanandan Achari (J-SA) Isotherm for Solid - Liquid Equilibria .....	126
3.5.9.1	John - Sivanandan Achari Isotherm for Phenol, <i>P</i> -Nitrophenol and Methylene Blue Adsorption on GACZR 1273 at Temperatures .....	132
3.6	Comparison of Adsorption Isotherms for the Adsorption of Phenol, <i>P</i> -Nitrophenol and Methylene Blue on GACZR 1273 .....	135
3.7	Adsorption Kinetic Studies .....	137
3.7.1	Kinetic Studies of Phenol, <i>P</i> -Nitrophenol and Methylene Blue .....	137
3.7.1.1	Pseudo-First Order Kinetic Study .....	138
3.7.1.2	Pseudo-Second Order Kinetic Study .....	138
3.7.1.3	Intraparticle Diffusion Model .....	138
3.7.2	Kinetic Study of Phenol on GACZR 1273, GAC 383, and GACO 383 at Temperatures.....	139

3.7.3	Kinetic Study of <i>P</i> -Nitrophenol on GACZR 1273, GAC 383 and GACO 383 at Temperatures .....	143
3.7.4	Kinetic Study of Methylene Blue (MB) on GACZR 1273, GAC 383 and GACO 383 at Temperatures .....	148
3.8	Thermodynamic Parameters .....	152
3.8.1	Thermodynamic Parameters from Distribution Coefficient .....	155
3.9	Diffusion Coefficient .....	159
3.9.1	Determination of Diffusivity for Phenol on GACZR 1273, GAC 383, GACO 383.....	159
3.9.2	Determination of Diffusivity for <i>P</i> -Nitrophenol on GACZR 1273, GAC 383, GACO 383. ....	160
3.9.3	Determination of Diffusivity for Methylene Blue on GACZR 1273, GAC 383, GACO 383 .....	161
3.10	Activation Energy .....	162
3.11	Design of Batch Adsorption from Isotherm Data .....	165
3.12	Adsorption of Trace Metal Ions by carbon GACZR Using Contaminated Groundwater .....	167
3.13	Statistical Analysis of the Data.....	169
3.14	Conclusions .....	173
	Reference .....	175

#### **Chapter 4**

#### **GRANULAR ACTIVATED CARBON OXIDISED AND ACTIVATED WITH ZIRCONYL CHLORIDE (GACOZR): PREPARATION, CHARACTERIZATION AND**

#### **ADSORPTION ISOTHERM STUDIES ..... 183 - 270**

4.1	Introduction .....	183
4.2	Granular Activated Carbons – GACOZR Series .....	184
4.3	Characterization Studies .....	184
4.3.1	Carbon Yield and Burn Off .....	184
4.3.2	Elemental Analysis .....	184
4.3.3	Boehm Analysis .....	185
4.3.4	Fourier Transform Infrared Spectroscopy (FTIR) Studies .....	186
4.3.5	X-ray Photoelectron Spectroscopy (XPS) Analysis .....	188
4.3.6	X-ray Diffraction (XRD) Analysis .....	190
4.3.7	Scanning Electron Microscopy (SEM) Analysis .....	191
4.3.8	Transmission Electron Microscopy (TEM) Analysis.....	192
4.4	Solid-Gas Adsorption Equilibria .....	193
4.4.1	Adsorption Isotherm Analysis.....	194
4.4.1.1	Brunauer-Emmett-Teller (BET) Isotherm Analysis .....	195

4.4.1.2	The BET–Scatchard (B–S) Plots ( <i>I</i> Point Method Analysis) .....	196
4.4.1.3	Langmuir Isotherm Analysis .....	198
4.4.1.4	Freundlich Isotherm Analysis .....	198
4.4.1.5	Dubinin-Radushkevich Isotherm (D-R) Analysis .....	200
4.4.1.6	Alpha S ( $\alpha_s$ ) Method.....	201
4.4.1.7	John Isotherm Analysis .....	203
4.4.1.8	<i>t</i> - Plot Method .....	205
4.4.1.9	Barrett-Joyner-Halenda (BJH) Method.....	206
4.5	Solid – Liquid Equilibria: Adsorption Studies .....	209
4.5.1	Adsorption Studies of Phenol, <i>P</i> -Nitrophenol and Methylene Blue .....	210
4.5.2	Adsorption of Phenol on GACOZR 1273, GAC 383, and GACO 383 at Temperatures .....	211
4.5.3	Adsorption of <i>P</i> -Nitrophenol on GACOZR 1273, GAC 383 and GACO 383 at Temperatures.....	216
4.5.4	Adsorption of Methylene Blue (MB) on GACOZR 1273, GAC 383 and GACO 383 at Temperatures .....	220
4.5.5	John-Sivanandan Achari (J-SA) Isotherm for Solid-Liquid Equilibria .....	224
4.5.5.1	John-Sivanandan Achari Isotherm for Phenol, <i>P</i> -Nitrophenol and MB Adsorption on GACOZR 1273 at Temperatures.....	228
4.6	Comparison of Adsorption Isotherms for Adsorption of Phenol, <i>p</i> -nitrophenol & Methylene Blue on GACOZR 1273 .....	231
4.7	Adsorption Kinetic Studies.....	233
4.7.1	Kinetic Study of Phenol on GACOZR 1273, GAC 383, and GACO 383 at Temperatures.....	233
4.7.2	Kinetic Study of <i>P</i> -Nitrophenol on GACOZR 1273, GAC 383 and GACO 383 at Temperatures .....	237
4.7.3	Kinetic Study of Methylene Blue (MB) on GACOZR 1273, GAC 383 and GACO 383 at Temperatures .....	241
4.8	Thermodynamic Parameters .....	245
4.8.1	Thermodynamic Parameters from Distribution Coefficient .....	249
4.9	Diffusion Coefficient .....	252
4.9.1	Determination of Diffusivity for Phenol on GACOZR 1273, GAC 383 and GACO 383.....	253
4.9.2	Determination of Diffusivity for <i>P</i> -Nitrophenol on GACOZR 1273, GAC 383 and GACO 383.....	254
4.9.3	Determination of Diffusivity for Methylene Blue (MB) on GACOZR 1273, GAC 383 and GACO 383.....	255



4.10	Activation Energy .....	256
4.11	Design of Batch Adsorption from Isotherm Data.....	258
4.12	Adsorption of Trace Metal Ions by GACOZR Using Contaminated Groundwater .....	260
4.13	Statistical Analysis of the Data.....	262
4.14	Conclusions .....	265
	Reference .....	267

## **Chapter 5**

### **GRANULAR ACTIVATED CARBON PREPARED BY ACTIVATION WITH ZIRCONIUM OXIDE (GACNZR): PREPARATION, CHARACTERIZATION AND**

### **ADSORPTION ISOTHERM STUDIES ..... 271 - 353**

5.1	Introduction .....	271
5.2	Granular Activated Carbons – GACNZR Series.....	272
5.3	Characterization of Nano Zirconia (ZrO <sub>2</sub> ).....	272
5.3.1	Effect of Zr <sup>4+</sup> / GAC Impregnation Ratio .....	274
5.4	Characterization Studies .....	275
5.4.1	Carbon Yield and Burn Off .....	275
5.4.2	Elemental Analysis.....	275
5.4.3	Boehm Surface Analysis.....	275
5.4.4	X-ray Diffraction (XRD) Analysis.....	276
5.4.5	Fourier Transform Infrared Spectroscopy (FTIR) Analysis.....	278
5.4.6	X-ray Photoelectron Spectroscopy (XPS) Analysis .....	280
5.4.7	Scanning Electron Microscopy (SEM) Analysis .....	282
5.4.8	Transmission Electron Microscopy (TEM) Analysis.....	283
5.5	Solid-Gas Adsorption Equilibria .....	283
5.5.1	Adsorption Isotherm Analysis .....	283
5.5.1.1	Brunauer-Emmett-Teller (BET) Isotherm Analysis.....	284
5.5.1.2	The BET–Scatchard (B–S) Plots ( <i>I</i> Point Analysis).....	286
5.5.1.3	Langmuir Isotherm Analysis .....	287
5.5.1.4	Freundlich Isotherm Analysis .....	288
5.5.1.5	Dubinin-Radushkevich (D-R) Isotherm Analysis .....	289
5.5.1.6	Alpha S ( $\alpha_s$ ) Method.....	290
5.5.1.7	John Isotherm Analysis .....	292
5.5.1.8	<i>t</i> -Plot Method .....	293
5.5.1.9	Barrett-Joyner-Halenda (BJH) Method.....	295
5.6	Solid-Liquid Equilibria: Adsorption Studies.....	297
5.6.1	Adsorption Studies of Phenol, <i>P</i> -Nitrophenol and Methylene Blue .....	298

5.6.2	Adsorption of Phenol on GACNZR 1073, GAC 383 and GACO 383 at Temperatures .....	299
5.6.3	Adsorption of <i>P</i> -Nitrophenol on GACNZR 1073, GAC 383 and GACO 383 at Temperatures.....	303
5.6.4	Adsorption of Methylene Blue on GACNZR 1073, GAC 383 and GACO 383 at Temperatures.....	307
5.6.5	John-Sivanandan Achari (J-SA) Isotherm Plots for Solid-Liquid Equilibria .....	310
5.6.5.1	John – Sivanandan Achari Isotherm for Phenol, <i>P</i> -Nitrophenol and Methylene Blue Adsorption on GACNZR 1073 at Temperatures.....	313
5.7	Comparison of Adsorption Isotherms for the Adsorption of Phenol, <i>P</i> -Nitrophenol and Methylene Blue on GACNZR1 073 .....	316
5.8	Adsorption Kinetic Studies.....	317
5.8.1	Kinetic Study of Phenol at Temperatures .....	317
5.8.2	Kinetic Study of <i>P</i> -Nitrophenol at Temperatures .....	322
5.8.3	Kinetic study of Methylene Blue (MB) at Temperatures .....	326
5.9	Thermodynamic Parameters .....	329
5.9.1	Thermodynamic Parameters from Distribution Coefficient .....	331
5.10	Diffusion Coefficient .....	336
5.10.1	Determination of Diffusivity for Phenol on GACNZR 1073, GAC 383 and GACO 383.....	336
5.10.2	Determination of Diffusivity for <i>P</i> -Nitrophenol on GACNZR 1073, GAC 383 and GACO 383 .....	338
5.10.3	Determination of Diffusivity for Methylene Blue (MB) on GACNZR 1073, GAC 383 and GACO 383.....	339
5.11	Activation Energy .....	340
5.12	Design of Batch Adsorption from Isotherm Data.....	342
5.13	Adsorption of Trace Metal Ions by GACNZR Using Contaminated Groundwater .....	343
5.14	Statistical Analysis of the Data.....	345
5.15	Conclusions .....	348
	Reference .....	350

## **Chapter 6**

### **GRANULAR ACTIVATED CARBON OXIDISED AND ACTIVATED WITH ZIRCONIUM OXIDE (GACONZR): PREPARATION, CHARACTERISATION AND ADSORPTION ISOTHERM STUDIES ..... 355 - 434**

6.1	Introduction.....	355
6.2	Granular Activated Carbons – GACONZR Series .....	355

6.3	Characterization Studies .....	356
6.3.1	Carbon Yield and Burn Off .....	356
6.3.2	Elemental Analysis .....	356
6.3.3	Boehm Analysis .....	357
6.3.4	Fourier Transform Infrared Spectroscopy (FTIR) Analysis .....	358
6.3.5	X-ray Photoelectron Spectroscopy (XPS) Analysis .....	359
6.3.6	X-ray Diffraction (XRD) Analysis .....	360
6.3.7	Scanning Electron Microscopy (SEM) Analysis .....	361
6.3.8	Transmission Electron Microscopy (TEM) Analysis .....	362
6.4	Solid-Gas Adsorption Equilibria.....	363
6.4.1	Adsorption Isotherm Analysis .....	363
6.4.1.1	Brunauer-Emmett-Teller (BET) Isotherm Analysis.....	364
6.4.1.2	The BET-Scatchard (B-S) Plots ( <i>I</i> Point Method Analysis) .....	366
6.4.1.3	Langmuir Isotherm Analysis.....	367
6.4.1.4	Freundlich Isotherm Analysis .....	368
6.4.1.5	Dubinin-Radushkevich Isotherm (D-R) Analysis .....	369
6.4.1.6	Alpha S ( $\alpha_s$ ) Method.....	370
6.4.1.7	John Isotherm Analysis .....	371
6.4.1.8	<i>t</i> – Plot Method.....	374
6.4.1.9	Barrett-Joyner-Halenda (BJH) Method.....	375
6.5	Solid – Liquid Equilibria: Adsorption Studies .....	377
6.5.1	Adsorption Studies of Phenol, <i>P</i> -Nitrophenol and Methylene Blue .....	378
6.5.2	Adsorption of Phenol on GACONZR 1273, GAC 383 and GACO 383 at Temperatures.....	379
6.5.3	Adsorption of <i>P</i> -Nitrophenol on GACONZR 1273, GAC 383 and GACO 383 at Temperatures .....	384
6.5.4	Adsorption of Methylene Blue (MB) on GACONZR 1273, GAC 383 and GACO 383 at Temperatures .....	388
6.5.5	John-Sivanandan Achari (J-SA) Isotherm for Solid- Liquid Equilibria .....	392
6.5.5.1	John - Sivanandan Achari Isotherm for Phenol, <i>P</i> -Nitrophenol and Methylene Blue (MB) Adsorption on GACONZR 1273 at Temperatures .....	395
6.6	Comparison of Adsorption Isotherms for the Adsorption of Phenol, <i>P</i> -Nitrophenol and Methylene Blue (MB) on GACONZR 1273 .....	398
6.7	Adsorption Kinetic Study .....	399
6.7.1	Kinetic Studies of Phenol on GACONZR 1273, GAC 383 and GACO 383 at Temperatures.....	399

6.7.2	Kinetic Study of <i>P</i> -Nitrophenol on GACONZR 1273, GAC 383 and GACO 383 at Temperatures .....	404
6.7.3	Kinetic Studies of Methylene Blue (MB) on GACONZR 1273, GAC 383 and GACO 383 at Temperatures .....	408
6.8	Thermodynamic Parameters .....	411
6.8.1	Thermodynamic Parameters from Distribution Coefficient .....	415
6.9	Diffusion Coefficient .....	418
6.9.1	Determination of Diffusivity for Phenol on GACONZR 1273, GAC 383 and GACO 383 .....	418
6.9.2	Determination of Diffusivity for <i>P</i> -Nitrophenol on GACONZR 1273, GAC 383 and GACO 383 .....	419
6.9.3	Determination of Diffusivity for Methylene Blue on GACONZR 1273, GAC 383 and GACO 383 .....	421
6.10	Activation Energy .....	422
6.11	Design of Batch Adsorption from Isotherm Data .....	424
6.12	Adsorption of Trace Metal Ions by GACONZR Using Contaminated Groundwater .....	426
6.13	Statistical Analysis of the Data .....	427
6.14	Conclusions .....	431
	Reference .....	432

## *Chapter 7*

<b>Summary and Conclusion</b> .....	<b>435 - 444</b>
Future Scope of The Study .....	444
<b>Publications</b> .....	<b>445 - 476</b>

## List of Tables

Table 3.1:	Effect of zirconyl chloride on carbon yield and burn off at 873K as a function of incorporation ratio $X_{ZrOCl_2}$ or $X_{Zr}$ .....	67
Table 3.2:	Burn off, carbon yield, elemental composition and Boehm titration analysis of carbons GAC 383, GACO 383 and GACZR series activated at temperatures 383-1273 K.....	70
Table 3.3:	Surface functional group analysis of carbons GAC 383, GACO 383, GACZR 1273 by XPS spectra.....	76
Table 3.4:	XRD crystalline parameters of GAC 383, GACO 383 and GACZR series activated at temperatures 383 – 1273 K.....	78
Table 3.5:	BET and <i>I</i> plot isotherm parameters for GAC 383, GACO 383, GACZR 873, GACZR 1073 & GACZR 1273 using $N_2$ at 77K .....	90
Table 3.6:	Langmuir and Freundlich isotherm parameters for carbons GAC 383, GACO 383, GACZR 873, GACZR 1073 & GACZR 1273 using $N_2$ at 77K.....	93
Table 3.7:	Dubinin-Radushkevich (D-R) & Alpha S ( $\alpha_S$ ) isotherm parameters of carbons GAC 383, GACO 383, GACZR 873, GACZR 1073 & GACZR 1273 using $N_2$ at 77K.....	97
Table 3.8:	John adsorption isotherm parameters of GAC 383, GACO 383 and GACZR 873, GACZR 1073 and GACZR 1273 .....	98
Table 3.9:	John, Dubinin-Radushkevich (D-R), Alpha S ( $\alpha_S$ ) and Langmuir isotherm: comparison of pore volume obtained from Isotherm models.....	100
Table 3.10:	<i>t</i> plot and BJH isotherm parameters of carbons GAC 383, GACO 383 GACZR 873, GACZR 1073 and GACZR 1273 using $N_2$ at 77K.....	105
Table 3.11:	Langmuir, Freundlich and Dubinin-Radushkevich isotherm parameters of phenol on GACZR 1273, GAC 383 and GACO 383 at temperatures of 283-323 K.....	117
Table 3.12:	Langmuir, Freundlich and Dubinin-Radushkevich isotherm parameters of <i>p</i> -nitrophenol on GACZR 1273, GAC 383, GACO 383 at temperatures of 283- 323K.....	121
Table 3.13:	Langmuir, Freundlich and Dubinin-Radushkevich isotherm parameters of methylene blue on GACZR 1273, GAC 383, GACO 383 at temperatures 283 – 323 K.....	126
Table 3.14:	Comparison of adsorption capacity (mg/g) and surface area ( $m^2/g$ ) for the adsorption of phenol, <i>p</i> -nitrophenol and methylene blue on carbon GACZR 1273, GAC 383 and GACO 383 using John-Sivanandan Achari, Langmuir, D-R and Freundlich isotherm models (T = 303 K).....	131

Table 3.15: John - Sivanandan Achari Isotherm parameter for the adsorption of phenol, <i>p</i> -nitrophenol and methylene blue on carbon GACZR 1273 at 283 – 323K.....	135
Table 3.16: The predicted non linear form of Freundlich, Langmuir, Dubinin – Radushkevich, and John –Sivanandan Achari isotherm equations for GACZR 1273.....	137
Table 3.17: Kinetic parameters of carbons GACZR 1273, GAC 383, GACO 383 for the adsorption of phenol at temperatures ranging from 283 - 323K [ $C_0 = 250$ mg/L].....	143
Table 3.18: Kinetic parameters of carbons GACZR 1273, GAC 383, GACO 383 for the adsorption of <i>p</i> -nitrophenol at temperatures ranging from 283 - 323K [ $C_0 = 250$ mg/L].....	147
Table 3.19: Kinetic parameters of carbons GACZR 1273, GAC 383, GACO 383 for the adsorption of methylene blue at temperatures ranging from 283 - 323K. [ $C_0 = 250$ mg/L].....	151
Table 3.20: Thermodynamic parameters for adsorption of phenol onto GAC 383, GACO 383 and GACZR 1273.....	152
Table 3.21: Thermodynamic parameters for adsorption of <i>p</i> -nitrophenol onto GAC 383, GACO 383 and GACZR 1273.....	153
Table 3.22: Thermodynamic parameters for adsorption of methylene blue (MB) onto GAC 383, GACO 383 and GACZR 1273.....	154
Table 3.23: Thermodynamic parameters obtained from plot of $\ln K_D$ versus $1/T$ for the adsorption of phenol.....	156
Table 3.24: Thermodynamic parameters obtained from plot of $\ln K_D$ versus $1/T$ for the adsorption of <i>p</i> -nitrophenol.....	157
Table 3.25: Thermodynamic parameters obtained from plot of $\ln K_D$ versus $1/T$ for the adsorption of methylene blue.....	157
Table 3.26: Effective diffusion coefficient of carbons for the adsorption of phenol, <i>p</i> -nitrophenol and methylene blue at 283-323K. ....	162
Table 3.27: Activation energy of carbons GAC 383, GACO 383 & GACZR 1273 for the adsorption of phenol, <i>p</i> -nitrophenol and methylene blue.....	164
Table 3.28: Efficiency of carbons GAC 383, GACO 383 and GACZR 1273 for removing trace metals in ground water.....	168
Table 3.29: Three way ANOVA analysis of pore volume and surface area obtained from BET and <i>I</i> -plot method.....	169
Table 3.30: Two way Anova analysis of pore volume obtained from Langmuir, Dubinin-Radsuhkevich (D-R), Alpha S ( $\alpha_s$ ) and John Isotherm.....	170
Table 3.31: Three way ANOVA statistical analysis of adsorption system in solid-liquid equilibria with respect to quantity of phenol, <i>p</i> -nitrophenol and methylene blue adsorbed on GACZR 1273, GAC 383 and GACO 383.....	171

Table 3.32:	Three way ANOVA statistical analysis of adsorption system in solid-liquid equilibria with respect to surface area of GACZR 1273, GAC 383 and GACO 383 .....	172
Table 4.1:	Burn off, carbon yield and elemental composition & Boehm titration analysis of GACOZR series activated at temperatures 383-1273K , GAC 383 and GACO 383.....	185
Table 4.2:	Surface functional groups analysis of carbons GAC 383, GACO 383 and GACOZR 1273 by XPS spectra .....	189
Table 4.3:	XRD crystalline parameters of GAC 383, GACO 383 and GACOZR series activated at temperatures 383 - 1273K.....	191
Table 4.4:	BET and <i>I</i> plot isotherm parameters for GAC 383, GACO 383, GACOZR 1073 & GACOZR 1273 using N <sub>2</sub> at 77K.....	197
Table 4.5:	Langmuir and Freundlich isotherm parameters for GAC 383, GACO 383, GACOZR 1073 & GACOZR 1273 using N <sub>2</sub> at 77K.....	199
Table 4.6:	Dubinin-Radushkevich (D-R) & Alpha S ( $\alpha_s$ ) isotherm parameters of GAC 383, GACO 383, GACOZR 1073 and GACOZR 1273K using N <sub>2</sub> at 77K .....	202
Table 4.7:	John adsorption isotherm parameters of GAC 383, GACO 383, GACOZR 1073 and GACOZR 1273.....	204
Table 4.8:	John, Dubinin-Radushkevich (D-R), Alpha S ( $\alpha_s$ ) and Langmuir isotherm: comparison of pore volume obtained from Isotherm models .....	205
Table 4.9:	<i>t</i> - plot and BJH isotherm parameters of carbons GAC 383, GACO 383, GACOZR 1073 and GACOZR 1273 .....	208
Table 4.10:	Langmuir, Freundlich and Dubinin-Radushkevich (D-R) isotherm parameters of phenol on GACOZR 1273, GAC 383 and GACO 383 at temperatures 283 - 323K.....	215
Table 4.11:	Langmuir, Freundlich and Dubinin-Radushkevich isotherm parameters of <i>p</i> -nitrophenol on GACOZR 1273, GAC 383, and GACO 383 at 283 - 323K.....	220
Table 4.12:	Langmuir, Freundlich and Dubinin-Radushkevich isotherm parameter of methylene blue on GACOZR 1273, GAC 383, GACO 383 at temperatures 283-323 K .....	224
Table 4.13:	Comparison of adsorption capacity (mg/g) and surface area (m <sup>2</sup> /g) for the adsorption of phenol, <i>p</i> -nitrophenol and methylene blue (MB) on carbon GACOZR 1273, GAC 383 and GACO 383 using John-Sivanandan Achari, Langmuir, D-R and Freundlich isotherm models (T = 303K).....	227
Table 4.14:	John - Sivanandan Achari Isotherm parameter for the adsorption of phenol, <i>p</i> -nitrophenol and methylene blue (MB) on carbon GACOZR 1273 at 283 - 323K.....	231
Table 4.15:	The predicted Freundlich, Langmuir, Dubinin – Radushkevich (D-R), John –Sivanandan Achari (J-SA) isotherm equations for GACOZR 1273.....	232

Table 4.16:	Kinetic parameters of carbons GACOZR 1273, GAC 383 and GACO 383 for the adsorption of phenol at temperatures ranging from 283 - 323K. [ $C_0 = 250$ mg/L].....	237
Table 4.17:	Kinetic parameters of carbons GACOZR 1273, GAC 383 and GACO 383 for the adsorption of <i>p</i> -nitrophenol at temperatures ranging from 283 - 323K. [ $C_0 = 250$ mg/L].....	241
Table 4.18:	Kinetic parameters of carbons GACOZR 1273, GAC 383 and GACO 383 for the adsorption of methylene blue (MB) at temperatures ranging from 283 – 323 K. [ $C_0 = 250$ mg/L].....	245
Table 4.19:	Thermodynamic parameters for adsorption of phenol onto GAC 383, GACO 383 and GACOZR 1273 .....	246
Table 4.20:	Thermodynamic parameters for adsorption of <i>p</i> -nitrophenol onto GAC 383, GACO 383 and GACOZR 1273 .....	247
Table 4.21:	Thermodynamic parameters for adsorption of methylene blue (MB) onto GACOZR 1273, GAC 383 and GACO 383.....	248
Table 4.22:	Thermodynamic parameters obtained from plot of $\ln K_D$ versus $1/T$ for the adsorption of phenol.....	250
Table 4.23:	Thermodynamic parameters obtained from plot of $\ln K_D$ versus $1/T$ for the adsorption of <i>p</i> -nitrophenol .....	250
Table 4.24:	Thermodynamic parameters obtained from plot of $\ln K_D$ versus $1/T$ for the adsorption of methylene blue (MB) .....	251
Table 4.25:	Effective diffusion coefficient of carbon for phenol, <i>p</i> -nitrophenol and methylene blue (MB).....	256
Table 4.26:	Activation energy obtained from Arrhenius equation .....	257
Table 4.27:	Efficiency of carbons GAC 383, GACO 383 and GACOZR 1273 for removing trace elements in groundwater. ....	261
Table 4.28:	Two way ANOVA analysis of pore volume and surface area obtained from BET and <i>I</i> -plot method.....	262
Table 4.29:	Statistical analysis of pore volume obtained from from Langmuir, Dubinin-Radushkevich, Alpha S and John isotherm by three way ANOVA .....	263
Table 4.30:	Statistical analysis of adsorption system in solid-liquid equilibria with respect to quantity of phenol, <i>p</i> -nitrophenol and methylene blue adsorbed on GACNZR 1073, GAC 383 and GACO 383 by three way ANOVA .....	264
Table 5.1:	Effect of $ZrO_2$ on carbon yield and burn off at 873K as a function of incorporation ratio $X_{ZrO_2}$ or $X_{Zr}$ .....	274
Table 5.2:	Burn off, carbon yield, elemental composition & Boehm titration analysis of GACNZR series at different temperature 383-1273K, GAC 383 and GACO 383.....	276
Table 5.3:	XRD crystalline parameters of carbons GAC 383, GACO 383 and GACNZR series at different temperature 383-1273K .....	278



Table 5.4:	BET and <i>I</i> plot isotherm parameters for GAC 383, GACO 383, GACNZR 1073 & GACNZR 1273 using N <sub>2</sub> /77K. ....	287
Table 5.5:	Langmuir and Freundlich isotherm parameters for GAC 383, GACO 383, GACNZR 1073 and GACNZR 1273 using N <sub>2</sub> /77K.....	289
Table 5.6:	Dubinin-Radushkevich (D-R) & Alpha S ( $\alpha_s$ ) isotherm parameters of GAC 383, GACO 383, GACNZR 1073 and GACNZR 1273 using N <sub>2</sub> /77K.....	291
Table 5.7:	John adsorption isotherm parameters of GAC 383, GACO 383, GACNZR 1073 and GACONZR 1273.....	293
Table 5.8:	<i>t</i> -plot and BJH isotherm parameters of GAC 383, GACO 383, GACNZR 1073 and GACNZR 1273.....	297
Table 5.9:	Langmuir, Freundlich and Dubinin-Radushkevich (D-R) isotherm parameters for the adsorption of phenol on carbons GACNZR 1073, GAC 383,GACO 383 at 283 – 323 K.....	303
Table 5.10:	Langmuir, Freundlich and Dubinin-Radushkevich (D-R) isotherm parameters for the adsorption of <i>p</i> -nitrophenol on carbons on GACNZR 1073,GAC 383,GACO 383 at 283 – 323 K. ....	306
Table 5.11:	Langmuir, Freundlich and Dubinin-Radushkevich isotherm parameters of methylene blue on carbons GACNZR 1073,GAC 383,GACO 383 at 283 – 323 K.....	310
Table 5.12:	John-Sivanandan Achari (J-SA), Langmuir, Dubinin-Radushkevich (D-R) and Freundlich isotherm models: comparison of adsorption capacity (mg/g) and surface area (m <sup>2</sup> /g) for the adsorption of phenol, <i>p</i> -nitrophenol and MB on carbon GACNZR 1073, GAC 383 and GACO 383 (T = 303K).....	312
Table 5.13:	John - Sivanandan Achari (J-SA) Isotherm parameter for the adsorption of phenol, <i>p</i> -nitrophenol and methylene blue on carbon GACNZR 1073 at 283 - 323K.....	315
Table 5.14:	The predicted non linear form of Freundlich, Langmuir, Dubinin-Radushkevich and John –Sivanandan Achari isotherm equations for GACNZR 1073.....	316
Table 5.15:	Kinetic parameters of carbons GACNZR 1073, GAC 383, GACO 383 for the adsorption of phenol at temperatures ranging from 283 – 323 K [C <sub>0</sub> = 250 mg/L] .....	321
Table 5.16:	Kinetic parameters of carbons GACNZR 1073, GAC 383, GACO 383 for the adsorption of <i>p</i> -nitrophenol at temperatures ranging from 283 – 323 K. [C <sub>0</sub> = 250 mg/L].....	325
Table 5.17:	Kinetic parameters of carbons GACNZR 1073, GAC 383, GACO 383 for the adsorption of methylene blue at temperatures ranging from 283 – 323 K. [C <sub>0</sub> = 250 mg/L].....	329
Table 5.18:	Thermodynamic parameters for adsorption of phenol onto carbons GAC 383, GACO 383 and GACNZR 1073 .....	330

Table 5.19:	Thermodynamic parameters for adsorption of <i>p</i> -nitrophenol onto GAC 383, GACO 383 and GACNZR 1073 .....	331
Table 5.20:	Thermodynamic parameters for adsorption of methylene blue (MB) onto GAC 383, GACO 383 and GACNZR 1073.....	331
Table 5.21:	Thermodynamic parameters obtained from plot of $\ln K_D$ versus $1/T$ for the adsorption of phenol on GACNZR 1073.....	333
Table 5.22:	Thermodynamic parameters obtained from plot of $\ln K_D$ versus $1/T$ for the adsorption of <i>p</i> -nitrophenol on GACNZR 1073 .....	334
Table 5.23:	Thermodynamic parameters obtained from plot of $\ln K_D$ versus $1/T$ for the adsorption of methylene blue (MB) on GACNZR 1073.....	335
Table 5.24:	Effective diffusion coefficient of carbon samples on phenol, <i>p</i> - nitrophenol and methylene blue (MB) .....	340
Table 5.25:	Activation energy obtained from Arrhenius equation .....	342
Table 5.26:	Efficiency of carbons GAC 383, GACO 383 and GACNZR 1073 for removing trace elements in ground water .....	344
Table 5.27:	Statistical analysis of pore volume obtained from BET and <i>I</i> plot using two way ANOVA .....	345
Table 5.28:	Statistical analysis of surface area obtained from BET and <i>I</i> plot using two way ANOVA .....	345
Table 5.29:	Statistical analysis of pore volume obtained from from Langmuir, Dubinin-Radushkevich (D-R), Alpha S ( $\alpha_s$ ) and John isotherm by two way ANOVA.....	346
Table 5.30:	Three way ANOVA statistical analysis of adsorption system in solid-liquid equilibria with respect to quantity of phenol, <i>p</i> -nitrophenol and methylene blue (MB) adsorbed on GACNZR 1073, GAC 383 and GACO 383 .....	347
Table 6.1:	Burn off, carbon yield, elemental composition & Boehm titration analysis of GACONZR series at different temperature 383-1273K, GAC 383 and GACO 383.....	357
Table 6.2:	XRD crystalline parameters of GACONZR series activated at different temperature 383-1273K, GAC 383 and GACO 383 .....	361
Table 6.3:	BET and <i>I</i> plot isotherm parameters for GAC 383, GACO 383, GACONZR 1073 & GACONZR 1273 using $N_2$ at 77K .....	367
Table 6.4:	Langmuir and Freundlich isotherm parameters for GAC 383, GACO 383, GACONZR 1073 and GACONZR 1273 using $N_2$ at 77K .....	369
Table 6.5:	Dubinin-Radushkevich (D-R) & Alpha S ( $\alpha_s$ ) isotherm parameters of GAC 383, GACO 383, GACONZR 1073 and GACONZR 1273 using $N_2$ at 77K .....	371
Table 6.6:	John isotherm parameters of GAC 383, GACO 383 GACONZR 1073 & GACONZR 1273 using $N_2$ /77K.....	373

Table 6.7:	John, Dubinin-Radushkevich (D-R), Alpha S ( $\alpha_s$ ) and Langmuir isotherm: comparison of pore volume obtained from isotherm models.....	373
Table 6.8:	$t$ -plot and BJH isotherm parameters of GAC 383, GACO 383, GACONZR 1073 and GACONZR 1273 using N <sub>2</sub> /77K.....	376
Table 6.9:	Adsorption isotherm parameter of phenol on GACONZR 1273, GAC 383 and GACO 383 at temperatures ranging from 283-323K.....	383
Table 6.10:	Adsorption isotherm parameter of <i>p</i> -nitrophenol on GACONZR 1273, GAC 383 and GACO 383 at temperatures ranging from 283-323K.....	387
Table 6.11:	Adsorption isotherm parameter of methylene blue (MB) on GACONZR 1273, GAC 383 and GACO 383 at temperatures ranging from 283-323K.....	391
Table 6.12:	John-Sivanandan Achari (J-SA), Langmuir, Dubinin-Radushkevich (D-R) and Freundlich isotherm models: comparison of adsorption capacity (mg/g) and surface area (m <sup>2</sup> /g) for the adsorption of phenol, <i>p</i> -nitrophenol and MB on carbon GACONZR 1273, GAC 383 and GACO 383 (T = 303K).....	394
Table 6.13:	John - Sivanandan Achari (J-SA) isotherm parameter for the adsorption of phenol, <i>p</i> -nitrophenol and methylene blue (MB) on carbon GACONZR 1273 at 283 - 323K.....	397
Table 6.14:	The predicted non linear form of Freundlich, Langmuir, Dubinin – Radushkevich, John-Sivanandan Achari isotherm equations for carbon GACONZR 1273.....	398
Table 6.15:	Kinetic parameters of carbons GACONZR 1273, GAC 383 and GACO 383 for the adsorption of phenol at temperatures 283 - 323K. [C <sub>0</sub> = 250 mg/L].....	403
Table 6.16:	Kinetic parameters of carbons GACONZR 1273, GAC 383, and GACO 383 for the adsorption of <i>p</i> -nitrophenol at temperatures 283 - 323K [C <sub>0</sub> = 250 mg/L].....	407
Table 6.17:	Kinetic parameters of carbons GACONZR 1273, GAC 383, and GACO 383 for the adsorption of methylene blue (MB) at temperatures 283 - 323K [C <sub>0</sub> = 250 mg/L].....	411
Table 6.18:	Thermodynamic parameters for the adsorption of phenol onto GAC 383, GACO 383 and GACONZR 1273.....	412
Table 6.19:	Thermodynamic parameters for <i>p</i> -nitrophenol adsorption on GAC 383, GACO 383 and GACONZR 1273.....	413
Table 6.20:	Evaluation of Thermodynamic parameters for methylene blue (MB) adsorption on GACONZR 1273, GAC 383 and GACO 383.....	414
Table 6.21:	Thermodynamic parameters obtained from plot of $\ln K_D$ versus 1/T for the adsorption of phenol on GACONZR 1273.....	416

Table 6.22: Thermodynamic parameters obtained from plot of $\ln K_D$ versus $1/T$ for the adsorption of <i>p</i> -nitrophenol on GACONZR 1273 .....	416
Table 6.23: Thermodynamic parameters obtained from plot of $\ln K_D$ versus $1/T$ for the adsorption of methylene blue (MB) on GACONZR 1273.....	417
Table 6.24: Effective diffusion coefficient of carbon on phenol, <i>p</i> -nitrophenol and methylene blue (MB) .....	422
Table 6.25: Activation energy obtained from Arrhenius equation .....	423
Table 6.26: Efficiency of GACONZR 1273 for removing Trace metals in contaminated groundwater.....	426
Table 6.27: Two way ANOVA analysis of pore volume obtained from BET and <i>I</i> -plot method.....	428
Table 6.28: Two way ANOVA analysis of surface area obtained from BET and <i>I</i> -plot method.....	428
Table 6.29: Two way Anova analysis of pore volume obtained from Langmuir, Dubinin-Radushkevich (D-R), Alpha S and John Isotherm.....	429
Table 6.30: Three way ANOVA statistical analysis of adsorption system in solid-liquid equilibria with respect to quantity of phenol, <i>p</i> -nitrophenol and methylene blue adsorbed on GACONZR 1273, GAC 383 and GACO 383.....	430

## ||| List of Figures |||

Figure 1.1:	Surface functional groups on activated carbon.....	06
Figure 1.2:	Schematic representation of pore structure of activated carbon .....	13
Figure 2.1:	The experimental setup for the carbonization of the native carbon char under steam flow in a temperature programmed furnace .....	36
Figure 2.2:	Schematic representation of newly prepared Zr incorporated granular activated carbons .....	36
Figure 2.3:	The IUPAC classification of adsorption isotherms .....	42
Figure 2.4:	The IUPAC classification of Hysteresis loops.....	42
Figure 2.5:	Schematic representation of the single stage batch adsorber system .....	59
Figure 3.1:	Variation of carbon yield and burn off with impregnation ratio.....	68
Figure 3.2:	Fourier transform infrared (FTIR) spectra of carbons (a) GAC 383 (b) GACO 383 (c)-(h) GACZR series of carbons activated at 383-1273K for the evaluation of functional groups.....	72
Figure 3.3:	X-ray photoelectron spectrum (XPS) of GACZR 1273 prepared by activating GAC 383 with $Zr^{4+}$ at 1273K. Deconvoluted peaks (a) C 1s, (b) O 1s (c) Zr 3d .....	74
Figure 3.4:	X-ray photoelectron spectrum (XPS) of GAC 383 (a) C 1s deconvoluted peaks (b) O 1s deconvoluted peaks .....	75
Figure 3.5:	X-ray photoelectron spectrum (XPS) of GACO 383 (a) C 1s deconvoluted peaks (b) O 1s deconvoluted peaks .....	75
Figure 3.6:	X-ray diffraction (XRD) spectra of (a) GAC 383 & GACO 383 (b) GACZR series of carbons activated at 383-1273K.....	77
Figure 3.7:	Scanning electron micrographs (SEM) at different magnifications (a) GAC 383 & (b) GACO 383 at 50 $\mu$ m resolution (c) GAC 383 & (d) GACO 383 at 10 $\mu$ m resolutions.....	79
Figure 3.8:	Scanning electron micrographs (SEM) of carbon GACZR 1273 at different resolution (a) 250-100 $\mu$ m (b) 500-50 $\mu$ m (c) 10 $\mu$ m & (d) 5 $\mu$ m.....	80
Figure 3.9:	High resolution transmission electron microscopy (HRTEM) of GAC 383 at different resolutions (a) 200 nm (b) 100 nm (c) 50 nm & (d) 20 nm .....	81
Figure 3.10:	High resolution transmission electron microscopy (HRTEM) of GACO 383 at different resolutions (a) 200 nm (b) 100 nm (c) 50 nm & (d) 20 nm .....	82
Figure 3.11:	High resolution transmission electron microscopy (HRTEM) of GACZR 1273 at different resolutions (a) 200 nm (b) 100 nm (c) 50 nm & (d) 20 nm.....	83
Figure 3.12:	N <sub>2</sub> adsorption isotherm for GAC 383, GACO 383 and GACZR series carbonized at temperature 873-1273 K.....	84

Figure 3.13: BET isotherm plot for carbons GAC 383, GACO 383, GACZR 873, GACZR 1073, GACZR 1273 (a) $p/p_0$ up to 0.3 and (b) $p/p_0$ up to 0.1 using $N_2$ at 77K.....	86
Figure 3.14: Nitrogen adsorption-desorption isotherms and the corresponding $I$ plots for (a) GAC 383 (b) GACO 383 (c) GACZR 873 (d) GACZR 1073 and (e) GACZR 1273 .....	89
Figure 3.15: Adsorption isotherm plots (a) Langmuir (b) Freundlich for carbons GAC 383, GACO 383, GACZR 873, GACZR 1073 & GACZR 1273 using $N_2$ at 77K.....	92
Figure 3.16: Adsorption isotherm plot (a) Dubinin- Radushkevich and (b) Alpha S ( $\alpha_s$ ) for GAC 383, GACO 383, GACZR 873, GACZR 1073, GACZR 1273 using $N_2$ at 77K.....	96
Figure 3.17: John Isotherm plot of carbons (a) – (c) GACZR series carbonized at temperature 873-1273 K, (d) GAC 383, & (e) GACO 383 using $N_2$ adsorption data at 77K.....	99
Figure 3.18: Comparison of pore volumes obtained from John (J) /D-R/ Alpha S/ Langmuir isotherm models.....	102
Figure 3.19: $t$ -plot analysis of GAC 383, GACO 383, GACZR 873, GACZR 1073 and GACZR 1273.....	102
Figure 3.20: BJH isotherm analysis (a) Adsorption cumulative pore volume (b) Desorption cumulative pore volume for GAC 383, GACO 383, GACZR 873, GACZR 1073 and GACZR 1273 using $N_2$ adsorption/desorption data at 77K.....	103
Figure 3.21: BJH isotherm analysis (a) Adsorption $dV/dw$ pore volume (b) Desorption $dV/dw$ pore volume for GAC 383, GACO 383, GACZR 873, GACZR 1073 and GACZR 1273 using $N_2$ adsorption/desorption data at 77K.....	103
Figure 3.22: BJH isotherm analysis (a) Adsorption $dV/dlogw$ pore volume and (b) Desorption $dV/dlogw$ pore volume for the carbons, GAC 383, GACO 383, GACZR 873, GACZR 1073 and GACZR 1273 using $N_2$ adsorption/desorption data at 77K.....	104
Figure 3.23: Specific amount of (a) phenol and (b) methylene blue (MB) adsorbed on different carbon dose in 50 ml solution of adsorbate.....	106
Figure 3.24: Effect of contact time for the adsorption of (a) phenol [ $C_0$ 1000mg/L], (b) $p$ -nitrophenol [ $C_0$ 1000mg/L] and (c) methylene blue [ $C_0$ 500mg/L].....	107
Figure 3.25: Adsorption efficiency of GACZR series of carbons in (a) 1000 mg/L phenol (b) 1000 mg/L $p$ -nitrophenol and (c) 500 mg/L methylene blue solution.....	108
Figure 3.26: Equilibrium adsorption isotherm plots for carbons GAC 383, GACO 383, and GACZR 1273 at 30 <sup>0</sup> C (a) phenol [ $C_0$ ; 25 - 3000 mg/L], (b) $p$ -nitrophenol [ $C_0$ ; 25-3000mg/L] and (c) methylene blue [ $C_0$ ; 25 -1500 mg/L].....	110

Figure 3.27: Langmuir isotherm plot for the adsorption of phenol on carbons at temperatures of 283 - 323 K and $C_0$ ; 25-3000mg/L (a) GACZR 1273, (b) GAC 383 and (c) GACO 383 .....	113
Figure 3.28: Freundlich isotherm plot for the adsorption of phenol on carbons at temperatures of 283 - 323 K and $C_0$ ; 25-3000mg/L (a) GACZR 1273, (b) GAC 383 and (c) GACO 383.....	114
Figure 3.29: Dubinin–Radushkevich (D-R) isotherm plot for the adsorption of phenol on carbons at temperatures of 283 - 323 K and $C_0$ ; 25-3000 mg/L (a) GACZR 1273, (b) GAC 383 and (c) GACO 383 .....	116
Figure 3.30: Langmuir isotherm plot for the adsorption of <i>p</i> -nitrophenol on carbons at temperatures of 283 - 323 K and $C_0$ ; 25-3000 mg/L (a) GACZR 1273, (b) GAC 383 and (c) GACO 383.....	118
Figure 3.31: Freundlich isotherm plot for the adsorption of <i>p</i> -nitrophenol on carbons at temperatures of 283 - 323 K and $C_0$ ; 25-3000 mg/L (a) GACZR 1273, (b) GAC 383 and (c) GACO 383.....	119
Figure 3.32: Dubinin–Radushkevich (D-R) isotherm plot for the adsorption of <i>p</i> -nitrophenol on carbons at temperatures of 283 - 323 K and $C_0$ ; 25-3000 mg/L (a) GACZR 1273, (b) GAC 383 and (c) GACO 383.....	120
Figure 3.33: Langmuir isotherm plot for the adsorption of methylene blue (MB) on carbons at temperatures of 283 - 323 K and $C_0$ ; 25 - 1500 mg/L (a) GACZR 1273, (b) GAC 383 and (c) GACO 383 .....	122
Figure 3.34: Freundlich isotherm plot for the adsorption of methylene blue (MB) on carbons at temperatures of 283 - 323 K and $C_0$ ; 25 - 1500 mg/L (a) GACZR 1273, (b) GAC 383 and (c) GACO 383 .....	124
Figure 3.35: Dubinin-Radushkevich (D-R) isotherm plot for the adsorption of methylene blue (MB) on carbons at temperatures of 283 - 323 K and $C_0$ ; 25 - 1500 mg/L (a) GACZR 1273, (b) GAC 383 and (c) GACO 383.....	125
Figure 3.36: John-Sivanandan Achari isotherm (J-SA) plot for the adsorption of methylene blue (MB) on carbons at 303 K and $C_0$ ; 25- 1500 mg/L (a) GAZR 1273 (b) GAC 383 and (c) GACO 383.....	128
Figure3. 37: John-Sivanandan Achari isotherm (J-SA) plot for the adsorption of phenol on carbons at 303 K and $C_0$ ; 25- 3000 mg/L (a) GACZR 1273 (b) GAC 383 and (c) GACO 383.....	129
Figure 3.38: John-Sivanandan Achari isotherm plot for the adsorption of <i>p</i> -nitrophenol on carbons at 303K and $C_0$ ; 25- 3000 mg/L (a) GAZR 1273 (b) GAC 383 (c) GACO 383.....	130
Figure 3.39: John –Sivanandan Achari isotherm plot for phenol adsorption on GACZR 1273 at temperatures (a) 283K (b) 293K (c) 313K and (d) 323K.....	132
Figure 3.40: John –Sivanandan Achari isotherm for <i>p</i> - nitrophenol adsorption on GACZR 1273 at temperatures (a) 283 K (b) 293 K (c) 313 K and (d) 323 K.....	133

Figure 3.41: John –Sivanandan Achari isotherm for methylene blue (MB) adsorption on GACZR 1273 at temperatures (a) 283 K (b) 293 K (c) 313 K and (d) 323 K.....	134
Figure 3.42: Comparison of the adsorption isotherms model to the observed isotherm data for the adsorption of (a) phenols, (b) <i>p</i> -nitrophenol and (c) methylene blue on to activated carbon GACZR 1273.....	136
Figure 3.43: Pseudo-first order kinetic plot of carbons for the adsorption of phenol at 283 – 323 K and $C_0$ ; 250 mg/L (a) GACZR 1273 (b) GAC 383 and (c) GACO 383 .....	139
Figure 3.44: Pseudo-second order kinetic plot of carbons for the adsorption of phenol at 283 – 323 K and $C_0$ ; 250 mg/L (a) GACZR 1273 (b) GAC 383 and (c) GACO 383.....	140
Figure 3.45: Intra-particle diffusion plot of carbons for the adsorption of phenol at 283 – 323 K and $C_0$ ; 250 mg/L (a) GACZR 1273 (b) GAC 383 and (c) GACO 383 .....	142
Figure 3.46: Pseudo-first order kinetic plot of carbons for the adsorption of <i>p</i> -nitrophenol at 283 – 323 K and $C_0$ ; 250 mg/L (a) GACZR 1273 (b) GAC 383 and (c) GACO 383.....	144
Figure 3.47: Pseudo-second order kinetic plot of carbons for the adsorption of <i>p</i> -nitrophenol at 283 – 323 K and $C_0$ ; 250 mg/L (a) GACZR 1273 (b) GAC 383 and (c) GACO 383.....	145
Figure 3.48: Intra-particle diffusion plot of carbons for the adsorption of <i>p</i> -nitrophenol at 283 – 323 K and $C_0$ ; 250 mg/L (a) GACZR 1273 (b) GAC 383 and (c) GACO 383.....	146
Figure 3.49: Pseudo-first order kinetic plot of carbons for the adsorption of methylene blue (MB) at 283 – 323 K and $C_0$ ; 250 mg/L (a) GACZR 1273 (b) GAC 383 and (c) GACO 383 .....	148
Figure 3.50: Pseudo-second order kinetic plot of carbons for the adsorption of methylene blue (MB) at 283 – 323 K and $C_0$ ; 250 mg/L (a) GACZR 1273 (b) GAC 383 and (c) GACO 383 .....	149
Figure 3.51: Intra-particle diffusion plot of carbons for the adsorption of methylene blue (MB) at 283 – 323 K and $C_0$ ; 250 mg/L (a) GACZR 1273 (b) GAC 383 and (c) GACO 383 .....	150
Figure 3.52: Plot of $\ln K_L$ versus $1/T$ for the estimation of thermodynamic parameters for the adsorption of (a) phenol, (b) <i>p</i> -nitrophenol and (c) methylene blue (MB) on carbons GACZR 1273, GAC 383, and GACO 383 .....	155
Figure 3.53: Plots of $\ln K_D$ versus $1/T$ of carbons GACZR 1273, GAC 383 and GACO 383 for the adsorption of (a-c) phenol, (d-f) <i>p</i> -nitrophenol and (g-i) methylene blue.....	158
Figure 3.54: Plot of $\ln[1/1-F^2(t)]$ versus time for the estimation of diffusion coefficient for the adsorption of phenol on carbons (a) GACZR 1273 (b) GAC 383 and (c) GACO 383.....	159



Figure 3.55: Plot of $\ln[1/1-F^2(t)]$ versus time for the estimation of diffusion coefficient for the adsorption of <i>p</i> -nitrophenol on carbons (a) GACZR 1273 (b) GAC 383 and (c) GACO 383 .....	160
Figure 3.56: Plot of $\ln[1/1-F^2(t)]$ versus time for the estimation of diffusion coefficient for the adsorption of methylene blue (MB) on carbons (a) GACZR 1273 (b) GAC 383 and (c) GACO 383 .....	161
Figure 3.57: Plot of $\ln K_2$ versus $1/T$ for the estimation of activation energy of carbons GACZR 1273, GAC 383, GACO 383 for the adsorption of (a) phenol, (b) <i>p</i> -nitrophenol and (c) methylene blue .....	163
Figure 3.58: Schematic representation of the single stage batch adsorber system .....	166
Figure 3.59: Adsorbent mass ( <i>M</i> ) against concentration of (a) phenol (b) <i>p</i> -nitrophenol (c) methylene blue (MB) for 99% removal of effluent in one liter of solution .....	167
Figure 4.1: FTIR spectra of carbons (a) GAC 383 (b) GACO 383 (c)-(h) GACOZR series of carbons activated at 383-1273K for the evaluation of functional groups. ....	187
Figure 4.2: X-ray photoelectron spectrum (XPS) of GACOZR 1273. Deconvoluted peaks (a) C 1s (b) O 1s and (c) Zr 3d .....	189
Figure 4.3: X-ray diffraction (XRD) spectra of (a) GAC 383 & GACO 383 (b) GACOZR series of carbons activated at 383-1273K.....	190
Figure 4.4: Scanning electron micrographs (SEM) of GACOZR 1273 at different resolution (a) 250-100 $\mu\text{m}$ (b) 500-50 $\mu\text{m}$ (c) 10 $\mu\text{m}$ and (d) 5 $\mu\text{m}$ .....	192
Figure 4.5: High resolution transmission electron microscopy (HRTEM) of GACOZR 1273 at different resolutions (a) 10nm (b) 5 nm (c) and (d) 2 nm.....	193
Figure 4.6: $\text{N}_2$ adsorption isotherm for GAC 383, GACO 383 and GACOZR carbonized at temperature 1073 and 1273 K.....	194
Figure 4.7: BET isotherm plot for GAC 383, GACO 383, GACOZR 1073 and GACOZR 1273 (a) $p/p_0$ up to 0.3 and (b) $p/p_0$ up to 0.1 .....	196
Figure 4.8: Nitrogen adsorption-desorption isotherms and the corresponding <i>I</i> plots for (a) GACOZR 1073 (b) GACOZR 1273 (c) GAC 383 and (d) GACO 383 carbons .....	197
Figure 4.9: Adsorption isotherm plots (a) Langmuir (b) Freundlich for GAC 383, GACO 383, GACOZR 1073 & GACOZR 1273 using $\text{N}_2$ at 77K.....	199
Figure 4.10: Adsorption isotherm plots (a) Dubinin - Radushkevich and (b) Alpha S ( $\alpha_s$ ) for GAC 383, GACO 383, GACOZR 1073 & GACOZR 1273 K using $\text{N}_2$ at 77K .....	201
Figure 4.11: John Isotherm plot for carbons (a) GACOZR 1073 (b) GACOZR 1273 (c) GAC 383 and (d) GACO 383 .....	204

Figure 4.12: Comparison of pore volumes obtained for John (J) /D-R/ Alpha S/ Langmuir models for the adsorption of N <sub>2</sub> at 77 K for newly prepared microporous carbons.....	206
Figure 4.13: <i>t</i> -plot analysis of carbons GAC 383, GACO383 and GACOZR 1073 and GACOZR 1273 .....	206
Figure 4.14: BJH isotherm analysis (a) Adsorption cumulative pore volume (b) Desorption cumulative pore volume for GAC 383, GACO 383, GACOZR 1073 & GACOZR 1273 .....	207
Figure 4.15: BJH isotherm analysis (a) Adsorption dV/dw pore volume (b) Desorption dV/dw pore volume for GAC 383, GACO 383, GACOZR 1073 & GACOZR 1273 .....	208
Figure 4.16: BJH isotherm analysis (a) Adsorption dV/dlogw pore volume and (b) Desorption dV/dlogw pore volume for the carbons, GAC 383, GACO 383, GACOZR 1073 & GACOZR 1273.....	208
Figure 4.17: Adsorption efficiency of GACOZR series of carbons in (a) 1000 mg/L phenol (b) 1000 mg/L <i>p</i> -nitrophenol and (c) 500 mg/L methylene blue (MB) .....	209
Figure 4.18: Equilibrium adsorption isotherm plots for carbons GAC 383, GACO 383 and GACOZR 1273 at 30 <sup>0</sup> C (a) Phenol [C <sub>0</sub> ; 25 - 3000 mg/L], (b) <i>p</i> -nitrophenol [C <sub>0</sub> ; 25-3000mg/L] and (c) Methylene Blue [C <sub>0</sub> ; 25 -1500 mg/L] .....	210
Figure 4.19: Langmuir isotherm plot for the adsorption of phenol on carbons at temperatures of 283 - 323 K and C <sub>0</sub> ; 25-3000mg/L (a) GACOZR 1273, (b) GAC 383 and (c) GACO 383 .....	212
Figure 4.20: Freundlich isotherm plot for the adsorption of phenol on carbons at temperatures of 283 - 323 K and C <sub>0</sub> ; 25 – 3000 mg/L (a) GACOZR 1273, (b) GAC 383 and (c) GACO 383 .....	213
Figure 4.21: Dubinin - Radushkevich (D-R) isotherm plot for the adsorption of phenol on carbons at temperatures of 283 - 323 K and C <sub>0</sub> ; 25 – 3000 mg/L (a) GACOZR 1273, (b) GAC 383 and (c) GACO 383 .....	214
Figure 4.22: Langmuir isotherm plot for the adsorption of <i>p</i> -nitrophenol on carbons at temperatures of 283 - 323 K and C <sub>0</sub> ; 25 – 3000 mg/L (a) GACOZR 1273, (b) GAC 383 and (c) GACO 383 .....	217
Figure 4.23: Freundlich isotherm plot for the adsorption of <i>p</i> -nitrophenol on carbons at temperatures of 283 - 323 K and C <sub>0</sub> ; 25 – 3000 mg/L (a) GACOZR 1273, (b) GAC 383 and (c) GACO 383 .....	218
Figure 4.24: Dubinin - Radushkevich (D-R) isotherm plot for the adsorption of <i>p</i> -nitrophenol on carbons at temperatures of 283 - 323 K and C <sub>0</sub> ; 25 – 3000 mg/L (a) GACOZR 1273, (b) GAC 383 and (c) GACO 383 .....	219
Figure 4.25: Langmuir isotherm plot for the adsorption of methylene blue on carbons at temperatures of 283 - 323 K and C <sub>0</sub> ; 25 – 1500 mg/L (a) GACOZR 1273, (b) GAC 383 and (c) GACO 383 .....	221

Figure 4.26: Freundlich isotherm plot for the adsorption of methylene blue (MB) on carbons at temperatures of 283 - 323 K and $C_0$ ; 25 – 1500 mg/L (a) GACOZR 1273, (b) GAC 383 and (c) GACO 383.....	222
Figure 4.27: Dubinin-Radushkevich (D-R) isotherm plot for the adsorption of methylene blue (MB) on carbons at temperatures of 283 - 323 K and $C_0$ ; 25 – 1500 mg/L (a) GACOZR 1273, (b) GAC 383 and (c) GACO 383.....	223
Figure 4.28: John-Sivanandan Achari isotherm plot for carbon GACOZR 1273 at 303 K for the adsorption of (a) methylene blue, $C_0$ 25 - 1500 mg/L (b) phenol, $C_0$ 25 -3000 mg/L and (c) <i>p</i> -nitrophenol, $C_0$ 25 - 3000 mg/L .....	228
Figure 4.29: John –Sivanandan Achari (J-SA) isotherm plot for phenol adsorption on GACOZR 1273 at selected temperatures (a) 283 K (b) 293 K (c) 313 K and (d) 323 K .....	229
Figure 4.30: John –Sivanandan Achari (J-SA) isotherm plot for <i>p</i> -nitrophenol adsorption on GACOZR 1273 at temperatures (a) 283 K (b) 293 K (c) 313 K and (d) 323 K.....	230
Figure 4.31: John –Sivanandan Achari (J-SA) isotherm plot for methylene blue (MB) adsorption on GACOZR 1273 at temperatures (a) 283 K (b) 293 K (c) 313 K and (d) 323 K.....	230
Figure 4.32: Comparison of the model fit of various isotherms to the observed isotherm data for the adsorption of (a) phenol (b) <i>p</i> -nitrophenol and (c) methylene blue (MB) onto activated carbon GACOZR 1273.....	232
Figure 4.33: Pseudo-first order kinetic plot of carbons for the adsorption of phenol at 283 – 323 K and $C_0$ ; 250 mg/L (a) GACOZR 1273 (b) GAC 383 and (c) GACO 383.....	233
Figure 4.34: Pseudo-second order kinetic plot of carbons for the adsorption of phenol at 283 – 323 K and $C_0$ ; 250 mg/L (a) GACOZR 1273 (b) GAC 383 and (c) GACO 383.....	234
Figure 4.35: Intra-particle diffusion kinetic plot of carbons for the adsorption of phenol at 283 – 323 K and $C_0$ ; 250 mg/L (a) GACOZR 1273 (b) GAC 383 and (c) GACO 383 .....	236
Figure 4.36: Pseudo-first order kinetic plot of carbons for the adsorption of <i>p</i> -nitrophenol at 283 – 323 K and $C_0$ ; 250 mg/L (a) GACOZR 1273 (b) GAC 383 and (c) GACO 383.....	238
Figure 4.37: Pseudo-second order kinetic plot of carbons for the adsorption of <i>p</i> -nitrophenol at 283 – 323 K and $C_0$ ; 250 mg/L (a) GACOZR 1273 (b) GAC 383 and (c) GACO 383 .....	239
Figure 4.38: Intra particle diffusion kinetic plot of carbons for the adsorption of <i>p</i> -nitrophenol at 283 – 323 K and $C_0$ ; 250 mg/L (a) GACOZR 1273 (b) GAC 383 and (c) GACO 383 .....	240
Figure 4.39: Pseudo-first order kinetic plot of carbons for the adsorption of methylene blue (MB) at 283 – 323 K and $C_0$ ; 250 mg/L (a) GACOZR 1273 (b) GAC 383 and (c) GACO 383 .....	242

Figure 4.40: Pseudo-second order kinetic plot of carbons for the adsorption of methylene blue (MB) at 283 – 323 K and $C_0$ ; 250 mg/L (a) GACOZR 1273 (b) GAC 383 and (c) GACO 383 .....	243
Figure 4.41: Intra particle diffusion kinetic plot of carbons for the adsorption of methylene blue (MB) at 283 – 323 K and $C_0$ ; 250 mg/L (a) GACOZR 1273 (b) GAC 383 and (c) GACO 383 .....	244
Figure 4.42: Plot of $\ln K_L$ versus $1/T$ for the estimation of thermodynamic parameters for the adsorption of (a) phenol, (b) <i>p</i> -nitrophenol and (c) methylene blue (MB) on carbons GACOZR 1273, GAC 383, and GACO 383.....	248
Figure 4.43: Plots of $\ln K_D$ versus $1/T$ of carbon GACOZR 1273 for the adsorption of (a) phenol, (b) <i>p</i> -nitrophenol and (c) methylene blue (MB) .....	252
Figure 4.44: Plot of $\ln[1/1-F^2(t)]$ versus time for the estimation of diffusion coefficient for the adsorption of phenol on carbons (a) GACOZR 1273 (b) GAC 383 and (c) GACO 383 .....	253
Figure 4.45: Plot of $\ln[1/1-F^2(t)]$ versus time for the estimation of diffusion coefficient for the adsorption of <i>p</i> -nitrophenol on carbons (a) GACOZR 1273 (b) GAC 383 and (c) GACO 383 .....	254
Figure 4.46: Plot of $\ln[1/1-F^2(t)]$ versus time for the estimation of diffusion coefficient for the adsorption of methylene blue (MB) on carbons (a) GACOZR 1273 (b) GAC 383 and (c) GACO 383.....	255
Figure 4.47: Plot of $\ln K_2$ versus $1/T$ for the estimation of activation energy of carbons GACOZR 1273, GAC 383, GACO 383 for the adsorption of (a) phenol, (b) <i>p</i> -nitrophenol and (c) methylene blue (MB) .....	258
Figure 4.48: Mass of adsorbent against concentration of (a) phenol, (b) <i>p</i> -nitrophenol, and (c) methylene blue (MB) solution.....	260
Figure 5.1: XRD spectra of Nano $ZrO_2$ prepared.....	273
Figure 5.2: EDS analysis of $ZrO_2$ prepared.....	273
Figure 5.3: TEM images of prepared nano $ZrO_2$ and its scattered area electron diffraction pattern .....	273
Figure 5.4: Variation of burn off with impregnation ratio .....	274
Figure 5.5: XRD spectra of (a) GAC 383 & GACO 383 (b) GACNZR series of carbons activated at 383-1273K.....	277
Figure 5.6: FTIR spectra of (a) GAC 383 (b) GACO 383 (c)-(h) GACNZR series of carbons activated at 383-1273K for the evaluation of functional groups .....	279
Figure 5.7: X-ray photo electron spectrum (a) C 1s spectrum of GAC 383, GACO 383 and GACNZR 1273 (b) O 1s spectrum of GAC 383, GACO 383 and GACNZR 1273 (c) Zr 3d spectrum of GACNZR 1273 .....	280
Figure 5.8: X-ray photoelectron spectrum (XPS) of GACNZR 1273. Deconvoluted peaks (a) C 1s and (b) O 1s .....	281

Figure 5.9: Scanning electron micrographs (SEM) of GACNZR 1273 at different resolution (a) 250-100 $\mu\text{m}$ (b) 500-50 $\mu\text{m}$ and (c) 10 $\mu\text{m}$ .....	282
Figure 5.10: High resolution transmission electron microscopy (HRTEM) of GACNZR 1273 at different resolutions (a) 50 nm and (b) 20 nm.....	283
Figure 5.11: N <sub>2</sub> adsorption isotherm for GAC 383, GACO 383 and GACNZR series carbonized at temperature 1073 and 1273 K.....	284
Figure 5.12: BET isotherm plot for GAC 383, GACO 383, GACNZR 1073 & GACNZR 1273 (a) p/p <sub>0</sub> up to 0.3 and (b) p/p <sub>0</sub> up to 0.1 using N <sub>2</sub> /77K.....	285
Figure 5.13: Nitrogen adsorption-desorption isotherms and the corresponding <i>I</i> plots (a) GACNZR 1073 (b) GACNZR 1273 (c) GAC 383 & (d) GACO 383 .....	286
Figure 5.14: Adsorption isotherm plots (a) Langmuir (b) Freundlich for GAC 383, GACO 383, GACNZR 1073 & GACNZR 1273 using N <sub>2</sub> /77K.....	289
Figure 5.15: Adsorption isotherm plots (a) Dubinin - Radushkevich (b) Alpha S ( $\alpha_s$ ) for GAC 383, GACO 383, GACNZR 1073 & GACNZR 1273 K using N <sub>2</sub> /77K.....	291
Figure 5.16: John Isotherm plot for carbons (a) GACNZR 1073 (b) GACNZR 1273.....	292
Figure 5.17: Comparison of Pore volumes obtained from John (J) , D-R, Alpha S and Langmuir models for the adsorption of N <sub>2</sub> at 77K for microporous carbons.....	294
Figure 5.18: <i>t</i> -plot analysis of GAC 383, GACO 383 and GACNZR series carbonized at temperature 1073- 1273 K.....	294
Figure 5.19: BJH isotherm analysis (a) Adsorption cumulative pore volume (b) Desorption cumulative pore volume for GAC 383, GACO 383, GACNZR 1073 & GACNZR 1273 .....	295
Figure 5.20: BJH isotherm analysis (a) Adsorption dV/dw pore volume (b) Desorption dV/dw pore volume for GAC 383, GACO 383, GACNZR 1073 & GACNZR 1273 .....	296
Figure 5.21: BJH isotherm analysis (a) Adsorption dV/dlogw pore volume and (b) Desorption dV/dlogw pore volume for the carbons, GAC 383, GACO 383, GACNZR 1073 & GACNZR 1273.....	296
Figure 5.22: Adsorption efficiency of GACNZR series of carbons in (a) 1000 mg/L phenol (b) 1000 mg/L <i>p</i> -nitrophenol and (c) 500 mg/L methylene blue (MB) .....	297
Figure 5.23: Equilibrium adsorption isotherm plots for carbons GAC 383, GACO 383, and GACNZR 1073 at 30 <sup>0</sup> C (a) Phenol [C <sub>0</sub> ; 25 - 3000 mg/L], (b) <i>p</i> -nitrophenol [C <sub>0</sub> ; 25-3000mg/L] and (c) methylene blue [C <sub>0</sub> ; 25 -1500 mg/L] .....	298
Figure 5.24: Langmuir isotherm plot for the adsorption of phenol on carbons at temperatures of 283 - 323 K and C <sub>0</sub> ; 25-3000 mg/L (a) GACNZR 1073, (b) GAC 383 and (c) GACO 383 .....	300

Figure 5.25: Freundlich isotherm plot for the adsorption of phenol on carbons at temperatures of 283 - 323 K and $C_0$ ; 25-3000 mg/L (a) GACNZR 1073, (b) GAC 383 and (c) GACO 383 .....	301
Figure 5.26: Dubinin-Radushkevich isotherm plot for the adsorption of phenol on carbons at temperatures of 283 - 323 K and $C_0$ ; 25-3000 mg/L (a) GACNZR 1073, (b) GAC 383 and (c) GACO 383.....	302
Figure 5.27: Langmuir isotherm plot for the adsorption of <i>p</i> -nitrophenol on carbons at temperatures of 283 - 323 K and $C_0$ ; 25-3000 mg/L (a) GACNZR 1073, (b) GAC 383 and (c) GACO 383 .....	304
Figure 5.28: Freundlich isotherm plot for the adsorption of <i>p</i> -nitrophenol on carbons at temperatures of 283 - 323 K and $C_0$ ; 25-3000 mg/L (a) GACNZR 1073, (b) GAC 383 and (c) GACO 383 .....	305
Figure 5.29: Dubinin-Radushkevich (D-R) isotherm plot for the adsorption of <i>p</i> -nitrophenol on carbons at temperature of 283 - 323 K and $C_0$ ; 25-3000 mg/L (a) GACNZR 1073, (b) GAC 383 and (c) GACO 383 .....	306
Figure 5.30: Langmuir isotherm plot for the adsorption of methylene blue (MB) on carbons at temperatures of 283 - 323 K and $C_0$ ; 25-1500 mg/L (a) GACNZR 1073, (b) GAC 383 and (c) GACO 383.....	307
Figure 5.31: Freundlich isotherm for the adsorption of methylene blue (MB) on carbons at temperatures of 283 - 323 K and $C_0$ ; 25-1500 mg/L (a) GACNZR 1073, (b) GAC 383 and (c) GACO 383 .....	308
Figure 5.32: Dubinin Radushkevich isotherm for the adsorption of methylene blue (MB) on carbons at temperatures of 283 - 323 K and $C_0$ ; 25-1500 mg/L (a) GACNZR 1073, (b) GAC 383 and (c) GACO 383 .....	309
Figure 5.33: John-Sivanandan Achari isotherm plot for the adsorption of (a) methylene blue (MB), (b) phenol and (c) <i>p</i> -nitrophenol on carbon GACNZR 1073 at 30 <sup>o</sup> C .....	311
Figure 5.34: John-Sivanandan Achari isotherm for phenol adsorption on GACNZR 1073 at temperatures (a) 283 K (b) 293 K (c) 313 K & (d) 323 K .....	313
Figure 5.35: John-Sivanandan Achari isotherm for <i>p</i> -nitrophenol adsorption on GACNZR 1073 at temperatures (a) 283 K (b) 293 K (c) 313 K (d) 323 K.....	314
Figure 5.36: John-Sivanandan Achari isotherm for methylene blue adsorption on GACNZR 1073 at temperatures (a) 283 K (b) 293 K (c) 313 K and (d) 323 K.....	315
Figure 5.37: Comparison of the model fit of various isotherms to the observed isotherm data for the adsorption of (a) phenol, (b) <i>p</i> -nitrophenol and (c) methylene blue (MB) onto activated carbon GACNZR 1073.....	317
Figure 5.38: Pseudo-first order kinetic plot of carbons for the adsorption of phenol at 283 – 323 K and $C_0$ ; 250 mg/L (a) GACNZR 1073 (b) GAC 383 and (c) GACO 383.....	318

Figure 5.39: Pseudo-second order plot of carbons for the adsorption of phenol at 283 – 323 K and $C_0$ ; 250 mg/L (a) GACNZR 1073 (b) GAC 383 and (c) GACO 383.....	319
Figure 5.40: Intra particle diffusion kinetic plot of carbons for the adsorption of phenol at 283 – 323 K and $C_0$ ; 250 mg/L (a) GACNZR 1073 (b) GAC 383 and (c) GACO 383.....	320
Figure 5.41: Pseudo first order kinetic plot of carbons for the adsorption of <i>p</i> -nitrophenol at 283 – 323 K and $C_0$ ; 250 mg/L (a) GACNZR 1073 (b) GAC 383 and (c) GACO 383.....	322
Figure 5.42: Pseudo second order kinetic plot of carbons for the adsorption of <i>p</i> -nitrophenol at 283 – 323 K and $C_0$ ; 250 mg/L (a) GACNZR 1073 (b) GAC 383 and (c) GACO 383 .....	323
Figure 5.43: Intra particle diffusion kinetic plot of carbons for the adsorption of <i>p</i> -nitrophenol at 283 – 323 K and $C_0$ ; 250 mg/L (a) GACNZR 1073 (b) GAC 383 and (c) GACO 383 .....	324
Figure 5.44: Pseudo first order kinetic plot of carbons for the adsorption of methylene blue (MB) at 283 – 323 K and $C_0$ ; 250 mg/L (a) GACNZR 1073 (b) GAC 383 and (c) GACO 383 .....	326
Figure 5.45: Pseudo second order kinetic plot of carbons for the adsorption of methylene blue (MB) at 283 – 323 K and $C_0$ ; 250 mg/L (a) GACNZR 1073 (b) GAC 383 and (c) GACO 383 .....	327
Figure 5.46: Intra particle diffusion kinetic plot of carbons for the adsorption of methylene blue (MB) at 283 – 323 K and $C_0$ ; 250 mg/L (a) GACNZR 1073 (b) GAC 383 and (c) GACO 383 .....	328
Figure 5.47: Plot of $\ln K_L$ versus $1/T$ for the estimation of thermodynamic parameters for the adsorption of (a) phenol, (b) <i>p</i> -nitrophenol and (c) methylene blue (MB) on carbons GACNZR 1073, GAC 383, and GACO 383 .....	332
Figure 5.48: Plots of $\ln K_D$ versus $1/T$ of carbon GACNZR 1073 for the adsorption of (a) phenol, (b) <i>p</i> -nitrophenol (c) methyleneblue (MB) .....	336
Figure 5.49: Plot of $\ln[1/1-F^2(t)]$ versus time for the estimation of diffusion coefficient for the adsorption of phenol on carbons (a) GACNZR 1073 (b) GAC 383 and (c) GACO 383 .....	337
Figure 5.50: Plot of $\ln[1/1-F^2(t)]$ versus time for the estimation of diffusion coefficient for the adsorption of <i>p</i> -nitrophenol on carbons (a) GACNZR 1073 (b) GAC 383 and (c) GACO 383 .....	338
Figure 5.51: Plot of $\ln[1/1-F^2(t)]$ versus time for the estimation of diffusion coefficient for the adsorption of methylene blue (MB) on carbons (a) GACNZR 1073 (b) GAC 383 and (c) GACO 383.....	339
Figure 5.52: Plot of $\ln K_2$ versus $1/T$ for the estimation of activation energy of carbons GACNZR 1073, GAC 383, GACO 383 for the adsorption of (a) phenol, (b) <i>p</i> -nitrophenol and (c) methylene blue (MB) .....	341

Figure 5.53: Adsorbent mass (M) against concentration of (a) phenol (b) p-nitrophenol (c) methylen blue (MB) for 99% removal of solute from one litre of aqueous solution .....	343
Figure 6.1: FTIR spectra of (a) GAC 383 (b) GACO 383 and (c)-(h) GACONZR series of carbons activated at 383-1273 K for the evaluation of functional groups .....	358
Figure 6.2: X-ray photoelectron spectrum (XPS) of GACONZR 1273. Deconvoluted peaks (a) C 1s, (b) O 1s and (c) Zr 3d .....	359
Figure 6.3: XRD spectra of (a) GAC 383 & GACO 383 (b) GACONZR series of carbons activated at 383-1273K .....	360
Figure 6.4: Scanning electron micrographs (SEM) of GACONZR 1273 at different resolution (a) 250-100 $\mu\text{m}$ (b) 500-50 $\mu\text{m}$ (c) 10 $\mu\text{m}$ and (d) 5 $\mu\text{m}$ .....	362
Figure 6.5: High resolution transmission electron microscopy (HRTEM) of GACONZR 1273 at different resolutions (a) 50 nm (b) 20 nm (c) 10 nm and (d) 5 nm .....	363
Figure 6.6: $\text{N}_2$ adsorption isotherm for carbons GAC 383, GACO 383, GACONZR 1073 and GACONZR 1273 at 77K .....	364
Figure 6.7: BET isotherm plot for GACONZR 1073, GACONZR 1273, GAC 383 and GACO 383 (a) $p/p_0$ up to 0.3 and (b) $p/p_0$ up to 0.1 using $\text{N}_2/77\text{K}$ .....	365
Figure 6.8: Nitrogen adsorption-desorption isotherms and the corresponding $I$ plots for (a) GACONZR1073 (b) GACONZR 1273 (c) GAC 383 & (d) GACO 383 .....	366
Figure 6.9: Adsorption isotherm plots (a) Langmuir (b) Freundlich for GAC 383, GACO 383, GACONZR 1073 & GACONZR 1273 using $\text{N}_2$ at 77K .....	368
Figure 6.10: Adsorption isotherm (a) Dubinin-Radushkevich (D-R) (b) Alpha S ( $\alpha_s$ ) plot of GAC 383, GACO 383, GACONZR 1073 & GACONZR 1273 .....	370
Figure 6.11: John Isotherm plot of GAC 383, GACO383, GACONZR 1073 and GACONZR 1273 using $\text{N}_2$ adsorption data at 77 K .....	372
Figure 6.12: Comparison of Pore volumes obtained for John (J) /D-R/ Alpha S ( $\alpha_s$ )/ Langmuir isotherm models .....	374
Figure 6.13: $t$ -plot analysis of GAC 383, GACO383 and GACONZR series carbonized at temperature 1073 and 1273 K .....	374
Figure 6.14: BJH isotherm analysis (a) Adsorption cumulative pore volume (b) Desorption cumulative pore volume for GAC 383, GACO 383, GACONZR 1073 & GACONZR 1273 .....	375
Figure 6.15: BJH isotherm analysis (a) Adsorption $dV/dw$ pore volume (b) Desorption $dV/dw$ pore volume for GAC 383, GACO 383, GACONZR 1073 & GACONZR 1273 .....	375
Figure 6.16: BJH isotherm analysis (a) Adsorption $dV/d\log w$ pore volume and (b) Desorption $dV/d\log w$ pore volume for the carbons, GAC 383, GACO 383, GACONZR 1073 & GACONZR 1273 .....	376



Figure 6.17: Adsorption efficiency of GACONZR series of carbons in (a) 1000 mg/L phenol (b) 1000 mg/L <i>p</i> -nitrophenol and (c) 500 mg/L methylene blue (MB) .....	377
Figure 6.18: Equilibrium adsorption isotherm plots for carbons GAC 383, GACO 383, and GACONZR 1273 at 30 <sup>0</sup> C (a) Phenol [C <sub>0</sub> ; 25 - 3000 mg/L], (b) <i>p</i> -nitrophenol [C <sub>0</sub> ; 25-3000mg/L] and (c) Methylene Blue [C <sub>0</sub> ; 25 -1500 mg/L] .....	378
Figure 6.19: Langmuir isotherm plot for the adsorption of phenol on carbons at temperature of 283 - 323 K and C <sub>0</sub> ; 25-3000mg/L (a) GACONZR 1273, (b) GAC 383 and (c) GACO 383 .....	380
Figure 6.20: Freundlich isotherm plot for the adsorption of phenol on carbons at temperature of 283 - 323 K and C <sub>0</sub> ; 25-3000 mg/L (a) GACONZR 1273, (b) GAC 383 and (c) GACO 383 .....	381
Figure 6.21: Dubinin – Radushkevich (D-R) isotherm plot for the adsorption of phenol on carbons at temperature of 283 - 323 K and C <sub>0</sub> ; 25-3000 mg/L (a) GACONZR 1273, (b) GAC 383 and (c) GACO 383 .....	382
Figure 6.22: Langmuir isotherm plot for the adsorption of <i>p</i> -nitrophenol on carbons at temperature of 283 - 323 K and C <sub>0</sub> ; 25-3000mg/L (a) GACONZR 1273, (b) GAC 383 and (c) GACO 383 .....	384
Figure 6.23: Freundlich isotherm plot for the adsorption of <i>p</i> -nitrophenol on carbons at temperature of 283 - 323 K and C <sub>0</sub> ; 25-3000mg/L (a) GACONZR 1273, (b) GAC 383 and (c) GACO 383 .....	385
Figure 6.24: Dubinin - Radushkevich isotherm plot for the adsorption of <i>p</i> -nitrophenol on carbons at temperature of 283 - 323 K and C <sub>0</sub> ; 25 – 3000 mg/L (a) GACONZR 1273, (b) GAC 383 and (c) GACO 383 .....	386
Figure 6.25: Langmuir isotherm plot for the adsorption of methylene blue (MB) on carbons at temperature of 283 - 323 K and C <sub>0</sub> ; 25 - 1500 mg/L (a) GACONZR 1273, (b) GAC 383 and (c) GACO 383 .....	388
Figure 6.26: Freundlich isotherm plot for the adsorption of methylene blue on carbons at temperature of 283 - 323 K and C <sub>0</sub> ; 25 - 1500 mg/L (a) GACONZR 1273 (b) GAC 383 and (c) GACO 383.....	389
Figure 6.27: Dubinin – Radushkevich (D-R) isotherm plot for the adsorption of methylene blue on carbons at temperature of 283 - 323 K and C <sub>0</sub> ; 25 - 1500 mg/L (a) GAC 383 (b) GACO 383 and (c) GACONZR 1273.....	390
Figure 6.28: John-Sivanandan Achari isotherm (J-SA) plot for the adsorption of (a) methylene blue (b) phenol (c) <i>p</i> -nitrophenol on carbons at 303 K and C <sub>0</sub> ; 25- 1500 mg/L GACONZR 1273 .....	393
Figure 6.29: John-Sivanandan Achari (J-SA) isotherm plot for phenol adsorption on GACONZR 1273 at temperatures (a) 283 K (b) 293K (c) 313K and (d) 323 K.....	395

Figure 6.30: John-Sivanandan Achari (J-SA) isotherm plot for <i>p</i> -nitrophenol adsorption on GACONZR 1273 at temperatures (a) 283 K (b) 293K (c) 313K and (d) 323 K.....	396
Figure 6.31: John-Sivanandan Achari (J-SA) isotherm plot for methylene blue adsorption on GACONZR 1273 at temperatures (a) 283 K (b) 293K (c) 313K and (d) 323 K.....	397
Figure 6.32: Comparison of the adsorption isotherms model to the observed isotherm data for the adsorption of (a) methylene blue (b) phenols, (c) <i>p</i> -nitrophenol on GACONZR 1273 .....	399
Figure 6.33: Pseudo-first order kinetic plot of carbons for the adsorption of phenol at 283 – 323 K and $C_0$ ; 250 mg/L (a) GACONZR 1273 (b) GAC 383 (c) GACO 383 .....	400
Figure 6.34: Pseudo second order kinetic plot for the adsorption of phenol at 283 – 323 K and $C_0$ ; 250 mg/L (a) GACONZR 1273 (b) GAC 383 and (c) GACO 383.....	401
Figure 6.35: Intra particle diffusion model plot for the adsorption of phenol at 283 – 323 K and $C_0$ ; 250 mg/L (a) GACONZR 1273 (b) GAC 383 and (c) GACO 383 .....	402
Figure 6.36: Pseudo first order kinetic plot for the adsorption of <i>p</i> -nitrophenol at 283 – 323 K and $C_0$ ; 250 mg/L (a) GACONZR 1273 (b) GAC 383 and (c) GACO 383.....	404
Figure 6.37: Pseudo second order kinetic plot for the adsorption of <i>p</i> -nitrophenol at 283 – 323 K and $C_0$ ; 250 mg/L (a) GACONZR 1273 (b) GAC 383 and (c) GACO 383.....	405
Figure 6.38: Intra particle kinetic plot for the adsorption of <i>p</i> -nitrophenol at 283 – 323 K and $C_0$ ; 250 mg/L (a) GACONZR 1273 (b) GAC 383 and (c) GACO 383.....	406
Figure 6.39: Pseudo first order kinetic plot for the adsorption of methylene blue (MB) at 283 – 323 K and $C_0$ ; 250 mg/L (a) GACONZR 1273 (b) GAC 383 and (c) GACO 383.....	408
Figure 6.40: Pseudo second order kinetic plot for the adsorption of methylene blue (MB) at 283 – 323 K and $C_0$ ; 250 mg/L (a) GACONZR 1273 (b) GAC 383 and (c) GACO 383.....	409
Figure 6.41: Intra particle kinetic plot for the adsorption of methylene blue (MB) at 283 – 323 K and $C_0$ ; 250 mg/L (a) GACONZR 1273 (b) GAC 383 and (c) GACO 383.....	410
Figure 6.42: Plot of $\ln K_L$ versus $1/T$ for the estimation of thermodynamic parameters for the adsorption of (a) phenol, (b) <i>p</i> -nitrophenol and (c) methylene blue (MB) on carbons GACONZR 1273, GAC 383, and GACO 383.....	415
Figure 6.43: Plots of $\ln K_D$ versus $1/T$ for the adsorption of (a) phenol, (b) <i>p</i> -nitrophenol and (c) methylene blue (MB) adsorption on GACONZR 1273.....	418

Figure 6.44: Plot of $\ln[1/1-F^2(t)]$ versus time for the estimation of diffusion coefficient for the adsorption of phenol on carbons (a) GACONZR 1273 (b) GAC 383 and (c) GACO 383 .....	419
Figure 6.45: Plot of $\ln[1/1-F^2(t)]$ versus time for the estimation of diffusion coefficient for the adsorption of <i>p</i> -nitrophenol on carbons (a) GACONZR 1273 (b) GAC 383 and (c) GACO 383 .....	420
Figure 6.46: Plot of $\ln[1/1-F^2(t)]$ versus time for the estimation of diffusion coefficient for the adsorption of methylene blue (MB) on carbons (a) GACONZR 1273 (b) GAC 383 and (c) GACO 383.....	421
Figure 6.47: Plot of $\ln K_2$ versus $1/T$ for the estimation of activation energy of carbons GACONZR 1273, GAC 383 and GACO 383 for the adsorption of (a) phenol, (b) <i>p</i> -nitrophenol and (c) methylene blue (MB) .....	424
Figure 6.48: Adsorbent mass (M) against concentration of (a) phenol (b) <i>p</i> -nitrophenol (c) methylene blue (MB) for 99% removal of effluent in one litre of solution .....	425



## ||| List of Figures |||

Figure 1.1:	Surface functional groups on activated carbon.....	06
Figure 1.2:	Schematic representation of pore structure of activated carbon .....	13
Figure 2.1:	The experimental setup for the carbonization of the native carbon char under steam flow in a temperature programmed furnace .....	36
Figure 2.2:	Schematic representation of newly prepared Zr incorporated granular activated carbons .....	36
Figure 2.3:	The IUPAC classification of adsorption isotherms .....	42
Figure 2.4:	The IUPAC classification of Hysteresis loops.....	42
Figure 2.5:	Schematic representation of the single stage batch adsorber system .....	59
Figure 3.1:	Variation of carbon yield and burn off with impregnation ratio.....	68
Figure 3.2:	Fourier transform infrared (FTIR) spectra of carbons (a) GAC 383 (b) GACO 383 (c)-(h) GACZR series of carbons activated at 383-1273K for the evaluation of functional groups.....	72
Figure 3.3:	X-ray photoelectron spectrum (XPS) of GACZR 1273 prepared by activating GAC 383 with $Zr^{4+}$ at 1273K. Deconvoluted peaks (a) C 1s, (b) O 1s (c) Zr 3d .....	74
Figure 3.4:	X-ray photoelectron spectrum (XPS) of GAC 383 (a) C 1s deconvoluted peaks (b) O 1s deconvoluted peaks .....	75
Figure 3.5:	X-ray photoelectron spectrum (XPS) of GACO 383 (a) C 1s deconvoluted peaks (b) O 1s deconvoluted peaks .....	75
Figure 3.6:	X-ray diffraction (XRD) spectra of (a) GAC 383 & GACO 383 (b) GACZR series of carbons activated at 383-1273K.....	77
Figure 3.7:	Scanning electron micrographs (SEM) at different magnifications (a) GAC 383 & (b) GACO 383 at 50 $\mu$ m resolution (c) GAC 383 & (d) GACO 383 at 10 $\mu$ m resolutions.....	79
Figure 3.8:	Scanning electron micrographs (SEM) of carbon GACZR 1273 at different resolution (a) 250-100 $\mu$ m (b) 500-50 $\mu$ m (c) 10 $\mu$ m & (d) 5 $\mu$ m.....	80
Figure 3.9:	High resolution transmission electron microscopy (HRTEM) of GAC 383 at different resolutions (a) 200 nm (b) 100 nm (c) 50 nm & (d) 20 nm .....	81
Figure 3.10:	High resolution transmission electron microscopy (HRTEM) of GACO 383 at different resolutions (a) 200 nm (b) 100 nm (c) 50 nm & (d) 20 nm .....	82
Figure 3.11:	High resolution transmission electron microscopy (HRTEM) of GACZR 1273 at different resolutions (a) 200 nm (b) 100 nm (c) 50 nm & (d) 20 nm.....	83
Figure 3.12:	$N_2$ adsorption isotherm for GAC 383, GACO 383 and GACZR series carbonized at temperature 873-1273 K.....	84

$q_I$ (J-SA)	Adsorbed quantity (mg/g) during 1 <sup>st</sup> phase of J-SA plot (solid-liquid equilibria)
$q_{II}$ (J-SA)	Adsorbed quantity (mg/g) during 2 <sup>nd</sup> phase of J-SA plot (solid-liquid equilibria)
$q_m$ (D-R)	Micropore adsorption capacity in Dubinin – Radushkevich isotherm
$q_m$ (L)	Monolayer adsorption capacity in Langmuir
$q_m$ (J-SA)	Monolayer adsorption capacity in J-SA isotherm plot.
$q_T$ (J-SA)	Total adsorbed quantity (mg/g) obtained in J-SA isotherm plots
R	Gas constant
$R^2$	Correlation co-efficient
$R_a$	Particle radius
$SA_{BET}$	BET surface area
$SA_{D-R}$	Dubinin-Radushkevich surface area (m <sup>2</sup> /g)
$SA_{ext(t)}$	External surface area in <i>t</i> - plot method
$SA_{ext}$	External surface area (m <sup>2</sup> /g)
$SA_L$	Langmuir Surface area (m <sup>2</sup> /g)
$SA_{mi(t)}$	Micropore surface area in <i>t</i> - plot method
$S_I$	I point surface area (m <sup>2</sup> /g)
$\Delta S$	Entroly change (J/mol.K)
T	Temperature (K)
t	Time
V	Adsorbed volume (solid-gas equilibrium) cm <sup>3</sup> /g STP or ml/g
$V_C$ (J)	Wider pore volume in John isotherm plot
$V_I$	Monolayer volume in I point (cm <sup>3</sup> /g.STP)
$V_m$ (BET)	Monolayer volume in BET (cm <sup>3</sup> /g.STP)
$V_m$ (L)	Monolayer volume in Langmuir (cm <sup>3</sup> /g.STP)
$V_m$ ( $\alpha_S$ )	Micropore volume in alpha S (cm <sup>3</sup> /g.STP)
$V_m$ (t)	Micropore volume in <i>t</i> -plot method
$V_m$ (J)	Monolayer volume in John isotherm plot
$V_{mse}$ (J)	Pore volume due to molecular sieve effect in John isotherm plot
$V_T$	Total pore volume (cm <sup>3</sup> /g.STP)
$\alpha_s$	Alpha S
$\beta$	Activity coefficient
$\varepsilon$	Polanyi potential

.....✪✪.....

### **1.1 Introduction**

Activated carbon is a unique form of carbonaceous material having properties of high surface area, porosity and pore size distribution; it helps to use them as special materials for purification and separation process [1]. The pores on carbon surface are created within the structure of activated carbon by reacting with activation gas or incorporated with chemical agents at high temperature. The relative proportions of pores generated within the activated carbon vary considerably according to the nature of raw material and carbonisation/activation conditions applied. The chemical activation of char/carbon improves porosity by incorporating metal ions in a single stage heat treatment process. Also, ion exchange properties can be imparted to the carbon surface by creating surface functional groups. For chemical activation of carbon and lignocellulosic materials, metal salts like KOH,  $Al_2SO_4$ , NaOH,  $ZnCl_2$ , etc. are generally used for this purpose and acids like  $H_2SO_4$ ,  $HNO_3$  and  $H_3PO_4$  are also used. Predominance of pores in the micropore range has been found ideal for the adsorption of small molecular weight species from gases and solution. The presence of active metal on an impregnated activated carbon surface greatly affects the adsorption affinity [2-5]. Therefore some organic and inorganic compounds will be adsorbed preferentially than that of plane activated carbon.

### **1.2 Activated Carbon**

Activated carbons are produced from organic parent sources (coal, coconut shells, wood, peat and petroleum based residues) by different carbonization and manufacturing processes. During carbonization, these pores are filled with the

tarry matter or blocked partially by disorganized carbon. This pore structure in carbonized char is further developed and enhanced during the activation process, which converts the carbonized raw char material into more efficient activated carbons. These have a highly developed porosity and strongly developed internal surfaces.

The adsorption behaviour of an activated carbon cannot be interpreted on the basis of surface area and pore size distribution alone. Other factors such as surface chemistry are considered when it comes to the commercial application of the activated carbon. Several inorganic and organic reagents present on the carbon surface modify the surface behaviour and adsorption characteristics of activated carbons. Surface chemistry make them useful for the removal of hazardous gases and vapors by chemisorptions and catalytic decomposition.

Random ordering of aromatic sheets in activated carbon causes variation in arrangement of carbon atoms. The carbon atoms at these places have unpaired electrons and residual valencies, and are richer in potential energy. These carbon atoms are highly reactive and known as active sites or active centres which determine the surface reactivity, surface reactions, and catalytic activity of carbons. The adsorptive properties of activated carbon includes very complex pore structure, large BET surface area, good catalytic activity, chemical and thermal stability, ease of processability and high density. Presence of variety of oxygen-containing functional groups on the carbon surface makes it an indispensable adsorbent for the national economy.

Cost, availability, and consistency of quality are considered importantly for selecting a source raw material, mostly lignocellulosic for the preparation of activated carbon. Due to environmental considerations, agricultural by-products are gaining great significance as precursors for the production of activated carbon [6].

Coconut shell is one of the best and finest raw materials used for the preparation of activated carbon. Compared to other types of activated carbons coconut shell-based carbon has the highest hardness, high density and less tarry materials are generated during carbonisation, which makes it the ideal carbon for separation and purification. Coconut shells (*Cocos nucifera* L.), is a common crop



and shell readily available in rural India from the agricultural sector. Indonesia, Philippines, India and Sri Lanka are the major countries known for production of coconut shell based carbon (which account for 87 % of world production). Several countries in the Association of South East Asian Nations (ASEAN) region in recent years have started doing so as well in this sector [7].

### **1.2.1 Preparation of Granular Activated Carbon**

Activated carbon is prepared by carbonizing base materials of vegetable origin. In the presence of specific organic or non organic compounds as impregnating agents offers activated carbon with controlled porous structure and high carbon yield.

Preparation of activated carbon mainly involves two steps, in the first step the carbonaceous raw material is carbonized at temperatures below 800°C (400 - 700°C) in the presence of dehydrating agent (e.g. H<sub>2</sub>SO<sub>4</sub>, ZnCl<sub>2</sub>, KOH and H<sub>3</sub>PO<sub>4</sub>) in an inert atmosphere. The carbonized product is further activated at higher temperature. Thus, all carbonaceous raw materials are converted into activated carbon. The final carbon product will have well developed porous structure and internal surfaces. The properties of the activated carbon will be different depending on the nature of the raw material used, the nature of the activating agent used, and the conditions of the carbonization and activation processes followed.

### **1.2.2 Physical Activation and Chemical Activation**

Most carbonaceous materials have well developed porosity and an internal surface area. This is sufficiently developed during activation of carbonized product. In physical activation method air, O<sub>2</sub>, CO<sub>2</sub>, steam or their mixtures are usually used for activating the precursor for developing pores and internal surfaces. The physical activation process is a two-step process, where pyrolysis in an inert atmosphere (usually nitrogen) of the precursor is done normally at 400-900°C. Thereafter the partial gasification using an oxidizing gas (steam or CO<sub>2</sub>) at 350-1000°C to develop the porosity and surface area. The chemical activation process is a one-step process, where the activating agent (typically an acid, strong base or a salt) is incorporated into the carbon precursor prior to pyrolysis at a temperature of 450-900°C. Chemical activation method involves carbonisation

with  $\text{ZnCl}_2$ ,  $\text{H}_3\text{PO}_4$ ,  $\text{KOH}$ ,  $\text{NaOH}$  etc in a single step. Zinc chloride promotes the extraction of water molecules from the lignocellulosic structures of parent materials. Phosphoric acid act chemically within the lignocellulosic structures and reduces the tar formation thereby increasing the carbon yield. The mechanisms by which potassium hydroxide activates an existing carbon are more complex and involve the disintegration of structure following intercalation as well as some gasification by the oxygen of hydroxide. The combination of both physical and chemical processes is also possible. The impregnation of metals as ions also modifies the gasification characteristics and varies the porous structure of the final product. The presence of oxygen is not essential for this type of activation. There are no carbon atoms are removed during the stage of activation therefore the carbonization yields are improved.

### **1.3 Literature Review**

#### **1.3.1 Activated Carbon Surface Chemistry**

Activated carbon can be represented by a model of a twisted network of defective hexagonal carbon layer planes which are cross-linked by aliphatic bridging groups. Heteroatoms are incorporated into to the edge of these planes. The heteroatoms bound to the surfaces react with many reagents during modification (treatment / oxidation) process and form surface functional groups. These surface groups are decisively influences physico-chemical and surface properties of activated carbon.

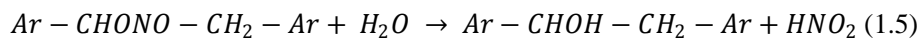
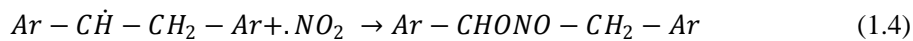
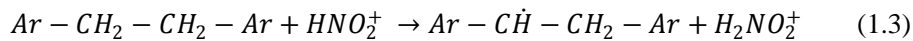
The presence of surface groups influence the surface characteristics such as the wettability, electrical resistivity, point of zero charge, polarity and acidity, Also, physico-chemical properties such as catalytic, and electrochemical interfacial state of the carbon surfaces and ion exchange capacity etc [8]. Moreno-Castilla, 2004 [9] suggested that surface chemistry of the carbon has a great influence on both electrostatic and non-electrostatic interactions. This can be considered the main factor in the adsorption mechanism from dilute aqueous solutions.

The modification of carbon with oxidizing agent (either in gas phase or in solution) instigates the formation of large amount of oxygen-containing surface complexes on the surface of activated carbons. Acidic C-O functional groups

make the activated carbon more hydrophilic and acidic. Although the chemical oxidation results in the fixation of both oxygen and nitrogen functional groups on the surface of activated carbon. It does not significantly modify the textural properties of activated carbon. This treatment enhances their adsorption efficiency and modifies selectivity to aqueous metal cation species [10].

For the oxidation treatment, various reagents including concentrated nitric acid ( $\text{HNO}_3$ ), concentrated sulphuric acid ( $\text{H}_2\text{SO}_4$ ), sodium hypochlorite ( $\text{NaClO}_2$ ), permanganate ( $\text{KMnO}_4$ ), dichromate ( $\text{K}_2\text{Cr}_2\text{O}_7$ ), hydrogen peroxide ( $\text{H}_2\text{O}_2$ ), transition metals and ozone-based gas mixtures have been used as oxidizers.

Oxidation of the new carbon with  $\text{HNO}_3$  is thought to proceed as shown below [2]



Oxygen and nitrogen were introduced into the carbon after nitric acid modifications.

The identification and estimation of the carbon-oxygen surface functional groups on carbons have been carried out using several physical, chemical, and physio-chemical techniques. This includes alkali titration and spectroscopic methods such as FTIR spectroscopy and x-ray photoelectron spectroscopy etc. Boehm titration methods are widely employed for the quantitative measurements of acidic and basic functional groups. In alkali titration method bases such as  $\text{NaHCO}_3$ ,  $\text{Na}_2\text{CO}_3$  and  $\text{NaOH}$  are used for quantitative measurement of carboxylic

acid group, acid anhydrides (lactones and lactols), and phenols. The basic groups on the surfaces, namely gamma pyrones and chromenes are quantitatively estimated by HCl titration.

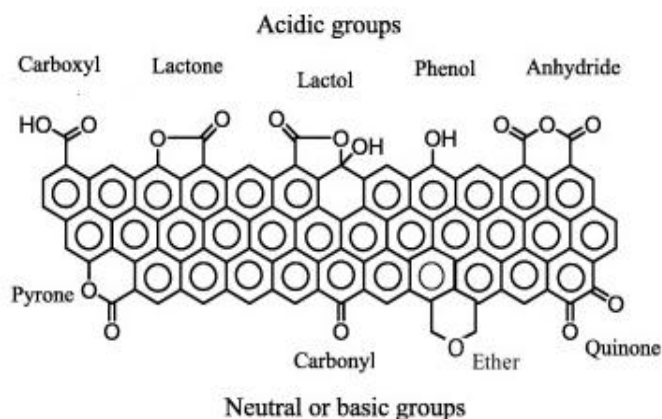


**Figure 1.1:** Surface functional groups on activated carbon

### 1.3.2 Application of Activated Carbon

Relatively simple and well-established production methods make activated carbons as one of the main candidates for many demanding applications. Mostly as catalyst supports, adsorbents, energy storage in super capacitors, Li-ion batteries, and CO<sub>2</sub> capture or hydrogen storage application. Carbon-based materials have attracted considerable interest in many energy-related applications due to their abundance, chemical and thermal stability, processability and controlled structural and chemical characteristics [11].

Due to the improved pore structure and low ash content, activated carbon is well- established for the anode reaction in fuel cell [12]. The ash content of the active carbon determines the amount of minerals present; it is also an important factor for the purification of organic solutions. Activated carbon containing oxygen surface functional groups, gives pseudocapacitance effect lead to increases the specific capacitance of amount of energy storing in the super capacitor [13].

Most of the commercial supercapacitors are based on powder activated carbon made from coconut shell. Porous carbons are used as electric double layer capacitor in electrode materials because of their higher specific capacitance, energy density, and power capability. The electric capacity of an electrode is affected by physical and chemical properties of activated carbon [14].

Activated carbons, activated carbon fibers and graphite nanofiber porous materials have been extensively studied as potential hydrogen storage materials, as they have high surface area, large pore volume, and good chemical stability. These properties enhance specific interaction between carbon atoms and gas molecules.

The major production of activated carbons in industrialized countries is utilised for the removal of hazardous substances from industrial exhaust gases. Also used for the separation of gas mixtures, recovery of useful and valuable components from industrial exhaust gases, purification of process gases from undesirable impurities, recovery of solvents and for refining liquid fuels.

Rodríguez-Reinoso et al. 2008 [15] studied the possibility of using chemically activated carbons for the storage of natural gas using a single experiment of immersion into dichloromethane. There is relatively a good correlation between the methane uptake and the microporosity data obtained from both the adsorption of N<sub>2</sub> and CO<sub>2</sub>.

### 1.3.3 Catalyst Supported Activated Carbon

Activated carbon impregnated with sodium hydroxide can be used for removing sulphur compounds, including mercaptans from gasoline [16, 17]. Activated carbons with better decolorizing power were prepared by the carbonization of wood and other high carbon content materials with zinc chloride.

Impregnation of activated carbon by chlorine using dilute solutions of hydrogen chloride or ZnCl<sub>2</sub> significantly increases adsorption of mercury species probably forming complexes with Hg as [HgCl]<sup>+</sup>, [HgCl<sub>2</sub>] and [HgCl<sub>4</sub>]<sup>2-</sup> [18]. Activated carbons impregnated with Fe (III) and Fe (II) can simultaneously remove arsenic and organic contaminants from water [19]. Adsorption for copper ion could be increased 2.2 times, by modifying coconut shell based activated carbon

with sodium acetate [20]. The effects of the addition of copper supported on activated carbon enhanced the chemical adsorption of NO, SO<sub>2</sub> and cyanide removal [21]. When the commercial activated carbon was loaded sodium and potassium, it could efficiently remove NO and SO<sub>2</sub> from waste gases by adsorption [22].

The impregnated potassium iodide in granular activated carbon reacts with the oxygen groups on the carbon surface and modifies their adsorption behaviour. Thereby improves the efficiency of the activated carbon to retain radioactive methyl iodide. This property makes to use in nuclear industry for the retention of radioactive iodine compounds from coolant release and ventilation systems [23].

Chen et al. 2002 [24] prepared activated carbon fibers (ACF) from sisal fiber as substrate, impregnated them with different concentrations of zinc chloride, and heat treated them in nitrogen at 800°C. These ACFs were tested for their antibacterial activity against *E. coli* and *S. aureus* bacteria. The ACF sample impregnated with zinc showed strong activity against *E. coli* and could kill almost all bacteria. Deposition of silver on ACF by treating with Ag (NH<sub>3</sub>)<sup>2+</sup> were found to improve the antibacterial activity against *S. aureus* considerably.

Modified rayon activated carbon fiber with nitrocellulose combustion, the nitrogen and oxygen groups could be increased, and it showed excellent adsorption for ammine and carbon disulfide [25]. Tannic acid was employed in the modification of the surface properties of granulated commercial activated carbon [26]. Tannic acid was found effective to enhance the metal adsorption capacity of activated carbon surfaces.

#### 1.3.4 Zirconium Based Carbon Materials

Zirconium ion impregnated fibre charcoal showed maximum fluoride up take and provided to be most effective de-fluoridating agent followed by groundnut shell and coconut shell. Adsorption of zirconium ion from solution by solid phase can occur with formation of surface complex between the oxygen containing functional group (COOH, -OH, >C=O) and the metal. Once this zirconium based Lewis acid sites are generated by chemisorptions on the activated charcoals as a monolayer, they are responsible for very strong adsorption of Lewis bases such as fluoride ion [27].

Peraniemi et al. 1994 [28] studied the adsorption efficiency of zirconium loaded activated carbon for the removal mercury, arsenic and selenium. The results showed that the loading of activated charcoal with zirconium significantly improved the adsorption power of charcoal towards arsenic selenium, and mercury. The oxidation state of metal is of little significance for the adsorption onto zirconium impregnated carbon, i.e. As (V) adsorbed better than As (III) and Hg(II) adsorbed better than Hg(I) onto zirconium based adsorbents.

Zirconium phosphate impregnated porous polymers shows higher adsorption preference towards lead ( $\text{Pb}^{2+}$ ) ions. So it can be used for removing  $\text{Pb}^{2+}$  ions from waters [29]. Activated carbon impregnated with zirconium hydroxide possesses significantly higher adsorption capacity towards toxic chemical gases such as  $\text{SO}_2$  and cyanogen chloride (CNCl) [30]. The metal anions of vanadium (V) and chromium (VI) in aqueous solution can be effectively adsorbed by Zr(IV)-impregnated collagen fiber (ZrICF) [31].

Juan et al. 2007 [32] studied the catalytic activity of zirconium sulphate supported activated carbon for the esterification of fatty acid. They found that it is an efficient catalyst for the esterification of oleic acid by n-butanol. Also they found that catalytic activity of supported zirconium sulphate is higher than that of conventional acidic resins.

### 1.3.5 Structural Characterization of Activated Carbons

Characterization of activated carbon has been important because a porous material is possessed by a wide distribution of pore sizes, shapes and the complexity of the pore network. Structural characterization of activated carbons includes: surface chemistry, porous texture, and morphology. This can be studied by using various techniques such as FTIR, XPS, XRD, SEM, HRTEM, etc.

In most of the pore size distribution (PSD) methods, pore size are evaluated by assuming the  $\text{N}_2$  molecules are get arranged into the pores according to their dimensions during adsorption. However each method has different theoretical approaches to the determination of the pore sizes.

Prauchner and Rodriguez-Reinoso, 2008 [33] prepared active carbons intended for adsorption of natural gas by combining chemical activation of coconut shell with  $\text{H}_3\text{PO}_4/\text{ZnCl}_2$  followed by physical activation with  $\text{CO}_2$ . It shows that chemical activation using less proportion of  $\text{H}_3\text{PO}_4$  or  $\text{ZnCl}_2$ , are enough to generate narrow micro porosity without significantly decreasing the bulk density. Subsequent physical activation develops the primary pore structure generated by added chemicals. This procedure made it possible to obtain materials with well developed porosity compatible with a relatively high bulk density.

Tan et al. 2008 [34] studied the effect of hydrochloric acid (HCl) treatment of activated carbon prepared from oil palm shell on methylene blue (MB) adsorption. It shows that, adsorption efficiency enhanced with HCl treatment. The Fourier transform infrared spectroscopy (FTIR) measurements showed that the surface chemistry of the activated carbon was influenced by the acid treatment and produced more acidic groups such as carboxylic and ether.

Jayabalan et al. 2009 [35] studied the influence of textural, chemical, and structural properties on the reactivity of coconut shell based activated carbons in air. The results suggest that oxygen present in the form of surface oxygenated groups, the mineral content, and the dimensions of the basic structural units influence the reactivity of activated carbons. Highly stable carbons were found to have less oxygen to carbon ratio, lower mineral content, and larger and better stacked polyaromatic layers.

Bouchelta et al. 2012 [36] prepared activated carbon from biomass of Algerian date pits. Pyrolysis process was optimized by varying parameters such as temperature, nitrogen flow, heating rate and pyrolysis hold time in order to determine their effects on the porous structure. Experimental results showed that pyrolysis conditions and activation hold time has significant effects on activated carbon porosity. In addition to that they suggested that carboxylic and a phenolic group at the surface of active carbon improves the cation-exchange and complexation properties.

Thommes et al. 2011 [37] assessing, surface chemistry and pore structure of active carbons by a combination of physisorption ( $\text{H}_2\text{O}$ , Ar,  $\text{N}_2$ ,  $\text{CO}_2$ ), XPS and



TPD-MS (Temperature Programmed Desorption with attached Mass Spectrometry). They clearly suggest that water adsorption is indeed a sensitive tool for detecting differences in surface chemistry between chemically and physically activated carbon materials with comparable ultramicropore structure. The occurrence of adsorption hysteresis associated with the filling of micro and narrow mesopores provides additional structural information, complementary to the insights from argon/nitrogen/carbon dioxide adsorption.

Oda et al. 2006 [38] compared the effect of the oxygen-containing functional group on activated carbon fiber in electrodes of an electric double-layer capacitor. It shows that larger number of phenolic hydroxyl groups on activated carbon fibre promoted the wettability of electrodes thus increasing the capacitance and producing pseudo capacitance effects.

Song et al. 2010 [39] studied surface modification of coconut-based activated carbon by liquid-phase oxidation and its effects on lead ion adsorption. It is found that adsorption capacity of activated carbon oxidized with  $\text{HNO}_3$  ( $10 \text{ mol L}^{-1}$ ) at 363 K was about 2.5 times higher than that of the original activated carbon. This is attributed to the increased oxygen groups, which enhanced the hydrophilicity of the activated carbon, and lowered the pH. This made the surface more negatively charged, and increased the amount of homogeneous active sites available for lead ions.

Velasco and Ania, 2011 [40] studied the phenol adsorption mechanism of activated carbon. It is found that physisorption of phenol depends strictly on the porosity of the activated carbons. Whereas chemisorption depends on the availability of the basal planes in the activated carbons

## 1.4 Adsorption Isotherms

The adsorption isotherm is the most extensively employed analytical method for representing the equilibrium states of an adsorption system. It can give useful information regarding the adsorbate, the adsorbent, and the adsorption process. It helps in the determination of the surface area of the adsorbent, the volume of the pores, and their size distribution, the heat of adsorption, and the relative absorbability of a gas or a vapour on a given adsorbent.

## 1.5 Porosity Study and Surface Area Determinations

Porosity/pore structure and surface area are the most important characteristics of activated carbon. The porosity of activated carbons offers a vast surface in which the adsorption can take place. Each type of carbon has its own unique distribution of pore sizes. These are classified into three groups, micropores (< 2 nm), mesopores (2 - 50 nm), and macropores (> 50 nm). Walls of the pores are comprised of two types of surfaces: the internal (microporous) surface and the external surface. Micropore surface area constitutes the walls of micropores whereas external surface area constitutes the walls of the meso and macropores. Surface area and pore size distribution of activated carbon is obtained by applying  $N_2$  adsorption data in various isotherm models. The most extended technique for the characterization of the porous texture of activated carbons is the physical adsorption of gases and vapours. BET nitrogen adsorption method introduced by Brunauer, Emmett, & Teller is now universally accepted as a standard procedure for the characterization of a variety of porous materials. Some other isotherm models like Langmuir, Freundlich, Dubinin- Radushkevich (D-R), John isotherm,  $t$ -plot method by Lippens De Boer, alpha S ( $\alpha_s$ ) method and BJH (Barrett-Joyner-Halenda) are also applied for the isotherm analysis for the specific surface area, porosity and pore size distributions.

Lozano-Castello et al. 2005 [41] studied the comparative characterization of micropore size distribution (MPSD) of activated carbons by HRTEM image analysis and isotherm analysis using Dubinin-Radushkevich isotherm equation (D-R equation to the  $N_2$  and  $CO_2$  adsorption isotherms). The MPSD obtained by high-resolution transmission electron microscopy (HRTEM) for the carbon molecular sieve is wider than that obtained by  $CO_2$  adsorption. Suggests that HRTEM is detecting the closed porosity existing in this sample, which is not accessible to gas adsorption. Thus, HRTEM combined with image analysis seems to be useful for structural analysis of narrow micropores including closed porosity.

Do et al. 2011 [42] develop a novel method which determined the accessible pore volume (the volume space that is accessible to the centre of an adsorbate molecule) and accessible pore size (largest sphere that can be accommodated in the accessible space) for pores having homogeneous surfaces.

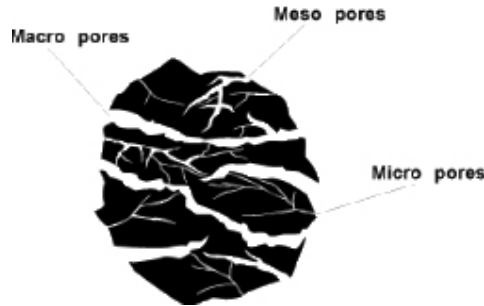


**Figure 1.2:** Schematic representation of pore structure of activated carbon

## 1.6 Adsorption Isotherm Models

The adsorption isotherm models describe the relation between the amount of gas adsorbed (specific amount adsorbed in liquid phase,  $q_e$ ) per gram of the solid adsorbent at the relative pressure  $p/p_0$  (equilibrium concentrations of the adsorptive in liquid phase,  $C_e$ ). Pore structure characteristics of activated carbons were determined by  $N_2$  adsorption at 77K. This is because of the nonpolar character of molecules and its relatively small cross-sectional area of  $0.162 \text{ nm}^2$ , hence easily accessible to their finer pores, micropores and mesopores. The data obtained from  $N_2$  gas sorption experiments were evaluated by different isotherm models. These models are successful either at lower pressures (higher adsorption potential), prior to monolayer formation or at higher pressure (lower adsorption potential) corresponding to the multilayer region in adsorption. Parameters obtained from these isotherm models are used for calculating surface area, porosity, pore volume, and pore size distribution of GAC.

### 1.6.1 Brunauer, Emmett and Teller (BET) Isotherm

Brunauer, Emmett and Teller (BET) proposed an equation based on the assumption of multilayer formation. These workers proposed that the forces acting in multimolecular adsorption are the same as those acting in the condensation of vapours [43].

The BET equation could be written as an equation (1.6)

$$\frac{1}{V \left( \frac{p_0}{p} - 1 \right)} = \frac{1}{V_m C} + \frac{C - 1}{V_m C} \left( \frac{p}{p_0} \right) \quad (1.6)$$


One important parameter for the characterization of porous materials is their specific surface area. The specific surface area ( $SA_{BET}$  m<sup>2</sup>/g) determined from monolayer volume  $V_m(BET)$  cm<sup>3</sup>/g obtained from the slope of the BET plot is the most widespread method.

$$SA_{BET} = \frac{V_m(\text{cm}^3/\text{g}) \times 6.023 \times 10^{23} \times 0.162 \times 10^{-18}}{22414} \quad (1.7)$$

### 1.6.2 I Plot Method

The *I* point method based on a modification of the original BET equation, (BET-Scatchard equation) proposed by Pomonis and collaborators [44]. The *I* point plot is nonlinear and gives the value of the specific area by identifying the inversion point, where the completion of monolayer occurs so-called *I* point. This SA (*I* plot) nearly equal to that of the usual BET procedure. Thus, there may be no need for a decision on an appropriate “range” of  $p/p_0$  to use in calculating both a slope and an intercept, as it is required for the usual BET procedure.

$$\frac{[V(1 - (p/p_0))]}{p/p_0} = CV_m - (C - 1)[V(1 - (p/p_0))] \quad (1.8)$$

The plot provides an inclined *V* shaped (  ) graph, i.e. a graph with an inversion point termed as *I* point; the extrapolation of this point towards the x-axis yields the monolayer capacity. From the monolayer capacity ( $V_m$ ), the surface area (SA) can be calculated

$$SA_{Ipoint} = 4.353 V_m \quad (1.9)$$

### 1.6.3 Langmuir Isotherm

The Langmuir isotherm equation is the first theoretically developed adsorption isotherm model. It assumes the concept that adsorption sites on solid surfaces are energetically homogeneous and there are no lateral interactions between the adsorbed molecules [45].

The well-known linear form of expression (solid-gas) system for the Langmuir model is given in equation (1.10)

$$\frac{P}{V} = \frac{1}{bV_m} + \frac{P}{V_m} \quad (1.10)$$

Linear form of Langmuir equation for solid –liquid equilibria is given by the equation (1.11)

$$\frac{C_e}{q_e} = \frac{1}{K_L} + \frac{a_L}{K_L} C_e \quad (1.11)$$

#### 1.6.4 Freundlich Isotherm

This isotherm is applicable only in the middle ranges of vapour pressure.

$$V = K_F P^{1/n} \quad (1.12)$$

The value of  $n$  is always greater than unity. The equation is of greater significance for physical adsorption system explained using equation [46].

Linear form of the Freundlich equation in the solid –liquid system is given in the equation (1.13)

$$\log q_e = \log K_F + \frac{1}{n} \log C_e \quad (1.13)$$

#### 1.6.5 Dubinin-Radushkevich Isotherm

Dubinin-Radushkevich equations have been developed primarily for microporous adsorbents. It can be expressed analytically by a Gaussian distribution equation between the total limiting volume of the adsorption space and the adsorption potential [47]. This is further made it possible to obtain an equation of the adsorption isotherms and to calculate the appropriate micropore volume.

Linear form the isotherm equation is given as

$$\ln V = \ln V_0 - D (\ln P_0/p)^2 \quad (1.14)$$

Linear form of equation in the solid –liquid system is given as

$$\ln q_e = \ln q_{mi} - \beta \varepsilon^2 \quad (1.15)$$

### 1.6.6 *t*-Plot Method

The *t*-plot is a plot of the amount of nitrogen adsorbed on the test sample as a function of the calculated thickness *t*, of the adsorbed layer. A straight line is drawn in the linear region of the *t* - plot and from the slope and intercept, the external surface area & micropore volume were obtained [48].

The *t*-plot procedure was evaluated during preliminary testing, using the equation (1.16)

$$t = [13.99 / (0.034 - \log \left( \frac{p}{p_0} \right))]^{0.5} \quad (1.16)$$

The external surface area  $SA_{Ext}$  of the microporous sample can be derived from the slope of the *t*-plot.

$$SA_{Ext} = \frac{Slope \times 10^{10} \times D}{F \times 10^6} \quad (1.17)$$

Where *D* is the density conversion factor 0.00015468 and *F* is a surface area correction factor, for most samples it is taken as 1.

### 1.6.7 Alpha S ( $\alpha_s$ ) Plots

Gregg and Sing, 1982 [49] proposed  $\alpha_s$  method as a variant of *t*-plot method. It involves a comparison in which the isotherm data of a test sample are plotted against the corresponding normalized isotherm data of an appropriate reference material. Surface chemistry of reference adsorbent should be same as that of porous material under investigation. The reference material should be free of micropore adsorption and capillary condensation in the relative pressure (*p/p*<sub>0</sub>) range used for the plot. Thus, the adsorption at a pre-selected *p/p*<sub>0</sub> is used to convert the standard amounts adsorbed into a dimensionless  $\alpha_s$  form. For this purpose, it is usually convenient to take *p/p*<sub>0</sub> = 0.4. The uptake of nitrogen *V*<sub>ads</sub> at each *p/p*<sub>0</sub> divided by that at 0.4 *p/p*<sub>0</sub> gives the  $\alpha_s$  value. The external surface area was calculated from the slope of the linear part of each  $\alpha_s$  plot by using the equation (1.18)

$$SA_{ext} = 2.86 V / \alpha_s \quad (1.18)$$

### 1.6.8 Barrett Joyner and Halenda (BJH) Method

The mesopore and micropore size distributions were determined using the Barret-Joyner-Halanda (BJH) isotherm method [50]. Pore radius is evaluated from adsorption and desorption isotherms. Isotherm analysis follows desorption of adsorbed volume from the multilayer completed.

The average pore diameters were calculated using the formula considering cylindrical form of the pores

$$d_{av} = 4 \frac{V_p}{SA_{BET}} \quad (1.19)$$

### 1.6.9 John Isotherm Model

P. T. John, an Indian Scientist, formerly developed a semi-empirical isotherm model known as John Isotherm for the evaluation of adsorption behaviour of porous and finely divided materials. Interaction between adsorbent-adsorbate differs in the extent of physisorption appears as a phase transition or a discontinuity, in John isotherm plots. Each phase on the plots is represented as micropore filling, submonolayer coverage, monolayer coverage, mesopore filling and capillary condensation [51, 52]. Linear form of isotherm model is given by

$$\log \log P = C + n \log V \quad (1.20)$$

### 1.6.10 John-Sivanandan Achari Isotherm Plots

This equation is further extended to study the adsorption potential of porous materials from solid - liquid adsorption system known as the John-Sivanandan Achari (J-SA) isotherm and given in the equation (1.21) [53-55]

$$\log \log C_e = C + n \log q_e \quad (1.21)$$

$C_e$  is the equilibrium adsorbate concentration,  $C$  is a constant,  $q_e$  is the equilibrium adsorbed quantity. Where  $n$  is the adsorption constant known as John adsorption capacity, is a measure of adsorption efficiency of the material. The extrapolation of the straight line curve to the point of saturation to the  $\log q_e$  axis gives the monolayer capacity  $q_m(J-SA)$ .

## 1.7 Aim and Scope of The Study

The aim of this research is to study the process of activation, material behaviour and adsorption isotherm studies of a series of zirconyl chloride ( $ZrOCl_2$ ) and nano zirconium oxide (zirconia- $ZrO_2$ ) activated granular carbon (GAC) under different carbonization/ activation temperatures. Also analysing their adsorption efficiency in solid-gas using  $N_2$  gas at 77K and solid –liquid adsorption using phenol, *p*-nitrophenol and methylene blue (MB).

This work is realised by preparing a series of granular activated carbon, activated with  $Zr^{4+}$  /nano  $ZrO_2$  in an inert atmosphere at different activation temperature 383 -1273K. This activated carbon is subjected to solid – gas equilibria using  $N_2$  at 77K to study the development of surface area, pore volume, micropore surface area and micropore volume of activated carbons. Evaluation of adsorption parameters with respect to solid – liquid equilibrium are used to determine the effect of various process parameters such as adsorbent dose, initial concentration, contact time, temperature effect and nature of thermodynamic parameters on the adsorption efficiency.

## 1.8 Objective of The Research Study

- 1) Preparation of granular activated carbons (GAC) based on coconut shells by chemical activation with zirconium compounds such as zirconyl chloride  $ZrOCl_2$  (marked as GACZR and GACZR) and nano zirconium oxide  $ZrO_2$  (designated as GACNZR and GACONZR) and study of activation conditions as a function of temperature.
- 2) Study of physico-chemical and the surface characteristics of the modified carbons incorporated with zirconyl chloride ( $ZrOCl_2$ ) and nano zirconium oxide ( $ZrO_2$ ) specifically, FTIR, XPS, XRD, SEM, and TEM methods.
- 3) Evaluation of adsorption isotherm behaviour of the modified materials with respect to solid-gas ( $N_2/77K$ ) equilibrium and determination of surface area, porosity and pore size distribution using standard isotherm models BET, *I* plot, Langmuir, Dubinin –Radushkevich (D-R), Alpha S ( $\alpha_s$ ), John isotherm, *t*-plot and BJH methods.



- 4) Evaluation of the adsorption isotherm behaviour, adsorption kinetics and thermodynamic parameters of the modified materials with respect to solid-liquid equilibrium using phenol, *p*-nitrophenol and methylene blue (MB) from the liquid phase for temperatures 10<sup>0</sup>C, 20<sup>0</sup>C, 30<sup>0</sup>C, 40<sup>0</sup>C and 50<sup>0</sup>C. Evaluation of adsorption isotherm behaviour of the new carbon adsorption system using Langmuir, Freundlich, Dubinin-Radushkevich (D-R), John – Sivanandan Achari (J-SA) isotherms and comparison of adsorption constants and parameters.
- 5) Evaluation of the adsorption efficiency of the carbons for trace metal ions in contaminated groundwater (collected from the field) using ICP-MS.
- 6) Testing and evaluation of the hypothesis using standard statistical methods to come out with useful findings.

There are four series of GAC's were prepared, and marked as

- a) **Carbon GACZR series** - Granular activated carbon incorporated with zirconyl chloride ( $ZrOCl_2$ ) and activated at 383K, 473K, 673K, 873K, 1073K and 1273K in a temperature – controlled muffle furnace under inert atmosphere.
- b) **Carbon GACOZR series** - Granular activated carbon oxidized with nitric acid, ( $HNO_3$ ) and activated with zirconyl chloride ( $ZrOCl_2$ ) at 383K, 473K, 673K, 873K, 1073K and 1273K in a temperature – controlled muffle furnace under inert atmosphere.
- c) **Carbon GACNZR series** - Granular activated carbon incorporated with nano zirconium oxide ( $ZrO_2$ ) and activated at 383K, 473K, 673K, 873K, 1073K and 1273K in a temperature – controlled muffle furnace under inert atmosphere.
- d) **Carbon GACONZR series** - Granular activated carbon oxidized with nitric acid, ( $HNO_3$ ) and activated with nano zirconium oxide ( $ZrO_2$ ) at 383K, 473K, 673K, 873K, 1073K and 1273K in a temperature – controlled muffle furnace under inert atmosphere.

In each study the specific material properties of the newly made carbons are compared with basic/native carbons GAC 383 and GACO 383

**GAC 383** Granular activated carbon washed and dried at 383K

**GACO 383** Nitric acid modified granular activated carbon, washed and dried at 383K

## 1.9 Hypothesis

1. Whether there is any significant difference in pore volume and surface area of  $Zr^{4+}/ZrO_2$  modified carbons compared to basic carbons GAC 383 and GACO 383 studied by using BET,  $I$  plot, Langmuir, Dubinin- Radushkevich (D-R), Alpha S ( $\alpha_s$ ), and John isotherm methods in solid-gas equilibria.
2. Whether there is any significant difference between the pore volumes determined for granular activated carbons prepared using Langmuir isotherm, Dubinin-Radushkevich isotherm, Alpha S ( $\alpha_s$ ) method and John isotherm.
3. Whether there is any significant difference in micropore surface area and external surface area with increase of activation temperature in  $Zr^{4+}/ZrO_2$  modified carbons.
4. Whether there is any significant difference in amount of phenol, *p*-nitrophenol and methylene blue (MB) adsorbed on  $Zr^{4+}/ZrO_2$  modified carbons compared to basic carbons GAC 383 and GACO 383 in solid-liquid equilibria.
5. Whether there is any significant difference in specific adsorption capacity determined for granular activated carbons prepared using Langmuir, Dubinin- Radushkevich (D-R), John –Sivanandan Achari isotherm models.
6. Whether there is any significant effect of temperature for the adsorption of phenol, *p*-nitrophenol and methylene blue (MB).

## 1.10 Structure of The Thesis

This bound thesis is organised in seven chapters.

Chapter 1: Introduction

Chapter 2: Materials and Methods

Chapter 3: Granular activated carbon prepared by activation with zirconyl chloride (GACZR): Preparation, characterization and adsorption isotherm studies

Chapter 4: Granular activated carbon oxidized and activated with zirconyl chloride (GACOZR): Preparation, characterization and adsorption isotherm studies.

Chapter 5: Granular activated carbon prepared by activation with zirconium oxide (GACNZR): Preparation, characterization and adsorption isotherm studies.

Chapter 6: Granular activated carbon oxidized and activated with zirconium oxide (GACONZR): Preparation, characterization and adsorption isotherm studies.

Chapter 7: Summary and Conclusion

These chapters are followed by a brief description of Future Scope of the study. The chapters and their contents are presented accordingly in the following sections for precise reference

### Chapter 1 Introduction

This chapter gives an overview of the current status of knowledge on carbon and carbon science; forms and classification, activated carbon preparation, the study of porosity and surface area, isotherm studies, isotherm models, and physicochemical methods of analysis. It also describes the review of the literature, aim and scope of the study, hypothesis, chapters followed by a description of the structure of the thesis.

## **Chapter 2 Materials and Methods**

This chapter describes in detail about materials and methods followed for the preparation of coconut shell based granular activated carbon (GAC) under chemical activation using zirconium ( $Zr^{4+}$ / nano  $ZrO_2$ ). It mainly includes materials, methods, instrumentation and theory followed with respect to different carbonization/activation conditions, preparation, characterization (FTIR, XPS, XRD, SEM, TEM) and adsorption studies. A detailed description of the various isotherm models are discussed for the evaluation of surface area, porosity and pore size distribution. The experimental procedures followed to study the liquid phase adsorption behaviour of the modified GACs under equilibrium conditions.

## **Chapter 3 Granular Activated Carbon Prepared by Activation with Zirconyl Chloride (GACZR): Preparation, Characterization and Adsorption Isotherm Studies**

In this chapter, preparation, characterization, and adsorption isotherm studies of GACZR series (granular activated carbon prepared by activation with zirconyl chloride,  $ZrOCl_2$ ) of activated carbons are discussed. Different activation conditions such as temperature and  $Zr^{4+}$ /GAC incorporation ratios are evaluated. Textural analysis of activated carbon was carried using established physicochemical and spectroscopic techniques. Their adsorption efficiency with respect to porosity parameters were determined by applying  $N_2$  adsorption desorption data in different standard isotherm models such as Brunauer-Emmett Teller (BET),  $I$  plot, Langmuir, Freundlich, Dubinin-Radushkevich (D-R), Alpha S ( $\alpha_s$ ), John isotherm,  $t$ -plot and Barrett- Joyner- Halenda (BJH) isotherms. Adsorption efficiency of carbon materials in solid-liquid adsorption system is tested using phenol, *p*-nitrophenol and methylene blue (MB). Adsorption data obtained at selected temperatures are subjected to Langmuir, Freundlich, Dubinin-Radushkevich (D-R) and John –Sivanandan Achari isotherm models to test the validity of isotherm equations. Kinetic models such as pseudo first order,

pseudo second order and intra particle diffusion mechanisms are applied to explain the controlling mechanisms. Thermodynamic parameters free energy change ( $\Delta G$ ), enthalpy change ( $\Delta H$ ) and entropy change ( $\Delta S$ ) were evaluated to understand whether the adsorption is exothermic/endothermic and spontaneous in nature. Field water collected from contaminated area is used to test the efficiency of carbons for trace metal ions. The Hypothesis is tested with statistical two factor ANOVA, three factor ANOVA, and t-test. This chapter ends with a summary followed by references.

#### **Chapter 4 Granular Activated Carbon Oxidized and Activated with Zirconyl Chloride (GACOZR): Preparation, Characterization and Adsorption Isotherm Studies.**

In this chapter the preparation, characterization, and adsorption isotherm studies of GACOZR series (granular activated carbon oxidized with nitric acid,  $\text{HNO}_3$  and activated with zirconyl chloride,  $\text{ZrOCl}_2$ ) of activated carbons are discussed. Textural analysis of activated carbon was carried out using several physicochemical techniques. The  $\text{N}_2$  adsorption-desorption isotherms data subjected to isotherm model analysis; Brunauer-Emmett-Teller (BET),  $I$  plot, Langmuir, Freundlich, Dubinin-Radushkevich (D-R), Alpha S ( $\alpha_s$ ),  $t$ -plot, John isotherm and Barrett- Joyner- Halenda (BJH) isotherms for assessing the surface area, pore size, and pore volume of the carbons. Solid-liquid equilibrium data obtained from phenol, *p*-nitrophenol and methylene blue subjected to Langmuir, Freundlich, Dubinin-Radushkevich (D-R) and John-Sivanandan Achari isotherms. Kinetic data obtained from different time interval is tested using mathematical expressions corresponding to various kinetic models, namely: Lagergren's first order equation, pseudo second-order reaction and intra particle diffusion. The thermodynamic parameters of Gibbs free energy change ( $\Delta G$ ), enthalpy change ( $\Delta H$ ), and entropy change ( $\Delta S$ ) for the adsorption processes are calculated and discussed. Field water collected from contaminated area is used to test the efficiency of carbons for trace metal ions. The Hypothesis is tested with statistical

two factor ANOVA, three factor ANOVA, and t-test. This chapter ends with summary followed by references.

**Chapter 5 Granular Activated Carbon Prepared by Activation with Zirconium Oxide (GACNZR): Preparation, Characterization and Adsorption Isotherm Studies.**

In this chapter, preparation, characterization, and adsorption isotherm studies of GACNZR series (granular activated carbon prepared by activation with nano zirconium oxide,  $ZrO_2$ ) of activated carbons are discussed. Different activation conditions of temperature and  $ZrO_2$ /GAC incorporation ratio are evaluated. Their adsorption efficiency and structural parameters were also determined by standard isotherm models such as Brunauer-Emmett-Teller (BET),  $I$  plot, Langmuir, Freundlich, Dubinin-Radushkevich (D-R), Alpha S ( $\alpha_s$ ),  $t$ -plot, John isotherm and Barrett- Joyner- Halenda (BJH). The evaluation of liquid phase isotherm study of the modified carbons with respect to their efficiency towards phenol, *p*-nitrophenol and methylene blue are presented. Adsorption isotherm analysis using Langmuir, Freundlich, Dubinin Radushkevich (D-R) and John – Sivanandan Achari isotherm methods are presented. Kinetic models such as Lagergren's first order equation, pseudo second-order reaction and intra particle diffusion is applied to predict the rate-limiting step in an adsorption process. Thermodynamic parameters, such as  $\Delta G$ ,  $\Delta H$ , and  $\Delta S$ , were calculated using adsorption equilibrium constant to conclude whether the process is spontaneous or not. Field water collected from contaminated area is used to test the efficiency of carbons for trace metal ions. The Hypothesis is tested with statistical two factors ANOVA, three factor ANOVA, and t-test. This chapter ends with summary followed by references.

**Chapter 6 Granular Activated Carbon Oxidized and Activated with Zirconium Oxide (GACONZR): Preparation, Characterization and Adsorption Isotherm Studies.**

In this chapter the preparation, characterization, and adsorption isotherm studies of GACONZR series (granular activated carbon

oxidized with nitric acid,  $\text{HNO}_3$  and activated with nano zirconium oxide,  $\text{ZrO}_2$ ) of activated carbons are discussed. Their porosity development, structural and textural characterization using  $\text{N}_2$  adsorption – desorption isotherm and the analysis of this data using various gas phase isotherm models such as Brunauer-Emmett-Teller (BET),  $I$  plot, Langmuir, Freundlich, Dubinin-Radushkevich (D-R), Alpha S ( $\alpha_s$ ), John isotherm,  $t$ -plot and Barrett-Joyner- Halenda (BJH) isotherm models are presented. The liquid phase isotherm studies are done to evaluate their adsorption efficiency towards phenol,  $p$ -nitrophenol and methylene blue. Adsorption data analysed using Langmuir, Freundlich, Dubinin-Radushkevich (D-R) isotherm, and John –Sivanandan Achari isotherm equations. Kinetic data were tested using pseudo-first-order, pseudo-second-order models and intraparticle diffusion models to evaluate the kinetic mechanism. The thermodynamic parameters of Gibbs free energy change,  $\Delta G$ , enthalpy change,  $\Delta H$ , and entropy change,  $\Delta S$ , for the adsorption processes are calculated and discussed in this chapter. Field water collected from contaminated area is used to test the efficiency of carbons for trace metal ions. The Hypothesis is tested with statistical two factor ANOVA, three factor ANOVA, and t-test. This chapter ends with summary followed by references.

## Chapter 7 Summary

This chapter summarizes the major outcome of this research based on critical analysis of the findings as well as on the basis of statistical analysis of adsorption isotherm parameter determined. The relative merits and demerits of the new activation procedures, the physics and chemistry of porosity and surface area development brought about by the optimization of activation parameters based on statistical principles, tests and evaluation methods followed are presented.

The thesis ends with concluding remarks and a discussion on the future scope of the study, followed by a list of publications.

## Reference

- [1] Juan, Y.; Ke-Qiang, Q. Preparation of Activated Carbon by Chemical Activation under Vacuum. *Environ. Sci. Technol.* **2009**, *43* (9), 3385–3390.
- [2] Achari, V. S. Modified Carbons and Wood Dust: Evaluation of Adsorption Properties. *Ph.D. Thesis* **1998**. Department of Chemistry, University of Kerala, Kariavattom, Thiruvananthapuram, Kerala, India.
- [3] Bindia Ravindran. Adsorption Isotherm Studies on Activated Carbon Prepared by Activation with Cerium Compounds. *Ph.D Thesis* **2016**. School of Environmental Studies, Cochin University of Science and Technology, Cochin, Kerala, India.
- [4] Achari, V.S.; Jayasree, S.; Rajalakshmi, A.S. Adsorption of *p* – nitrophenol on Coconut Shell Granular Activated Carbon: Isotherms, Kinetics and Thermodynamics. *Indian Journal of Chemical Technology.* **2017**, *24*,471-478
- [5] Achari, V.S.; Rajalakshmi, A.S.; Jayasree, S. Surface Area and Porosity Development on Granular Activated Carbon by Zirconium: Adsorption Isotherm Studies. *Journal of Applied Research and Technology*, **2017** (Accepted November 2017).
- [6] Girgis, B. S.; Yunis, S. S.; Soliman, A. M. Characteristics of Activated Carbon from Peanut Hulls in Relation to Conditions of Preparation. *Mater. Lett.* **2002**, *57* (1), 164–172.
- [7] Gunasekaran, K.; Annadura,R.; Kumar,P.S. A study on some durability properties of coconut shell aggregate concrete. *Materials and Structures* **2015**, *48*, 1253–1264.
- [8] Pandolfo, A. G.; Hollenkamp, A. F. Carbon Properties and Their Role in Supercapacitors. *Journal of Power Sources* **2006**, *157* (1), 11–27.
- [9] Moreno-Castilla, C. Adsorption of Organic Molecules from Aqueous Solutions on Carbon Materials. *Carbon* **2004**, *42* (1), 83–94.
- [10] Song, X.; Liu, H.; Cheng, L.; Qu, Y. Surface Modification of Coconut-Based Activated Carbon by Liquid-Phase Oxidation and Its Effects on Lead Ion Adsorption. *Desalination* **2010**, *255* (1–3), 78–83.
- [11] Sevilla, M.; Mokaya, R. Environmental Science Energy Storage Applications of Activated Carbons : Supercapacitors and Hydrogen Storage. *Environmental science and Technology* **2014**, 1250–1280.
- [12] Zhang, J.; Zhong, Z.; Shen, D.; Zhao, J.; Zhang, H.; Yang, M.; Li, W. Preparation of Bamboo-Based Activated Carbon and Its Application in Direct Carbon Fuel Cells. *Energy and Fuels* **2011**, *25* (5), 2187–2193.



- [13] Ma, M.; Zhang, C.; Huang, G.; Xing, B.; Duan, Y.; Wang, X.; Yang, Z.; Zhang, C. Synthesis and Electrochemical Performance of Polyacrylonitrile Carbon Nanostructure Microspheres for Supercapacitor Application. *J. Nanomater.* **2015**, Article ID 246093, 1-10.
- [14] Lozano-Castello, D.; Cazorla-Amoros, D.; Linares-Solano, A.; Shiraiishi, S.; Kurihara, S.; Oya, H. Influence of pore structure and surface chemistry on electric double layer capacitance in non- aqueous electrolyte. *Carbon* **2003**, *41*, 1765-1775.
- [15] Rodríguez-Reinoso, F.; Nakagawa, Y.; Silvestre-Albero, J.; Juárez-Galán, J. M.; Molina-Sabio, M. Correlation of Methane Uptake with Microporosity and Surface Area of Chemically Activated Carbons. *Microporous Mesoporous Mater.* **2008**, *115* (3), 603–608.
- [16] Bagreev, A.; Bandosz, T. J. A Role of Sodium Hydroxide in the Process of Hydrogen Sulfide Adsorption/Oxidation on Caustic-Impregnated Activated Carbons. *Ind. Eng. Chem. Res.* **2002**, *41* (4), 672–679.
- [17] Removing Mercaptans From Hydrocarbons With Active Carbon Impregnated With Alkali, PATENT US2748059 A, **1956**.
- [18] Ghorishi, S. B.; Keeney, R. M.; Serre, S. D.; Gullett, B. K.; Jozewicz, W. S. Development of a Cl - Impregnated Activated Carbon for Entrained-Flow Capture of Elemental Mercury. *Environ. Sci. Technol.* **2002**, *36* (20), 4454–4459.
- [19] Sharma, A.; Verma, N.; Sharma, A.; Deva, D.; Sankararamakrishnan, N. Iron Doped Phenolic Resin Based Activated Carbon Micro and Nanoparticles by Milling: Synthesis, Characterization and Application in Arsenic Removal. *Chem. Eng. Sci.* **2010**, *65* (11), 3591–3601.
- [20] Mugisidi, D.; Rinaldo, A.; Soedarsono, J.W.; Hikam, M. Modification of activated carbon using sodium acetate and its regeneration using sodium hydroxide for the adsorption of copper from aqueous solution. *Carbon* **2007**, *45*, 1081-1084.
- [21] López, D.; Buitrago, R.; Sepúlveda-Escribano, A.; Rodríguez-Reinoso, F.; Mondragón, F. Low-Temperature Catalytic Adsorption of NO on Activated Carbon Materials. *Langmuir* **2007**, *23* (18), 12131–12137.
- [22] Zhu, J.L.; Wang, Y.H.; Zhang, J.C.; Ma, R.Y. Experimental investigation of adsorption of NO and SO<sub>2</sub> on modified activated carbon sorbent from flue gases. *Energy Convers Manage* **2005**, *46*, 2173-2184.
- [23] Chieh, C.C.; Huang, Y.P.; Wang, W.C.; Chao, J.H.; Wei, Y.Y. Efficiency of moso bamboo charcoal and activated carbon for adsorbing radioactive Iodine. *CLEAN-Soil Air Water* **2011**, *39*, 103-108.

- [24] Chen, S.; Liu, J.; Zhana, X.; Zeng, H. Studies on the preparation of zinc containing activated carbon fibres and their antibacterial activity. *Chin.J.React.Polym.* **2002**, *11*(2), 113-117.
- [25] Shen, W.; Li, Z.; Liu, Y. Surface Chemical Functional Groups Modification of Porous Carbon. *Recent Patents Chem. Eng.* **2008**, *1* (1), 27–40.
- [26] Üçer, A.; Uyanik, A.; Çay, S.; Özkan, Y. Immobilisation of Tannic Acid onto Activated Carbon to Improve Fe (III) Adsorption. *Sep. Purif. Technol.* **2005**, *44* (1), 11–17.
- [27] Sathish, R. S.; Raju, N. S. R.; Raju, G. S.; Rao, G. N.; Kumar, K. A.; Janardhana, C. Equilibrium and Kinetic Studies for Fluoride Adsorption from Water on Zirconium Impregnated Coconut Shell Carbon. *Sep. Sci. Technol.* **2007**, *42* (4), 769–788.
- [28] Peräniemi, S.; Hannonen, S.; Mustalahti, H.; Ahlgrén, M. Zirconium-Loaded Activated Charcoal as an Adsorbent for Arsenic, Selenium and Mercury. *Fresenius J. Anal. Chem.* **1994**, *349*, 510–515.
- [29] Zhang, Q.; Jiang, P.; Pan, B.; Zhang, W.; Lv, L. Impregnating Zirconium Phosphate onto Porous Polymers for Lead Removal from Waters: Effect of Nanosized Particles. *Ind. Eng. Chem. Res.* **2009**, *48*(9), 4495–4499.
- [30] Li, L.; Li, K.; Ma, L.; Luan, Z.O. Activated carbon impregnated with zirconium hydroxide for toxic chemical removal. *Material Science and Environmental Engineering* **2015**, ISBN: 978-1-138-02938-5,759–762.
- [31] Liao, X. P.; Tang, W.; Zhou, R. Q.; Shi, B. Adsorption of metal anions of vanadium (V) and chromium(VI) on Zr (IV)-impregnated collagen fiber. *Adsorption* **2007**, *14*(1), 55–64.
- [32] Juan, J. C.; Zhang, J.; Jiang, Y.; Cao, W.; Ambar, M. Zirconium Sulfate Supported on Activated Carbon as Catalyst for Esterification of Oleic Acid by N -Butanol under Solvent-Free Conditions. *Catalysis Letters* **2007**, *117*(3-4), 153–158.
- [33] Prauchner, M. J.; Rodriguez-Reinoso, F. Preparation of Granular Activated Carbons for Adsorption of Natural Gas. *Microporous Mesoporous Mater.* **2008**, *109* (1–3), 581–584.
- [34] Tan, I. A. W.; Ahmad, A. L.; Hameed, B. H. Enhancement of Basic Dye Adsorption Uptake from Aqueous Solutions Using Chemically Modified Oil Palm Shell Activated Carbon. *Colloids Surfaces A Physicochem. Eng. Asp.* **2008**, *318* (1–3), 88–96.

- [35] Jayabalan, T.; Pré, P.; Héquet, V.; Umr-cnrs, G.; Nantes, E. M. Material Properties Influencing the Reactivity of Activated Carbons : Thermal Analysis, and HRTEM study and Statistical Modelling. *Energy & Fuels* **2009**, *23*, 4051–4058.
- [36] Bouchelta, C.; Medjram, M. S.; Zoubida, M.; Chekkat, F. A.; Ramdane, N.; Bellat, J. P. Effects of pyrolysis conditions on the porous structure development of date pits activated carbon. *Journal of Analytical and Applied Pyrolysis* **2012**, *94*, 215–222.
- [37] Thommes, M.; Morlay, C.; Ahmad, R.; Joly, J. P. Assessing surface chemistry and pore structure of active carbons by a combination of physisorption (H<sub>2</sub>O, Ar, N<sub>2</sub>, CO<sub>2</sub>), XPS and TPD-MS. *Adsorption* **2011**, *17*(3), 653–661.
- [38] Oda, H.; Yamashita, A.; Minoura, S.; Okamoto, M.; Morimoto, T. Modification of the oxygen-containing functional group on activated carbon fiber in electrodes of an electric double-layer capacitor. *J Power Sources* **2006**, *158*, 1510-1516.
- [39] Song, X.; Liu, H.; Cheng, L.; Qu, Y. Surface Modification of Coconut-Based Activated Carbon by Liquid-Phase Oxidation and Its Effects on Lead Ion Adsorption. *Desalination* **2010**, *255* (1–3), 78–83.
- [40] Velasco, L. F.; Ania, C. O. Understanding phenol adsorption mechanisms on activated carbons. *Adsorption* **2011**, *17*(1), 247–254.
- [41] Lozano-Castello, D.; Cazorla-Amoros, D.; Linares-Solano, A.; Oshida, K.; Miyazaki, T.; Kim, Y. J.; Endo, M. Comparative Characterization Study of Microporous Carbons by HRTEM Image Analysis and Gas Adsorption. *The Journal of Physical Chemistry B* **2005**, *109*(31), 15032–15036.
- [42] Do, D. D.; Herrera, L. F.; Nicholson, D. A method for the determination of accessible surface area, pore volume, pore size and its volume distribution for homogeneous pores of different shapes. *Adsorption* **2011**, *17*(2), 325–335.
- [43] Brunauer, S.; Emmett, P. H.; Teller, E. Adsorption of Gases in Multimolecular Layers, *J. Am. Chem. Soc.* **1938**, *60*, 309–319.
- [44] Pomonis, P. J.; Armatas, G. S. A Method for the Estimation of Pore Anisotropy in Porous. *Langmuir* **2004**, *10*, 6719–6726.
- [45] Langmuir, I. The Adsorption of Gases on Plane Surfaces of Glass, Mica and Platinum. *Journal of the American Chemical Society* **1918**, *40* (9), 1361–1403
- [46] Freundlich, H.M. Over the Adsorption in Solution. *Journal of Physical Chemistry A* **1906**, *57*, 385-470.
- [47] Dubinin, M.M.; Radushkevich, L.V. The Equation of the Characteristic Curve of Activated Charcoal. Proceedings of the Academy of Sciences, *Physical Chemistry Section* **1947**, *55*, 331.

- [48] Lippens, B. C.; De Boer, J. H. Studies on Pore Systems in Catalysts. *J. Catalysis* **1965**, *4*, 319–323.
- [49] Gregg, S. J.; Sing, K. S. W. Adsorption Surface area and Porosity. **1982**, Academic Press, London.
- [50] Barrett, E. P.; Joyner, L. G.; Halenda, P. P. The Determination of Pore Volume and Area Distributions in Porous Substances. I. Computations from Nitrogen Isotherms. *J. Am. Chem. Soc.* **1951**, *73*, 373-380.
- [51] John, P.; Nagpal, K.; Suri, D. Determination of Surface Area/ monolayer Capacity or Limiting Micropore Volume of Carbons from Binary and Ternary Mixtures. *Carbon* **1984**, *22* (6), 575-578.
- [52] John, P. T.; Achari, V.S. Characterisation of Structural Parameters of Finely Divided and Porous Materials by a New Adsorption Isotherm. *Journal of Materials Science* **2002**, *37*, 885-893.
- [53] Achari, V.S. John Isotherm for Liquid Phase Adsorption: Comparison with Langmuir and Freundlich Models. *International Carbon Conference, Carbon 2006*, Robert Gordon University, Aberdeen, Scotland, UK. Extended Abstract, ISBN 0- 9553365-1-1, 3P 107.
- [54] Jayasree, S.; Rajalakshmi A. S.; Achari, V. S. Determination of Surface Area of Activated Carbons using John- Sivanandan Achari Isotherm Plots. *Proceedings of the 26<sup>th</sup> Kerala Science Congress, 2014*, Kerala Veterinary and Animal Sciences University, Pookode Wayanad, 1362-1371.
- [55] Mercy Thomas. Adsorption Isotherm Characterization of Porous Materials Using John Isotherm. *Ph.D Thesis 2016*, School of Environmental Studies, Cochin University of Science and Technology, Cochin, India.

.....✉.....

### 2.1 Introduction

This chapter describes in detail about materials and methods followed for the preparation of coconut shell based Granular Activated Carbon (GAC) under chemical activation using zirconium ( $Zr^{4+}$ / nano  $ZrO_2$ ). It mainly includes materials, methods, instrumentation and theory followed with respect to carbonization/activation conditions, preparation, characterization (FTIR, XPS, XRD, SEM, TEM) and adsorption studies. A detailed description of the various isotherm models are discussed for the evaluation of surface area, porosity and pore size distribution. The experimental procedures followed to study the liquid phase adsorption behaviour of the modified GACs under equilibrium conditions.

The basic/native carbon is procured from a nearby carbon manufacturing industry (Indo-German Carbons Limited, Cochin, India) and is purified under laboratory conditions, which used as the starting material for the preparation of a new series of carbon. The change in the chemical composition of activated carbon brought by chemical/thermal treatment has been assessed by different analytical techniques. The surface area of carbon is determined by BET method. Batch experiments were done to optimize maximum adsorption efficiency of the prepared samples using, phenol, *p*-nitrophenol and methylene blue. Thermodynamic study was carried out at 10-50<sup>0</sup>C in 10<sup>0</sup>C steps.

Zirconia ( $ZrO_2$ ) which prepared under laboratory conditions and  $ZrOCl_2$  (99 % purity) purchased from Spectrochem are used as an activating agent in the present study. The  $Zr^{4+}/ZrO_2$  impregnated granular carbon was activated systematically at 383 - 1273 K under inert conditions with steam. Each series of carbons were suitably labelled with a number that specifically indicating their respective activation temperature.

Surface area, pore volume, and pore size distributions are determined by  $N_2$  adsorption data at 77K. Solid-liquid equilibrium studies were carried using phenol, *p*-nitrophenol and methylene blue (MB) for evaluating adsorption isotherm behaviour, adsorption kinetics and thermodynamics of a new series of carbons produced under laboratory conditions.

## 2.2 Materials

The basic/native carbon is procured from a nearby carbon manufacturing industry Indo-German Carbons Limited, Binanipuram, Cochin, Kerala, India [Particle size (US mesh) 12 x 40, Iodine No. 1100 mg/g, apparent density 0.50 g/cc, moisture 5 %, ash 4 %] is used throughout the study as the starting material.

### 2.2.1 Preparation of GAC Series

The granular activated carbon (GAC) washed thoroughly with distilled water. The carbon was taken into a glass column and it was washed with 0.5M aqueous NaOH solution. Sufficient bed volumes of distilled water were passed to remove the traces of alkali left till pH 7.0 is noted in the washings. Then washing is repeated with 0.5M HCl. Finally, more than 1L bed volume of distilled water is passed through a glass column until a neutral pH was noted. Washed carbon was then dried in an air oven at 383 K, it is represented as GAC 383.

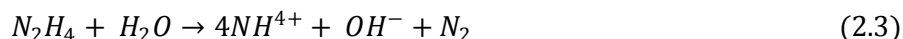
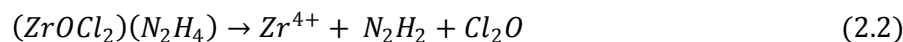
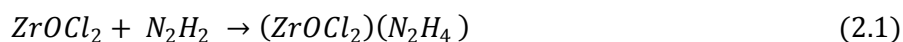
### 2.2.2 Preparation of GACO Series

The oxidation of GAC was done in a reaction mixture consisting of 100 g acid washed activated carbon, 130ml of 12.94%  $HNO_3$  and 540ml of distilled water. It is refluxed for 3 hour. After filtration the procedure was repeated by adding fresh solution of  $HNO_3$  and distilled water in the same ratio as the previous for 1 hour. After oxidation, the samples were filtered and thoroughly washed with hot distilled

water until the pH became neutral, then dried in an air oven at 383K. This nitric acid treated activated carbon was represented as GACO 383 [1, 2].

### 2.2.3 Preparation of ZrO<sub>2</sub>

The hydrothermal method has been widely applied for the preparation of fine ZrO<sub>2</sub> powders due to its low crystallization temperature simplicity and low cost. The starting reagents used in these experiments were analytical grade zirconium oxychloride (ZrOCl<sub>2</sub>.8H<sub>2</sub>O) and 85% hydrazine hydrate. 0.04M zirconium oxychloride and 0.2 M concentration of hydrazine hydrate were mixed under continuous magnetic stirring. After 10 minutes of stirring the final solution was transferred into a Teflon lined stainless steel autoclave maintained at 150 °C for 4 hours and then cooled naturally to room temperature. The product was centrifuged, filtered out and rinsed with alcohol and deionised water several times to remove the ions possibly remaining in the final products. Finally, the product was dried at 60<sup>0</sup>C in air [3, 4].



### 2.2.4 Preparation of GACZR Carbons

Different weight of zirconyl chloride (ZrOCl<sub>2</sub>.8H<sub>2</sub>O) noted as an impregnation ratio (X<sub>Zr</sub> is weight of ZrOCl<sub>2</sub>.8H<sub>2</sub>O to carbon GAC weight for every 10 g carbon) 0.0065, 0.026, 0.052 and 0.078 is used for impregnation. Impregnation was done by mixing the GAC 383 and activating agent of zirconyl chloride at 85°C for 2 hours with a magnetic stirrer. After stirring samples were placed in a water bath for about 5-6 hours and finally dried in an air oven at 383 K. The samples thus obtained are known hereafter as GACZR 383 [5].

Best  $Zr^{4+}$  impregnation ratio for carbon was selected by the value of burn off / carbon yield. It is further activated under steam in a temperature programmed furnace designed/maintained in the laboratory at different activation temperatures, such as 473 K, 673 K, 873 K, 1073 K and 1273 K. The resulted products were labelled as GACZR 473, GACZR 673, GACZR 873, GACZR 1073 and GACZR 1273.

### 2.2.5 Preparation of GACOZR Carbons

Impregnation was done by mixing the GACO 383 and activating agent of zirconyl chloride (same  $Zr^{4+}$ /carbon ratio, which is chosen for GACZR series) at  $85^{\circ}C$  for 2h with a magnetic stirrer. After stirring, samples were placed in a water bath for about 5-6 hrs and finally dried in an air oven at 383K. The samples thus obtained are known hereafter as GACOZR 383. It is further activated with steam in a temperature programmed furnace designed/maintained in the laboratory at different selected activation temperatures (473 K, 673 K, 873 K, 1073 K and 1273 K). The resulted products were labelled as GACOZR 473, GACOZR 673, GACOZR 873, GACOZR 1073 and GACOZR 1273

### 2.2.6 Preparation of GACNZR Carbons

Different weight of  $ZrO_2$  (zirconia) noted as an impregnation ratio ( $X_{Zr}$  weight of  $ZrO_2$  to carbon GAC weight for every 10g carbon) 0.0025, 0.01, 0.02 and 0.03 is used for impregnation. Impregnation was done by mixing the GAC 383 and activating agent of zirconia at  $85^{\circ}C$  for 2 hours with a magnetic stirrer. After stirring samples were placed in a water bath for about 5-6 hours and finally dried in an air oven at 383K. The samples thus obtained are known hereafter as GACNZR 383.

Best  $Zr^{4+}$  impregnation ratio for carbon was selected by the value of burn off / carbon yield. It is further activated under steam in a temperature programmed furnace designed/maintained in the laboratory at different activation temperatures (473 K, 673 K, 873 K, 1073 K and 1273 K). The resulted products were labelled as GACNZR 473, GACNZR 673, GACNZR 873, GACNZR 1073 and GACNZR 1273.



### **2.2.7 Preparation of GACONZR Carbons**

Impregnation was done by mixing the GACO 383 and activating agent of zirconia (same  $Zr^{4+}$ /carbon ratio, which is chosen for GANZR series) at 85°C for 2 hours with a magnetic stirrer. After stirring samples were placed in a water bath for about 5-6 hours and finally dried in an air oven at 383 K. The carbon thus obtained is known hereafter as GACONZR 383. It was further activated under steam in a temperature programmed furnace designed/maintained in the laboratory at different activation temperatures (473 K, 673 K, 873 K, 1073 K and 1273 K). The resulted products were labelled as GACONZR 473, GACONZR 673, GACONZR 873, GACONZR 1073 and GACONZR 1273.

### **2.3 Carbonisation Procedure**

Carbonisation is a process in which starting material is subjected to heat treatment in an inert atmosphere, where volatile components are burned off at higher temperatures. This results in a consolidation of the char where carbon micro-crystallites are getting reorganised preserving the interlayer lattices. During this process of activation carbon content of the resulting product becomes high and decreases in the contents of heteroatom due to decomposition of some groups which are readily destroyed. The carbonized materials have a developed pore structure. These pores on carbonised char is furthermore developed and enhanced during the course of the activation process. This converts the carbonized raw material into a form that contains the greatest possible number of randomly distributed pores of various sizes and shapes. Hence gives extended and extremely high surface area of the product. Prior to carbonisation the impregnated carbon was transferred into a clean and pre-weighed crucible. It is then placed in a temperature-controlled muffle furnace with 50 cm internal diameter and heated at different temperature of 383 K, 473 K, 673 K, 873 K, 1073 K and 1273 K in a continuous flow of steam into the heating chamber. After this process, the carbon was allowed to cool within the furnace to room temperature, and then it is taken out and stored in air tight container.

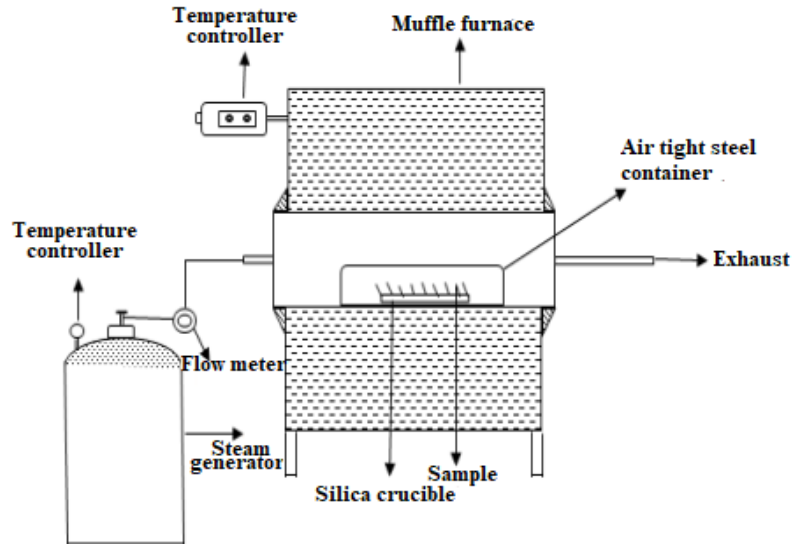


**Figure 2.1:** The experimental setup for the carbonization of the native carbon char under steam flow in a temperature programmed furnace

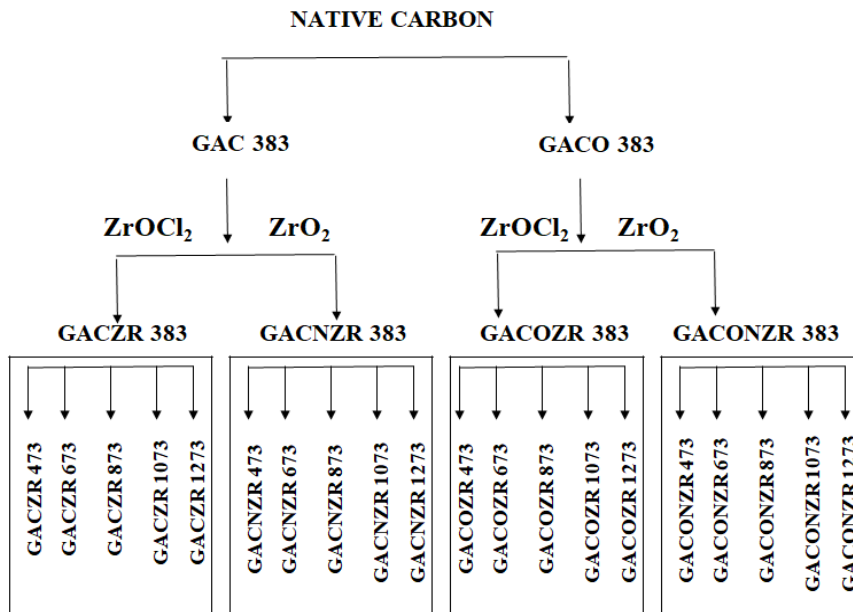


**Figure 2.2:** Schematic representation of newly prepared Zr incorporated granular activated carbons

## 2.4 Methods

### 2.4.1 Carbon Yield and Burn Off

The yield of activated carbon can be regarded as an indicator of the efficiency for the activation process. The yield of activated carbon is calculated as the percentage weight of the resultant activated carbon divided by weight of raw carbons.

$$\text{Carbon yield (\%)} = \frac{(W_t)}{(W_i)} \times 100 \quad (2.5)$$

$W_t$  is the weight of activated carbon after activation;  $W_i$  is the weight of raw carbon. Burn off refers to the weight difference between the weight of activated carbon after activation and weight of raw carbon divided by the weight of raw carbon.

$$\text{Burn off (\%)} = \frac{W_i - W_t}{W_i} \times 100 \quad (2.6)$$

### 2.4.2 Elemental Analysis

The percentage of prominent elements C, H, N, and S present in the new carbons are analyzed using Elementar Vario EL III, the percentage of oxygen was calculated by the difference using the formula

$$\text{Oxygen (\%)} = 100 - (C\% + H\% + N\% + S\%) \quad (2.7)$$

### 2.4.3 Boehm Titration

The Boehm titration method was used for the quantitative measurement of surface functional groups on the activated carbon. The characterization of acidic functional groups carboxyl, lactones and phenols are determined by neutralization with 0.05 N solutions of  $\text{NaHCO}_3$ ,  $\text{Na}_2\text{CO}_3$  and  $\text{NaOH}$ , respectively. A small quantity (0.15g) of powdered carbon was shaken with 30 ml of 0.05N  $\text{NaHCO}_3$ ,  $\text{Na}_2\text{CO}_3$  and  $\text{NaOH}$  for 20 hours. The content was separated and the filtrate collected for the analysis, further this aliquot of the solution was titrated with 0.05N  $\text{HCl}$ . Similarly, basic functional groups were estimated by neutralization with 30 ml of 0.05 N  $\text{HCl}$  for 20 hours after that solution is filtered and titrated against 0.05N  $\text{NaOH}$  [6].

#### 2.4.4 Fourier Transform Infrared Spectroscopy (FTIR)

Fourier transform infrared (FTIR) spectroscopy is the most commonly used spectroscopic techniques for the analysis of chemical structure of activated carbons. The surface groups of different oxides present on activated carbon were identified using “Thermo Nicolet, Avatar 370”. The FTIR spectra were measured using KBr disks containing wt % finely ground carbon samples, with a spectral resolution of  $4\text{ cm}^{-1}$  in the range  $4000\text{-}400\text{ cm}^{-1}$ .

#### 2.4.5 X-ray Photoelectron Spectroscopy (XPS)

X-ray photoelectron spectroscopy (XPS) is used to characterize the chemical structure such as carbon oxygen complexes on surfaces of granular activated carbon. This technique measures the kinetic energy of electrons emitted from atoms under the influence of irradiation of the sample with x-rays. XPS analysis of carbons was made with a spectrometer (AXIS Supra) equipped with a 500 mm Rowland circle monochromated Al  $K_{\alpha}$  X-rays source.

#### 2.4.6 X-ray Powder Diffractometry (XRD)

X-ray powder diffractometry is one of the most powerful and established technique for material structural analysis and it is capable of providing information about the structure of a material at the atomic level. An XRD analyzer (Bruker AXS D8 Advance) was used to measure powder x-ray diffraction patterns of the new GAC series.

Scherrer equation is used to estimate the crystalline size  $L$  ( $L_a$  or  $L_c$ ) of nanophase material.

$$L = \frac{K\lambda}{B\cos\theta} \quad (2.8)$$

Where  $L_c$  is crystalline height along  $c$ -axis,  $L_a$  is the crystalline width along  $a$ -axis.  $\lambda$  is the wavelength of the x-ray used to measure the diffractograms,  $\theta$  is the diffraction angle (Bragg angle) and  $K$  is the Scherrer constant. For carbonaceous materials, values of  $K$  for  $L_a$  and  $L_c$  are 1.84 and 0.94.

#### **2.4.7 Scanning Electron Microscopy (SEM) and Energy Dispersive Spectroscopy (EDS)**

Scanning electron microscope (JOEL Model JSM - 6390LV) and energy dispersive spectrometer (JOEL Model JED - 2300) used for high resolution surface imaging and elemental analysis. Different elements and surface topographies emit different proportion of electrons, due to which the contrast in a SEM micrograph is representative of the surface topography and distribution of elemental composition on the surface.

#### **2.4.8 High Resolution Transmission Electron Microscopy (HRTEM)**

High resolution transmission electron microscopy is a microscopy technique. HRTEM JOEL/JEM 2100 model is used for producing images of carbon. In this technique image is formed from the interaction of the electrons transmitted through an ultra-thin specimen.

#### **2.4.9 UV-Visible Spectrophotometry**

Ultraviolet-visible spectrophotometry is used for the quantitative determination of different analyte. Cary 50 Probe Spectrophotometer was used for the estimation of phenol, *p*-nitrophenol, and methylene blue (MB) in the batch adsorption studies.

#### **2.4.10 Inductively Coupled Plasma–Mass Spectrometry (ICP-MS)**

Inductively coupled plasma–mass spectrometry (ICP-MS) combines of two well-established techniques, namely the inductively coupled plasma and mass spectrometry. The concentrations of trace elements were measured by ICP-MS (Thermo scientific iCAP Qc) including QCell technology combining proven He KED (kinetic energy discrimination) interference reduction capabilities with a flatpole low mass cut-off.

### **2.5 Other Instruments**

#### **2.5.1 Water Bath**

Labline water bath incubator Model No. WBIS-3 with temperature control was used to get the modified carbons dried.

### **2.5.2 Water Bath Shaker**

LABLINE shaking water bath having a temperature variation of  $\pm 1.0^\circ$  was used for all the equilibrium batch experiment studies.

### **2.5.3 Air Oven**

LABLINE oven is used for drying the sample.

### **2.5.4 Autoclave**

KEMI (15 lbs) made stainless steel autoclave are used for steam generation.

### **2.5.5 Muffle Furnace**

A Fourtech model muffle furnace was used for heat treatment steps. The temperature range varied between 20-1500  $^\circ\text{C}$  with an accuracy of 5  $^\circ\text{C}$ .

### **2.5.6 Weighing Balance**

Reagents were weighed on SARTORIUS BP 211D digital weighing device.

### **2.5.7 pH**

pH measurements were made using the Digital pH meter MK VI with a sensitivity of  $\pm 0.01$  was used.

## **2.6 Glass Wares**

All the glassware's (Borosil make of Grade A) were cleaned with a concentrated chromic acid solution followed by rinsing with distilled water.

## **2.7 Chemicals**

All the chemicals used were of analytical reagent grade of purity 98% purchased from Merck, Alpha chemicals, Spectrochem etc.

## **2.8 Solid –Gas Equilibria: Adsorption Studies**

Characterization of GAC by  $N_2$  adsorption-desorption isotherms at 77 K was carried out volumetrically using Micromeritics TriStar 3000 V6.07 A. Total surface area, micropore and mesopore surface area, total pore volume, micropore

and mesopore volume, and pore size distribution of the carbons are determined. The porous structure of new GACs are analyzed by applying various isotherm equations like Langmuir, Freundlich, Brunauer-Emmett-Teller (BET), Dubinin-Radushkevich (D-R), Alphas S ( $\alpha_s$ ),  $t$  - plot, BJH, and John isotherm etc.

## 2.9 Solid – Liquid Equilibria: Batch Adsorption Studies

The adsorption efficiency of the modified GAC's with respect to selected organic compounds; phenol, *p*-nitrophenol, and methylene blue (MB) were determined using a batch adsorption method. The effect of various parameters like initial concentration, contact time and temperature on the efficiency to remove adsorbate was investigated. The ultimate analysis was carried out by UV-Visible spectrophotometer at 268 nm (phenol), 317 nm (*p*-nitrophenol), and 650 nm (methylene blue) respectively. The adsorption equilibrium data were well explained by Langmuir, Freundlich, Dubinin-Radushkevich, and John - Sivanandan Achari (J-SA) isotherm models. Adsorption data obtained from different time interval are subjected to pseudo first order, pseudo second order and intra particle diffusion models to determine the rate controlling parameters. The thermodynamic behaviour of adsorption system was evaluated by conducting batch experiments at five selected temperatures (283, 293, 303, 313 & 323 K).

## 2.10 Adsorption – Desorption Isotherm Procedure

The  $N_2$  adsorption-desorption isotherm data were obtained by using Micromeritics (TriStar 3000 V6.07 A). The adsorption data are represented by several isotherm equations for the determination of the surface area of the adsorbent, the volume of the pores, and their size distribution.

### 2.10.1 Type of Adsorption Isotherm

Experimental adsorption isotherms measured on a wide variety of gas-solid systems were grouped into six classes in the IUPAC classification [7]

The Langmuirian isotherm or *Type I* isotherms are characterized by a plateau that is almost horizontal and parallel to the relative pressure axis. The adsorption in *Type I* isotherms does not increase continuously, but attains a limiting value shown by the plateau is due to the pores being so narrow that they

cannot accommodate more than a single molecular layer. These types of isotherms are exhibited by microporous solids having relatively small external surface area. The *Type II* isotherm corresponds to multilayer physical adsorption. The shape of isotherm is concave to the  $x$ -axis at low relative pressures then almost long linear and finally convex to the  $p/p_o$  axis. The point at which the linear portion begins was termed as *point B* and this point was taken as the point at which the monolayer is completed. The *Type III* and *Type V* isotherms are not common and are characterized by being convex to the pressure axis. *Type III* isotherms are convex to the  $p/p_o$  axis over the complete range; it also indicates unrestricted multilayer formation process. Adsorption on mesoporous solids proceeds via multilayer adsorption followed by capillary condensation results in *Type IV* and *Type V* isotherms. The most significant characteristic of *Type IV* and *Type V* isotherms is adsorption-desorption hysteresis. *Type V* isotherm reaches a plateau at fairly high relative pressures, often at  $p/p_o$  higher than 0.51, i.e., in the multilayer region. *Type VI* isotherm or stepped isotherm is relatively rare and is associated with layer-by-layer adsorption on a highly uniform surface. The step height and sharpness depend on the system and temperature. Amongst the best examples for *Type VI* isotherms are those obtained with Ar or Kr on graphitized carbon blacks at liquid nitrogen temperature [8].

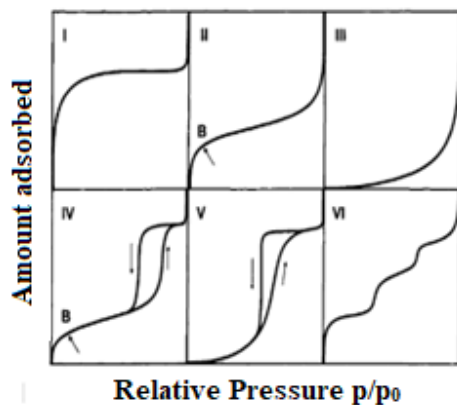


**Figure 2.3:** The IUPAC classification of adsorption isotherms

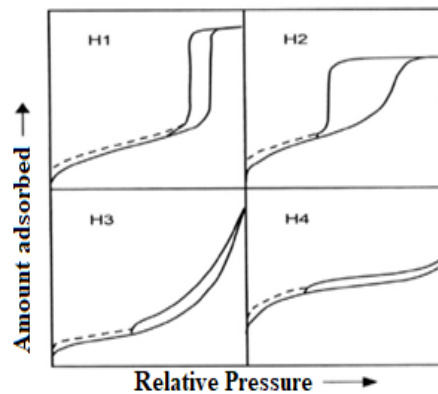


**Figure 2.4:** The IUPAC classification of Hysteresis loops



Figure 2.4 shows the IUPAC classification of hysteresis loops. According to IUPAC, *Type H1* is often associated with porous materials consisting of well-defined cylindrical-like pore channels or agglomerates of approximately uniform spheres. *Type H2* ascribes materials that are often disordered where the distribution of pore size and shape is not well defined and also indicative of bottle neck constrictions. Materials that give rise to *H3* hysteresis have slit-shaped pores. *Type H4* hysteresis is also often associated with narrow slit pores [9].

### 2.10.2 Determination of Porosity and Surface area

The physical properties of the GACs such as specific surface area, pore volume and pore size distribution can be found out using Nitrogen ( $N_2$ ) gas adsorption-desorption isotherms at 77 K. Some of the isotherms which are frequently used by researchers are applied in this study and is discussed in detail in the following sections.

The most commonly used equations to interpret adsorption isotherms are Brunauer-Emmet-Teller (BET),  $I$  plot method, Langmuir, Freundlich, Dubinin-Radushkevich (D-R), Alpha S ( $\alpha_S$ ), John Isotherm,  $t$  - plot, and BJH isotherm.

#### 2.10.2.1 Brunauer-Emmett-Teller (BET) Model

The basic assumption of the BET theory is that the first layer of adsorbed molecules acts as a support for the adsorption of the second layer of molecules, which in turn acts as a support for the third layer, and so on, so that the concept of localization is maintained in all layers. Furthermore, the forces of interaction between the adsorbed molecules are neglected [10].

The simple or infinity form of the BET equation is given as

$$V = \frac{V_m C p}{(p_0 - p)[1 + (C - 1)p/p_0]} \quad (2.9)$$

It can be rewritten in the linear form as

$$\frac{1}{V(p_0/p - 1)} = \frac{1}{V_m C} + \frac{C - 1}{V_m C} \left(\frac{p}{p_0}\right) \quad (2.10)$$

A plot gives a straight line with intercept  $\frac{1}{V_m C}$  and slope  $\frac{C-1}{V_m C}$ , from these the monolayer volume  $V_m$  and the constant  $C$  can be calculated.

$$C = \frac{\text{slope} + \text{intercept}}{\text{intercept}} \quad (2.11)$$

$$V_m = \frac{1}{\text{slope} + \text{intercept}} \quad (2.12)$$

From monolayer volume,  $V_m$  the specific surface area can be calculated by using the relationship

$$SA_{BET} = a_m N \cdot V_m \quad (2.13)$$

Where  $V_m$  is the volume of gas adsorbed,  $N$  is the Avogadro number ( $6.023 \times 10^{23}$  molecules/ mole).

According to the classical BET method, the specific surface area of the adsorbent is usually measured by adsorption of nitrogen at 77 K using molecular area of nitrogen as  $0.162 \text{ nm}^2$

$$SA_{BET} = \frac{V_m (\text{cm}^3/\text{g}) \times 6.023 \times 10^{23} \times 0.162 \times 10^{-18}}{22414} \quad (2.14)$$

### 2.10.2.2 I Plot Method

The  $I$  point method is the one alternative procedure to obtain specific area described by Pomonis and collaborators. It uses a nonlinear form of the original BET equation, i.e. BET-Scatchard (B-S) equation [11].

$$(p/p_0)[V(1 - (p/p_0))] = 1/CV_m + \frac{(C-1)(p/p_0)}{CV_m} \quad (2.15)$$

$$\frac{V(1 - (p/p_0))}{p/p_0} = CV_m - (C-1) \left[ V(1 - (p/p_0)) \right] \quad (2.16)$$

A plot of  $V[1-(p/p_0)]/(p/p_0)$  versus  $V[1-(p/p_0)]$  provided an inclined V-shaped graph, i.e. similar to the notation  $\blacktriangleright$  with an inversion point termed as  $I$  point. The extrapolation of this point towards the x-axis yields the monolayer capacity  $V_I$ , and from this surface area ( $SA_I$ ), is calculated.

$$SA_I = 4.353 V_m \quad (2.17)$$

### 2.10.2.3 Langmuir Isotherm Model

The Langmuir equation was originated from the basis of dynamic equilibrium meaning that the rate of molecules being adsorbed onto the surface equal the rate of removing of the adsorbed molecules from the surface i.e. rate of adsorption is equal to rate of desorption [12].

$$\text{The rate of adsorption, } r_{ad} = K_a P(1 - \theta) \quad (2.18)$$

$$\text{The rate of desorption, } r_{de} = K_d \theta \quad (2.19)$$

Where  $\theta$  is a fraction of the total sites occupied by the vapour at an equilibrium partial pressure,  $K_d$  desorption rate constant, and  $K_a$  adsorption rate constant

$$\text{At equilibrium, } K_d \theta = K_a P(1 - \theta) \quad (2.20)$$

$$\theta = \frac{K_a P}{K_d + K_a P} = \frac{(K_a/K_d)P}{1 + (K_a/K_d)P} \quad (2.21)$$

$$\theta = \frac{bP}{1 + bP} \quad (2.22)$$

The fraction  $\theta$  of the surface covered can also be written as the ratio of volume  $V$  of the gas or vapour adsorbed at pressure  $P$  and  $V_m$ , the volume of the adsorbate required to form a monomolecular layer. Thus, Equation (2.22) can also written as

$$\frac{V}{V_m} = \frac{bP}{1 + bP} \quad (2.23)$$

Rearrangement of the above equation gives the linear form of Langmuir Isotherm equation

$$\frac{P}{V} = \frac{1}{bV_m} + \frac{P}{V_m} \quad (2.24)$$

From this surface area ( $SA_L$ ) can be calculated as

$$SA_L = \frac{V_m (\text{cm}^3/\text{g}) \times 6.023 \times 10^{23} \times 0.162 \times 10^{-18}}{22414} \quad (2.25)$$

#### 2.10.2.4 Freundlich Isotherm Model

It is applicable only in the middle ranges of vapour pressures. The general form of the Langmuir isotherm is written as

$$V = \frac{V_m bP}{1 + bP} \quad (2.26)$$

At low pressures,  $bP$  is much smaller than unity and, therefore, can be neglected in the denominator so that the equation becomes.

$$V = V_m bP \quad (2.27)$$

Indicating that the amount adsorbed is proportional to the first power of the pressure.

$$\text{At high pressures, } V = V_m \quad (2.28)$$

The amount adsorbed becomes independent of the pressure. It is thus apparent that in the middle ranges of pressure, the amount adsorbed can be represented by a fractional exponent  $1/n$ . This will tend to vary between zero and unity, depending upon whether the pressure increases or decreases. This can be expressed by a general form of the adsorption equation

$$V = V_m bp^{1/n} \quad (2.29)$$

$$V = K_F P^{1/n} \quad (2.30)$$

on linearization the equation becomes

$$\log V = \log K_F + 1/n \log P \quad (2.31)$$

#### 2.10.2.5 Dubinin- Radushkevich (D-R) Isotherm Model

Dubinin - Radushkevich (D-R) model is basically developed for the prediction of adsorption process in microporous materials. Dubinin and Radushkevich postulated an equation which allows the micropore volume to be calculated from the adsorption isotherm [13] [1].

They suggested that for microporous active carbons (or porous materials), volume of adsorption space can be expressed as a Gaussian function of the corresponding adsorption potential

$$V = V(e) \quad (2.32)$$

$$V = V_0 \exp(-\varepsilon_0^2) \quad (2.33)$$

Where  $V_0$  is the total volume of all the micropores,  $\varepsilon$  is Polanyi potential

$$\varepsilon = \frac{\epsilon}{\beta E} \quad (2.34)$$

Where  $\beta$  is a constant called the affinity coefficient (0.33 for nitrogen),  $E$  is the characteristic energy

$$V = V_0 \exp\left(\frac{-\varepsilon}{\beta E}\right)^2 \quad (2.35)$$

$$\varepsilon = RT \ln \frac{p_0}{p} \quad (2.36)$$

$$V = V_0 \exp\left(\frac{-RT \ln p_0/p}{\beta E}\right)^2 \quad (2.37)$$

$$\ln V = \ln V_0 - \left(\frac{RT}{\beta E}\right)^2 \left(\ln \frac{p_0}{p}\right)^2 \quad (2.38)$$

$$\ln V = \ln V_0 - D \left(\ln p_0/p\right)^2 \quad (2.39)$$

$$D = \left(\frac{RT}{\beta E}\right)^2 \quad (2.40)$$

A plot of  $\log V$  versus  $(\log p_0/p)^2$  gives a straight line at very low  $p/p_0$  value where the micropores are considered to be completely filled. From the intercept of the linear plot the micropore volume can be calculated. Where  $V$  is the volume of nitrogen adsorbed,  $V_0$  is the micropore volume,  $p/p_0$  is relative pressure and  $D$  is a constant related to the micro pore structure.

$$E = \frac{RT}{\beta} \sqrt{\frac{2.303}{D}} \quad (2.41)$$

Dubinin and Stoeckli proposed that  $E$  can be related to the average micropore width  $L$ , for a carbonaceous adsorbent by the following simple formula

$$L = 6.6 - 1.79 \ln E \text{ nm} \quad (2.42)$$

micropore surface area ( $SA_{mi}$ ) related to pore width according to the following empirical formula.

$$SA_{D-R} = 2 \times \frac{10^3 V_0}{L} \text{ m}^2/\text{g} \quad (2.43)$$

#### 2.10.2.6 Alpha S ( $\alpha_s$ ) Method

The Alpha S ( $\alpha_s$ ) method allows assessing the effective micropore volume and external surface area of microporous solid. The  $\alpha_s$  method is based on the comparison of the experimental physisorption isotherm of the studied porous sample to that of a non-porous material chosen as a reference. The reference isotherm in the Alpha S method is a plot of the amount of gas adsorbed, normalized by the amount of gas adsorbed at a fixed relative pressure versus  $p/p_0$ . The reference relative pressure is usually taken as  $p/p_0 = 0.4$ , and the normalized  $V_{ads}/V_{ads(0.4)}$  is plotted. The slope of the plot is equal to the ratio of external surface area [14].

The external surface area,  $SA_{ext}$ , is calculated using the equation,

$$SA_{ext} = 2.86 \times \frac{V}{\alpha_s} \quad (2.44)$$

Where  $V$  is the amount of  $N_2$  gas adsorbed at  $p/p_0 = 0.4$  ( $\text{cm}^3/\text{g}$  STP) and the factor 2.86 is obtained by calibrating against the BET area of sooty silica's.

#### 2.10.2.7 John Isotherm Model

John isotherm models are used to express the adsorption phenomena exhibited by numerous porous materials. It is applied to various adsorption systems in its general form.

$$\log \log P = C + n \log V \quad (2.45)$$

$$\text{Where, } P = p/p_0 \times 10^N \quad (2.46)$$

Where  $p/p_0$  is the relative pressure,  $C$  is a constant,  $n$  is the slope of john isotherm plot is a measure of adsorption efficiency of the porous material reported as adsorbability constant [1].

' $N$ ' is taken conveniently to make  $\log P$  positive thereby  $\log \log P$  could be found. Different phases of adsorption can be identified that constitute the distinct pore filling mechanism. The finer micropore filling, sub monolayer filling, monolayer completion has been observed as distinct phases for adsorption on microporous carbons [15-17].

### 2.10.2.8 $t$ -Plot Method

Lippens and de Boer made use of the universal  $t$ -plot method as a standard isotherm for nitrogen adsorption at 77 K for assessing the micropore volume and the external area. It is a plot of the volume of gas adsorbed as a function of  $t$ , (standard multilayer thickness). By this method, specific surface area, can be calculated from the slope [18, 19].

The  $t$  values are calculated as a function of the relative pressure using the equation.

$$t = [13.99 / (0.034 - \log \left( \frac{p}{p_0} \right))]^{0.5} \quad (2.47)$$

Where  $t$  is the thickness of the pores and  $p/p_0$  is the relative pressure.

The external surface area  $SA_{Ext}$  of the microporous carbon can be derived from the slope of the  $t$ -plot

$$SA_{Ext} = \frac{Slope \times 10^{10} \times D}{F \times 10^6} \quad (2.48)$$

Where  $D$  is the density conversion factor 0.00015468 and  $F$  is surface area correction factor, for most samples it is taken as 1.

Micropore volume ( $\text{cm}^3$  liquid/g) is determined by

$$V_{mi} = \text{Intercept (cm}^3/\text{g STP)} \times D \quad (2.49)$$

The micropore surface area ( $SA_{mi}$ ) can be calculated from the relation

$$SA_{mi} = SA_{BET} - SA_{Ext} \quad (2.50)$$

Where  $SA_{BET}$  is the BET surface area and  $SA_{Ext}$  is the external surface area

### 2.10.2.9 Barrett Joyner and Halenda (BJH) Method

In the year 1951 Barrett, Joyner and Halenda proposed a method for the estimation of pore volume and surface area of various adsorbents using  $N_2$  isotherm. They proposed this as a correction term for the theories proposed by Wheeler, Shull and Outlon, as most of them are insufficient to deal with adsorbents with high pore size. The BJH theory is based on the assumption that the nitrogen adsorption in the pores takes place by physical adsorption as well as capillary condensation. These two factors determine the equilibrium between the gas and liquid phase at high  $p/p_0$ . With this assumption they calculated the pore volume and surface area distribution with respect to the pore radius [20].

In the BJH method, the distribution curves of pore volume and surface area are drawn as a function of pore diameter from the  $N_2$  adsorption desorption isotherm. The cumulative surface areas, pore volumes and pore width were computed from the adsorption as well as desorption branch of the  $N_2$  isotherm.

The cumulative surface area was calculated using the equation

$$SA_{cum} = 2 \sum V_{pi} / r_{pi} \quad (2.51)$$

The Kelvin equation provides the relationship between the cylindrical pore radius ( $r$ ), adsorbed layer thickness ( $t$ ), and the adsorbed liquid  $N_2$  meniscus radius ( $r_K$ )

$$r_p = t + r_K = t - \frac{4.5}{\log\left(\frac{p}{p_0}\right)} \quad (2.52)$$

$$t = [13.99 / (0.034 - \log(p/p_0))]^{0.5} \quad (2.53)$$

The average pore diameters were calculated using the formula considering cylindrical form of the pores

$$d_{av} = 4 \frac{V_p}{S}, \quad \text{where } S \text{ denotes } SA_{BET} \quad (2.54)$$

The accessibility of pores on new prepared carbon to molecules of given size and shape is determined by their pore size distribution (PSD).



## 2.11 Solid-Liquid Equilibrium

### 2.11.1 Phenol (P) and *P*-Nitrophenol (PNP)

Phenol is an organic pollutant has a molecular weight of 94.11 g/mol, appears as transparent crystalline solid. Chemically it is slightly acidic. Inhalation of phenol can cause irritate the nose, throat, and lungs. Higher exposures may cause a build-up of fluid in the lungs. Ingestion of as little as 1 gram of phenol can be fatal to humans. It can also cause severe eye damage, including blindness. *P*-Nitrophenol is used in this study as an adsorbate/pollutant molecule has molecular weight of 139.11 g/mol and appears as light yellow crystalline solid.

*Reagents:* The phenol and *p*-nitrophenol used in the present study were of analytical reagent grade (99.99 % pure) supplied by Merck. The stock solution containing 3000 mg/L of standard phenol, as well as *p*-nitrophenol, was prepared by dissolving 3g of AR grade reagent in distilled water and made upto 1000ml. Standard solution of phenol and *p*-nitrophenol (25, 50, 75, 100, 150, 200, 250, 350, 500, 750, 1000, 1250, 1500, 2000, 2500 mg/L) were prepared by diluting the stock solution into appropriate volume by using distilled water.

### 2.11.2 Methylene Blue (MB)

Methylene blue is cationic dyes have been classified as one of the toxic colorants. It has a molecular weight of 319.85 g/mol. It causes irritation to the gastrointestinal tract with symptoms of vomiting and diarrhoea. Among the various industries involved in process of dyes, textile industry ranks first in usage of dyes.

*Reagents:* A stock solution of methylene blue (MB) was prepared by weighing a given quantity of the chemical and dissolving it in an appropriate volume of distilled water. From the stock solution, dilution was done to prepare the desired concentration of MB solutions (25, 50, 75, 100, 150, 200, 250, 350, 500, 750, 1000, and 1500 mg/L).

### 2.11.3 Equilibrium Batch Tests

Adsorption batch experiments were carried out by contacting 0.05g of carbon particle with 50 ml of adsorbate solution of different initial concentration.

The adsorbant – adsorbate contact was made in 100 ml Erlenmeyer flasks using temperature controlled water bath shaker. At the end of the predetermined time interval bottles were withdrawn one by one from the water bath shaker and adsorbent was filtered off using Whatmann No.1 filter paper. The remaining solution has been quantitatively analysed by using UV-Visible spectrophotometer. Absorbance of phenol measurements were made at 268 nm, nitrophenol at 317 nm and methylene blue were done at 650 nm. The adsorption isotherm plots analysis as a function of contact time revealed that 8 hour is enough to reach the adsorption equilibrium for phenol and *p*-nitrophenol. Whereas equilibrium time of 10 hour is required for methylene blue. Adsorption data obtained from solid-liquid equilibrium is subjected to various isotherm models such as Langmuir, Freundlich, Dubinin –Radushkevich and John-Sivanandan Achari isotherms.

### 2.11.3.1 Langmuir Isotherm

The relationship between the amount adsorbed and the corresponding equilibrium concentration can be expressed by Langmuir isotherm in solid-liquid equilibria. The linearized form of Langmuir equation is

$$\frac{C_e}{q_e} = \frac{1}{K_L} + \frac{a_L}{K_L} C_e \quad (2.55)$$

Where  $C_e$  (mg/l) is the equilibrium concentration of the adsorbate,  $q_e$  (mg/g) is the amount of adsorbate adsorbed per unit mass of adsorbent,  $K_L$  ( $\text{dm}^3/\text{g}$ ) and  $a_L$  ( $\text{dm}^3/\text{mg}$ ) are the Langmuir constants related to maximum adsorption capacity and the energy of adsorption. These constants are evaluated from slope and intercept of the linear plot.

The favourability of a Langmuir adsorption process can be determined by a dimensionless constant separation factor  $R_L$

$$R_L = \frac{1}{1 + a_L C_o} \quad (2.56)$$

$R_L$  value implies the adsorption to be unfavourable ( $R_L > 1$ ), linear ( $R_L = 1$ ), favourable ( $0 < R_L < 1$ ), or irreversible ( $R_L = 0$ ).

### 2.11.3.2 Freundlich Isotherm

The Freundlich isotherm is an empirical equation that can be used for heterogeneous systems with interaction between the molecules adsorbed.

The linear form of the Freundlich isotherm model is given by the following equation

$$q_e = K_F C_e^{1/n} \quad (2.57)$$

$$\log q_e = \log K_F + \frac{1}{n} \log C_e \quad (2.58)$$

The parameter  $K_F$  is a measure of the adsorption capacity and  $1/n$  determines intensity of adsorption. If  $1/n$  is below one it indicates a normal adsorption. A plot of  $\log q_e$  versus  $\log C_e$  gives a straight line whose intercept is  $\log K_F$  and slope is  $1/n$ , from that the values of  $n$  and  $K_F$  can be calculated

### 2.11.3.3 Dubinin-Radushkevich (D-R) Isotherm

In the case of liquid-phase adsorption Dubinin-Radushkevich equation assumes that the adsorption in micropores is limited to a monolayer. The linear form of D-R equation for liquid phase is expressed as

$$q = q_m \exp(-\beta \varepsilon^2) \quad (2.59)$$

$$\ln q = \ln q_m - \beta \varepsilon^2 \quad (2.60)$$

Where  $q_m$  is the maximum sorption capacity,  $\beta$  is the activity coefficient related to mean adsorption energy, and  $\varepsilon$  is the Polanyi potential, which is defined as

$$\varepsilon = RT \ln \left[ 1 + \frac{1}{C_e} \right] \quad (2.61)$$

The mean free energy,  $E$  per molecule of adsorbate (for removing a molecule from its location in the sorption space to the infinity) can be computed by the relationship

$$E = \frac{1}{\sqrt{2\beta}} \quad (2.62)$$

#### 2.11.3.4 John – Sivanandan Achari Isotherm

The originally developed equation for solid - gas equilibria was modified for solid-liquid equilibria as John-Sivanandan Achari (*J-SA*) equation [21-23]

$$\log \log C_e = C + n \log q_e \quad (2.63)$$

Where,  $C_e$  is equilibrium adsorbate concentration  $C_e = C_e \times 10^N$  and the significance of  $N$  is already mentioned above.  $C$  is a constant and  $n$  is the adsorbability constant.

From equation 2.63,

$$\log q_e = \frac{\log \log C_e - C}{n} \quad (2.64)$$

Where  $C$  and ' $n$ ' are the intercept and slope respectively. ' $n$ ' referred as adsorbability constant of John isotherm is a measure of adsorption efficiency.

#### 2.11.4 Kinetic Studies

In order to optimise the design of sorption system we need to analyse the data by using kinetic equations which provide valuable insights into the reaction mechanism so that it is important to predict the rate at which the pollutant is removed.

The kinetics of adsorption of organic molecules is described by the solute uptake rate that determines the residence time required for the adsorption reaction. It is well established that the adsorption kinetics ultimately controls the process efficiency. The sorption of organic compounds from liquid phase to a solid phase can be considered as a reversible process, with equilibrium being established between the two phases. To analyse the adsorption rate of adsorbate on GACs, kinetic study was carried out using concentration of 250 mg/L. Adsorption data were correlated by using simplified kinetic models including pseudo first order, pseudo second order and intra particle diffusion models.

##### 2.11.4.1 Lagergren Pseudo-First Order Kinetics

Pseudo first order equation proposed by Lagergren, 1898 [24] based on the assumption that the rate of adsorption is proportional to the difference between the maximum capacity  $q_e$ , at equilibrium and the capacity  $q_t$  at any time,  $t$ .

$$\frac{dq}{dt} = K_1 (q_e - q_t) \quad (2.65)$$

After integration by applying the initial conditions  $q = 0$  at  $t = 0$  and  $q = q_t$  at  $t = t$ , Equation (2.65) becomes:

$$\log\left(\frac{q_e}{q_e - q_t}\right) = \frac{k_1 t}{2.303} \quad (2.66)$$

Linearised form of equation is given by

$$\log(q_e - q_t) = \log q_e - \frac{K_1 t}{2.303} \quad (2.67)$$

Where  $q_e$  and  $q_t$  are amounts of adsorbate adsorbed (mg/g) at equilibrium and at time  $t$  respectively,  $K_1$  is the first order rate constant for adsorption ( $\text{min}^{-1}$ ).

#### 2.11.4.2 Ho Pseudo-Second Order Kinetics

It is assumed that the adsorption capacity is proportional to the number of active sites occupied on the adsorbent, then the kinetic rate law can be rewritten as [25, 26].

$$\frac{dq}{dt} = K_2 (q_e - q_t)^2 \quad (2.68)$$

$K_2$  is the rate constant of sorption (g/mg min),  $q_e$  is the amount of solute adsorbed at equilibrium (mg/g), and  $q_t$  (mg/g) is amount of solute adsorbate on the surface of the sorbent at any time  $t$ .

Integrating above equation at boundary condition  $t = 0$  to  $t = t$  and  $q_t = 0$  to  $q_t = q_t$  gives

$$\frac{1}{q_e - q_t} = \frac{1}{q_e} + Kt \quad (2.69)$$

Rearrangement of the above equation gives linearised form of equation

$$\frac{t}{q_t} = \frac{1}{K_2 q_e^2} + \frac{1}{q_e} t \quad (2.70)$$

Equation (2.70) can be rearranged to obtain a linear form

$$\frac{t}{q_t} = \frac{1}{h} + \frac{1}{q_e} t \quad (2.71)$$

Where  $h = K_2 q_e^2$  ( $\text{mg g}^{-1} \text{min}^{-1}$ ) can be regarded as the initial adsorption rate as  $t \rightarrow 0$

#### 2.11.4.3 Intraparticle Diffusion Model

The possibility of intraparticle diffusion was examined using the intraparticle diffusion model, taking into account that during the course of adsorption the adsorbed amount is proportional to the square root of the contact time,  $t$  [27]. The rate parameters for intraparticle diffusion ( $K_{id}$ ) at different initial concentrations are determined using the following equation.

$$q_t = K_{id} t^{1/2} \quad (2.72)$$

Where  $K_{id}$  is the intraparticle diffusion constant ( $\text{mg/gmin}^{1/2}$ ). It calculated from linear plot of  $q_t$  versus  $t^{1/2}$ .

#### 2.11.5 Diffusion Coefficient

Diffusion coefficient, also called diffusivity, is an important parameter indicative of the diffusion mobility. This kinetic expression given by Boyd et al. predicts the actual slowest step involved in the adsorption process for different adsorbent - adsorbate systems. It is given by [28]

$$F(t) = 1 - \frac{6}{\pi^2} \sum \frac{1}{z^2} \exp \left[ \frac{-Z^2 \pi^2 D_e t}{R_a^2} \right] \quad (2.73)$$

$F(t) = q_t / q_e$  is the fractional attainment of equilibrium at time  $t$ ,  $D_e$  the effective diffusion coefficient of adsorbates in the adsorbent phase ( $\text{m}^2/\text{s}$ ),  $R_a$  the radius of the adsorbent particle and  $Z$  is an integer.

Vermeulen's approximation of the above equation fits the whole range  $0 < F(t) < 1$ , for adsorption on spherical particles.

$$F(t) = \left[ 1 - \exp \left( \frac{-\pi^2 D_e t}{R_a^2} \right) \right]^{1/2} \quad (2.74)$$

This equation could further be simplified to cover most of the data points for calculating effective particle diffusivity.

$$\ln \left[ \frac{1}{1 - F^2(t)} \right] = \frac{\pi^2 D_e t}{R_a^2} \quad (2.75)$$

Thus the slope of the linear plot of  $\ln \left[ \frac{1}{1 - F^2(t)} \right]$  versus  $t$  would give  $D_e$ .

### 2.11.6 Thermodynamic Studies

In order to understand the nature of adsorption the thermodynamic parameters such as free energy change ( $\Delta G$ ) and enthalpy change ( $\Delta H$ ) and entropy change ( $\Delta S$ ) are calculated. They are calculated using Van't-Hoff equation.

$$\Delta G = -RT \ln K_L \quad (2.76)$$

$K_L$  is Langmuir constant,  $T$  is the temperature in Kelvin and  $R$  is the gas constant (8.314 Jmol<sup>-1</sup>K<sup>-1</sup>)

$$\ln K_L = \frac{\Delta S}{R} - \frac{\Delta H}{RT} \quad (2.77)$$

The slope and intercept of the plot of  $\ln K_L$  versus  $1/T$  were used to determine the values of  $\Delta S$  and  $\Delta H$ .

Then, the influence of temperature on free energy of the system was evaluated using the equations

$$\Delta G = \Delta H - T\Delta S \quad (2.78)$$

In general these parameters indicate that the adsorption process is spontaneous or not and exothermic or endothermic. The standard enthalpy change ( $\Delta H$ ) for the adsorption process is: (i) positive value indicates that the process is endothermic in nature (ii) negative value indicates that the process is exothermic in nature. The ( $\Delta S$ ) indicate measure of disorder/ degree of randomness of the adsorbed species [29].

The variations of the thermodynamic parameters with distribution coefficient ( $K_D$ ) can be obtained by the relation

$$\ln K_D = \frac{\Delta S}{R} - \frac{\Delta H}{RT} \quad (2.79)$$

### 2.11.7 Activation Energy

The apparent activation energy gives an idea about the influence of temperature on diffusivity. The activation energy  $E_a$ , was obtained from the Arrhenius equation, which is given as follows:

$$K = A e^{E_a/RT} \quad (2.80)$$

$$\ln K_2 = \ln A - E_a/RT \quad (2.81)$$

Where  $E_a$  is the activation energy (kJ/mol),  $K_2$  is the pseudo-second- order rate constant,  $A$  is the Arrhenius constant,  $R$  is the gas constant (8.314 J/mol/K), and  $T$  is the solution temperature (K). The plots of  $\ln K_2$  versus  $1/T$  were found to be straight lines and the values of  $E_a$  were determined from the slope of linear plots.

### 2.12 Design of Batch Adsorption from Isotherm Data

Adsorption isotherms can be used to predict the design of single-stage batch adsorption system. Based on the best fitting isotherm, a single stage adsorber as shown in Figure 2.5 as designed for different solution concentrations [30].

The design objective is to reduce the concentration of known volume ( $V$ ) of solution from an initial concentration of  $C_0$  to  $C_1$  (mg/l). The mass of adsorbent is  $M$  and the solute adsorbed on the adsorbent changes from  $q_0$  (mg/g) to  $q_1$  (mg/g). At time  $t = 0$ ,  $q_0 = 0$  and as time proceeds the mass balance equation for the sorption system in Figure 2.5 can be written as

The mass balance equation for adsorbent system can be written as

$$V(C_0 - C_e) = M(q_0 - q_1) = Mq_e \quad (2.82)$$

Under equilibrium condition  $C_1 \rightarrow C_0$  and  $q_1 \rightarrow q_e$

$$\frac{M}{V} = \frac{C_0 - C_e}{q_e} \quad (2.83)$$



Langmuir isotherm is used for batch adsorber design. Equation rewritten as

$$\frac{M}{V} = \frac{C_0 - C_e}{\frac{q_0 K_L C_e}{1 + K_L C_e}} \quad (2.84)$$

Where  $q_e$  is obtained from rearranging the Langmuir equation  $q_e = \frac{q_0 K_L C_e}{1 + K_L C_e}$

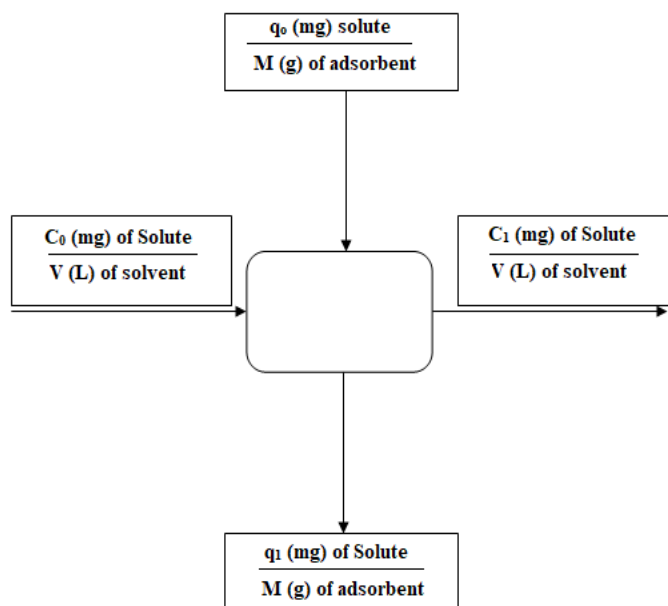


**Figure 2.5:** Schematic representation of the single stage batch adsorber system

### 2.13 Trace Elements Removal by Activated Carbon

To determine the ability of granular activated carbons to remove trace elements, ground water collected from contaminated site with trace elements are used in this study. Physico-chemical parameters of this water are known as it is collected from fireworks accident (occurred on 10<sup>th</sup> april 2016) site of Puttingal Devi Temple, Paravoor, Kollam. Adsorption experiments were performed using 50 ml solution with activated carbon dose of 0.05g. Samples were shaken using water bath shaker at 30<sup>o</sup>C. The samples were taken at 8hours after reaction time and filtered through Whatmann No.1 filter paper. The concentration of trace elements was measured by inductively coupled plasma- mass spectroscopy (ICP-MS).

## 2.14 Statistical Analysis

Data collected for the study were compiled and analysed statistically using the following significant tests. (a) **Two factor ANOVA** technique for comparison of row and column effects (b) **Three factor ANOVA** technique for comparison of row, column and treatment effects, (c) **t- test** for testing the significance of an observed correlation coefficient

The mathematical model used for framing the two factor anova is

$$X_{ij} = \mu + \alpha_i + \beta_j + \epsilon_{ij} \quad (2.85)$$

$X_{ij}$  is the observation in the  $i^{\text{th}}$  row and  $j^{\text{th}}$  column,  $\mu$  = overall effect

$\alpha_i = i^{\text{th}}$  row effect,  $\beta_j = j^{\text{th}}$  column effect,  $\epsilon_{ij}$  is the random error

Wherever the treatment effects were found to be significant, least significant difference (LSD) at 5 % level was calculated in order to identify the significant treatment effects.

The mathematical model used for the construction of three factors ANOVA is

$$X_{ijk} = \mu + \alpha_i + \beta_j + \gamma_k + \epsilon_{ijk} \quad (2.86)$$

$\gamma_k = k^{\text{th}}$  treatment effect,  $\epsilon_{ijk} = \text{Random error}$

Karl Pearson's coefficient of correlation was worked out using the formula

$$r = \frac{n \sum xy - \sum x \sum y}{\sqrt{\sqrt{n \sum x^2 - (\sum x)^2} \times \sqrt{n \sum y^2 - (\sum y)^2}}} \quad (2.87)$$

The significance of the observed correlation coefficient was tested using 't' test

$$t = \frac{r\sqrt{n-2}}{\sqrt{1-r^2}} \quad (2.88)$$

$n-2$  is the degree of freedom

These analytical procedures, methodologies and statistical tools are applied to the respective stages of studies to come out with valuable observations. The results are discussed with a sound scientific background in the following chapters.

## Reference

- [1] Achari, V. S. Modified Carbons and Wood Dust: Evaluation of Adsorption Properties. *Ph.D. Thesis* **1998**. Department of Chemistry, University of Kerala, Kariavattom, Thiruvananthapuram, Kerala, India.
- [2] Bindia Ravindran. Adsorption Isotherm Studies on Activated Carbon Prepared by Activation with Cerium Compounds. *Ph.D Thesis* **2016**. School of Environmental Studies, Cochin University of Science and Technology, Cochin, Kerala, India.
- [3] Zhu, H.; Yang, D.; Xi, Z.; Zhu, L. Hydrothermal Synthesis and Characterization of Zirconia Nanocrystallites. *J. Am. Ceram. Soc.* **2007**, *90* (4), 1334–1338.
- [4] Cui, H.; Li, Q.; Gao, S.; Ku, J. Strong Adsorption of Arsenic Species by Amorphous Zirconium Oxide Nanoparticles. *Journal of Industrial and Engineering Chemistry* **2012**, *18*, 1418–1427
- [5] Achari, V.S.; Rajalakshmi, A.S.; Jayasree, S. Surface Area and Porosity Development on Granular Activated Carbon by Zirconium: Adsorption Isotherm Studies. *Journal of Applied Research and Technology* **2017** (Accepted November 2017).
- [6] Boehm, H. Surface Oxides on Carbon and Their Analysis: A Critical Assessment. *Carbon* **2002**, *40* (2), 145–149.
- [7] Thommes, M.; Kaneko, K.; Neimark, A. V; Olivier, J. P.; Rodriguez-Reinoso, F.; Rouquerol, J.; Sing, K. S. W. Physisorption of Gases, with Special Reference to the Evaluation of Surface Area and Pore Size Distribution ( IUPAC Technical Report ). *Pure Applied Chemistry* **2015**, *87* (9-10), 1051 -1061.
- [8] Bansal, R.C.; Goyal, M. Activated carbon adsorption **2005**, ISBN-10: 0-8247-5344-5, Taylor & Francis Group.
- [9] Alothman, Z. A. A Review: Fundamental Aspects of Silicate Mesoporous Materials. *Materials* **2012**, *5* (12), 2874–2902.
- [10] Brunauer, S.; Emmett, P. H.; Teller, E. Adsorption of Gases in Multimolecular Layers, *J. Am. Chem. Soc.* **1938**, *60*, 309–319.
- [11] Pomonis, P. J. The I-Point Method for Estimating the Surface Area of Solid Catalysts and the Variation of C -Term of the BET Equation. *Catal. Commun.* **2005**, *6*, 93–96.
- [12] Langmuir, I. The Adsorption of Gases on Plane Surfaces of Glass, Mica and Platinum. *J. Am. Chem. Soc.* **1918**, *40* (9), 1361–1403.

- [13] Dubinin, M. M.; Kadlec, O. New Ways in Determination of the Parameters of Porous Structure of Microporous. *Carbon* **1975**, *13* (1), 263–265.
- [14] Sing, K. S. W. Reporting Physisorption Data for Gas/solid Systems with Special Reference to the Determination of Surface Area and Porosity (Recommendations 1984). *Pure Appl. Chem.* **1985**, *57* (4), 603–61
- [15] John, P. T.; Suri D. K.; Nagpal, K. C. Degree and Volume of Microporosity and a Measure of Size Range of Micropores of Adsorbents from the Parameters of John's Isotherm. *Indian J. Technol.* **1980**, *18*, 225.
- [16] John, P. T.; Achari, V. S. Characterisation of Structural Parameters of Finely Divided and Porous Materials by a New Adsorption Isotherm. *Journal of Materials Science* **2002**, *37* (4), 885–893.
- [17] Mercy Thomas. Adsorption Isotherm Characterization of Porous Materials Using John Isotherm. *Ph.D Thesis* **2016**, School of Environmental Studies, Cochin University of Science and Technology, Cochin, India.
- [18] Lippens, B. C.; de Boer, J. H. Studies on Pore Systems in Catalysts Systems Distribution Curves in Aluminum Oxide. *J. of Catalysis* **1964**, *3*, 44–49.
- [19] Lippens, B. C.; Linsen, B. G.; de Boer, J. H. Studies on Pore Systems in Catalysts I. The Adsorption of Nitrogen ; Apparatus and Calculation. *J. of Catalysis* **1964**, *3*, 32–37.
- [20] Barrett, E. P.; Joyner, L. G.; Halenda, P. P. The Determination of Pore Volume and Area Distributions in Porous Substances. I. Computations from Nitrogen Isotherms. *J. Am. Chem. Soc.* **1951**, 73.
- [21] Achari, V.S.; Jayasree, S.; Rajalakshmi, A.S. Adsorption of *p* – nitrophenol on Coconut Shell Granular Activated Carbon: Isotherms, Kinetics and Thermodynamics. *Indian Journal of Chemical Technology* **2017**, *24*,471-478.
- [22] Achari, V.S. John Isotherm for Liquid Phase Adsorption: Comparison with Langmuir and Freundlich Models. *International Carbon Conference, Carbon* **2006**, Robert Gordon University, Aberdeen, Scotland, UK. Extended Abstract, 16-21. ISBN 0- 9553365-1-1, 3P 107.
- [23] Jayasree, S.; Rajalakshmi A. S.; Achari, V. S. Determination of Surface Area of Activated Carbons using John- Sivanandan Achari Isotherm Plots. *Proceedings of the 26<sup>th</sup> Kerala Science Congress* **2014**, Kerala Veterinary and Animal Sciences University, Pookode, Wayanad, 1362-1371.
- [24] Lagergren, S. About the theory of so-called adsorption of soluble substances, Zur theorie der sogenannten adsorption gelster stoffe, Kungliga Svenska Vetenskapsakademiens, *Handlingar* **1898**, *24*, 1-39.

- [25] Ho, Y. S.; McKay, G. Pseudo-Second Order Model for Sorption Processes. *Process Biochem.* **1999**, *34* (5), 451–465.
- [26] Senthil Kumar, P.; Gayathri, R. Adsorption of  $Pb^{2+}$  ions from aqueous solutions onto bael tree leaf powder: Isotherms, kinetics and thermodynamics study. *Journal of Engineering Science and Technology* **2009**, *4*(4), 381–399.
- [27] Macedo, J. D. S.; da Costa Júnior, N. B.; Almeida, L. E.; Vieira, E. F. D. S.; Cestari, A. R.; Gimenez, I. D. F.; Villarreal Carreño, N. L.; Barreto, L. S. Kinetic and Calorimetric Study of the Adsorption of Dyes on Mesoporous Activated Carbon Prepared from Coconut Coir Dust. *J. Colloid Interface Sci.* **2006**, *298* (2), 515–522.
- [28] Boyd, G.E; Adamson, A.W.; Myers, L.S. The exchange adsorption of ions from aqueous solutions by organic zeolites. II. Kinetics. *Journal of the American Chemical Society* **1947**, *69*, 2836-2848.
- [29] Al-Anber, M. A. Thermodynamics Approach in the Adsorption of Heavy Metals. *J. C* **2011**, 737–764.
- [30] Vadivelan, V.; Vasanth Kumar, K. Equilibrium, kinetics, mechanism, and process design for the sorption of methylene blue onto rice husk. *Journal of Colloid and Interface Science* **2005**, *286* (1), 90-100.

.....✂.....



**GRANULAR ACTIVATED CARBON PREPARED BY  
ACTIVATION WITH ZIRCONYL CHLORIDE (GACZR):  
PREPARATION, CHARACTERIZATION AND ADSORPTION  
ISOTHERM STUDIES**

---

### **3.1 Introduction**

Granular activated carbons (GACs) have been widely used in separation and purification process, particularly in water treatments to remove organic or inorganic pollutants. They are good adsorbents for gases because of their extended surface area, high affinity, reaction rate, and specific surface reactivity. Adsorption of activated carbons depends largely on many kinds of factors, as raw materials used, activation process, the nature of pore structure, and their surface functionality. Addition of activating agent during carbonisation, space between the aromatic sheets of elementary carbon may get filled with tarry matter (or blocked partially by the disorganized carbon) is preferentially burnt out. Therefore, the closed and clogged pores between the sheets are getting opened. This ultimately contributes to the extra number of voids these are termed as pores which make activated carbons excellent adsorbents. The impregnation of carbon char with metals and their oxides makes them extremely good catalysts for industrial processes. The impregnation of metals modifies the carbonisation character and alter the porous structure of the final product. It is seen that, the adsorption efficiency of carbon can be better improved by the treating carbon char with zirconium ions. Zirconium and its compounds are reported to be environmentally safe as having low biotoxicity and are relatively cost effective. The most important characteristics are their catalytic potential, high reactivity,

relatively large surface area, ease of separation, and a large number of active sites for interaction with a number of contaminants [1].

In this chapter, the porous structure and surface area developments of a series of granular activated carbon (GAC) based on coconut shell prepared under different activation conditions and  $Zr^{4+}$ /GAC incorporation ratio are evaluated. Their adsorption efficiency with respect to structural parameters was determined using standard isotherm models. Carbon products are referred to as GACZR carbons.

### 3.2 Granular Activated Carbons – GACZR Series

There are eight carbons labelled/ nomenclatures as GAC 383, GACO 383, GACZR 383, GACZR 473, GACZR 673, GACZR 873, GACZR 1073, and GACZR 1273 are prepared and tested under lab conditions. GAC 383 is the native carbon based on coconut shell, GACO 383 is acid oxidised and others are  $Zr^{4+}$  activated carbons of GAC 383. The methods of preparation and experimental setup for furnace based thermal activation were already discussed in Chapter 2.

#### 3.2.1 Effect of $Zr^{4+}$ / GAC Impregnation Ratio

The effect of the impregnation ratio of  $Zr^{4+}$  ions on the yield of granular activated carbon was determined by treating different amounts of zirconyl chloride with 10 g of granular activated carbon (GAC).

Table 3.1 shows the different ratio of zirconyl chloride ( $ZrOCl_2$ ), and its percentage used for the activation of GAC, incorporation ratio ( $X_{ZrOCl_2}$  or  $X_{Zr}$ ) together with carbon yield, and burn off of the modified carbon produced. The percentage of zirconyl chloride [(weight of zirconyl chloride/ weight of carbon) X 100] and the weight of  $Zr^{4+}$  [molecular weight of Zr/ (molecular weight of  $ZrOCl_2 \cdot 8 H_2O$ ) X weight of  $ZrOCl_2 \cdot 8 H_2O$ ] are given.  $X_{Zr}$  is the surface loading ratio of the activating agent obtained by dividing the weight of zirconium by the weight of carbon.  $X_{ZrOCl_2}$  is the incorporating ratio of  $ZrOCl_2$  obtained by dividing the weight of  $ZrOCl_2$  by the weight of carbon.



**Table 3.1:** Effect of zirconyl chloride on carbon yield and burn off at 873K as a function of incorporation ratio  $X_{ZrOCl_2}$  or  $X_{Zr}$

Amount of ( $ZrOCl_2 \cdot 8H_2O$ )	% of $ZrOCl_2 \cdot 8H_2O$	% of zirconium	$X_{ZrOCl_2}$	$X_{Zr}$	Carbon yield%	Burn off%
0.065	0.65	0.185	0.0065	0.0018	86.89	13.11
0.261	2.61	0.740	0.0261	0.0074	85.68	14.32
0.523	5.23	1.48	0.0523	0.0148	84.72	15.28
0.785	7.85	2.22	0.0784	0.0222	82.72	17.28

Burn off of carbon is the weight loss during the process of activation. Figure 3.1 shows that burn off are found to be varied with increasing amount of zirconium (as zirconyl chloride) impregnated. An incorporation ratio 0.2 % shows 13.1% burn off. Low burn off of active carbon are usually undesirable as they lead to the formation of carbon with a low surface area. This in turn may lead to low adsorption capacity for target molecules during reactor operations.

In the present study, burn off is reported to be 13-17 % (Table 3.1), the largest development of microporosity in the char without a noticeable increase in the volume of micropores is obtained preferentially when the burn off is in between 10- 25 % [2, 3].

The optimum carbon yield 84.7 % with a burn off of 15.3 % is given by an impregnation of 1.5 % zirconium, indicate a stage of progressive carbonization (Figure 3.1). Further, incorporation of  $Zr^{4+}$  (2.2 %) exhibited marked enhancement in burn off (17.28 %) leads to results a lower carbon yield (82.72 %), It is presumed that, the impregnation of 1.5 % attributes to a better carbon yield due to uniform distribution and large dispersion of  $Zr^{4+}$  ions throughout the accessible interior of the carbon granules [4].

Based on this result, carbons loaded with 1.5 % of zirconium (0.523g  $ZrOCl_2$ ) are used for further steam activation at higher temperature for better yield and burn off. Because, further impregnation of zirconium may cause the widening

of the existing pores as well as the formation of large pores by extra burn off of the walls between the adjacent pores in the later stages of activation.

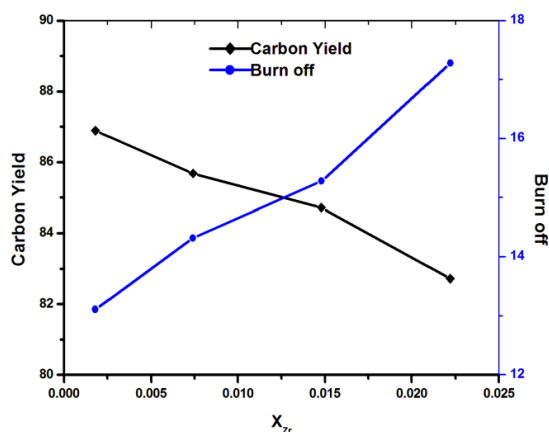


**Figure 3.1:** Variation of carbon yield and burn off with impregnation ratio

### 3.3 Characterization Studies

#### 3.3.1 Carbon Yield and Burn Off

Zirconium impregnated carbon activated with steam at different activation temperatures ranging from 473 K to 1273K (Table 3.2) shows a continuous decrease in carbon yield with increase of activation temperature. As the activation temperature increased the hydrogen (H) and oxygen (O) elements decreased progressively due to the steady release of volatile matter leaving a high carbon content. Successive burn off at a higher activation temperature decreased the yield of total active carbon from 94.5 % to 82.2 %. It shows maximum burn off 17.78 % for GACZR 1273. This low burn off even at higher activation temperature (1273 K) indicates the thermal stability of GAC achieved by successive impregnation by  $Zr^{4+}$  ions.

#### 3.3.2 Elemental Analysis

During the process of carbonization the bond at the edge of aromatic sheet in activated carbon is broken. This caused the formation of edge carbon atoms with unsaturated valencies. These carbon atoms interact with hetero atom like nitrogen, hydrogen, oxygen and sulfur. Activated carbons associated with these elements are studied using elemental composition analysis.

CHNS analysis shows that carbon percentage of GACZR series was found to be in the range of 72 - 88 % as shown in the Table 3.2. The percentage of carbon was found to be higher at a higher activation temperature of 1073K (88 %) and 1273K (86 %). The carbon percentage at these temperatures lies in the range of typical activated carbon. The edge carbon atoms are highly reactive and are called active sites or active centers that determine the surface reactivity, surface reactions, and catalytic reactions of carbons. The percentage of hydrogen in GACZR series was found to be gradually decreased with heating temperature and lies in the range of 2.8 - 0.24 %. For typical activated carbon the percentage of hydrogen usually shows 0.5 %. The presence of oxygen on the activated carbon surface has an important effect on the adsorption capacity. In GACZR series, the percentage of oxygen lies in the range of 25 - 11%. Heat treatment at higher temperature resulted in a significant decrease in the oxygen content. Successive decomposition of active surface functional groups releases CO<sub>2</sub>, CO and H<sub>2</sub>O. The nitrogen content of GACZR carbons is very low as compared to that of GAC 383 (0.36 %) and GACO 383 (0.58 %). From the Table 3.2 we can see that carbon content is inversely proportional to percentage of hydrogen and oxygen. Elements such as oxygen, hydrogen, nitrogen, and sulfur are eliminated as volatile gaseous products during the pyrolytic decomposition.

### **3.3.3 Boehm Surface Analysis**

Surface oxygen groups on carbon with acidic character, namely carboxylic (-C-OO-H), phenolic (-OH), and lactonic groups are determined by neutralization with a base of NaHCO<sub>3</sub>, NaOH and Na<sub>2</sub>CO<sub>3</sub> respectively whereas basic groups are determined by neutralization with HCl. The Boehm titration data of carbon series in Table 3.2 shows that the native carbon (GAC 383) has surface groups carboxylic (0.40 meq/g), lactones (0.18 meq/g), pyrones (0.5 meq/g), and phenols (0.45 meq/g). On HNO<sub>3</sub> oxidised carbon (GACO 383) the proportions of surface groups are more, as regards to carboxylic (1.38 meq/g), lactones (1.34 meq/g), phenols (2.1 meq/g) and pyrones (0.2 meq/g). This indicates that surface modification with nitric acid treatment enhances the oxygenation of C - O acid functional groups on the other hand the number of basic sites is reduced.

Activation of GAC after incorporation with  $ZrOCl_2$  brought marked changes in the content of oxygen surface groups that ranges carboxyl (0.393 - 0.743 meq/g), lactone (0.202 - 0.707 meq/g), pyrone (0.2 - 0.55 meq/g), and phenols (0.444 - 0.888 meq/g). Quantitative measurement of surface functional groups indicated that surface of carbon is acidic in nature. Carbon- oxygen surface functional groups make the carbon surface hydrophilic and polar in character. The surface acidities due to carboxylic and lactonic groups are evolved as  $CO_2$  and  $H_2O$  on heat treatment. This tends to decrease for the value of carboxylic group from 0.74 to 0.39 meq/g and decreasing the lactonic group from 0.70 to 0.20 meq/g during activation from 383 to 1273 K. The higher temperature treatment causes the removal of hydrogen, oxygen, and nitrogen, resulted the carbon network in activated carbon becomes more carbonaceous and aromatic in nature.

**Table 3.2:** Burn off, carbon yield, elemental composition and Boehm titration analysis of carbons GAC 383, GACO 383 and GACZR series activated at temperatures 383-1273 K

Carbons	Activation T (K)	Burn off %	Carbon yield %	Elemental composition (%)				Boehm titration analysis (meq/g)			
				C%	H%	N%	O%	Carboxylic/	Phenolic/	lactones/	yield/g
GACZR	383	NA	NA	72.2	2.9	0.05	25.0	0.74	0.56	0.71	0.20
	473	5.5	94.5	74.3	0.9	ND	24.7	0.61	0.89	0.51	0.40
	673	10.2	89.9	85.2	0.4	0.06	14.4	0.52	0.62	0.40	0.55
	873	15.6	84.7	83.7	0.5	ND	15.8	0.47	0.80	0.30	0.50
	1073	17.1	83.0	88.2	0.3	0.09	11.6	0.44	0.62	0.30	0.55
	1273	17.8	82.2	86.4	0.2	0.02	13.4	0.39	0.44	0.20	0.60
GAC 383	383	NA	NA	89.4	0.6	0.36	9.6	0.40	0.45	0.18	0.50
GACO 383	383	NA	NA	65.1	2.6	0.58	31.7	1.38	2.10	1.34	0.20

### 3.3.4 Fourier Transform Infrared Spectroscopy (FTIR) Analysis

The active adsorption sites on new activated carbons can be divided into two major types: (i) hydrophobic surfaces comprising of the graphene layers and (ii) oxygen functional groups which are primarily hydrophilic. The carbon surface of coconut shell activated charcoals has many unsaturated C = C bonds. This on

oxidation with concentrated nitric acid enhances the amount of carbon-oxygen surface chemical structures by generating more oxygen-containing groups. The originally present and surface groups evolved upon oxidation with  $\text{HNO}_3$  and respective temperature treatment under the inert condition is analysed by FTIR method and is shown in Figure 3.2 (a) – (h).

An intensive peak at  $3600 - 3100 \text{ cm}^{-1}$  in the FTIR spectrum of all the carbon is the characteristic of O - H stretching vibrations of surface hydroxyl groups and chemisorbed water. Absorbance at  $2600 - 3000 \text{ cm}^{-1}$  is due to presence of C - H stretching bond. The presence of overlapping bands between  $1300$  and  $1000 \text{ cm}^{-1}$  are assigned to C - O stretching and O - H bending modes of alcoholic, phenolic, and carboxylic groups existing in different structural environments. A peak at  $1121 - 992 \text{ cm}^{-1}$  is observed in GACO 383 because of C -OH stretching in carboxylic acid. This is the evidence for the generation of more oxygen complexes by the surface oxidation of active sites on graphene edges. This is further confirmed by the presence of peak at  $1029 \text{ cm}^{-1}$  (C- O -C) in GACO 383. FTIR spectrum revealed that, peaks at  $1700 \text{ cm}^{-1}$  were missing. This could be due to the decomposition of  $-\text{COOH}$ , which result in a peak due to quinone structure ( $1627 \text{ cm}^{-1}$ ) and it is stronger as shown in the Figure 3.2 (b) due to surface oxidation as more are generated in addition to [5-7].

Figure 3.2(c)–(d) is the FTIR profile of GACZR 383 and GACZR 473. It gives prominent peaks at  $3429 \text{ cm}^{-1}$  due to adsorbed water molecule,  $2910 \text{ cm}^{-1}$  due to O - H stretching vibration and  $1623 \text{ cm}^{-1}$  due to quinone structure. Figure 3.2(e)–(h) is the FTIR profile of GACZR series of carbon activated at 673 K, 873 K, 1073 K and 1273 K. It shows that there are peaks around at  $3429 \text{ cm}^{-1}$ ,  $2910 \text{ cm}^{-1}$ ,  $2840 \text{ cm}^{-1}$ ,  $1620 \text{ cm}^{-1}$ ,  $1450 \text{ cm}^{-1}$ ,  $1057 \text{ cm}^{-1}$  and  $589 \text{ cm}^{-1}$ . Bands at  $2910$  and  $2840 \text{ cm}^{-1}$  are associated with the stretching of the methylene ( $\text{CH}_2$ ) groups. The presence of the peaks around  $1600$  and  $1620 \text{ cm}^{-1}$  suggests the presence of carbonyls C = O groups coming from the stretching of the C = C bond. The lines observed around  $1450 - 1500 \text{ cm}^{-1}$  could correspond to the vibrations in the plane of the aromatic rings. The peak  $1050 \text{ cm}^{-1}$  and  $1100 \text{ cm}^{-1}$  due to C - OH stretching vibration characteristic respectively of primary and secondary alcohols. The band appears at  $589 \text{ cm}^{-1}$  is due to the Zr - O bending mode [8].

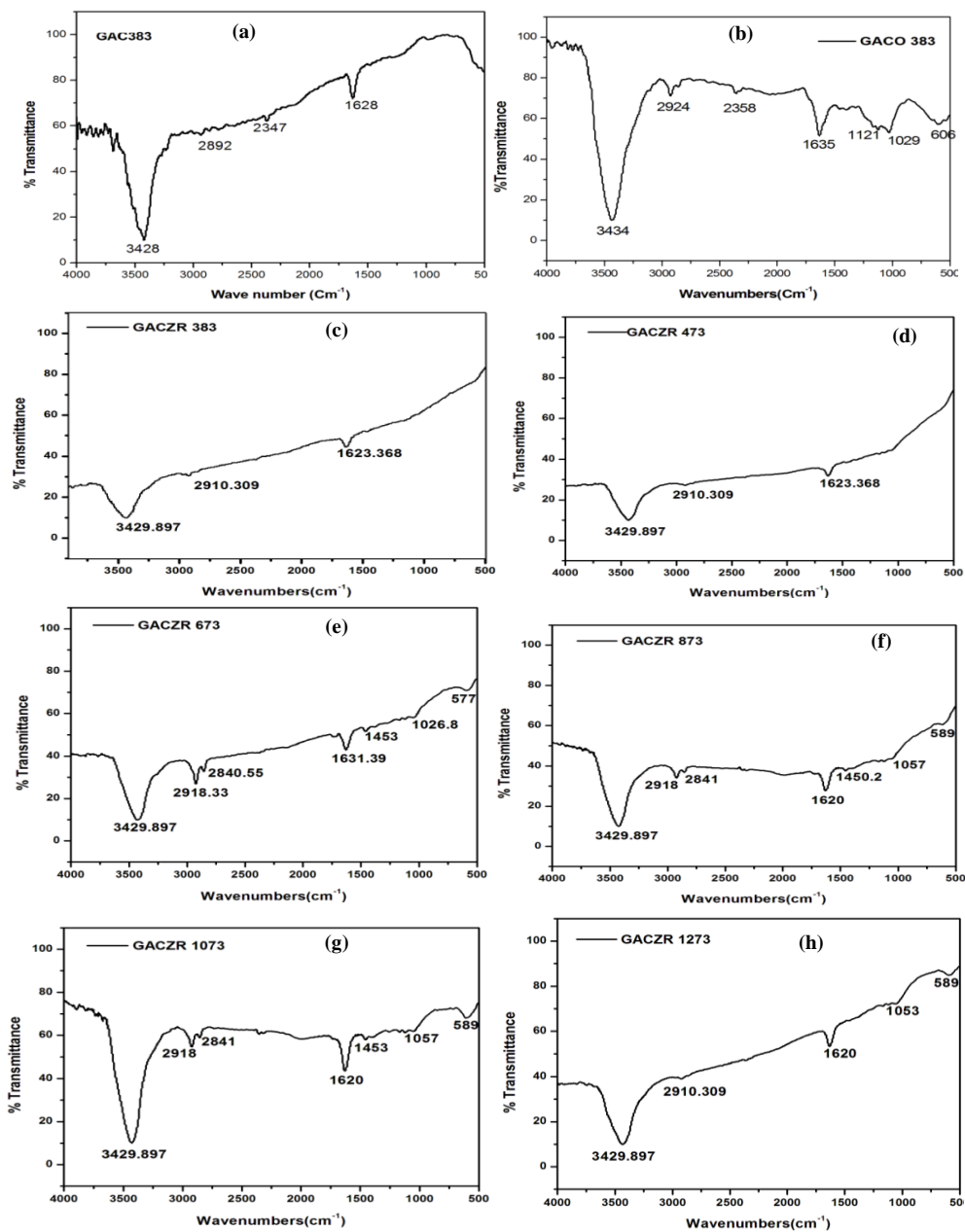


**Figure 3.2:** Fourier transform infrared (FTIR) spectra of carbons (a) GAC 383 (b) GACO 383 (c)-(h) GACZR series of carbons activated at 383-1273K for the evaluation of functional groups

The broadening of the spectra at  $3423 - 2857 \text{ cm}^{-1}$  in GACZR series of carbon compared to GAC 383 and GACO 383 shows the elimination of aromatic and aliphatic chains to a small extent and was convinced by a new peak at  $1453 \text{ cm}^{-1}$ . This shows the presence of hydrogen-bonded highly conjugated CO near one of the carbon atoms. This observation was supported by a peak at  $1057 \text{ cm}^{-1}$  due to COC asymmetric stretch in carbon GACZR 873, GACZR 1073 and GACZR 1273.

### **3.3.5 X- ray Photoelectron Spectroscopy (XPS) Analysis**

The surface chemistry of the carbonaceous adsorbent was studied using an XPS. It provides information corresponding to the outer surface of the studied activated carbon particles. The electron binding energies (eV) of the photoelectron peaks of C 1s, O 1s, Zr 3d for GACZR 1273 are shown in Figure 3.3(a) - (c).

With this analysis, it is possible to determine how much oxygen is bound to the carbon. An asymmetric photoelectron peak of C1s observed in Figure 3.3 (a) which can be decomposed into six peaks at 283.5 eV, 284.0 eV, 285.3 eV, 286.7 eV, 287.9 eV and 288.95 eV representing carbon states C1, C2, C3, C4, C5 and C6. The binding energy of 285.3 eV, associated with C – C and/or C – H groups. The binding energy of 286.7 eV, associated with C – O – H/C– O – C groups. The binding energy of 287.9 eV associated with C = O groups, 288.95 eV representing O –C = O.

The photoelectron peak of O1s observed in Figure 3.3 (b). The binding energy of O1s in between 531.3–532.6 eV associated with C = O groups (carbonyl). Binding energy in between 533.0–534.1 eV associated with C– O– (C or H) groups (ether or phenol). Peak at binding energies between 534.4 and 535.0 eV suggest the presence of chemisorbed water and/or oxygen on carbons. The binding energy 530.4 eV of O1s associated with O in  $\text{ZrO}_2$  [9, 10].

XPS measurements give information about the changes in the electronic states and chemical environment of Zr and O atoms in  $\text{ZrO}_2$ . It can be seen that Zr 3d had strong spin orbit doublet of  $3d_{5/2}$  (182.6 eV) and  $3d_{3/2}$  (185.3 eV) and

maintain a distance of about 2.7 eV between them. The region of binding energy in the Zr 3d spectrum is corresponding to  $Zr^{4+}$  in  $ZrO_2$ . Binding energy in the region of Cl 2p was not detected in Figure 3.3. The BE shift to higher energy and the shoulder peak on the lower binding energy side can arise due to the existence of sub oxide of zirconium. The existence of sub oxide component (with oxidation state less than + 4) suggests the occurrence of some reduction in the  $ZrO_2$  samples. Zr 3d  $_{5/2}$  binding energies (BE) are 182.4, 183.7 and the Zr 3d  $_{3/2}$  peak shows a BE around at 186.6, 187.2, 188, 189.6, and 189 eV. The narrowing of Zr 3d peak indicates the more uniform nature of the zirconium chemical state in  $ZrO_2$ .

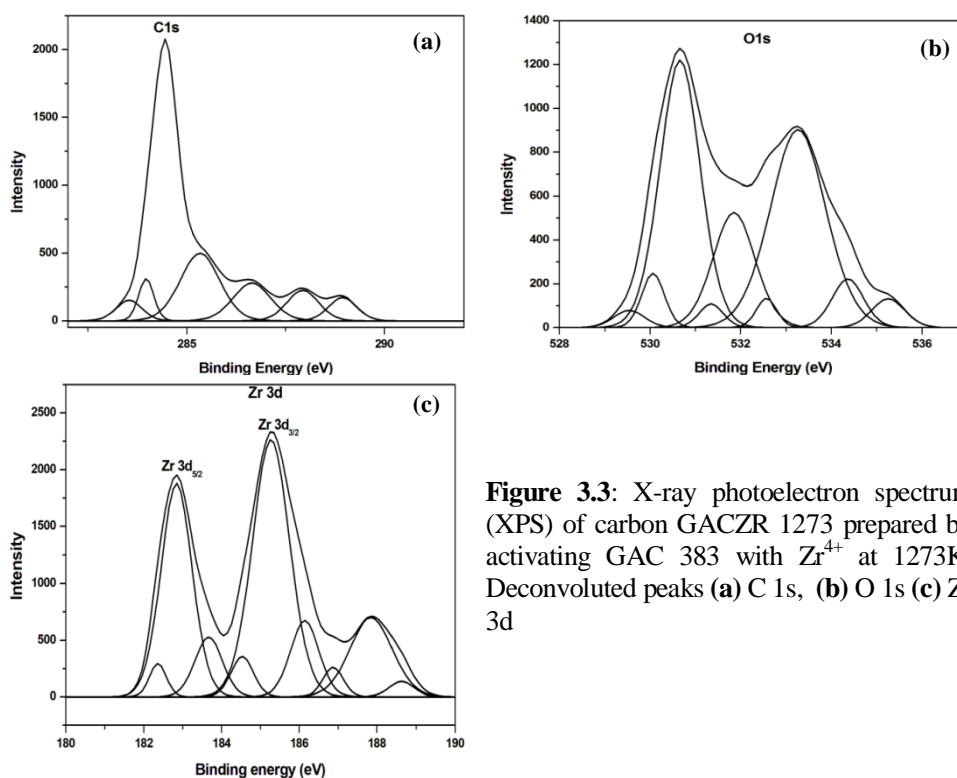


**Figure 3.3:** X-ray photoelectron spectrum (XPS) of carbon GACZR 1273 prepared by activating GAC 383 with  $Zr^{4+}$  at 1273K. Deconvoluted peaks (a) C 1s, (b) O 1s (c) Zr 3d

A detailed examination of the C 1s and O 1s regions of GAC 383 and GACO 383 reveals a number of overlapping features corresponding to different chemical functionality (Figure 3.4 and Figure 3.5).



The C 1s signal of GAC 383 and GACO 383 consists of different chemically shifted components which can be deconvoluted into different peaks. The component at 284.3 eV attributed to graphitic carbon (C – C), 284.7 – 285.1 eV due to ether or hydroxyl group (C – O), 285.6 eV assigned to C – O single bond and component at 286.1 eV corresponds to –C– OH, C– O– C≡, C– O– R and 287.0 – 287.9 eV is assigned to carbonyl groups or quinone group.

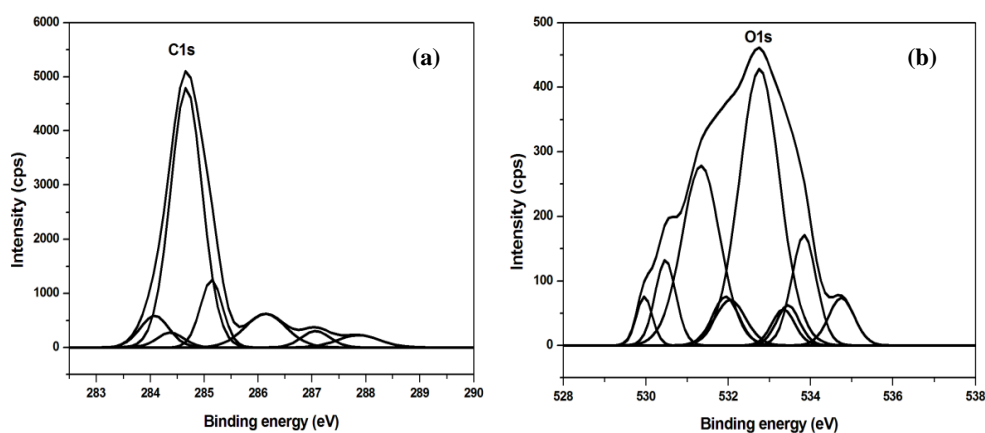


**Figure 3.4:** X-ray photoelectron spectrum (XPS) of GAC 383 (a) C 1s deconvoluted peaks (b) O 1s deconvoluted peaks

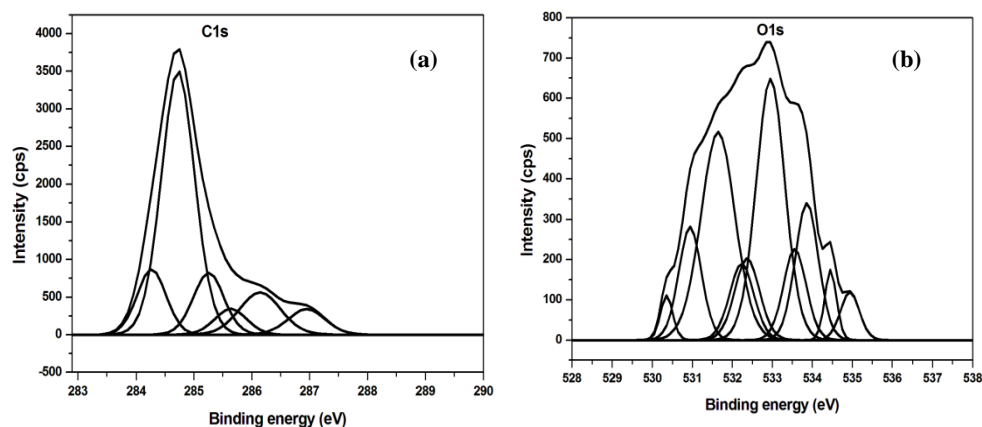


**Figure 3.5:** X-ray photoelectron spectrum (XPS) of GACO 383 (a) C 1s deconvoluted peaks (b) O 1s deconvoluted peaks

The O 1s XPS spectra for GAC 383 and GACO 383 present one peak centred at  $532.7 \pm 0.1$  eV, which is due to oxygen singly bound to  $sp^2$  carbons. 531.3 eV owing to oxygen bound to carbon by a double bond (C = O from carboxyl groups linked to aromatic rings) and the other at 533.1 eV assigned to oxygen singly bound to  $sp^2$  carbons. Peak at 532.03 eV assigned to oxygen singly bonded to aliphatic carbon (C – O), 534.7 eV assigned chemisorbed / adsorbed H<sub>2</sub>O molecule. Peaks at 533.4 eV denoted as phenolic groups (oxygen singly bonded to aromatic carbon). Intensity of peak in the O 1s XPS spectra of GACO 383 is more prominent than GAC 383 reveals formation of additional oxygen surface groups [11, 12].

**Table 3.3:** Surface functional groups analysis of carbons GAC 383, GACO 383, GACZR 1273 by XPS spectra

C1s		O1s	
285.3eV	- C-C and/or C-H groups	531.3–532.6 eV	- C = O groups (carbonyl)
286.7 eV	- C-O-H/C-O-C groups	533.0–534.1 eV	- C-O-(C,H) groups (ether or phenol)
287.9 eV	- C=O groups	534.4 – 535.0 eV	- chemisorbed water or oxygen on carbons
288.95 eV	- O-C=O groups	530.4 eV	- Oxygen in ZrO <sub>2</sub>
Zr 3d			
182.6 eV	- Zr-AC and ZrOx-AC		
183.6 eV	- Zr <sup>4+</sup> in ZrO <sub>2</sub> (3d <sub>5/2</sub> )		
184.5 eV	- Zr 3d <sub>3/2</sub> suboxide		
185.3 eV	- 3d <sub>3/2</sub> region of ZrO <sub>2</sub>		

### 3.3.6 X-ray Diffraction (XRD) Analysis

The XRD profile for the carbons GAC 383, GACO 383, and GACZR series of carbons are given in Figure 3.6. The occurrence of the broad peak at 25° and 43° shows the diffraction from (002) and (100) plane of the carbon structures. It indicates a well defined regular crystal structure for the carbon that resulted in better layer alignment. This microcrystalline structure differs from that of graphite with respect to interlayer spacing. For graphitized carbon interlayer spacing  $d_{002}$  is found to be 0.335 nm but here  $d_{002}$  for all the carbons studied are found to be in between the range of 0.35 to 0.37 nm. This indicates that the

GAC samples are non graphitized carbons. Generally, non graphitized carbon shows well developed microporous structure that is preserved even during the high carbon series temperatures. The nitric acid oxidation caused changes in the micro crystallinity of the carbon layers as evidenced by the  $L_a$ ,  $L_c$  and  $d_{002}$  values as given in Table 3.4.

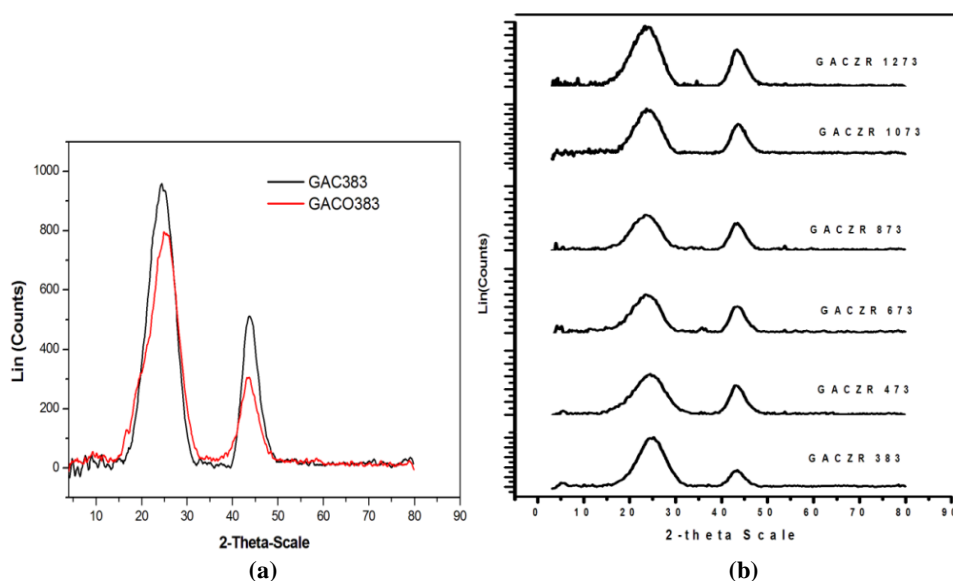


**Figure 3.6:** X-ray diffraction (XRD) spectra of (a) GAC 383 & GACO 383 (b) GACZR series of carbons activated at 383-1273K

XRD peak intensity becomes more prominent at higher activation temperatures. Three common structural changes could increase the (002) monolithic XRD peak intensity (1) an increased average number of graphene sheets per turbostratic crystallite (an  $L$  growth effect) (2) a narrower distribution of graphene sheet spacing in the turbostratic crystallites (a strain distribution effect); or (3) an increased amount of carbon from large turbostratic crystallites. The first two structural changes would cause a change in the FWHM. Since the FWHM did not change appreciably, the increase in (002) monolithic XRD peak intensity was attributed to an increased amount of carbon from large turbostratic crystallites [13].

$L_a$  and  $L_c$  values are found to be decreased with increase of temperature,  $L_c$  varies as 1.24 nm – 0.979 nm (GACZR series), 1.14 nm (GAC 383) and 0.97 nm

(GACO 383),  $L_a$  varies as 2.53 – 2.0 nm (GACZR series), 2.28 nm (GAC 383) and 1.94 nm (GACO 383). Growth effect or strain distribution effect would cause a lower FWHM and greater peak intensity. At higher temperature as we can see the broadening of the peak was small, which results small FWHM value.

The sharp 002 diffraction peak at  $26.4^\circ$  indicated a highly organized crystal structure, revealing an interlayer spacing of about  $d_{002} > 0.335$  nm. Oxidation treatment caused a decrease in the 002 peak intensity. The orientation of the stacks of aromatic sheets is also different, being less ordered in activated carbon which leaves free interstices. These interstices give rise to pores, which make activated carbons excellent adsorbents

**Table 3.4:** XRD crystalline parameters of GAC 383, GACO 383 and GACZR series activated at temperatures 383 – 1273 K

Carbons	$L_c$ (0.9) nm	$L_a$ (1.84)nm	$d_{002}$ nm
GAC 383	1.14	2.28	0.364
GACO 383	0.97	1.94	0.356
GACZR 383	1.24	2.53	0.352
GACZR 473	1.07	2.20	0.366
GACZR 673	1.13	2.30	0.379
GACZR 873	1.13	2.30	0.382
GACZR 1073	1.01	2.07	0.377
GACZR 1273	0.979	2.00	0.371

### 3.3.7 Scanning Electron Microscopy (SEM) Analysis

The surface morphology of the prepared activated carbons was examined by scanning electron microscope (SEM), and the images are shown in Figure 3.7 & 3.8. It was clear that the pore structure of the original carbon was originated from the basic lignocellulosic fibers of coconut shell (Figure 3.7(a)–(c)). The acidic treatment of GAC 383 with con  $HNO_3$  showed some distorted pattern in the arrangement of stacks. This may be due to the widening of pores and destruction of pore walls as seen in the Figure 3.7(d). Compared to GAC 383, pores in GACO 383 are apparently more open and broad.

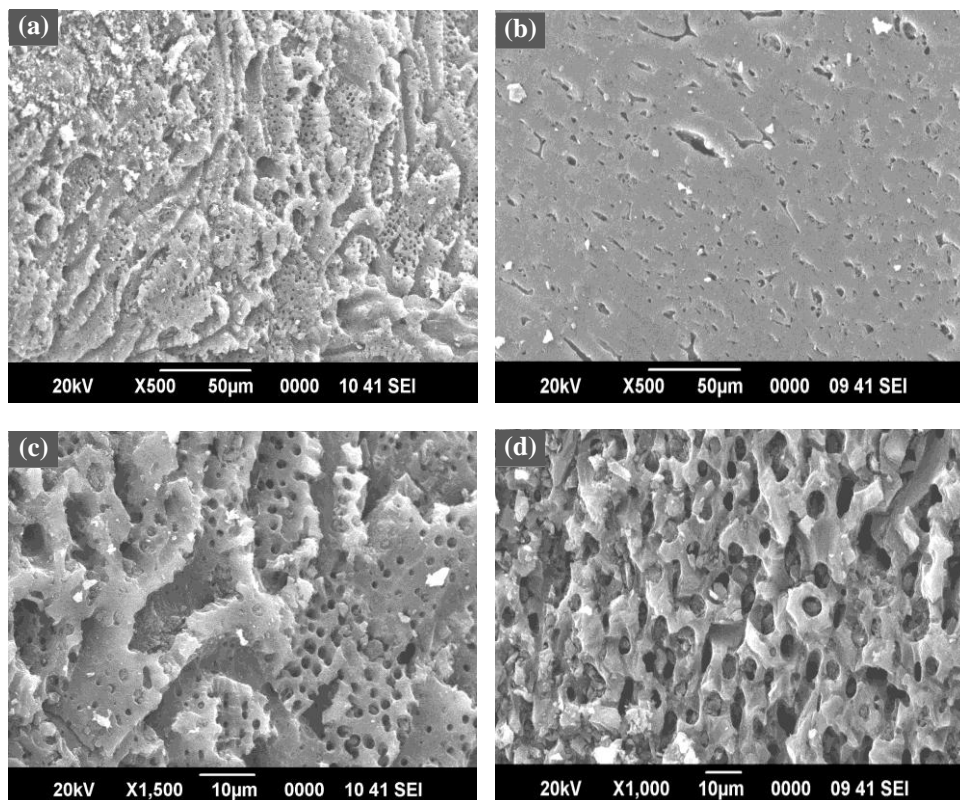


**Figure 3.7:** Scanning electron micrographs (SEM) at different magnifications (a) GAC 383 & (b) GACO 383 at 50µm resolution (c) GAC 383 & (d) GACO 383 at 10 µm resolutions

Similar to GAC 383, carbon GACZR 1273 is having a heterogeneous surface and a variety of randomly distributed pore sizes as seen in Figure 3.8(a)-(d). In all three activated carbon materials, well-developed porous surface was observed at higher magnification. The pores observed from SEM images are having a diameter in micrometer ( $\mu\text{m}$ ) range. These pores are considered as channels to the microporous network. This porous structure of the GAC imparts high surface area essential for the adsorption purposes. From the Figure 3.8(a)-(d), it can be observed that all the adsorbents have a rough texture.

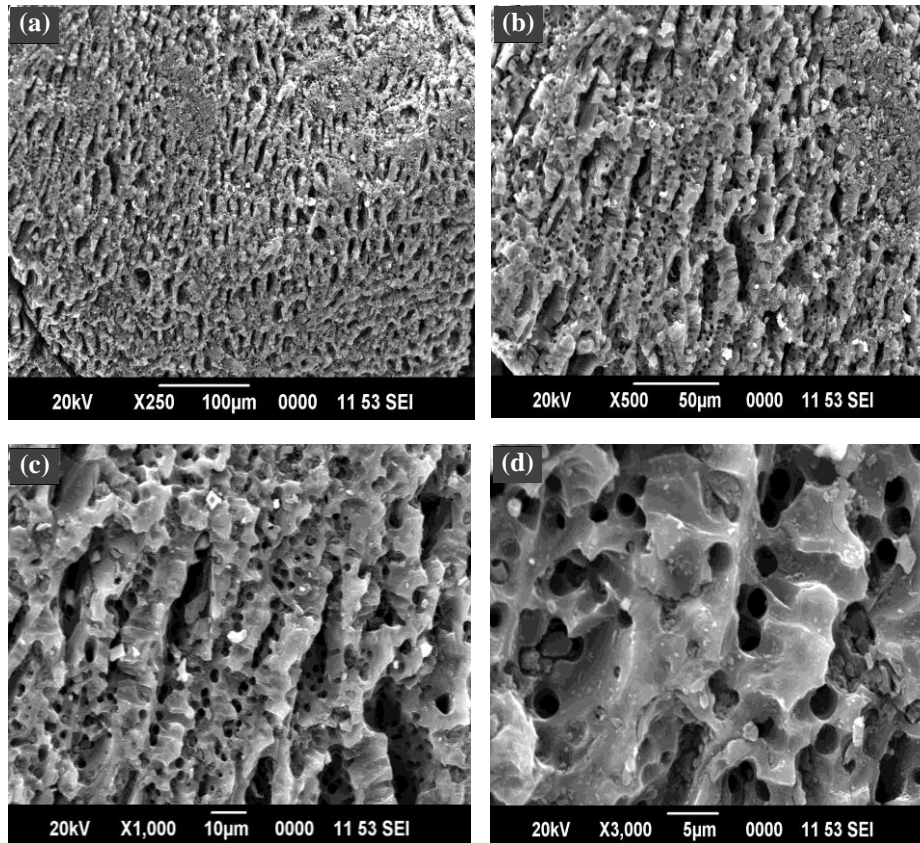


**Figure 3.8:** Scanning electron micrographs (SEM) of carbon GACZR 1273 at different resolution (a) 250-100  $\mu\text{m}$  (b) 500-50  $\mu\text{m}$  (c) 10  $\mu\text{m}$  & (d) 5  $\mu\text{m}$

### 3.3.8 Transmission Electron Microscopy (TEM) Analysis

Activated carbon prepared at optimum conditions by different chemical activations were characterized by transmission electron microscope (TEM) to observe the internal microporous network structure. From the Figure 3.9 – 3.11, it is clearly observed that the prepared GACs are highly micropores of uniform pore size.

High-resolution transmission electron microscopy (HRTEM) image indicated that the basic carbon material GAC 383 has a uniform micro porosity. The dark regions are the bulk surface of the carbon and light (bright) regions are the pore structures. At high resolution (20 nm) the pores were getting visible due to the high electron density field of micropore area. These pores were inherent

throughout the surface and are slit-shaped. They were responsible for high energy sites of graphene layers (Figure 3.9(a)-(d)).

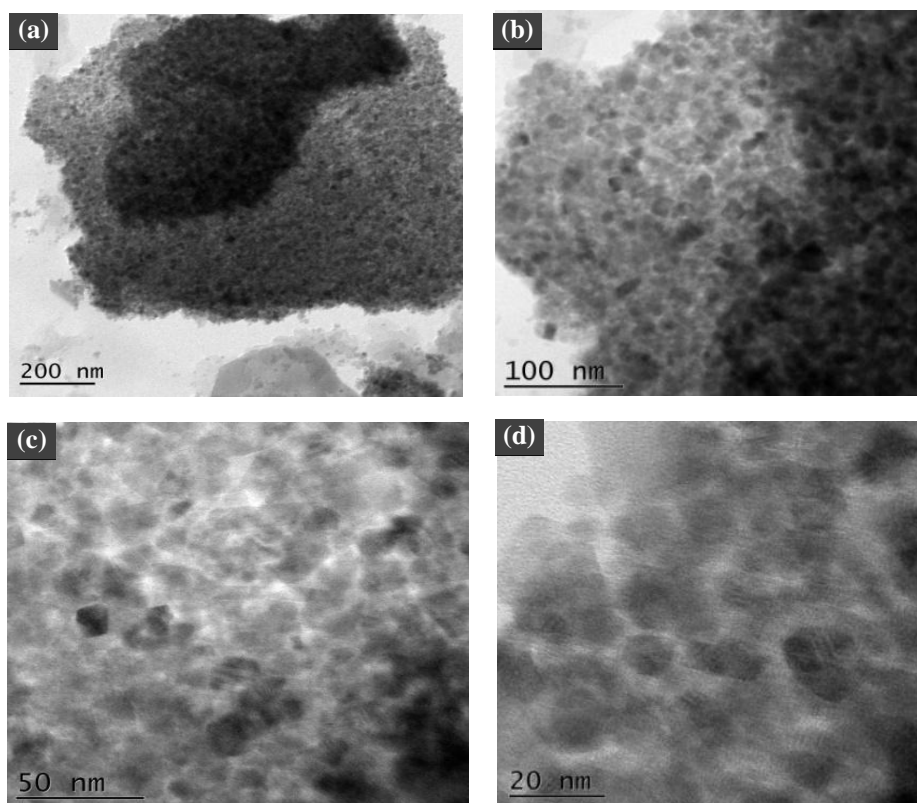


**Figure 3.9:** High resolution transmission electron microscopy (HRTEM) of GAC 383 at different resolutions (a) 200 nm (b) 100 nm (c) 50 nm & (d) 20 nm

GAC 383 carbons on chemical activation/oxidation gave GACO 383 with dramatic changes on the carbon surface as revealed by HRTEM images of nitric acid oxidized carbons. GACO 383 showed a more prominent distribution of pores as revealed in Figure 3.10(a)–(d) with a wider dispersion of the bright area. Nitric acid treatment etches the surface and oxidises any adsorbed fines and tar forms, therefore the inner layers of graphitic spacing become visible. The crystal lattice has a circular/ hexagon shaped layers with a thickness of less than 10 nm. Fringes patterns are becoming more apparent (Figure 3.10(c) – (d)). The smooth surfaces

of GAC 383 become irregular, and the surface appears to have a collapsed and irregular pattern. High-resolution transmission electron microscopic (HRTEM) images of GACZR 1273 are given in Figure 3.11. The shapes of the particles observed were almost similar to that of GAC 383 [14].

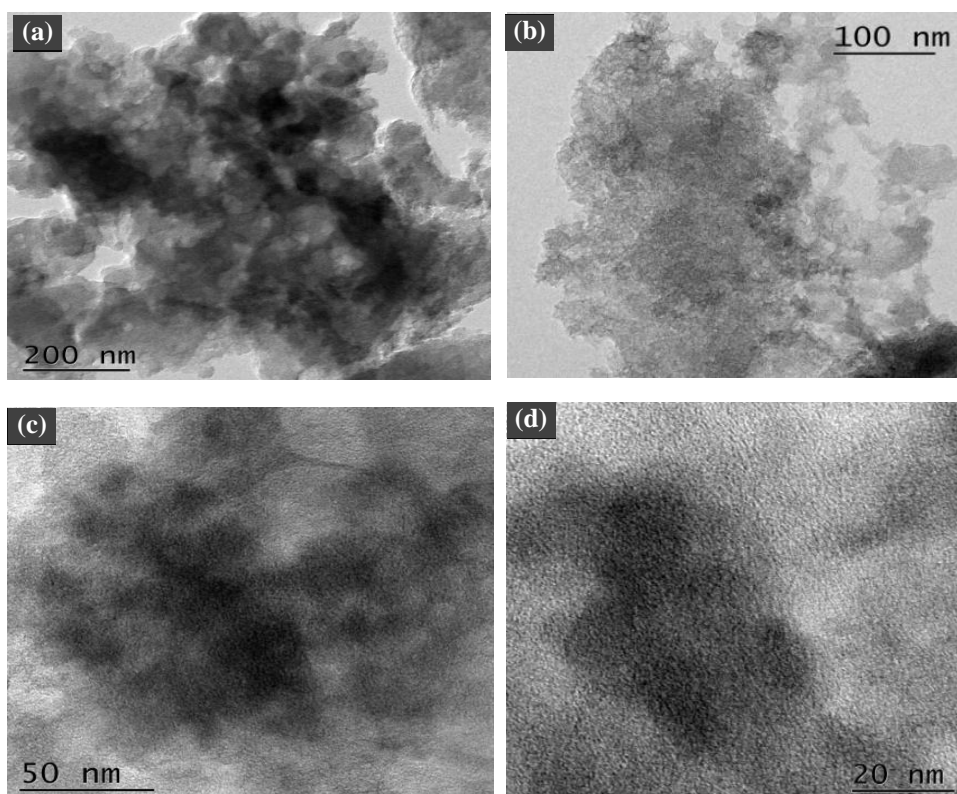


**Figure 3.10 :** High resolution transmission electron microscopy (HRTEM) of GACO 383 at different resolutions (a) 200 nm (b) 100 nm (c) 50 nm & (d) 20 nm

The obtained micrographs reveal agglomerated microstructures. However, plain faces of crystallites can be seen in Figure 3.11(c). Carbon pores are assumed to have slit shaped structures, confirmed by parallel planes. GACZR 1273 has high disordered and porous microstructure consisting of mainly tightly curled single carbon layers. The hexagonal shapes were clearly dominant in GACZR 1273 but pentagonal arrangements are also seen [15].



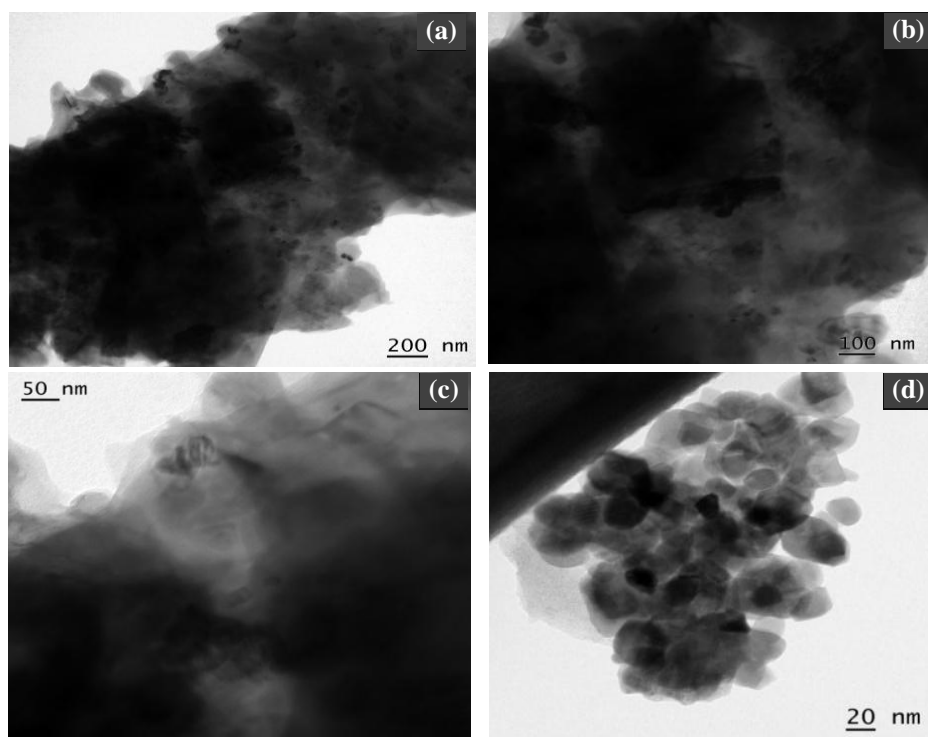


**Figure 3.11:** High resolution transmission electron microscopy (HRTEM) of GACZR 1273 at different resolutions (a) 200 nm (b) 100 nm (c) 50 nm & (d) 20 nm

The HRTEM image of GACZR 1273 shows a void region representing the pore widening occurs extensively throughout the structure. Figure 3.11(a)-(d) indicates the arrangement of microcrystalline lattice fringes with the presence of  $Zr^{4+}$  deposited/ dispersed on the carbon supports with small particle size (as dark areas) due to high electron density. The white regions are purely amorphous  $Zr^{4+}$  formed on the carbons. They were deposited on the carbon surfaces and were not uniformly distributed. The stack arrangements are the evidence for the graphene layers. This indicates that  $Zr^{4+}$  based carbon oxidation resulted in pore widening at high temperature and their distribution is homogeneous on the carbon surface.

### 3.4 Solid-Gas Adsorption Equilibria

When a porous material is exposed to a gas, an attractive force acts between the exposed surface of the solid and the gas molecules. Liquid nitrogen at a temperature of 77 K is used for measuring surface area and pore size distribution.

The  $N_2$  adsorption-desorption isotherms (at 77 K) of the GAC impregnated with zirconyl chloride prepared at different temperatures ranging from 873 K to 1273 K were carried out to investigate the porous characteristics.

### 3.4.1 Adsorption Isotherm Analysis

In an adsorption, dynamic phase equilibrium exists between the adsorbent and adsorbate. The equilibrium is usually expressed in terms of partial pressure and volume of  $N_2$  adsorbed per unit mass.

Figure 3.12 indicates the adsorption isotherm of  $N_2$  gas adsorbed on GAC 383, GACO 383, GACZR 873, GACZR 1073, and GACZR 1273. Isotherm gives the features of *Type I* isotherm i.e. concave to the relative pressure ( $p/p_0$ ) axis. It rises sharply at low relative pressures and reaches a plateau: the amount adsorbed by the unit mass of carbon studied, approaches a limiting value as  $p/p_0 \rightarrow 1$ . *Type I* isotherms are observed for the adsorption of gases on micro porous solids.

The micropore filling process is dependent on both the ratio of the pore width to the molecular diameter ( $w/d$ ) and the pore shape. If the pore width ( $w$ ) is no more than a few molecular diameters ( $d$ ), the enhanced interactions lead to complete pore filling at very low  $p/p_0$ .

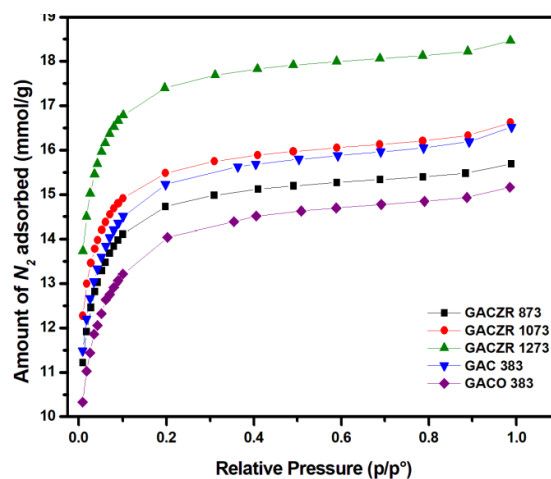


**Figure 3.12:**  $N_2$  adsorption isotherm for GAC 383, GACO 383 and GACZR series carbonized at temperature 873-1273 K

As shown in the Figure 3.12 the isotherms have a steep rise in the initial stage of adsorption at lower  $p/p_0$  ranges, progressed well to attain saturation at higher pressure ranges. Most of the  $N_2$  molecule adsorbed at low  $p/p_0 < 0.1$  indicates the filling of narrow micropores. The surface of solid having micropores (micropores adsorbent) generally gives *Type 1* isotherm. Shape of the isotherm is a clear indication of small external surface area due to wide micropores and absence of significant mesoporosity. Pores preferentially filled at very low  $p/p_0$ , has been called 'primary micropore filling'. Wider micro pores are filled by a 'secondary', or co-operative, process over a range of higher  $p/p_0$ .

To represent the equilibrium isotherm data different isotherm models such as Brunauer- Emmett-Teller (BET),  $I$  plot, Langmuir, Freundlich, Dubinin Radushkevich (D-R), alpha S ( $\alpha_s$ ), John isotherm,  $t$ -plot and BJH are used. Many of these isotherm equations are valid over small relative pressure ranges and not fit experimental data over the full range of relative pressures.

#### **3.4.1.1 Brunauer-Emmett-Teller (BET) Isotherm Analysis**

The BET equation is used to give the volume of gas needed to form a monolayer on the surface of the sample. This is the first method to measure the specific surface of the finely divided and porous solids.

The original BET treatment involved an extension of the Langmuir kinetic theory of monomolecular adsorption to the formation of an infinite number of adsorbed layers.

According to the BET model, the adsorbed molecules in one layer can act as adsorption sites for molecules in the next layer and, at any pressure below the saturation vapour pressure fractions of the surface are covered by layers of adsorbed molecules.

This linear transformed BET Equation (3.1) provides the basis for the BET plot of experimental isotherm data.

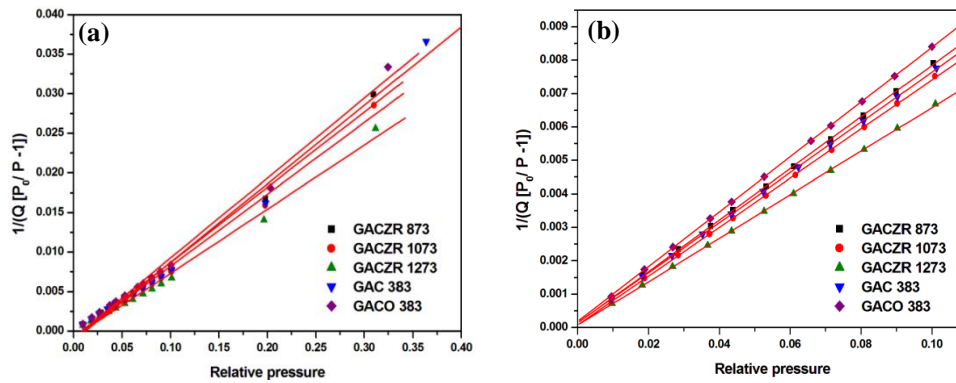
$$\frac{1}{V(p_0/p - 1)} = \frac{1}{V_m C} + \frac{C - 1}{V_m C} (p/p_0) \quad (3.1)$$

Figure 3.13 shows a linear plot of  $\frac{1}{V(p_0/p-1)}$  versus  $p/p_0$  for GAC 383, GACO 383, GACZR 873, GACZR 1073, and GACZR 1273 carbon which gives a straight line with intercept  $\frac{1}{V_m C}$  and slope  $\frac{C-1}{V_m C}$ . From these, the monolayer volume  $V_m$  and  $C$  were calculated and given in Table 3.5. The linear part of the plot usually extended in the range  $0.05 < p/p_0 < 0.25$ . The constant  $C$ , which is given by Equation (3.2)

$$C \approx \exp\left(\frac{q_1 - q_L}{RT}\right) \quad (3.2)$$

Here,  $q_1$  is the heat of adsorption in the first layer and  $q_L$  is the heat of condensation. It corresponds approximately to the value of the  $C$ -parameter at the point where the adsorbed monolayer is formed. The determination of  $C$ -parameter in the whole range of adsorption ( $0 < P < 1$ ) is unattainable [16].

The specific surface area  $SA_{BET}$ ,  $V_m$  and  $C$  values are given in Table 3.5 along with total volume  $V_{Total}$ . The  $C$  value in many cases is not positive, but for an ideal microporous material it has to be greater than 150 to get full information regarding material characteristics [17].



**Figure 3.13:** BET isotherm plot for carbons GAC 383, GACO 383, GACZR 873, GACZR 1073, GACZR 1273 (a)  $p/p_0$  up to 0.3 and (b)  $p/p_0$  up to 0.1 using  $N_2$  at 77K

BET specific surface area of modified GAC are given as; GAC 383 (997 m<sup>2</sup>/g), GACO 383 (974 m<sup>2</sup>/g), GACZR 873 (1035 m<sup>2</sup>/g), GACZR 1073 (1085 m<sup>2</sup>/g), GACZR 1273 (1217 m<sup>2</sup>/g). Surface area and pore volume varies as per the order of GACZR 1273 > GACZR 1073 > GACZR 873 > GAC 383 > GACO 383. Which indicate that Zr<sup>4+</sup> impregnation on GAC and the steam activation at temperature ranges from 873 – 1273K enhances the specific surface area.

In some cases the range of linearity of BET plot is not extending more than  $p/p_0 \approx 0.35$  and in some cases not more than  $p/p_0 \approx 0.1$ . Surface area and pore volume obtained from linear plot of BET in both  $p/p_0 \approx 0.35$  and  $p/p_0 \approx 0.1$  is given in Table 3.5. It indicates that value of surface area increases when the relative pressure range changes from  $p/p_0 \approx 0.35$  to  $p/p_0 \approx 0.1$  i.e. surface area measurement in BET strongly depends on the range of relative vapour pressure used for determination.

BET surface area ( $SA_{BET}$ ) and monolayer volume of GAC 383, GACO 383, GACZR 1073 and GACZR 1273 carbons increases about 22 – 23% by shifting the relative pressure range from 0.3 to 0.1 in the BET plot (Figure 3.13 (b)).

The linear part of traditional BET-plots are not well determined, then there might be some ambiguities in the determination of  $V_m$  and therefore of the surface area. In order to overcome these difficulties, the BET equation could be treated in the form which separates the  $C$  and  $V_m$  parameters. This can be done by re-arranging the BET equation in a Scatchard type form.

### 3.4.1.2 The BET–Scatchard (B–S) Plots (I Point Analysis)

The BET–Scatchard (B–S) plots in the form given by Equation (3.3)

$$\frac{[V(1 - P)]}{P} = CV_m - (C - 1)[V(1 - P)] \quad (3.3)$$

Where  $P$  is  $p/p_0$ , plots  $V(1 - P)/P$  versus  $V(1 - P)$  should provide lines with slope equal to  $(C - 1)$  at any  $P$  and  $V$  values.

It provides an inclined V shape curve ( ) with an inversion point, termed *I* point. The calculation of the specific surface area requires the estimation of  $V_m$ . The Projection of the *I* point on the  $V(I - P)$  axis corresponds exactly to  $V_m$ , i.e.,  $[V(I - P)]_{I\text{-point}} = V_m$  [4]. Then the specific surface areas can be calculated easily from the trivial relationship Equation (3.4) without any knowledge of  $C$ .

$$\text{Specific surface area, } SA_I (m^2 g^{-1}) = 4.356 V_m \quad (3.4)$$

The inversion points (*I*-points) of the carbons GAC 383, GACO 383, GACZR 873, GACZR 1073 and GACZR 1273 are schematically represented in Figure 3.14.

Most carbon has a  $C$  parameter (BET) positive for further plotting at  $p/p_0 \leq 0.1$  and simultaneously fitting the BET model for confirmation. The surface area of materials with positive  $C$  values in new BET analysis plots ( $p/p_0 = 0.1$ ) has obtained comparable surface area similar to that obtained from *I* plot.

Monolayer capacity  $V_I$  and surface area  $SA_I$  obtained for the modified carbons are given as; GACZR 873 ( $V_I$  285.69  $\text{cm}^3/\text{g}$  &  $SA_I$  1243.64  $\text{m}^2/\text{g}$ ); GACZR 1073 ( $V_I$  303.04  $\text{cm}^3/\text{g}$  &  $SA_I$  1319.21  $\text{m}^2/\text{g}$ ); GACZR 1273 ( $V_I$  340.46  $\text{cm}^3/\text{g}$  &  $SA_I$  1482.10  $\text{m}^2/\text{g}$ ).

Monolayer capacity and surface area obtained from series of zirconium impregnated carbons activated at different temperature shows that there is a progressive development of porosity and surface area (6 %) during activation from 873K to 1073K. Further rise of temperature from 1073 K to 1273 K, leads to enhancement up to 12 % in porosity. On comparing with basic carbon GAC 383 ( $V_I$  292.98  $\text{cm}^3/\text{g}$  &  $SA_I$  1275.39  $\text{m}^2/\text{g}$ )  $\text{Zr}^{4+}$  modified carbon GACZR 1073 has 3.4% and GACZR 1273 has 16.2 % increment in monolayer volume and surface area. Treatment with nitric acid causes, the reduction of monolayer volume and surface area as regards to GACO 383. It decreases about 8.68 % of  $V_I$  and  $SA_I$  compared to basic GAC 383.

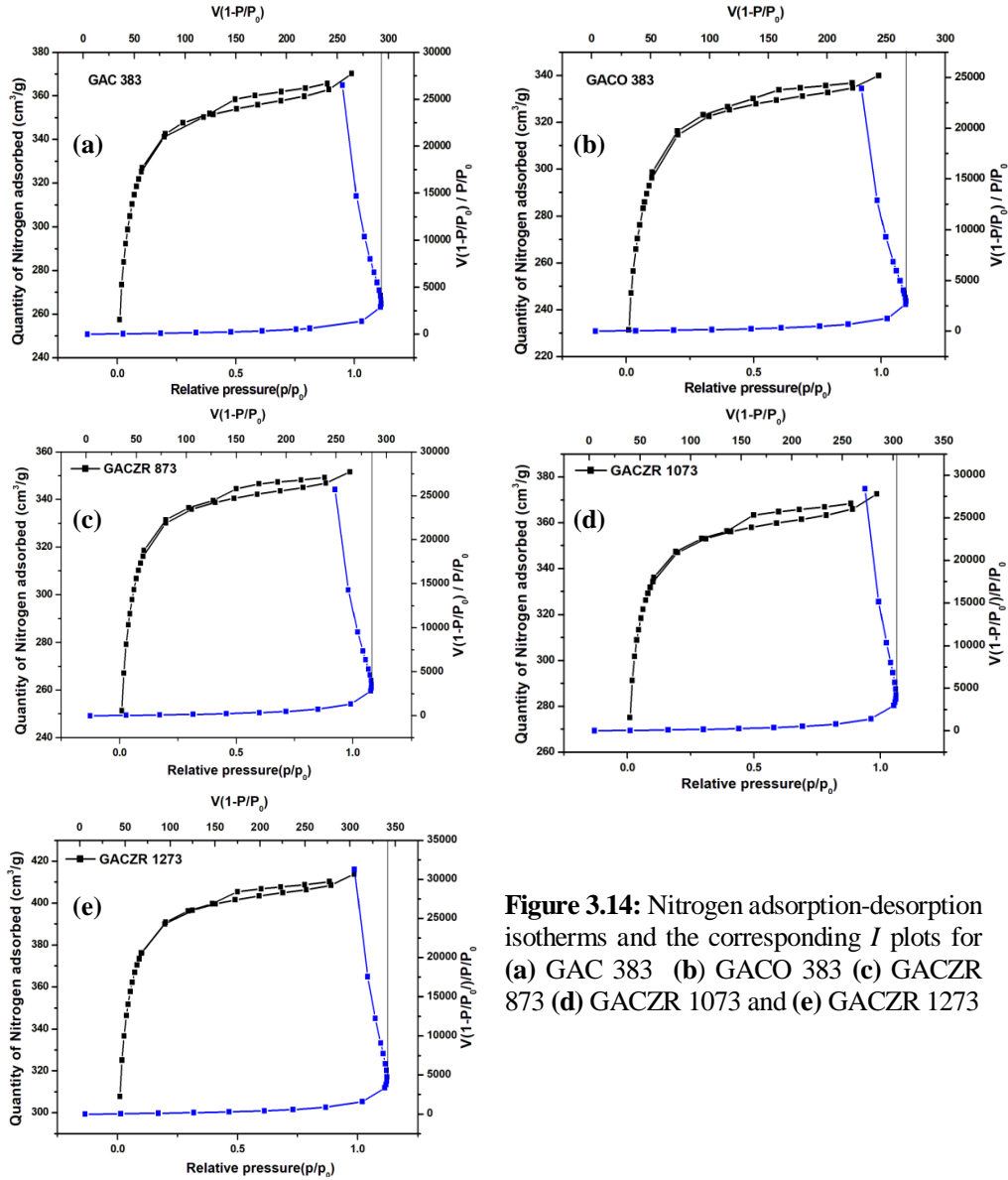


**Figure 3.14:** Nitrogen adsorption-desorption isotherms and the corresponding  $I$  plots for (a) GAC 383 (b) GACO 383 (c) GACZR 873 (d) GACZR 1073 and (e) GACZR 1273

$C$  obtained from the linear plot of BET  $p/p_0$  up to 0.1 is greater than 200 which shows significant micropore filling contribution or localized adsorption on specific sites. The negative intercept of the BET plot indicates that data are outside the valid range of BET equation. The pore volume and surface area

obtained from BET  $p/p_0 \approx 0.1$  is close agreement with  $I$  point method. It supports the validity of linear BET plot up to  $p/p_0 \approx 0.1$ .

**Table 3.5:** BET and  $I$  plot isotherm parameters for GAC 383, GACO 383, GACZR 873, GACZR 1073 & GACZR 1273 using  $N_2$  at 77K

Carbon	Total pore volume $V_T$ cm <sup>3</sup> /g.STP	BET $p/p_0$ upto 0.3			I plot method		BET $p/p_0$ upto 0.1			
		$S_{A\text{ BET}}$ m <sup>2</sup> /g	$V_m$ cm <sup>3</sup> /g. STP	$C_{\text{BET}}$	$S_{A\text{ I}}$ m <sup>2</sup> /g	$V_I$ cm <sup>3</sup> /g. STP	$S_{A\text{ BET}}$ m <sup>2</sup> /g	$V_m$ cm <sup>3</sup> /g. STP	$C_{\text{BET}}$	Pore width(mm)
GAC 383	370.4	996.8	229.0	-816	1275.4	293.0	1298.5	298.3	524	1.76
GACO 383	340.2	974.3	223.8	-119	1164.7	267.5	1186.5	272.6	439	1.77
GACZR 873	351.8	1035.2	237.8	-114	1243.6	285.7	1263.6	290.3	560	1.72
GACZR1073	372.8	1085.5	249.4	-105	1319.2	303.0	1328.7	305.2	988	1.73
GACZR 1273	414.1	1217.2	279.6	-104	1482.1	340.5	1497.3	344.0	873	1.71

### 3.4.1.3 Langmuir Isotherm Analysis

Adsorption isotherm model based on scientific and empirical observation was first proposed by Irving Langmuir in 1918 [18]. The Langmuir isotherm model assumes monolayer adsorption of molecules on a homogeneous surface. Langmuir adsorption isotherms for the adsorption of  $N_2$  gases for GAC 383, GACO 383, GACZR 873, GACZR 1073 and GACZR 1273 are shown in Figure 3.15(a). This isotherm is generally valid for adsorption of gases on most microporous carbonaceous materials. *Type I* isotherms appear to obey a simple form of Langmuir equation over a wide range of pressure. The linear form of the Langmuir is given by the Equation (3.5)

$$\frac{P}{V} = \frac{1}{bV_m} + \frac{P}{V_m} \quad (3.5)$$

Where  $V$  is the specific amount of gas adsorbed at the equilibrium pressure  $P$  and  $V_m$  is the monolayer capacity. From the graph of  $P/V$  versus  $P$ , a straight line is obtained and from the slope and intercept  $V_m$  monolayer volume and constant  $b$  can be calculated.



As shown in the Figure 3.15(a) Langmuir isotherm plot assumes perfect linearity ( $R^2=0.999$ ) with a clear evidence for well defined microporosity (monolayer capacity). The respective surface area obtained is high. This indicated that the monolayer coverages of these carbons are associated with micropore filling. The Langmuir equation is valid only within a small restricted range in most cases below a relative pressure range  $p/p_0 < 0.1$ . The monolayer volume  $V_m (L)$  obtained from the linear plots differed by 10.5 – 11.5 % from the values of surface area measured by BET methods. Though the difference is acceptable for physical systems, further evaluation is needed for the material characterization and optimization of carbon properties. The linearity of Langmuir isotherm does not mean that the adsorption process follows localized monolayer model. This is due to the fact that perfectly energetically homogeneous surfaces are rare and difficult to obtain. In some cases, the effect of non homogeneity of the surface may be compensated by adsorbate – adsorbent interactions and thus give rise to linear Langmuir plot.

The monolayer volume  $V_m (L)$  and surface area  $SA_L$  obtained from Langmuir adsorption isotherm of carbon samples are GAC 383 ( $V_m$  336.6  $\text{cm}^3/\text{g}$  &  $SA_L$  1465.27  $\text{m}^2/\text{g}$ ), GACO 383 ( $V_m$  304.5  $\text{cm}^3/\text{g}$  &  $SA_L$  1325.54  $\text{m}^2/\text{g}$ ), GACZR 873 ( $V_m$  327.36  $\text{cm}^3/\text{g}$  &  $SA_L$  1425.04  $\text{m}^2/\text{g}$ ), GACZR 1073 ( $V_m$  343.88  $\text{cm}^3/\text{g}$  &  $SA_L$  1496.97  $\text{m}^2/\text{g}$ ) and GACZR 1273 ( $V_m$  387.58  $\text{cm}^3/\text{g}$  &  $SA_L$  1687.23  $\text{m}^2/\text{g}$ ).

For comparing the monolayer volume and surface area of series of zirconium impregnated carbon activated at different temperature ranging from 873 K to 1273 K shows that monolayer volume and surface area increases with increase of activation temperature. It is seen that as the activation temperature rises from 873 K to 1073 K there is 5 % increment and from 1073 K to 1273 K there is 11 % increment in monolayer adsorption capacity and surface area in 1.5 % of  $\text{Zr}^{4+}$  ion activated GAC. The variation of monolayer volume and surface area of GACZR 1073 and GACZR 1273 made from basic GAC 383 indicates that the impregnation of zirconium and activation with steam above 1073 K enhances the adsorption capacity.

### 3.4.1.4 Freundlich Isotherm Analysis

Freundlich, 1906 [19] expressed an empirical equation for representing the isothermal variation of adsorption of a gas adsorbed by unit mass of solid adsorbent with pressure. Physisorption of  $N_2$  gas on the new carbons was evaluated using the Freundlich isotherm given by the relationship;

$$V = K_F P^{1/n} \quad (3.6)$$

$$\log V = \log K_F + \frac{1}{n} \log P \quad (3.7)$$

Figure 3.15(b) indicates Freundlich isotherm plot of carbons GAC 383, GACO 383, GACZR 873, GACZR 1073 and GACZR 1273. The straight line plot with high  $R^2$  value suggested that the Freundlich adsorption isotherm features are followed by the carbons.

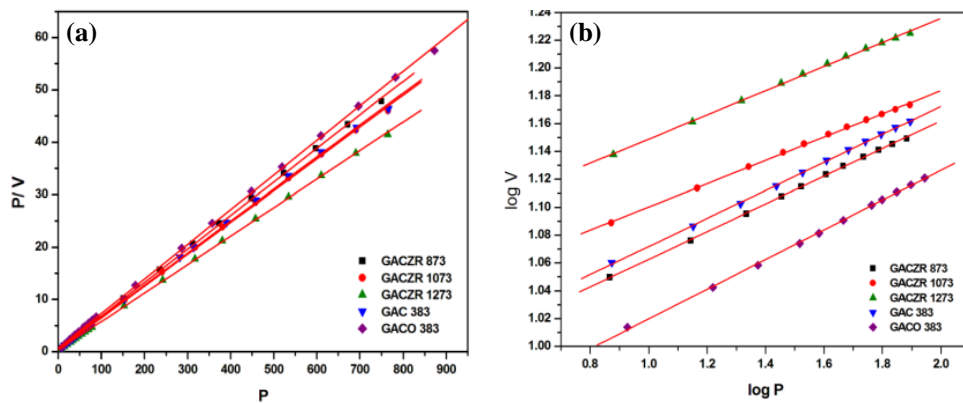


**Figure 3.15:** Adsorption isotherm plots (a) Langmuir (b) Freundlich for carbons GAC 383, GACO 383, GACZR 873, GACZR 1073 & GACZR 1273 using  $N_2$  at 77K

$K_F$  and  $n$  are constants obtained from the slope and intercept of isotherm plot. It depends upon the nature of adsorbent and  $N_2$  gas at a particular temperature (Table 3.6). Most cases  $n$  should be greater than one ( $n > 1.0$ ). Value of ' $n$ ' for zirconium impregnated sample (10.06 – 11.51) is quiet high suggests, that the interaction between carbon and  $N_2$  gas is prominent than GAC 383 ( $n = 9.94$ ) and GACO 383 ( $n = 9.37$ ).

Freundlich constant  $K_F$  is related to measures of adsorption capacity. The  $K_F$  and  $n$  value of carbons are given as GAC 383 ( $K_F=209.82$  &  $n = 9.94$ ), GACO 383 ( $K_F = 183.51$  &  $n = 9.36$ ), GACZR 873 ( $K_F = 205.99$  &  $n=10.06$ ), GACZR 1073 ( $K_F= 232.99$  &  $n =11.97$ ) and GACZR 1273 ( $K_F= 258.62$  &  $n = 11.51$ ).

Freundlich isotherm studies show that GACZR 1073 has 13% more adsorption of  $N_2$  than GACZR 873. Carbon GACZR 1273 shows 11% more adsorption of  $N_2$  than GACZR 1073. Progressive activation of basic carbon (GAC 383) brought about 23% more adsorption capacity in GACZR 1273.

The isotherm behaviour and porosity development of the new carbon have been further evaluated applying the Dubinin - Radushkevich isotherm model [20]. Thereafter analyses of  $N_2$  isotherm data using the ‘ $t$ ’ plot method adopted by Harkins and Jura was also applied in the following sections.

**Table 3.6:** Langmuir and Freundlich isotherm parameters for carbons GAC 383, GACO 383, GACZR 873, GACZR 1073 & GACZR 1273 using  $N_2$  at 77K

Carbon	Langmuir				Freundlich		
	$V_{m(L)}$ $cm^3/g, STP$	$SA_L (m^2/g)$	$bx10^3$	$R^2$	$n$	$K_F L/g$	$R^2$
GAC 383	336.6	1465.3	278	0.99	9.9	209.8	0.99
GACO 383	304.5	1325.5	246	0.99	9.4	183.5	0.99
GACZR 873	327.4	1425.0	292	0.99	10.1	206.0	0.99
GACZR 1073	343.9	1497.0	351	0.99	11.9	233.0	0.99
GACZR 1273	387.6	1687.2	340	0.99	11.5	258.6	0.99

### 3.4.1.5 Dubinin - Radushkevich (D-R) Isotherm Analysis

Adsorption isotherms of pure gases on microporous adsorbents can be described by means of Polanyi's potential theory. Each adsorbent system is characterized by an adsorption potential  $E$  which is influenced in particular by the chemical properties of the adsorbent. Dubinin -Radushkevich isotherm analysis is used for determining the microporosity of activated carbons. According to Dubinin, the adsorption potential equals the work required to bring an adsorbed molecule into the gas phase.

Adsorption process on microporous activated carbons involves the filling of the micropores before the adsorption occurs on surface of wider pores. Adsorption isotherm analysis by Dubinin - Radushkevich model (Equations 3.8) provide the micropore volume  $V_{mi}$  is more acceptable than the BET method [21]. The D-R isotherms are written in logarithmic form so as to give a straight line.

$$\log V = \log V_0 - D \log^2 (p_0/p) \quad (3.8)$$

$$D = 2.303 \left( \frac{RT}{\beta E_0} \right)^2 \quad (3.9)$$

Where  $E_0$  (or  $E$ ) is the characteristic adsorption energy for the adsorption of  $N_2$  on carbon,  $\beta$  is the affinity co-efficient or similarity co-efficient (for  $N_2$  it is 0.33),  $R$  is gas constant (8.314 J/K/mol) and  $T$  is the temperature (77 K).

D-R analysis was carried out by applying  $N_2$  isotherm data of GAC 383, GACO 383, GACZR 873, GACZR 1073 and GACZR 1273 (Figure 3.16 (a)). It is seen that a plot of  $\log V$  versus  $\log^2 p_0/p$  confirms to straight line at a very low  $p/p_0$  where the micropores were considered to be completely filled [22]. From the intercept of the linear plot, the micropore volumes  $V_0$  or  $V_{mi}$  (D-R) are calculated and from the slope the characteristic energy  $E$  is calculated.

To evaluate the data, the region of relative pressure  $0.009754 < p/p_0 < 0.3$  is preferred. The entire data in this region assumes a straight line. The parameters  $V_{mi}$  (D-R),  $SA_{D-R}$ , and  $E$  (kJ/mol) called the characteristic energy of adsorption were calculated.  $E$  is related to the average pore width “ $L$ ” and micropore surface area ( $SA_{D-R}$ ) according to the following empirical formula.

$$L = 6.6 - 1.79 \ln E \text{ nm} \quad (3.10)$$

Characteristic energy large in magnitude causes the decreasing of pore width. Respective pore width calculated by using the Equation (3.10) is given in Table 3.7 reveals that the carbon prepared by the activation with  $Zr^{4+}$  ion had a pore width within the range of 1.53 -1.65 nm.

The micropores contribute a large proportion of surface area and micropore volume, hence it determines the adsorption capacity of a given active carbon to a

great extent. There are two types of surfaces; external surface ( $S_{ex}$ ) and internal surface ( $S_{mi}$ ). Internal surface represents within the walls of the pores and has an area of several hundred square meters per gram of the carbon. It is given by the relationship (Equation 3.11).

$$SA_{D-R} = \frac{2 \times 10^3 V_{mi} (cm^3/g)}{L(nm)} \quad (3.11)$$

Where  $SA_{D-R}$  is the micropore surface area in  $m^2/g$ ,  $V_{mi} (D-R)$  is the micropore volume in  $cm^3/g$ , and  $L$  is the accessible pore width in nanometers. If the pore width is very small  $SA_{D-R}$  is very large. This surface area is contained predominantly within micropores which have an effective diameter less than 2.0 nm.

The micropore volume and pore width calculated are given in Table 3.7. The average pore width of GACZR 1073 ( $L = 1.50$ ) and GACZR 1273 ( $L = 1.53$ ) gives values less than 2 nm and its value is comparatively smaller than the average pore width of GAC 383 ( $L = 1.68$ ). It indicates that pore having a width less than 2 nm are more generated by chemical activation by incorporating with  $Zr^{4+}$  on coconut shell based precursor.

Extra microporosity of GACZR 1073 and GACZR 1273 has been confirmed by the value of the micropore volume analysis. GACZR 1073 ( $356.4 cm^3/g$ ) and GACZR 1273 ( $401.7 cm^3/g$ ) have found to be quiet higher micropore volume  $V_{mi} (D-R)$  than the basic carbon GAC 383 ( $351.28 cm^3/g$ ). There has been a 14.34 % increase of  $V_{mi} (D-R)$  in GACZR 1273 compared to that of GAC 383.

The micropore surface area calculated as per the Equation 3.11 shows that impregnation of  $Zr^{4+}$  and steam activation at higher temperature enhances the micropore surface area. On comparing with GAC 383 ( $SA_{D-R} = 646.5 m^2/g$ ), a modified carbon GACZR 1073 has 14 % ( $SA_{D-R} = 735.1 m^2/g$ ) and GACZR 1273 has 26 % ( $SA_{D-R} = 814.3 m^2/g$ ) enhancement in micropore surface area.

#### **3.4.1.6 Alpha S ( $\alpha_s$ ) Method**

The Gregg and Sing [23] developed a method known as Alpha S ( $\alpha_s$ ) to estimate the micropore volume and external surface area by comparing the experimental physisorption isotherm of porous material to be studied with that of a

non-porous material chosen as a reference. Alpha S ( $\alpha_s$ ) is the ratio of the amount of gas adsorbed to the amount of gas adsorbed at a fixed relative pressure, ( $p/p_0 = 0.4$ ).

$$\alpha_s = \frac{V_{ads}}{V_{ads}(\frac{p}{p_0}=0.4)} \quad (3.12)$$

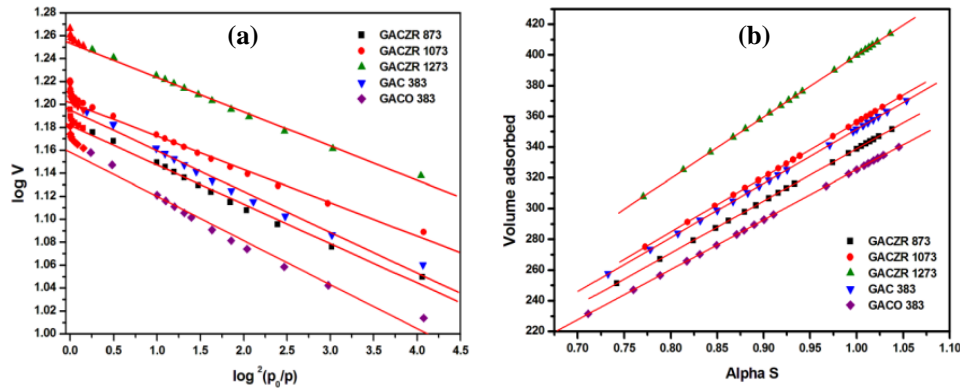


**Figure 3.16:** Adsorption isotherm plot (a) Dubinin- Radushkevich and (b) Alpha S ( $\alpha_s$ ) for GAC 383, GACO 383, GACZR 873, GACZR 1073, GACZR 1273 using  $N_2$  at 77K

The plot is obtained by plotting the volume of gas adsorbed by sample versus  $\alpha_s$ . The calculation of the surface area is obtained by relating the slope of the  $\alpha_s$  -plot of the carbon to the slope of the corresponding plot for a standard sample of known surface area. In principle,  $\alpha_s$  method has many advantages can be used with any adsorptive gas, and can be used to re-evaluate the BET surface area, and to assess micro and mesoporosity.

$$SA_{Ext} = 2.86 * slope \quad (3.13)$$

The  $\alpha_s$  plots of the new carbons plotted are given in Figure 3.16(b). The micropore volume and external surface area of samples are listed in Table 3.7. All the carbons have a linear straight line plot. Straight line of Alpha S ( $\alpha_s$ ) plot indicates adsorption of  $N_2$  in micropores. The micropore volume  $V_{mi}(\alpha_s)$  obtained from an isotherm plot of carbons are GAC 383 (351.49  $cm^3/g$ ), GACO 383 (325.28  $cm^3/g$ ), GACZR 873 (338.82  $cm^3/g$ ), GACZR 1073 (356.07  $cm^3/g$ ) and GACZR 1273 (399.59  $cm^3/g$ ). The micropore volumes provided by D-R i.e.  $V_{mi}$  (D-R) and Alpha S ( $V_{mi} \alpha_s$ ) methods are in excellent agreement for all carbons.

**Table 3.7:** Dubinin-Radushkevich (D-R) & Alpha S ( $\alpha_s$ ) isotherm parameters of carbons GAC 383, GACO 383, GACZR 873, GACZR 1073 & GACZR 1273 using  $N_2$  at 77K

Carbon	Dubinin-Radushkevich (D-R)					Alpha S ( $\alpha_s$ )	
	$V_{mi}^{(D-R)}$ cm <sup>3</sup> /g.STP	$SA_{D-R}$ m <sup>2</sup> /g	L nm	E kJ/mol	$R^2$	$V_{mi}^{(\alpha_s)}$ cm <sup>3</sup> /g.STP	$SA_{ext}$ (m <sup>2</sup> /g)
GAC 383	351.3	646.5	1.68	15.6	0.99	351.5	1005.3
GACO 383	322.8	570.2	1.75	15.0	0.98	325.3	930.3
GACZR 873	340.5	638.4	1.65	15.9	0.99	338.8	969.03
GACZR 1073	356.4	735.1	1.50	17.3	0.99	356.1	1018.4
GACZR 1273	401.7	814.3	1.53	17.0	0.99	399.6	1142.8

### 3.4.1.7 John Isotherm Analysis

John isotherm models can be used for the evaluation of adsorption behaviour of porosity on microporous (as well as mesoporous) materials [24] [49].

The general form of the John isotherm equation is

$$\log \log P = C + n \log V \quad (3.14)$$

Where  $P = p/p_0 \times 10^N$ ,  $N$  is taken conveniently to make  $\log P$  positive thereby  $\log \log P$  could be found.  $C$  is a constant, and  $n$  is adsorbability constant

The equation (3.14) is further extended to study the adsorption potential of porous materials, from solid - liquid adsorption system known as the John - Sivanandan Achari isotherm given by [50].

$$\log \log C_e = C + n \log q_e \quad (3.14 a)$$

The John isotherm plots, based upon  $N_2$  uptake data (Equation 3.14) provide three distinct phases for GAC 383, GACO 383, GACZR 873, GACZR 1073, and GACZR 1273 are presented in a Figure 3.17. Overall adsorption comprises of three phases. For all these carbons molecular sieve effect (*phase I*) occurs within the range of relative pressure ( $p/p_0$ ;  $9.6 \times 10^{-3}$  -  $3.5 \times 10^{-2}$ ), monolayer completion (*phase II*) occurs within the range ( $p/p_0$ ;  $3.5 \times 10^{-2}$  -  $1.97 \times 10^{-1}$ ) and finally saturation (*phase III*) within the relative pressure range ( $p/p_0$   $1.97 \times 10^{-1}$  -  $9.85 \times 10^{-1}$ ). This suggests

the prominences of three different pore filling mechanisms operating from the lower to the higher relative pressure range. Total pore volume ( $V_T$ ) obtained from the John isotherm plot is the sum of  $V_{mse}$ ,  $V_m(J)$  and  $V_c(J)$  it is found to be well in agreement with the total pore volume obtained from BET.

From the first phase of the isotherm plot, we can calculate the molecular sieve effect which is mainly due to the finer micropores (ultra micropore) having a width less than 0.8 nm. The  $V_{mse}$  (*phase I*) of carbons are given as follows GAC 383 (289.95 cm<sup>3</sup>/g), GACO 383 (264.10 cm<sup>3</sup>/g), GACZR 873 (283.38 cm<sup>3</sup>/g), GACZR 1073 (305.92 cm<sup>3</sup>/g) and GACZR 1273 (340.45 cm<sup>3</sup>/g). Out of the total pore volume  $V_T(J)$ , the molecular sieve effect  $V_{mse}(J)$  contributes more than 75 % for all carbon studied. The percentage contribution of  $V_{mse}(J)$  in  $V_T(J)$  for each carbon given as follows GAC 383 (80.9 %), GACO 383 (82.9 %), GACZR 873 (82.86 %), GACZR 1073 (79.30 %) and GACZR 1273 (78.20 %). The molecular sieve effect is prominent for  $N_2$  atoms for all the carbon studied, suggest that micropore filling of carbon pores smaller than 1nm occurs at very low pressures, i.e. contribution of finer micropores in total pore volume is higher for all these carbons.

**Table 3.8:** John adsorption isotherm parameters of GAC 383, GACO 383 and GACZR 873, GACZR 1073 and GACZR 1273

Carbons	Adsorption Capacity (cm <sup>3</sup> /g)			
	$V_{mse}(J)$ cm <sup>3</sup> /g. STP	$V_m(J)$ cm <sup>3</sup> /g. STP	$V_c(J)$ cm <sup>3</sup> /g. STP	$V_T(J)$ cm <sup>3</sup> /g. STP
GAC 383	289.95 n = 3.76	43.61 n = 2.85	32.05 n = 3.60	365.61
GACO 383	264.10 n = 3.43	52.06 n = 2.42	21.55 n = 3.78	337.72
GACZR 873	283.38 n = 3.74	46.50 n = 3.03	20.16 n = 4.79	350.04
GACZR 1073	305.92 n = 4.33	36.30 n = 3.58	26.66 n = 4.32	368.88
GACZR 1273	340.45 n = 4.13	47.95 n = 3.51	22.46 n = 5.11	410.85

From the second phase of the John isotherm plot, we can calculate monolayer volume (or limiting micropore volume) due to pores having a width in between 0.8 - 2.0 nm in range. The  $V_m(J)$  (*phase II*) of carbons are given as follows GAC 383 (43.61 cm<sup>3</sup>/g), GACO 383 (52.06 cm<sup>3</sup>/g), GACZR 873 (46.50 cm<sup>3</sup>/g), GACZR 1073 (36.30 cm<sup>3</sup>/g) and GACZR 1273 (47.95 cm<sup>3</sup>/g).



This part of pore volume is contributed by pores having a width in between 0.8 - 2.0 nm. GAC 383 contributes 11.67 %  $V_m(J)$  in total micropore volume  $V_T(J)$ . The percentage contribution of  $V_m$  in total pore volumes for other carbons are GACO 383 (15.42 %), GACZR 873 (13.28 %), GACZR 1073 (9.84 %), GACZR 1273 (11.67 %).

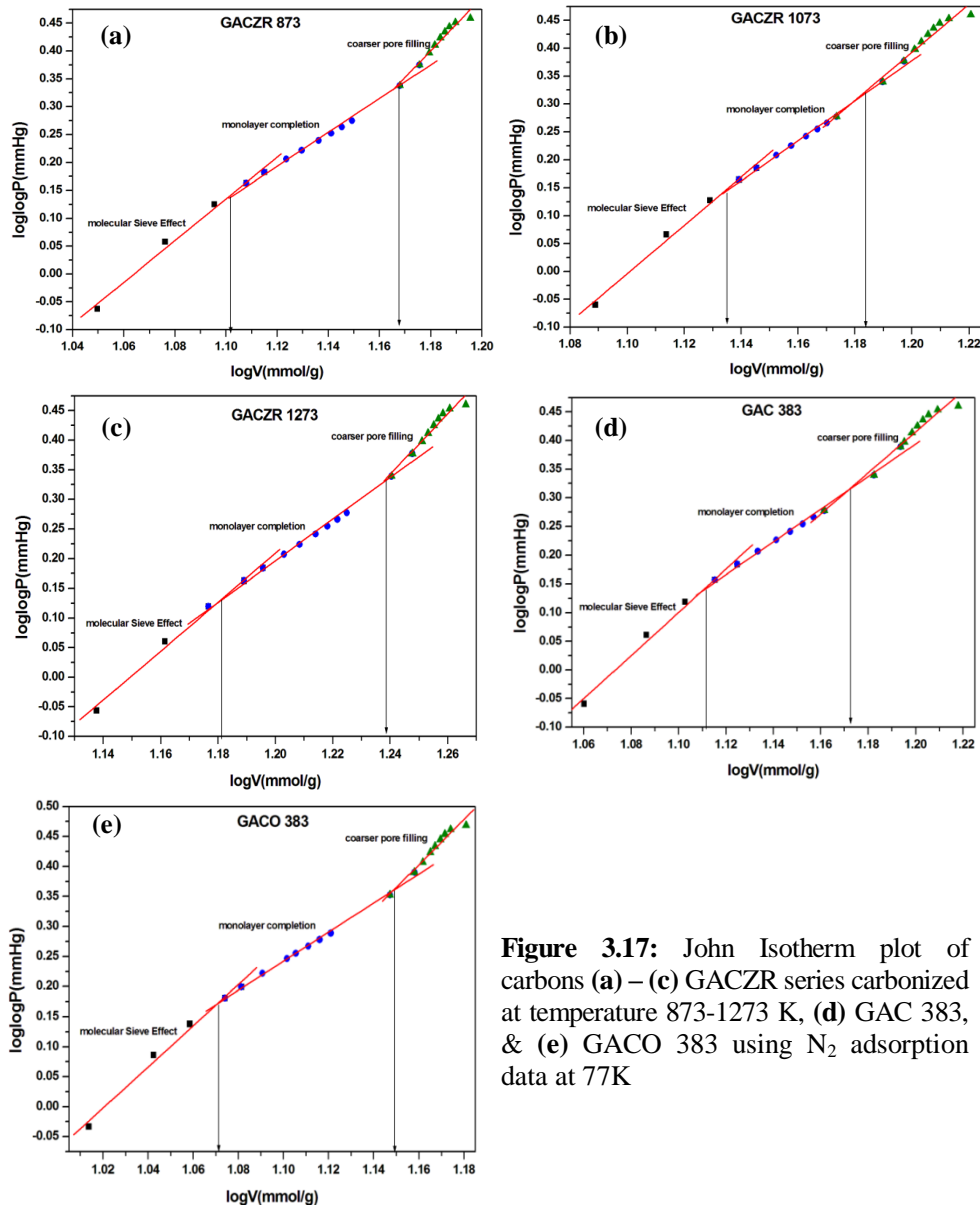


**Figure 3.17:** John Isotherm plot of carbons (a) – (c) GACZR series carbonized at temperature 873-1273 K, (d) GAC 383, & (e) GACO 383 using  $N_2$  adsorption data at 77K

Wider micropores  $V_c$  ( $J$ ) (pore width greater than 2 nm) contribution in GACZR 1273 shows comparatively less than that of GAC 383. It is clearly indicated that impregnation of zirconium in GAC preserves most of the existing micropores without changing the pore size even at higher activation temperature. Also, it will help to create new additional micropores on GAC surfaces during the process of progressive activation.

Boehm data for phenolic surface groups have been GACZR 873 (0.799 meq/g), GACZR 1073 (0.622 meq/g) and GACZR 1273 (0.444 meq/g). Content of phenolic groups on the surface of carbon decreases the  $V_m$  ( $J$ ) value, this indicate marked changes in the surface chemistry and porosity of the carbon [25].

A comparison of total micropore volume ( $V_{mse} + V_m$ ) obtained from the John isotherm model with other isotherm models (D-R, Alpha S, and Langmuir) are schematically represented in the Figure 3.18. It shows that John (J), and Langmuir (L) isotherm models offer almost identical values of monolayer volumes for all the carbon studied. Whereas micropore volume obtained from D-R and Alpha S ( $\alpha_s$ ) isotherm shows comparatively higher values than obtained from John isotherm. However the value obtained from D-R and Alphas S ( $\alpha_s$ ) does not deviate more than 5 % from the value obtained from John isotherm.

**Table 3.9:** John, Dubinin-Radushkevich (D-R), Alpha S ( $\alpha_s$ ) and Langmuir isotherm: comparison of pore volume obtained from Isotherm models

Carbon	Pore volume			
	John ( $V_{mse} + V_m$ ) cm <sup>3</sup> /g STP	D-R $V_m$ (D-R) cm <sup>3</sup> /g STP	$\alpha_s$ $V_m$ ( $\alpha_s$ ) cm <sup>3</sup> /g STP	Langmuir $V_m$ (L) cm <sup>3</sup> /g STP
GAC 383	333.56	351.28	351.49	336.60
GACO 383	316.16	322.75	325.28	304.5
GACZR 873	329.88	340.54	338.82	327.36
GACZR 1073	342.22	356.43	356.07	343.88
GACZR 1273	388.39	401.7	399.59	387.58

#### 3.4.1.8 $t$ - Plot Method

In porosimetry study both the microporous and mesoporous volumes are determined by the  $t$ -plot method. Lippens and de Boer [26, 27] proposed a method for the determination of micropore volume and external surface area by plotting

the thickness of adsorbed layer  $t$  against quantity of  $N_2$  adsorbed. This has been applied to test the new carbon materials as shown in the Figure 3.19. It gives isotherms uptake specific to micropore and mesopore filling. Evaluated external surface area  $SA_{ext}$ , micro pore surface area, and micropore volume for carbons are given in the Table 3.10.

The GAC has the distinct steep rise with respect to quantity adsorbed (mmol/g) in ' $t$ '- plot in the initial range of adsorbed thickness, to attain maximum with a round knee. Finally become oriented slightly parallel to the  $x$ -axis at the higher ranges of adsorbed thickness. A straight line is drawn in the linear region of the  $t$  plot, and from the slope and intercept the external surface area and micropore volume were calculated respectively.

$$t = \left[ \frac{13.99}{0.034 - \log (p/p_0)} \right]^{0.5} \quad (3.15)$$

Where  $t$  is the thickness of the pores and  $p/p_0$  is the relative pressure. External surface area of the microporous materials can be determined from the slope of the  $t$ -plot,

$$SA_{ext} = \frac{\text{slope} \times (10^{10} A^0/m) \times D}{F \times 10^6} \quad (3.16)$$

Where  $D$  is the density conversion factor and is equal to  $0.0015468$ .  $F$  is a surface area correction factor, for most samples it is taken as 1.

From the intercept of isotherm plot we can calculate micropore volume

$$V_{mi} = \text{intercept} (cm^3/g STP) \times D \quad (3.17)$$

The micropore surface area ( $SA_{mi}$ ) can be calculated from the relation as given below, Here BET surface area is taken as total surface area

$$\text{Micropore surface area (m}^2/\text{g), } SA_{mi} = SA_{BET} - SA_{EXT}. \quad (3.18)$$

Where  $SA_{BET}$  is the BET surface area and  $SA_{EXT}$  is the external surface area. The region between the two linear portions represents the transition that occurs as

the micropores become filled while multilayer adsorption continues to occur in the larger pores. The  $t$ -plot (Figure 3.19) indicates that there is curve between two linear portions it is an indication of wider distribution of micropores.

High external surface area of GACO 383 reveals that nitric acid modified carbon possesses a significant amount of larger pores. This is evidenced, by an increase in the external surface area up to 6.28 % compared to basic carbon GAC 383. Increasing of external surface area is being caused by reduction of micropore volume up to 15.32 % due to the widening of existing micropore. Activation of carbon granules GAC 383 with  $Zr^{4+}$  enhances 28.40 % (GACZR 1273) of the micropore volume, shows that the activated carbon GACZR 1273 generated is consisting of predominantly micropores. In fact, of the total surface area of this carbon ( $S_T$ ), micropore surface area contributes 70.0 % and the remaining 30 % contribute external surface area, i.e.  $Zr^{4+}$  activation leads to the acceleration of porosity development on the activated carbon matrix of GAC 383.

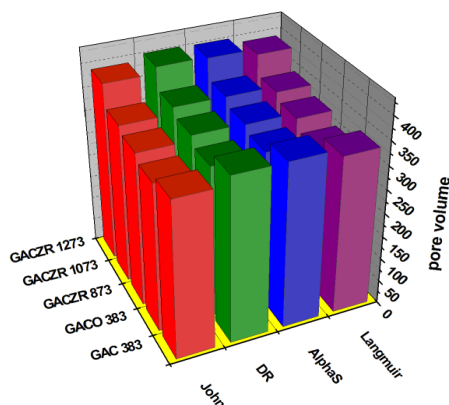


**Figure 3.18:** Comparison of pore volumes obtained from John, D-R, Alpha S, & Langmuir isotherm models

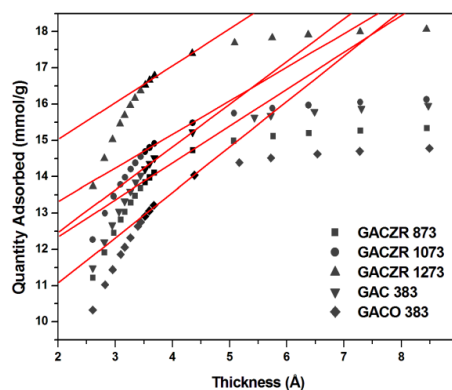


**Figure 3.19:**  $t$ -plot analysis of GAC 383, GACO 383, GACZR 873, GACZR 1073, and GACZR 1273

#### 3.4.1.9 Barrett-Joyner-Halenda (BJH) Method

Distribution of pores with respect to their volume or surface area as a function of pore diameter based on adsorption-desorption isotherm branches of  $N_2$  uptake at 77K is regarded as a significant step for the characterisation of porous

materials. This can be measured, and distribution pattern can be studied in terms of cumulative surface area in the region of the hysteresis loop. The pore size distributions were obtained from desorption branches of nitrogen isotherms by using the Barrett-Joyner-Halenda (BJH) method [28].

The distribution functions of mesopore volume calculated for nitrogen desorption isotherms by using the BJH method. In Table 3.10, the BJH average pore diameters are also given.

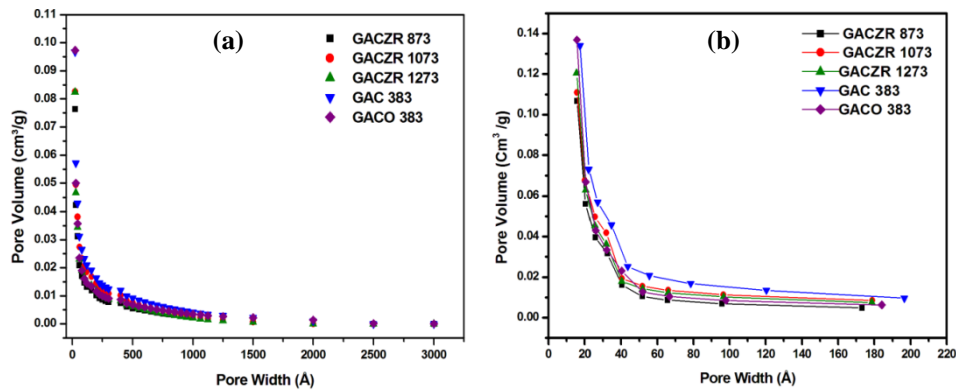


**Figure 3.20:** BJH isotherm analysis (a) Adsorption cumulative pore volume (b) Desorption cumulative pore volume for GAC 383, GACO 383, GACZR 873, GACZR 1073 and GACZR 1273 using  $N_2$  adsorption/desorption data at 77K

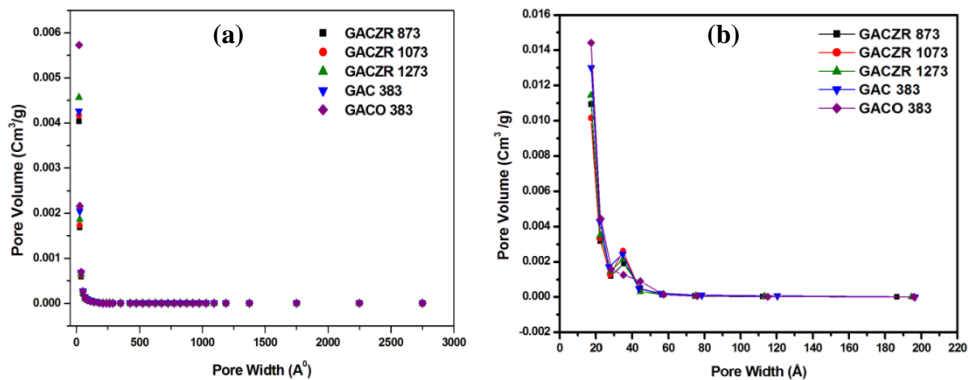


**Figure 3.21:** BJH isotherm analysis (a) Adsorption  $dV/dw$  pore volume (b) Desorption  $dV/dw$  pore volume for GAC 383, GACO 383, GACZR 873, GACZR 1073 and GACZR 1273 using  $N_2$  adsorption/desorption data at 77K

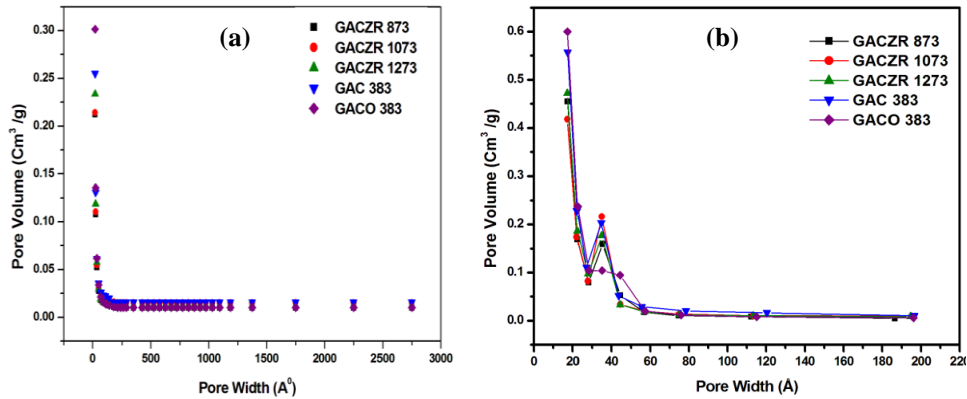


**Figure 3.22:** BJH isotherm analysis (a) Adsorption  $dV/d\log w$  pore volume and (b) Desorption  $dV/d\log w$  pore volume for the carbons, GAC 383, GACO 383, GACZR 873, GACZR 1073 and GACZR 1273 using  $N_2$  adsorption/desorption data at 77K

The pore size distribution was determined by the BJH method from both adsorption and desorption values of  $N_2$  isotherm. The nitrogen adsorption–desorption isotherms of GACs and its corresponding pore width distribution are shown in Figure 3.20 - 3.22. BJH analysis indicated that the maxima pore size distribution centers at approximately 3.5 nm. This result reveals the widening of micropores occurs due to extra burn off. The adsorption cumulative surface area ( $ADCSA$ ) of GAC 383 was found to be  $226.2 \text{ m}^2/\text{g}$  for an equivalent adsorption cumulative pore volume ( $ACPV$ ) of  $0.138 \text{ cm}^3/\text{g}$  ( $89.26 \text{ cm}^3/\text{g.STP}$ ). The desorption cumulative surface area ( $DCSA$ ) of the respective pore are  $220.5 \text{ m}^2/\text{g}$  for a desorption cumulative pore volume ( $DCPV$ ) of  $0.134 \text{ cm}^3/\text{g}$  ( $86.67 \text{ cm}^3/\text{g.STP}$ ). The respective adsorption pore width and desorption pore width of the GAC 383 carbon are  $24.35 \text{ \AA}$  ( $2.44 \text{ nm}$ ) and  $24.3 \text{ \AA}$  ( $2.43 \text{ nm}$ ).

The adsorption and desorption cumulative surface area of nitric acid modified carbon sample GACO 383 are high ( $ADCSA$ ;  $250 \text{ m}^2/\text{g}$  and  $DCSA$ ;  $242.8 \text{ m}^2/\text{g}$ ) compared to the starting carbon GAC 383. This constitutes adsorption and desorption cumulative pore volume of  $0.142 \text{ cm}^3/\text{g}$  ( $91.85 \text{ cm}^3/\text{g.STP}$ ) and  $0.137 \text{ cm}^3/\text{g}$  ( $88.61 \text{ cm}^3/\text{g}$ ) respectively. The respective adsorption-desorption pore widths are 2.28 and 2.26 nm respectively for this carbon.

For GACZR 1273, the adsorption cumulative surface area (ADCSA) of the respective pore is 196.07 m<sup>2</sup>/g for a cumulative pore volume (ACPV) of 0.117 cm<sup>3</sup>/g (75.68 cm<sup>3</sup>/g.STP). Their desorption cumulative surface area (DCSA) found to be 207.5 m<sup>2</sup>/g for a cumulative pore volume (DCPV) of 0.121 cm<sup>3</sup>/g (78.26 cm<sup>3</sup>/g.STP). The respective adsorption pore width and desorption pore width are 2.39 nm and 2.32 nm. However, this value is comparatively lower than the starting carbon GAC 383. The lower adsorption and desorption cumulative surface area indicates that small proportions of mesopores is formed during activation with Zr<sup>4+</sup> at 1273K.

**Table 3.10:** *t*-plot and BJH isotherm parameters of carbons GAC 383, GACO 383 GACZR 873, GACZR 1073 and GACZR 1273 using N<sub>2</sub> at 77K

Carbon	t-plot			Barrett-Joyner-Halenda (BJH)					
	V <sub>mi</sub> (t) cm <sup>3</sup> /g.STP	SA <sub>mi</sub> (t) m <sup>2</sup> /g	SA <sub>ext</sub> (t) m <sup>2</sup> /g	ADCSA m <sup>2</sup> /g	DCSA m <sup>2</sup> /g	*ACPV cm <sup>3</sup> /g	*DCPV cm <sup>3</sup> /g	Pore width ( Ads) nm	Pore width ( des) nm
GAC 383	226.7	588.7	408.1	226.2	220.5	0.138	0.134	2.44	2.43
GACO 383	192.0	540.3	433.7	250.0	242.8	0.142	0.137	2.28	2.26
GACZR 873	231.2	683.0	352.2	193.2	183.5	0.113	0.107	2.33	2.33
GACZR 1073	257.0	763.9	321.1	182.5	178.2	0.114	0.114	2.50	2.49
GACZR 1273	291.1	863.8	353.4	196.1	207.5	0.117	0.121	2.39	2.32

$$* V_m (cm^3/g) = \frac{V_m (cm^3/g).STP \times 28}{22414 \times 0.808}$$

Among the four carbons selected, desorption pore size distribution has a peak within the range 2.0 - 4.0 nm supports the existence of the fractional mesoporosity. The adsorption pore width and desorption pore width for zirconium impregnated activated carbon are less (in the range 2.26 - 2.39 nm) compared to GAC 383 (2.43 nm). A decrease in the micropore width enhances the adsorption energy and hence micropore filling occurs at a lower relative pressure ( $p/p_0 \leq 0.1$ ) as evidenced by BET and *I* plot method (Table 3.5).

### 3.5 Solid – Liquid Equilibria: Adsorption Studies

The adsorption efficiency of the modified GAC's with respect to selected organic compounds; phenol, *p*-nitrophenol, and methylene blue (MB) are determined using a batch adsorption method. The effect of various parameters like initial concentration, contact time and temperature on the efficiency to remove adsorbate is analysed.

#### 3.5.1 Effect of Adsorbent Dose

The effect of adsorbent dose was studied by using four different adsorbent dosage 0.05 g, 0.1 g, 0.2 g and 0.3 g in 50 ml solution of phenol (1000 mg/L) and MB (500 mg/L). The results are shown in Figures 3.23(a)&(b).

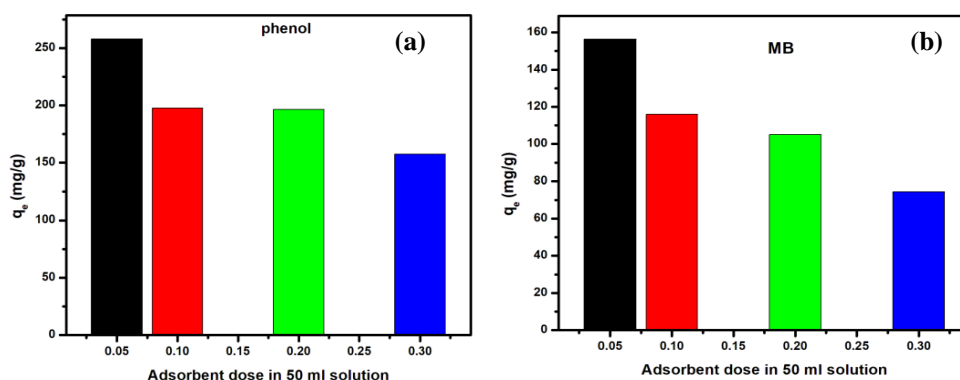


**Figure 3.23:** Specific amount of (a) phenol and (b) methylene blue (MB) adsorbed on different carbon dose in 50 ml solution of adsorbate

The increases in the adsorbent carbon dose causes the decrease in the amount of phenol and methylene blue (MB) adsorbed per gram of the adsorbents ( $q_e$ ). This is mainly because of unsaturation of adsorption sites through the adsorption process or may be due to the aggregation of adsorbent particles that leads to a decrease in the effective surface area of adsorbent available for adsorption. Therefore 0.05 g of carbon was selected as the optimum adsorbent dosage for further research studies [29, 30].



### 3.5.2 Effect of Contact Time

A preliminary kinetic analysis with each adsorbent (carbon) - adsorbate (phenol, *p*-nitrophenol and methylene blue) system was carried out to determine the required equilibration time. The equilibrium time for the adsorption of phenol and *p*-nitrophenol on GAC is found to be 8 hours but for methylene blue it has been 10 hours.

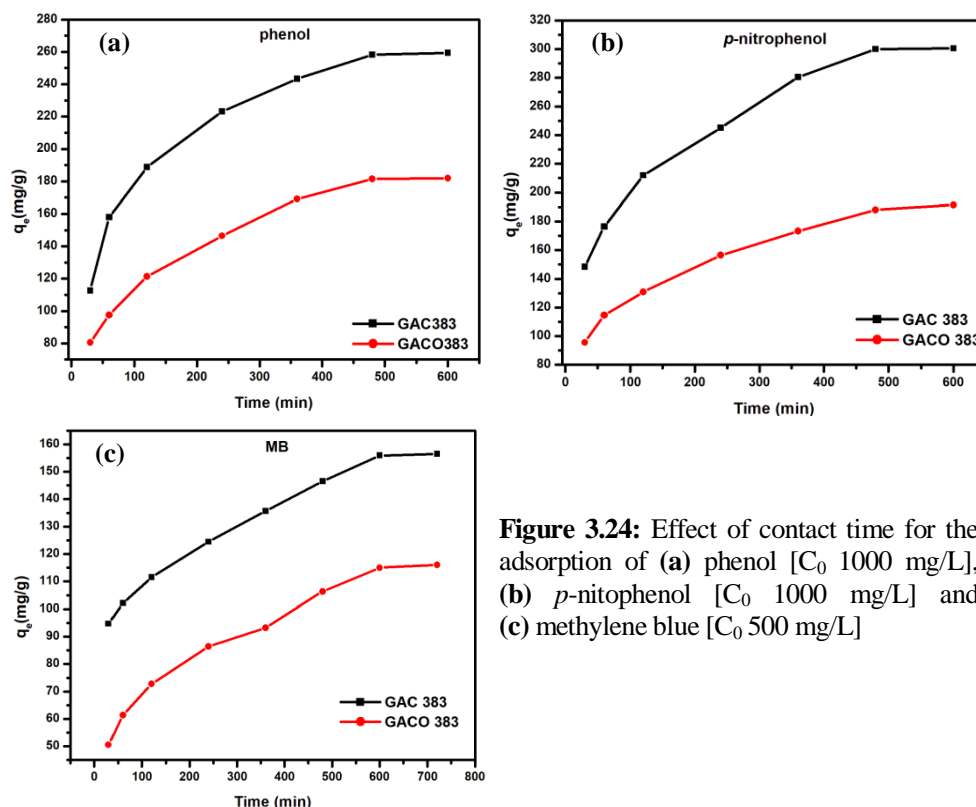


**Figure 3.24:** Effect of contact time for the adsorption of (a) phenol [ $C_0$  1000 mg/L], (b) *p*-nitrophenol [ $C_0$  1000 mg/L] and (c) methylene blue [ $C_0$  500 mg/L]

### 3.5.3 Selection of Carbon in GACZR Series for Solid-Liquid Equilibria

To choose the best carbon from the GACZR series for solid –liquid adsorption studies were noted by shaking 0.05 g carbon in 50 ml solution of phenol (1000 mg/L), *p*-nitrophenol (1000 mg/L) and methylene blue (500 mg/L) and it was placed on a water bath shaker for required equilibration time at 30°C. The residual adsorbate solution concentration was determined at a corresponding

absorbance ( $\lambda$  max) in UV-Visible spectrophotometer. Among the series of GACZR carbons studied, GACZR 1273 shows comparatively higher adsorption efficiency in liquid phase than others, which also possess a high surface area and pore volume. So this carbon has been selected for further solid-liquid equilibrium studies along with basic carbons GAC 383 and GACO 383.

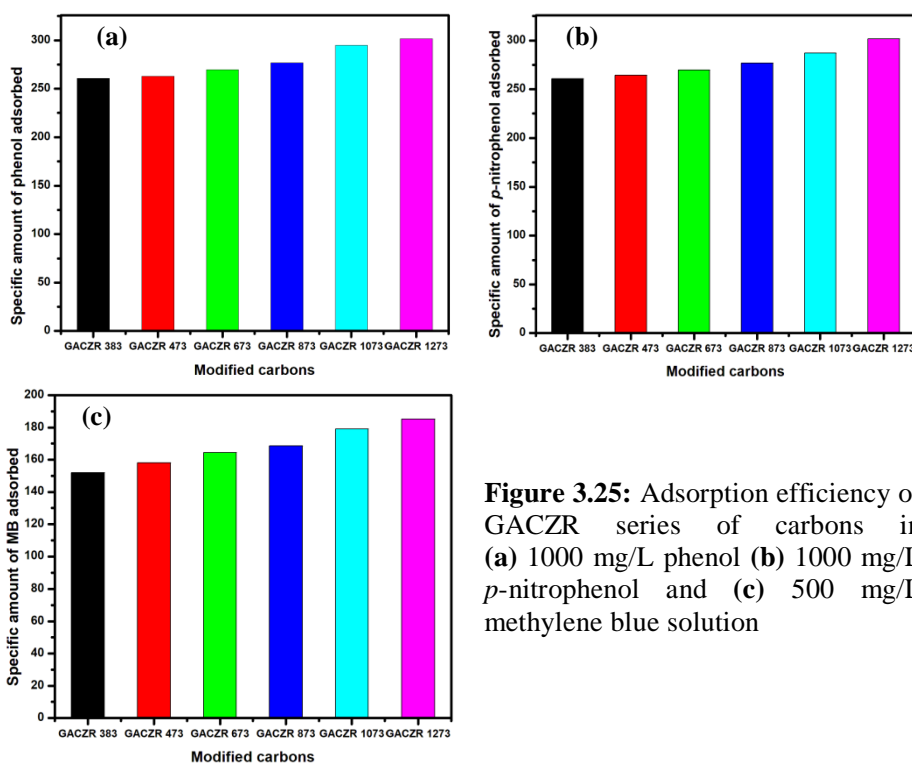


**Figure 3.25:** Adsorption efficiency of GACZR series of carbons in (a) 1000 mg/L phenol (b) 1000 mg/L *p*-nitrophenol and (c) 500 mg/L methylene blue solution

### 3.5.4 Adsorption Studies of Phenol, *P*-Nitrophenol and Methylene Blue

The equilibrium experimental data obtained from the solution of non electrolyte by the adsorption of microporous adsorbent is of great significance. The need for efficient removal of organic pollutants is becoming increasingly important. Phenols being anionic in natural waters are highly toxic and are present in the effluents of a number of industrial units. Here, also methylene blue was selected as an organic and cationic dye. This dye has been chosen to study because of its known strong adsorption onto solids, and it often serves as a model

compound for removal/adsorption study of organic contaminants from aqueous solutions [31]. In this section an attempt is made to report the adsorption characteristics of phenol (P), *p*- nitrophenol (PNP) and methylene blue (MB) on GAC 383, GACO 383 and zirconyl chloride impregnated granular activated carbon (GACZR 1273).

### 3.5.5 Equilibrium Adsorption Isotherm

Equilibrium isotherm data obtained from batch experiments were subjected to different isotherm models of Langmuir, Freundlich, and Dubinin-Radushkevich equations to optimize the design of specific adsorbent/adsorbate system. Figure 3.26(a)-(c) shows adsorption isotherm of phenol, *p*-nitrophenol and methylene blue on GAC 383, GACO 383, and GACZR 1273 at 303K.

The experimental data obtained from the adsorption isotherm studies show that adsorption of phenol, *p*-nitrophenol and methylene blue on GAC 383, GACO 383 and GACZR 1273 appears to be a *Type I* isotherm according to IUPAC classification (Figure 3.26(a)-(c)). Isotherms of *Type I* or *L* type are concave to the concentration axis (IUPAC 2015). *Type L* isotherm having a long well-defined plateau is generally associated with monolayer adsorption of the solute and minimal competition from the solvent [32].

It can be seen that the adsorption capacity of activated carbon increased progressively with the equilibrium concentration of solute (phenol, *p*-nitrophenol and MB) and reached saturation. This could be due to the increasing driving force of the concentration gradient. The increase in solute concentration could accelerate the diffusion of adsorbate molecules onto granular activated carbons. The adsorption capacity of activated carbons was calculated according to the following Equation (3.19)

$$q_e = \frac{(C_0 - C_e)V}{M} \quad (3.19)$$

Where  $C_0$  and  $C_e$  represent the initial and equilibrium concentrations of adsorbate (phenol, *p*-nitrophenol and MB) in aqueous solution (mg/L),  $V$  is the volume of the solution (L), and  $M$  is the mass of the adsorbent (g).

Nitric acid oxidised carbon (GACO 383) showed comparatively less adsorption among all the three adsorbate. This is due to the presence of extra C - O acidic functional groups, that (carboxylic/lactonic) suppresses the adsorption of phenol, *p*-nitrophenol and methylene blue.

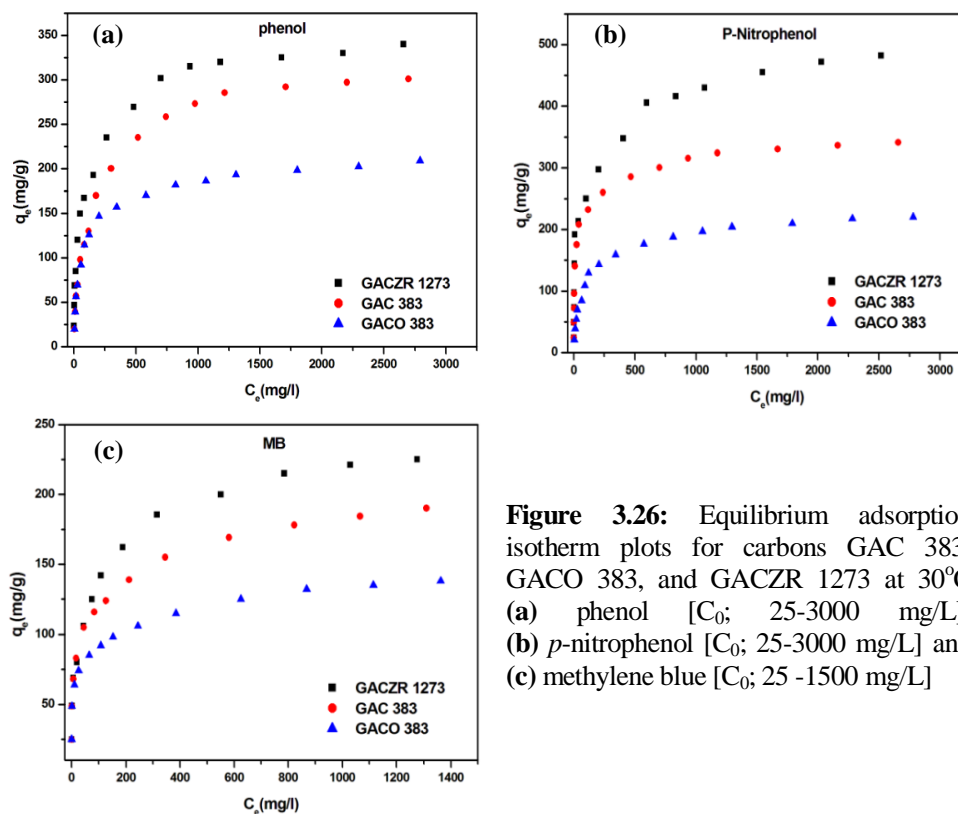


**Figure 3.26:** Equilibrium adsorption isotherm plots for carbons GAC 383, GACO 383, and GACZR 1273 at 30°C (a) phenol [ $C_0$ ; 25-3000 mg/L], (b) *p*-nitrophenol [ $C_0$ ; 25-3000 mg/L] and (c) methylene blue [ $C_0$ ; 25 -1500 mg/L]

The adsorption affinity of GAC towards selected adsorbate varies in the order *p*-nitrophenol > phenol > methylene blue. The presence of the nitro group on para position make the phenol ring more positive (electron acceptor) and therefore increasing electron donor acceptor interaction between adsorbent and adsorbate. This results more adsorption of *p*-nitrophenol on the carbon surface compared to phenol molecule. The adsorption rate of methylene blue is comparatively lower than phenolic compounds. It was suggested that some of the micropores in active carbons were not accessible to methylene blue dye molecules due to large molecular size (cross sectional area is 1.2 nm<sup>2</sup>).

Equilibrium data analysed by using various solid-liquid isotherm models such as Langmuir, Freundlich, Dubinin – Radushkevich and John – Sivanandan Achari isotherm models are discussed in the following sections.

### **3.5.5.1 Langmuir Isotherm for Solid – Liquid Equilibria**

The Langmuir Isotherm model assumes that adsorption occurs on a homogeneous surface by monolayer coverage and there is no subsequent interaction occurs between adsorbed species. The isotherm is based on the theoretical principle that only a single adsorption layer (monolayer) exists on an adsorbent. The linear form of Langmuir equation is given as follows [33].

$$\frac{C_e}{q_e} = \frac{1}{K_L} + \frac{a_L}{K_L} C_e \quad (3.20)$$

Where  $q_e$  is the adsorbed amount per gram of adsorbent (mg/g),  $C_e$  represents the equilibrium concentration of the adsorbate in solution (mg/L),  $K_L$  and  $a_L$  is the Langmuir constants (L/mg), is related to the affinity of the binding sites, and  $K_L/a_L$  (or  $q_m$ ) represents the monolayer adsorption capacity of the adsorbent (mg/g). The values of  $q_m$  and  $K_L$  are calculated from the slope and intercept of the linear plot of  $C_e/q_e$  against  $C_e$ .

### **3.5.5.2 Freundlich Isotherm for Solid – Liquid Equilibria**

The Freundlich model is an empirical model based on multilayer adsorption on heterogeneous surfaces. The equation is commonly described as

$$q_e = K_F C_e^{1/n} \quad (3.21)$$

$$\log q_e = \log K_F + \frac{1}{n} \log C_e \quad (3.22)$$

$K_F$  and  $n$  are the Freundlich constants that represent the adsorption capacity and adsorption strength, respectively. The magnitude of  $1/n$  quantifies the favourability of adsorption and the degree of heterogeneity of the surface. If  $n > 1$ , suggesting favourable adsorption, then the adsorption capacity increases and new adsorption sites are formed.  $K_F$  and  $n$  can be obtained from the intercept and slope of the linear plot of  $\log q_e$  versus  $\log C_e$ .

### 3.5.5.3 Dubinin-Radushkevich Isotherm for Solid-Liquid Equilibria

Equilibrium data are applied to the linear form of the Dubinin-Radushkevich isotherm model to test the nature of adsorption assigned as chemical or physical. The equation is represented as

$$q_e = q_{mi} e^{-\beta \varepsilon^2} \quad (3.23)$$

$$\ln q_e = \ln q_{mi} - \beta \varepsilon^2 \quad (3.24)$$

Where  $q_{mi}$  (*D-R*) is the Dubinin-Radushkevich adsorption capacity (mg/g),  $\beta$  is activity coefficient related to the mean free energy, and  $\varepsilon$  is the Polanyi potential which is related to the equilibrium concentration as follows

$$\varepsilon = RT \ln \left( 1 + \frac{1}{C_e} \right) \quad (3.25)$$

Where  $R$  is the gas constant (8.314 J/mol K) and  $T$  (K) is the absolute temperature. The constant  $\beta$  gives the mean free energy ( $E$ ) of adsorption. It is energy per molecule of the adsorbate for transferring to the surface of the solid from infinity in the solution and can be computed using the relationship

$$E = \frac{1}{\sqrt{2\beta}} \quad (3.26)$$

The saturation limit  $q_{mi}$  (*D-R*) may represent the adsorption monolayer in micropores. The slope of the plot of  $\ln q_e$  versus  $\varepsilon^2$  gives  $\beta$  ( $\text{mol}^2/\text{J}^2$ ) and the intercept yields the adsorption capacity,  $q_{mi}$  (*D-R*) (mg/g).

### 3.5.6 Adsorption of Phenol on GACZR 1273, GAC 383 and GACO 383 at Temperatures

The effect of temperature on the adsorption system was studied by performing experiments at different temperatures.

The equilibrium adsorption isotherms for phenol at 283 K, 293 K, 303 K, 313 K, & 323 K on GAC 383, GACO 383 and GACZR 1273 from an aqueous solution were measured at contact time 8 hour, concentration of phenol ranges from 25 - 3000 mg/L, and adsorbent dose taken as 1 g/L (0.05g carbon in 50 ml solution of phenol).

The variation of Langmuir, Freundlich and Dubinin – Radushkevich isotherm parameter of phenol at above temperatures are noted quantitatively evaluate the adsorption capacities.

The Langmuir plots of phenol adsorption on GAC 383, GACO 383 and GACZR 1273 with respect to five temperatures are given in Figure 3.27(a)–(c). The monolayer capacity  $q_m$  ( $K_L/a_L$ ) and Langmuir constant  $K_L$  were calculated from the slope and intercept of the corresponding plots. The  $K_L/a_L$  increases with temperature, suggesting that the adsorption is favoured at high temperatures. This suggests an endothermic adsorption mechanism. The high Langmuir constants  $K_L/a_L$  ( $q_m$ ) and  $K_L$  are because of the highest uptake capacity and strong affinity for adsorbate. The monolayer capacity of new carbons at 323 K are given as follows; GACZR 1273 ( $q_m = 467.29$  mg/g &  $K_L = 5.79$  Lg<sup>-1</sup>), GAC 383 ( $q_m = 352.11$  mg/g &  $K_L = 2.68$  Lg<sup>-1</sup>), GACO 383 ( $q_m = 237.0$  mg/g &  $K_L = 2.59$  Lg<sup>-1</sup>).

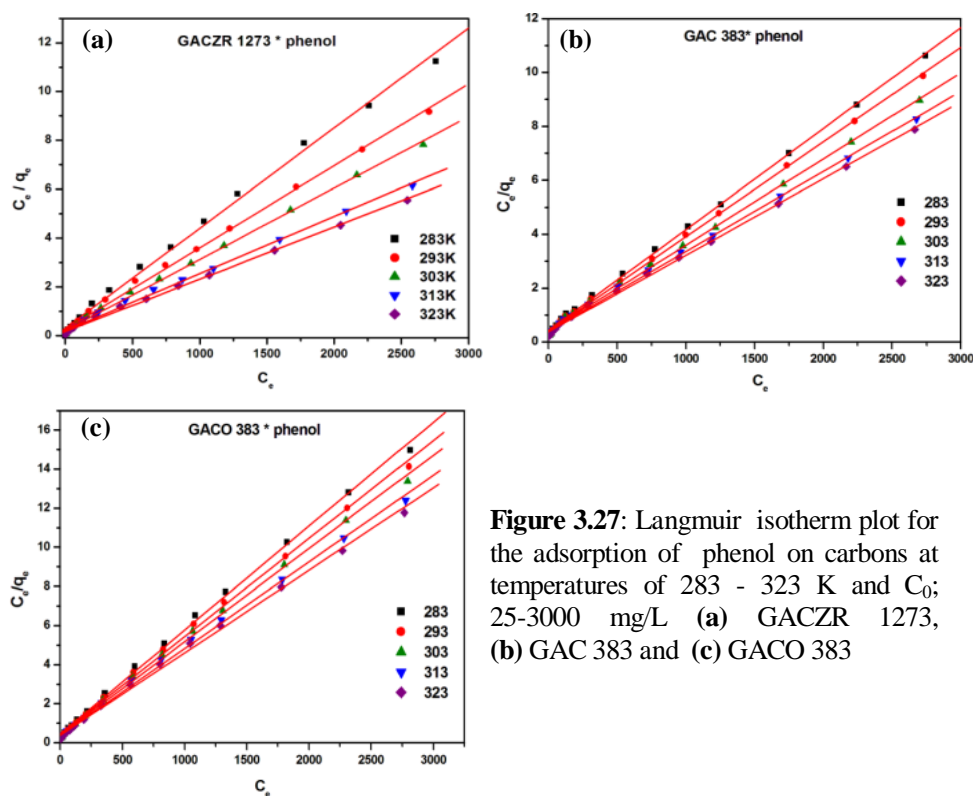


**Figure 3.27:** Langmuir isotherm plot for the adsorption of phenol on carbons at temperatures of 283 - 323 K and  $C_0$ ; 25-3000 mg/L (a) GACZR 1273, (b) GAC 383 and (c) GACO 383

The phenol molecules find large potential adsorption sites on the GACZR 1273 sample compared to GAC 383 and GACO 383. At 323 K (50°C) zirconium impregnated GACZR 1273 shows 32 % increment in monolayer capacity compared to the GAC 383. Whereas nitric acid modified GACO 383 shows 33 % decrease in monolayer volume. Langmuir constant  $K_L$  is related to the equilibrium adsorption and enthalpy change and it varies for new carbons as GACZR 1273 (3.25 – 5.79  $\text{Lg}^{-1}$ ), GAC 383 (2.33 – 2.68  $\text{Lg}^{-1}$ ), and GACO 383 (2.17 – 2.59  $\text{Lg}^{-1}$ ). Phenol adsorption on carbon involves dispersive forces between the  $\pi$  electrons in phenol and the  $\pi$  electrons in carbons.

The Freundlich plots of phenol adsorption on GAC 383, GACO 383 and GACZR 1273 with respect to five temperatures are given in Figures 3.28(a) –(c). The  $K_F$  and  $n$  were calculated from the intercept and slope of the linear plots of Freundlich isotherm and are given in Table 3.11. The Freundlich constant,  $1/n$  between  $0.1 < 1/n < 1.0$  represent relatively good adsorption of phenols onto activated carbon.

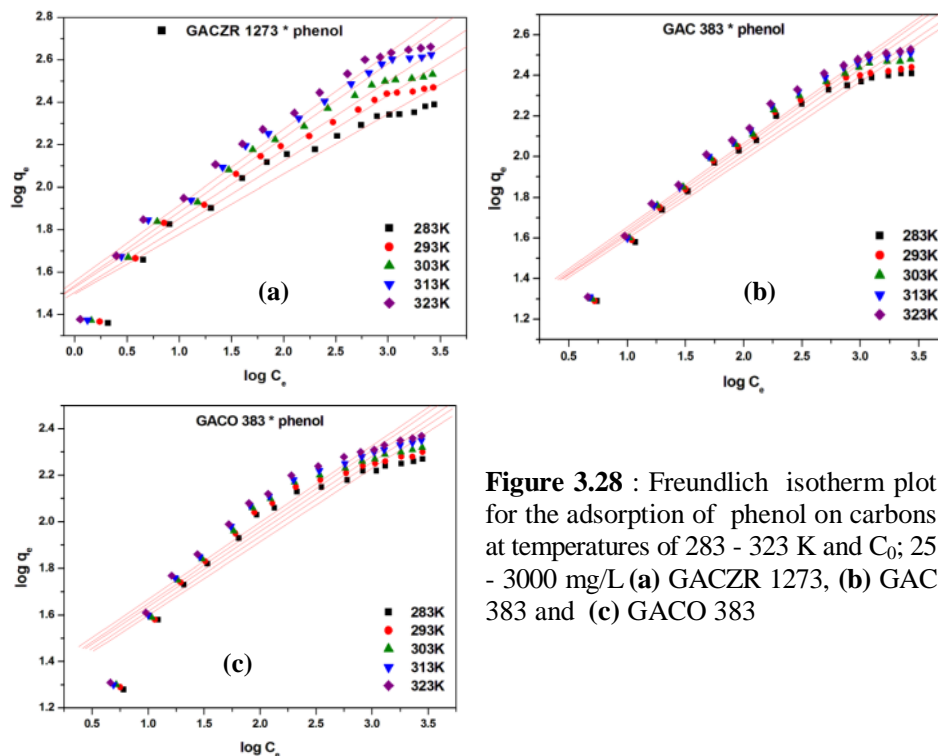


**Figure 3.28** : Freundlich isotherm plot for the adsorption of phenol on carbons at temperatures of 283 - 323 K and  $C_0$ ; 25 - 3000 mg/L (a) GACZR 1273, (b) GAC 383 and (c) GACO 383



The Freundlich constant,  $K_F$  for phenol adsorption at 283 – 323K on GAC has been found to be varies as GACZR 1273 (31.44 – 36.17 L/g), GAC 383 (16.38 – 17.38 L/g), GACO 383 (19.16 – 21.66 L/g) respectively. It is noted that the measured  $K_F$  increased with increasing solution temperature and reached a maximum at 323 K, results easy uptake of adsorbates with relatively high temperatures.

The increase in  $K_F$  can be attributed to the increase in surface area and porosity. The increased porosity due to impregnation of zirconium influences the adsorption of phenol. Adsorption of phenol at low and moderate concentrations are very much dependant on the microporous nature and surface area of the activated carbons. Hence, the increase of porosity and surface area of GACZR 1273 promotes adsorption of large numbers of phenol molecules into it compared to GAC 383 and GACO 383. The high  $K_F$  of phenol adsorption on GACZR 1273 carbon can be ascribed strong interaction of the  $\pi$  electrons of the aromatic nucleus of phenol with surface of GACZR 1273.

The Dubinin–Radushkevich (D-R) plot of  $\ln q_e$  against  $[RT \ln (1+1/C_e)]^2$  of phenol adsorption on GAC 383, GACO 383 and GACZR 1273 with respect to five temperatures are given in Figure 3.29(a)–(c). The parameters such as  $q_{mi}$  (D-R),  $\beta$ , and the mean free energy ( $E$ ) were determined from the appropriate plot and are given in Table 3.11.

Schematic representation of D-R isotherm shows an increasing trend of  $q_{mi}$  (D-R) with temperature for all GACs and only lower points is connected to the straight line. The adsorption capacity increased with rise of temperature from 283 to 323K. The percentage of increment for GAC is given as GACZR 1273 (11 %), GAC 383 (7 %), and for GACO 383 (6.3 %). The mean energy ‘ $E$ ’ gives an idea about the type of adsorption. The  $E$  increases slightly with temperature for all GACs but not exceed the limit of physisorption ( $< 8$  kJ/mol) [34].

The results showed that the phenol uptake is dependent on both the porosity and surface chemistry of the carbons. Phenol adsorption has strong dependence on the number of carboxylic acid groups due to two factors: (1) phenol reacts with carboxylic groups on the carbon surface, forming an ester bond, and (2) carboxylic

groups on the carbon surface, remove the  $\pi$ -electron from the activated carbon aromatic ring matrix, causing a decrease in the strength of interactions between the benzene ring of phenol and the carbons basal planes, which decreases the uptake of phenol on GACO 383 [35].

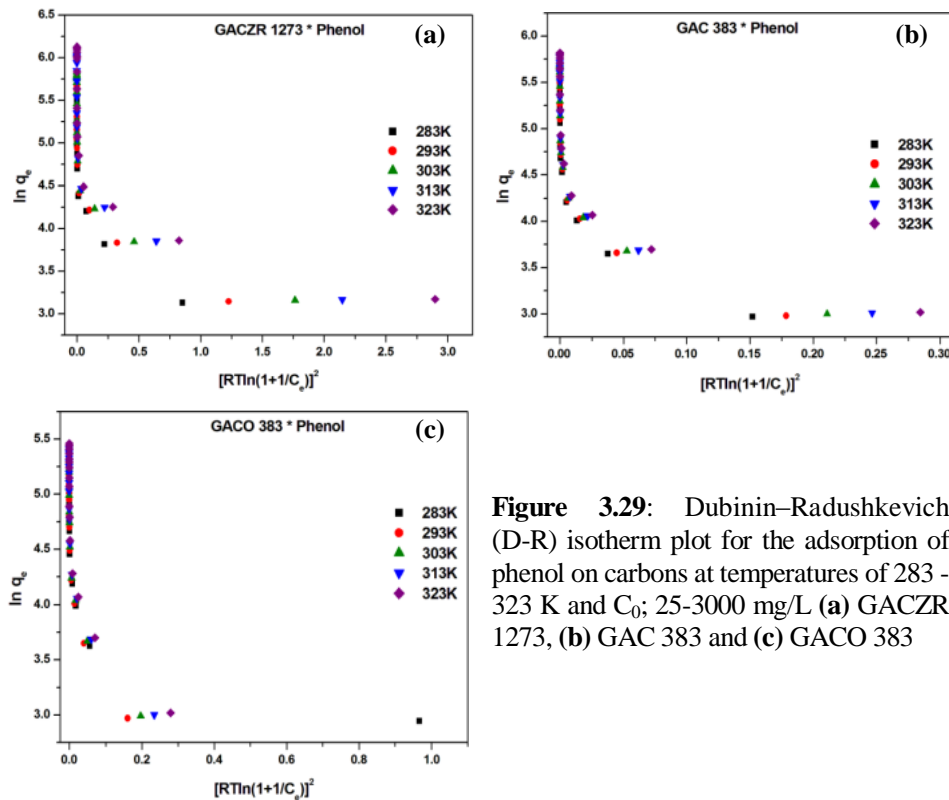


**Figure 3.29:** Dubinin–Radushkevich (D-R) isotherm plot for the adsorption of phenol on carbons at temperatures of 283 - 323 K and  $C_0$ ; 25-3000 mg/L (a) GACZR 1273, (b) GAC 383 and (c) GACO 383

Overall analysis indicates, the fitness of Langmuir isotherm model to Phenol-GAC adsorption system, suggesting a monolayer adsorption of phenol on the surface of GAC. Quantitative evaluation of adsorption efficiency of GAC in aqueous solution of phenol shows that at higher temperatures the rate of diffusion of phenol molecule within the pores of the GAC leads to a high rate of adsorption. Higher adsorption with temperature may also be due to increase in the number of adsorption sites generated as results of breaking of some internal bonds near edge of active surface sites of GAC [36-38].

**Table 3.11:** Langmuir, Freundlich and Dubinin-Radushkevich isotherm parameters of phenol on GACZR 1273, GAC 383 and GACO 383 at temperatures of 283-323 K

Carbons	Temperature (K)	Langmuir				Freundlich			Dubinin -Radushkevich			
		$K_L/a_L$ (mg/g)	$K_L$ (Lg <sup>-1</sup> )	$a_L \times 10^{-4}$ (Lg <sup>-1</sup> )	$R^2$	$n$	$K_F$ (Lg <sup>-1</sup> )	$R^2$	$q_{mi}$ (D-R) (mg/g)	$\beta$ mol <sup>2</sup> /kJ <sup>2</sup>	$R^2$	$E$ (kJ/mol)
GACZR 1273	283	243.9	3.25	133	0.996	3.54	31.4	0.922	67.7	1.30	0.966	0.622
	293	298.5	3.91	131	0.998	3.24	32.0	0.943	68.4	0.89	0.970	0.747
	303	342.5	4.83	141	0.998	3.10	33.9	0.947	69.2	0.62	0.968	0.897
	313	427.4	4.88	114	0.996	2.87	34.3	0.960	73.2	0.54	0.968	0.966
	323	467.3	5.79	124	0.998	2.80	36.2	0.962	72.8	0.39	0.970	1.130
GAC 383	283	266.7	2.33	87.3	0.998	2.60	16.4	0.935	55.5	7.00	0.966	0.267
	293	284.9	2.46	86.5	0.998	2.56	16.7	0.935	56.6	6.00	0.966	0.288
	303	312.5	2.48	79.4	0.998	2.49	16.7	0.945	57.4	5.10	0.966	0.293
	313	336.7	2.53	75.1	0.998	2.44	17.0	0.951	58.4	4.40	0.966	0.338
	323	352.1	2.68	76	0.998	2.42	17.4	0.951	59.2	3.80	0.966	0.362
GACO 383	283	188.3	2.17	115	0.998	3.17	19.2	0.885	46.9	0.94	0.906	0.258
	293	199.6	2.34	117	0.998	3.13	19.9	0.889	56.1	6.70	0.966	0.273
	303	209.6	2.48	119	0.998	3.12	20.7	0.895	57.4	5.50	0.970	0.302
	313	225.7	2.52	112	0.998	3.05	21.1	0.903	58.8	4.70	0.968	0.328
	323	237.0	2.59	109	0.998	3.02	21.7	0.904	59.3	3.90	0.966	0.359

### 3.5.7 Adsorption of *P*-Nitrophenol on GACZR 1273, GAC 383 and GACO 383 at Temperatures

Batch adsorption isotherm studies for *p*-nitrophenol were carried out at five selected temperatures, 283 K, 293 K, 303 K, 313 K and 323 K (at contact time 8hour, concentration of *p*-nitrophenol 25 – 3000 mg/L, adsorbent dose 1 g/L) .

Equilibrium data of *p*-nitrophenol at five temperatures is applied to linear form of Langmuir equation and is schematically represented in Figure 3.30(a) – (c). Linear plots with high correlation coefficients suggest that the adsorption of *p*-nitrophenol on these carbons is in agreement with the Langmuir equation. The asymptotic nature of the Langmuir model gives stable adsorption at the maximum adsorptive capacity. Therefore, it will perform better when used in industrial applications [39].

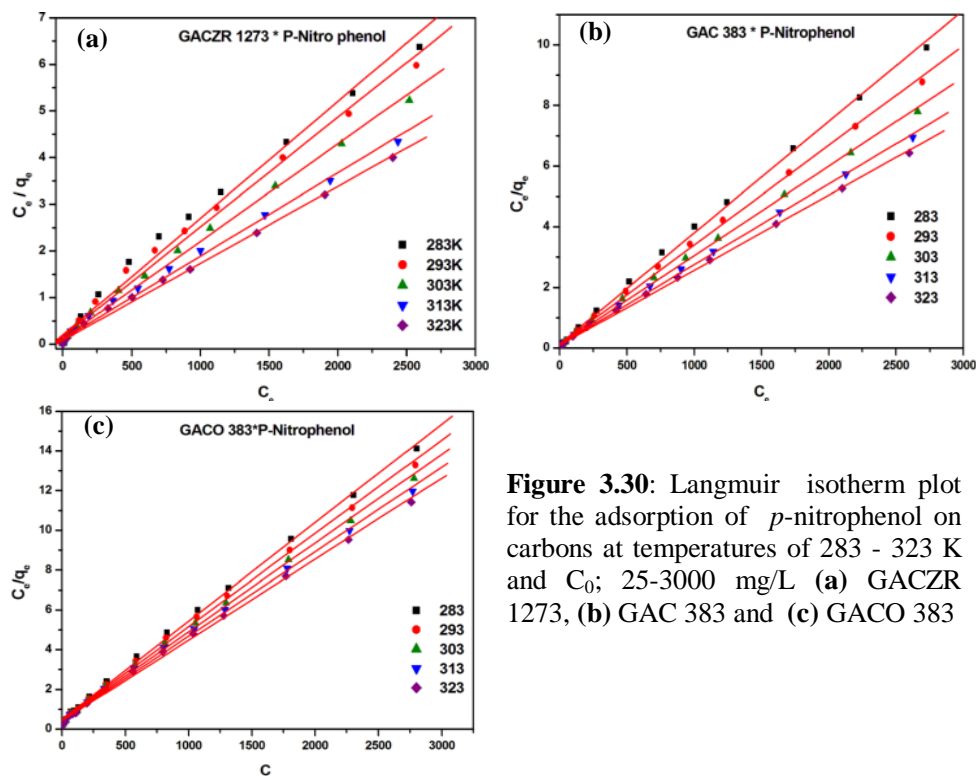


**Figure 3.30:** Langmuir isotherm plot for the adsorption of *p*-nitrophenol on carbons at temperatures of 283 - 323 K and  $C_0$ ; 25-3000 mg/L (a) GACZR 1273, (b) GAC 383 and (c) GACO 383

The monolayer capacity  $K_L/a_L$  ( $q_m$ ) of GACZR 1273, for *p*-nitrophenol adsorption is as high as 564 mg/g at 323 K. The corresponding monolayer adsorption capacities at other temperatures are given as; 283 K (400 mg/g), 293 K (425.5 mg/g), 303 K (478.5 mg/g), and 313K (518.1 mg/g) respectively. The monolayer capacity increases up to 41 % with rising the temperature from 283 K to 323 K. Whereas, GAC 383 shows 48 % increase in monolayer capacity and GACO 383 shows 22 % increment in uptake. This indicates that, adsorption of *p*-nitrophenol on activated carbon is favoured at high temperatures. Zirconium impregnation is shown to have significant influence on the monolayer capacity of the new carbon.

Monolayer capacities of activated carbon for phenol and *p*-nitrophenol, shows that at low concentration range, *p*-nitrophenols gives more intense adsorption capacity compared to phenol. This higher adsorption can be related to the electron withdrawing properties of the  $-NO_2$  group at the para position in the

phenol ring [40]. The adsorption of phenolic compounds on GAC can be explained by interactions of  $\pi$   $e^-$  in aromatic rings and graphene layers. Electron withdrawing groups on the aromatic rings reduces the electron density of  $\pi$  electrons thus enhance the  $\pi - \pi$  interactions by diminishing the repulsive electrostatic interactions between the aromatic rings [41-43].

The Freundlich plots of *p*-nitrophenol adsorption on GAC 383, GACO 383 and GACZR 1273 with respect to five temperatures are given in Figures 3.31(a)–(c). It shows the deviation from linearity at higher concentration indicating that significant adsorption takes place at low concentrations [44].

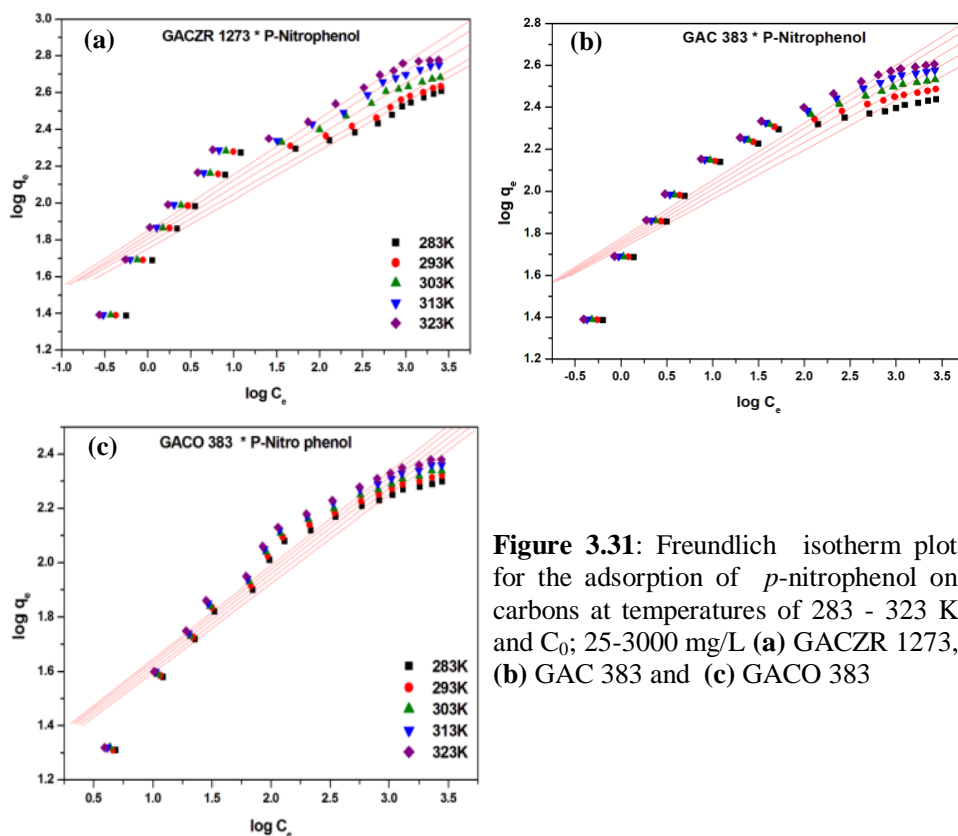


**Figure 3.31:** Freundlich isotherm plot for the adsorption of *p*-nitrophenol on carbons at temperatures of 283 - 323 K and  $C_0$ ; 25-3000 mg/L (a) GACZR 1273, (b) GAC 383 and (c) GACO 383

The Freundlich constants  $K_F$  and  $n$  are determined is given in Table 3.12. The Freundlich constant,  $K_F$ , varies at 283 – 323 K is given as; GACZR 1273 (56.53 – 70.80 L/g), GAC 383 (53.49 – 59.9 L/g) and GACO 383 (18.48 – 20.04 L/g).

Large  $K_F$  can be attributed to large adsorption of *p*-nitrophenol and it increases with solution temperature. Impregnation of  $Zr^{4+}$  on GAC also makes the  $K_F$  into a high value. The extra porosity due to activation with zirconium influences the adsorption of *p*-nitrophenol at low and moderate concentrations. This is very much dependant on the microporous nature and surface area of the activated carbons.

The Dubinin–Radushkevich plot of  $\ln q_e$  against  $[RT \ln(1+1/C_e)]^2$  of *p*-nitrophenol adsorption on GAC 383, GACO 383 and GACZR 1273 with respect to five temperatures are given in Figures 3.32(a)–(c). The parameters  $q_{mi}$  (*D-R*),  $\beta$  and the mean free energy,  $E$  were determined from the appropriate plot and are given in Table 3.12.

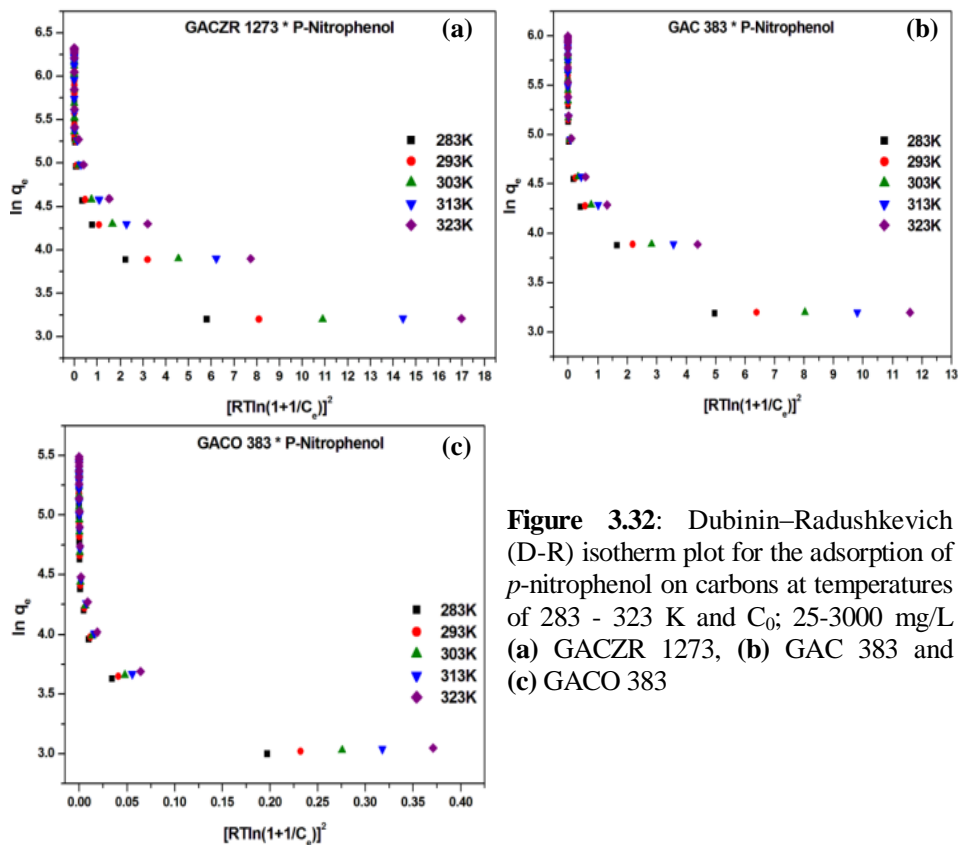


**Figure 3.32:** Dubinin–Radushkevich (D-R) isotherm plot for the adsorption of *p*-nitrophenol on carbons at temperatures of 283 - 323 K and  $C_0$ ; 25-3000 mg/L (a) GACZR 1273, (b) GAC 383 and (c) GACO 383

The percentages of micropore adsorption capacity  $q_{mi}(D-R)$  increases for new carbons by rising the solution temperature from 283 K to 323 K is given as follows; GACZR 1273 (10 %), GAC 383 (7 %) and GACO 383 (6.3 %). The mean energy gives an idea about the type of adsorption. The value of mean free energy  $E$  obtained from Dubinin - Radushkevich isotherm has value less than 3 kJ/mol for GAC 383, GACO 383 and GACZR1273. This suggested that physical adsorption is dominating in the adsorption process between the *p*-nitrophenol and new carbons.

**Table 3.12:** Langmuir, Freundlich and Dubinin-Radushkevich isotherm parameters of *p*-nitrophenol on GACZR 1273, GAC 383, GACO 383 at temperatures of 283- 323K

Carbons	Temperature (K)	Langmuir isotherm				Freundlich			Dubinin -Radushkevich			
		$K_L/a_L$ (mg/g)	$K_L$ (Lg <sup>-1</sup> )	$a_L \times 10^4$ (Lg <sup>-1</sup> )	$R^2$	$n$	$K_F$ (Lg <sup>-1</sup> )	$R^2$	$q_{mi}$ (D-R) mg/g	$\beta$ mol <sup>2</sup> /kJ <sup>2</sup>	$R^2$	$E$ (kJ/mol)
GACZR 1273	283	400.0	4.99	125	0.990	3.76	56.5	0.897	92.5	0.24	0.970	1.45
	293	425.5	5.99	141	0.992	3.73	60.5	0.906	93.4	0.17	0.972	1.72
	303	478.5	8.39	175	0.996	3.55	64.0	0.918	96.5	0.13	0.978	1.97
	313	518.1	11.9	229	0.998	3.45	67.1	0.925	98.2	0.10	0.980	2.26
	323	564.9	14.7	261	0.998	3.35	70.8	0.929	103	0.09	0.984	2.42
GAC 383	283	272.5	7.61	279	0.998	4.26	53.5	0.861	75.8	0.23	0.966	1.60
	293	304.9	8.36	274	0.998	4.06	55.0	0.880	77.0	0.18	0.966	1.75
	303	340.1	9.03	265	0.998	3.88	56.6	0.893	78.2	0.15	0.966	1.90
	313	377.4	9.40	249	0.998	3.73	58.1	0.906	79.5	0.12	0.966	2.07
	323	403.2	10.7	265	0.998	3.64	59.9	0.914	81.2	0.10	0.966	2.21
GACO 383	283	201.6	2.06	102	0.998	3.05	18.5	0.925	49.6	4.63	0.951	0.33
	293	213.2	2.14	101	0.998	3.01	18.9	0.927	50.6	3.97	0.953	0.36
	303	224.2	2.24	100	0.998	2.97	19.3	0.929	51.3	3.35	0.951	0.39
	313	235.3	2.31	98	0.998	2.94	19.7	0.931	52.1	2.92	0.951	0.41
	323	245.7	2.41	98	0.998	2.91	20.0	0.933	52.7	2.51	0.949	0.45

### 3.5.8 Adsorption of Methylene Blue (MB) on GACZR 1273, GAC 383, and GACO 383 at Temperatures

The equilibrium adsorption capacity of GAC 383, GACO 383, and GACZR 1273 towards methylene blue is evaluated at five temperatures (283 K, 293 K,

303 K, 313 K and 323 K). The isotherm experiments were carried out at contact time of 10 hours at which the equilibrium is attained. Batch experiments were conducted by taking the methylene blue (MB) concentration ranges from 25 - 1500 mg/L and also keeping the adsorbent dosage as 1 g/L.

The linear form of the Langmuir equation was applied to evaluate the adsorption characteristics of methylene blue adsorption on the equilibrium adsorption data. The plots of  $C_e/q_e$  versus  $C_e$ , at five different temperatures are given in Figure 3.33(a)–(c). The linearity of plots suggests that methylene blue adsorption agrees with the Langmuir model. The parameters  $K_L/a_L$  (or  $q_m$ ),  $K_L$  and  $a_L$  are given in Table 3.13.

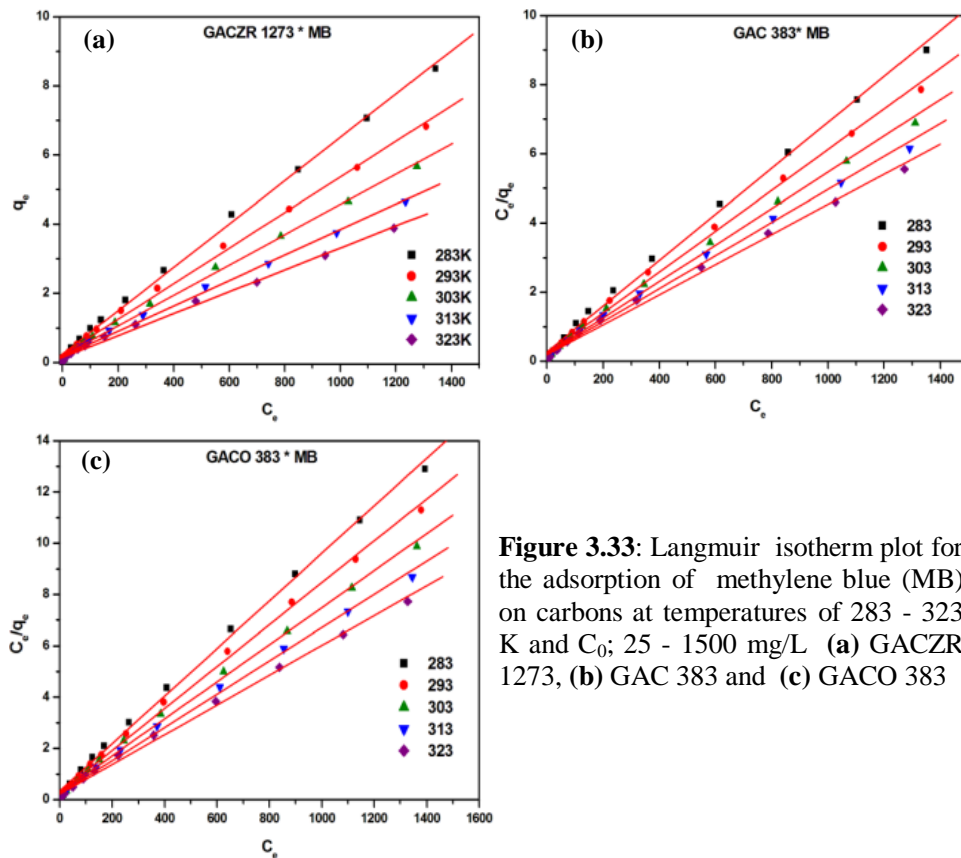


**Figure 3.33:** Langmuir isotherm plot for the adsorption of methylene blue (MB) on carbons at temperatures of 283 - 323 K and  $C_0$ ; 25 - 1500 mg/L (a) GACZR 1273, (b) GAC 383 and (c) GACO 383



The Langmuir isotherm plots for GAC 383, GACO 383, and GACZR 1273 are found to be smooth straight line graphs with intercept near to origin. At the higher concentrations, the spread of the data varies widely. This may be due to the preferential filling of the mesopores by the dye molecules rather than its limited accessibility to the micropores. Being the molecule is larger in size the micropores are not much exposed for adsorption. At higher equilibrium concentrations, mass transfer occurs to mesopores by diffusion. Langmuir  $K_L/a_L$  varies at 283 - 323K for GAC are given as GACZR 1273 (159.7 – 315.5 mg/g), GAC 383 (150.6 – 229.4 mg/g) and GACO 383 (108.0 – 172.4 mg/g). This suggested that increasing of solution temperatures enhanced the adsorption capacity due to penetration of more MB into pores of GAC [45, 46].

The monolayer capacity,  $K_L/a_L$  for methylene blue adsorption on all carbon is lower than that for phenol and *p*-nitrophenol adsorption. This can be explained by considering the size of these molecules. When a large molecule, like methylene blue, and smaller, or solvent molecules, like water, are adsorbed on a porous solid with a distribution of pore sizes the effective adsorbent surface available to the larger molecule is limited by pore screening or molecular sieving. The cross sectional area occupied by a molecule of methylene blue has been reported to be 1.2 nm<sup>2</sup>. Hence the finer micropores in the activated carbon structure are not available as adsorption sites for methylene blue molecules due to their large size. Hence, methylene blue adsorption on activated carbons is less compared to phenol and *p*-nitrophenol molecule.

Freundlich constants  $K_F (Lg^{-1})$  and  $n$  are given in Table 3.13 and is seen that  $K_F$  increases with temperature. As regards to Freundlich isotherm constants the zirconium modified carbon (GACZR 1273) exhibit relatively high dye uptake.

The value of  $1/n < 1$  is an indication of favorable adsorption and is classified to *L*-type isotherm. This isotherm reflects a relatively high affinity between the solute and the solid phase.

$K_F$  increased with increasing solution temperature and reached a maximum at 323K, indicating that easy uptake of methylene blue (MB) with high adsorptive capacity would be achieved at relatively high solution temperatures

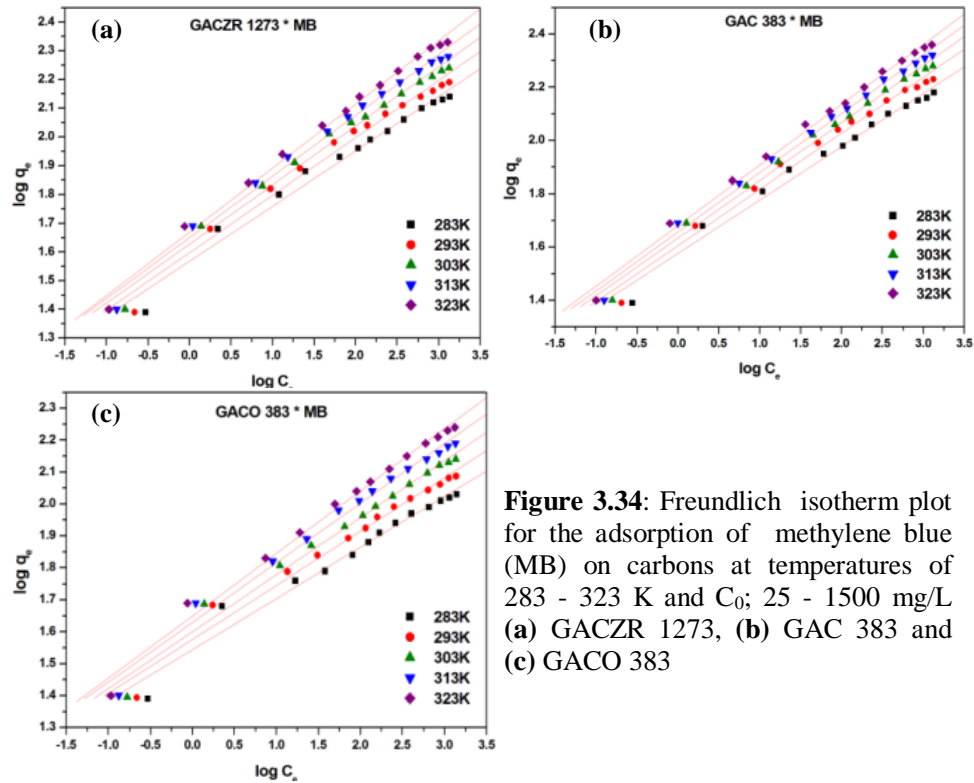


**Figure 3.34:** Freundlich isotherm plot for the adsorption of methylene blue (MB) on carbons at temperatures of 283 - 323 K and  $C_0$ : 25 - 1500 mg/L (a) GACZR 1273, (b) GAC 383 and (c) GACO 383

The equilibrium data were also applied to the linear form of the Dubinin–Radushkevich isotherm model to test the nature of adsorption assigned as chemical or physical. The isotherm constants were calculated from this isotherm and given in Table 3.13.

The micropore adsorption capacity  $q_{mi}(D-R)$  of GACZR 1273 increases 10 %, GAC 383 increases 9 % and GACO 383 increases 12.6 % by rising the solution temperature from 283 K to 323 K. Energy constant  $E$  calculated are all below 5 kJ/mol, suggesting that physical adsorption was dominating in the adsorption process.

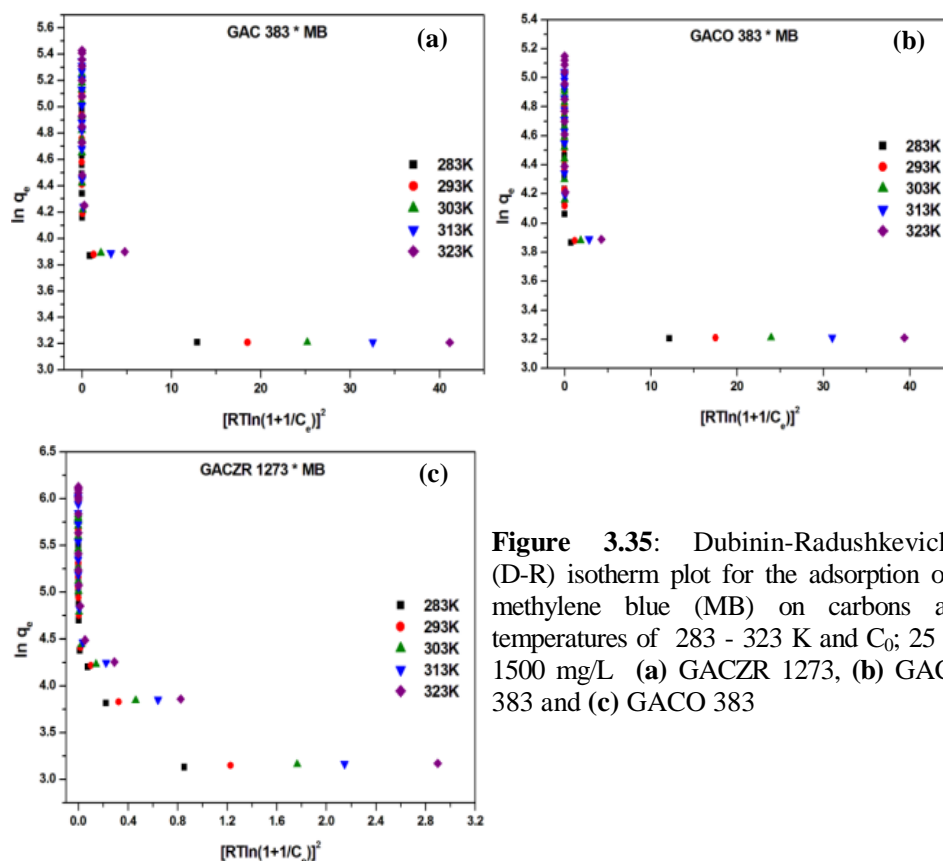


**Figure 3.35:** Dubinin-Radushkevich (D-R) isotherm plot for the adsorption of methylene blue (MB) on carbons at temperatures of 283 - 323 K and  $C_0$ ; 25 - 1500 mg/L (a) GACZR 1273, (b) GACO 383 and (c) GAC 383

Adsorption mechanism that may occur in the case of solutes containing conjugated system such as the dye molecules studied here corresponds to  $\pi$ - $\pi$  dispersive interactions. This mode of interaction can take place between the aromatic rings and  $-N=C-C=C-$  system of methylene blue (MB) [47].

**Table 3.13:** Langmuir, Freundlich and Dubinin-Radushkevich isotherm parameters of methylene blue on GACZR 1273, GAC 383, GACO 383 at temperatures 283 – 323 K

Carbons	Temperature (K)	Langmuir isotherm				Freundlich			Dubinin-Radushkevich				
		$K_L/a_L$ (mg/g)	$K_L$ ( $Lg^{-1}$ )	$a_L \times 10^{-4}$ ( $Lg^{-1}$ )	$R^2$	$n$	$K_F$ ( $Lg^{-1}$ )	$R^2$	$\ln q_{mi}$	$q_{mi}$ (D-R) mg/g	$\beta \times 10^3$ mol <sup>2</sup> /kJ <sup>2</sup>	$R^2$	$E$ (kJ/mol)
GACZR 1273	283	159.7	4.04	253	0.996	4.67	36.7	0.982	4.06	57.8	71	0.939	2.66
	293	194.6	4.45	229	0.992	4.33	39.5	0.990	4.09	59.5	50	0.933	3.16
	303	228.3	5.29	232	0.992	4.08	42.4	0.990	4.11	61.1	37	0.937	3.65
	313	271.7	6.01	221	0.992	3.84	45.4	0.992	4.13	62.2	32	0.939	3.93
	323	315.5	6.92	219	0.988	3.66	48.4	0.994	4.15	63.5	23	0.943	4.64
GAC 383	283	150.6	3.74	248	0.992	1.58	37.7	0.982	4.05	57.4	66	0.943	2.75
	293	169.5	4.54	268	0.992	1.61	40.7	0.984	4.07	58.8	47	0.935	3.26
	303	190.1	4.80	252	0.992	1.63	42.9	0.990	4.10	60.3	36	0.935	3.75
	313	209.6	5.13	245	0.988	1.66	45.3	0.992	4.12	61.6	28	0.937	4.21
	323	229.4	5.51	240	0.988	1.68	47.8	0.994	4.14	62.8	23	0.941	4.68
GACO383	283	108.0	2.89	268	0.996	6.27	35.1	0.968	3.99	54.2	65	0.972	2.77
	293	122.4	3.37	275	0.992	5.92	37.7	0.976	4.03	56.3	47	0.960	3.26
	303	138.7	3.60	259	0.992	5.61	39.8	0.982	4.06	58.0	36	0.955	3.74
	313	154.3	4.31	279	0.992	5.33	42.3	0.984	4.09	59.5	28	0.951	4.19
	323	172.4	4.59	266	0.992	5.12	44.6	0.988	4.11	61.0	23	0.953	4.66

### 3.5.9 John-Sivanandan Achari (J-SA) Isotherm for Solid- Liquid Equilibria

John and Achari [48] extended the application of John isotherm model originally designed for solid-gas equilibrium to solid-liquid equilibrium, applicable over a wide range of concentration. The separation of adsorption and pore filling phenomena as visible through different phases in the solid-liquid adsorption in John –Sivanandan Achari (*J-SA*) isotherm [ $\log \log C_e = C + n \log q_e$ ] are very much helpful to recognize and thereby interpret both specific and non-specific interactions occur during the adsorption process [49, 50].

John–Sivanandan Achari (J-SA) isotherm for solid-liquid is expressed as

$$\log \log C_e = C + n \log q_e \quad (3.27)$$

$$\text{Where; } C_e = C_e \times 10^N \quad (3.28)$$

$$q_e = q_I + q_{II} + q_{III} \quad (3.29)$$

The newly developed carbons GACZR 1273, GAC 383 and GACO 383 are evaluated for their adsorption efficiency using John-Sivanandan Achari isotherm models for methylene blue (MB), phenol (P) and *p*-nitrophenol (PNP) adsorption. The adsorption efficiency on GACZR 1273 obtained from J-SA isotherm model is compared to Langmuir (L), Dubinin-Radushkevich (D-R) and Freundlich (F) isotherm models. The John-Sivanandan Achari isotherm plots of methylene blue adsorption exhibited three distinct phases (marked by lines) of adsorption. The different pore filling mechanisms are explained over distinct phases. Isotherm has three distinct phases marked by kinks or distinct lines for phase change

The adsorption of MB on activated carbon in *phase I*,  $q_I(J)$  is found to be GACZR 1273 (79.50 mg/g), GAC 383 (67.48 mg/g), GACO 383 (66.62 mg/g) and the total adsorption capacity  $q_T(J)$  determined from  $\log q_T(J)$  corresponding to the highest  $\log \log C_e$  is given as GACZR 1273 (226.06 mg/g), GAC 383 (191.87 mg/g), GACO 383 (138.41 mg/g). This means 34.5 % of the total adsorption takes place during the *phase I* with specific adsorption mechanism. Low concentration adsorption given in the *phase I* is generally attributed to the presence of surface functional groups. While in *phase II*, adsorption given by GAC follows as, GACZR 1273 – 126.43 mg/g (61.8 %), GAC 383 – 124.39 mg/g (64.8 %), GACO 383 – 71.79 mg/g (51.9 %) adsorption. It is the highest adsorption quantity noted among three phases. The remaining 3.67 % of adsorption in GACZR 1273 is contributed by *phase III* ( $q_{III}(J)$  8.3mg/g) it is probably due to the adsorption of methylene blue in accessible mesopores.

A comparison of adsorption capacity  $V(J)$  and surface area  $SA(J)$  determined in comparison with other isotherm models are given in Table 3.14. There is an almost perfect agreement between  $q_T$  (J-SA) and  $q_m$  (L).

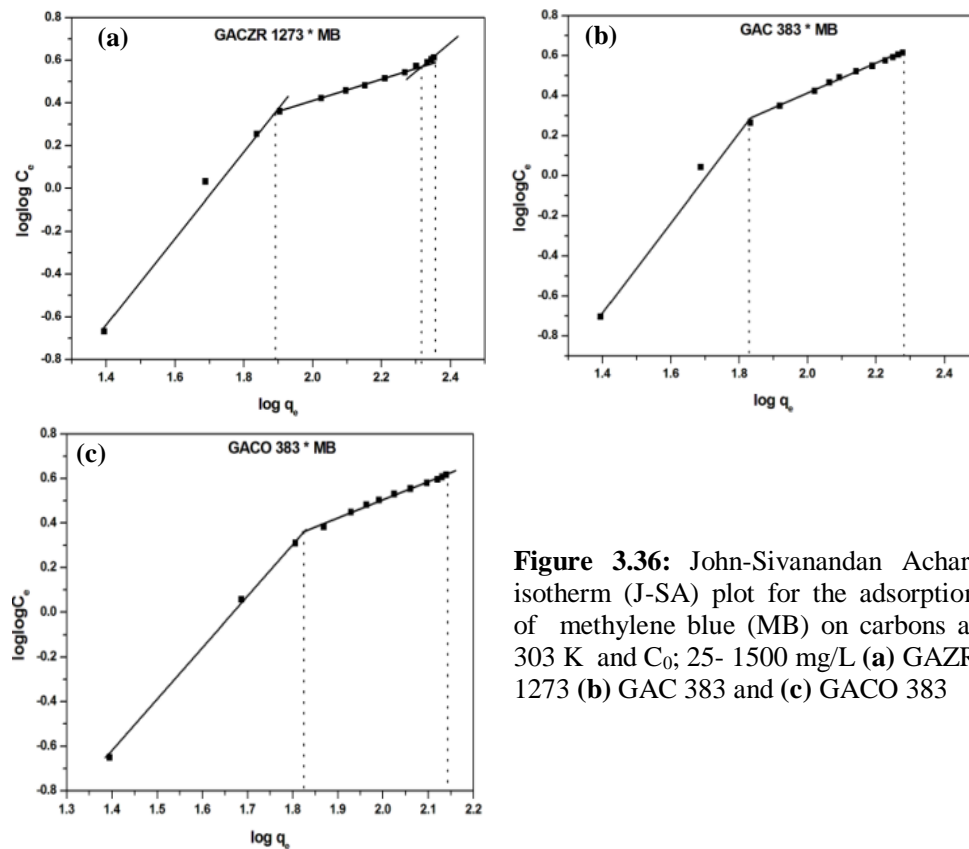


**Figure 3.36:** John-Sivanandan Achari isotherm (J-SA) plot for the adsorption of methylene blue (MB) on carbons at 303 K and  $C_0$ ; 25- 1500 mg/L (a) GAZR 1273 (b) GAC 383 and (c) GACO 383

The successive filling of phenol on GACZR 1273, GAC 383 and GACO 383 is represented by three distinct phases. Adsorption of phenol in *phase I* of *J-SA* isotherm plots given as GACZR 1273 (85.15 mg/g), GAC 383 (72.87 mg/g), GACO 383 (56.39 mg/g). The percentage contribution of *phase I* in total adsorption for GAC is calculated and given as GACZR 1273 –24.9 %, GAC 383 – 24.13% and GACO 383 – 26.58 %. Whereas *phase II* indicate extensive interaction of finer micropores (0.8 – 2 nm) and phenol molecule. The foremost adsorption in GACZR 1273 and GAC 383 i.e. about 65% adsorption will occur in *phase II*. Adsorption of phenol in *phase II* of GAC follows GACZR 1273 - 220.26 mg/g (64.5%), GAC 383 – 209.82 mg/g (69.5%), GACO 383 – 93.11 mg/g (43.8%). The remaining adsorption is contributed by *phase III* in John –Sivanandan Achari isotherm; GACZR 1273 - 35.99 mg/g (10.5%), GAC 383 -19.24 mg/g (6.4%) and

GACO 383 – 62.68 mg/g (25.9%) which is probably due to the adsorption of phenol in mesopores.

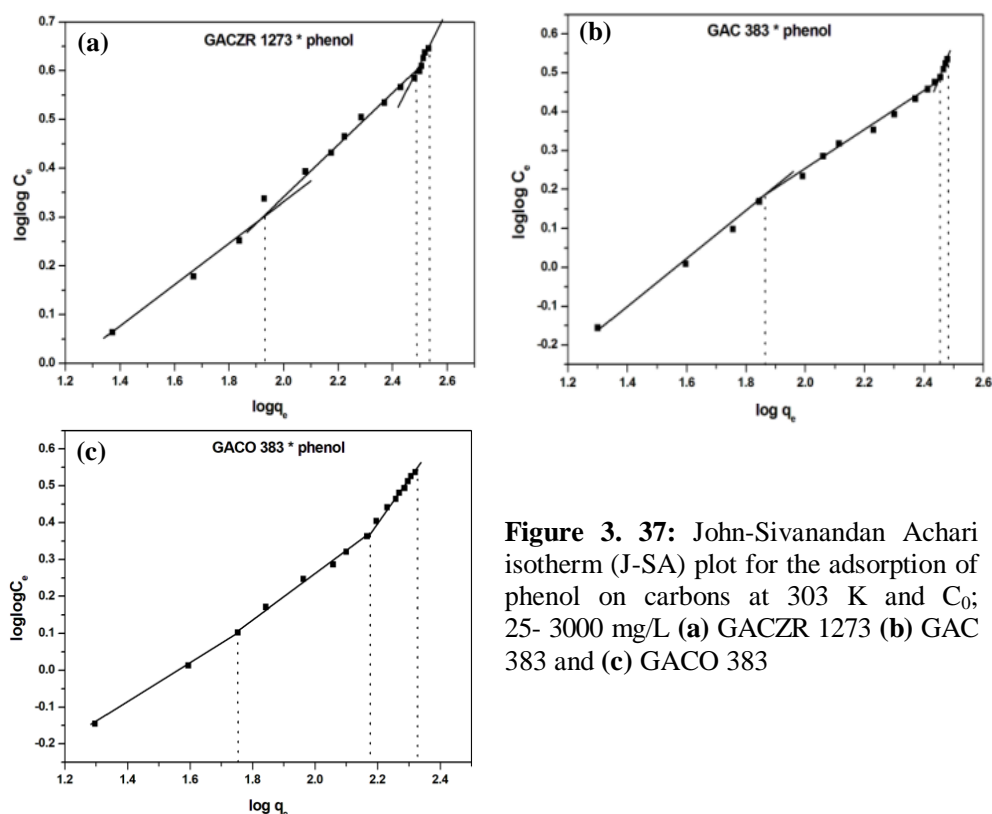


**Figure 3. 37:** John-Sivanandan Achari isotherm (J-SA) plot for the adsorption of phenol on carbons at 303 K and  $C_0$ ; 25- 3000 mg/L (a) GACZR 1273 (b) GAC 383 and (c) GACO 383

The *J-SA* plots of *p*-nitrophenol adsorption exhibited three phases of adsorption for GACZR 1273 and GACO 383, whereas GAC 383 shows only two distinct phases. In *phase I* GACZR 1273 adsorb 159.01 mg/g out of total adsorption  $q_T$  (*J*) of 478.63 mg/g and GACO 383 adsorb 52.27 mg/g of *p*-nitrophenol. The percentage contribution of *phase I* in total adsorption is given as GACZR 1273 (32.68 %), GACO 383 (23.53 %). There is no separation between molecular sieve effect and monolayer filling for adsorption of *p*-nitrophenol in GAC 383. Adsorption of *p*-nitrophenol in *phase II* for carbons are GACZR 1273 (141.84 mg/g), and GACO 383 (85.59 mg/g). The total adsorption (*Phase I* + *phase II*) constitutes monolayer filling in GAC 383 give 210.15 mg/g. The contribution of

phase III in *p*-nitrophenol adsorption is given by GACZR 1273 (185.74 mg/g), GAC 383 (134.1 mg/g) GACO 383 (84.24 mg/g).

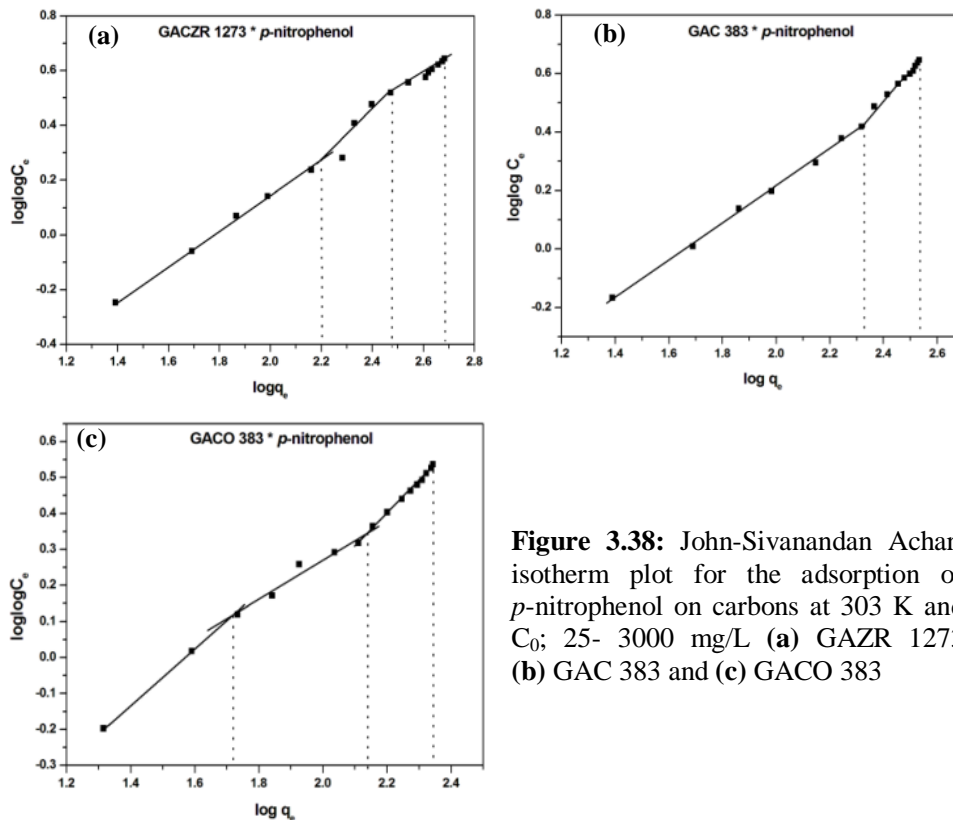


**Figure 3.38:** John-Sivanandan Achari isotherm plot for the adsorption of *p*-nitrophenol on carbons at 303 K and  $C_0$ ; 25- 3000 mg/L (a) GAZR 1273 (b) GAC 383 and (c) GACO 383

The comparison of adsorption capacities of J-SA isotherm model  $q_T$  (J-SA) mg/g, with Langmuir isotherm model  $q_m(L)$  are presented in Table 3.14. Total adsorption capacity of carbons obtained from J-SA isotherm  $q_T$  (J-SA) for the adsorption of phenol, *p*-nitrophenol and methylene blue are found to be close agreement with  $q_m(L)$ .



**Table 3.14:** Comparison of adsorption capacity (mg/g) and surface area (m<sup>2</sup>/g) for the adsorption of phenol, *p*-nitrophenol and methylene blue on carbon GACZR 1273, GAC 383 and GACO 383 using John-Sivanandan Achari, Langmuir, D-R and Freundlich isotherm models (T = 303 K)

	Adsorbate (cross sectional area nm <sup>2</sup> )	J-SA adsorption capacity mg/g				Langmuir q <sub>m</sub> (L) mg/g (*SA m <sup>2</sup> /g)	q <sub>m</sub> (D-R) mg/g (*SA m <sup>2</sup> /g)	Freundlich q <sub>F</sub> (Fr) mg/g (*SA m <sup>2</sup> /g)
		q <sub>I</sub> (J-SA) mg/g (*SA m <sup>2</sup> /g)	q <sub>II</sub> (J-SA) mg/g (*SA m <sup>2</sup> /g)	q <sub>III</sub> (J-SA) mg/g (*SA m <sup>2</sup> /g)	q <sub>r</sub> (J-SA) mg/g (*SA m <sup>2</sup> /g)			
GACZR 1273	*MB (1.2)	79.5 (179.7)	126.4 (285.7)	21.2 (47.9)	226.1 (510.8)	228.3 (515.9)	73.0 (165.0)	42.4 (95.9)
	*P (0.522)	85.2 (284.5)	220.3 (735.9)	36.0 (120.2)	341.4 (1140.0)	342.5 (1144.0)	76.1 (254.4)	33.9 (76.9)
	*PNP (0.525)	159.0 (361.4)	141.8 (322.4)	185.7 (422.2)	478.6 (1088.0)	478.5 (1087.6)	96.5 (255.7)	64.0 (145.4)
GAC 383	MB	67.5 (152.5)	124.4 (281.1)	*ND	191.9 (433.6)	190.1 (429.6)	60.3 (136.3)	42.9 (96.9)
	P	72.9 (243.4)	209.8 (701.0)	19.2 (64.3)	301.9 (1008.7)	312.5 (1044.0)	57.4 (191.7)	16.7 (55.9)
	PNP	*ND	210.2 (477.7)	134.1 (304.8)	345.2 (784.7)	334.5 (760.2)	78.2 (177.7)	60.7 (138.1)
GACO 383	MB	66.6 (150.5)	71.8 (162.2)	*ND	138.4 (312.8)	138.7 (313.4)	58.0 (131.0)	39.8 (90.0)
	PNP	56.4 (188.4)	93.1 (311.1)	62.7 (209.4)	212.2 (708.8)	209.6 (700.2)	57.4 (191.8)	20.7 (69.2)
	P	52.3 (118.8)	85.6 (194.6)	84.2 (191.5)	222.1 (504.9)	224.2 (509.7)	51.3 (116.6)	19.3 (43.9)

\*MB - Methylene blue \*P - phenol, \*PNP - *p*-nitrophenol, \*ND – not detected

$$*SA(m^2/g) = \frac{q \text{ (mg/g)} \times 6.022 \times 10^{23} \times \text{cross sectional area of adsorbate (nm}^2\text{)}}{\text{Molecular weight of adsorbate}}$$

### 3.5.9.1 John - Sivanandan Achari Isotherm for Phenol, *p*-Nitrophenol and Methylene Blue Adsorption on GACZR 1273 at Temperatures

John – Sivanandan isotherm plots are made at temperature 283 – 323 K. Distinct phase changes in the plot with respect to adsorption of phenol, *p*-nitrophenol and methylene blue on carbon GACZR 1273 are given in Table 3.15. The temperature rise shows a systematic quantitative enhancement in adsorption.

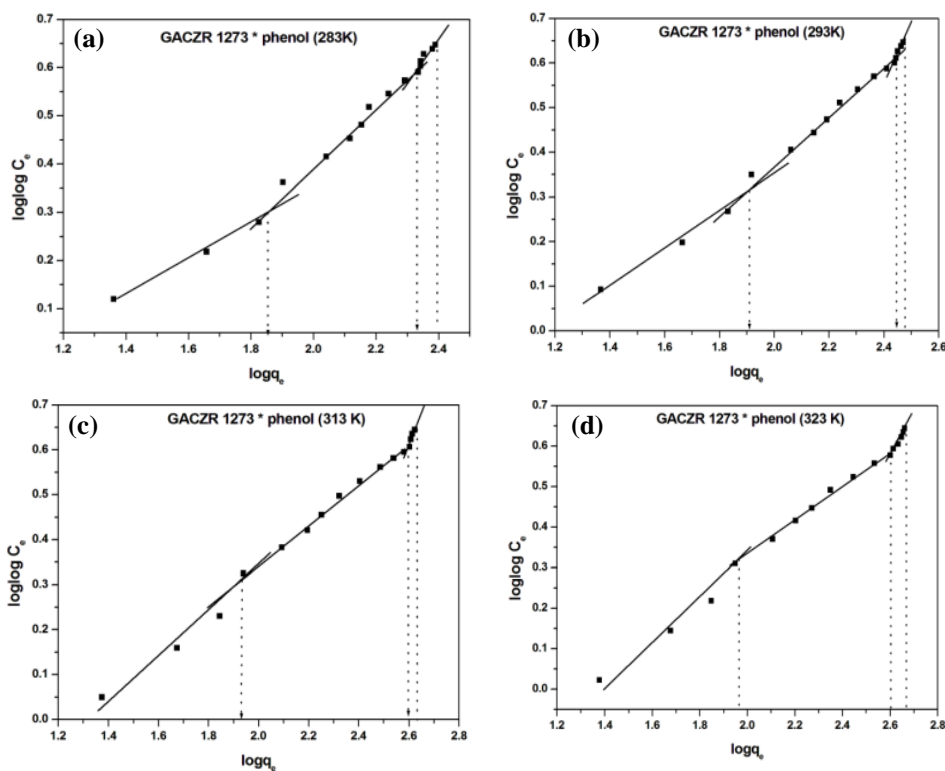


**Figure 3.39:** John –Sivanandan Achari isotherm plot for phenol adsorption on GACZR 1273 at temperatures (a) 283K (b) 293K (c) 313K and (d) 323K

For phenol adsorption on carbon GACZR 1273 in *phase I* show only a slight enhancement from 71.23 mg/g to 91.76 mg/g by rising the solution temperature from 283K to 323K. However, in *phase II* shows significant enhancement from 143.15 mg/g to 308.9 mg/g by rising the solution temperature.

This is because more and more adsorption sites are activated and becomes accessible with increase of temperature. Further increment of solution temperature causes the diffusion of more phenol molecules into wider pores. As there are few wider pores available for effective uptake of phenol at lower solution temperature (32.77 mg/g at 283K) however, as the solution temperature increases more phenol molecule get diffused into wider pores and adsorption in *phase III* increased to 65.09 mg/g at 323K.

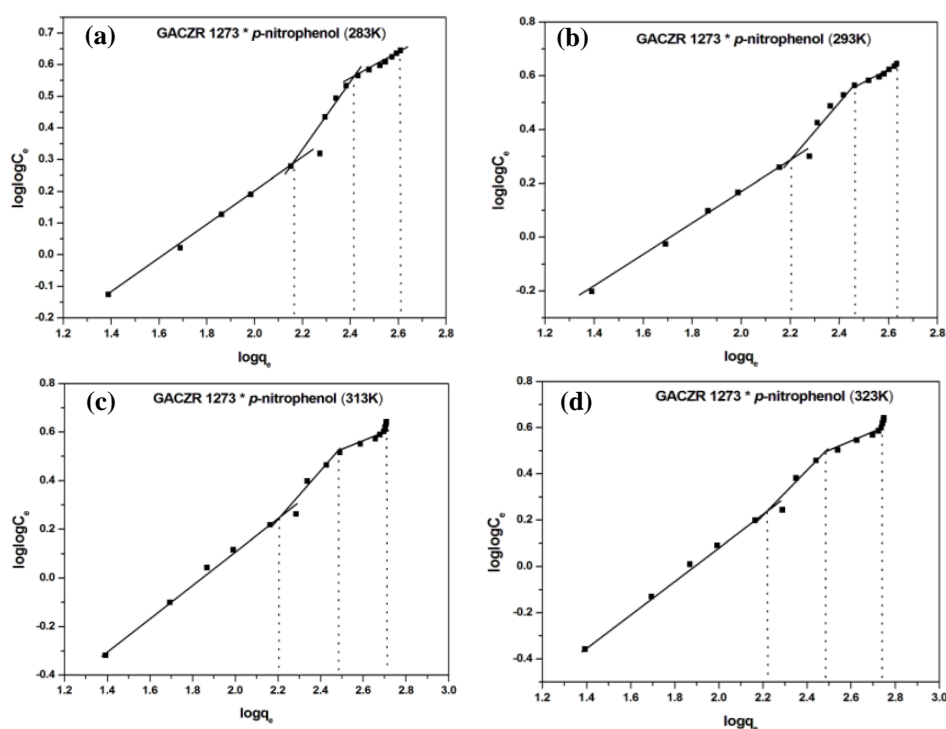


**Figure 3.40:** John –Sivanandan Achari isotherm for *p* - nitrophenol adsorption on GACZR 1273 at temperatures (a) 283 K (b) 293 K (c) 313 K and (d) 323 K

Compared to phenol molecules, the amount of *p*-nitrophenol adsorbed in the first phase is two times more than that of phenol molecule. It indicates that  $\pi - \pi$  interaction between *p*-nitrophenol and GACZR 1273 is more prominent than phenol molecule. Quantity of *p*-nitrophenol adsorbed in first phase increases from 146.55 mg/g to 163.53 mg/g, whereas in *phase II* it increases from 113.9 mg/g to

142.16 mg/g and in *phase III* quantity of adsorption increased from 145.41 mg/g to 242.30 mg/g by rising the solution temperature from 283 K to 323 K. It can be seen that as the solution temperature increases more *p*-nitrophenol molecule get diffused into wider pores.

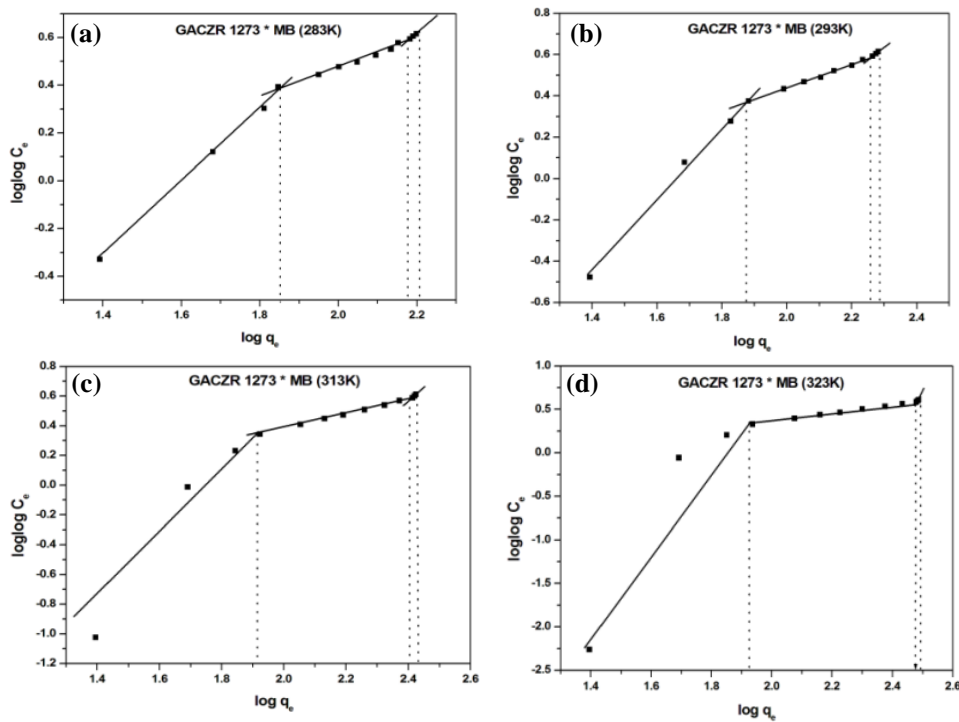


**Figure 3.41:** John –Sivanandan Achari isotherm for methylene blue (MB) adsorption on GACZR 1273 at temperatures (a) 283 K (b) 293 K (c) 313 K and (d) 323 K

Compared to phenol and *p*-nitrophenol adsorption  $q_T$  (J), methylene blue (MB) adsorption is less favoured. Small micropores hinder the entry of methylene blue molecules inside micropores due to size restrictions. This pore restriction during adsorption towards large molecules is well indicated by an additional phase for the John-Sivanandan Achari isotherm plots (Figure 3.41).

**Table 3.15:** John - Sivanandan Achari Isotherm parameter for the adsorption of phenol, *p*-nitrophenol and methylene blue on carbon GACZR 1273 at 283 - 323K

Carbon	Temperature (K)	Phenol			<i>p</i> -nitrophenol			Methylene Blue (MB)		
		$q_I$ (J-SA) mg/g (SA m <sup>2</sup> /g)	$q_{II}$ (J-SA) mg/g (SA m <sup>2</sup> /g)	$q_{III}$ (J-SA) mg/g (SA m <sup>2</sup> /g)	$q_I$ (J-SA) mg/g (SA m <sup>2</sup> /g)	$q_{II}$ (J-SA) mg/g (SA m <sup>2</sup> /g)	$q_{III}$ (J-SA) mg/g (SA m <sup>2</sup> /g)	$q_I$ (J-SA) mg/g (SA m <sup>2</sup> /g)	$q_{II}$ (J-SA) mg/g (SA m <sup>2</sup> /g)	$q_{III}$ (J-SA) mg/g (SA m <sup>2</sup> /g)
GACZR 1273	283	71.2 (238.0)	143.2 (478.2)	32.8 (109.5)	146.6 (333.1)	113.9 (258.9)	145.4 (330.5)	71.3 (161.1)	79.0 (178.4)	10.4 (23.5)
	293	80.9 (270.1)	184.0 (614.7)	33.7 (112.6)	159.0 (361.4)	130.6 (296.9)	139.7 (317.6)	75.1 (169.8)	105.5 (238.3)	14.0 (31.7)
	303	85.2 (284.5)	220.3 (735.9)	36.0 (120.2)	159.0 (361.4)	141.8 (322.4)	185.7 (422.2)	79.5 (179.7)	126.4 (285.7)	21.2 (47.9)
	313	86.2 (288.0)	297.5 (993.9)	43.0 (143.6)	161.2 (366.5)	142.3 (323.5)	210.9 (479.3)	81.8 (184.9)	172.0 (388.8)	14.6 (33.0)
	323	91.8 (306.6)	309.0 (1032)	65.1 (217.5)	163.5 (371.7)	142.2 (323.1)	242.3 (550.8)	83.9 (189.6)	213.3 (482.0)	13.9 (31.4)

### 3.6 Comparison of Adsorption Isotherms for the Adsorption of Phenol, *P*-Nitrophenol and Methylene Blue on GACZR 1273

In order to assess the different isotherms and their ability to correlate with experimental results, the theoretical isotherm plot has been made by the experimental data. The predicted Freundlich, Langmuir, D-R, J-SA isotherm equation for phenol, *p*-nitrophenol and methylene blue (MB) onto GACZR 1273 is given in the Table 3.16.

Figure 3.42(a) shows the different isotherm curve for phenol onto GACZR 1273 at a constant solution temperature of 30<sup>0</sup>C along with experimental data. It is plotted in the form of an amount adsorbed ( $q_e$ ) per unit mass of GACZR 1273, against the concentration of phenol remaining in solution ( $C_e$ ). It was observed that equilibrium data are well represented by Langmuir and John – Sivanandan Achari isotherm compared to Freundlich and Dubinin – Radushkevich isotherm

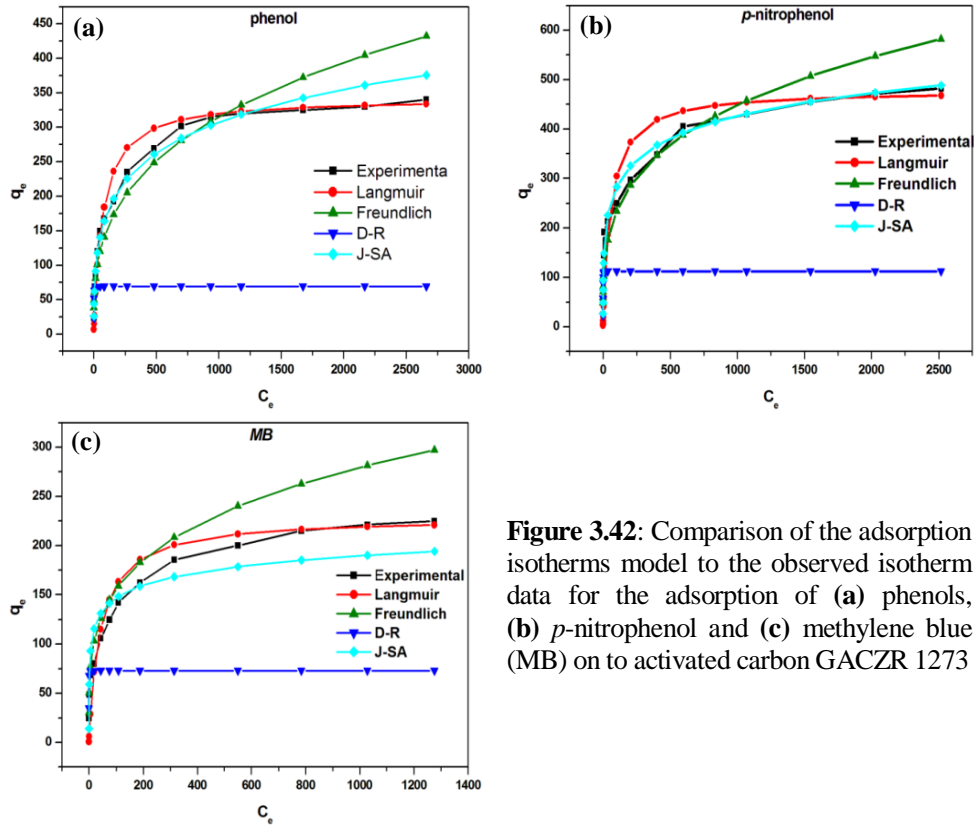


**Figure 3.42:** Comparison of the adsorption isotherms model to the observed isotherm data for the adsorption of (a) phenols, (b) *p*-nitrophenol and (c) methylene blue (MB) on to activated carbon GACZR 1273

Comparison of the model fit of various isotherms to the observed isotherm data for the adsorption of *p*-nitrophenols onto activated carbon GACZR 1273 is given in the Figure 3.42(b). It shows the best fit of equilibrium data in the Langmuir isotherm equation and J-SA isotherm equation. It indicates that adsorption of *p*-nitrophenol on GACZR 1273 confirms equilibrium data are well represented by these two isotherm equations.

Comparison of the model fit of various isotherms to the observed isotherm data for the adsorption of methylene blue (MB) onto activated carbon GACZR 1273 is given in the Figure 3.42(c). It indicates that in the entire concentration range of equilibrium data of methylene blue best fitted to Langmuir isotherm model.

**Table 3.16:** The predicted non linear form of Freundlich, Langmuir, Dubinin – Radushkevich, and John –Sivanandan Achari isotherm equations for GACZR 1273

Isotherms	Phenol	<i>p</i> -nitrophenol	Methylene Blue
Langmuir	$q_e = \frac{C_e \times 4.83}{1 + 0.0141C_e}$	$q_e = \frac{C_e \times 8.39}{1 + 0.0175C_e}$	$q_e = \frac{C_e \times 5.29}{1 + 0.02319C_e}$
Freundlich	$q_e = 33.85 \times C_e^{0.323}$	$q_e = 63.97 \times C_e^{0.282}$	$q_e = 42.32 \times C_e^{0.2451}$
*D-R	$q_e = 69.21 \times e^{0.6221\varepsilon^2}$	$q_e = 96.47 \times e^{0.1286\varepsilon^2}$	$q_e = 61.07 \times e^{0.0374\varepsilon^2}$
*J-SA	$q_e = e^{\frac{\log\log C_e + 0.6487}{0.5028}}$	$q_e = e^{\frac{\log\log C_e + 1.246}{0.7028}}$	$q_e = e^{\frac{\log\log C_e + 1.9653}{1.13}}$

\*D-R Dubinin-Radushkevich isotherm \*J-SA John-Sivanandan Achari isotherm

### 3.7 Adsorption Kinetic Studies

In order to examine the controlling mechanism of adsorption processes, including mass transfer and chemical reaction, a suitable kinetic model is applied and analyzed.

#### 3.7.1 Kinetic Studies of Phenol, *P*-Nitrophenol and Methylene Blue

Adsorption kinetics expressed as the adsorbate removal rate that controls the residence time of the molecules in solid-solution interface. The procedure used for kinetic tests was identical to that used for adsorption equilibrium experiments. The kinetic studies were carried out at a fixed initial concentration of 250 mg/L with an adsorbent dosage of 0.05 g in 50 ml solution of adsorbate at five different temperatures.

The aqueous samples of phenol and *p*-nitrophenol were taken at time intervals of 10 - 360 min (10 min, 20 min, 30 min, 40 min, 60 min, 120 min, 180 min, 240 min, and 360 min). Whereas, methylene blue adsorption taken at time intervals of 10 - 480 min. The concentrations of phenol, *p* - nitrophenol and methylene blue (MB) were measured by UV-Visible spectrophotometer at their corresponding wavelength. The uptake of phenol, *p*-nitrophenol and methylene blue at time *t* was calculated by using the Equation (3.30).

$$q_t = \frac{(C_0 - C_t)V}{M} \tag{3.30}$$

The three basic models such as pseudo-first order model [51], pseudo-second order model [52] and intraparticle diffusion model [53] were applied to analyze the kinetic data of phenol, *p*-nitrophenol and MB adsorption on GACZR 1273, GAC 383 and GACO 383.

### 3.7.1.1 Pseudo-First Order Kinetic Study

The integral form of the pseudo-first order equation proposed by Lagergren to describe the adsorption system expressed as follows [51] [54].

$$\log(q_e - q_t) = \log q_e - \frac{K_1 t}{2.303} \quad (3.31)$$

Where  $q_e$  and  $q_t$  (mg/g) are the amount of adsorbate (phenol, *p*-nitrophenol and methylene blue) adsorbed at the equilibrium and at time  $t$  (min), respectively and  $K_1$  ( $\text{min}^{-1}$ ) is the rate constant. The values of  $K_1$  and  $q_e$  were calculated from the slopes and intercepts of  $\log(q_e - q_t)$  against the  $t$  plots.

### 3.7.1.2 Pseudo-Second Order Kinetic Study

The adsorption kinetics may also be described by a pseudo-second order kinetic model. The linearized integral form of the model is represented as

$$\frac{t}{q_t} = \frac{1}{K_2 q_e^2} + \frac{1}{q_e} t \quad (3.32)$$

Where  $q_e$  and  $q_t$  (mg/g) are the amount adsorbed at the equilibrium and at time  $t$  (min), respectively, and  $K_2$  is the pseudo-second order rate constant of adsorption ( $\text{g/mg min}$ ). The initial adsorption rate,  $h$  ( $K_2 q_e^2$ ), has been widely used for evaluation of the adsorption rates. This model is based on the assumption that the rate of occupation of adsorption sites is proportional to the square of the number of unoccupied sites [55, 56].

### 3.7.1.3. Intraparticle Diffusion Model

To predict the rate limiting step in an adsorption process it is important to understand the mechanism associated with it. The intra-particle diffusion model is used to study the functioning of diffusion controlled adsorption system [57].



The intra-particle diffusion equation is expressed in the following form

$$q_t = K_{id} t^{1/2} + C \quad (3.33)$$

Where  $q_t$  is the amount adsorbed (mg/g) at time,  $t$  (min),  $K_{id}$  is the intra particle diffusion coefficient and  $C$  represent the thickness of the boundary layer.

### 3.7.2 Kinetic Study of Phenol on GACZR 1273, GAC 383, and GACO 383 at Temperatures

The first order kinetic plots of phenol adsorption onto three adsorbents (GAC 383, GACO 383 and GACZR 1273) at 283, 293, 303, 313 and 323 K temperatures are given in Figure 3.43(a)–(c).

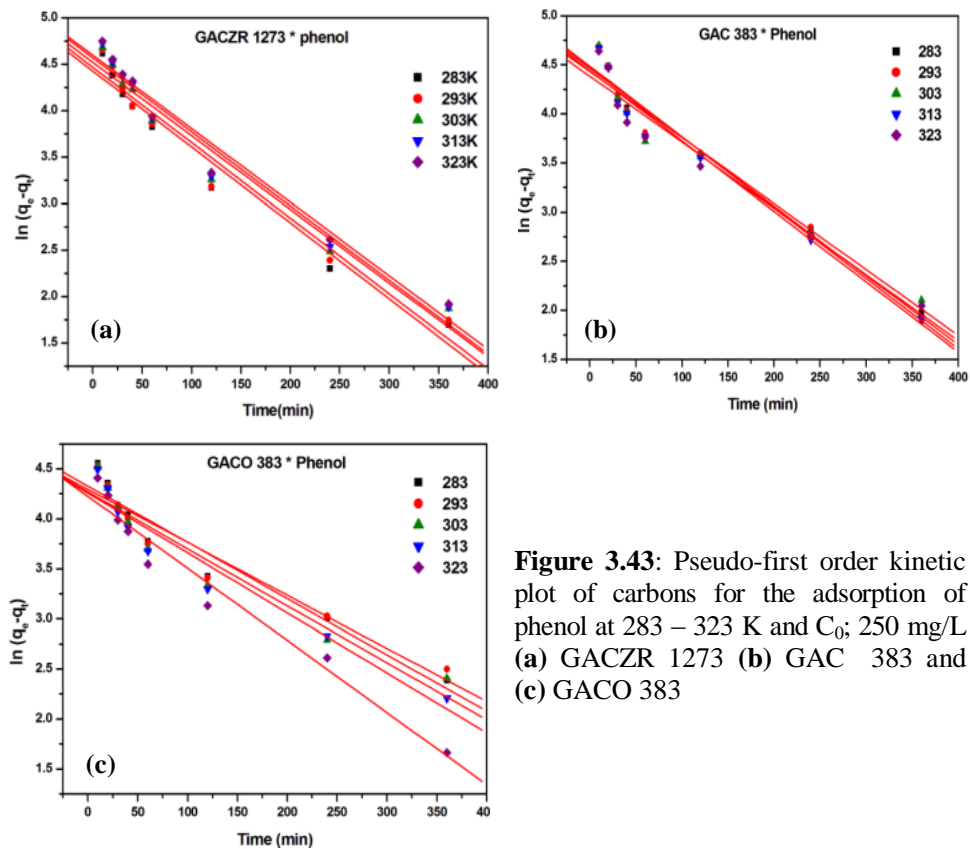


**Figure 3.43:** Pseudo-first order kinetic plot of carbons for the adsorption of phenol at 283 – 323 K and  $C_0$ ; 250 mg/L (a) GACZR 1273 (b) GAC 383 and (c) GACO 383

Conformity between the experimental data  $q_e (exp)$  and the model predicted data  $q_e (cal)$  was expressed by the correlation co-efficient. Theoretical  $q_e$  value obtained from the pseudo-first order kinetic model doesn't vary with  $q_e$  experimental value. Linear plot shows lower regression co-efficient, this suggest that this adsorption system is not a pseudo-first order reaction. Deviation from straight line can be attributed to the control of boundary layer over phenol adsorption at the initial stages [58]. The percentage of error between the experimental  $q_e (exp)$  and calculated  $q_e (cal)$  of GACZR 1273 shows 43 – 46 %, GAC 383 shows 34 – 58%, and GACO 383 shows 42 – 63 %. The percentage of error is more prominent at higher solution temperatures.

The second order kinetic plots of phenol adsorption onto three adsorbents (GAC 383, GACO 383 and GACZR 1273) at five temperatures are given in Figure 3.44(a)-(c). Kinetic parameters along with correlation co-efficient for pseudo-second order kinetic model are listed in the Table 3.17.

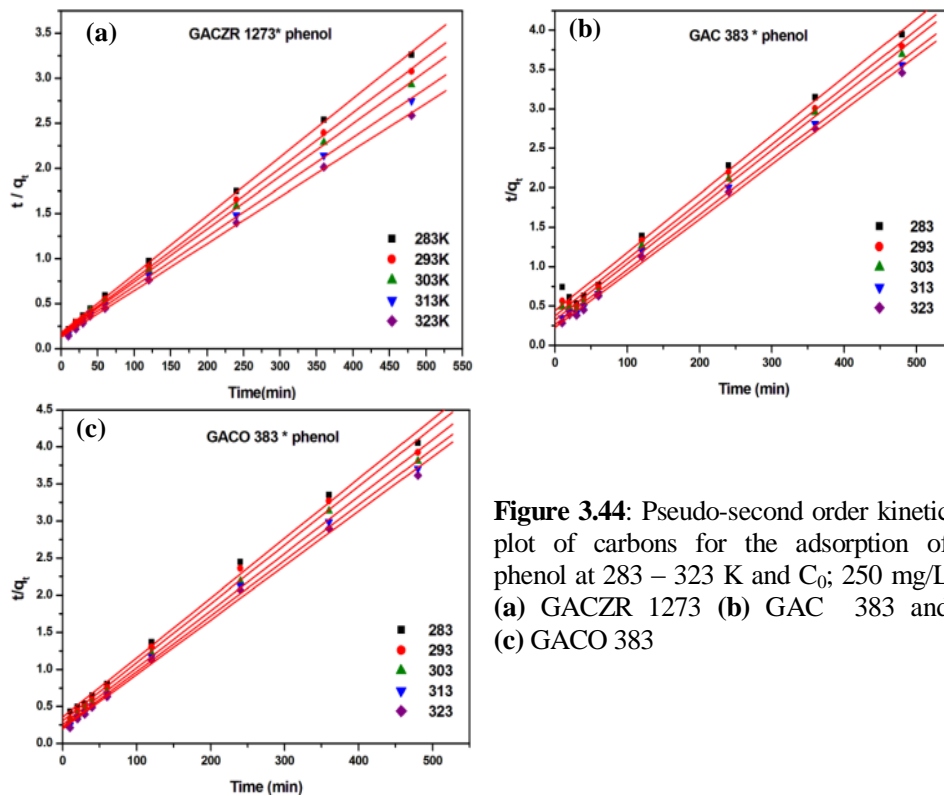


**Figure 3.44:** Pseudo-second order kinetic plot of carbons for the adsorption of phenol at 283 – 323 K and  $C_0$ ; 250 mg/L (a) GACZR 1273 (b) GAC 383 and (c) GACO 383

The correlation coefficient of the second order kinetic model was found to be higher than that of pseudo-first order kinetic model. The calculated  $q_e$  (*cal*) obtained from the pseudo-second order also agree well with the experimental  $q_e$ . The difference between the experimental  $q_e$  and calculated  $q_e$  of pseudo-second order kinetic are GACZR 1273 (3.4 – 5.3 %), GAC 383 (4.3 – 10%), and GACO 383 (2.6 – 5.0 %) for the temperatures studied. The difference between  $q_e$  (*exp*) and  $q_e$  (*cal*) is decreased with rise of temperature for all carbons. These indicate that the adsorption system studied belongs to the second order kinetic model.

An assumption made on pseudo-second order kinetics is that the number of molecules adsorbed on the surface of carbon is proportional to the square of the number of vacant sites. The initial adsorption rate,  $h$  ( $K_2q_e^2$ ) obtained from the intercept of the pseudo-second order plot, has been widely used for evaluation of the adsorption rates. The values of ' $h$ ' increase with rise of temperature for all carbons, indicating that more phenol molecule gets adsorbed on activated carbon with rise of temperature.

Two phases in the intra-particle diffusion plot suggest that the adsorption process proceeds by surface adsorption and intra-particle diffusion. The  $K_{id}$  is the intra-particle diffusion coefficient and  $C$  is the boundary layer effect. Higher the intercept more the contribution of surface adsorption in the rate limiting step. The intra-particle diffusion starts with a rapid transport of adsorbate molecules into macropores and wider mesopores and then, penetrating the smaller meso and micropores at much slower speed.

The plot of  $q_t$  versus  $t^{0.5}$  shows two stages of adsorption with deviation of a straight line from the origin that may be because of the difference in the rate of mass transfer between initial and final stages of adsorption. The initial steep portion is a measure of boundary layer diffusion effects [59] i.e. instantaneous adsorption on the external surface of the carbon. The second linear portion shows a steady increase in adsorption result of intraparticle diffusion effects, i.e. the transfer of adsorbed molecule from the surface to the intra-particle active sites which determine the rate limiting step [60].

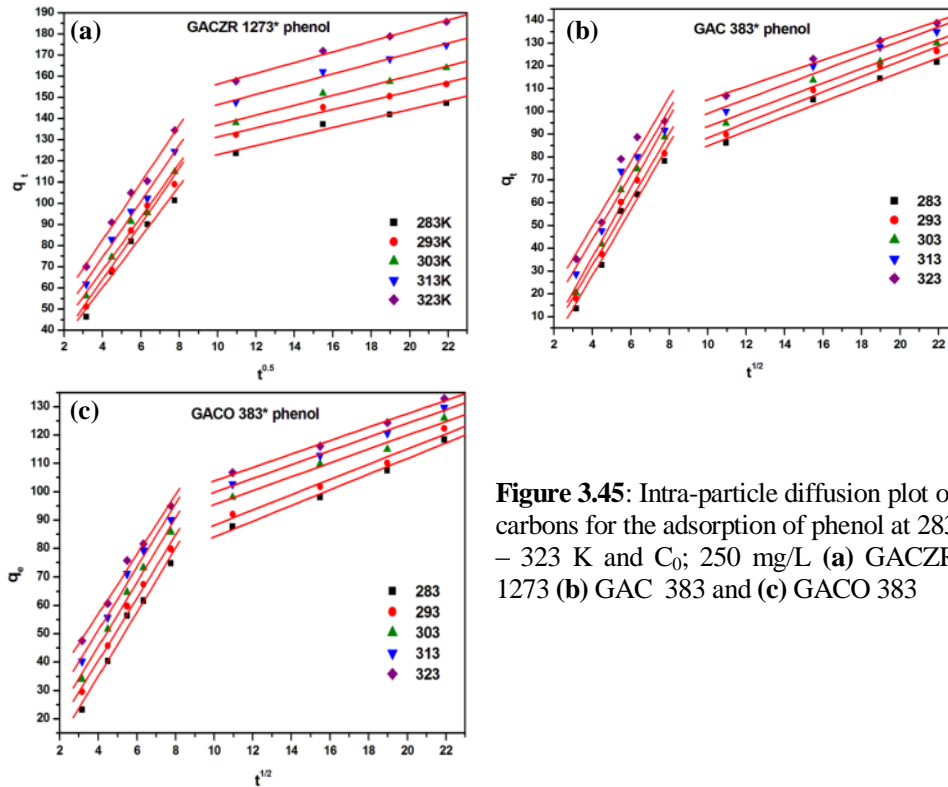


**Figure 3.45:** Intra-particle diffusion plot of carbons for the adsorption of phenol at 283 – 323 K and  $C_0$ : 250 mg/L (a) GACZR 1273 (b) GAC 383 and (c) GACO 383

Slope of the first linear portion is high due to the availability of larger surface area and adsorption sites. The lower slopes of second portion due to the gradual decrease in the concentration of an adsorbate in a solution, which makes the diffusion of adsorbate in to the micropores of the adsorbent, it indicate that intra particle diffusion is slowing down the adsorption process.

The value of  $C$  increases directly with the temperature shows temperature affects both the adsorption capacity and the adsorption mechanism of phenol.

**Table 3.17:** Kinetic parameters of carbons GACZR 1273, GAC 383, GACO 383 for the adsorption of phenol at temperatures ranging from 283 - 323K [ $C_0 = 250$  mg/L]

Carbons	T (Kelvin)	$q_e$ (exp) mg/g	Pseudo-first order kinetics			Pseudo-second order kinetics				Intra-particle diffusion					
			$q_e$ (cal) mg/g	$K_1 \times 10^4$ min <sup>-1</sup>	R <sup>2</sup>	$q_e$ (cal) mg/g	$K_2 \times 10^5$ g mg <sup>-1</sup> min <sup>-1</sup>	$h$ mg g <sup>-1</sup> min <sup>-1</sup>	R <sup>2</sup>	$K_{id1}$ mg/g min <sup>1/2</sup>	C <sub>1</sub>	R <sup>2</sup>	$K_{id2}$ mg/g min <sup>1/2</sup>	C <sub>2</sub>	R <sup>2</sup>
GACZR 1273	283	147	84	82	0.98	154	23	5.6	0.99	14	6	0.99	1.8	109	0.98
	293	156	87	81	0.98	164	24	6.4	0.99	14	9	0.99	2.2	110	0.99
	303	164	92	79	0.98	171	24	7.1	0.99	14	16	0.99	2.2	118	0.99
	313	175	96	80	0.98	182	25	8.1	0.99	13	28	0.99	2.2	127	0.99
	323	186	99	79	0.98	192	25	9.3	0.99	14	33	0.99	2.2	138	0.99
GAC 383	283	122	87	71	0.98	135	12	2.3	0.99	15	-30	0.98	3.2	53	0.99
	293	126	89	72	0.98	138	14	2.7	0.99	14	-25	0.98	3.4	55	0.99
	303	130	84	67	0.97	140	16	3.1	0.99	15	-25	0.98	3.2	62	0.99
	313	135	85	72	0.98	143	18	3.8	0.99	14	-13	0.97	3.2	67	0.98
	323	139	80	67	0.97	145	21	4.4	0.99	14	-7	0.96	2.9	76	0.99
GACO 383	283	118	76	56	0.97	125	18	2.8	0.99	11	-10	0.9	2.8	56	0.99
	293	122	73	53	0.96	126	21	3.3	0.99	11	-4	0.99	2.7	61	0.98
	303	126	71	57	0.96	130	23	3.9	0.99	11	0	0.99	2.4	71	0.98
	313	130	70	60	0.97	134	25	4.5	0.99	11	7	0.99	2.4	76	0.99
	323	133	69	61	0.97	136	27	5.0	0.99	11	15	0.99	2.4	80	0.99

### 3.7.3 Kinetic Study of *P*-Nitrophenol on GACZR 1273, GAC 383, and GACO 383 at Temperatures

The first order kinetic plots of *p*-nitrophenol adsorption onto three adsorbents (GAC 383, GACO 383 and GACZR 1273) at five temperatures are given in Figure 3.46 (a)–(c). The adsorption capacity at equilibrium obtained from both experimentally  $q_e(exp)$  and kinetic model  $q_e(cal)$  are given in Table 3.18. It shows the percentages of difference between these two values are more prominent with increasing of temperature. For GACZR 1273 shows 25 – 46 %, GAC 383 shows 24 – 35%, and GACO 383 shows 31 – 44 %. Rate constant  $K_1$  obtained from the slope of the plot for GACZR 1273 increases from  $78.9 \times 10^{-4} \text{ min}^{-1}$  to  $84.2 \times 10^{-4} \text{ min}^{-1}$  with rise of temperature from 283 K to 323 K.

The deviation of straight line plot and non conformity between the experimental data and the model predicted values indicate that, the adsorption of *p*-nitrophenol on GAC 383, GACO 383 and GACZR 1273 is not following a pseudo-first order reaction similar to that of phenol for all temperatures studied.

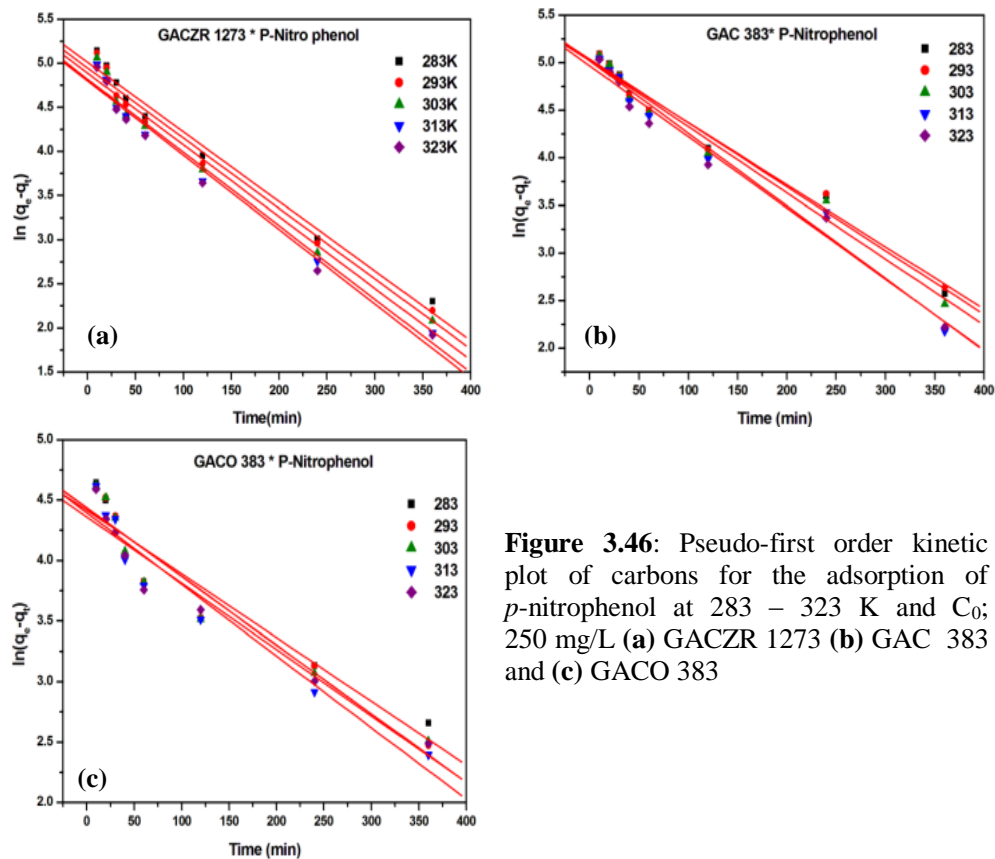


**Figure 3.46:** Pseudo-first order kinetic plot of carbons for the adsorption of *p*-nitrophenol at 283 – 323 K and  $C_0$ ; 250 mg/L (a) GACZR 1273 (b) GAC 383 and (c) GACO 383

Figure 3.47 (a)-(c) shows the second order kinetic plots of *p*-nitrophenol adsorption onto three adsorbents (GAC 383, GACO 383 and GACZR 1273) at five temperatures. The rate constant  $K_2$ , initial adsorption rate  $h$ , and predicted  $q_e$  can be calculated from the plot and the corresponding linear correlation coefficient are given in the Table 3.18.

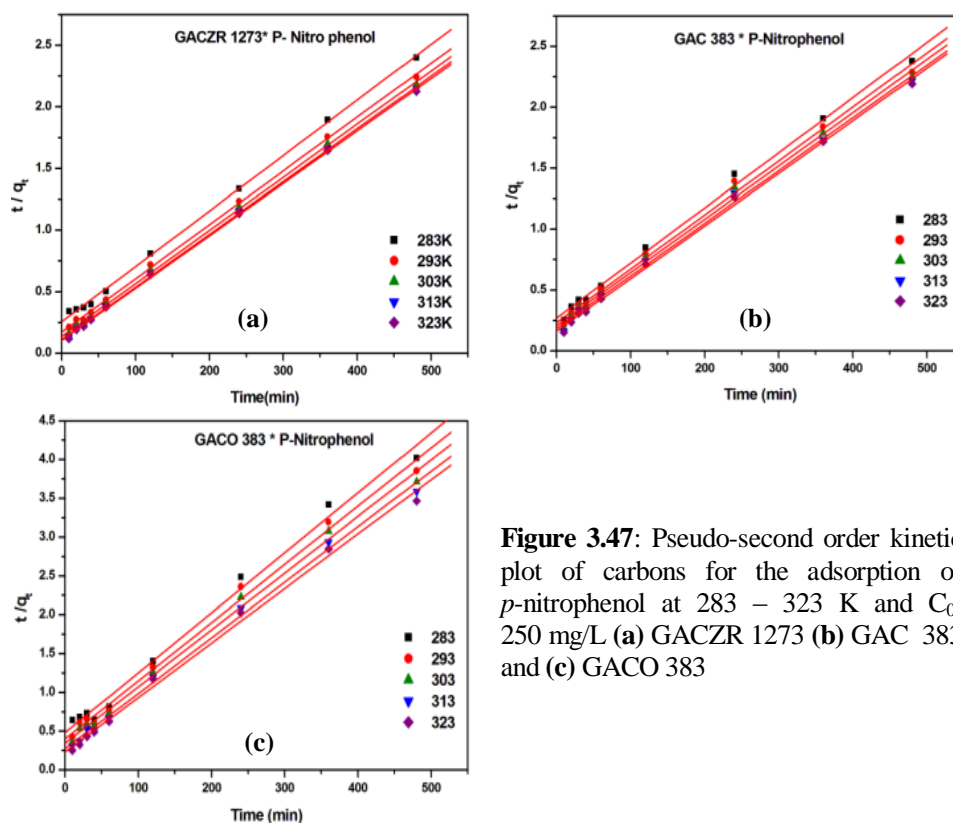


**Figure 3.47:** Pseudo-second order kinetic plot of carbons for the adsorption of *p*-nitrophenol at 283 – 323 K and  $C_0$ ; 250 mg/L (a) GACZR 1273 (b) GAC 383 and (c) GACO 383

All the three activated carbons show high correlation coefficient (close to unity) for second order kinetic model compared to pseudo-first order kinetics. It is confirmed that the adsorption of *p*-nitrophenol by the new activated carbons followed pseudo second order kinetics. The calculated  $q_e$  obtained from pseudo-second order also agrees well with the experimental  $q_e$ . The percentages of difference between the experimental  $q_e$  and calculated  $q_e$  of pseudo-second order kinetic at five different temperatures varies as GACZR 1273 (4.1 -11.1 %), GAC 383 (5.9 -10 %), and GACO 383 (2.8 - 8.4 %). This shows adsorption system studied belongs to the second order kinetic model. The values of ‘*h*’ followed the trend GACZR 1273 > GAC 383 > GACO 383 indicating that GACZR 1273 adsorbs *p*-nitrophenol more rapidly than GAC 383 and GACO 383.

The intra-particle diffusion plots of *p*-nitrophenol adsorption onto three adsorbents (GAC 383, GACO 383 and GACZR 1273) from 283 to 323K are given in Figure 3.48(a)–(c) The plots of  $q_t$  against  $t^{1/2}$  at different temperature showed multi-linearity with two steps occurred during the adsorption process.

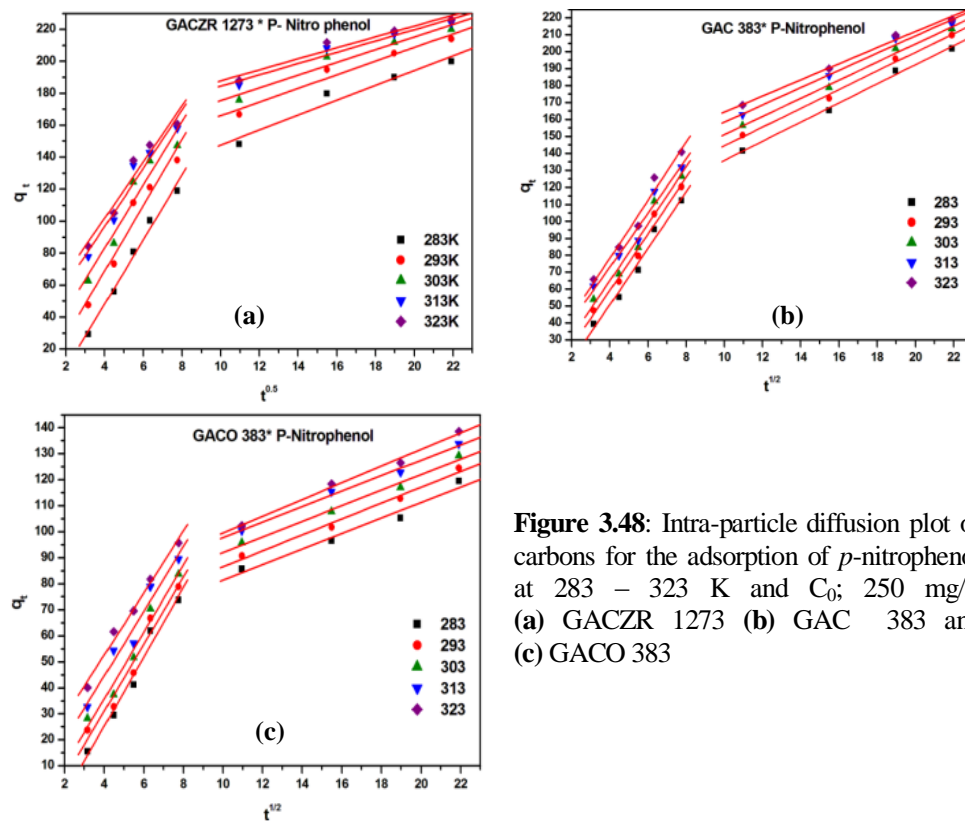


**Figure 3.48:** Intra-particle diffusion plot of carbons for the adsorption of *p*-nitrophenol at 283 – 323 K and  $C_0$ ; 250 mg/L (a) GACZR 1273 (b) GAC 383 and (c) GACO 383

The initial steep portion is due to the instantaneous adsorption of *p*-nitrophenol on the external surface and the second step is the gradual adsorption stage, where intra-particle diffusion is the rate controlling. The larger slopes of the initial step sections indicate that the rate of *p*-nitrophenol adsorption is higher in the beginning due to the instantaneous availability of larger surface area and adsorption sites. The lower slope of the second portion is due to the decreased concentration gradient which makes the diffusion of *p*-nitrophenol ions into the micropores of the adsorbent. The two steps of the process suggested that, the



intra-particle diffusion is not only the rate controlling step for the adsorption of *p*-nitrophenol on GAC 383, GACO 383 and GACZR 1273.

**Table 3.18:** Kinetic parameters of carbons GACZR 1273, GAC 383, GACO 383 for the adsorption of *p*-nitrophenol at temperatures ranging from 283 - 323K [ $C_0=250$  mg/L]

Carbons	T (Kelvin)	$q_e$ (exp) (mg/g)	Pseudo-first order			Pseudo-second order			Intra-particle diffusion						
			$q_e$ (cal) (mg/g)	$K_1 \times 10^4 \text{ min}^{-1}$	$R^2$	$q_e$ (cal) (mg/g)	$K_2 \times 10^5 \text{ gm}^{-1} \text{ min}^{-1}$	$R^2$	$h \text{ mg g}^{-1} \text{ min}^{-1}$	$K_{id1} \text{ mg/g min}^{1/2}$	$C_1$	$R^2$	$K_{id2} \text{ mg/g min}^{1/2}$	$C_2$	$R^2$
GACZR 1273	283	200	150	79	0.98	222	8	0.99	3.9	20	-33	0.99	5	101	0.95
	293	214	141	80	0.98	229	11	0.99	5.9	21	-14	0.95	4	123	0.96
	303	220	133	81	0.98	232	14	0.99	7.4	20	4	0.93	4	135	0.95
	313	224	124	83	0.98	234	17	0.99	9.0	18	24	0.95	4	149	0.96
	323	226	121	84	0.98	235	18	0.99	9.7	18	32	0.95	3	154	0.95
GAC 383	283	202	154	67	0.98	221	8	0.99	3.7	17	-16	0.98	6	80	0.99
	293	210	152	65	0.98	226	9	0.99	4.3	17	-8	0.98	5	89	0.99
	303	213	151	69	0.98	229	9	0.99	4.8	17	-2	0.97	5	98	0.99
	313	217	151	76	0.98	232	10	0.99	5.5	16	9	0.96	5	108	0.99
	323	219	143	75	0.98	232	12	0.99	6.2	17	10	0.97	5	117	0.99
GACO 383	283	120	83	53	0.91	130	12	0.99	2.1	13	-28	0.98	3	52	0.97
	293	125	85	57	0.93	133	14	0.99	2.5	13	-21	0.96	3	56	0.99
	303	129	84	57	0.93	137	16	0.99	2.9	13	-16	0.97	3	62	0.99
	313	134	81	59	0.94	140	19	0.99	3.7	12	-5	0.96	3	68	0.99
	323	139	78	55	0.94	143	21	0.99	4.3	12	5	0.99	3	67	0.99

Rate constants ( $K_{id}$ ) and correlation coefficients ( $R^2$ ) were presented in Table 3.18. It was observed that the  $K_{id}$  continuously decreased with increase in temperature for GACZR 1273 and GAC 383.

### 3.7.4 Kinetic Study of Methylene Blue (MB) on GACZR 1273, GAC 383 and GACO 383 at Temperatures

Kinetic studies were performed at five different temperatures. The first order kinetic plots of methylene blue (MB) adsorption onto three adsorbents (GAC 383, GACO 383 and GACZR 1273) at five temperatures are given in Figure 3.49(a)–(c). The parameters  $K_1$ ,  $q_e$ , and the correlation coefficient ( $R^2$ ) are given in Table 3.19.

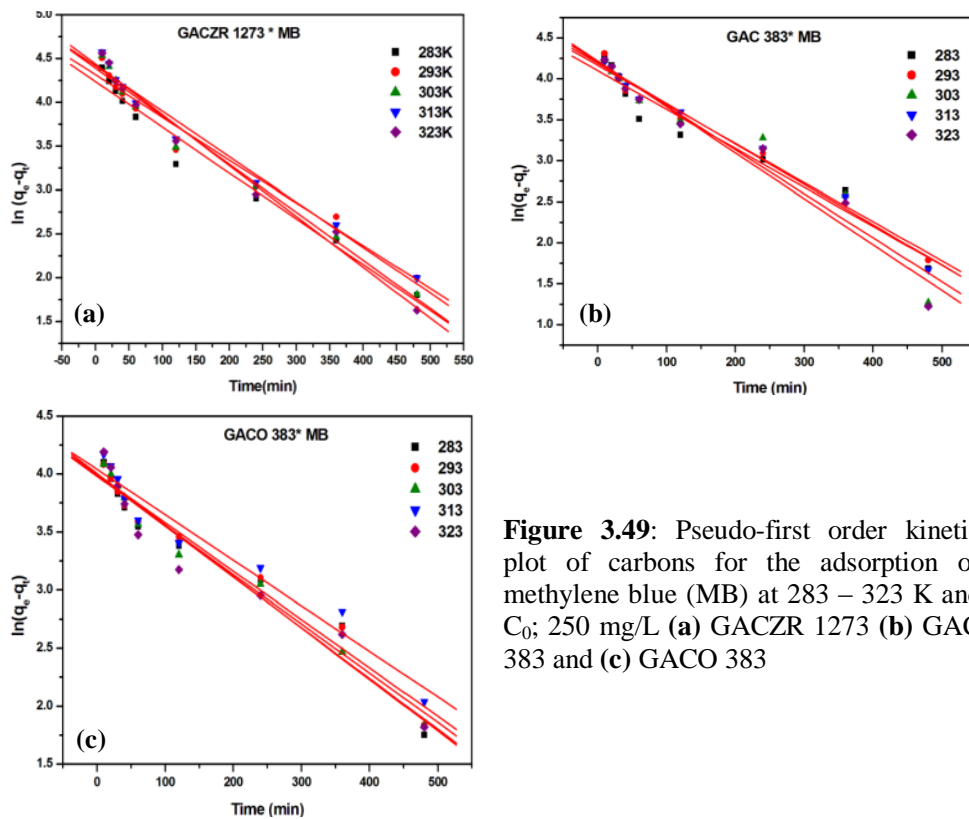


**Figure 3.49:** Pseudo-first order kinetic plot of carbons for the adsorption of methylene blue (MB) at 283 – 323 K and  $C_0$ ; 250 mg/L (a) GACZR 1273 (b) GAC 383 and (c) GACO 383

The correlation coefficient  $R^2$  for pseudo-first order kinetic plot has low value, i.e. equation of Lagergren does not fit well with the whole range of contact time. The difference between the experimental  $q_e$  and calculated  $q_e$  for GACZR 1273 varies 33.6 - 38.0 %, whereas GAC 383 shows 40.9 - 50.9 %, and GACO 383 shows 33.6 - 54.3 %. The percentage difference between the experimental

and calculated  $q_e$  increase with temperature for all the three carbon samples. The large difference between theoretical  $q_e$  and experimental  $q_e$  and lower correlation coefficient of linear plot suggest that this adsorption system is not following pseudo-first order reaction.

The straight line fit of the experimental data of methylene blue (MB) to pseudo-second order kinetic model at different temperatures (Figure 3.50) indicate the favourability of pseudo-second order kinetic model for all adsorbents. The kinetic constant and parameters are given in Table 3.19.

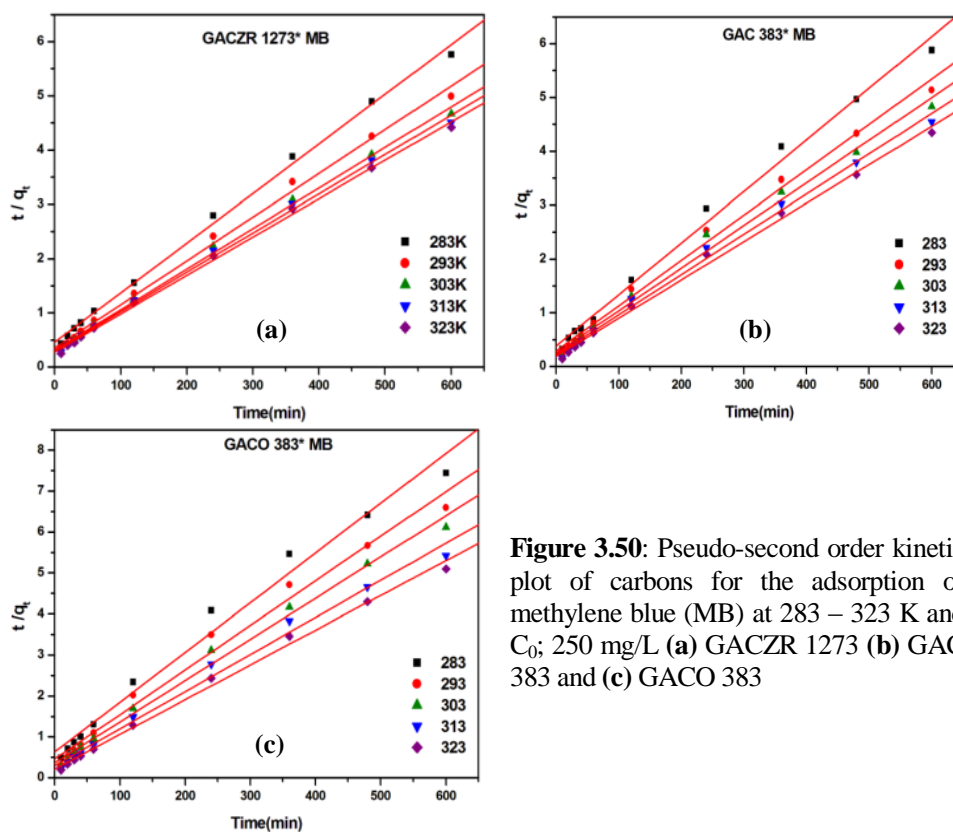


**Figure 3.50:** Pseudo-second order kinetic plot of carbons for the adsorption of methylene blue (MB) at 283 – 323 K and  $C_0$ ; 250 mg/L (a) GACZR 1273 (b) GAC 383 and (c) GACO 383

The correlation coefficient of the second order kinetic model is found to be higher than that of pseudo-first order kinetic model. The calculated  $q_e$  obtained from pseudo-second order agrees well with the experimental  $q_e$ . The difference between the experimental  $q_e$  and calculated  $q_e$  of pseudo-second order kinetic for

carbons at 283 -323 K is given as; GACZR 1273 (2.3 – 5%), GAC 383 (1.6 – 2.3 %) and GACO 383 (0.3 – 2.2 %). Initial adsorption rate indicated by ' $h$ ' increased with temperature due to increased mobility of the methylene blue solute and an enhanced diffusion at higher temperature.

Intra particle diffusion model at different temperature for the adsorption of methylene blue on GACZR 1273, GAC 383 and GACO 383 are shown in the Figure 3.51(a)-(c). The rate constants and correlation coefficient are given in Table 3.19.

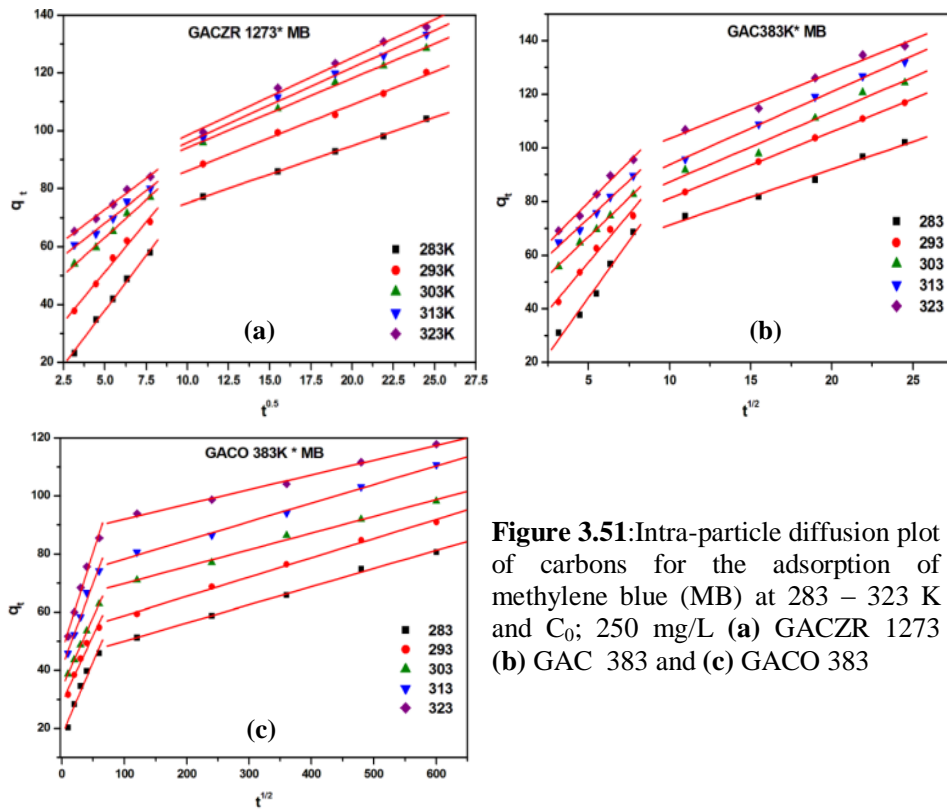


**Figure 3.51:** Intra-particle diffusion plot of carbons for the adsorption of methylene blue (MB) at 283 – 323 K and  $C_0$ ; 250 mg/L (a) GACZR 1273 (b) GAC 383 and (c) GACO 383

Double linear plot indicates that more than one step involved in the adsorption process, i.e. external mass transfer, intra-particle diffusion or both. The external mass transfer is significant only in the early stages of adsorption is represented by the first sharper portion. The second linear portion is the gradual adsorption stage which controlling intra-particle diffusion.

**Table 3.19:** Kinetic parameters of carbons GACZR 1273, GAC 383, GACO 383 for the adsorption of methylene blue at temperatures ranging from 283 - 323K. [ $C_0 = 250$  mg/L]

Carbons	T (Kelvin)	$q_e$ (exp) mg/g	Pseudo-first order			Pseudo-second order				Intra-particle diffusion					
			$q_e$ (cal) mg/g	$K_1 \times 10^4$ min <sup>-1</sup>	$R^2$	$q_e$ (cal) (mg/g)	$K_2 \times 10^5$ g/mg min <sup>-1</sup>	$h$ mg/g min <sup>-1</sup>	$R^2$	$K_{i01}$ mg/g min <sup>1/2</sup>	$C_1$	$R^2$	$K_{i02}$ mg/g min <sup>1/2</sup>	$C_2$	$R^2$
GACZR 1273	283	104	69	52	0.97	109	19	2.2	0.99	7.6	0.10	0.99	2.0	55	0.99
	293	120	75	49	0.97	124	20	3.0	0.99	6.9	16.7	0.99	2.3	63	0.99
	303	128	81	55	0.98	134	21	3.8	0.99	5.2	37.3	0.99	2.4	70	0.99
	313	133	83	52	0.98	136	22	4.1	0.99	4.5	45.8	0.98	2.6	70	0.99
	323	136	84	58	0.98	139	23	4.5	0.99	4.3	51.4	0.99	2.7	72	0.99
GAC 383	283	102	60	48	0.94	104	24	2.6	0.99	8.5	1.80	0.98	2.1	51	0.96
	293	117	64	48	0.98	119	25	3.5	0.99	7.2	21.2	0.97	2.5	56	0.99
	303	124	67	54	0.94	126	25	4.0	0.99	5.8	38.0	1.00	2.6	61	0.94
	313	132	66	49	0.98	134	26	4.6	0.99	5.6	45.8	0.99	2.7	67	0.99
	323	138	68	56	0.96	140	27	5.4	0.99	6.1	49.3	0.98	2.5	79	0.99
GACO 383	283	81	54	42	0.96	82	23	1.6	0.99	0.51	17.6	0.96	0.06	44	0.99
	293	91	54	42	0.97	92	26	2.2	0.99	0.46	28.9	0.96	0.07	52	0.99
	303	98	55	44	0.98	100	28	2.7	0.99	0.48	34.0	1.00	0.06	64	0.99
	313	111	57	39	0.95	110	28	3.4	0.99	0.58	41.0	0.98	0.06	72	0.99
	323	118	54	44	0.94	118	33	4.6	0.99	0.68	46.5	0.98	0.05	87	0.99

The slope of the second stage characterizes the rate parameter corresponding to the intra-particle diffusion, whereas the intercept of this portion is proportional to the boundary layer thickness ( $C$ ) and is found to be increased with temperature.

Larger rate of surface adsorption of methylene blue than intra-particle diffusion is proven by the high value of slope obtained from the first linear portion. The  $R^2$  value for first and second linear portion is  $\approx 0.99$ . This indicates that the adsorption of methylene blue onto GAC 383, GACO 383 and GACZR 1273 can be followed by both external mass transfer and intra-particle diffusion simultaneously.

### 3.8 Thermodynamic Parameters

Thermodynamic behaviour of the adsorption of phenol, *p*-nitrophenol and methylene blue on GAC 383, GACO 383 and GACZR 1273 is investigated using thermodynamic parameters such as change in free energy ( $\Delta G$ ), enthalpy ( $\Delta H$ ), and entropy ( $\Delta S$ ) based on isotherm studies conducted at 283 K – 323 K for every 10 °C step wise rise.

The thermodynamic parameters obtained from Langmuir constant ( $K_L$ ) indicate a chemical, feasible, spontaneous and endothermic adsorption. The thermodynamic parameters obtained from Langmuir constant ( $K_L$ ) are given by Equation (3.34). The  $\Delta H$  and  $\Delta S$  parameters for phenol, *p*-nitrophenol and methylene blue on GAC 383, GACO 383 and GACZR 1273 carbons can be calculated from the slope and intercepts of the plot of  $\ln K_L$  versus  $1/T$  (Figure. 3.51).

$$\ln K_L = \frac{\Delta S}{R} - \frac{\Delta H}{RT} \quad (3.34)$$

The values of  $\Delta H$  and  $\Delta S$  were computed from the slope and intercept of the plot. From the value of  $\Delta H$  and  $\Delta S$  calculated the change in free energy using the following Equation (3.35).

$$\Delta G = \Delta H - T\Delta S \quad (3.35)$$

The free energy change ( $\Delta G$ ) indicates the degree of spontaneity of the adsorption process.  $\Delta H$  explains the nature of adsorption, i.e. whether it is exothermic or endothermic and the value of  $\Delta S$  is the measure of degree of disorder.

**Table 3.20:** Thermodynamic parameters for adsorption of phenol onto GAC 383, GACO 383 and GACZR 1273

Carbon	$\Delta H$ kJ/mol	$\Delta S$ J/mol.K	$\Delta G$ (kJ/mol)				
			283K	293K	303K	313K	323K
GAC 383	2.33	15.32	-2.00	-2.15	-2.31	-2.46	-2.61
GACO 383	3.28	18.20	-1.86	-2.05	-2.23	-2.41	-2.59
GACZR 1273	10.51	47.17	-2.84	-3.31	-3.78	-4.25	-4.73

The value of  $\Delta H$ ,  $\Delta S$  and  $\Delta G$  for the adsorption of phenol are given in Table 3.20. The  $\Delta H$  calculated for phenol adsorption on GAC 383 gives the value of 2.33 kJ/mol, GACO 383 give 3.28 kJ/mol and GACZR 1273 give 10.51 kJ/mol

respectively. The positive  $\Delta H$  of all adsorbents indicates the endothermic nature of adsorption i.e the adsorption of phenol is favoured at higher temperatures it follows the order of GACZR 1273 > GACO 383 > GAC 383. Also, magnitude of  $\Delta H$  gives knowledge on the type of adsorption, which can be either physical or chemical. For all this adsorbent,  $\Delta H$  doesn't exceed the 40 kJ/mol indicate the physisorption process.

The positive  $\Delta S$  suggests the randomness of the adsorption process, also greater stability of an adsorption process with no structural changes at the solid-liquid interface. The magnitude of  $\Delta S$  for GAC is given as GAC 383 (15.32 J/mol.K), GACO 383 (18.20 J/mol.K) and GACZR 1273 (47.17 J/mol.K) respectively. The high positive  $\Delta S$  of GACZR 1273 suggests an increase in the randomness at adsorbate-solution interface during the adsorption process by the impregnation of  $Zr^{4+}$  in GAC.

$\Delta G$  indicates spontaneous adsorption and the degree of spontaneity of the reaction as it is negative. Gibbs free energy change ( $\Delta G$ ) ranges from -2.0 to -2.61 kJ/mol for GAC 383 at temperature from 283 K to 323 K. For GACO 383 it ranges from -1.86 to -2.59 kJ/mol and for GACZR 1273 ranges from -2.84 to -4.726 kJ/mol. The increasing negative value of  $\Delta G$  with temperature indicates an increase in the feasibility of adsorption at higher temperatures due to the increase in number of adsorption sites generated as a result of breaking of some internal bonds near edge of active surface sites of adsorbent [35].

$\Delta H$ ,  $\Delta S$  and  $\Delta G$  for the adsorption of *p*-nitrophenol are given in Table 3.21. The  $\Delta H$  calculated for adsorption of *p*-nitrophenol on GAC are given as; GAC 383 (6.04 kJ/mol), GACO 383 (2.94 kJ/mol) and GACZR 1273 (21.6 kJ/mol) respectively.

**Table 3.21:** Thermodynamic parameters for adsorption of *p*-nitrophenol onto GAC 383, GACO 383 and GACZR 1273

Carbon	$\Delta H$ kJ/mol	$\Delta S$ J/mol. K	$\Delta G$ (kJ/mol)				
			283K	293K	303K	313K	323K
GAC 383	6.04	38.2	-4.77	-5.15	-5.53	-5.92	-6.30
GACO383	2.94	16.4	-1.70	-1.87	-2.03	-2.19	-2.36
GACZR 1273	21.6	89.3	-3.67	-4.56	-5.46	-6.35	-7.24

The thermodynamic parameter of *p*-nitrophenol adsorption on all the three carbons shows the positive value of  $\Delta H$ , which shows 21.6 kJ/mol for zirconium activated carbon same as that of phenol adsorption but comparatively higher than that for phenol adsorption. Positive value of  $\Delta H$  indicates the endothermic nature of adsorption process. This is attributed to an increase in the entropy of the adsorbate due to the dissociation of the molecule during the process of adsorption.

$\Delta S$  for the adsorption of *p*-nitrophenol on zirconium impregnated carbon shows 89.3 J/mol.K which is comparatively higher than for GAC 383 (38.2 J/mol.K) and GACO 383 (16.4 J/mol.K). The high value of  $\Delta S$  indicates degree of disorder for the adsorption of *p*-nitrophenol on GAC increase by modification with zirconium and the degree of disorder for the adsorption of *p*-nitrophenol is comparatively higher than that of phenol.

Gibbs free energy change ( $\Delta G$ ) for the adsorption of *p*-nitrophenol on GAC 383 ranges from -4.77 to -6.30 kJ/mol, for GACO 383 it ranges from -1.70 to -2.36 kJ/mol and for GACZR 1273 this ranges from -3.67 to -7.24 kJ/mol. The negative value of  $\Delta G$  indicates spontaneous adsorption and the degree of spontaneity of the reaction increases with rise of temperature. Higher negative  $\Delta G$  reflects a more energetically favourable adsorption.

**Table 3.22:** Thermodynamic parameters for adsorption of methylene blue (MB) onto GAC 383, GACO 383 and GACZR 1273

Carbon	$\Delta H$ kJ/mol	$\Delta S$ J/mol. K	$\Delta G$ (kJ/mol)				
			283K	293K	303K	313K	323K
GAC 383	6.87	35.60	-3.20	-3.56	-3.92	-4.27	-4.63
GACO383	8.91	40.35	-2.51	-2.91	-3.32	-3.72	-4.12
GACZR 1273	10.44	48.31	-3.23	-3.71	-4.20	-4.68	-5.16

$\Delta H$ ,  $\Delta S$  and  $\Delta G$  for the adsorption of methylene blue are given in Table 3.22. The  $\Delta H$  calculated for methylene blue adsorption gives; GAC 383 (6.87 kJ/mol), GACO 383 (8.91 kJ/mol) and GACZR 1273 (10.44 kJ/mol) respectively. Positive  $\Delta H$  indicates the endothermic nature of the reaction which is an indication of the existence of strong interaction between activated carbon and methylene blue. For the movement of methylene blue through solution and reaching the adsorption sites, it is necessary for them first to become out of their



hydration shell, this process requires enough energy input. Thus the positive  $\Delta H$  indicates that adsorption is increased with temperature [61].

The thermodynamic parameters suggested that the adsorption of methylene blue onto GACZR 1273, GAC 383 and GACO 383 is physisorption, spontaneous and endothermic in nature.

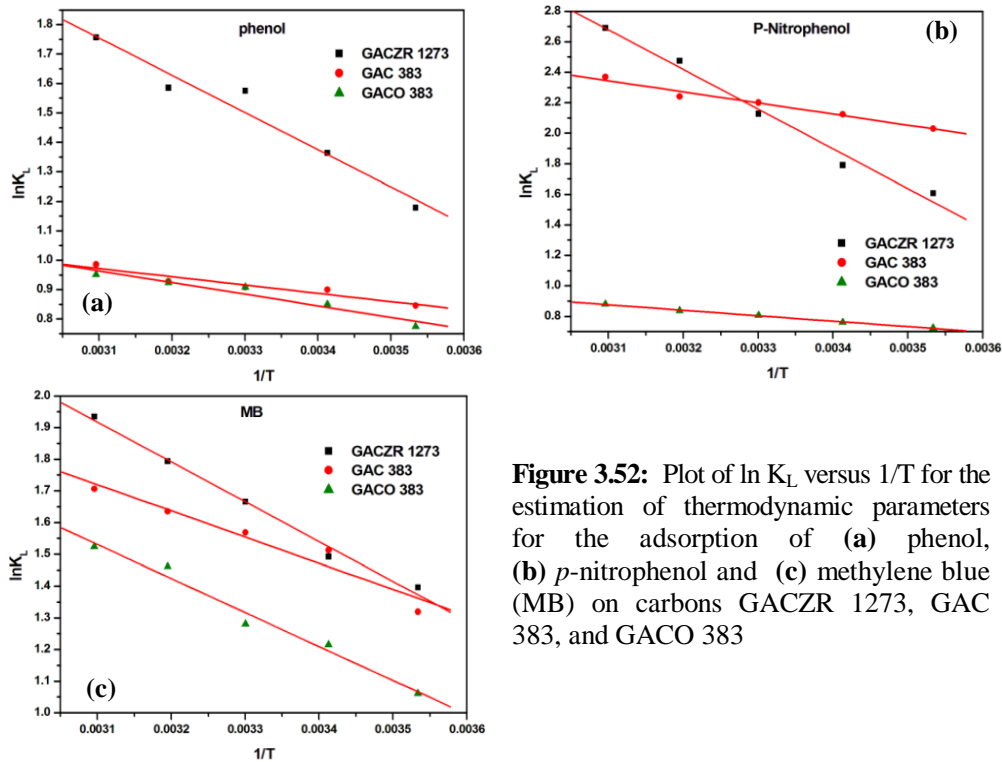


**Figure 3.52:** Plot of  $\ln K_L$  versus  $1/T$  for the estimation of thermodynamic parameters for the adsorption of (a) phenol, (b) *p*-nitrophenol and (c) methylene blue (MB) on carbons GACZR 1273, GAC 383, and GACO 383

### 3.8.1 Thermodynamic Parameters from Distribution Coefficient

To understand how the thermodynamic parameters change with concentration of solution can be explained by plotting thermodynamic equilibrium constant ( $K_D$ )  $\ln K_D$  versus  $1/T$ . Then the slope and intercept of the lines are used to determine the values of  $\Delta H$  and  $\Delta S$  for each concentration of a solution using the equation (3.36).

$$\ln K_D = \frac{\Delta S}{R} - \frac{\Delta H}{RT} \quad (3.36)$$

The distribution coefficient  $K_D$  is defined as the ratio of solute concentration in the adsorbed phase to solute concentration in the equilibrium phase [62].

$$\text{where } K_D = \frac{C_o - C_e}{C_e} \quad (3.37)$$

It is clear that distribution coefficient decreases with increase the equilibrium concentration of adsorbate.

**Table 3.23:** Thermodynamic parameters obtained from plot of  $\ln K_D$  versus  $1/T$  for the adsorption of phenol

$C_0$ mg/L	GACZR 1273 - phenol							GAC 383 - phenol						GACO 383 - phenol							
	$\Delta S$ J/mol.K	$\Delta H$ kJ/mol	$\Delta G$ kJ/mol					$\Delta S$ J/mol.K	$\Delta H$ kJ/mol	$\Delta G$ kJ/mol					$\Delta S$ J/mol.K	$\Delta H$ kJ/mol	$\Delta G$ kJ/mol				
			283	293	303	313	323			283	293	303	313	323			283	293	303	313	323
25	63	12	-6	-6	-7	-8	-8	27	5	-3	-3	-3	-4	-4	32	6	-3	-3	-3	-4	-4
50	63	12	-6	-6	-7	-7	-8	27	5	-3	-3	-3	-4	-4	32	6	-3	-3	-3	-4	-4
75	62	13	-5	-6	-6	-7	-7	26	5	-2	-3	-3	-3	-3	30	6	-2	-3	-3	-3	-3
100	59	13	-3	-4	-4	-5	-6	23	5	-2	-3	-2	-2	-3	27	6	-2	-2	-2	-2	-3
150	58	14	-2	-3	-4	-4	-5	22	5	-1	-1	-2	-2	-2	24	6	-1	-1	-1	-1	-2
200	57	14	-2	-3	-3	-4	-4	19	5	0	-1	-1	-1	-1	21	6	0	-1	-1	-1	-1
250	57	15	-1	-1	-2	-2	-3	18	5	0	0	0	0	-1	18	5	0	0	0	0	0
350	55	16	1	0	-1	-1	-2	16	5	1	0	0	0	0	16	6	1	1	1	1	1
500	53	16	2	1	0	0	-1	14	5	1	1	1	1	1	11	5	2	2	2	2	2
750	49	16	3	2	2	1	1	11	5	2	2	2	2	2	7	5	3	3	3	3	3
1000	48	17	3	3	2	2	1	10	6	3	2	2	2	2	2	4	4	4	4	4	4

The change in  $\Delta H$  for the adsorption of phenol (in the concentration range of 25 mg/L - 1000 mg/L) on GAC are given as follows GACZR 1273 (12 - 16 kJ/mol), GAC 383 (4.9 - 5.5 kJ/mol), and GACO 383 (4.4 - 6.4 kJ/mol), The change in  $\Delta S$  for phenol adsorption on GAC are given as GACZR 1273 (63 - 48 J/mol.K), GAC 383 (27.2 - 10.4 J/mol.K), GACO 383 (32.2 - 2.1 J/mol.K).

The change in  $\Delta H$  values for the adsorption of *p*-nitrophenol (25 mg/L - 1000 mg/L) on GAC varies in the range; GACZR 1273 (13.7 - 16.5 kJ/mol), GAC 383 (9.4 - 10.8 kJ/mol), and GACO 383 (4.3 - 4.7 kJ/mol). The change in entropy  $\Delta S$  for *p*-nitrophenol adsorption on GAC are given as GACZR 1273 (80 - 51 J/mol.K), GAC 383 (64 - 29 J/mol.K), GACO 383 (28 - 2.0 J/mol.K).

**Table 3.24:** Thermodynamic parameters obtained from plot of  $\ln K_D$  versus  $1/T$  for the adsorption of *p*-nitrophenol

$C_0$ mg/L	GACZR 1273 - <i>p</i> -nitrophenol						GAC 383- <i>p</i> -nitrophenol						GACO 383- <i>p</i> -nitrophenol								
	$\Delta S$ J/mol.K	$\Delta H$ kJ/mol	$\Delta G$ kJ/mol					$\Delta S$ J/mol.K	$\Delta H$ kJ/mol	$\Delta G$ kJ/mol					$\Delta S$ J/mol.K	$\Delta H$ kJ/mol	$\Delta G$ kJ/mol				
			283	293	303	313	323			283	293	303	313	323			283	293	303	313	323
25	80	14	-9	-10	-11	-11	-12	64	9	-9	-9	-10	-11	-11	29	5	-3	-4	-4	-4	-5
50	80	14	-9	-10	-11	-11	-12	63	10	-8	-9	-10	-10	-11	26	5	-3	-3	-3	-3	-4
75	79	14	-8	-9	-10	-10	-11	62	10	-7	-8	-9	-9	-10	23	5	-2	-2	-2	-3	-3
100	78	14	-8	-9	-9	-9	-11	59	10	-7	-8	-8	-9	-9	22	5	-2	-2	-2	-2	-3
150	76	15	-7	-8	-8	-9	-10	55	10	-6	-6	-7	-7	-8	17	5	0	0	-1	-1	-1
200	76	15	-6	-7	-8	-9	-10	49	10	-4	-5	-5	-5	-6	16	5	0	0	-1	-1	-1
250	68	16	-3	-4	-4	-5	-6	47	10	-3	-4	-5	-5	-5	16	5	0	0	0	0	0
350	61	16	-1	-2	-2	-3	-4	40	10	-1	-1	-2	-2	-3	12	4	1	1	1	1	1
500	57	16	0	0	-1	-2	-2	35	11	1	0	-1	-1	-1	8	4	2	2	2	2	2
750	53	17	1	1	0	2	-1	31	11	2	2	1	1	1	5	4	3	3	3	3	3
1000	51	17	2	2	1	1	0	29	11	3	2	2	2	2	2	4	4	4	4	4	4

**Table 3.25:** Thermodynamic parameters obtained from plot of  $\ln K_D$  versus  $1/T$  for the adsorption of methylene blue

$C_0$ mg/L	GACZR 1273 - MB						GAC 383- MB						GACO 383- MB								
	$\Delta S$ J/mol.K	$\Delta H$ kJ/mol	$\Delta G$ kJ/mol					$\Delta S$ J/mol.K	$\Delta H$ kJ/mol	$\Delta G$ kJ/mol					$\Delta S$ J/mol.K	$\Delta H$ kJ/mol	$\Delta G$ kJ/mol				
			283	293	303	313	323			283	293	303	313	323			283	293	303	313	323
25	110	21	-11	-12	-13	-14	-15	106	19	-11	-12	-13	-14	-15	105	19	-11	-12	-13	-14	-15
50	97	20	-7	-8	-9	-10	-11	91	18	-7	-8	-9	-10	-11	91	19	-7	-8	-9	-10	-11
75	83	19	-4	-5	-6	-7	-8	79	18	-4	-5	-6	-7	-7	75	18	-3	-4	-4	-5	-6
100	73	19	-2	-3	-4	-4	-5	61	14	-3	-4	-4	-5	-5	67	18	-1	-2	-3	-3	-4
150	68	18	-1	-2	-2	-3	-4	53	14	-1	-1	-2	-3	-3	57	17	0	0	-1	-1	-2
200	64	18	0	-1	-1	-2	-3	44	13	0	0	-1	-1	-2	44	14	1	1	0	0	-1
250	61	18	1	0	-1	-1	-2	35	11	1	0	0	0	-1	36	12	2	1	1	1	0
350	55	17	1	1	0	0	-1	31	10	2	1	1	1	0	28	11	3	2	2	2	1
500	51	17	2	2	1	1	0	26	10	3	2	2	2	2	25	11	4	3	3	3	3
750	47	17	3	3	3	2	2	21	10	4	3	3	3	3	21	10	4	4	4	4	4
1000	44	17	4	4	3	3	2	18	9	4	4	4	4	4	18	10	5	5	5	5	4

The change in  $\Delta H$  values for the adsorption of methylene blue (25 mg/L - 1000 mg/L) on GAC varies in the range; GACZR 1273 (20.6 - 16.6 kJ/mol), GAC 383 (19.3 - 9.3 kJ/mol), and GACO 383 (19.3 - 10.1 kJ/mol). The change in entropy  $\Delta S$  for MB adsorption on GAC are given as GACZR 1273 (109.7 - 44.4 J/mol. K), GAC 383 (105.6 - 18 J/mol. K), GACO 383 (105.3 - 17.6 J/mol. K).

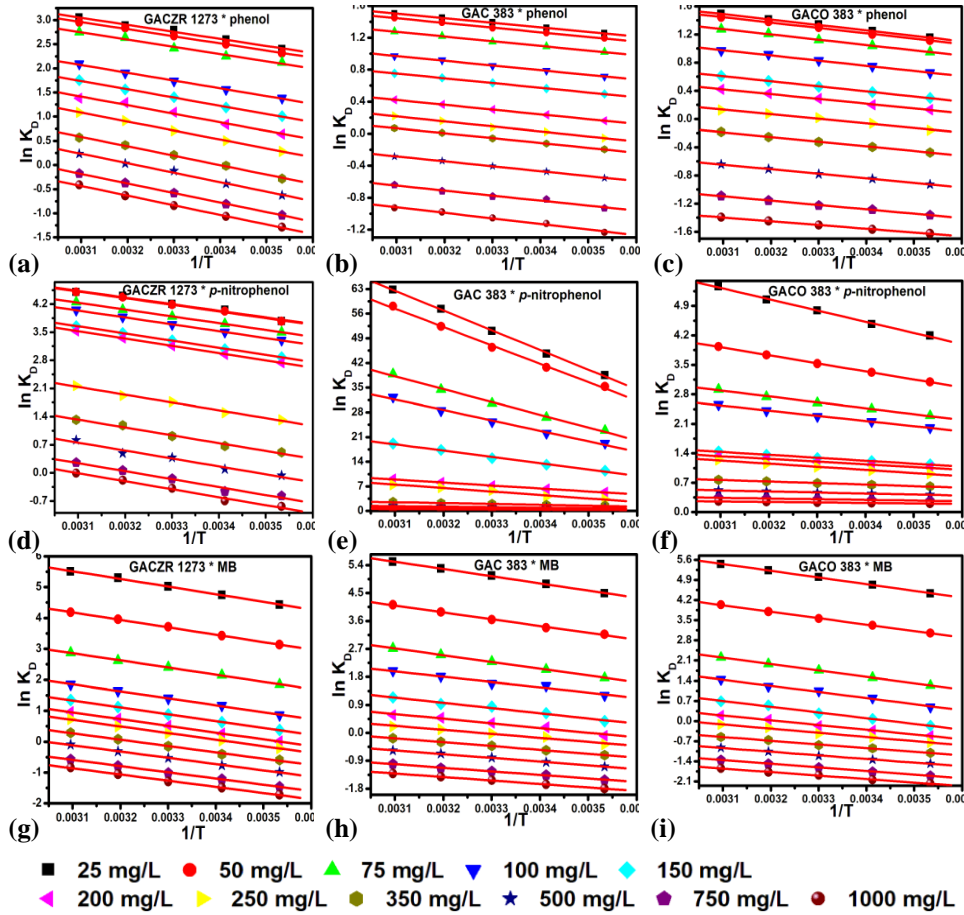


**Figure 3.53:** Plots of  $\ln K_D$  versus  $1/T$  of carbons GACZR 1273, GAC 383 and GACO 383 for the adsorption of (a-c) phenol, (d-f) *p*-nitrophenol and (g-i) methylene blue

For the range of concentrations studied for phenol, *p*-nitrophenol and methylene blue (MB) shows that adsorption system belongs to an endothermic nature. Its value does not vary much more even at wide concentration range. It indicates the physical adsorption. The degree of disorder  $\Delta S$  decreases with increase in solution concentration. Means that the adsorbent – adsorbate interaction decreases with increase of solution concentration. The small value of  $-\Delta G$  with increasing concentration indicate the lower feasibility of adsorption.

### 3.9 Diffusion Coefficient

The effective diffusion co-efficient for adsorption onto activated carbon was computed by assessing particle phase control govern by Fickien law.

$$\ln \left[ \frac{1}{1 - F^2(t)} \right] = \frac{\pi^2 D_e t}{R_a^2} \quad (3.38)$$

Where  $F = q_t / q_e$ ,  $q_t$  and  $q_e$  are the amounts of uptake at time  $t$  and equilibrium respectively.  $R_a$  is the particle radius and  $D_e$  is the diffusion coefficient. From the slope of a straight line plot of  $\ln [1/1-F^2(t)]$  versus  $t$ , the diffusion coefficient  $D_e$  is calculated.

#### 3.9.1 Determination of Diffusivity for Phenol on GACZR 1273, GAC 383, and GACO 383

The diffusion coefficient of adsorption of phenol on GAC 383, GACO 383 and GACZR 1273 are determined from the linear plot of  $\ln [1/1-F^2(t)]$  versus  $t$  which is given in the Figure 3.54(a)-(c) and are listed in the Table 3.25.

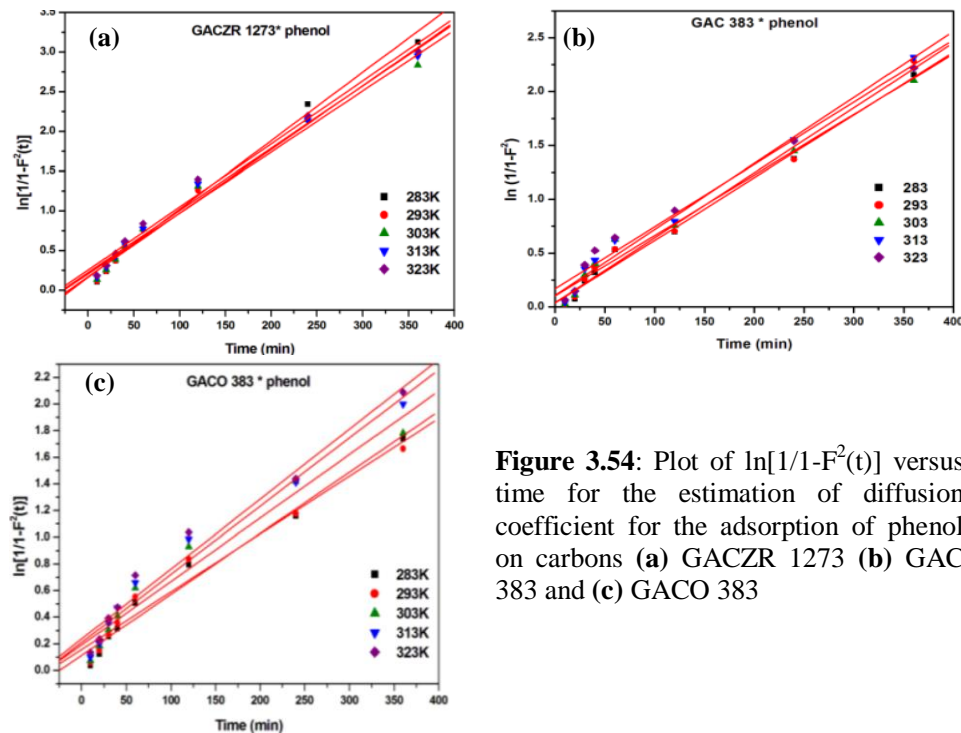


**Figure 3.54:** Plot of  $\ln[1/1-F^2(t)]$  versus time for the estimation of diffusion coefficient for the adsorption of phenol on carbons (a) GACZR 1273 (b) GAC 383 and (c) GACO 383

The effective diffusion coefficient of phenol on GACZR 1273 lies within the range of  $2.14 \times 10^{-10}$  -  $2.41 \times 10^{-10}$  m<sup>2</sup>/s. For GAC 383 it is found to be in the range of  $1.5 \times 10^{-10}$  -  $1.71 \times 10^{-10}$ . For GACO 383 it is  $1.21 \times 10^{-10}$  -  $1.47 \times 10^{-10}$  m<sup>2</sup>/s, respectively, for phenol. The overall pore diffusion rate of GACZR 1273 has high comparing with GAC 383 and GACO 383. This indicates that diffusion of phenol occurs within the pores and electrostatic interaction at the surface of GAC increased by the activation of zirconium. It is known that structural and chemical changes on GAC affected the adsorption process of the phenol [63].

### 3.9.2 Determination of Diffusivity for *p*-Nitrophenol on GACZR 1273, GAC 383 and GACO 383.

The diffusion coefficient of adsorption of *p*-nitrophenol on GAC 383, GACO 383 and GACZR 1273 are determined from the linear plot of  $\ln [1/(1-F^2(t))]$  versus  $t$  which is given in the Figure 3.55(a)-(c) and values are listed in the Table 3.25.

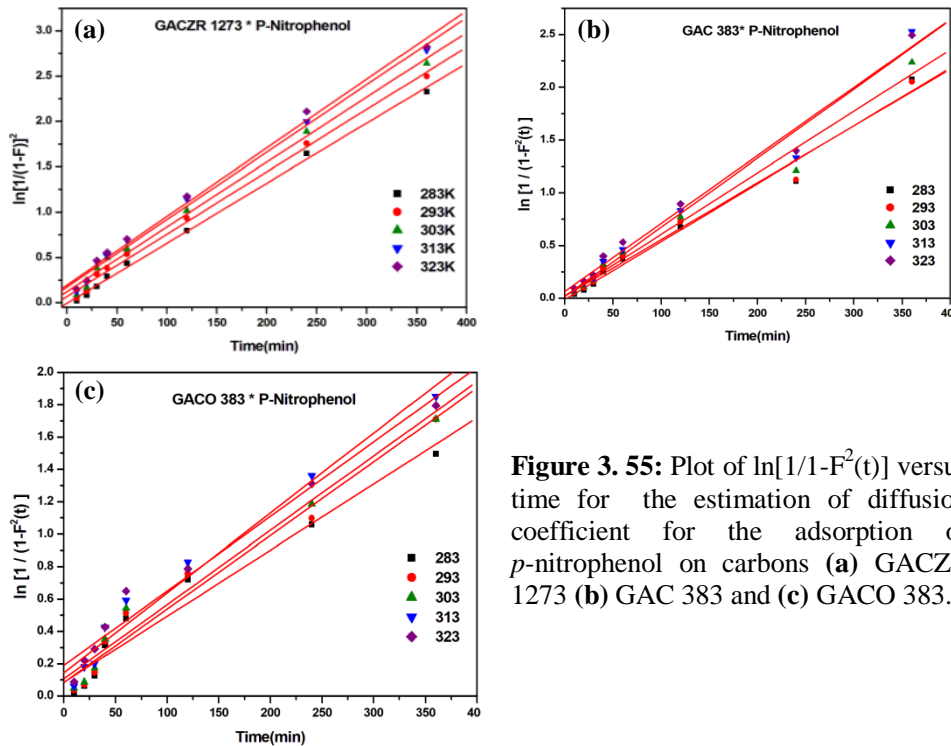


**Figure 3. 55:** Plot of  $\ln[1/(1-F^2(t))]$  versus time for the estimation of diffusion coefficient for the adsorption of *p*-nitrophenol on carbons (a) GACZR 1273 (b) GAC 383 and (c) GACO 383.

The effective diffusion coefficient of *p*-nitrophenol on GACZR 1273 lies within the range of  $2.23 - 2.48 \times 10^{-10} \text{ m}^2/\text{s}$  which is higher than the diffusion coefficient of phenol. Similarly, GAC 383 ( $1.5 - 1.71 \times 10^{-10}$ ) and GACO 383 ( $1.14 - 1.29 \times 10^{-10}$ ) also gave higher diffusion coefficient of *p*-nitrophenol. Large diffusion coefficient suggested that diffusion of *p*-nitrophenol on GACZR 1273, GAC 383 and GACO 383 is higher than for phenol molecule. Adsorbent-adsorbate interactions will change the diffusivity of each component and alter its adsorption energy, leading to changes in adsorption capacities [64].

### 3.9.3 Determination of Diffusivity for Methylene Blue (MB) on GACZR 1273, GAC 383 and GACO 383

The diffusion coefficient of adsorption of MB on GAC 383, GACO 383 and GACZR 1273 are determined from the linear plot of  $\ln [1/(1-F^2(t))]$  versus  $t$  which is given in the Figure 3.56(a)-(c) and are listed in the Table 3.26. Straight line plot for different temperature indicate the validity of the equation.

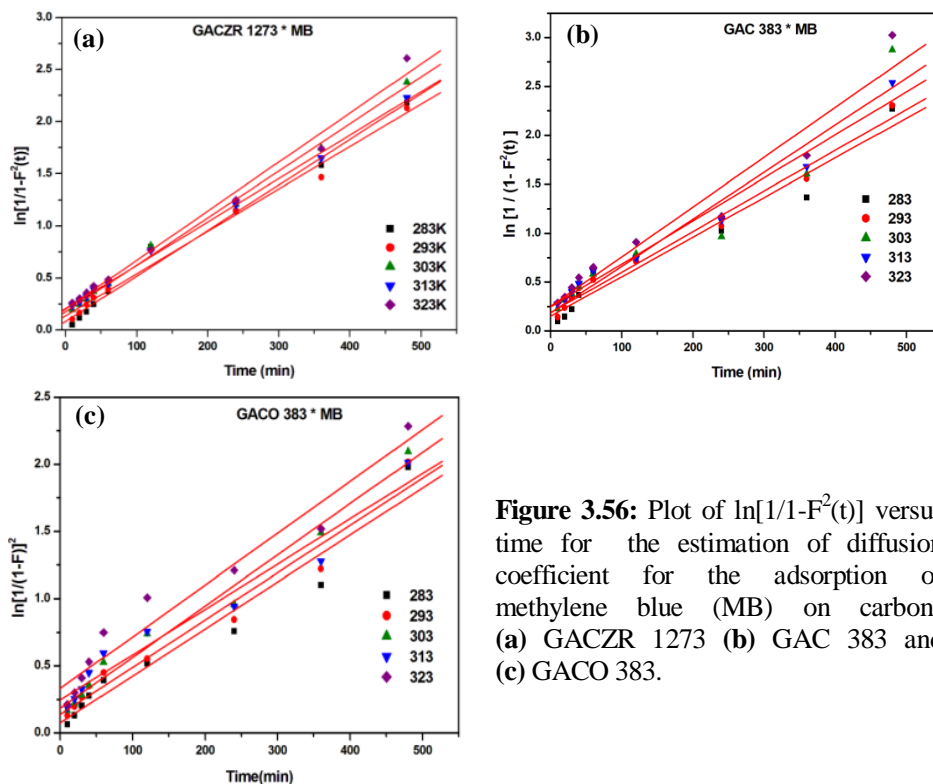


**Figure 3.56:** Plot of  $\ln[1/(1-F^2(t))]$  versus time for the estimation of diffusion coefficient for the adsorption of methylene blue (MB) on carbons (a) GACZR 1273 (b) GAC 383 and (c) GACO 383.

The effective diffusion coefficient of methylene blue (MB) on GACZR 1273 lies within the range of  $1.13 - 1.32 \times 10^{-10} \text{ m}^2/\text{s}$ . For GAC 383 it is found to be in the range of  $0.25 \times 10^{-10} - 1.34 \times 10^{-10}$ . For GACO 383 it is  $0.98 \times 10^{-10} - 1.08 \times 10^{-10} \text{ m}^2/\text{s}$  for methylene blue adsorption. These results suggest that, diffusion on the activated carbons GAC 383, GACO 383 and GACZR 1273 was not much faster for methylene blue than phenol and *p*-nitrophenol according to the value of the effective diffusion coefficient.

**Table 3.26:** Effective diffusion coefficient of carbons for the adsorption of phenol, *p*-nitrophenol and methylene blue at 283-323K.

Carbons	T ( K )	Phenol		<i>p</i> -nitrophenol		Methylene Blue	
		$D_e \times 10^{10}$ ( $\text{m}^2/\text{S}$ )	$R^2$	$D_e \times 10^{10}$ ( $\text{m}^2/\text{S}$ )	$R^2$	$D_e \times 10^{10}$ ( $\text{m}^2/\text{S}$ )	$R^2$
GACZR 1273	283	2.41	0.988	2.41	0.998	1.22	0.988
	293	2.24	0.990	2.49	0.992	1.14	0.986
	303	2.15	0.984	2.23	0.992	1.26	0.996
	313	2.19	0.990	2.23	0.992	1.17	0.998
	323	2.22	0.986	2.40	0.992	1.32	0.990
GAC 383	283	1.63	0.988	1.53	0.984	1.13	0.984
	293	1.69	0.986	1.50	0.984	1.16	0.984
	303	1.57	0.980	1.63	0.982	1.34	0.982
	313	1.71	0.986	1.83	0.980	1.230	0.980
	323	1.62	0.978	1.80	0.984	0.250	0.984
GACO 383	283	1.28	0.976	1.14	0.958	0.978	0.958
	293	1.21	0.964	1.27	0.968	0.984	0.968
	303	1.33	0.958	1.28	0.968	1.070	0.968
	313	1.43	0.970	1.38	0.974	0.940	0.974
	323	1.47	0.970	1.29	0.972	1.080	0.972

### 3.10 Activation Energy

The nature of the forces involved in the process of adsorption can be determined by their activation energy value. Arrhenius relationship was used to evaluate the activation energy of adsorption represent the minimum energy that reactants must have for the reaction to proceed.



$$\ln K_2 = \ln A - \frac{E_a}{RT} \quad (3.39)$$

Where  $K_2$  is the rate constant obtained from the pseudo-second order kinetic model,  $E_a$  the Arrhenius activation energy of adsorption,  $A$  is the Arrhenius factor,  $R$  is the gas constant, and is equal to  $8.314 \text{ J mol}^{-1} \text{ K}^{-1}$ , and  $T$  is the solution temperature. When  $\ln K_2$  is plotted against  $1/T$ , a straight line with slope  $-E_a/R$  is obtained.

$\ln K_2$  versus  $1/T$  plot of phenol on GACZR 1273, GAC 383, GACO 383 is given in the Figure 3.57 and activation energy obtained is given in Table 3.27.

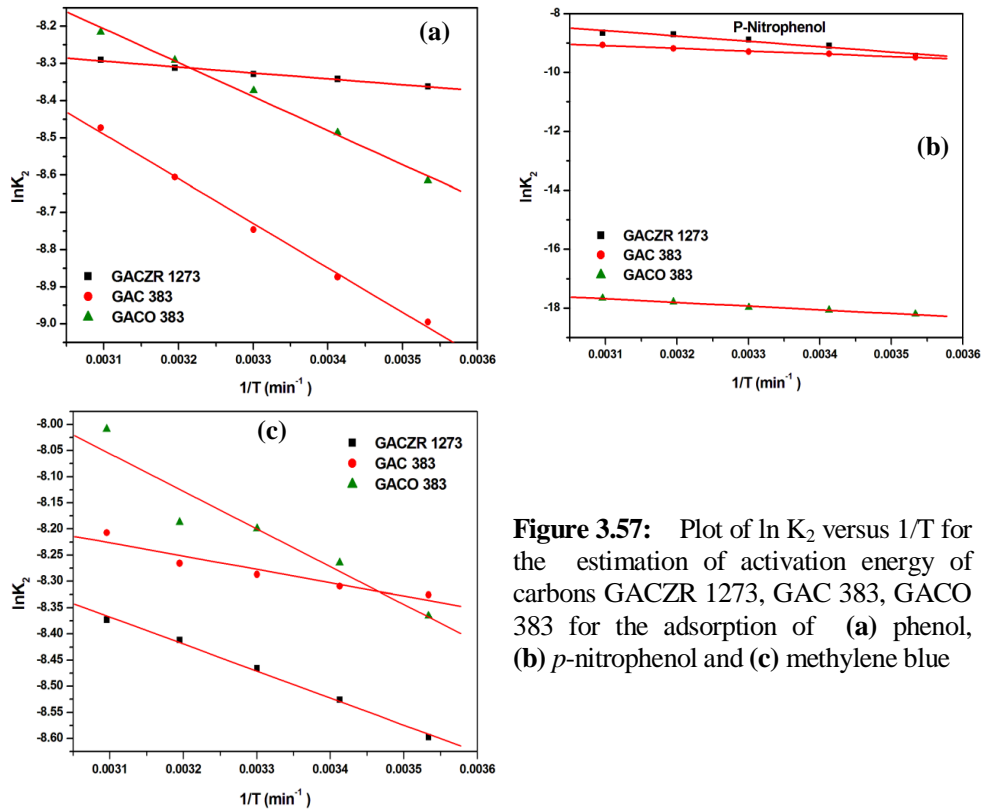


**Figure 3.57:** Plot of  $\ln K_2$  versus  $1/T$  for the estimation of activation energy of carbons GACZR 1273, GAC 383, GACO 383 for the adsorption of (a) phenol, (b) *p*-nitrophenol and (c) methylene blue

The magnitude of activation energy gives an idea of a type of adsorption, which is mainly physical or chemical. In the case of physical adsorption, the heat of adsorption is of the same order as the heat of condensation and does not usually

exceed 40 kJ/mol. Whereas in chemisorption the heat of adsorption is usually 40 to 400 kJ/mol.

The activation energy of any reaction process depicts the energy barrier that the reactants must overcome before any reaction could take place. The activation energy obtained for the adsorption of phenols on carbons is given as GAC 383 (9.95 kJ/mol), GACO 383 (7.59 kJ/mol) and GACZR 1273 (1.32 kJ/mol). This indicates that the adsorption of phenol on all the three activated carbon can be due to physical adsorption. This result is also consistent with thermodynamic results. It suggests that molecules of phenol are bound to the surface of GAC by relatively weak van der Waals forces.

$\ln K_2$  versus  $1/T$  plot of *p*-nitrophenol on GACZR 1273, GAC 383, GACO 383 are given in the Figure 3.57(b) and activation energy obtained is given in Table 3.27. The activation energy for the adsorption of *p*-nitrophenol on GAC is found to be GAC 383 (7.71 kJ/mol), GACO 383 (10.32 kJ/mol) and GACZR 1273 (15.10 kJ/mol) respectively. This indicates that the adsorption of *p*-nitrophenol onto all the three activated carbon occurs by physical adsorption as evidenced by thermodynamic principle and parameters determined.

$\ln K_2$  versus  $1/T$  plot of methylene blue on GACZR 1273, GAC 383, GACO 383 are given in the Figure 3.57(c) and activation energy obtained is given in Table 3.27

Activation energy for the adsorption of MB in this study is found to be GAC 383 (2.14 kJ/mol), GACO 383 (7.59 kJ/mol) and GACZR 1273 (4.29 kJ/mol) respectively. This indicates that the adsorption of MB onto all the three activated carbon can be assigned that physical adsorption controls the adsorption of methylene blue (MB) on GAC.

**Table 3.27:** Activation energy of carbons GAC 383, GACO 383 & GACZR 1273 for the adsorption of phenol, *p*-nitrophenol and methylene blue

Carbon	phenol		<i>p</i> -nitrophenol		Methylene blue	
	$E_a$ kJ/mol	A x 10 <sup>4</sup>	$E_a$ kJ/mol	A	$E_a$ kJ/mol	A x 10 <sup>4</sup>
GAC 383	9.95	84.00	7.71	0.001995	2.14	5.95
GACO 383	7.59	46.30	10.33	9.84E-07	7.59	46.22
GACZR 1273	1.32	4.06	15.10	0.052241	4.29	11.52

GACZR 1273 shows activation energy 15.10 kJ/mol for *p*-nitrophenol adsorption whereas for phenol adsorption  $E_a$  is 1.32 kJ/mol and for methylene blue  $E_a$  is given as 4.29 kJ/mol. This shows that diffusion of *p*-nitrophenol into the finer pores of GACZR 1273 may require more activation energy than phenol and methylene blue.

### 3.11 Design of Batch Adsorption from Isotherm Data

Adsorption isotherms can be used to predict the design of single-stage batch adsorption system. Based on the best fitting isotherm, a single stage adsorber as shown in Figure 3.58 are designed for different solution concentrations [65].

The design objective is to reduce the solution of volume  $V$ , from an initial concentration of  $C_0$  to  $C_1$  (mg/L). The mass of adsorbent is  $M$  and the solute adsorbed on the adsorbent changes from  $q_0$  (mg/g) to  $q_1$  (mg/g). At time  $t = 0$ ,  $q_0 = 0$  and as time proceeds the mass balance equation for the adsorption system in Figure 3.58 can be written as equation 3.40

The mass balance equation for adsorbent system can be written as

$$V(C_0 - C_e) = M(q_0 - q_1) = Mq_e \quad (3.40)$$

Under equilibrium condition  $C_1 \rightarrow C_0$  and  $q_1 \rightarrow q_e$

$$\frac{M}{V} = \frac{C_0 - C_e}{q_e} \quad (3.41)$$

Adsorption isotherm studies confirm that the equilibrium data for phenol, *p*-nitrophenol and methylene blue onto GAC 383, GACO 383 and GACZR 1273 fitted well in Langmuir isotherm. So the Langmuir isotherm is used for batch adsorber design. So equation rewritten as

$$\frac{M}{V} = \frac{C_0 - C_e}{\frac{q_0 K_L C_e}{1 + K_L C_e}} \quad (3.42)$$

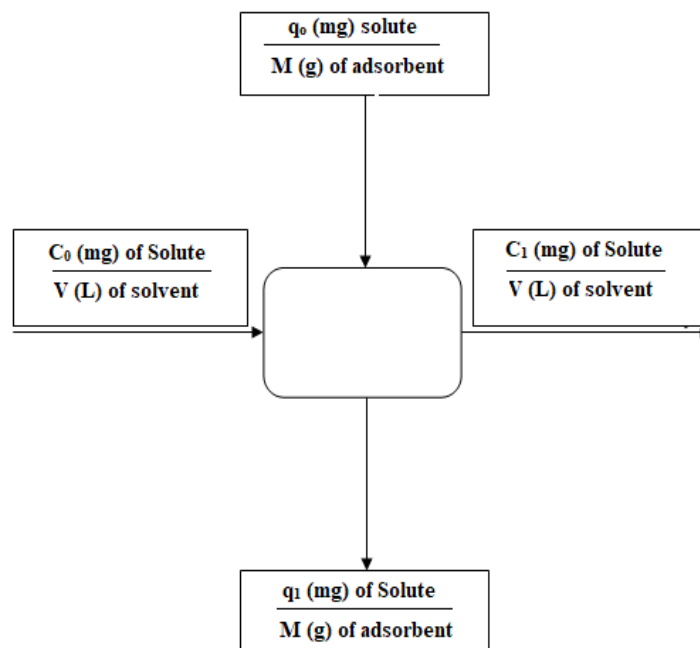


**Figure 3.58:** Schematic representation of the single stage batch adsorber system

The amounts of carbon required for treating different adsorbate (phenol, *p*-nitrophenol and methylene blue) at different concentrations are given in the Figure 3.59(a)-(c). It shows that for treating all the three adsorbate the amount required for GACZR 1273 is comparatively lower than that of GAC 383 and GACO 383. It indicates the efficiency of materials varies as per the order of GACZR 1273 > GAC 383 > GACO 383.

The amount of GAC required for treating 3000 mg/L phenol in one liter solution is given as GACZR 1273 (7.53 g), GAC 383 (11.7 g), GACO 383 (17.54 g). For attaining the same efficiency for removing the phenol pollutant GAC 383 needed more than 55 % weight and GACO 383 requires more than 2.3 times weight compared to GACZR 1273.

For treating *p*-nitrophenol (3000 mg/L) the amount of carbon is given as follows GACZR 1273 (5.67 g), GAC 383 (8.13 g) and GACO 383 (17.28 g). It indicates GAC 383 requires more than 43 % weight compared to  $Zr^{4+}$  loaded carbon, whereas GACO 383 requires 3times more weight.

The amount of carbon required for the 99 % removal of methylene blue (1500 mg/L) from one litre of aqueous solution is given as GACZR 1273 (5.4 g), GAC 383 (9.53 g) and GACO 383 (10.59 g). Basic carbon GAC 383 and nitric acid modified GACO 383 requires approximately 2 times more weight compared to GACZR 1273 for achieving the same efficiency.

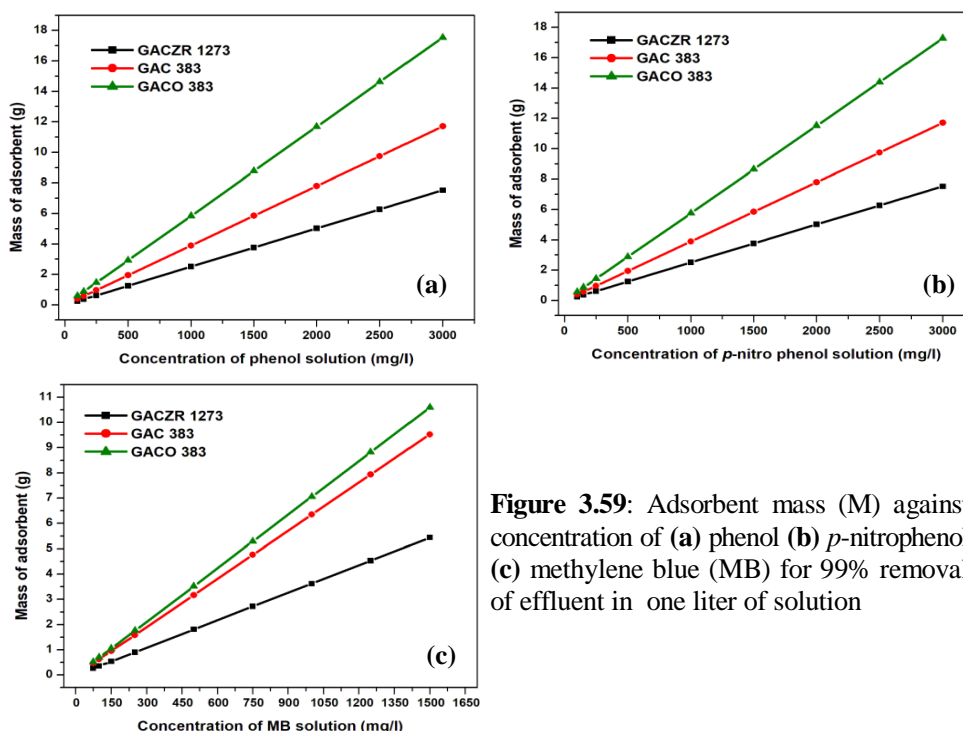


**Figure 3.59:** Adsorbent mass (M) against concentration of (a) phenol (b) *p*-nitrophenol (c) methylene blue (MB) for 99% removal of effluent in one liter of solution

### 3.12 Adsorption of Trace Metal Ions by carbon GACZR Using Contaminated Groundwater

To determine the ability of granular activated carbons to remove trace metal ions, contaminated ground water (whose initial parameters are already known) with trace elements is used in this study. Adsorption experiments were performed by batch experiments using field ground water with 8 hours of contact time.

**Table 3.28:** Efficiency of carbons GAC 383, GACO 383 and GACZR 1273 for removing trace metals in ground water

Trace metals	Initial concentration (ppb)	Concentration after adsorption (ppb)		
		GACZR 1273	GAC 383	GACO 383
<sup>7</sup> Li	4.5 (% Removal)	3.94 (12.4)	4.29 (4.7)	3.83 (14.9)
<sup>9</sup> Be	0.22 (% Removal)	ND (100.0)	0.01 (95.5)	ND (100.0)
<sup>24</sup> Mg	2905.63 (% Removal)	2341.45 (19.4)	2802.3 (3.6)	2395.43 (17.6)
<sup>27</sup> Al	257.22 (% Removal)	6.46 (97.5)	2.84 (98.9)	2.18 (99.2)
<sup>52</sup> Cr	1.5 (% Removal)	0.64 (57.3)	0.92 (38.7)	1.05 (30.0)
<sup>55</sup> Mn	85.73 (% Removal)	22.71 (73.5)	7.34 (91.4)	10.05 (88.3)
<sup>56</sup> Fe	48.78 (% Removal)	23.36 (52.1)	33.15 (32.0)	27.34 (44.0)
<sup>58</sup> Ni	5.46 (% Removal)	2.02 (63.0)	1.82 (66.7)	4.51 (17.4)
<sup>59</sup> Co	2.81 (% Removal)	0.04 (98.6)	0.13 (95.4)	0.23 (91.8)
<sup>63</sup> Cu	21.90 (% Removal)	2.44 (88.9)	3.17 (85.5)	4.46 (79.6)
<sup>64</sup> Zn	40.77 (% Removal)	7.58 (81.4)	17 (58.3)	28.46 (30.2)
<sup>75</sup> As	1.89 (% Removal)	0.4 (78.8)	0.34 (82.0)	0.27 (85.7)
<sup>114</sup> Cd	0.62 (% Removal)	0.21 (66.1)	0.16 (74.2)	0.57 (8.1)
<sup>138</sup> Ba	89.02 (% Removal)	38.26 (57.0)	42.77 (52.0)	21.25 (76.1)
<sup>205</sup> Tl	0.08 (% Removal)	0.02 (75.0)	0.04 (50.0)	0.04 (50.0)
<sup>208</sup> Pb	6.18 (% Removal)	0.06 (99.0)	0.24 (96.1)	0.23 (96.3)

The Percentage removals of each trace element with respect to their initial concentration by carbons are given in the Table 3.28. Granular activated carbons have more than 95 % removal efficiency towards Be Al, Co and Pb elements with respect to their initial concentration. Among the carbon studied, GACZR 1273 has more than 80 % efficiency towards Cu (88.9 %) and Zn (81.4 %), more than 75 % efficiency towards As (78.8 %) and Tl (75 %) whereas GAC 383 and GACO 383 shows only 58.3 % and 30.2 % efficiency towards Zn and 50 % removal efficiency towards Tl. The removal efficiency of GACZR 1273 for Cr and Cd gives 57.3 % and 66.1 % respectively, which is comparatively higher than basic carbons.

Trace elemental analysis by activated carbons GAC 383, GACO 383 and GACZR 1273 reveals that there are several factors, such as specific surface area, pore-size distribution, pore volume, surface charge, and presence of surface functional groups, affect the adsorption of metal ions on activated carbon.

### 3.13 Statistical Analysis of the Data

The statistical significance of the ratio of mean square variation due to regression and mean square residual error was tested using ANOVA.

**Hypothesis 1:** Whether there is any significant difference in pore volume and surface area of carbons obtained from BET and *I*-plot method

To test the **Hypothesis 1**, pore volume and surface area obtained from BET and *I* plot for GAC 383, GACO 383, GACZR 873, GACZR 1073 and GACZR 1273 is given in Table 3.5 are analysed statistically using three way ANOVA test by keeping GACO 383 as constant.

Based on the statistical parameters given in Table 3.29 i.e. sum of squares (SS), degree of freedom (df), mean square (ms), variance ratio (F) and level of significance (P value) observations are summarised below.

**Table 3.29:** Three way ANOVA analysis of pore volume and surface area obtained from BET and *I*-plot method

Source	SS	df	ms	F	P-value
Total	4191142.5429	15			
<i>I</i> point and BET carbons	417.8959	1	417.8959	0.130	P>0.05
SA and V <sub>m</sub>	81266.0366	3	27088.6789	8.4392	P< 0.05
Residual	4077360.0466	1	4077360.047	1270.262	P< 0.001
	32098.5638	10	3209.8564		

$P$  less than 0.05 indicate model is significant. Here the pore volume obtained from both BET and  $I$  plot shows significant differences between carbons ( $P < 0.05$ ). GACZR 1273 gives significantly higher values than the rest. Whereas no significant difference is shown between BET ( $p/p_0$  0.1) and  $I$  plot method ( $P > 0.05$ ).  $P$  less than 0.001, indicates very high significant difference between surface area and pore volume ( $P < 0.001$ ).

**Hypothesis 2:** Whether there is any significant difference between the pore volume of carbons ( $N_2/77K$  adsorption isotherm data) obtained from Langmuir, Dubinin-Radushkevich (D-R), Alpha S ( $\alpha_s$ ) and John isotherm.

To test the **Hypothesis 2**, pore volume obtained from Langmuir, Dubinin-Radushkevich (D-R), Alpha S ( $\alpha_s$ ) and John isotherm for GAC 383 GACO 383, GACZR 873, GACZR 1073 and GACZR 1273 is given in Table 3.9 are statistically analysed by two way ANOVA test. The results are interpreted based on the constants in Table 3.30.

**Table 3.30:** Two way Anova analysis of pore volume obtained from Langmuir, Dubinin-Radushkevich (D-R), Alpha S ( $\alpha_s$ ) and John Isotherm

Source	SS	df	ms	F	P-value
Total	14243.44	19	3621.667		
methods	906.1883	3	302.0628	41.07119	$P < 0.05$
carbons	13249	4	3312.25	450.3635	$P < 0.001$
Residual	88.25537	12	7.354614		

High significant difference ( $P < 0.001$ ) indicates the large difference exists in pore volume between the carbons. GACZR 1273 gives significantly higher values than rest. Statistical analysis reveals that there is a significant difference exists between pore volumes ( $P < 0.05$ ), which obtained from four isotherm methods (Langmuir, D-R, Alpha S, and John isotherms). Among the four isotherms studied D-R and Alpha S is comparatively higher than Langmuir and John isotherm.



**Hypothesis 3:** Whether there is any correlation between activation temperature and micropore volume [Karl Pearson's Coefficient of correlation/ t-test].

To test the **Hypothesis 3**, correlation between micropore volume and activation temperature is statistically analysed by Karl Pearson's co-efficient of correlation using Dubinin–Radushkevich micropore volume ( $V_m$  (D-R)) of GACZR series of carbons (Table 3.9) activated at different temperatures (873 K, 1073 K, 1273 K). It gives a significant positive correlation between activation temperature and micro pore volume ( $r = 0.99674$ ,  $t = 12.35$ ,  $P < 0.01$ ). This indicates that with increasing of activation temperature micropore volume also increases.

**Hypothesis 4:** Whether there is any significant difference in quantity adsorbed and surface area between the samples for the adsorption of phenol, *p*-nitrophenol and methylene blue (MB).

To test the **Hypothesis 4**, adsorption rate and surface area of carbons GACZR 1273, GAC 383 and GACO 383 with respect to solid –liquid equilibria using phenol, *p*-nitrophenol and MB obtained from Langmuir, D-R and J-SA isotherms (Table 3.14) are analysed statistically using three way ANOVA test. The results are interpreted based on the constants in Table 3.29

**Table 3.31:** Three way ANOVA statistical analysis of adsorption system in solid-liquid equilibria with respect to quantity of phenol, *p*-nitrophenol and methylene blue adsorbed on GACZR 1273, GAC 383 and GACO 383

Source	SS	df	ms	F	P-value
Total	628403.0304	26			
Phenol, PNP,MB carbons	108617.4512	2	54308.7560	51.547	P< 0.001
methods	11238.5767	2	5619.2884	5.339	P<0.05
Residual	487495.3055	2	243747.6828	231.578	P< 0.001
	21051.6970	20	1052.55		

Three way ANOVA method is used for analysing the adsorption rate of carbons towards different adsorbate. Between phenol, *p*-nitrophenol and methylene blue adsorption rate varies significantly ( $P < 0.001$ ). Significant difference between carbons with respect to adsorption rate indicates by  $P < 0.05$

and GACZR 1273 is having a significantly higher adsorption rate than GAC 383 and GACO 383. Different isotherm methods also exhibit a significant difference in adsorption rate ( $P < 0.001$ ). Between the John-Sivanandan Achari isotherm and Langmuir the difference is not significant.

**Table 3.32:** Three way ANOVA statistical analysis of adsorption system in solid-liquid equilibria with respect to surface area of GACZR 1273, GAC 383 and GACO 383

Source	SS	df	ms	F	P-value
Total	3182711.8535	26			
carbons	293640.9700	2	146820.4850	6.7075	$P < 0.01$
methods	1916774.3012	2	958387.1506	43.784	$P < 0.001$
Phenol, PNP,MB	534518.8357	2	267259.4179	12.2098	$P < 0.001$
Residual	437777.7466	20	21888.8873		

There is a significant difference between carbon with respect to surface area and GACZR 1273 is having significantly higher surface area compared to others ( $P < 0.01$ ). Phenol showed a significant high surface area compared to nitrophenol and methylene blue.

**Hypothesis 5:** whether there is any correlation between temperature and adsorption of phenol, temperature and adsorption of *p*-nitrophenol & temperature and adsorption of methylene blue [Karl Pearson's Co efficient of correlation/ t-test].

To test the **Hypothesis 5**, Langmuir adsorption capacity of GACZR 1273 towards phenol (Table 3.11), *p*-nitrophenol (Table 3.12) and methylene blue (Table 3.13) at five solution temperature (283 K, 293 K, 303 K, 313 K and 323 K) are correlated by Karl Pearson's Coefficient.

There is a significant positive correlation between temperature and adsorption of phenol on GACZR 1273 ( $r = 0.9941$ ,  $t = 15.82$ ,  $df = 3$ ,  $P < 0.01$ ). This indicates that as temperature increases adsorption of phenol also increases. There is a significant positive correlation between temperature and adsorption of *p*-nitrophenol on GACZR 1273 ( $r = 0.9957$ ,  $t = 18.51$ ,  $df = 3$ ,  $P < 0.01$ ). This indicates that as temperature increases adsorption of *p*-nitrophenol also increases.

There is a significant positive correlation between temperature and adsorption of methylene blue on GACZR 1273 ( $r = 0.9980$ ,  $t = 27.5$ ,  $df = 3$ ,  $P < 0.01$ ). This indicates that as temperature increases adsorption of methylene blue also increases.

### 3.14 Conclusions

Chemical activation of GAC with  $ZrOCl_2 \cdot 8H_2O$  brought marked changes in the surface chemistry of GAC. Successive burn off at a higher activation temperature decreases the yield of total active carbon from 94.53 % to 82.22 % in GACZR series. High temperature treatment of GACZR series carbons, burn off does not exceed more than 20 %. It indicates that the thermal stability of GAC is achieved by successive impregnation of  $Zr^{4+}$  into it.

On heat treatment from 383 to 1273 K surface oxygen group varies as carboxylic group (0.74 - 0.39 meq/g), phenolic group (0.56 - 0.89 meq /g), lactonic group (0.70 - 0.20 meq/g), pyrone (0.2 - 0.6 meq/g) for the new series of carbon. A spectroscopic technique such as FTIR and XPS indicates the presence of  $Zr^{4+}$  in GAC. FTIR band appears at  $589\text{ cm}^{-1}$  is attributed to the Zr - O bending on the surface of GAC. The binding energy of Zr 3d region corresponding to Zr - AC and  $ZrO_x$  - AC at 182.4 eV is associated with  $Zr^{4+}$  in  $ZrO_2$ . This again showed, that the  $Zr^{4+}$  is better dispersed on the carbon surface of zirconium impregnated carbon. The nitric acid oxidation of GAC 383 caused changes in the micro crystallinity of the carbon layers as evidenced by the  $L_w$ ,  $L_c$  and  $d_{002}$  with distinct changes. The sharp 002 diffraction peak at  $26.4^\circ$  indicated a highly organized crystal structure, revealing an interlayer spacing of about  $d_{002} > 0.335$  nm. Carbon has well-defined and well-interconnected pore structure as evidenced by SEM and HRTEM results. The acidic treatment of GAC 383 with con. $HNO_3$  showed some distorted pattern in the arrangement of stacks.

The pore volume and surface area obtained from BET  $p/p_0 \approx 0.1$  is close agreement with I point method. It supports the validity of linear BET plot up to  $p/p_0 \approx 0.1$ . The critical evaluation of isotherm constants by BET and I-plot method shows that monolayer volume and surface area of zirconium impregnated carbon samples increases with activation temperature from 873K to 1273K. The

Dubinin-Radushkevich isotherm shows that  $Zr^{4+}$  modified carbon GACZR 1073 has 14% ( $SA_{mi} = 735.1 \text{ m}^2/\text{g}$ ) and GACZR 1273 has 26 % ( $SA_{mi} = 814.3 \text{ m}^2/\text{g}$ ) enhancement in micropore surface area compared to basic carbon GAC 383 ( $SA_{mi} = 646.5 \text{ m}^2/\text{g}$ ). The micropore volumes provided by D-R and  $\alpha_s$  methods are in excellent agreement with all carbons. John isotherm suggests the three different pore filling mechanisms of  $N_2$  molecule in GAC. The molecular sieve effect is found to be prominent for  $N_2$  atoms for all the carbon studied. This suggests that most of the  $N_2$  molecules fill in carbon pores smaller than 1 nm in size. The  $t$  - plot method shows that among the total surface area of GACZR 1273 ( $S_T$ ), micropore surface area contribute 70.0 % and external surface area contribute 30 % i.e.  $Zr^{4+}$  activation leads to the acceleration of micropores on the activated carbon matrix of GAC 383. Pore size distribution studies (PSD) showed that adsorption and desorption pore width ranges 2.3 -2.5 nm for zirconium activated carbon series.

The experimental data obtained from the adsorption isotherm studies shows that nitric acid oxidised carbon (GACO 383) showed comparatively less adsorption among all the three adsorbate. The adsorption affinity of GAC towards selected adsorbate varies in the order of  $p$ -nitrophenol > phenol > methylene blue. Nitro group in para position enhances electron donor acceptor interaction between adsorbent and adsorbate which results more adsorption of  $p$ -nitrophenol on carbon surface compared to phenol molecule. Adsorption rate of methylene blue is comparatively lower than phenolic compounds. It was suggested that some of the micropores in active carbons were not accessible to methylene blue dye molecules (cross sectional area is  $1.2 \text{ nm}^2$ ). Best fitting of isotherm models to the observed isotherm data for the adsorption of phenols,  $p$ -nitrophenol and methylene blue onto activated carbon gives the order Langmuir > John – Sivanandan Achari > Freundlich > Dubinin-Radushkevich.

A kinetic study shows that the adsorption system studied belongs to the second order kinetic model. Two phases in the intraparticle diffusion plot suggest that adsorption process proceeds by surface adsorption and intraparticle diffusion. Activation energy obtained from Arrhenius equation shows that physical adsorption control the adsorption of phenol,  $p$ -nitrophenol and methylene blue. The positive  $\Delta H$  of all adsorbents indicates endothermic nature of adsorption i.e

the adsorption is favoured at higher temperatures. The high positive  $\Delta S$  suggests an increase in the randomness at adsorbate-solution interface during the adsorption process. The increase in  $-\Delta G$  values with increasing temperature shows an increase in feasibility of adsorption at higher temperatures due to the increase in number of adsorption sites generated as a result of breaking of some internal bonds near edge of active surface sites of adsorbent. Trace elemental analysis by ICP-MS shows that granular activated carbon can effectively remove trace elements from field groundwater. Statistical analysis shows that there is significant difference exist between surface area and pore volume of carbon samples ( $P < 0.001$ ). A positive correlation exists between activation temperature and micro pore volume of GACZR series of carbons. The significant difference exists between carbons with respect to the adsorption rate in solid liquid equilibria. GACZR 1273 is having a significantly higher adsorption rate ( $P < 0.05$ ) for phenol, *p*-nitrophenol and methylene blue. Different isotherm methods also exhibit a significant difference in adsorption rate ( $P < 0.001$ ). Between the John-Sivanandan Achari isotherm and Langmuir the difference is not significant. There is a significant positive correlation between temperature and adsorption rate of phenol, *p*-nitrophenol and MB on GACZR 1273.

## Reference

- [1] Holmes, H. F.; Fuller, E. L.; Gammage, R. B. Heats of Immersion in the Zirconium Oxide Water System. *The Journal of Physical Chemistry* **1972**, *76* (10), 1497–1502.
- [2] Molina-Sabio, M.; Sánchez-Montero, M. J.; Juárez-Galan, J. M.; Salvador, F.; Rodríguez-Reinoso, F.; Salvador, A. Development of Porosity in a Char during Reaction with Steam or Supercritical Water. *The journal of physical chemistry B* **2006**, *110* (25), 12360–12364.
- [3] Garrido, J.; Linares-Solano, A.; Martín-Martínez, J. M.; Molina-Sabio, M.; Rodríguez-Reinoso, F.; Torregrosa, R. Use of  $N_2$  vs.  $CO_2$  in the Characterization of Activated Carbons. *Langmuir* **1987**, *3* (10), 76–81.
- [4] Achari, V.S.; Rajalakshmi, A.S.; Jayasree, S. Surface Area and Porosity Development on Granular Activated Carbon by Zirconium: Adsorption Isotherm Studies. *Journal of Applied Research and Technology*, **2017** (Accepted November 2017).

- [5] He, Q.; Xu, Y.; Wang, C.; She, S.; Zhou, S.; Wang, R. Silane Modification and Characterization of Activated Carbon. *Adsorption* **2012**, *18* (1), 23–29.
- [6] Shen, W.; Li, Z.; Liu, Y. Surface Chemical Functional Groups Modification of Porous Carbon. *Recent Patents on Chemical Engineering* **2008**, *1* (1), 27–40.
- [7] Ketcha, J. M.; Dina, D. J. D.; Ngomo, H. M.; Ndi, N. J. Preparation and Characterization of Activated Carbons Obtained from Maize Cobs by Zinc Chloride Activation. *American Chemical Science Journal* **2012**, *2* (4), 136–160.
- [8] Bortun, A. I.; Bortun, L. N.; Clearfield, A. Hydrothermal Synthesis of Sodium Zirconium Silicates and Characterization of Their Properties. *Chemistry of Materials* **1997**, *9* (8), 1854–1864.
- [9] Fang, P.; Cen, C.; Chen, D.; Tang, Z. Carbonaceous Adsorbents Prepared from Sewage Sludge and Its Application for Hg<sup>0</sup> Adsorption in Simulated Flue Gas. *Chinese Journal of Chemical Engineering* **2010**, *18* (2), 231–238.
- [10] Matos, J.; Nahas, C.; Rojas, L.; Rosales, M. Synthesis and Characterization of Activated Carbon from Sawdust of Algarroba Wood. 1. Physical Activation and Pyrolysis. *Journal of Hazardous Materials* **2011**, *196*, 360–369.
- [11] Hontoria-Lucas, C.; Lopez-Peinado, A.J.; Lopez-Gonzalez De, D. J.; Rojas-Cervantes, M.L.; Martin – Aranda, R.M. Study of oxygen-containing groups in a series of graphite oxides: physical and chemical characterization. *Carbon* **1995**, *33* (11), 1585–1592.
- [12] Ganguly, A.; Sharma, S.; Papakonstantinou, P.; Hamilton, J. Probing the Thermal Deoxygenation of Graphene Oxide Using High-Resolution In Situ X-ray-Based Spectroscopies. *J. Phys. Chem. C* **2011**, *115*, 17009–1701.
- [13] Kercher, A. K.; Nagle, D. C. Microstructural Evolution during Charcoal Carbonization by X-Ray Diffraction Analysis. *Carbon* **2003**, *41*, 15–27.
- [14] Bindia Ravindran. Adsorption Isotherm Studies on Activated Carbon Prepared by Activation with Cerium Compounds. *Ph.D Thesis* **2016**. School of Environmental Studies, Cochin University of Science and Technology, Cochin, India.
- [15] Harris, P.J.F.; Liu, Z.; Suenaga, K. Imaging the structure of activated carbon using aberration corrected TEM. *J. Phys. Condens. Matter* **2008**, *20*, 362201.
- [16] Pomonis, P. J.; Petrakis, D. E.; Ladavos, A. K.; Kolonia, K. M.; Pantazis, C. C.; Giannakas, A. E.; Leontiou, A. A. The I-Point Method for Estimating the Surface Area of Solid Catalysts and the Variation of C-Term of the BET Equation. *Catalysis Communications* **2005**, *6* (1), 93–96.

- [17] Sing, K. The Use of Nitrogen Adsorption for the Characterisation of Porous Materials. *Colloids and Surfaces A: Physicochemical and Engineering Aspects* **2001**, 187–188, 3–9.
- [18] Langmuir, I. The Adsorption of Gases on Plane Surfaces of Glass, Mica and Platinum. *Journal of the American Chemical Society* **1918**, 40 (9), 1361–1403.
- [19] Freundlich, H.M. Over the Adsorption in Solution. *Journal of Physical Chemistry A* **1906**, 57, 385–470.
- [20] Dubinin, M.M.; Radushkevich, L.V. The Equation of the Characteristic Curve of Activated Charcoal. Proceedings of the Academy of Sciences, Physical Chemistry Section. **1947**, 55, 331.
- [21] Gonzalez, M.; T. Escribano A.S.; Sabiano, M.M.; Reinoso, R.F. Correlation between Surface Areas and Micropore Volumes of Activated Carbons Obtained from Physical Adsorption and Immersion Calorimetry. *Langmuir* **1996**, No. 7, 2151–2155.
- [22] El-Hendawy, A. A. An Insight into the KOH Activation Mechanism through the Production of Microporous Activated Carbon for the Removal of  $Pb^{2+}$  Cations. *Applied Surface Science* **2009**, 255, 3723–3730.
- [23] Gregg, S. J.; Sing, K. S.W. Adsorption surface area and porosity. Academic Press. London. **1982**.
- [24] John, P.T.; Suri, D. K.; Nagpal, K. C. Characterization of structural parameters of porous materials by a new adsorption isotherm. *Journal of material science* **1985**, 20 (6), 2071–2086.
- [25] Mercy Thomas. Adsorption Isotherm Characterization of Porous Materials Using John Isotherm. *Ph.D Thesis* **2016**, School of Environmental Studies, Cochin University of Science and Technology, Cochin, India.
- [26] Lippens, B. C.; de Boer, J. H. Studies on Pore Systems in Catalysts Systems Distribution Curves in Aluminum Oxide. *journal of Catalysis* **1964**, 3, 44–49.
- [27] Lippens, B. C.; Linsen, B. G.; de Boer, J. H. Studies on Pore Systems in Catalysts I. The Adsorption of Nitrogen ; Apparatus and Calculation. *journal of Catalysis* **1964**, 3, 32–37.
- [28] Deryło-Marczewska, A.; Goworek, J.; Pikus, S.; Kobylas, E.; Zgrajka, W. Characterization of Melamine-Formaldehyde Resins by XPS, SAXS, and Sorption Techniques. *Langmuir* **2002**, 18 (20), 7538–7543.
- [29] Sarker, N.; Fakhrudin, A. N. M. Removal of Phenol from Aqueous Solution Using Rice Straw as Adsorbent. *Appl. Water Sci.* **2015**, 7 (3), 1459–1465.

- [30] Singh, H.; Roohi, S. Removal of Basic Dyes from Aqueous Solutions Using Mustard Waste Ash and Buffalo Dung Ash. *International journal of environmental sciences* **2013**, 3 (5), 1711–1725.
- [31] Hameed, B. H.; Din, A. T. M.; Ahmad, A. L. Adsorption of Methylene Blue onto Bamboo-Based Activated Carbon: Kinetics and Equilibrium Studies. *Journal of Hazardous Materials* **2007**, 141 (3), 819–825.
- [32] Rouquerol, F.; Rouquerol, J.; Sing, K. S. W. Adsorption by powders and porous solids, Academic Press, London, **1999**.
- [33] Xu, J.; Wang, L.; Zhu, Y. Decontamination of Bisphenol A from Aqueous Solution by Graphene Adsorption. *Langmuir* **2012**, 28, 8418–8425.
- [34] Basu, T.; Gupta, K.; Ghosh, U. C. Equilibrium and Thermodynamics on arsenic(III) Sorption Reaction in the Presence of Background Ions Occurring in Groundwater with Nanoparticle Agglomerates of Hydrous iron(III) + chromium(III) Mixed Oxide. *Journal of Chemical and Engineering Data* **2010**, 55 (5), 2039–2047.
- [35] Achari, V. S. Modified Carbons and Wood Dust: Evaluation of Adsorption Properties. *Ph.D. Thesis* **1998**. Department of Chemistry, University of Kerala, Kariavattom, Thiruvananthapuram.
- [36] Namasivayam, C.; Yamuna, R. T. Adsorption of Direct Red 12 B by Biogas Residual Slurry: Equilibrium and Rate Processes. *Environ. Pollut.* **1995**, 89, 1-7.
- [37] Pandey, K.K.; Prasad, G.; Singh, V.N. Use of wollastonite for the treatment of Cu(II) rich effluent. *Water Air and Soil Pollution* **1986**, 27, 287-296.
- [38] Ramakrishna, G.; Susmita, M. Application of response surface methodology for optimization of Cr(III) and Cr(VI) adsorption on commercial activated carbons, *Research Journal of Chemical Sciences* **2012**, 2(2), 40-48.
- [39] Bello-Huitle, V.; Atenco-Fernández, P.; Reyes-Mazzoco, R. Adsorption Studies of Methylene Blue and Phenol Onto Pecan and Castile Nutshells Prepared By Chemical Activation. *Revista Mexicana de Ingenieria Química* **2010**, 9 (3), 313–322.
- [40] Morrison, R.T.; Boyd, R.N. Organic Chemistry, 4<sup>th</sup> Ed., Allyn and Bacon, Inc. Boston, **1983**, 338.
- [41] Liu, Q.-S.; Zheng, T.; Wang, P.; Jiang, J.-P.; Li, N. Adsorption Isotherm, Kinetic and Mechanism Studies of Some Substituted Phenols on Activated Carbon Fibers. *Chemical Engineering Journal* **2010**, 157 (2–3), 348–356.



- [42] Achari, V.S.; Jayasree, S.; Rajalakshmi, A.S. Adsorption of *p* – nitrophenol on Coconut Shell Granular Activated Carbon: Isotherms, Kinetics and Thermodynamics. *Indian Journal of Chemical Technology*. **2017**, *24*, 471-478.
- [43] Achari, V. S.; Rajalakshmi, A.S. Adsorption of phenol using Zirconium impregnated activated carbon: Equilibrium and Kinetic study, *24<sup>th</sup> Swadeshi Science Congress 2014*, Thunchath Ezhuthachan Malayalam University. ISBN: 978-81-928129-2-2, 314-319.
- [44] Teng, H.; Hsieh, C.-T. Influence of Surface Characteristics on Liquid-Phase Adsorption of Phenol by Activated Carbons Prepared from Bituminous Coal. *Industrial & Engineering Chemistry Research* **1998**, *37* (9), 3618–3624.
- [45] Chen, L.; Bai, B. Equilibrium, Kinetic, Thermodynamic, and in Situ Regeneration Studies about Methylene Blue Adsorption by the Raspberry-like TiO<sub>2</sub>@yeast Microspheres. *Industrial & Engineering Chemistry Research* **2013**, *52*, 15568–15577.
- [46] Sharma, Y. C.; Uma. Optimization of Parameters for Adsorption of Methylene Blue on a Low-Cost Activated Carbon. *Journal of Chemical and Engineering Data* **2010**, *55* (1), 435–439.
- [47] Macedo, J. D. S.; Costa Júnior, N. B.; Almeida, L. E.; Vieira, E. F. D. S.; Cestari, A. R.; Gimenez, I. D. F.; Villarreal Carreño, N. L.; Barreto, L. S. Kinetic and Calorimetric Study of the Adsorption of Dyes on Mesoporous Activated Carbon Prepared from Coconut Coir Dust. *Journal of Colloid and Interface Science*. **2006**, *298* (2), 515–522.
- [48] John, P. T.; Achari, V. S. Characterisation of Structural Parameters of Finely Divided and Porous Materials by a New Adsorption Isotherm. *Journal of Materials Science* **2002**, *37* (4), 885–893.
- [49] Achari, V.S. John Isotherm for Liquid Phase Adsorption: Comparison with Langmuir and Freundlich Models. *International Carbon Conference, Carbon 2006*, Robert Gordon University, Aberdeen, Scotland, UK. Extended Abstract, 16-21. ISBN 0- 9553365-1-1, 3P 107.
- [50] Jayasree, S.; Rajalakshmi A. S.; Achari, V. S. Determination of Surface Area of Activated Carbons using John- Sivanandan Achari Isotherm Plots. *Proceedings of the 26<sup>th</sup> Kerala Science Congress 2014*, Kerala Veterinary and Animal Sciences University, Pookode Wayanad , 1362-1371.
- [51] Lagergren, S. Zur theorie der sogenannten adsorption gelöster stoffe, Kungliga Svenska Vetenskapsakademiens. *Handlingar* **1898**, *24*, 1-39.

- [52] Ho, Y. S.; McKay, G. Pseudo-Second Order Model for Sorption Processes. *Process Biochemistry* **1999**, *34* (5), 451–465.
- [53] Weber, W.J.; Morris, J.C. Kinetics of adsorption carbon from solutions. *Journal Sanitary Engineering Division Proceedings. American Society of Civil Engineers* **1963**, *89*, 31-60.
- [54] Achari, V. S.; Anirudhan, T. S. Phenol Removal from Aqueous Systems by Sorption on Jackwood Sawdust. *Indian Journal of Chemical Technology* **1995**, *2*, 137–141.
- [55] Karthikeyan, S.; Balasubramanian, R.; Iyer, C.S.P. Evaluation of the marine algae *Ulva fasciata* and *Sargassum* sp. For the biosorption of Cu(II) from aqueous solutions. *Bioresource Technology* **2007**, *98* (2), 452-455.
- [56] Sag, Y., Aktay, Y. Kinetic studies on sorption of Cr(VI) and Cu(II) ions by chitin, chitosan and *Rhizopus arrhizus*. *Biochemical Engineering Journal* **2002**, *12* (2), 143-153.
- [57] M. Dogan, M.; Alkan, M. Adsorption kinetics of methyl violet onto perlite. *Chemosphere* **2003**, *50*, 517–528.
- [58] Boudrahem, F.; Aissani-Benissad, H. Batch sorption dynamics and equilibrium for the removal of lead ions from aqueous phase using activated carbon developed from coffee residue activated with zinc chloride. *Journal of Environmental Management* **2009**, *90*, 3031-3039.
- [59] Crank, The Mathematics of Diffusion. first ed, Oxford Clarendon Press, London, **1965** vol. 84.
- [60] Chingombe, P.; Saha, B.; Wakeman, R.J. Sorption of atrazine on conventional and surface modified activated carbons. *Journal of Colloid and Interface Science* **2006**, *302*, 408-416.
- [61] Shahryari, Z.; Goharrizi, A .S.; Azadi, M. Experimental study of methylene blue adsorption from aqueous solution onto carbon nano tubes. *International Journal of Water Resource and Environmental Engineering* **2010**, *2* (2), 016-028.
- [62] Rahmani-Sani, A.; Shan, R. ran; Yan, L. guo; Hosseini-Bandegharaei, Minor Correction to the Thermodynamic Calculation Using the Distribution Constant *J. Hazard. Mater.* **2016**, *325*, 367–368.
- [63] Varghese, S.; Vinod, V. P.; Anirudhan, T. S. Kinetic and Equilibrium Characterization of Phenols Adsorption onto a Novel Activated Carbon in Water Treatment. *Indian Journal of Chemical Technology* **2004**, *11* (6), 825–833.

- [64] Srivastava, V. C.; Swamy, M. M.; Mall, I. D.; Prasad, B.; Mishra, I. M. Adsorptive Removal of Phenol by Bagasse Fly Ash and Activated Carbon: Equilibrium, Kinetics and Thermodynamics. *Colloids and Surfaces A: Physicochemical and Engineering Aspects* **2006**, 272 (1–2), 89–104.
- [65] Vadivelan, V.; Vasanth Kumar, K. Equilibrium, kinetics, mechanism, and process design for the sorption of methylene blue onto rice husk. *Journal of Colloid and Interface Science* **2005**, 286 (1), 90-100.

.....❧.....



## GRANULAR ACTIVATED CARBON OXIDISED AND ACTIVATED WITH ZIRCONYL CHLORIDE (GACOZR): PREPARATION, CHARACTERIZATION AND ADSORPTION ISOTHERM STUDIES

### 4.1 Introduction

The presence of carbon-oxygen surface functional groups on GAC has a strong influence on the adsorption capacity in solid - gas /solid - liquid equilibria. Chemical structure of the carbon surface is one of the important factors as that of surface area and porosity to determine its efficiency. The identification and estimation of the carbon-oxygen surface groups have been carried out using several physical, chemical, and physicochemical techniques. The acidic functional groups present on the surface of activated carbon have been identified as carboxyl, lactones, and phenols. Basic groups have been postulated as pyrones and chromene structures. Acidic groups on the surface of the activated carbons make it more hydrophilic. They affect the surface area and pore texture of the activated carbons. The incorporation of surface groups by reactions modify the surface behaviour and adsorption characteristics of activated carbons and these surface functional groups interact differently in different environments. Presence of oxygen-containing surface functional group on GAC determines the ion exchange capacities of carbon material.

This chapter insightfully discusses the preparation, characterization, and adsorption isotherm studies of zirconium as zirconyl chloride impregnated nitric acid modified granular activated carbons (GACOZR). The carbon, whose textural analysis was previously done, was further subjected to adsorption isotherm studies ( $N_2$ /gas at 77K), and solid –liquid equilibrium studies using phenol, *p*-nitrophenol and methylene blue to identify their material applications.

## 4.2 Granular Activated Carbons – GACOZR Series

There are eight carbons GAC 383, GACO 383, GACOZR 383, GACOZR 473, GACOZR 673, GACOZR 873, GACOZR 1073, and GACOZR 1273 are used in this study. GAC 383 is the native carbon based on coconut shell, GACO 383 is acid oxidized and others are  $Zr^{4+}$  activated carbons of GACO 383. The methods of preparation and experimental setup for furnace based thermal activation were discussed in Chapter 2.

## 4.3 Characterization Studies

### 4.3.1 Carbon Yield and Burn Off

Burn off of GACOZR series of carbon was calculated by dividing the weight loss during carbonisation between the original carbon and the final carbon product by the weight of the original carbon. GACOZR series gives the various extent of burn off depending upon their activation temperature. At the higher activation temperature the observed carbon yield is low. The maximum burn off of 23.62 % is obtained in activation temperature 1273 K and lowest burn off about 14.53 % is obtained in activation temperature of 473 K. After that there is a less noticeable change in burn off when activating up to 673 K (15.28 %). Increasing the activation at 873K (21.02 %) gives comparatively higher burn off than at 673K. This is almost consistent upto 1073 K and there is a small increment in burn off (23.62 %) for further rise of the temperature upto 1273 K. Burn off of GACOZR series of carbon lies in between 14 - 24 % in the temperature range of 473 - 1273K; it means that thermal decomposition of GAC is prevented by the presence of  $Zr^{4+}$  in GAC.

### 4.3.2 Elemental Analysis

Elemental composition of GACOZR series activated at different activation temperatures varies as, C (65.77 % - 89.71 %), O (8.83 % - 32.9 %), H (0.3 % - 3 %), and N (0.47 % - 0.60 %) given in the Table 4.1.

It can be seen that oxidation with nitric acid increases the oxygen content of granular activated carbon GACOZR. This is due to the formation of surface oxygen complexes by the oxidation of surface carbons. At the higher activation

temperatures, oxygen percentage is found to decrease from 32.9 % to 8.83 %. Sure to believe that more C - O functional groups is evolved as a volatile substance during activation. The oxygen percentage level maintains 10 – 8 % at the activation temperature of 1073 – 1273 K. An increase in carbon percent was observed with the rise of temperature and it is found to be in the range of 65.8 - 89.7 % for GACOZR series. For typical activated carbon, the carbon percentage is reported to be 88 % [1]. And this can be achieved by GACOZR series when activating at temperatures above 873 K.

### 4.3.3 Boehm Analysis

The surface oxygen groups on a GAC with acidic (carboxyl, lactone, phenol), as well as basic properties are determined by the Boehm titrimetric method. The surface functional groups, which differ in their acidities, are distinguished by neutralization with different solutions, i.e. HCl (for basic groups) and NaHCO<sub>3</sub>, Na<sub>2</sub>CO<sub>3</sub> and NaOH (for acidic groups).

**Table 4.1:** Burn off, carbon yield and elemental composition & Boehm titration analysis of GACOZR series activated at temperatures 383-1273K, GAC 383 and GACO 383

Carbons	Activation T (K)	Burn off %	Carbon yield %	C%	H%	N%	O%	Carboxylic/ meq/g	Phenolic/ meq/g	Lactones/ meq/g	Base/ meq/g
GACOZR	383	NA	NA	65.8	1.3	0.60	32.9	1.38	2.8	1.5	0.01
	473	14.5	85.5	67.5	3.0	0.54	29.5	1.20	3.7	1.3	0.01
	673	15.3	84.7	76.7	3.0	0.47	20.3	0.69	1.9	0.99	0.09
	873	21.0	79.0	76.4	0.7	0.50	22.8	1.01	2.2	1.2	0.24
	1073	21.7	78.3	89.2	0.3	0.57	10.5	0.32	1.9	0.29	0.38
	1273	23.6	76.4	89.7	1.5	0.53	8.8	0.23	1.5	0.18	0.38
GAC 383	383	NA	NA	89.4	0.6	0.36	9.6	0.40	0.45	0.18	0.5
GACO 383	383	NA	NA	65.1	2.6	0.58	31.7	1.38	2.10	1.34	0.2

Surface oxygen complexes on carbon materials are found to be decreased during chemical activation at higher temperatures. The variation observed in the quantity of functional groups is given as follows, carboxylic (1.38 - 0.229 meq/g), lactonic (1.52 - 0.175 meq/g) and phenolic (2.83 - 1.52 meq/g). Surface oxygen

complexes on carbon materials decompose upon heating by releasing CO and CO<sub>2</sub>. The desorption of CO<sub>2</sub> from carboxylic group is prominent at the temperature range of 383 – 673 K. This is attributed to the reduction of carboxylic group from 1.38 to 0.689 meq/g. The lactonic group gets decomposed at the temperature range of 473 – 973 K and this is the main reason for the reduction of lactonic groups from 1.52 to 0.292 meq/g.

These functional groups on the surface of carbon modify the surface behaviour and adsorption characteristics of activated carbons. It can be observed, that the amount of basic groups was significantly lower than the total amount of acidic groups on all the activated carbons studied. This suggests that all carbons in GACOZR series had an acidic character due to the presence of carbon-oxygen surface chemical structures, decided by carboxyl and lactones. It can be stated that acidic character of GAC makes the carbon surface hydrophilic and polar in nature.

#### 4.3.4. Fourier Transform Infrared Spectroscopy (FTIR) Studies

The FTIR spectra of GAC 383, GACO 383 and GACOZR series are given in Figure 4.1(a)-(h). Most FTIR spectra give broad peaks at 3430 cm<sup>-1</sup> (interstitially adsorbed H<sub>2</sub>O) and 3362 cm<sup>-1</sup> (OH stretching vibrations). The intensity of peaks in this region is relatively less for GACOZR series activated in 873 and 1073K compared to those at 473 and 673K Figure 4.1(d)-(g). Results of elemental analysis results support this observation, as we can see the loss of hydrogen content from 3.03 to 0.30 % at this temperature range. Peak at 2924 and 2881 cm<sup>-1</sup> can be assigned to the –C – H – stretching of methyl group [2]. The intensity of this peak is sharper in GACO 383 compared to GAC 383.

FTIR spectra of Figure 4.1(c)&(d) shows band at 1365 - 1385 cm<sup>-1</sup> attributed to the O - H bending deformation or C = O stretching in carboxylic acid (it is almost absent in GAC 383). At higher temperature this signal shifted to 1403 - 1429 cm<sup>-1</sup> as seen in Figure 4.1(e)-(h) can be assigned to ν(C - O) vibration in the carboxylate group.

The band located at about 1584 - 1638 cm<sup>-1</sup> is attributed to the carbonyl group (C = O) in quinones. The intensity of this peak in GACOZR series is gradually decreased by increasing the activation temperature from 673 - 1073K.



Compared to GAC 383, sharp peak is visible at  $1635\text{ cm}^{-1}$  (C = O) for GACO 383. The band at  $1112$  and  $1030\text{ cm}^{-1}$  could be assigned to the alcohol (R - OH) groups [3]. The presence of carboxylic and phenolic groups improves the cation-exchange and complexation properties of new carbon materials [4].

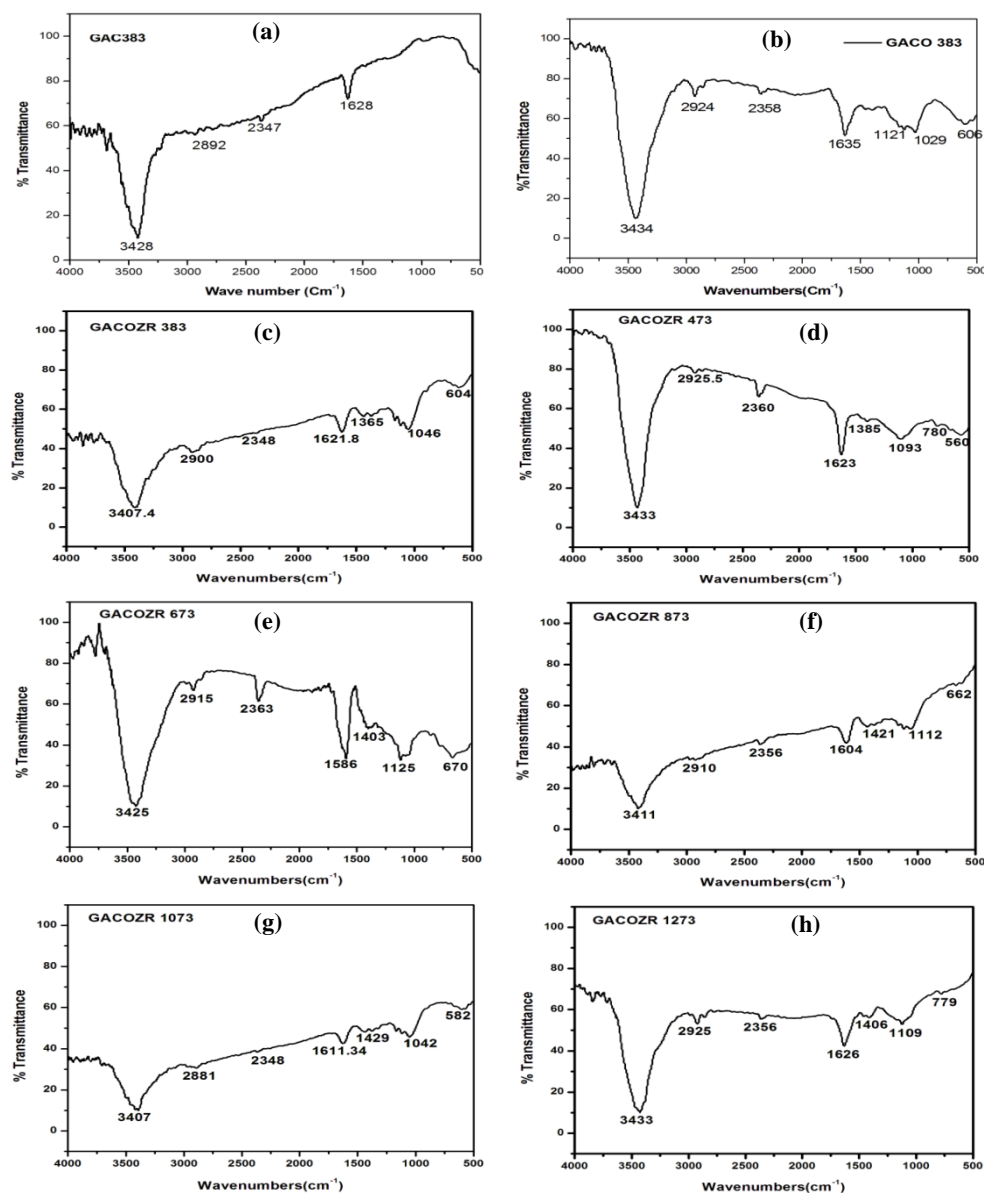


**Figure 4.1:** FTIR spectra of carbons (a) GAC 383 (b) GACO 383 (c)-(h) GACOZR series of carbons activated at 383-1273K for the evaluation of functional groups

### 4.3.5 X-ray Photoelectron Spectroscopy (XPS) Analysis

X-ray photoelectron spectroscopy (XPS) has been frequently used as a technique for the investigation of the surface chemical composition of carbon materials. The XPS spectra of C 1s and O 1s indicates that carbonyl groups were introduced to the surface at low oxidation potentials, and the concentration of alcohol-ether groups increased at high oxidation potentials.

Deconvolution of the O 1s, C 1s and Zr 3d peaks are shown in Figures 4.2. An asymmetric photoelectron peak of C 1s gives the binding energy of 284.0 eV indicate graphite (C - C), 284.4 eV associated with  $-C = C-$  non functionalised  $sp^2$  carbon, 285.3 eV associated with C - C and/or C - H groups. The binding energy of 286.4 eV associated with C - O -H/C - O -C,  $-C-O-C \equiv$  groups, 287.6 eV is associated with  $-COOC-$  groups, and 289.07 eV representing COOH carboxylic acid group.

The binding energy of 531.0 – 531.8 eV is associated with C = O group (oxygen doubly bonded to aromatic carbon), 533.1 eV attributed to the C - O group (oxygen singly bonded to  $sp^2$  carbon) or  $-C(O)OH$  groups, 534 eV is related with anhydride is observed, 534.6 eV is due to the chemisorbed  $H_2O$  molecule and the binding energy 530.4 eV of O 1s associated with O in  $ZrO_2$  [5, 6].

Most of the XPS measurements of the Zr 3d photoelectron spectrum had main peaks in between 180 eV – 190 eV. The peaks located at 181.3 and 186.8 eV are attributed to the spin-orbit splitting of the Zr 3d components, i.e. Zr  $3d_{5/2}$  and Zr  $3d_{3/2}$ . The binding energy of O 1s in  $ZrO_2$  is located at 530.4 eV. The Zr 3d spectrum had the strong spin-orbit doublet Zr  $3d_{5/2}$  - Zr  $3d_{3/2}$  with splitting of 2.3 eV. It was fitted by a single component (Zr - O) with the binding energy of  $182.76 \pm 0.2$  eV for the Zr  $3d_{5/2}$ .

The values of 182.03 eV, 183.3 eV, 182.2 eV and 182.60 eV have been associated with the presence of pure  $ZrO_2$  phase [7].

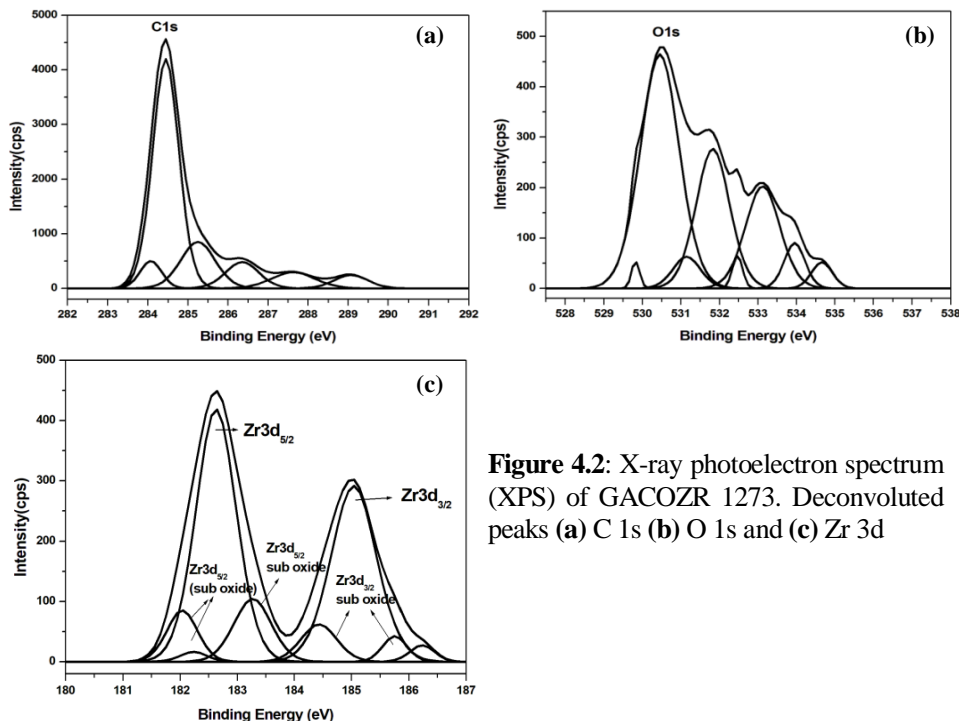


**Figure 4.2:** X-ray photoelectron spectrum (XPS) of GACOZR 1273. Deconvoluted peaks (a) C 1s (b) O 1s and (c) Zr 3d

The average binding energy (BE) values of  $180.996 \pm 0.05$  eV, and  $182.106 \pm 0.05$  eV gives a strong evidence for the formation of Zr sub-valence states  $Zr^{2+}$  and  $Zr^{3+}$  components [8].

**Table 4.2:** Surface functional groups analysis of carbons GAC 383, GACO 383 and GACOZR 1273 by XPS spectra

C1s		O1s	
284.5 eV	- C =C bonds with $sp^2$ hybridization	532.3 eV	- presence of C O/C O bonds
284.8 eV	- C -C bonds with $sp^3$ hybridization	533.3 eV	- C-OH bonds
285.7 eV	- C -O and C -OH functionalities	534.7 eV	- oxygen in water molecules
286.7 eV	- epoxide groups	532.0 eV	- carboxylic acid
289.4 eV	- carboxyl groups	[531.1, 532.3, 533.1 eV]	- single and double bond between O and C.
Zr 3d			
182.3 eV	- $ZrO_2$		
$180.99 \pm 0.05$ eV	- Zr sub-valence states $Zr^{2+}$		
$182.10 \pm 0.05$ eV	- Zr sub-valence states $Zr^{2+}$		

### 4.3.6 X-ray Diffraction (XRD) Analysis

Crystalline nature of the carbon was studied by using x-ray powder diffractometry. The crystalline size data were calculated from the XRD profiles using Scherrer analysis. X-ray diffractograms for activated carbon GAC 383, GACO 383 and GACOZR series are shown in Figures 4.3. The interlayer spacing values,  $d_{002}$ , and the crystallite size along the  $c$  ( $L_c$ ) and  $a$  ( $L_a$ ) axis of the carbon are given in Table 4.3.

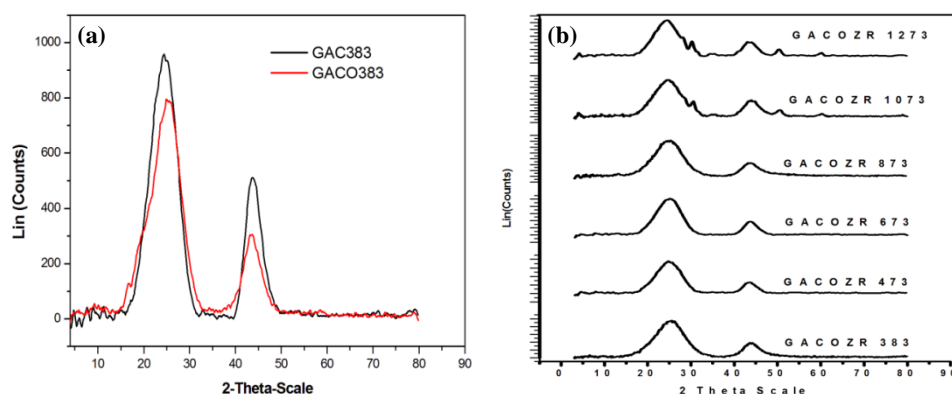


**Figure 4.3:** X-ray diffraction (XRD) spectra of (a) GAC 383 & GACO 383 (b) GACOZR series of carbons activated at 383-1273K

The two broad peak around  $2\theta = 25^\circ$  and  $43.6^\circ$  is ascribed to (002) and (100) diffraction peak of turbostratic carbon structure. Broad peak at  $25^\circ$  obtained instead of the sharp peak indicate the poor crystalline nature, which is one of the beneficial property for most well defined carbon materials [9].

The crystalline sizes vary as  $L_c$  (1.15 - 1.36 nm),  $L_a$  (2.35 - 2.77 nm) for GACOZR series. The interlayer spacing  $d_{002}$ , are in the range of 0.349 to 0.364 nm, which is slightly larger than that of graphitic carbon structure. It might be due to the presence of hetero atoms such as oxygen and hydrogen between the graphene layers of GAC [10]. These non graphitized carbons have well developed micropore structure during high temperature activation treatment.

**Table 4.3:** XRD crystalline parameters of GAC 383, GACO 383 and GACOZR series activated at temperatures 383 - 1273K

Carbons	$L_c$ (0.9) nm	$L_a$ (1.84)nm	$d_{002}$ nm
GAC 383	1.14	2.28	0.364
GACO 383	0.97	1.94	0.356
GACOZR 383	1.15	2.35	0.352
GACOZR 473	1.28	2.61	0.358
GACOZR 673	1.21	2.47	0.354
GACOZR 873	1.16	2.38	0.349
GACOZR 1073	1.36	2.77	0.356
GACOZR 1273	1.31	2.68	0.362

No visible structural changes were observed in the crystallinity for GACOZR series of carbons upon successive activation until 873 K. The new peak at  $2\theta = 30^\circ$  is obtained in activation temperature of 1073 and 1273 K for GACOZR series. This is attributed to the diffraction from (101) plane of tetragonal  $ZrO_2$ . It indicates, generation of  $ZrO_2$  from  $ZrOCl_2$  into the porous structure of GAC at a higher activation temperature [11].

#### 4.3.7 Scanning Electron Microscopy (SEM) Analysis

The SEM micrographs of GACOZR 1273 are given in the Figure 4.4. In SEM micrographs, a beam of electrons is used to scan the surface of a carbon. This analysis makes possible the direct observation of its surface features at the micro and submicro levels. There are several well developed pores are formed on the surface of GACOZR 1273. Comparison of these micrographs with GAC 383 indicates that the activation process enlarges the diameters of the pores on the surface of GACOZR 1273. The nitric acid oxidation/modification causes the widening of existing pores and the formation of large pores by burn out of the walls between the adjacent pores.

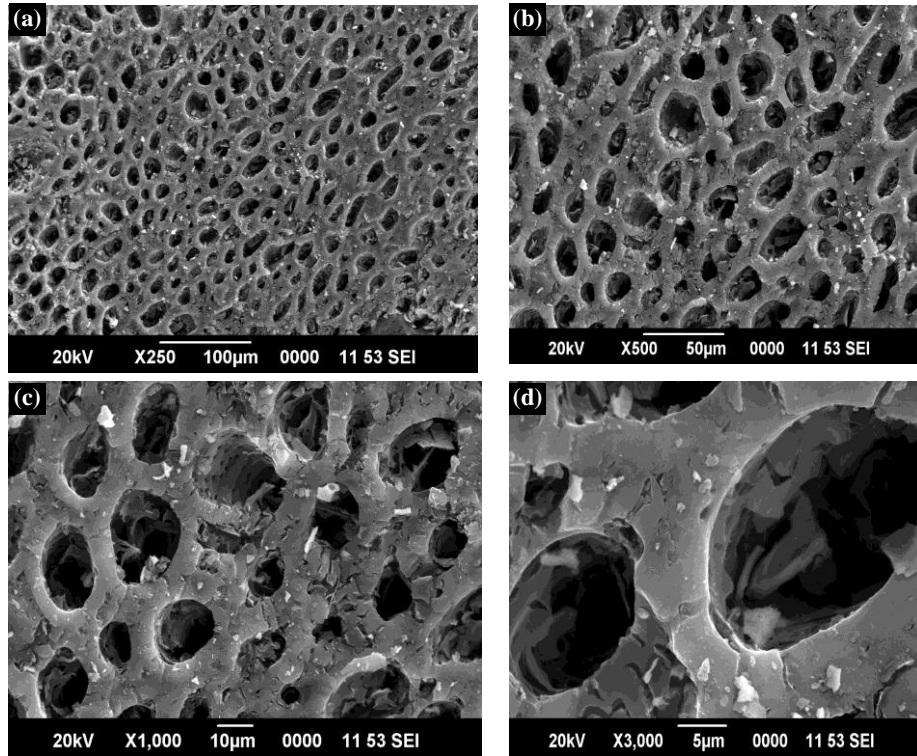


**Figure 4.4:** Scanning electron micrographs (SEM) of GACOZR 1273 at different resolution (a) 250-100  $\mu\text{m}$  (b) 500-50  $\mu\text{m}$  (c) 10  $\mu\text{m}$  and (d) 5  $\mu\text{m}$

Different size of pores are distributed over the surface of carbon, which is due to the removal of volatiles during carbonization and activation, leads to the creation of additional pores and widening of existing pore networks. Largest possible number of randomly distributed pores of various shapes and sizes, give rise to a carbon product with an extended and extremely high surface area.

#### 4.3.8. Transmission Electron Microscopy (TEM) Analysis

The structure of GACOZR 1273 is studied by using TEM images (Figure 4.5(a)-(d)). It shows very complex pore configurations, having various dimensions and irregular shapes.

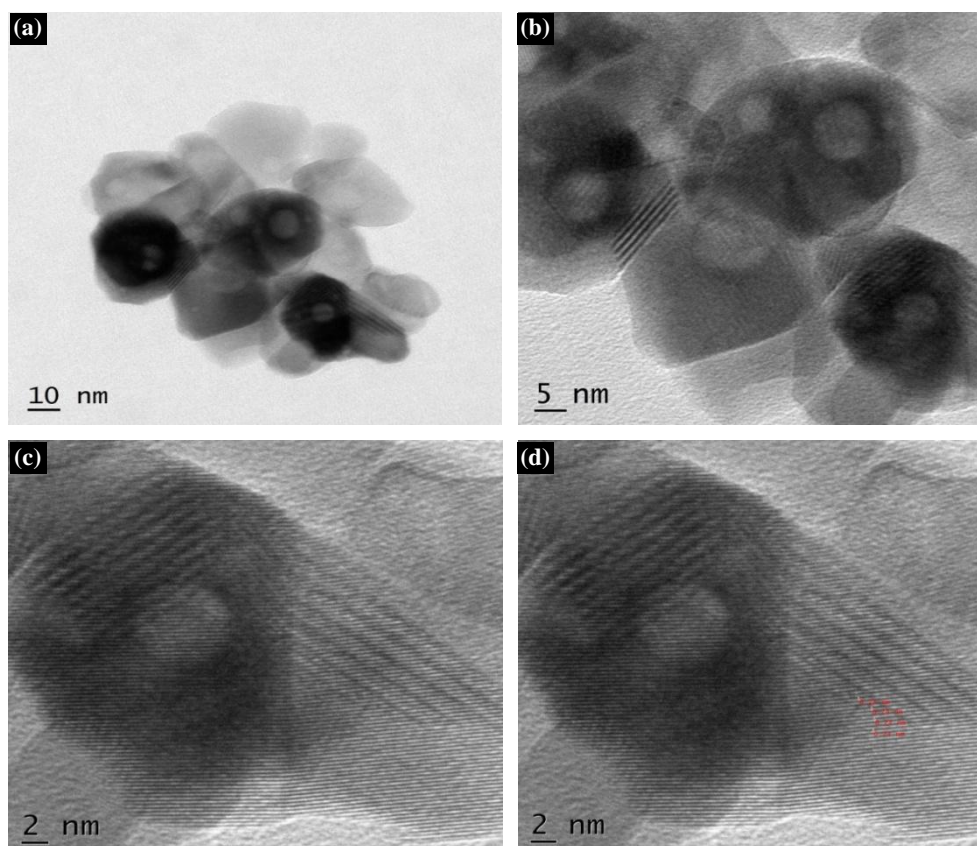


**Figure 4.5:** High resolution transmission electron microscopy (HRTEM) of GACOZR 1273 at different resolutions (a) 10nm (b) 5 nm (c) and (d) 2 nm

TEM image shows that carbon has a highly disordered and porous microstructure. Here the bright spots represent the centres of the individual rings of carbon atoms. Pores are having slit shaped structure confined by parallel planes and in some parts of the carbon GACOZR 1273, activation has produced cavities of mesopore size.

#### 4.4 Solid-Gas Adsorption Equilibria

The equilibrium and dynamic adsorption behaviour of active carbon have been studied by using  $N_2$  adsorption data for assessing the surface area, pore size, and pore volume of the carbons.

The  $N_2$  adsorption-desorption isotherms of the oxidised granular activated carbon impregnated with zirconyl chloride and activated at 1073 and 1273 K were carried out to investigate the porous characteristics.

#### 4.4.1 Adsorption Isotherm Analysis

The adsorption isotherm of  $N_2$  (77K) gas adsorbed on GAC 383, GACO 383, GACOZR 1073 and GACOZR 1273 are given in Figure 4.6.

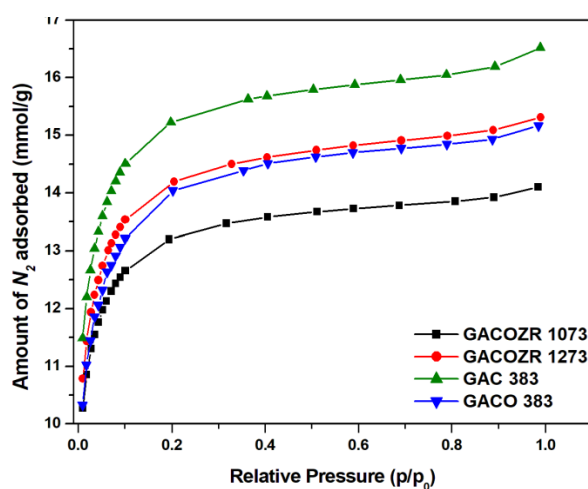


**Figure 4.6:**  $N_2$  adsorption isotherm for GAC 383, GACO 383 and GACOZR carbonized at temperature 1073 and 1273 K

It is expected to give the same isothermal behaviour as that of GACZR series (discussed in Chapter 3). *Type I* isotherm behaviour of GACOZR 1073 and GACOZR 1273 indicates that  $N_2$  molecules are progressively getting adsorbed on the micropores of these carbons, which are developed during activation process.

The nitrogen equilibrium data analysed by Brunauer-Emmett-Teller (BET), Langmuir, Freundlich, Dubinin-Radushkevich (D-R), Alpha S ( $\alpha_s$ ), John isotherm,  $t$ -plot and Barrett Joyner Halenda (BJH) models are used for comparing the porosity and surface area.



#### 4.4.1.1 Brunauer-Emmett-Teller (BET) Isotherm Analysis

The surface area of carbons is determined from the  $N_2$  isotherm by the BET method, based on surface coverage mechanism. This linearised BET equation provides the basis for the BET plot of experimental isotherm data.

$$\frac{1}{V(p_0/p - 1)} = \frac{1}{V_m C} + \frac{C - 1}{V_m C} (p/p_0) \quad (4.1)$$

Since the range of linearity of BET plot is usually taken in the relative pressure upto  $p/p_0 \approx 0.35$  and in some cases not more than  $p/p_0 \approx 0.1$ . Surface area and pore volume obtained from a linear plot of BET at  $p/p_0 \approx 0.35$  and  $p/p_0 \approx 0.1$  is given in Table 4.4.

Surface area and pore volume obtained from BET ( $p/p_0$  0.3) increases as per the order of GAC 383 ( $SA_{BET} = 997 \text{ m}^2/\text{g}$  &  $V_m = 228.97 \text{ cm}^3/\text{g}$ ) > GACOZR 1273 ( $SA_{BET} = 976.25 \text{ m}^2/\text{g}$  &  $V_m = 224.26 \text{ cm}^3/\text{g}$ ) > GACO 383 ( $SA_{BET} = 974 \text{ m}^2/\text{g}$  &  $V_m = 223.81 \text{ cm}^3/\text{g}$ ) > GACOZR 1073 ( $SA_{BET} = 920.15 \text{ m}^2/\text{g}$  &  $V_m = 211.37 \text{ cm}^3/\text{g}$ ).

All the carbons show surface area greater than  $900 \text{ m}^2/\text{g}$ . But surface modification with nitric acid (GACO 383) reduces the specific surface area by 7 % compared to basic GAC 383. The reduction in surface area is more pronounced in oxidised carbon GACOZR 1073 (specific surface area less by 13 % than GAC 383). Degree of activation makes the pore walls thinner and is easily destroyed by the  $\text{HNO}_3$  treatment [12]. GACOZR 1073 ( $920.15 \text{ m}^2/\text{g}$ ) and GACOZR 1273 ( $976.25 \text{ m}^2/\text{g}$ ) clearly shows that surface area and pore volume of GACOZR series is enhanced by activation temperature.

$SA_{BET}$  calculated from  $p/p_0$  upto 0.1 and 0.3 are different as shown in the Table 4.3 which indicate that  $SA_{BET}$  depends on the range of  $p/p_0$  used for the determination. The relative pressure range when shifted from 0.3 to 0.1 there is an increment of the surface area about 30.3 % in GAC 383 ( $1298.483 \text{ m}^2/\text{g}$ ), 21.8 % in GACO 383 ( $1186.476 \text{ m}^2/\text{g}$ ), 22.8 % in GACOZR 1073 ( $1130.349 \text{ m}^2/\text{g}$ ) and 24.2 % in GACOZR 1273 ( $1212.188 \text{ m}^2/\text{g}$ ).

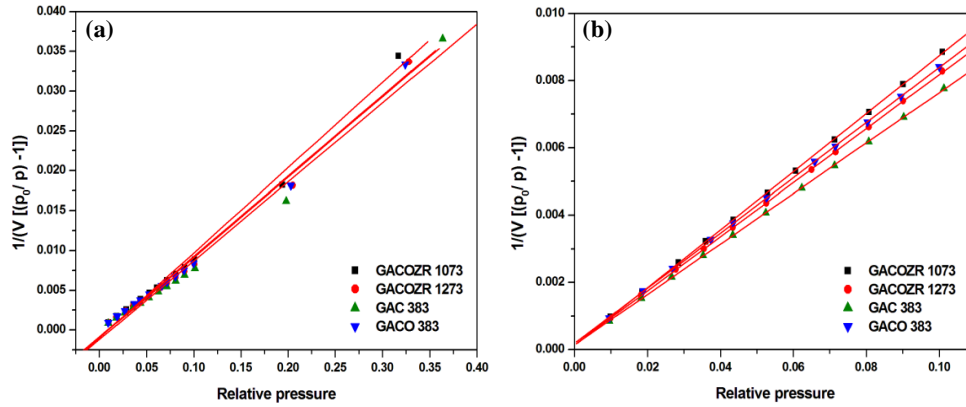


**Figure 4.7:** BET isotherm plot for GAC 383, GACO 383, GACOZR 1073 and GACOZR 1273 (a)  $p/p_0$  up to 0.3 and (b)  $p/p_0$  up to 0.1

#### 4.4.1.2 The BET–Scatchard (B–S) Plots (*I* Point Method Analysis)

The rearrangement of BET equation for calculating the specific surface area is given by the equation (4.2)

$$\frac{[V(1 - P)]}{P} = CV_m - (C - 1)[V(1 - P)] \quad (4.2)$$

Where  $P$  is  $p/p_0$ , it provides inclined  $V$  type graphs, (i.e.  $>$ ) with an inversion point, termed *I* point. The calculation of the specific surface area requires the estimation of  $V_m$ . The projection of the *I* point on the  $V(I - P)$  axis corresponds exactly to  $V_m$ , i.e.,  $[V(I - P)]_{I\text{-point}} = V_m$ . Then the specific surface areas can be calculated easily from the trivial relationship equation (4.3) without any knowledge of  $C$ .

$$\text{Specific surface area, } SA_I (m^2 g^{-1}) = 4.356 V_m \quad (4.3)$$

The plots are shown in Figure 4.8, and the results are given in Table 4.4.

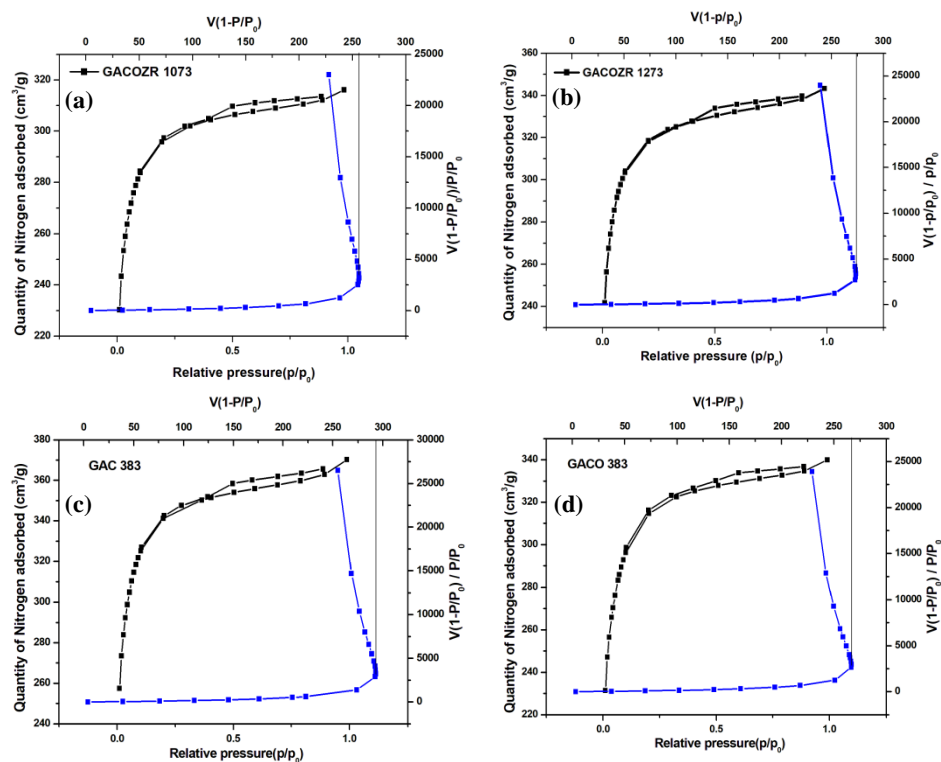


**Figure 4.8 :** Nitrogen adsorption-desorption isotherms and the corresponding *I* plots for (a) GACOZR 1073 (b) GACOZR 1273 (c) GAC 383 and (d) GACO 383 carbons

**Table 4.4:** BET and *I* plot isotherm parameters for GAC 383, GACO 383, GACOZR 1073 & GACOZR 1273 using N<sub>2</sub> at 77K

Carbons	Total pore volume $V_T$ cm <sup>3</sup> /g.STP	BET $p/p_0$ upto 0.3			I plot method		BET $p/p_0$ upto 0.1			
		$S_{BET}$ m <sup>2</sup> /g	$V_m$ cm <sup>3</sup> /g .STP	$C_{BET}$	$S_I$ m <sup>2</sup> /g	$V_I$ cm <sup>3</sup> /g.STP	$S_{BET}$ m <sup>2</sup> /g	$V_m$ cm <sup>3</sup> /g.STP	$C_{BET}$	Pore Width (nm)
GAC 383	370.4	996.8	229.0	-816	1275.4	293.0	1298.5	298.3	524	1.76
GACO 383	340.2	974.3	223.8	-119	1164.7	267.5	1186.5	272.6	439	1.77
GACOZR 1073	316.3	920.2	211.4	-106	1114.8	256.1	1130.4	259.7	715	1.73
GACOZR 1273	343.4	976.3	224.3	-103	1193.2	274.1	1212.2	278.5	563	1.75

The monolayer capacity  $V_l$  and surface area  $SA_l$  obtained for the modified carbons are GACOZR 1073 ( $V_l = 256.09 \text{ cm}^3/\text{g}$  &  $SA_l = 1114.83 \text{ m}^2/\text{g}$ ) and GACOZR 1273 ( $V_l = 274.10 \text{ cm}^3/\text{g}$  &  $SA_l = 1193.23 \text{ m}^2/\text{g}$ ). The pore volume and surface area obtained from BET  $p/p_0 \approx 0.1$  is close agreement with  $I$  point method. It supports the validity of linear BET plot up to  $p/p_0 \approx 0.1$  [13, 14].

#### 4.4.1.3 Langmuir Isotherm Analysis

Adsorption equilibrium in homogeneous adsorbents can be measured by using the standard Langmuir isotherm model. The linear form of the equation is

$$\frac{P}{V} = \frac{1}{bV_m} + \frac{P}{V_m} \quad (4.4)$$

Where  $V$  is the specific amount of gas adsorbed at the equilibrium pressure  $P$  and  $V_m$  is the monolayer capacity. From the graph of  $P/V$  versus  $P$ , a straight line is obtained and from the slope and intercept  $V_m$  ( $L$ ) monolayer volume and constant  $b$  is calculated. Langmuir adsorption isotherms for the adsorption of  $N_2$  gases on GAC 383, GACO 383, GACOZR 1073 and GACOZR 1273 are shown in Figure 4.9(a)

The straight line plot indicates that the Langmuir equation is valid for this entire range. The monolayer volume obtained for GAC 383 is  $336.60 \text{ cm}^3/\text{g}$ , whereas GACO 383 is  $304.5 \text{ cm}^3/\text{g}$ , indicates 9.5 % decrease in monolayer volume by surface modification with nitric acid. For GACOZR 1073 shows monolayer volume  $292.8 \text{ cm}^3/\text{g}$ , reveals that activation of GACO 383 with  $Zr^{4+}$  at 1073K further decrease the monolayer volume up to 3.8 %. At the activation temperature of 1273K, carbon GACOZR 1273 ( $314.1 \text{ cm}^3/\text{g}$ ) shows an enhancement in monolayer volume of 7.2 % compared to that of GACOZR 1073.

#### 4.4.1.4 Freundlich Isotherm Analysis

The relationship between the magnitude of adsorption (amount of gas adsorbed) and relative pressure,  $P$  can be expressed mathematically by an empirical equation of Freundlich isotherm model.

$$V = K_F P^{1/n} \quad (4.5)$$

$$\log V = \log K_F + \frac{1}{n} \log P \quad (4.6)$$

Freundlich adsorption isotherm plot of GAC 383, GACO 383, GACOZR 1073 and GACOZR 1273 are shown in the Figure 4.9 (b)

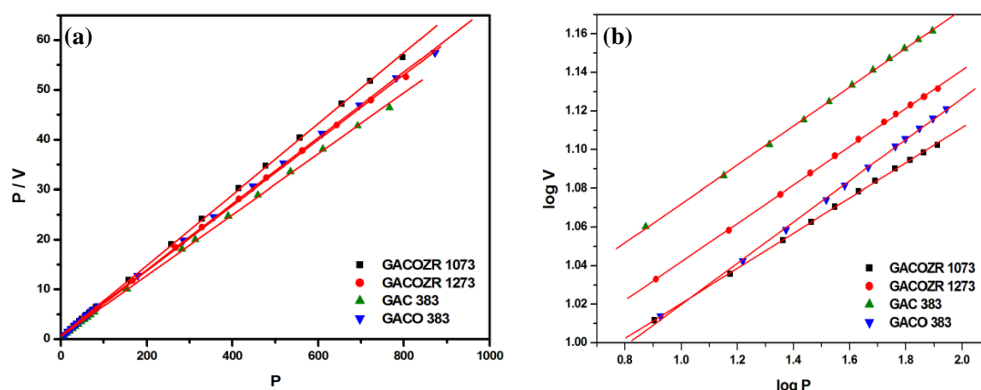


**Figure 4.9:** Adsorption isotherm plots (a) Langmuir (b) Freundlich for GAC 383, GACO 383, GACOZR 1073 & GACOZR 1273 using  $N_2$  at 77K

On plotting  $\log V$  versus  $\log P$  gives a straight line with intercept  $\log K_F$  and slope  $1/n$ . The constant are given in Table 4.5.  $K_F$  and  $n$  are depends upon carbon and  $N_2$  gas at a particular temperature. Straight line with high correlation coefficient ( $R^2 = 0.99$ ) shows the strong interaction of  $N_2$  molecule on the surface of carbons.

The  $K_F$  and  $n$  obtained for new carbons are GAC 383 ( $K_F$  is 209.82 &  $n$  is 9.94), GACO 383 ( $K_F$  is 183.51 &  $n$  is 9.36), GACOZR 1073 ( $K_F$  is 190.58 &  $n$  is 11) and GACOZR 1273 ( $K_F$  is 196.45 &  $n$  is 10.08) respectively.

**Table 4.5:** Langmuir and Freundlich isotherm parameters for GAC 383, GACO 383, GACOZR 1073 & GACOZR 1273 using  $N_2$  at 77K

Carbons	Langmuir				Freundlich		
	$V_m$ (L) $cm^3/g,STP$	$S_{A_L}$ ( $m^2/g$ )	$b$	$R^2$	$n$	$K_F$ L/g	$R^2$
GAC 383	336.6	1465.3	0.278	0.999	9.9	209.8	0.999
GACO 383	304.5	1325.5	0.246	0.999	9.4	183.5	0.999
GACOZR 1073	292.8	1274.6	0.301	0.999	11.0	190.6	0.999
GACOZR 1273	314.1	1367.3	0.274	0.999	10.1	196.5	0.999

Freundlich parameter  $n$  value, which is regarded as adsorption intensity is comparatively lower for nitric acid modified carbons (GACO 383, GACOZR 1073 and GACOZR 1273) than basic carbon GAC 383.

#### 4.4.1.5 Dubinin-Radushkevich Isotherm (D-R) Analysis

The D-R isotherm measures the pore filling mechanism within the micropores. The micropore volume  $V_{mi}(D-R)$  (or  $V_0$ ) and characteristic adsorption energy  $E$  (or  $E_0$ ) within micropore is obtained from the intercept and slope of the plot  $\log V$  versus  $\log^2(p_0/p)$ . This method makes possible to calculate micropore volume at low relative vapour pressure

$$\log V = \log V_0 - D \log^2(p_0/p) \quad (4.7)$$

$$D = 2.303 \left( \frac{RT}{\beta E_0} \right)^2 \quad (4.8)$$

$E_0$  is related to the average pore width ' $L$ ' according to the following empirical formula.

$$L = 6.6 - 1.79 \ln E_0 \text{ nm} \quad (4.9)$$

Relationship between  $L$  value and surface area are given by the equation.

$$SA_{D-R} = \frac{2 \times 10^3 V_{mi} (\text{cm}^3/\text{g})}{L(\text{nm})} \quad (4.10)$$

Where  $SA_{D-R}$  is the surface area in  $\text{m}^2/\text{g}$ .  $V_{mi}(D-R)$  is the micropore volume in  $\text{cm}^3/\text{g}$ , and  $L$  is the accessible pore width in nanometres. Parameters are calculated and given in Table 4.6.

Figure 4.10(a) shows that equation is valid over a range of relative pressures  $p/p_0$  0.00998 to 0.3 which corresponds to 85 to 95% filling of the micropores. GACO 383 ( $V_{mi} = 322.75 \text{ cm}^3/\text{g}$ ) shows 8.1% decreases of micropore volume compared to that of GAC 383 ( $V_{mi} = 351.3 \text{ cm}^3/\text{g}$ ). The  $\text{Zr}^{4+}$  activated oxidised carbons GACOZR 1073 ( $V_{mi} = 304.5 \text{ cm}^3/\text{g}$ ) shows 5.65 % lesser micropore volume compared to that of GACO 383 and 13.3 % decrease of micropore volume compared to that of GAC 383 ( $V_{mi} = 351.3 \text{ cm}^3/\text{g}$ ). By rising the activation temperature up to 1273K, the  $\text{Zr}^{4+}$  impregnated oxidised carbon

samples GACOZR 1273 (327.76 cm<sup>3</sup>/g) shows 7.6 % enhancement in micropore volume compared to that of GACOZR 1073 but lower than that of GAC 383. All these results indicate that oxidation of GAC with HNO<sub>3</sub> and activation of GACO with Zr<sup>4+</sup> could not achieve higher micropore volume compared to GAC 383. Calculated pore width (equation (4.9) increases from 1.59 nm to 1.66 nm for Zr<sup>4+</sup> impregnated oxidised GAC by rising the temperature from 1073 K to 1273 K.

#### 4.4.1.6 Alpha S ( $\alpha_s$ ) Method

The external surface area ( $SA_{ext}$ ) and micropore volume ( $V_{mi}$ ) can be calculated by using Alpha S ( $\alpha_s$ ) plots. The fitting of isotherm data on equations gives plot with respect to the carbon samples GACOZR 1073, GACOZR 1273, GAC 383 and GACO 383 (Figure 4.10 (b)). It is obtained by plotting the volume of gas adsorbed by carbon versus  $\alpha_s$  and it is directly proportional to specific surface area of carbons.

$$\alpha_s = \frac{V_{ads}}{V_{ads}(\frac{p}{p_0}=0.4)} \quad (4.11)$$

The plot gives a straight line from the region of  $0.7 > \alpha_s < 1.10$ . From the slope and intercept of plot, the external surface area (corresponds to mesopore) and micropore volume can be calculated (values are listed in Table 4.6). The micropore volume obtained from two independent methods i.e Dubinin – Radushkevich (D-R) and Alphas S ( $\alpha_s$ ) method shows close agreement.

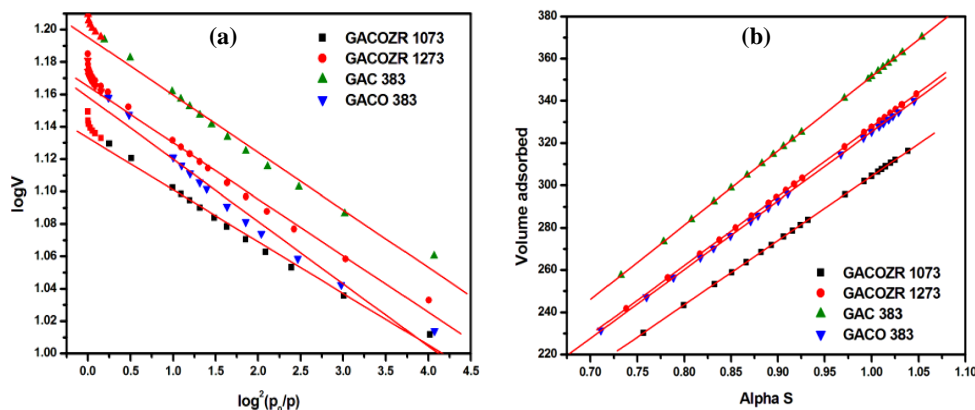


**Figure 4.10:** Adsorption isotherm plots (a) Dubinin - Radushkevich and (b) Alpha S ( $\alpha_s$ ) for GAC 383, GACO 383, GACOZR 1073 & GACOZR 1273 K using N<sub>2</sub> at 77K

Surface modification of GAC 383 with  $\text{HNO}_3$  decreases the external surface area from  $1005.27 \text{ m}^2/\text{g}$  (GAC 383) to  $930.30 \text{ m}^2/\text{g}$  (GACO 383) and pore volume from  $351.5 \text{ cm}^3/\text{g}$  (GAC 383) to  $325.3 \text{ cm}^3/\text{g}$  (GACO 383) respectively. It is noted that 7.45 % decrease in the external surface area and pore volume in GACO 383 compared to GAC 383. Further modification of GACO 383 with  $\text{Zr}^{4+}$  (GACOZR 1073) gives 6.4 % decrease in  $SA_{ext}$  and  $V_{mi}$  compared to GACO 383. This result shows that surface modification with nitric acid (GACO 383) and their higher degree of activation (GACOZR 1073) cause decrease in the external surface area compared to basic GAC 383. This might be due to the partial destruction of meso and macropore network of thinner pore walls.

The carbon GACOZR 1273 gives 7.6 % enhancement of external surface area and pore volume compared to that of GACOZR 1073. Increasing of  $SA_{ext}$  suggests the widening of the micropores without the destruction of pore walls. Increases of micropore volume from  $304.43 \text{ cm}^3/\text{g}$  to  $327.65 \text{ cm}^3/\text{g}$  indicates the generation of new micropores in GACOZR 1273 compared to GACOZR 1073.

**Table 4.6:** Dubinin-Radushkevich (D-R) & Alpha S ( $\alpha_s$ ) isotherm parameters of GAC 383, GACO 383, GACOZR 1073 and GACOZR 1273K using  $\text{N}_2$  at 77K

Carbons	Dubinin-Radushkevich (D-R)					Alpha S	
	$SA_{D-R}$ ( $\text{m}^2/\text{g}$ )	$V_{mi}$ (D-R) ( $\text{cm}^3/\text{g.STP}$ )	L mm	E kJ/mol	$R^2$	$V_{mi}$ ( $\alpha_s$ ) ( $\text{cm}^3/\text{g.STP}$ )	$SA_{ext}$ ( $\text{m}^2/\text{g}$ )
GAC 383	646.5	351.3	1.68	15.6	0.986	351.5	1005.3
GACO 383	570.2	322.8	1.75	15.0	0.979	325.3	930.3
GACOZR 1073	593.9	304.5	1.59	16.5	0.990	304.4	870.7
GACOZR 1273	609.0	327.8	1.66	15.8	0.991	327.7	937.1

Comparison of the relative values of the micropore volume ( $V_{mi}/V_T$ ) and the mesopore surface area ( $SA_{ext}/SA_{BET}$ ) shows similar value for GAC 383, ( $V_{mi}/V_T = 0.95$ ,  $SA_{ext}/SA_{BET} = 0.77$ ), GACOZR 1273 ( $V_{mi}/V_T = 0.95$ ,  $SA_{ext}/SA_{BET} = 0.77$ ), GACO 383 ( $V_{mi}/V_T = 0.95$ ,  $SA_{ext}/SA_{BET} = 0.78$ ) and GACOZR 1073 ( $V_{mi}/V_T = 0.96$ ,



$SA_{ext}/SA_{BET} = 0.77$ ). This means that these carbons have rather uniform microporous structure [15].

#### 4.4.1.7. John Isotherm Analysis

The general form of John isotherm equation applied to the  $N_2$  adsorption data to study the pore filling mechanism [16].

$$\log \log P = C + n \log V \quad (4.12)$$

Where  $P = p/p_0 \times 10^N$  'N' is taken conveniently to make  $\log P$  positive thereby  $\log \log P$  could be found, and  $n$  is adsorbability constant.

The equation (4.12) is further extended to study the adsorption potential of porous materials, from solid - liquid adsorption system known as the John - Sivanandan Achari isotherm given by

$$\log \log C_e = C + n \log q_e \quad (4.12 a)$$

The John isotherm plots, based upon  $N_2$  uptake data provide three distinct phases for GAC 383, GACO 383, GACOZR 1073, and GACOZR 1273 are presented in a Figure 4.11.

Total pore volume ( $V_T$ ) calculated by John isotherm method shows good agreement with the total pore volume obtained at  $p/p_0$  0.9 (Table 4.4). The total pore volume  $V_T$  ( $J$ ) comprises into three different phases. Molecular sieve effects ( $mse$ ), cause major adsorption to take place in *phase I* i.e.  $V_{mse}(J)$ , equal to an adsorption capacity 289.95  $\text{cm}^3/\text{g}$  (GAC 383), 264.10  $\text{cm}^3/\text{g}$  (GACO 383), 255.82  $\text{cm}^3/\text{g}$  (GACOZR 1073), 270.59  $\text{cm}^3/\text{g}$  (GACOZR 1273). This indicates that the majority of  $N_2$  molecule will get adsorbed into the pores having dimensions less than 0.8 nm.

The presence of micropores having width 0.8 – 2.0 nm indicated by *Phase II* i.e.  $V_m(J)$  and it is equal to 43.61  $\text{cm}^3/\text{g}$  (GAC 383), 52.06  $\text{cm}^3/\text{g}$  (GACO 383), 37.06  $\text{cm}^3/\text{g}$  (GACOZR 1073) and 41.84  $\text{cm}^3/\text{g}$  (GACOZR 1273). Contribution of wider pores (pore width > 2nm) represented by *phase III* its value  $V_c$  is obtained by subtracting the ( $V_{mse} + V_m$ ) from  $V_T$ . The lower values of  $V_c(J)$  indicate the lower contribution of wider micropore in total pore volume i.e it contribute 6.4 - 8.9 % only in total pore volume whereas  $V_{mse}(J)$  contribute 78 - 80% in total pore volume  $V_T(J)$ .

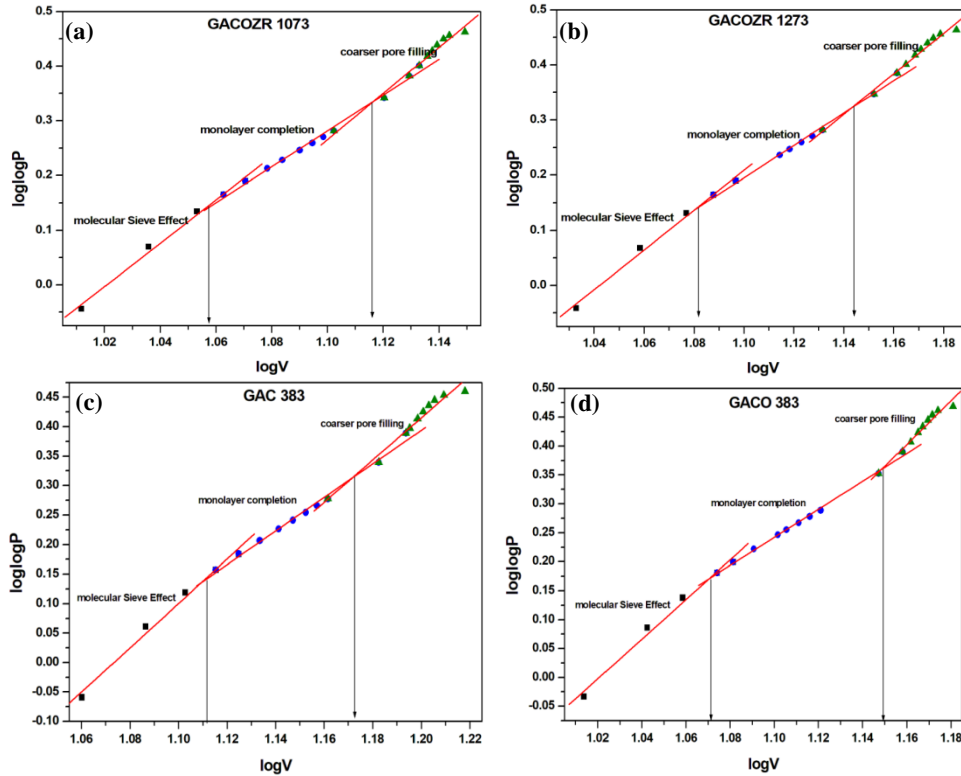


**Figure 4.11:** John Isotherm plot for carbons (a) GACOZR 1073 (b) GACOZR 1273 (c) GAC 383 and (d) GACO 383

**Table 4.7 :** John adsorption isotherm parameters of GAC 383, GACO 383, GACOZR 1073 and GACOZR 1273

Carbons	Adsorption Capacity (cm <sup>3</sup> /g)			
	V <sub>mse</sub> (J) cm <sup>3</sup> /g.STP	V <sub>m</sub> (J) cm <sup>3</sup> /g.STP	V <sub>c</sub> (J) cm <sup>3</sup> /g.STP	V <sub>T</sub> (J) cm <sup>3</sup> /g.STP
GAC 383	289.95 n = 3.76	43.61 n = 2.85	32.05 n = 3.60	365.61
GACO 383	264.10 n = 3.43	52.06 n = 2.42	21.55 n = 3.78	337.72
GACOZR 1073	255.82 n = 3.96	37.06 n = 3.27	23.19 n = 4.21	316.07
GACOZR 1273	270.59 n = 3.61	41.84 n = 2.93	30.58 n = 3.67	343.008

A comparison of total micropore volume ( $V_{mse} + V_m$ ) obtained from the john isotherm model with other isotherm models (D-R, Alpha S, and Langmuir) are schematically represented in the Figure 4.12. All the isotherm model offer almost identical values of monolayer volumes for all the carbon studied.

**Table 4.8:** John, Dubinin-Radushkevich (D-R), Alpha S ( $\alpha_s$ ) and Langmuir isotherm: comparison of pore volume obtained from Isotherm models

Carbons	Pore volume			
	John ( $V_{mse} + V_m$ ) cm <sup>3</sup> /g STP	D-R $V_m$ (D-R) cm <sup>3</sup> /g STP	Alpha S $V_m$ ( $\alpha_s$ ) cm <sup>3</sup> /g STP	Langmuir $V_m$ (L) cm <sup>3</sup> /g STP
GAC 383	333.6	351.3	351.5	336.6
GACO 383	316.2	322.8	325.3	304.5
GACOZR 1073	292.9	304.5	304.4	292.8
GACOZR 1273	312.4	327.8	327.7	314.1

#### 4.4.1.8. *t*- Plot Method

The *t* - plot isotherm analysis was done for the GACOZR carbon series, and the thickness of the pores was calculated using the equation

$$t = \left[ \frac{13.99}{0.034 - \log (P/p_0)} \right]^{0.5} \quad (4.13)$$

The *t* - plot method is applied to calculate the micropore volume and external surface area. The mesopore volume was calculated by subtracting the micropore volume from the total pore volume. Figure 4.13 gives the plot of mmol/g of  $N_2$  gas adsorbed versus thickness for carbon GAC 383, GACO 383, GACOZR 1073 and GACOZR 1273. A straight line is drawn in the linear region of the *t* - plot, and from the slope and intercept the external surface area and micropore volume are calculated.

The external surface area obtained from the slope of the *t*-plot is given in the Table 4.9. It shows that surface modification of GAC with  $HNO_3$  enhances 6.27 % external surface area compared to that of GAC 383, is a marked evidence for enlargement of microporosity. But the chemical activation of GACO with  $Zr^{4+}$  lowers the external surface area by 27.2 % in GACOZR 1073 and 19.8 % decreases in GACOZR 1273 compared to basic GAC 383.

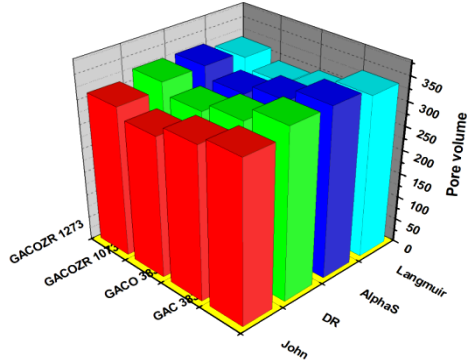


**Figure 4.12:** Comparison of pore volumes obtained for John (J) /D-R/ Alpha S/ Langmuir models for the adsorption of  $N_2$  at 77 K for newly prepared microporous carbons

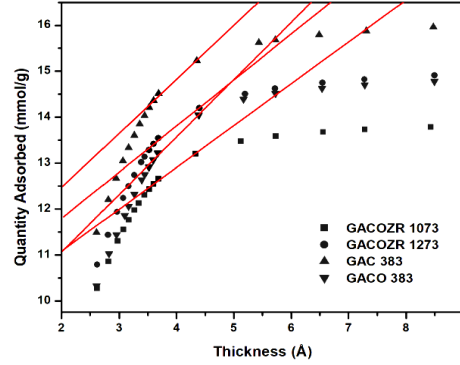


**Figure 4.13:**  $t$ -plot analysis of carbons GAC 383, GACO 383 and GACOZR 1073 and GACOZR 1273

Micropore surface area obtained by subtracting the  $SA_{ext(t)}$  from  $SA_{BET}$  is given in Table 4.9 for all carbon studied. It can be seen that micropore surface area  $SA_{mi(t)}$  and external surface area ( $SA_{ext(t)}$ ) are inversely related. Carbon which has a less external surface area (GACOZR 1073 and GACOZR 1273) provides high micropore surface area.

Comparison of GACOZR 1073 and GACOZR 1273 shows that, micropore surface area  $SA_{mi(t)}$  and micropore volume  $V_{mi}(t)$  of GACOZR 1273 ( $SA_{mi} 628.4 \text{ m}^2/\text{g}$  &  $V_{mi} 219.58 \text{ cm}^3/\text{g}$ ) is high compared to GACOZR 1073 ( $SA_{mi} 604.44 \text{ m}^2/\text{g}$  &  $V_{mi} 207.7 \text{ cm}^3/\text{g}$ ). It illustrates that the extent of pore formation in GACOZR series is continued even at higher activation temperatures (1273K) without the loss of porosity or destruction of pore wall.

#### 4.4.1.9 Barrett-Joyner-Halenda (BJH) Method

BJH analysis used to determine pore area and specific pore volume using  $N_2$  adsorption and desorption techniques. The pore size distribution obtained by the BJH method for the activated carbons GAC 383, GACO 383, GACOZR 1073 and GACOZR 1273 is given in the Figure 4.14–4.16.

Barrett-Joyner-Halenda (BJH) pore-size distributions were determined from both the adsorption and desorption techniques of the isotherms of  $N_2$  gas for the carbons.

Pore size distribution obtained from desorption shows a single peak near to 30 Å. For all the carbons main peak is located at same pore width except GACO 383, which is shifted to higher pore width region (near to 50 Å).

The area under the pore size distribution curves of GAC 383 is higher compared to that of GACOZR 1273, GACOZR 1073 and GACO 383.

For GACOZR 1073 the adsorption cumulative surface area (ADCSA) of the respective pore is 174.7 m<sup>2</sup>/g for a cumulative pore volume (ACPV) of 0.102544 cm<sup>3</sup>/g (66.30 cm<sup>3</sup>/g.STP) and corresponding desorption cumulative surface area (DCSA) is found to be 181.1 m<sup>2</sup>/g for a cumulative pore volume (DCPV) of 0.10348 cm<sup>3</sup>/g (66.94 cm<sup>3</sup>/g.STP). The respective adsorption pore width and desorption pore width are 2.35 nm and 2.29 nm.

For GACOZR 1273 the adsorption cumulative surface area (ADCSA) of the respective pore is 204.04 m<sup>2</sup>/g for a cumulative pore volume (ACPV) of 0.12294 cm<sup>3</sup>/g (79.49 cm<sup>3</sup>/g.STP) and corresponding desorption cumulative surface area (DCSA) found to be 205.76 m<sup>2</sup>/g for a cumulative pore volume (DCPV) of 0.12275 cm<sup>3</sup>/g (79.36 cm<sup>3</sup>/g.STP). The respective adsorption pore width and desorption pore width are 2.41 nm and 2.39 nm. The adsorption pore width and desorption pore width for zirconium impregnated oxidised granular activated carbon are high (in the range 2.35 – 2.41 nm) compared to GACO 383 (2.25 - 2.28 nm).

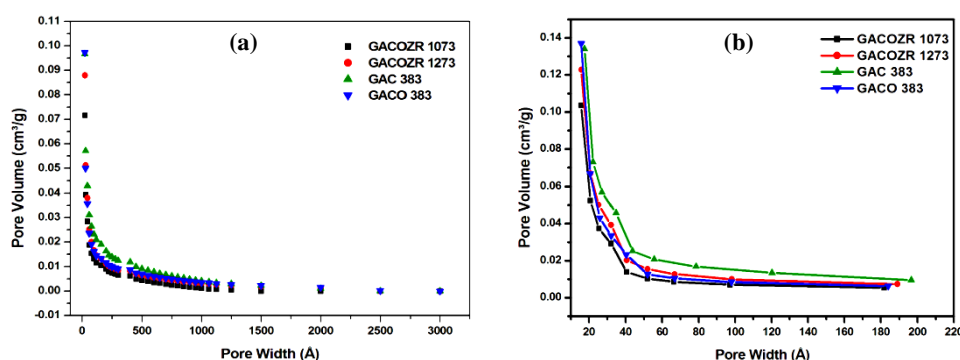


**Figure 4.14:** BJH isotherm analysis (a) Adsorption cumulative pore volume (b) Desorption cumulative pore volume for GAC 383, GACO 383, GACOZR 1073 & GACOZR 1273

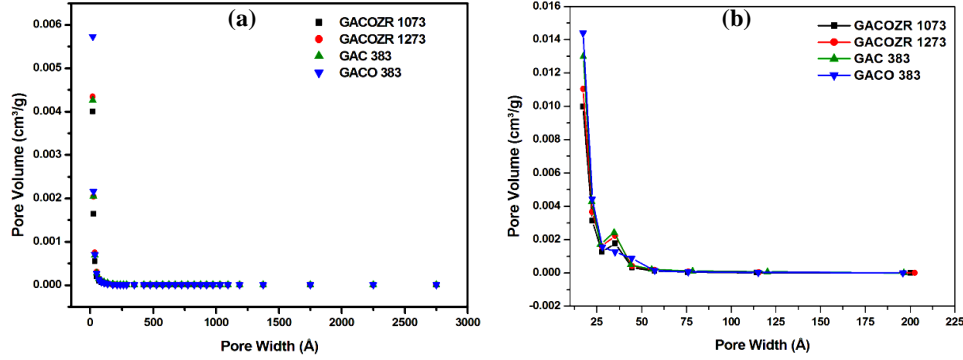


**Figure 4.15:** BJH isotherm analysis (a) Adsorption  $dV/dw$  pore volume (b) Desorption  $dV/dw$  pore volume for GAC 383, GACO 383, GACOZR 1073 & GACOZR 1273

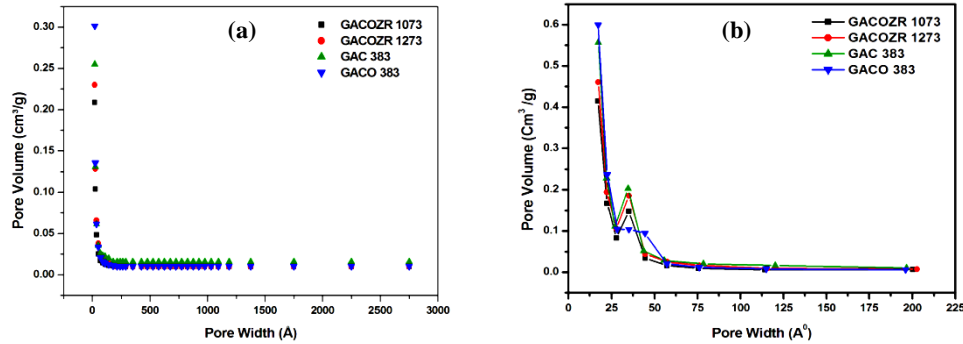


**Figure 4.16:** BJH isotherm analysis (a) Adsorption  $dV/d\log w$  pore volume and (b) Desorption  $dV/d\log w$  pore volume for the carbons, GAC 383, GACO 383, GACOZR 1073 & GACOZR 1273

**Table 4.9:**  $t$  - plot and BJH isotherm parameters of carbons GAC 383, GACO 383, GACOZR 1073 and GACOZR 1273

Carbons	t-plot			Barrett-Joyner-Halenda					
	$V_{mi} (t)$ $cm^3/g.STP$	$SA_{mi} (t)$ $m^2/g$	$SA_{ext} (t)$ $m^2/g$	ADCSA $m^2/g$	DCSA $m^2/g$	*ACPV $cm^3/g$	*DCPV $cm^3/g$	Pore width (ads) nm	Pore width(des) nm
GAC 383	226.7	588.7	408.1	226.2	220.5	0.138	0.134	2.44	2.43
GACO 383	192.0	540.3	433.7	250.0	242.8	0.142	0.137	2.28	2.25
GACOZR 1073	207.7	604.4	315.7	174.7	181.1	0.103	0.104	2.35	2.29
GACOZR 1273	219.6	628.5	347.8	204.0	205.8	0.123	0.123	2.41	2.39

$$* V_m (cm^3/g) = \frac{V_m (cm^3/g).STP \times 28}{22414 \times 0.808}$$

#### 4.5 Solid – Liquid Equilibria: Adsorption Studies

To choose the best carbon in GACOZR series for solid –liquid adsorption, batch adsorption experiments were performed by contacting 0.05 g of selected carbons in 100 ml Erlenmeyer flask with 50ml solutions of phenol ( $C_0$  1000 mg/L, equilibrium time 8hours), *p*-nitrophenol ( $C_0$  1000 mg/L, equilibrium time 8hours) and MB ( $C_0$  500 mg/L, equilibrium time 10 hours). The experiments were performed in a water bath shaker at controlled temperature ( $30 \pm 2^\circ\text{C}$ ) for a period of appropriate equilibrium time. The residual adsorbate solution concentration was determined by UV-Visible spectrophotometer at 268 nm for phenol, 317 nm for *p*-nitrophenol and 650 nm for MB. Among the series of GACOZR carbons studied, GACOZR 1273 shows comparatively higher adsorption efficiency in liquid phase than others. So this carbon is selected for further solid-liquid equilibrium studies together with basic carbons GAC 383 and GACO 383.

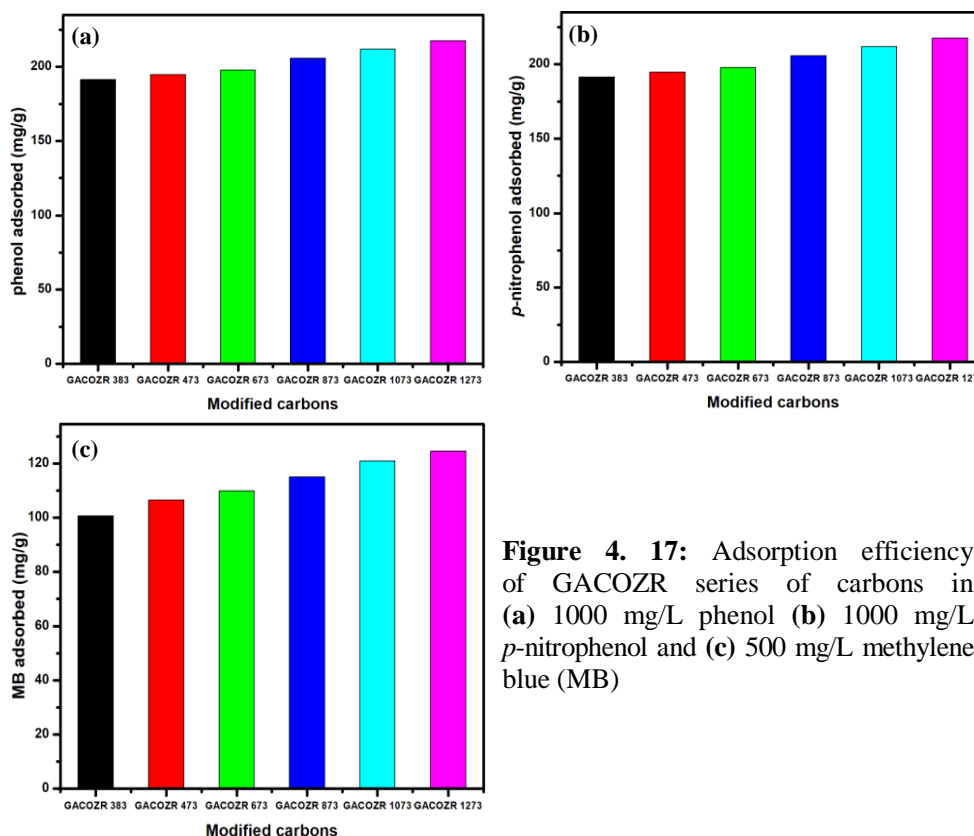


**Figure 4. 17:** Adsorption efficiency of GACOZR series of carbons in (a) 1000 mg/L phenol (b) 1000 mg/L *p*-nitrophenol and (c) 500 mg/L methylene blue (MB)

#### 4.5.1 Adsorption Studies of Phenol, *P*-Nitrophenol and Methylene Blue

Equilibrium isotherm data obtained from batch experiments were subjected to different isotherm models such as Langmuir, Freundlich, and Dubinin - Radushkevich (D-R) to optimize the design of specific adsorbent/adsorbate system. Figure 4.18(a)-(c) shows adsorption isotherm of phenol, *p*-nitrophenol and methylene blue on GAC 383, GACO 383, and GACOZR 1273 at 303K.

The amount of phenol adsorbed on the GAC is given as follows GACOZR 1273 (275 mg/g), GAC 383 (301 mg/g) and GACO 383 (209 mg/g). The amount of *p*-nitrophenol adsorbed is given as GACOZR 1273 (410 mg/g), GAC 383 (341 mg/g) and GACO 383 (220 mg/g). Methylene blue adsorbed on GAC given as GACOZR 1273 (140 mg/g), GAC 383 (190 mg/g) and GACO 383 (138 mg/g).

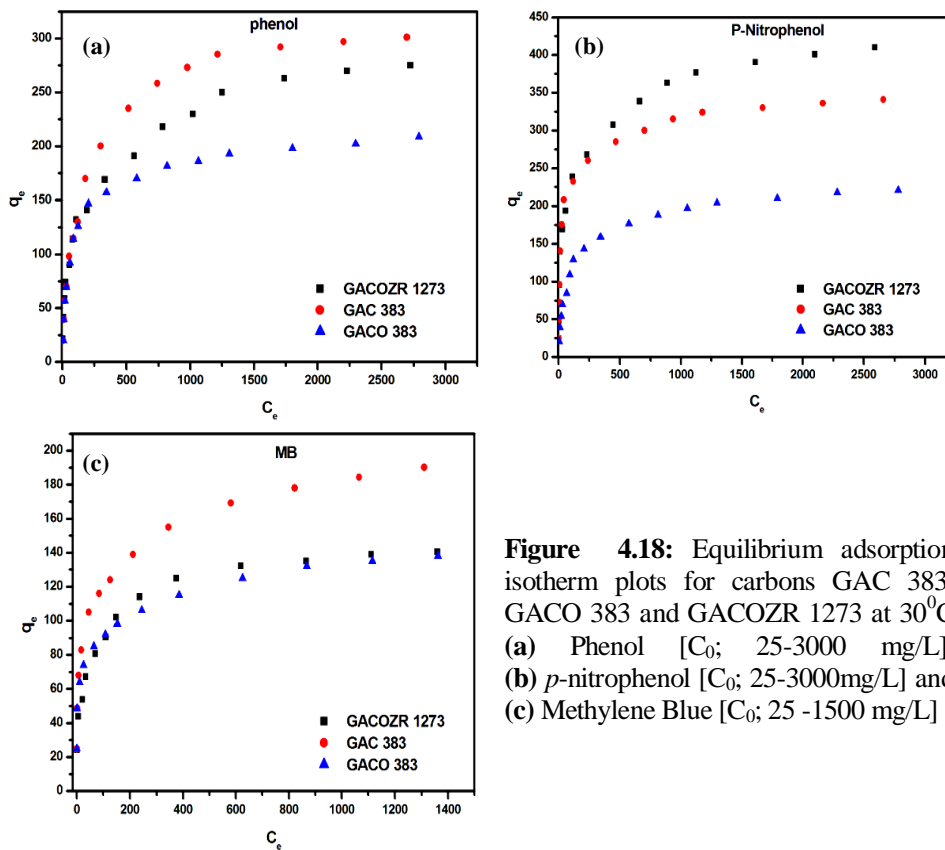


**Figure 4.18:** Equilibrium adsorption isotherm plots for carbons GAC 383, GACO 383 and GACOZR 1273 at 30°C (a) Phenol [ $C_0$ ; 25-3000 mg/L], (b) *p*-nitrophenol [ $C_0$ ; 25-3000mg/L] and (c) Methylene Blue [ $C_0$ ; 25 -1500 mg/L]



Zirconyl chloride impregnated oxidised GAC (*i.e.* GACOZR 1273) shows high adsorption ( $\approx 32\%$  more phenol adsorption,  $86\%$  increment in *p*-nitrophenol adsorption and  $1.45\%$  increment in methylene blue adsorption) compared to that of GACO 383.

Adsorption of methylene blue on oxidised carbon such as GACOZR 1273 and GACO 383 has no significant difference in adsorbed quantity. Adsorption of methylene blue (MB) on activated carbon depends on the pH of the solution. Adsorption of this cationic dye is favoured by an increase in initial solution pH. As the surface functional group content is more on activated carbon it causes a decrease of solution pH. Therefore, it decreases the electrostatic interaction between the oxidised carbon samples and dye molecules [17].

#### **4.5.2 Adsorption of Phenol on GACOZR 1273, GAC 383 and GACO 383 at Temperatures**

Adsorption of phenol on GACOZR 1273, GAC 383 and GACO 383 at five temperatures from 283 to 323 K is studied and plotted as per isotherm models. The parameters obtained from Langmuir, Freundlich and Dubinin - Radushkevich isotherm equations along with the values of the correlation coefficient determined ( $R^2$ ) for the best fits of adsorption data at various temperatures are given in Table 4.10. A linearised form of Langmuir isotherm equation applied is [18-20]

$$\frac{C_e}{q_e} = \frac{1}{K_L} + \frac{a_L}{K_L} C_e \quad (4.14)$$

The Langmuir plots of phenol adsorption on GAC 383, GACO 383 and GACOZR 1273 with respect to five temperatures are given in Figures 4.19(a)–(c). Straight line plot of  $C_e/q_e$  versus  $C_e$  at each temperature has  $R^2$  value 0.99 indicates the applicability of Langmuir isotherm.

The  $q_m$  and  $K_L$  are given in Table 4.10. Isotherm constants obtained from GACOZR 1273 are compared with the values obtained for GAC 383 and GACO 383.

The  $q_m$  (or  $K_L/a_L$ ) increases with solution temperature, for GACOZR 1273 it is given as; 283K (250.0 mg/g), 293K (266.0 mg/g), 303 K (280.9 mg/g), 313 K

(303.95 mg/g) and 323 K (315.46 mg/g), suggesting that the adsorption is favoured at high temperatures. This shows an endothermic adsorption mechanism.

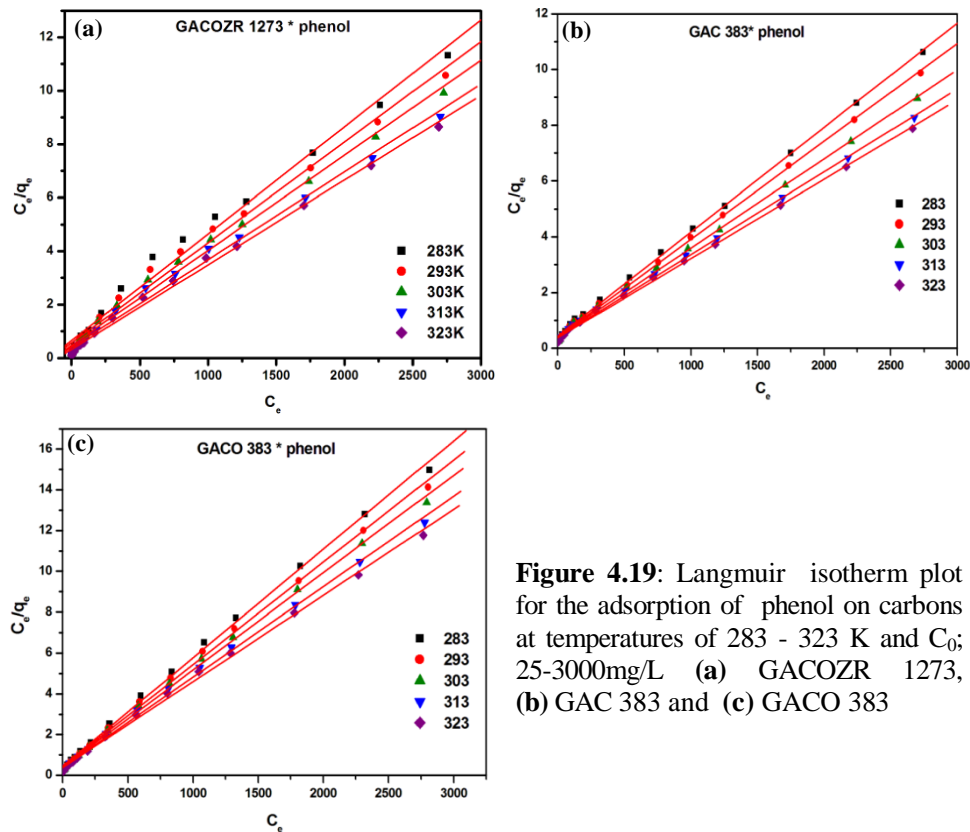


**Figure 4.19:** Langmuir isotherm plot for the adsorption of phenol on carbons at temperatures of 283 - 323 K and  $C_0$ ; 25-3000mg/L (a) GACOZR 1273, (b) GAC 383 and (c) GACO 383

For every temperature the monolayer adsorption capacity of GACOZR 1273 is found to be comparatively lesser than basic carbon GAC 383. At higher temperature (303 K, 313 K and 323 K) the difference in the monolayer adsorption capacity of GACOZR 1273 and GAC 383 is greater than 10%.

The adsorption equilibrium constant  $K_L$  for new carbons varies as; GACOZR 1273 ( $1.54 - 3.13 \text{ Lg}^{-1}$ ), GAC 383 ( $2.33 - 2.68 \text{ Lg}^{-1}$ ) and GACO 383 ( $2.17 - 2.59 \text{ Lg}^{-1}$ ) for the temperature range of 283 K to 323 K. An increase of Langmuir constant ( $K_L$ ) with temperatures indicates that higher heat of adsorption by the rise of temperature [21]. It is clearly suggesting the endothermic nature of

adsorption i.e. the adsorption rate of phenol on GACOZR 1273, GAC 383 and GACO 383 is favoured at higher temperatures. Weak hydrogen bonding at higher temperature makes the phenol molecules freely available for adsorption [22]. The increasing order of adsorption rate of phenol at different temperatures is given as 323K > 313K > 303K > 293K > 283K.

The linearized form of Freundlich isotherm equation applied is given by the following equation

$$\log q_e = \log K_F + \frac{1}{n} \log C_e \quad (4.15)$$

Plot of  $\log q_e$  versus  $\log C_e$  at five different temperatures are given in the Figure 4.20(a)-(c). The calculated Freundlich constant and correlation coefficient are given in the Table 4.10.

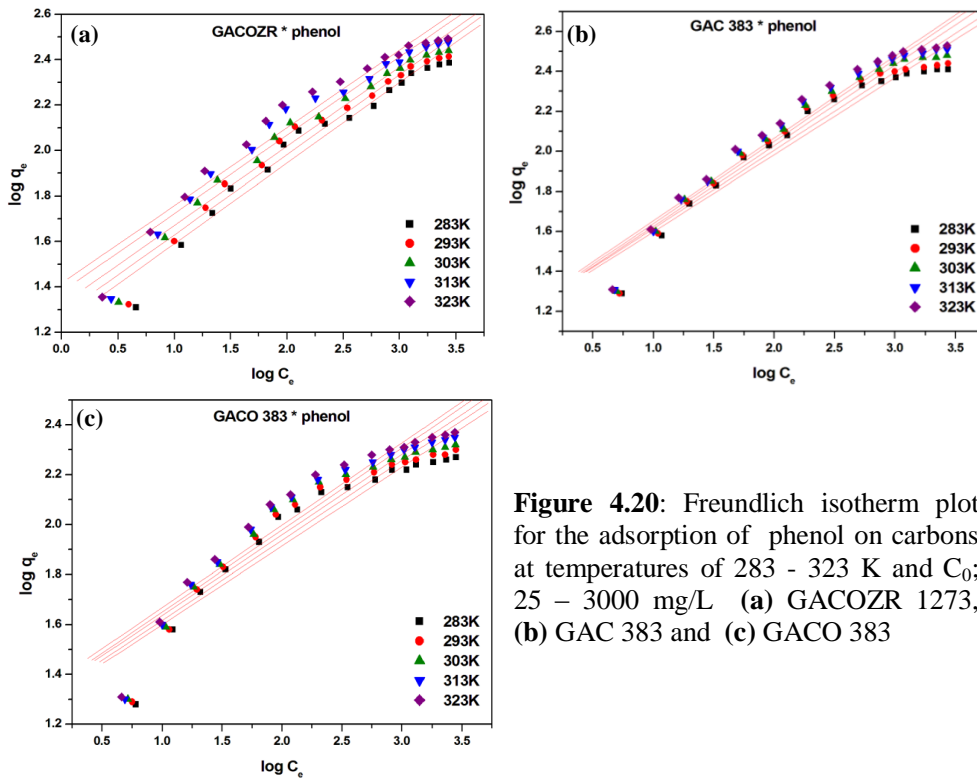


**Figure 4.20:** Freundlich isotherm plot for the adsorption of phenol on carbons at temperatures of 283 - 323 K and  $C_0$ ; 25 – 3000 mg/L (a) GACOZR 1273, (b) GAC 383 and (c) GACO 383

The  $n$  indicates favourability of adsorption, it lies in the range  $1 < n < 10$ . It varies at 283 – 323 K for new carbons as, GACOZR 1273 (3.92 - 4.08), GAC 383 (4.02 - 4.08) and GACO 383 (3.85 - 4.05). Therefore, the adsorption of phenol on GACOZR 1273, GAC 383 and GACO 383 appears to be favourable.

For GACOZR 1273,  $K_F$  is increasing with solution temperature and varies from  $17.18 \text{ Lg}^{-1}$  to  $26.02 \text{ Lg}^{-1}$ . It indicates that adsorption rate also increases with the solution temperature [23].

The linear form of the Dubinin - Radushkevich (D-R) isotherm model applied to the data is

$$\ln q_e = \ln q_{mi} - \beta \varepsilon^2 \quad (4.16)$$

The Dubinin - Radushkevich plot of  $\ln q_e$  against  $[RT \ln(1+1/C_e)]^2$  of phenol adsorption on GAC 383, GACO 383 and GACOZR 1273 with respect to five temperatures are given in Figures 4.21(a)–(c).

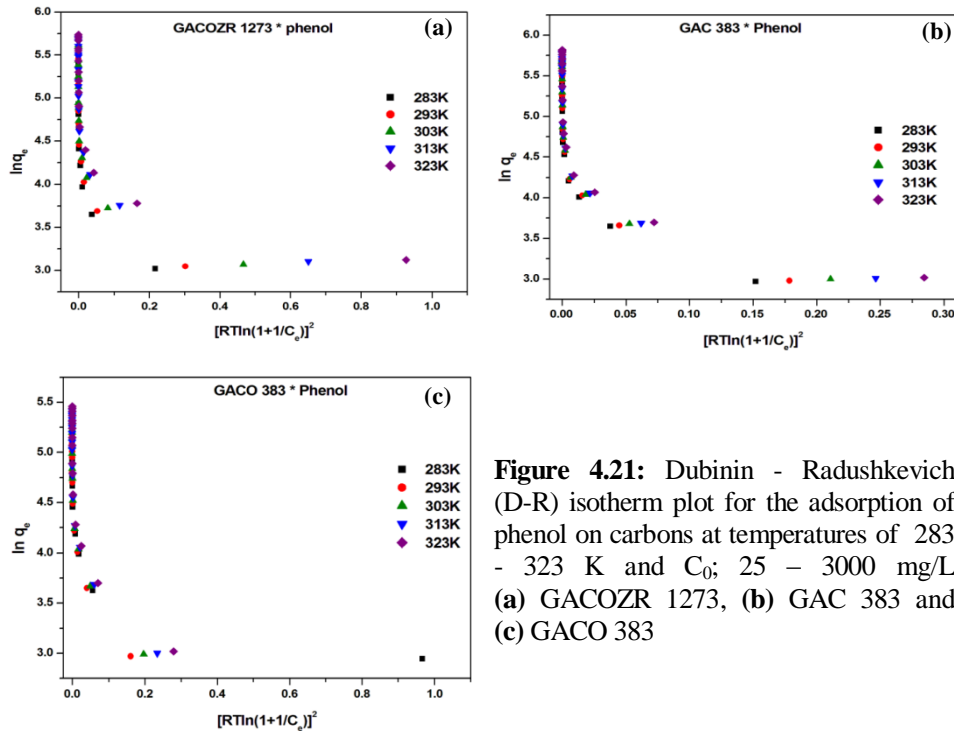


**Figure 4.21:** Dubinin - Radushkevich (D-R) isotherm plot for the adsorption of phenol on carbons at temperatures of 283 - 323 K and  $C_0$ ; 25 – 3000 mg/L (a) GACOZR 1273, (b) GAC 383 and (c) GACO 383

Isotherm parameters  $q_{mi}(D-R)$ ,  $\beta$  and the mean free energy ( $E$ ) are determined from the appropriate plot and are given in Table 4.10. Dubinin-Radushkevich (D-R) isotherm assumes that characteristics of the adsorption curves are related to the porosity of the adsorbent. From the linear plot of D-R isotherm of GACOZR 1273, micropore adsorption capacity  $q_{mi}$  (D-R) is determined and is given as; 283 K ( $q_{mi} = 50.45$  mg/g &  $E = 0.344$  kJ/mol), 293 K ( $q_{mi} = 53.13$  mg/g &  $E = 0.401$  kJ/mol), 303 K ( $q_{mi} = 55.51$  mg/g &  $E = 0.492$  kJ/mol), 313 K ( $q_{mi} = 57.71$  mg/g &  $E = 0.579$  kJ/mol) and 323 K ( $q_{mi} = 58.97$  mg/g &  $E = 0.690$  kJ/mol). Mean free energy  $E$  indicates the nature of physisorption process. As the increasing of temperature, more phenol molecules are occupied on the available pores on carbon therefore increasing the  $q_{mi}$  (D-R) with temperature.

**Table 4.10:** Langmuir, Freundlich and Dubinin-Radushkevich (D-R) isotherm parameters of phenol on GACOZR 1273, GAC 383 and GACO 383 at temperatures 283 – 323K

Carbons	T ( Kelvin)	Langmuir isotherm				Freundlich			Dubinin-Radushkevich			
		$K_L/a_L$ (mg/g)	$K_L(Lg^{-1})$	$a_L \times 10^4 (Lg^{-1})$	$R^2$	n	$K_F (Lg^{-1})$	$R^2$	$q_{mi} (D-R)$ (mg/g)	$\beta \text{ mol}^2/kJ^2$	$R^2$	E (kJ/mol)
GACOZR 1273	283	250.0	1.54	62	0.994	2.82	17.2	0.979	50.5	4.2	0.977	0.344
	293	266.0	1.81	68	0.996	2.84	18.9	0.98	53.1	3.1	0.975	0.401
	303	281.0	2.11	75	0.997	2.87	21.0	0.981	55.5	2.1	0.974	0.492
	313	304.0	2.53	83	0.996	2.90	23.9	0.975	57.7	1.5	0.973	0.579
	323	315.5	3.13	99	0.998	2.92	26.0	0.974	59.0	1.1	0.975	0.690
GAC 383	283	266.7	2.33	87	0.999	2.60	16.4	0.967	55.5	7.0	0.983	0.267
	293	284.9	2.46	87	0.999	2.56	16.7	0.967	56.6	6.0	0.983	0.288
	303	312.5	2.48	79	0.999	2.49	16.7	0.972	57.4	5.1	0.983	0.293
	313	336.7	2.53	75	0.999	2.44	17.0	0.975	58.4	4.4	0.983	0.338
	323	352.1	2.68	76	0.999	2.42	17.4	0.975	59.2	3.8	0.983	0.362
GACO 383	283	188.3	2.17	115	0.999	3.17	19.2	0.941	46.9	0.9	0.952	0.258
	293	199.6	2.34	117	0.999	3.13	19.9	0.943	56.1	6.7	0.983	0.273
	303	209.6	2.48	119	0.999	3.12	20.7	0.946	57.4	5.5	0.985	0.302
	313	225.7	2.52	112	0.999	3.05	21.1	0.950	58.8	4.7	0.984	0.328
	323	237.0	2.59	109	0.999	3.02	21.7	0.951	59.3	3.9	0.983	0.359

A comparison of coefficient of determination for three isotherms has been made and listed in Table 4.10. The high value of the correlation coefficient in case of Langmuir models compared to Freundlich and Dubinin - Radushkevich (D-R) isotherm models suggest that the Langmuir isotherm model is the best fit model for equilibrium isotherm data. This concludes the fact that all the three adsorbent follows monolayer adsorption on a surface that is homogenous.

#### **4.5.3 Adsorption of *P*-Nitrophenol on GACOZR 1273, GAC 383 and GACO 383 at Temperatures**

The effect of temperature for the removal of *p*-nitrophenol on GAC 383, GACO 383 and GACOZR 1273 is studied in the temperature range of 283 – 323 K. The removal efficiency of *p*-nitrophenol increases with solution temperature and maximum adsorption take place at 323 K due to dispersive interaction between the *p*-nitrophenol and GACs is increasing at high solution temperature.

The Langmuirian isotherm curve (*L* curve) obtained for the adsorption of *p*-nitrophenol on new carbon indicates that there is no strong competition between solvent and the adsorbate to occupy the adsorbent surface sites [24].

Langmuir, Freundlich and Dubinin-Radushkevich (D-R) isotherm models are used to describe the mechanism and adsorption behaviour of *p*-nitrophenol on GAC 383, GACO 383 and GACOZR 1273 at selected temperatures.

The Langmuir plots of *p*-nitrophenol adsorption on GAC 383, GACO 383 and GACOZR 1273 with respect to five temperatures are given in Figures 4.22(a)–(c). The monolayer capacity  $K_L/a_L$  (or  $q_m$ ) and Langmuir constant  $K_L$  are calculated from the slope and intercept of the corresponding plots and are given in Table 4.11. The monolayer capacity ( $q_m$ ) increases with temperature, suggesting that the adsorption is favoured at high temperature.

The percentage increments of monolayer adsorption capacity for new carbons on rising the adsorption reactor temperature from 283 K to 323 K are given as; GACOZR 1273 (19 %), GAC 383 (48 %) and GACO 383 (22 %). The maximum monolayer capacities of new carbons at 323 K are given as; GACOZR 1273 (448.43 mg/g), GAC 383 (403.23 mg/g) and GACO 383 (245.7 mg/g).

On comparing with GAC 383, the percentage increments of monolayer adsorption capacity of GACOZR 1273 at different temperatures are 283 K (28 %), 293 K (23 %), 303 K (17 %), 313 K (13 %) and 323 K (10 %) respectively. Similarly for comparing with GACO 383 the  $q_m$  of GACOZR 1273 is, 283 K (47 %), 293 K (46 %), 303 K (45 %), 313 K (46 %) and 323 K (45 %).

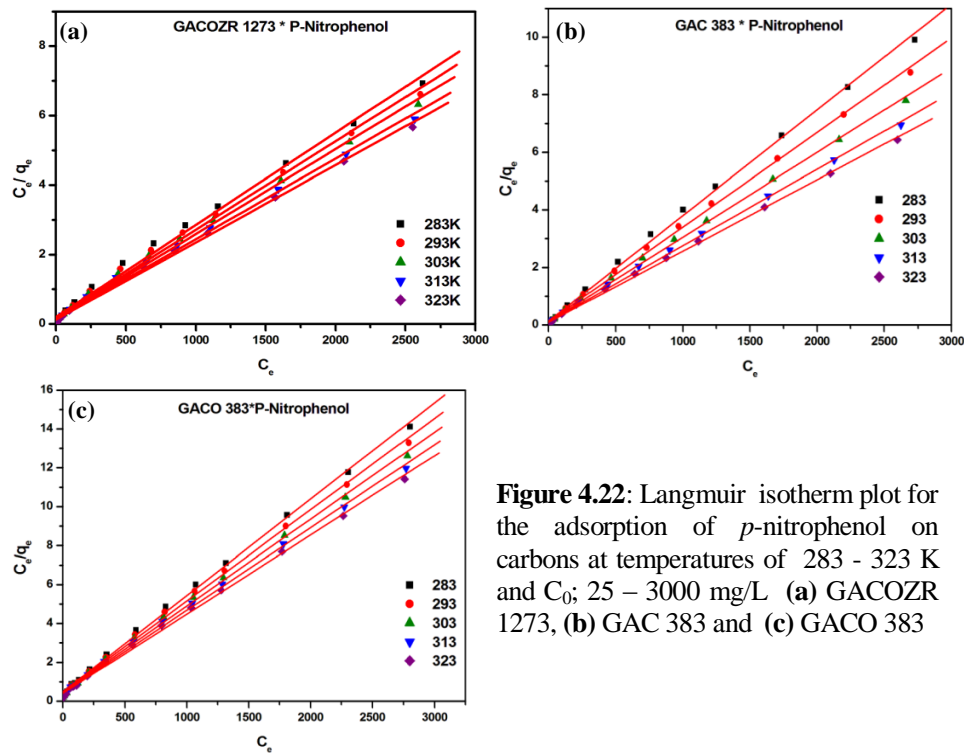


**Figure 4.22:** Langmuir isotherm plot for the adsorption of *p*-nitrophenol on carbons at temperatures of 283 - 323 K and  $C_0$ ; 25 – 3000 mg/L (a) GACOZR 1273, (b) GAC 383 and (c) GACO 383

Large Langmuir constant ( $K_L$ ) implied a strong bonding on a finite number of binding sites. Langmuir constants (Table 4.11) slightly increased with temperature indicating an endothermic process of the *p*-nitrophenol adsorption on studied activated carbons. This observation could be attributed to the strong interaction between adsorbent carbon and adsorbates at higher temperatures [25].

The coefficient of correlation ( $R^2$ ) obtained from Langmuir isotherm give  $\approx 0.99$  which indicate that the adsorption of *p*-nitrophenol on GAC follows the Langmuir isotherm.

The isotherm data for *p*-nitrophenol adsorption on GAC 383, GACO 383 and GACOZR 1273 were fitted into the Freundlich equation. Plots of  $\log C_e$  versus  $\log q_e$  are given in Figures 4.23(a)–(c). The  $K_F$  and  $1/n$  were evaluated from the intercept and slope of the linear plot of  $\log q_e$  versus  $\log C_e$  and are listed in Table 4.11.

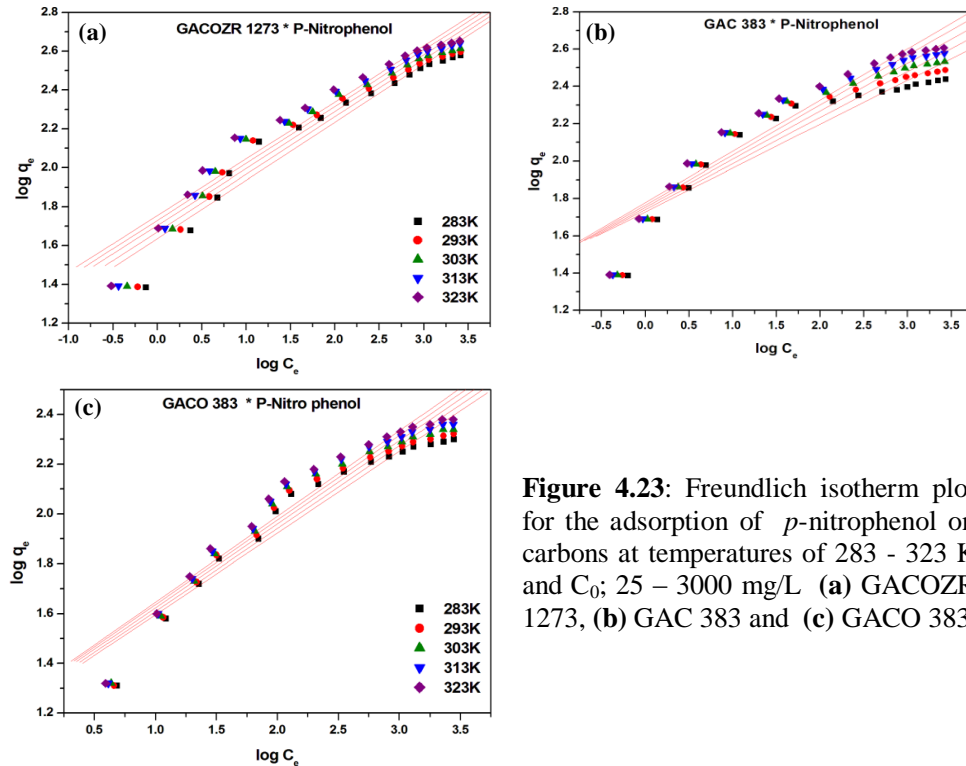


**Figure 4.23:** Freundlich isotherm plot for the adsorption of *p*-nitrophenol on carbons at temperatures of 283 - 323 K and  $C_0$ ; 25 – 3000 mg/L (a) GACOZR 1273, (b) GAC 383 and (c) GACO 383

The Freundlich constant, ' $n$ ' varies for new GAC are given as GACOZR 1273 (3.35 - 4.44), GAC 383 (3.64 - 4.26), GACO 383 (2.91 - 3.05). For all the carbons ' $n$ ' lies within the range of  $1 < n < 10$ . It represents good adsorption of *p*-nitrophenols onto activated carbon. Larger the ' $n$ ' indicates the stronger the interaction between adsorbent and adsorbate.

Freundlich constant  $K_F$  related to adsorption capacity. For GACOZR 1273, its value at different solution temperatures are given as; 283 K ( $43.27 \text{ Lg}^{-1}$ ), 293 K ( $46.89 \text{ Lg}^{-1}$ ), 303 K ( $50.52 \text{ Lg}^{-1}$ ), 313 K ( $53.69 \text{ Lg}^{-1}$ ), and 323 K ( $56.85 \text{ Lg}^{-1}$ ).  $K_F$  increases with temperature suggest the endothermic nature of adsorption i.e. adsorption is favoured at high temperature.



The Dubinin-Radushkevich (D-R) plot of  $\ln q_e$  against  $[RT \ln(1+1/C_e)]^2$  for *p*-nitrophenol adsorption on GAC 383, GACO 383 and GACOZR 1273 with respect to five temperatures are given in Figures 4.24(a) –(c).

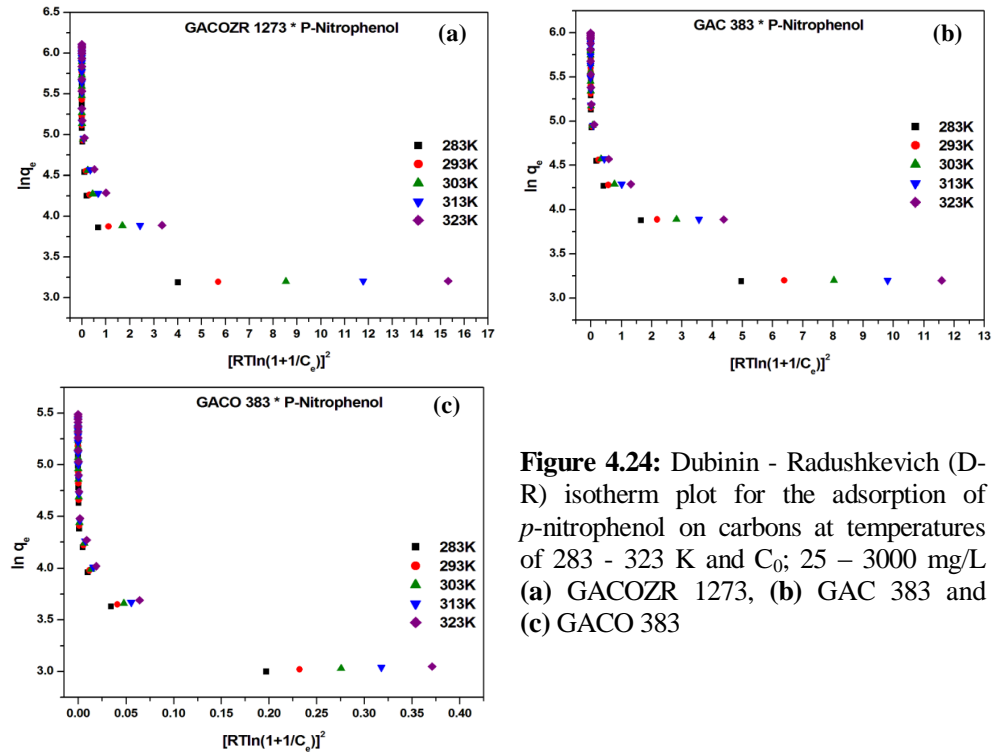


**Figure 4.24:** Dubinin - Radushkevich (D-R) isotherm plot for the adsorption of *p*-nitrophenol on carbons at temperatures of 283 - 323 K and  $C_0$ ; 25 – 3000 mg/L (a) GACOZR 1273, (b) GAC 383 and (c) GACO 383

Intercept of the Dubinin-Radushkevich (D-R) plots defines the micropore adsorption capacity ( $q_{mi}$ ) and slope  $\beta$  related to the adsorption energy. Parameters were determined from the appropriate plot and are given in Table 4.11. With the increasing of solution temperature from 283 K to 323 K, the micropore adsorption capacity,  $q_{mi}$  (D-R) of GACOZR 1273 increases from 75.87 mg/g to 81.21 mg/g, for GAC 383, it increases from 75.77 mg/g to 81.24 mg/g and for GACO 383 increases from 49.61 mg/g to 52.74 mg/g.

The magnitude of  $E$  are found to be varying and it ranges for new carbons are; GACOZR 1273 (1.31-2.49 kJ/mol), GAC 383 (1.6-2.2 kJ/mol) GACO 383 (0.329-0.414 kJ/mol).

**Table 4.11:** Langmuir, Freundlich and Dubinin-Radushkevich isotherm parameters of *p*-nitrophenol on GACOZR 1273, GAC 383, and GACO 383 at 283 - 323K

Carbons	Temperature (K)	Langmuir isotherm				Freundlich			Dubini -Radushkevich			
		$K_L/a_L$ (mg/g)	$K_L$ (Lg <sup>-1</sup> )	$a_L \times 10^{-4}$ Lg <sup>-1</sup>	$R^2$	$n$	$K_F$ (Lg <sup>-1</sup> )	$R^2$	$q_{mi}$ (D-R) (mg/g)	$\beta$ mol <sup>2</sup> /kJ <sup>2</sup>	$R^2$	$E$ (kJ/mol)
GACOZR 1273	283	377.4	4.90	13.0	0.994	3.35	43.3	0.941	75.9	0.29	0.872	1.31
	293	393.7	5.75	14.6	0.996	3.38	46.9	0.941	78.1	0.21	0.889	1.54
	303	409.8	6.68	16.3	0.996	3.42	50.5	0.943	78.7	0.14	0.889	1.88
	313	432.9	7.15	16.5	0.996	3.42	53.7	0.947	79.8	0.10	0.895	2.20
	323	448.4	8.21	18.3	0.996	3.44	56.9	0.949	81.2	0.08	0.899	2.49
GAC 383	283	272.5	7.61	27.9	0.998	4.26	53.5	0.861	75.8	0.23	0.966	1.60
	293	304.9	8.36	27.4	0.998	4.06	55.0	0.880	77.0	0.18	0.966	1.75
	303	340.1	9.03	26.5	0.998	3.88	56.6	0.893	78.2	0.15	0.966	1.90
	313	377.4	9.40	24.9	0.998	3.73	58.1	0.906	79.5	0.12	0.966	2.07
	323	403.2	10.7	26.5	0.998	3.64	59.9	0.914	81.2	0.10	0.966	2.21
GACO 383	283	201.6	2.06	10.2	0.998	3.05	18.5	0.925	49.6	4.63	0.951	0.33
	293	213.2	2.14	10.1	0.998	3.01	18.9	0.927	50.6	3.97	0.953	0.36
	303	224.2	2.24	10.0	0.998	2.97	19.3	0.929	51.3	3.35	0.951	0.39
	313	235.3	2.31	9.8	0.998	2.94	19.7	0.931	52.1	2.92	0.951	0.41
	323	245.7	2.41	9.8	0.998	2.91	20.0	0.933	52.7	2.51	0.949	0.45

#### 4.5.4 Adsorption of Methylene Blue (MB) on GACOZR 1273, GAC 383 and GACO 383 at Temperatures

Equilibrium adsorption isotherm for the removal of methylene blue (MB) from aqueous solution using activated carbons GAC 383, GACO 383 and GACOZR 1273 has been investigated at different temperature 283, 293, 303, 313 and 323 K. It shows that adsorption capacity of all the carbon studied increases with solution temperature. An increasing number of molecules acquire sufficient energy to undergo an interaction with active sites at the surface with rise of temperature [26].

The amount of methylene blue (MB) adsorbed at the equilibrium time reflects its maximum adsorption efficiency of the carbons. The amount of MB adsorbed increases with initial concentration and solution temperature. The mass transfer driving force become larger, when the initial concentration is increased and hence resulting in higher adsorption of MB [27].

Adsorption equilibrium is represented with Langmuir, Freundlich and Dubinin - Radushkevich (D-R) isotherm models.

The Langmuir plots of MB adsorption on GAC 383, GACO 383 and GACOZR 1273 with respect to five temperatures are given in Figures 4.25(a)–(c).

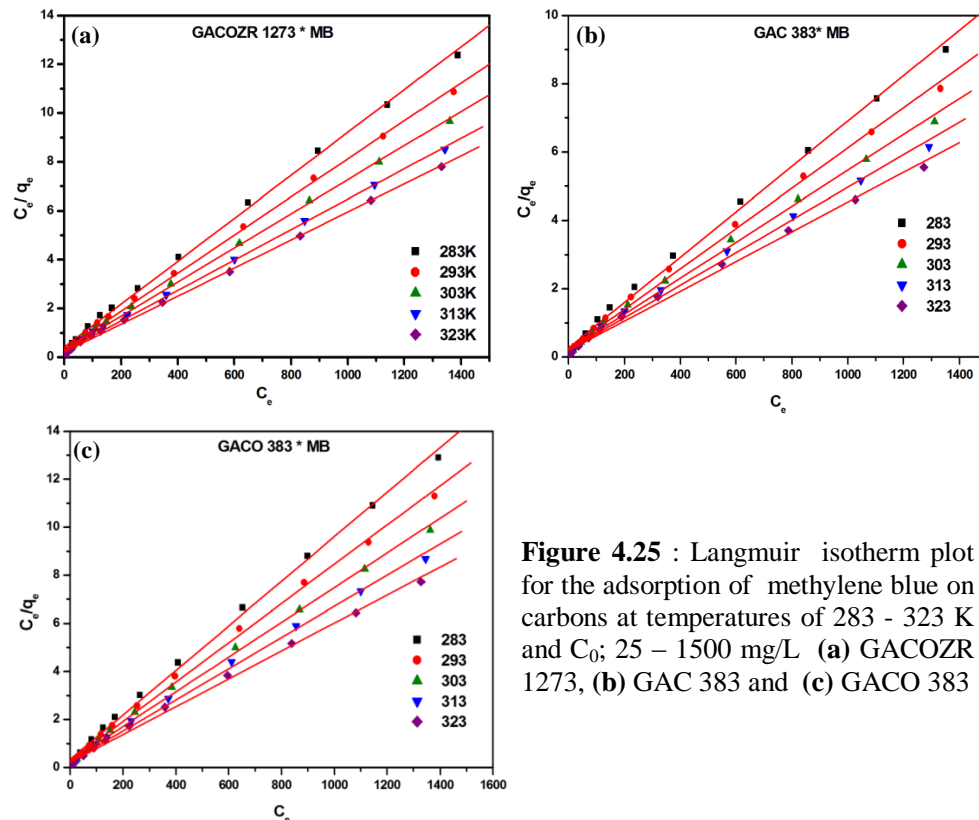


**Figure 4.25 :** Langmuir isotherm plot for the adsorption of methylene blue on carbons at temperatures of 283 - 323 K and  $C_0$ ; 25 – 1500 mg/L (a) GACOZR 1273, (b) GAC 383 and (c) GACO 383

Straight line plot of  $C_e/q_e$  versus  $C_e$  indicates that the adsorption of MB follows Langmuir isotherm model. As shown in the Table 4.12 the monolayer capacity ( $K_L/a_L$ ) and  $K_L$  increases with temperature for all the carbons. Increasing the solution temperature from 283 K to 323 K, the monolayer volume of new carbons increases as; GACOZR 1273 (113.77 mg/g to 174.22 mg/g), GAC 383 (150.60 mg/g to 229.36 mg/g), and GACO 383 (107.99 mg/g to 172.41 mg/g). This means that a rise of solution temperature makes MB molecule free to move, i.e. mobility of dye molecule increases and more MB get adsorbed on the surface of

the carbon. Adsorption is said to be an endothermic in nature. Increasing the temperature reduces the swelling effect within the internal structure of adsorbent, which causes further penetration of larger dye molecules within the pores [28, 29].

The high value of correlation coefficient ( $R^2$  is 0.99) of Langmuir isotherm assumes a monolayer coverage and uniform activity distribution on the adsorbent surface.

The Freundlich plots of methylene blue (MB) adsorption on GACOZR 1273, GACO 383 and GACOZR 1273 with respect to five temperatures are given in Figures 4.26(a)–(c).  $K_F$  and  $n$  obtained from the slope and intercept of the straight line plot  $\log C_e$  versus  $\log q_e$  are given in the Table 4.12.

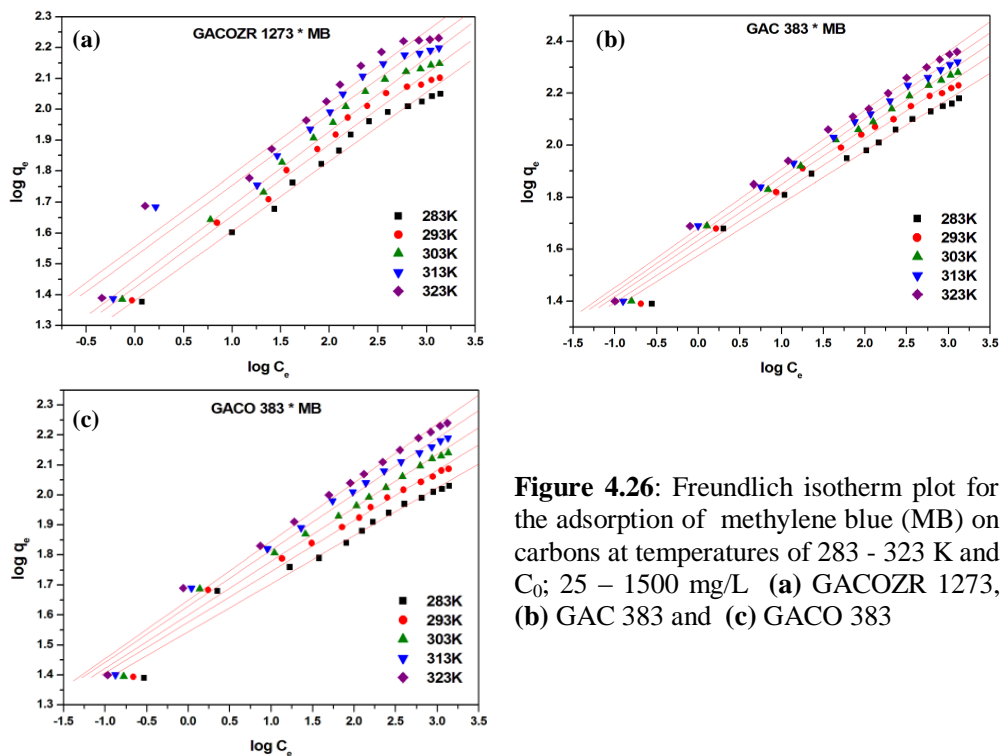


**Figure 4.26:** Freundlich isotherm plot for the adsorption of methylene blue (MB) on carbons at temperatures of 283 - 323 K and  $C_0$ ; 25 - 1500 mg/L (a) GACOZR 1273, (b) GAC 383 and (c) GACO 383

Favourability of adsorbent/adsorbate system indicate by the  $n$  value, which varies as GACOZR 1273 (4.45 - 4.29), GAC 383 (1.58 - 1.68) and GACO 383 (5.12 - 6.27). These values confirm the favourability of the adsorption.

$K_F$  is a measure of adsorption capacity. The variation of  $K_F$  for GACOZR 1273 at different temperature is, 283 K (24.08 Lg<sup>-1</sup>), 293 K (26.54 Lg<sup>-1</sup>), 303 K (28.11 Lg<sup>-1</sup>), 313 K (33.45 Lg<sup>-1</sup>) and 323 K (35.94 Lg<sup>-1</sup>).

The Dubinin - Radushkevich (D-R) plot of  $\ln q_e$  against  $[RT \ln(1+1/C_e)]^2$  for methylene blue (MB) adsorption on GAC 383, GACO 383 and GACOZR 1273 with respect to five temperatures is given in Figures 4.27 (a)–(c).

$q_{mi}$  (D-R) obtained from isotherm plot is increased with temperature, which is related to maximum adsorption efficiency. The micropore adsorption capacity increment for new carbons by rising the solution temperature from 283 K to 323 K is given as; GACOZR 1273 (44.07 - 60.55 mg/g), GAC 383 (57.43 - 62.78 mg/g) and GACO 383 (54.15- 60.98 mg/g). GACOZR 1273 shows the highest increment in  $q_{mi}$  (D-R) i.e. about 37.4 %, whereas GAC 383 shows 9.32 % and GACO 383 shows 12.61 % increment by rising solution temperature.

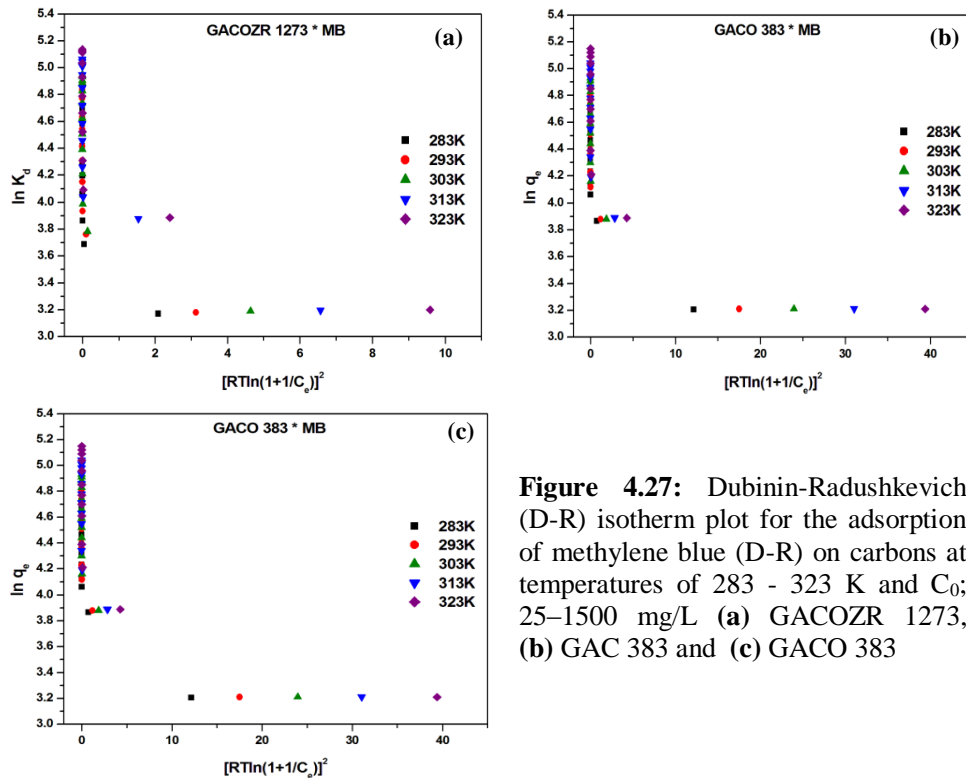


**Figure 4.27:** Dubinin-Radushkevich (D-R) isotherm plot for the adsorption of methylene blue (D-R) on carbons at temperatures of 283 - 323 K and  $C_0$ ; 25–1500 mg/L (a) GACOZR 1273, (b) GAC 383 and (c) GACO 383

$E$  calculated for carbons given as, GACOZR 1273 (1.30 - 2.31 kJ/mol), GAC 383 (2.75 - 4.68 kJ/mol), GACO 383 (2.77- 4.66 kJ/mol). This indicates the adsorption process occurs through physical interaction, i.e. forces existing between the adsorbent and adsorbate is Van der Waals forces.

**Table 4.12:** Langmuir, Freundlich and Dubinin-Radushkevich isotherm parameter of methylene blue on GACOZR 1273, GAC 383, GACO 383 at temperatures 283-323 K

Carbons	Temperature (K)	Langmuir isotherm				Freundlich			Dubinin-Radushkevich			
		$K_L/a_L$ (mg/g)	$K_L$ (Lg <sup>-1</sup> )	$a_L \times 10^{-4}$ (Lg <sup>-1</sup> )	$R^2$	$n$	$K_F$ (Lg <sup>-1</sup> )	$R^2$	$q_{mi}$ (D-R) mg/g	$\beta$ mol <sup>2</sup> /kJ <sup>2</sup>	$R^2$	$E$ (kJ/mol)
GACOZR 1273	283	113.8	2.39	210	0.998	4.45	24.1	0.984	44.1	0.296	0.949	1.30
	293	128.4	3.00	234	0.998	4.33	26.5	0.980	47.6	0.218	0.962	1.51
	303	143.3	3.40	237	0.998	4.17	28.1	0.982	49.4	0.154	0.953	1.80
	313	160.8	4.00	249	0.998	4.36	33.5	0.958	57.9	0.130	0.998	1.96
	323	174.2	4.81	276	0.998	4.29	35.9	0.960	60.6	0.094	0.998	2.31
GAC 383	283	150.6	3.74	248	0.996	1.58	37.7	0.982	57.4	0.066	0.943	2.75
	293	169.5	4.54	268	0.996	1.61	40.7	0.984	58.8	0.047	0.935	3.26
	303	190.1	4.80	252	0.994	1.63	42.9	0.990	60.3	0.036	0.935	3.75
	313	209.6	5.13	245	0.994	1.66	45.3	0.992	61.6	0.028	0.937	4.21
	323	229.4	5.51	240	0.994	1.68	47.8	0.994	62.8	0.023	0.941	4.68
GACO 383	283	108.0	2.89	268	0.996	6.27	35.1	0.968	54.2	0.065	0.972	2.77
	293	122.4	3.37	275	0.996	5.92	37.7	0.976	56.3	0.047	0.960	3.26
	303	138.7	3.60	259	0.996	5.61	39.8	0.982	58.0	0.036	0.955	3.74
	313	154.3	4.31	279	0.996	5.33	42.3	0.984	59.5	0.028	0.951	4.19
	323	172.4	4.59	266	0.996	5.12	44.6	0.988	61.0	0.023	0.953	4.66

#### 4.5.5 John-Sivanandan Achari (J-SA) Isotherm for Solid-Liquid Equilibria

The separation of adsorption and pore filling phenomena of adsorbate (phenol, *p*-nitrophenol and methylene blue) on newly developed carbons GACOZR 1273, GAC 383 and GACO 383 are evaluated in the solid-liquid equilibria using John –Sivanandan Achari (J-SA) isotherm models [30, 31]. The adsorption efficiency obtained from J-SA isotherm model is compared to Langmuir (L), Dubinin-Radushkevich (D-R) and Freundlich (F) isotherm models.

John–Sivanandan Achari (J-SA) isotherm model is given by

$$\log \log C_e = C + n \log q_e \quad (3.27)$$

$$\text{Where ; } C_e = C_e \times 10^N \quad (3.28)$$

$$q_e = q_I + q_{II} + q_{III} \quad (3.29)$$

$C$  and ' $n$ ' are the intercept and slope of the plot  $\log \log C_e$  versus  $\log q_e$

The  $J$ -SA plots of methylene blue adsorption exhibited three distinct phases of adsorption. Steep rise in *phase I* indicate prominent molecular sieve effects. The adsorption of MB on activated carbon in *phase I*,  $q_I(J)$  is given as; GACOZR 1273 (54.13 mg/g), GAC 383 (67.48 mg/g), GACO 383 (66.62 mg/g) and the total adsorption capacity  $q_T(J)$  determined from  $\log q_T(J)$  corresponding to the highest  $\log \log C_e$  is given as GACOZR 1273 (141.5 mg/g), GAC 383 (191.87 mg/g), GACO 383 (138.41 mg/g). After the molecular sieve effect the monolayer adsorption capacity is revealed by *phase II*. Adsorption in *phase II* is given by GAC follows as, GACOZR 1273 – 73.39 mg/g (51.87%), GAC 383 – 124.39 mg/g (64.8%), GACO 383 – 71.79 mg/g (51.9%) adsorption. It is the highest adsorption noted among three phases. The remaining 9.87 % of adsorption in GACOZR 1273 is contributed by a third phase ( $q_{III} J$  - 13.97mg/g) it is probably due to the adsorption of MB in mesopores/large- wide micropores.

The successive filling of phenol on GACOZR 1273, GAC 383 and GACO 383 is represented by three distinct phases. The carbonyl surface oxygen groups act as an electron donor and the aromatic ring of the phenol molecule act as electron acceptors and the adsorption becomes effective probably constitute the *phase I* of John-Sivanandan Achari ( $J$ -SA) isotherm plot.

Adsorption of phenol in *phase I* of  $J$ -SA isotherm plots is given as GACOZR 1273 (58.86 mg/g) GAC 383 (72.87 mg/g), GACO 383 (56.39 mg/g). The percentage contribution of *phase I* in total adsorption for GAC is calculated and is given as GACOZR 1273 (21.16 %), GAC 383 (24.13 %) and GACO 383 (26.58 %).

The phenol adsorption in micropores is given by *phase II*. Here phenol adsorption might have dominantly governed by the dispersion interaction between the basal plane of carbon and the aromatic ring of the adsorbate. Adsorption of phenol in *phase II* and the percentage of the contribution in the total adsorption of GAC is given as GACOZR 1273 – 200.18 mg/g (71.95 %), GAC 383 – 209.82 mg/g (69.5 %), GACO 383 – 93.11 mg/g (43.8 %).

The third phase in *J-SA* isotherm is due to the adsorption of phenol in wide micropores/ mesopores. The total contribution of wider pores for the adsorption of phenol on GAC is given as GACOZR 1273 – 19.17 mg/g (6.89 %), GAC 383 – 19.24 mg/g (6.4%) and GACO 383 – 62.68 mg/g (25.9%).

The interaction between *p*-nitrophenol and GAC is the same as that of phenol. But electron withdrawing groups on para position make it more electron deficient and increases the donor acceptor interaction. So more *p*-nitrophenol get adsorbed on GAC compared to phenol molecule.

The John –Sivanandan Achari plots of *p*-nitrophenol adsorption exhibited three phases of adsorption for GACOZR 1273 and GACO 383 whereas GAC 383 shows only two distinct phases. The percentage contribution of *phase I* in total adsorption is given as GACOZR 1273 (33.26 %), GACO 383 (23.53 %). In GAC 383 molecular sieve effect is not clearly separated from monolayer filling. In *phase II*, adsorption of *p*-nitrophenol is given as GACOZR 1273 (165.13 mg/g), GAC 383 (210.15 mg/g) and GACO 383 (85.59 mg/g). The contribution of *phase III* for *p*-nitrophenol adsorption is given by GACOZR 1273 (114.49 mg/g), GAC 383 (134.07mg/g) and GACO 383 (84.24 mg/g). A comparison of adsorption capacity  $q_T(J)$  and surface area  $SA(J)$  determined from *J-SA* isotherm model is in excellent agreement with Langmuir isotherm. Accordingly, the results of the above set of isotherm data are presented in Table 4.13. The above results indicate that the adsorption efficiency of the same carbon is different towards different adsorbates.



**Table 4.13:** Comparison of adsorption capacity (mg/g) and surface area (m<sup>2</sup>/g) for the adsorption of phenol, *p*-nitrophenol and methylene blue (MB) on carbon GACOZR 1273, GAC 383 and GACO 383 using John-Sivanandan Achari, Langmuir, D-R and Freundlich isotherm models (T = 303K)

Carbons	Adsorbate (cross sectional area nm <sup>2</sup> )	J-SA adsorption capacity mg/g				Langmuir q <sub>m</sub> (L) mg/g (*SA m <sup>2</sup> /g)	q <sub>m</sub> (D-R) mg/g (*SA m <sup>2</sup> /g)	Freundlich q <sub>F</sub> (mg/g) (*SA m <sup>2</sup> /g)
		q <sub>I</sub> (J-SA) mg/g (*SA m <sup>2</sup> /g)	q <sub>II</sub> (J-SA) mg/g (*SA m <sup>2</sup> /g)	q <sub>III</sub> (J-SA) mg/g (*SA m <sup>2</sup> /g)	q <sub>IV</sub> (J-SA) mg/g (*SA m <sup>2</sup> /g)			
GACOZR 1273	*MB (1.2)	54.1 (122.3)	73.4 (165.85)	14.0 (31.56)	141.5 (319.7)	143.3 (323.8)	49.4 (111.6)	28.1 (63.5)
	*P (0.522)	58.86 (196.6)	200.18 (668.8)	19.17 (64.0)	278.21 (929.4)	281.0 (938.7)	55.51 (185.4)	21.0 (70.2)
	*PNP (0.525)	139.3 (316.7)	165.1 (375.4)	114.5 (260.3)	418.9 (952.3)	409.8 (931.5)	78.7 (179.0)	50.5 (114.8)
GAC 383	MB	67.5 (152.5)	124.4 (281.1)	ND	191.9 (433.6)	190.1 (429.6)	60.3 (136.3)	42.9 (96.9)
	P	72.9 (243.4)	209.8 (700.9)	19.2 (64.3)	301.9 (1008.7)	312.5 (1044.0)	57.4 (191.7)	16.7 (55.9)
	PNP	ND	210.15 (477.7)	134.07 (304.8)	345.22 (784.7)	334.5 (760.2)	78.2 (177.7)	60.7 (138.1)
GACO 383	MB	66.6 (150.5)	71.8 (162.2)	ND	138.4 (312.7)	138.7 (313.4)	58.0 (131.0)	39.8 (90.0)
	PNP	56.4 (188.4)	93.1 (311.1)	62.7 (209.4)	212.2 (708.8)	209.6 (700.2)	57.4 (191.8)	20.7 (69.2)
	P	52.3 (118.8)	85.6 (194.6)	84.2 (191.5)	222.1 (504.9)	224.2 (509.7)	51.3 (116.6)	19.3 (43.9)

\*MB - Methylene blue \*P - phenol, \*PNP - *p*-nitrophenol, \*ND – not detected

$$*SA(m^2/g) = \frac{q \text{ (mg/g)} \times 6.022 \times 10^{23} \times \text{cross sectional area of adsorbate}(nm^2)}{\text{Molecular weight of adsorbate}}$$

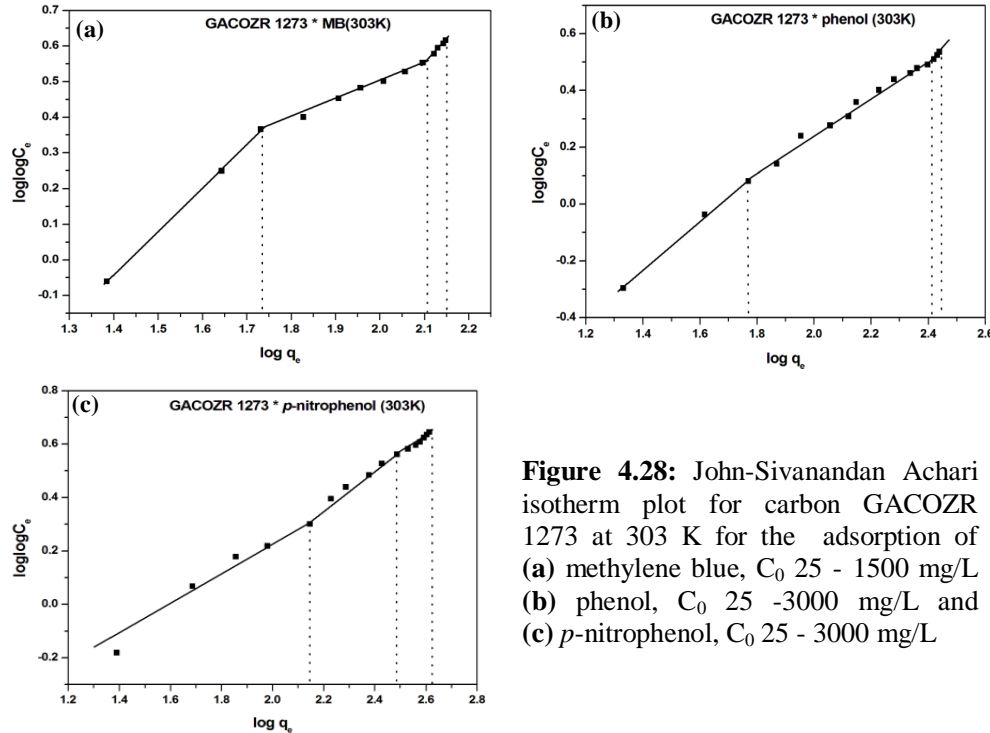


**Figure 4.28:** John-Sivanandan Achari isotherm plot for carbon GACOZR 1273 at 303 K for the adsorption of (a) methylene blue,  $C_0$  25 - 1500 mg/L (b) phenol,  $C_0$  25 - 3000 mg/L and (c) *p*-nitrophenol,  $C_0$  25 - 3000 mg/L

#### 4.5.5.1 John-Sivanandan Achari Isotherm for Phenol, *P*-Nitrophenol and Methylene Blue (MB) Adsorption on GACOZR 1273 at Temperatures

Selected phase changes for the adsorption of phenol, *p*-nitrophenol and methylene blue (MB) at 283, 293, 303, 313 and 323 K in John – Sivanandan Achari isotherm plots are given in Table 4.14.

The temperature enhancement is showing systematic quantitative enhancement in adsorption. For phenol adsorption in *phase I* show only a slight enhancement from 52.77 mg/g to 63.57 mg/g by rising the solution temperature. However, in *phase II* shows significant enhancement from 169.33 mg/g to 230.31mg/g by rising the solution temperature. This is because more and more adsorption sites are activated and becomes accessible with increase of temperature. The wider micropores provided an easy access of phenol molecules to the finer micropores and results in the *phase II* adsorption in J-SA isotherm plot.

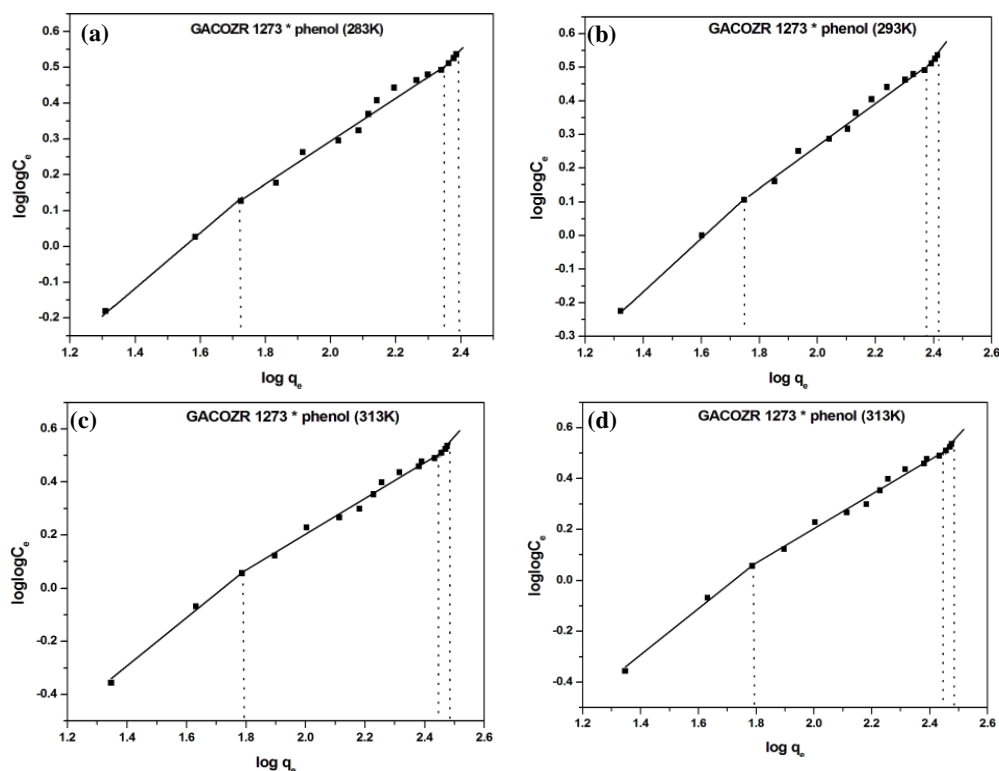


**Figure 4.29:** John –Sivanandan Achari (J-SA) isotherm plot for phenol adsorption on GACOZR 1273 at selected temperatures (a) 283 K (b) 293 K (c) 313 K and (d) 323 K

Total adsorption of *p*-nitrophenol (PNP) is found highest than phenol. Hydrophobic group present in *p*-nitrophenol make it to be less soluble in water and therefore adsorbed strongly than phenol. Quantity of *p*-nitrophenol adsorbed in first phase increases from 133.64 mg/g to 143.9 mg/g, whereas in *phase II* increases from 134.75 mg/g to 201.13 mg/g.

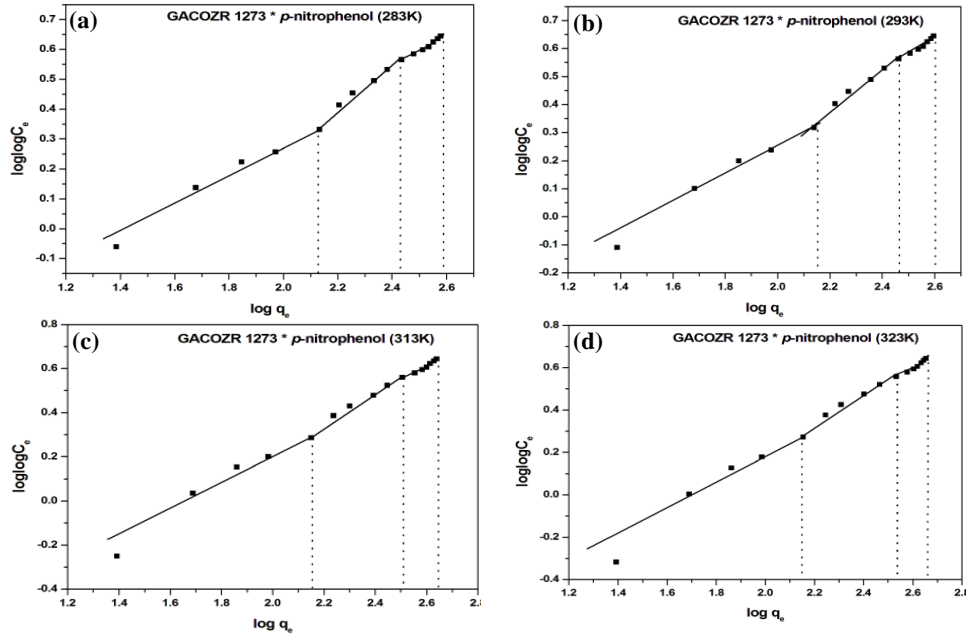


**Figure 4.30:** John –Sivanandan Achari (J-SA) isotherm plot for *p*-nitrophenol adsorption on GACOZR 1273 at temperatures (a) 283 K (b) 293 K (c) 313 K and (d) 323 K

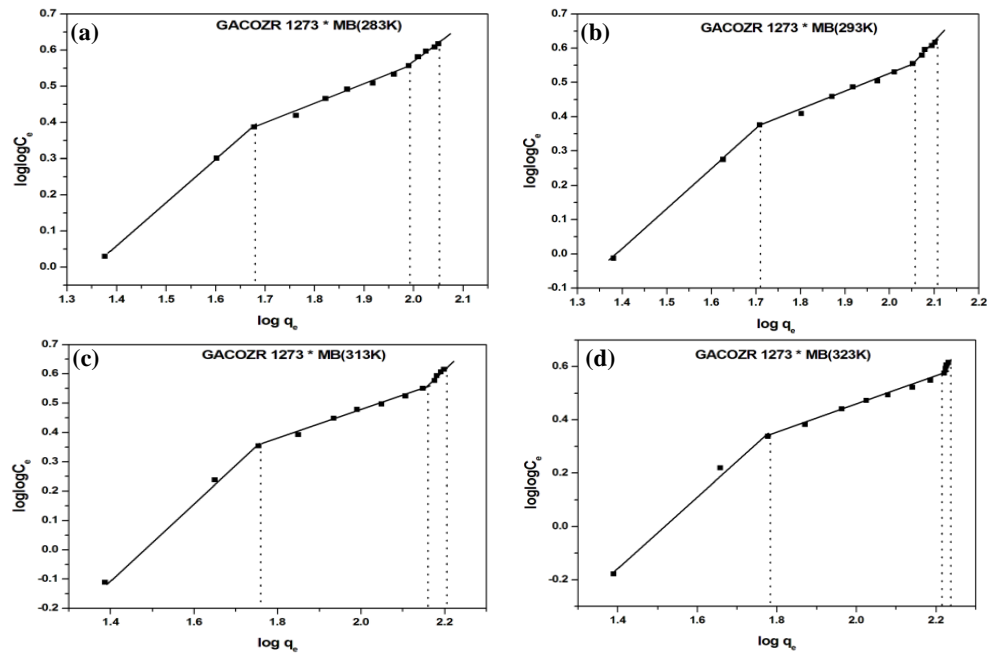


**Figure 4.31:** John –Sivanandan Achari (J-SA) isotherm plot for methylene blue (MB) adsorption on GACOZR 1273 at temperatures (a) 283 K (b) 293 K (c) 313 K and (d) 323 K

John –Sivanandan Achari isotherm plot of methylene blue (MB) on GACOZR 1273 at different temperatures shows that isotherm become steeper with a rise in solution temperatures. It indicates that more adsorption sites are activated and becomes accessible for MB.

Quantity of methylene blue (MB) adsorbed on GACOZR in *phase I* increases from 47.78 mg/g to 60.48 mg/g, whereas in *phase II* quantity adsorbed enhanced from 50.42 mg/g to 101.96 mg/g. Methylene blue molecule has molecular cross sectional area 1.2 nm<sup>2</sup> and the carbon has large micropores of pore diameter greater than 1.5 nm so that the adsorptive removal of the target adsorbate (MB) is enhanced.

**Table 4.14:** John - Sivanandan Achari Isotherm parameter for the adsorption of phenol, *p*-nitrophenol and methylene blue (MB) on carbon GACOZR 1273 at 283 - 323K

Carbons	Temperatures (K)	Phenol			<i>p</i> -nitrophenol			Methylene blue		
		q <sub>I</sub> (J-SA) mg/g (SA m <sup>2</sup> /g)	q <sub>II</sub> (J-SA) mg/g (SA m <sup>2</sup> /g)	q <sub>III</sub> (J-SA) mg/g (SA m <sup>2</sup> /g)	q <sub>I</sub> (J-SA) mg/g (SA m <sup>2</sup> /g)	q <sub>II</sub> (J-SA) mg/g (SA m <sup>2</sup> /g)	q <sub>III</sub> (J-SA) mg/g (SA m <sup>2</sup> /g)	q <sub>I</sub> (J-SA) mg/g (SA m <sup>2</sup> /g)	q <sub>II</sub> (J-SA) mg/g (SA m <sup>2</sup> /g)	q <sub>III</sub> (J-SA) mg/g (SA m <sup>2</sup> /g)
GACOZR 1273	283	52.8 (176.3)	169.3 (565.7)	25.0 (83.7)	133.6 (303.8)	134.7 (306.3)	117.5 (267.1)	47.8 (108.0)	50.4 (113.9)	13.5 (30.6)
	293	56.0 (187.2)	180.0 (601.5)	28.8 (96.2)	137.7 (312.9)	152.1 (345.6)	110.2 (250.5)	51.2 (115.6)	62.5 (141.2)	14.0 (31.6)
	303	58.9 (196.6)	200.2 (668.8)	19.2 (64.0)	139.3 (316.7)	165.1 (375.4)	114.5 (260.3)	54.1 (122.3)	73.4 (165.9)	14.0 (31.6)
	313	61.8 (206.6)	217.9 (728.1)	23.8 (79.7)	143.0 (325.0)	181.1 (411.7)	116.3 (264.3)	57.3 (129.4)	87.3 (197.2)	13.6 (30.6)
	323	63.6 (212.4)	230.3 (769.4)	23.3 (77.8)	143.9 (327.1)	201.1 (457.2)	115.0 (261.3)	60.5 (136.7)	102.0 (230.4)	10.1 (22.9)

#### 4.6 Comparison of Adsorption Isotherms for Adsorption of Phenol, *P*-Nitrophenol & Methylene Blue on GACOZR 1273

In order to assess different isotherms and their ability to correlate with experimental results, the theoretical plots from each isotherm have been shown by the experimental data. The predicted Freundlich, Langmuir, Dubinin-Radushkevich, John –Sivanandan Achari isotherm equation for phenol, *p*-nitrophenol and MB onto GACOZR 1273 is given in Table 4.15

**Table 4.15** : The predicted Freundlich, Langmuir, Dubinin – Radushkevich (D-R), John – Sivanandan Achari (J-SA) isotherm equations for GACOZR 1273

Isotherms	Phenol	<i>p</i> -nitrophenol	Methylene Blue
Langmuir	$q_e = \frac{C_e \times 3.13}{1 + 0.0099C_e}$	$q_e = \frac{C_e \times 8.21}{1 + 0.0183C_e}$	$q_e = \frac{C_e \times 4.81}{1 + 0.0276C_e}$
Freundlich	$q_e = 26.02 \times C_e^{0.3422}$	$q_e = 56.85 \times C_e^{0.2911}$	$q_e = 35.94 \times C_e^{0.2329}$
*D-R	$q_e = 67.38 \times e^{-1.22\varepsilon^2}$	$q_e = 81.21 \times e^{-0.0806\varepsilon^2}$	$q_e = 60.55 \times e^{-0.1041\varepsilon^2}$
*J-SA	$q_e = e^{\frac{\log \log C_e + 1.424}{0.7869}}$	$q_e = e^{\frac{\log \log C_e + 1.237}{0.7099}}$	$q_e = e^{\frac{\log \log C_e + 1.177}{0.8052}}$

\*D-R Dubinin Radushkevich \* J-SA John-Sivanandan Achari isotherm

Figure 4.32(a)–(c) shows the different isotherm curve for phenol, *p*-nitrophenol and methylene blue onto GACOZR 1273 at a constant solution temperature of 303 K. It is plotted in the form of an amount adsorbed ( $q_e$ ) per unit mass of GACOZR 1273, against the concentration of adsorbate remaining in solution,  $C_e$ . It was observed that equilibrium data were well represented by Langmuir and John –Sivanandan Achari isotherm compared to Freundlich and Dubinin-Radsuhkevich (D-R).

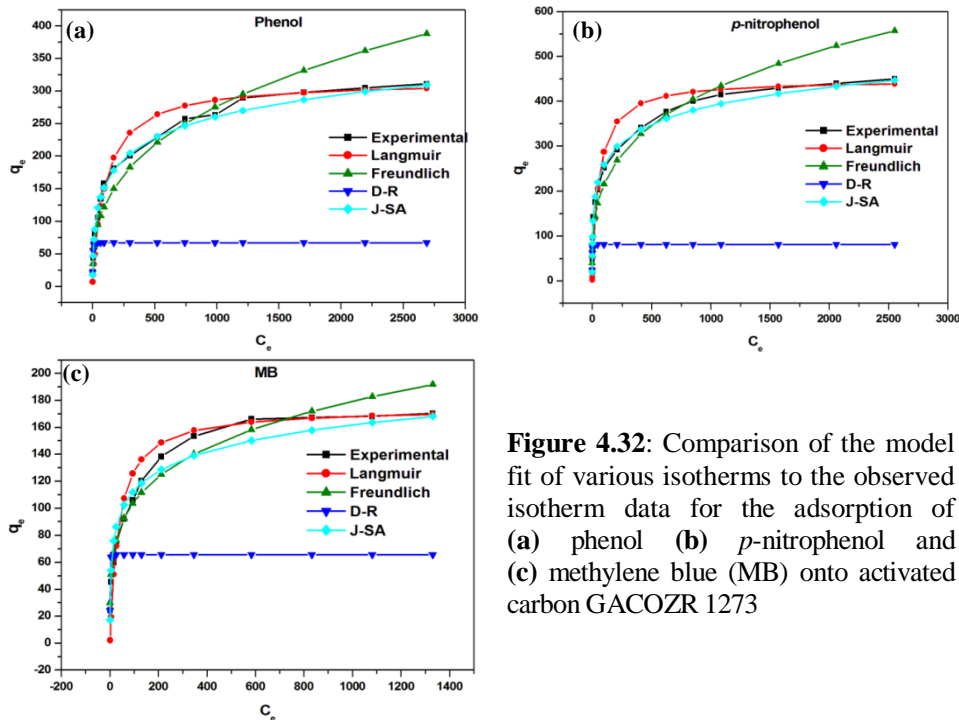


**Figure 4.32:** Comparison of the model fit of various isotherms to the observed isotherm data for the adsorption of (a) phenol (b) *p*-nitrophenol and (c) methylene blue (MB) onto activated carbon GACOZR 1273

The best fit of equilibrium data in the Langmuir isotherm equation and John – Sivanandan Achari isotherm indicates that adsorption data of phenol, *p*-nitrophenol and MB on GACOZR 1273 are well represented by these equations.

#### 4.7 Adsorption Kinetic Studies

To analyze the adsorption kinetics, data obtained from different time interval is tested using mathematical expressions corresponding to various models, namely: Lagergren’s first order equation, pseudo-second order reaction and intra particle diffusion model.

##### 4.7.1 Kinetic Study of Phenol on GACOZR 1273, GAC 383 and GACO 383 at Temperatures

The first order kinetic plots of phenol adsorption onto three adsorbents GAC 383, GACO 383 and GACOZR 1273 at 283, 293, 303, 313 and 323 K are given in Figure 4.33(a)–(c).

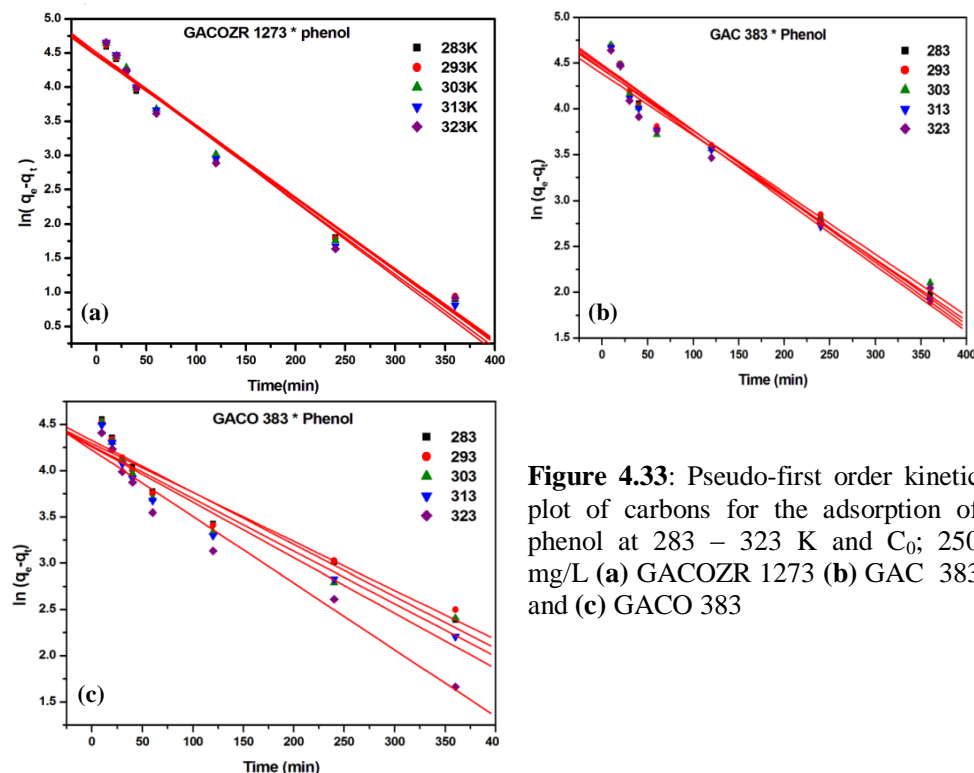


**Figure 4.33:** Pseudo-first order kinetic plot of carbons for the adsorption of phenol at 283 – 323 K and  $C_0$ ; 250 mg/L (a) GACOZR 1273 (b) GAC 383 and (c) GACO 383

The linear form of pseudo-first order equation is

$$\log(q_e - q_t) = \log q_e - \frac{K_1 t}{2.303} \quad (4.17)$$

The slope and intercept obtained from the straight line plot of  $\log(q_e - q_t)$  versus  $t$  are used to determine the first-order rate constant  $K_1$ . Rate along with correlation coefficient are given in Table 4.16.

The second order kinetic plots of phenol onto three carbons GACOZR 1273, GAC 383 and GACO 383 at five different temperatures are given in Figure 4.34 (a)-(c).

Linear form of pseudo-second order equation is

$$\frac{t}{q_t} = \frac{1}{K_2 q_e^2} + \frac{1}{q_e} t \quad (4.18)$$

A plot of  $t/q_t$  versus  $t$  should give a straight line from which  $q_e$  and  $K_2$  can be determined. These are listed in the Table 4.16.

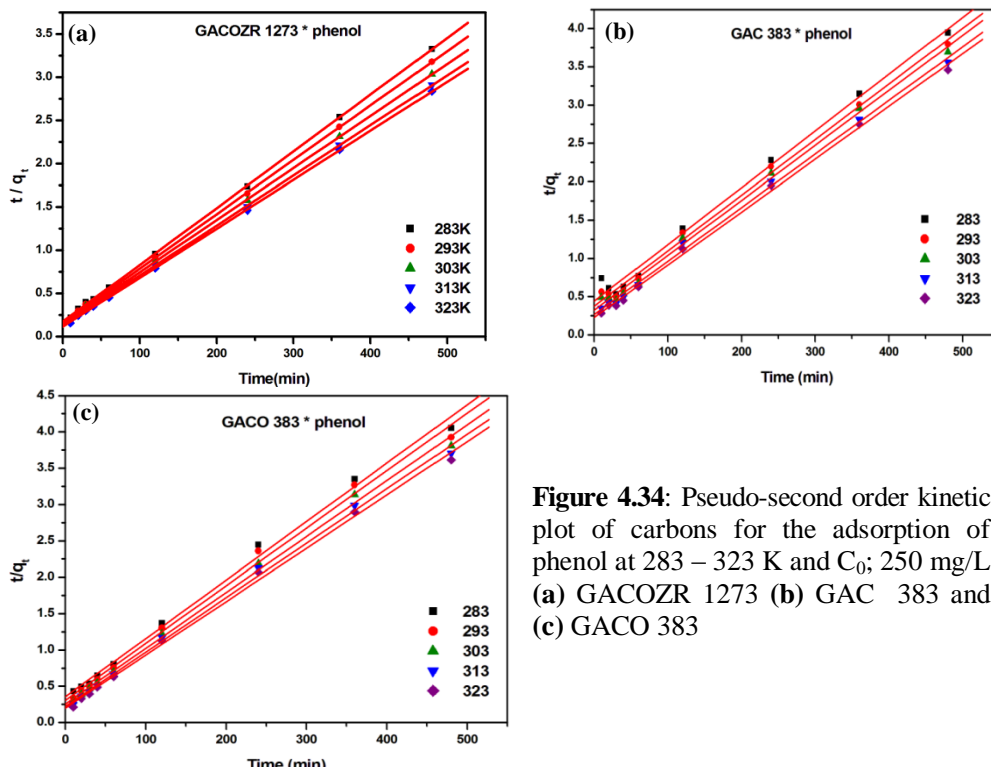


**Figure 4.34:** Pseudo-second order kinetic plot of carbons for the adsorption of phenol at 283 – 323 K and  $C_0$ ; 250 mg/L (a) GACOZR 1273 (b) GAC 383 and (c) GACO 383



Percentages of error between the experimental  $q_e$  and calculated  $q_e$  (pseudo-second order kinetics) of carbon GACOZR 1273 are given as follows; 283 K (5.74 %), 293 K (5.39 %), 303 K (5.17 %), 313 K (4.85 %), 323 K (4.49 %). Percentages of error vary with temperature for GAC 383 is (10 % - 4.5 %) and GACO 383 is (11 % - 4.5 %). This shows that the error percentage between  $q_e$  experimental and  $q_e$  calculated from pseudo-second order is within the limit of 10%. Less percentage of error between the  $q_e$  experimental with  $q_e$  calculated suggested that adsorption of phenol on all these carbons following the pseudo-second order kinetics. Less percentage of error at higher temperature indicates that adsorption system follows more favourably the pseudo-second order kinetics at higher temperatures. Conformity between the experimental  $q_e$  and calculated  $q_e$  is also given by straight line plot with the high correlation coefficient ( $R^2 \approx 0.99$ ).

To describe whether the adsorption process is controlled by diffusion in the adsorbent particles and consecutive diffusion in the bulk of the solution, the plot of  $q_t$ , (the amount of adsorbate adsorbed per unit weight of adsorbent) versus square root of time  $t$  has been used. The plot of  $q_t$  versus  $t^{1/2}$  for adsorption of phenol on GACOZR 1273, GAC 383 and GACO 383 at five temperatures are given in the Figure 4.35 (a)-(c).

$$q_t = k_{id} t^{1/2} + C \quad (4.19)$$

From the slope and intercept, intra particle diffusion parameters  $K_{id1}$ ,  $K_{id2}$  and  $C$  are obtained which are given in the Table 4.16

Two linear plots suggest that the adsorption process proceeds by surface adsorption and intraparticle diffusion.  $K_{id}$  is the intraparticle diffusion coefficient and  $C$  is the boundary layer effect. Greater the intercept greater the contribution of surface adsorption in the rate limiting step.

The plot of  $q_t$  versus  $t^{0.5}$  shows two stages of adsorption with deviation of a straight line from the origin that may be because of the difference in the rate of mass transfer between initial and final stages of adsorption. The initial linear portion refers to the external mass transfer effect or boundary layer effect and the latter portion is due to the intra particle diffusion. External mass transfer

coefficient  $K_{id1}$  given by GACOZR 1273 at different temperatures are 283K (13.58), 293K (13.92), 303K (14.39), 313K (14.88) and 323K (15.26), found to be increased with temperature. Whereas, intraparticle diffusion coefficient  $K_{id2}$  is 283K (1.71), 293K (1.76), 303K (1.83), 313K (1.72), and 323K (1.6). Higher  $K_{id1}$  value compared to  $K_{id2}$  indicates that external mass transfer is more predominating than intra particle diffusion for the adsorption of phenol on GACOZR 1273. This could be attributed to the limitation of the available vacant sites for the diffusion and nature of pore blockage [32, 33].

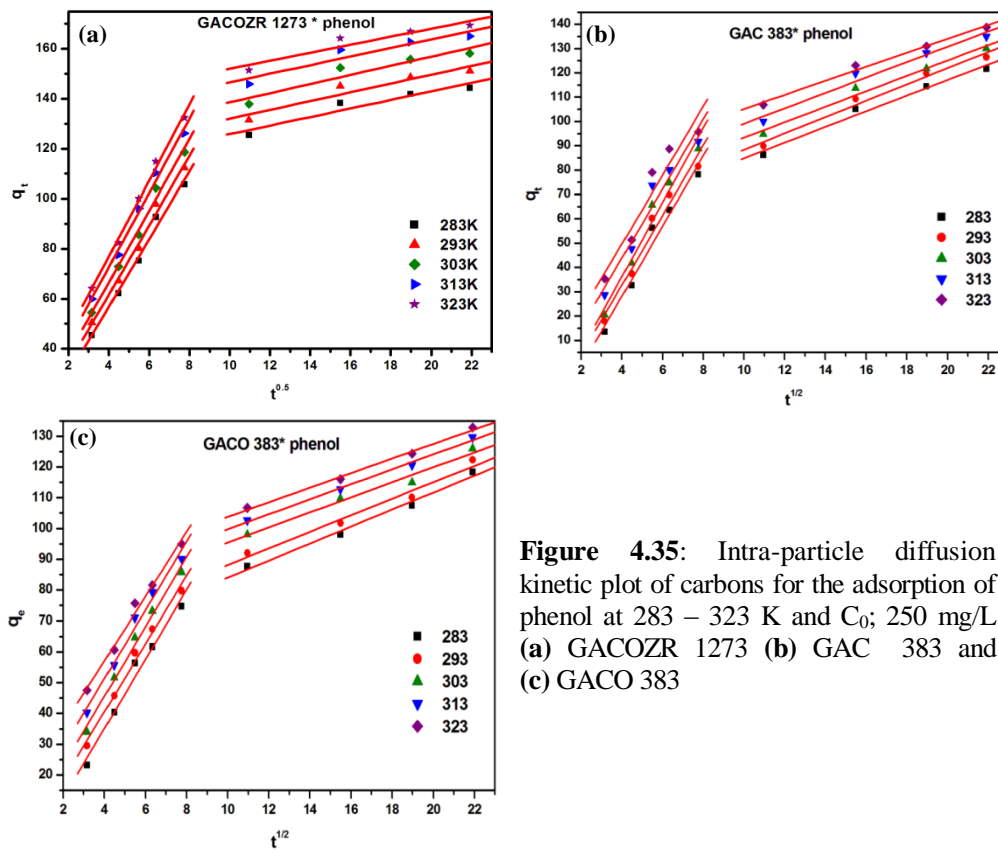


**Figure 4.35:** Intra-particle diffusion kinetic plot of carbons for the adsorption of phenol at 283 – 323 K and  $C_0$ ; 250 mg/L (a) GACOZR 1273 (b) GAC 383 and (c) GACO 383

The  $C$  increases directly with the temperatures, suggests a high boundary layer effect. This indicates that temperature affect both the adsorption capacity and the adsorption mechanism of phenol.

**Table 4.16:** Kinetic parameters of carbons GACOZR 1273, GAC 383 and GACO 383 for the adsorption of phenol at temperatures ranging from 283 - 323K [ C<sub>0</sub> = 250 mg/L]

Carbons	T (Kelvin)	Pseudo-first order				Pseudo-second order				Intra particle diffusion					
		q (exp) mg/g	q <sub>e</sub> (cal) mg/g	K <sub>1</sub> x 10 <sup>-4</sup> min <sup>-1</sup>	R <sup>2</sup>	q <sub>e</sub> (cal) mg/g	K <sub>2</sub> x 10 <sup>5</sup> g mg <sup>-1</sup> min <sup>-1</sup>	h mg g <sup>-1</sup> min <sup>-1</sup>	R <sup>2</sup>	K <sub>id1</sub> mg/g min <sup>1/2</sup>	C <sub>1</sub>	R <sup>2</sup>	K <sub>id2</sub> mg/g min <sup>1/2</sup>	C <sub>2</sub>	R <sup>2</sup>
GACOZR 1273	283	144	87	105	0.98	153	24	5.7	0.99	14	2	0.99	1.7	109	0.97
	293	151	88	104	0.98	159	25	6.2	0.99	14	6	0.99	1.8	114	0.98
	303	158	91	107	0.98	166	25	6.8	0.99	14	9	0.99	1.8	120	0.98
	313	165	91	110	0.98	173	26	7.8	0.99	15	13	0.99	1.7	129	0.98
	323	169	88	107	0.97	177	27	8.5	0.99	15	16	0.99	1.6	136	0.99
GAC383	283	122	87	71	0.96	135	12	2.3	0.99	15	-30	0.97	3.2	53	0.98
	293	126	89	72	0.97	138	14	2.7	0.99	14	-25	0.97	3.4	55	0.98
	303	130	84	67	0.95	140	16	3.1	0.99	15	-25	0.97	3.2	62	0.98
	313	135	85	72	0.96	143	18	3.8	0.99	14	-13	0.95	3.2	67	0.97
	323	139	80	67	0.95	145	21	4.4	0.99	14	-7	0.93	2.9	76	0.99
GACO383	283	118	76	56	0.94	125	18	2.8	0.99	11	-10	0.98	2.8	56	0.99
	293	122	73	53	0.93	126	21	3.3	0.99	11	-4	0.99	2.7	61	0.97
	303	126	71	57	0.93	130	23	3.9	0.99	11	0	0.99	2.4	71	0.98
	313	130	71	60	0.94	134	25	4.5	0.99	11	7	0.98	2.4	76	0.99
	323	133	69	61	0.95	136	27	5.0	0.99	11	15	0.99	2.4	80	0.99

#### 4.7.2 Kinetic Study of P-Nitrophenol on GACOZR 1273, GAC 383 and GACO 383 at Temperatures

The slope and intercept obtained from the straight line plot of  $\log(q_e - q_t)$  versus  $t$  were used to determine the first-order rate constant  $K_1$ . The rate constant along with correlation coefficient are given in Table 4.17 .

Percentages of error calculated between the experimental  $q_e$  and calculated  $q_e$  of GACOZR 1273 is given as; at 283K (25.9 %), 293K (26.98 %), 303K (30.85 %), 313K (35.32 %), 323K (45.18 %). This shows that the error percentage between  $q_e$  experimental and  $q_e$  calculated from pseudo-first order is increased with temperature and varies for new carbons as; GACOZR 1273 (25.9 % - 45.18

%), GAC 383 (23.80 % - 34.63 %), and GACO 383 (30.79 % - 43.58 %) for the temperature range of 283 to 323K. The high percentage error between the  $q_e$  experimental with  $q_e$  calculated suggested adsorption of *p*-nitrophenol on all these carbons is not following the pseudo-first order kinetics.

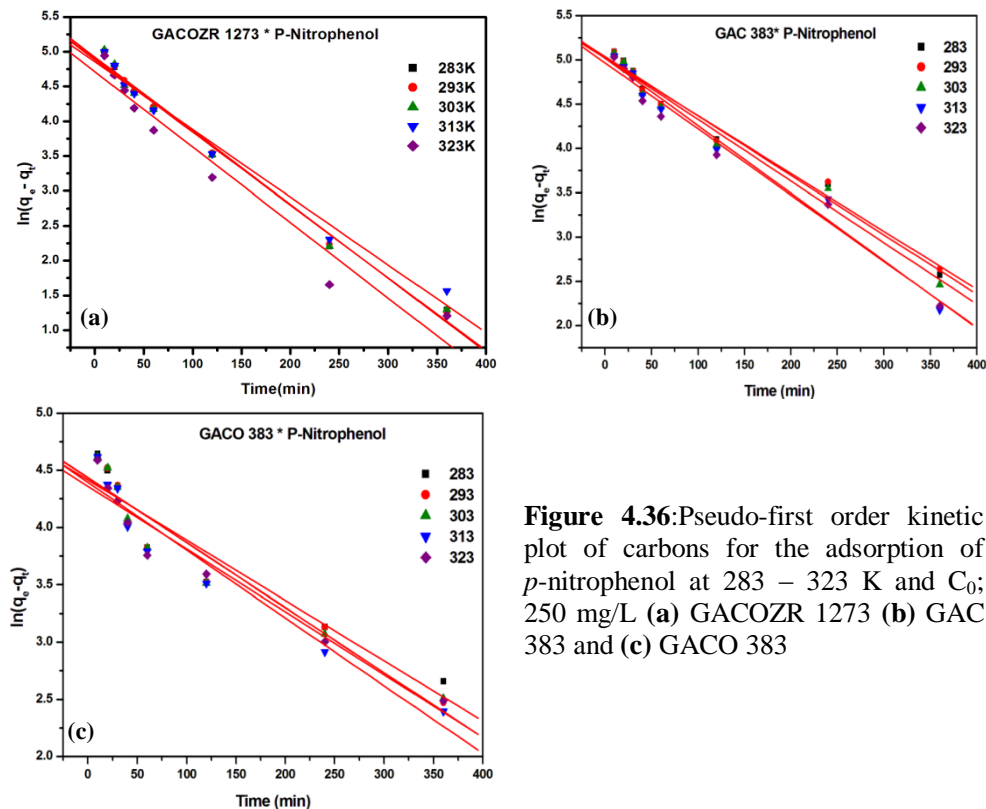


**Figure 4.36:** Pseudo-first order kinetic plot of carbons for the adsorption of *p*-nitrophenol at 283 – 323 K and  $C_0$ ; 250 mg/L (a) GACOZR 1273 (b) GAC 383 and (c) GACO 383

The second order kinetic plots of *p*-nitrophenol adsorption onto three adsorbents GACOZR 1273, GAC 383, and GACO 383 at five temperatures are given in Figure 4.37 (a)-(c). Plots of  $t/q_t$  versus  $t$  should give straight lines from which  $q_e$  and  $K_2$  can be determined are listed in the Table 4.17.

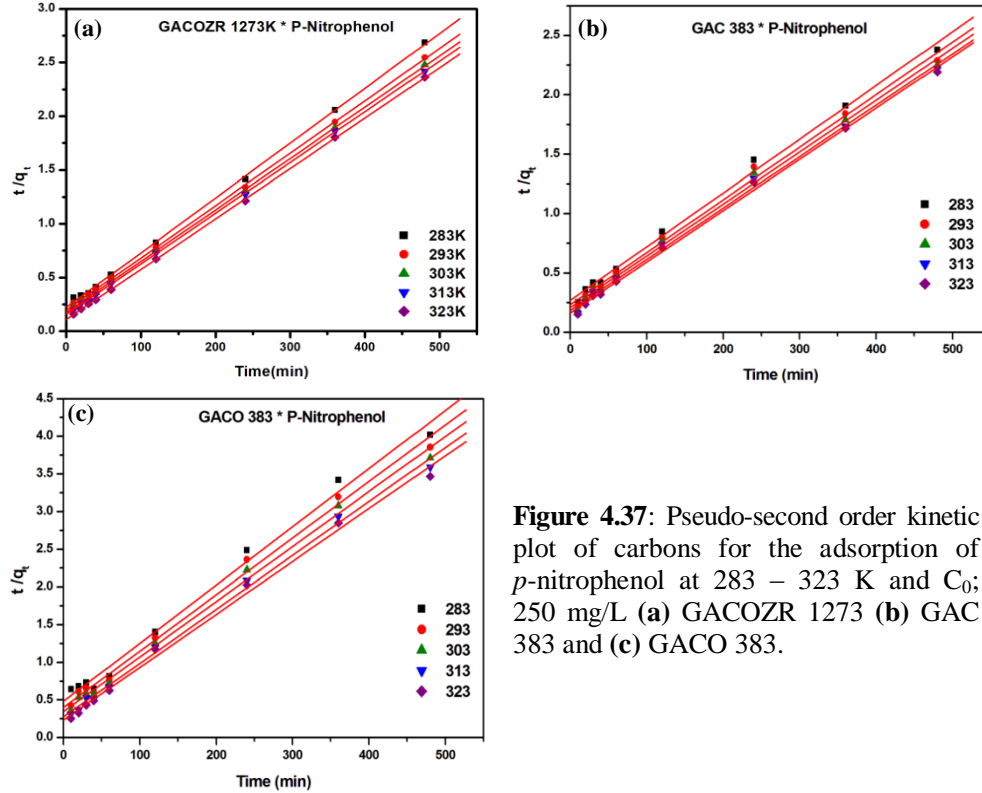


**Figure 4.37:** Pseudo-second order kinetic plot of carbons for the adsorption of *p*-nitrophenol at 283 – 323 K and  $C_0$ ; 250 mg/L (a) GACOZR 1273 (b) GAC 383 and (c) GACO 383.

Percentages of error calculated between the experimental  $q_e$  and calculated  $q_e$  (second order kinetics) of GACOZR 1273 at 283 - 323K are given as 283 K (9.69 %), 293 K (8.94 %), 303 K (7.97 %), 313 K (6.80 %), 323 K (4.98 %). Close agreement between two  $q_e$  values (calculated and experimental) and correlation coefficient  $R^2 \approx 0.99$  suggest that adsorption system follows pseudo-second order kinetics.

Intra particle diffusion plot of ( $q_t$  versus  $t^{1/2}$ ) *p*-nitrophenol at five different temperatures are given in the Figure 4.38. From the slope and intercept intra particle diffusion parameters  $K_{id1}$ ,  $K_{id2}$  and  $C$  are obtained which are given in the Table 4.17.

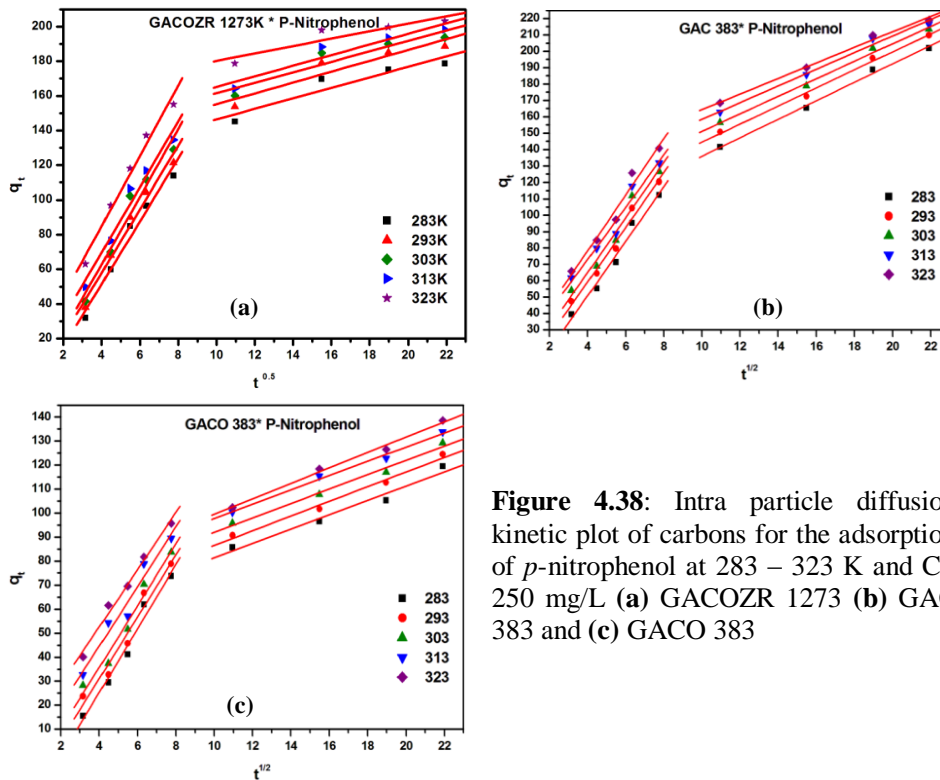


**Figure 4.38:** Intra particle diffusion kinetic plot of carbons for the adsorption of *p*-nitrophenol at 283 – 323 K and  $C_0$ ; 250 mg/L (a) GACOZR 1273 (b) GAC 383 and (c) GACO 383

The plots consisted of two linear sections indicating that two steps contribute to the adsorption process. This suggested that the adsorption of *p*-nitrophenol on GACOZR 1273, GAC 383 and GACO 383 was controlled by external mass transfer followed by intra particle diffusion. External mass transfer coefficient  $K_{id1}$  given by GACOZR 1273 at 283 - 323K are given as; at 283K (18.15), 293 K (18.37), 303 K (19.56), 313 K (18.96) and 323 K (20.29 mg/g min<sup>1/2</sup>) where as intraparticle diffusion coefficient  $K_{id2}$  at temperatures are 283K (3.03), 293K (3.13), 303K (3.03), 313K (3.06), and at 323K (2.144 mg/g min<sup>1/2</sup>).

**Table 4.17:** Kinetic parameters of carbons GACOZR 1273, GAC 383 and GACO 383 for the adsorption of *p*-nitrophenol at temperatures ranging from 283 - 323K [ C<sub>0</sub> = 250 mg/L]

Carbons	T (Kelvin)	q <sub>e</sub> (exp) mg/g	Pseudo-first order			Pseudo-second order				Intra particle diffusion					
			q <sub>e</sub> (cal) mg/g	K <sub>1</sub> × 10 <sup>-4</sup> min <sup>-1</sup>	R <sup>2</sup>	q <sub>e</sub> (cal) mg/g	K <sub>2</sub> × 10 <sup>5</sup> g mg <sup>-1</sup> min <sup>-1</sup>	R <sup>2</sup>	h mg g <sup>-1</sup> min <sup>-1</sup>	K <sub>id1</sub> mg/g min <sup>1/2</sup>	C <sub>1</sub>	R <sup>2</sup>	K <sub>id2</sub> mg/g min <sup>1/2</sup>	C <sub>2</sub>	R <sup>2</sup>
GACOZR 1273	283	179	133	104	0.99	196	12	0.99	4.5	18	-21	0.97	3.0	116	0.89
	293	189	138	106	0.99	205	12	0.99	5.1	18	-15	0.98	3.1	124	0.89
	303	194	134	105	0.99	209	13	0.99	5.8	20	-15	0.96	3.0	131	0.89
	313	198	128	97	0.98	212	14	0.99	6.4	19	-6	0.97	3.1	135	0.90
	323	203	111	108	0.96	213	20	0.99	9.3	20	4	0.98	2.1	159	0.85
GAC 383	283	202	154	67	0.98	221	8	0.99	3.7	17	-16	0.98	5.6	80	1.00
	293	210	152	65	0.98	226	9	0.99	4.3	17	-8	0.98	5.1	89	0.99
	303	213	151	69	0.98	229	9	0.99	4.8	17	-2	0.97	5.3	98	0.99
	313	217	151	76	0.98	232	10	0.99	5.5	16	9	0.96	5.1	108	0.99
	323	219	143	75	0.98	232	12	0.99	6.2	17	10	0.97	4.8	117	0.99
GACO 383	283	120	83	53	0.91	130	12	0.99	2.1	13	-28	0.98	3.0	52	0.97
	293	125	85	57	0.93	133	14	0.99	2.5	13	-21	0.96	3.1	56	0.99
	303	129	84	57	0.93	137	16	0.99	2.9	13	-16	0.97	3.0	62	0.99
	313	134	81	59	0.94	140	19	0.99	3.7	12	-5	0.96	3.0	68	0.99
	323	139	78	55	0.94	143	21	0.99	4.3	12	5	0.99	3.2	67	0.99

#### 4.7.3 Kinetic Study of Methylene Blue (MB) on GACOZR 1273, GAC 383 and GACO 383 at Temperatures

The effect of temperature on the adsorption of methylene blue dye onto GACOZR 1273, GAC 383 and GACO 383 was studied by batch contact-time experiments. Adsorption data are applied to kinetic models such as Lagergren pseudo-first order, Ho pseudo-second order and intra particle diffusion models.

Pseudo-first order plot  $\log (q_e - q_t)$  versus  $t$  at five different temperatures on GACOZR 1273, GAC 383 and GACO 383 is given by the Figure 4.39 (a)-(c).

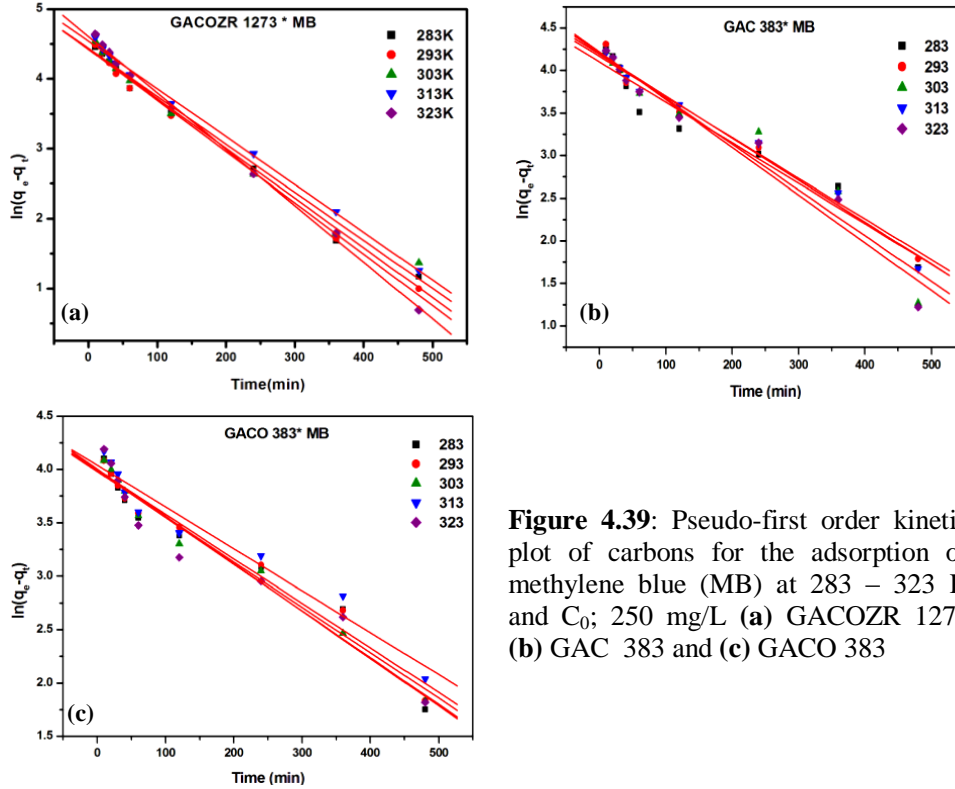


**Figure 4.39:** Pseudo-first order kinetic plot of carbons for the adsorption of methylene blue (MB) at 283 – 323 K and  $C_0$ ; 250 mg/L (a) GACOZR 1273 (b) GAC 383 and (c) GACO 383

The calculated equilibrium adsorption capacities  $q_e$  (cal) were by far lower than the experimental values. Percentages of error calculated between the experimental  $q_e$  and calculated  $q_e$  value of GACOZR 1273 at 283-323K are determined as; at 283K (12.87 %), 293K (17.14 %), 303K (23.99 %), 313K (21.68 %), 323K (22.09 %). Percentages of error vary for new carbons at 283 - 323 K are given as; GACOZR 1273 (12.87 % - 22.09 %), GAC 383 (40.86 % - 50.88 %) and GACO 383 (33.60 % - 54.27 %). The straight line relationship was not valid in the whole range of contact time, i.e. the adsorption of methylene blue by the carbons GACOZR 1273, GAC 383 and GACO 383 investigated is not an ideal first order reaction.

Figure 4.40 represents the plot of  $t/q_t$  versus  $t$  for the adsorption of methylene blue onto GACOZR 1273, GAC 383 and GACO 383 at 283, 293, 303,



313 and 323K. Kinetic parameters  $K_2$ ,  $q_e$  and  $R^2$  for methylene blue - activated carbons system at five different temperatures are listed in Table 4.18.

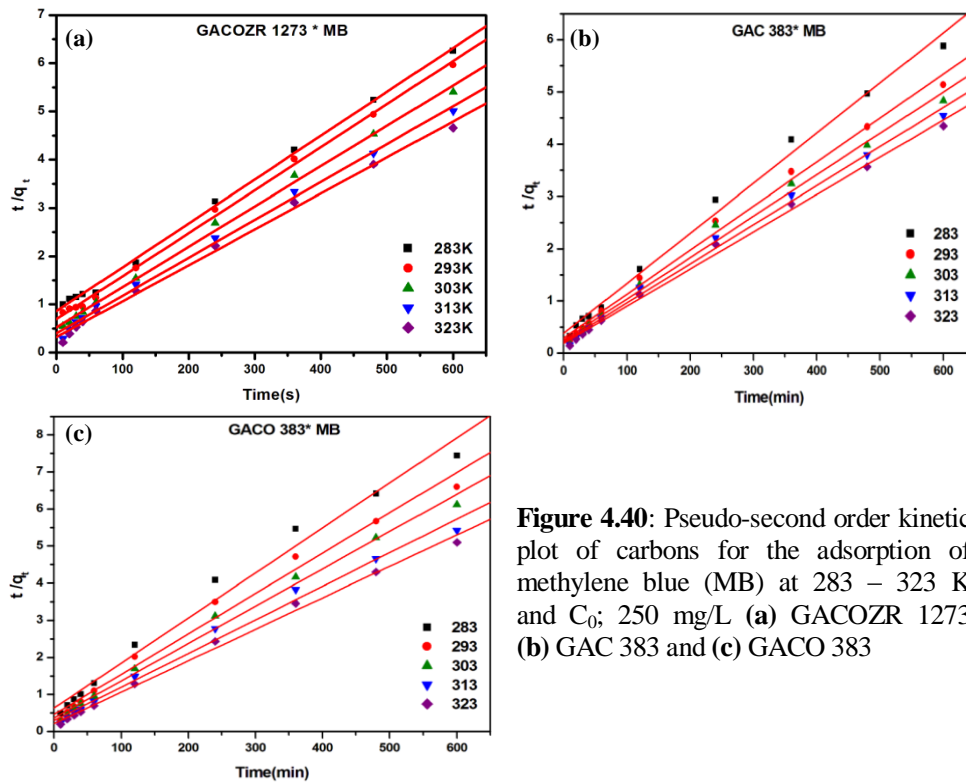


**Figure 4.40:** Pseudo-second order kinetic plot of carbons for the adsorption of methylene blue (MB) at 283 – 323 K and  $C_0$ ; 250 mg/L (a) GACOZR 1273 (b) GAC 383 and (c) GACO 383

Percentages of error calculated between the experimental  $q_e$  and calculated  $q_e$  value of GACOZR 1273 shows 14.61 % (at 283 K), 11.59 % (at 293 K), 7.97 % (at 303 K), 6.41 % (at 313 K) and 4.20 % (at 323K). The lower percentage of error indicates calculated  $q_e$  is more close to experimental  $q_e$  and the value of  $R^2$  is close to unity indicating that the adsorption of methylene blue fits very well with the pseudo-second order kinetics.

The possibility of intra-particle diffusion for the adsorption of methylene blue on activated carbon can be explained by using the intra-particle diffusion model. A plot of  $q_t$  versus  $t^{1/2}$  is given in the Figure 4.41(a)–(c). Adsorption of methylene blue on GACOZR 1273, GAC 383 and GACO 383 are influenced by a two step process confirmed by the two linear plots.

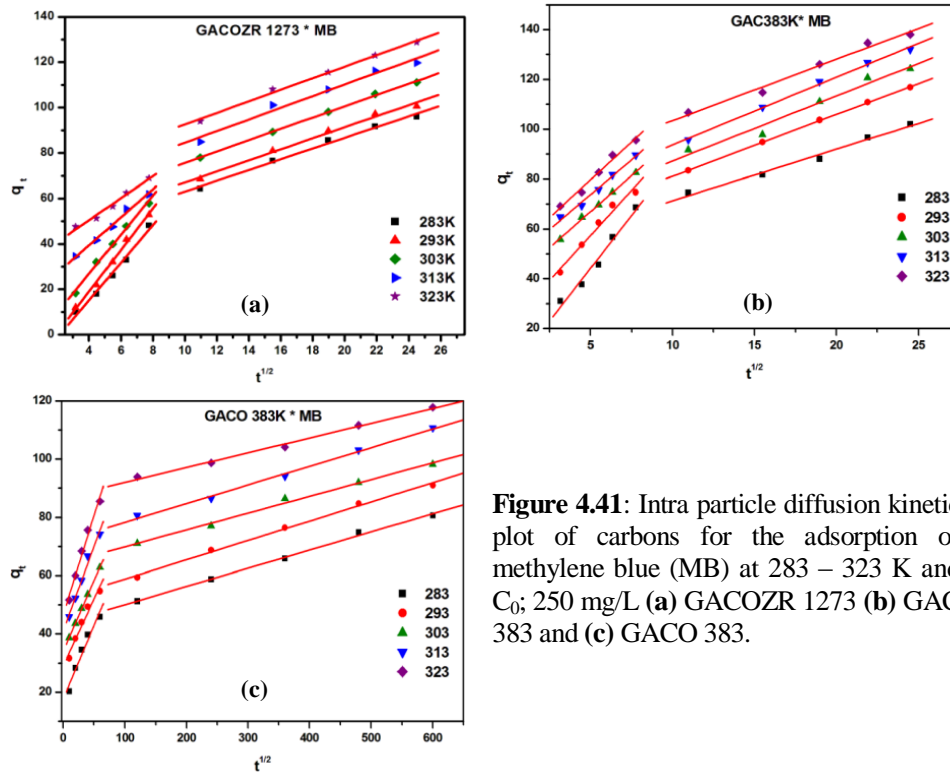


**Figure 4.41:** Intra particle diffusion kinetic plot of carbons for the adsorption of methylene blue (MB) at 283 – 323 K and  $C_0$ ; 250 mg/L (a) GACOZR 1273 (b) GAC 383 and (c) GACO 383.

The first sharper linear portion evidence that, the external resistance to mass transfer surrounding the particles is significant in the early stages of adsorption followed by controlled intra particle diffusion as indicated by the second linear portion.

External mass transfer coefficient  $K_{id1}$  given by new carbons at 283 - 323 K are; GACOZR 1273 (4.85 - 9.16 mg/g min<sup>1/2</sup>), GAC 383 (5.59 – 8.49 mg/g min<sup>1/2</sup>) and GACO 383 (0.460 - 0.678 mg/g min<sup>1/2</sup>). Where, intraparticle diffusion coefficient  $K_{id2}$  is given as; GACOZR 1273 (2.36-2.54 mg/g min<sup>1/2</sup>), GAC 383 (2.07 -2.72 mg/g min<sup>1/2</sup>) and GACO 383 (0.051-0.066 mg/g min<sup>1/2</sup>).

Extrapolation of the linear portions of the plots back to the y-axis gives the intercepts, which provide the measure of the boundary layer thickness. Higher the  $C$  value indicates higher boundary layer effect.

**Table 4.18 :** Kinetic parameters of carbons GACOZR 1273, GAC 383 and GACO 383 for the adsorption of methylene blue (MB) at temperatures ranging from 283 – 323 K [ C<sub>0</sub> = 250 mg/L]

Carbons	T ( Kelvin)	q <sub>e</sub> (exp) mg/g	Pseudo-first order			Pseudo-second order				Intra particle diffusion					
			q <sub>e</sub> (cal) mg/g	K <sub>1</sub> × 10 <sup>-4</sup> min <sup>-1</sup>	R <sup>2</sup>	q <sub>e</sub> (cal) mg/g	K <sub>2</sub> × 10 <sup>5</sup> g mg <sup>-1</sup> min <sup>-1</sup>	h mg g <sup>-1</sup> min <sup>-1</sup>	R <sup>2</sup>	K <sub>id1</sub> mg/g min <sup>1/2</sup>	C <sub>1</sub>	R <sup>2</sup>	K <sub>id2</sub> mg/g min <sup>1/2</sup>	C <sub>2</sub>	R <sup>2</sup>
GACOZR 1273	283	96	84	71	0.99	110	10	1.2	0.99	8.3	-18	0.98	2.4	39	0.99
	293	101	83	73	0.99	112	11	1.4	0.99	9.2	-17	0.99	2.4	43	0.99
	303	111	85	69	0.99	120	13	1.9	0.99	8.6	-8	0.99	2.5	51	0.99
	313	120	94	68	0.99	127	16	2.5	0.99	6.2	15	0.99	2.6	59	0.98
	323	129	100	81	0.99	134	17	3.1	0.99	4.9	31	0.98	2.5	67	0.99
GAC 383	283	102	60	48	0.94	104	24	2.6	0.99	8.5	2	0.98	2.1	51	0.97
	293	117	65	48	0.98	119	25	3.5	0.99	7.2	21	0.97	2.5	56	0.99
	303	124	67	54	0.94	126	25	4.0	0.99	5.8	38	0.99	2.6	61	0.97
	313	132	66	49	0.98	134	26	4.6	0.99	5.6	46	0.98	2.7	67	0.99
	323	138	68	56	0.96	140	27	5.4	0.99	6.1	49	0.98	2.5	79	0.98
GACO 383	283	81	54	42	0.96	82	23	1.6	0.99	0.51	18	0.96	0.06	44	0.99
	293	91	54	42	0.97	92	26	2.2	0.99	0.46	29	0.96	0.07	52	0.99
	303	98	55	44	0.98	100	28	2.7	0.99	0.48	34	0.99	0.06	64	0.99
	313	111	57	39	0.95	110	28	3.4	0.99	0.58	41	0.98	0.06	72	0.99
	323	118	54	44	0.94	118	33	4.6	0.99	0.68	47	0.98	0.05	87	0.99

#### 4.8 Thermodynamic Parameters

Thermodynamic parameter  $\Delta H$  and  $\Delta S$  is obtained from the slope and intercept of the plot of adsorption equilibrium constant obtained from Langmuir isotherm ( $\ln K_L$ ) versus  $1/T$ . The  $\Delta G$  obtained from the relationship between  $\Delta H$ ,  $\Delta S$  and reaction temperature.

$$\ln K_L = \frac{\Delta S}{R} - \frac{\Delta H}{RT} \tag{4.20}$$

$$\Delta G = \Delta H - T\Delta S \tag{4.21}$$

The thermodynamic study of phenol adsorption on GACOZR 1273, GAC 383 and GACO 383 are given in the Figure 4.42(a). The thermodynamic parameters of Gibbs free energy change  $\Delta G$ , enthalpy change  $\Delta H$  and entropy change  $\Delta S$ , for the adsorption processes are calculated and are given in Table 4.19.

**Table 4.19:** Thermodynamic parameters for adsorption of phenol onto GAC 383, GACO 383 and GACOZR 1273

Carbons	$(\Delta H)$ kJ/mol	$(\Delta S)$ J/mol.K	$\Delta G$ (kJ/mol)				
			283K	293K	303K	313K	323K
GAC 383	2.33	15.32	-2.0	-2.15	-2.31	-2.46	-2.61
GACO 383	3.28	18.20	-1.87	-2.05	-2.23	-2.41	-2.59
GACOZR 1273	13.28	50.32	-0.96	-1.46	-1.97	-2.47	-2.97

The  $\Delta H$  calculated for phenol adsorption on GAC is given as; GAC 383 (2.33 kJ/mol), GACO 383 (3.28 kJ/mol) and GACOZR 1273 (13.28 kJ/mol). These enthalpies represent the interaction energy of the amount adsorbed on the adsorbent - adsorbate interface. The positive  $\Delta H$  of all adsorbents indicates the endothermic nature of adsorption i.e. large amount of heat must be input into the phenol-solvent systems for adsorption of phenol on GAC 383, GACO 383 and GACOZR 1273 [34]. Also magnitude of  $\Delta H$  differentiates between physical and chemical adsorption processes. Enthalpy change values are less than 20 kJ/mol therefore; it follows behaviour of physisorption in the process.

The spontaneity of the process appears to be associated with a highly ordered system going to a less-ordered. The positive value of  $\Delta S$  suggests the randomness of the adsorption process. It indicates the greater stability of an adsorption process with no structural changes at the solid-liquid interface. The magnitude of  $\Delta S$  for GAC is given as GAC 383 (15.32 J/mol.K), GACO 383 (18.20 J/mol.K) and GACOZR 1273 (50.32 J/mol.K). Positive  $\Delta S$  value for the adsorption of phenol on GAC means that the increase in the degrees of freedom at the phenol-solvent interface during the process of adsorption of phenol molecules on the active sites of the adsorbent.

Negative  $\Delta G$  indicates spontaneous adsorption and the degree of spontaneity of the reaction. The Gibbs free energy change ( $\Delta G$ ) obtained ranges from 283 to

323 K for respective GAC are given as; GAC 383 ( - 2.0 to - 2.61 kJ/mol), GACO 383 (-1.86 to -2.59 kJ/mol) and for GACOZR 1273 (-0.96 to -2.97 kJ/mol). It was also observed that with an increase in temperature the  $\Delta G$  become more negative. It indicates that adsorption of phenol on GAC studied, was spontaneous and thermodynamically favourable by an increase in temperature.

Figure 4.42 (b) indicates thermodynamic study of adsorption process of *p*-nitrophenol on GACOZR 1273, GAC 383 and GACO 383. The thermodynamic parameters of Gibbs free energy change  $\Delta G$ , enthalpy change  $\Delta H$ , and entropy change  $\Delta S$  for the adsorption processes are calculated and are given in Table 4.20.

**Table 4.20:** Thermodynamic parameters for adsorption of *p*-nitrophenol onto GAC 383, GACO 383 and GACOZR 1273

Carbon	$\Delta H$ kJ/mol	$\Delta S$ J/mol.K	$\Delta G$ (kJ/mol)				
			283K	293K	303K	313K	323K
GAC 383	6.04	38.2	-4.77	-5.15	-5.53	-5.92	-6.30
GACO383	2.94	16.4	-1.70	-1.87	-2.03	-2.19	-2.36
GACOZR 1273	9.53	6.98	-3.77	-4.24	-4.71	-5.18	-5.65

The  $\Delta H$  calculated for *p*-nitrophenol adsorption on GAC follows, GAC 383 (6.04 kJ/mol), GACO 383 (2.94 kJ/mol) and GACOZR 1273 (9.53 kJ/mol) respectively. The positive  $\Delta H$  of all carbon adsorbents indicates the endothermic nature of adsorption. The Low value of the adsorption energy indicates the physical nature of adsorption. The high degree of disorder of an adsorption system gives a positive value of  $\Delta S$  as it varies for carbons as; GAC 383 (38.2 J/mol.K), GACO 383 (16.4 J/mol.K) and GACOZR 1273 (46.98 J/mol.K) respectively.

The negative values of  $\Delta G$  confirm the feasibility of the process and the spontaneous nature of adsorption with a high preference of *p*-nitrophenol by GACOZR 1273, GAC 383 and GACO 383. The Gibbs free energy change ( $\Delta G$ ) determined ranges at temperature 283 K to 323 K for new carbons are; GAC 383 ( -4.77 to -6.30 kJ/mol), GACO 383 ( -1.70 to -2.36 kJ/mol) and GACOZR 1273 (-3.77 to -5.65 kJ/mol). The decrease in the negative value of  $\Delta G$  with an increase

in temperature indicates that the adsorption process of *p*-nitrophenol on GAC studied becomes more favourable at higher temperatures.

Figure 4.42(c) shows thermodynamic study of adsorption process of methylene blue on GACOZR 1273, GAC 383 and GACO 383. The thermodynamic parameters of Gibbs free energy change  $\Delta G$ , enthalpy change  $\Delta H$ , and entropy change  $\Delta S$  for the adsorption processes are calculated and are given in Table 4.21.

**Table 4.21:** Thermodynamic parameters for adsorption of methylene blue (MB) onto GACOZR 1273, GAC 383 and GACO 383

Carbon	$(\Delta H)$ kJ/mol	$(\Delta S)$ J/mol.K	$\Delta G$ (kJ/mol)				
			283K	293K	303K	313K	323K
GAC 383	6.87	35.60	-3.20	-3.56	-3.92	-4.27	-4.63
GACO 383	8.91	40.35	-2.51	-2.91	-3.32	-3.72	-4.12
GACOZR 1273	12.81	52.59	-2.08	-2.60	-3.13	-3.65	-4.18

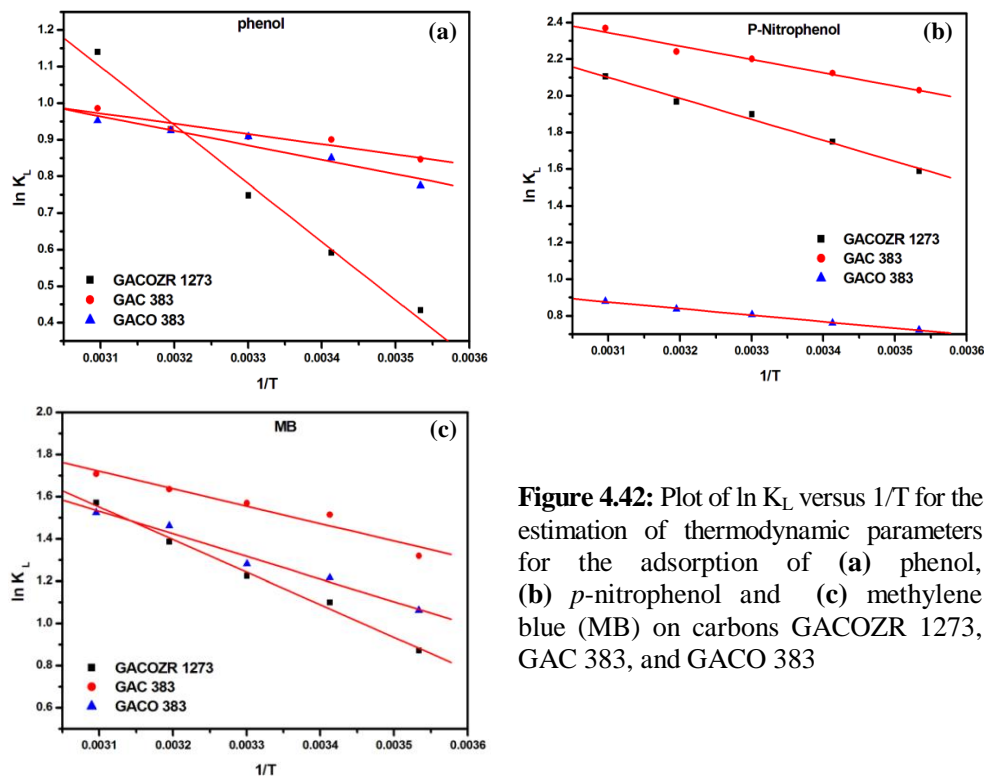


**Figure 4.42:** Plot of  $\ln K_L$  versus  $1/T$  for the estimation of thermodynamic parameters for the adsorption of (a) phenol, (b) *p*-nitrophenol and (c) methylene blue (MB) on carbons GACOZR 1273, GAC 383, and GACO 383

As seen in Table 4.21, positive values of  $\Delta H$  (GAC 383: 6.87 kJ/mol, GACO 383: 8.91 kJ/mol, and GACOZR 1273: 12.81 kJ/mol) show the endothermic nature of adsorption. The negative values of  $\Delta G$  indicate the spontaneous nature of adsorption for methylene blue. It varies for new carbons as; GAC 383 (- 3.20 to - 4.63 kJ/mol), GACO 383 (- 2.51 to - 4.12 kJ/mol) and GACOZR 1273 (-2.08 to -4.18 kJ/mol). The high negative value of  $\Delta G$  indicates higher adsorption capability at higher temperature. At higher temperature organic molecule could overcome space hindrance while diffusing into GACs [35]. The positive values of  $\Delta S$  (GAC 383: 35.60 J/mol.K, GACO 383: 40.35 J/mol.K, and GACOZR 1273: 52.59 J/mol.K) suggest the increased randomness at the solid/solution interface during the adsorption of methylene blue on GAC 383, GACO 383 and GACOZR 1273.

#### 4.8.1 Thermodynamic Parameters from Distribution Coefficient

Thermodynamic parameters were calculated from the variations of the thermodynamic equilibrium constant ( $K_D$ ) by plotting of  $\ln K_D$  versus  $1/T$  [36].

$$\ln K_D = \frac{\Delta S}{R} - \frac{\Delta H}{RT} \quad (4.22)$$

The slope and intercept of the lines are used to determine the  $\Delta H$  and  $\Delta S$  using the equations (4.23).

Distribution coefficient ( $K_D$ ) is defined as the ratio of the quantity of the adsorbate adsorbed per mass of the solid to the amount of the adsorbate remaining in solution [37].

$$\text{where } K_D = \frac{C_o - C_e}{C_e} \quad (4.23)$$

The obtained values of  $\Delta H$ ,  $\Delta S$  and  $\Delta G$  for the adsorption of phenol uptake on the new carbons are summarized in Table 4.22.

**Table 4.22:** Thermodynamic parameters obtained from plot of  $\ln K_D$  versus  $1/T$  for the adsorption of phenol

$C_0$ mg/L	GACOZR 1273 - phenol							GAC 383 - phenol					GACO 383 - phenol								
	$\Delta S$ J/mol.K	$\Delta H$ kJ/mol	$\Delta G$ kJ/mol					$\Delta S$ J/mol.K	$\Delta H$ kJ/mol	$\Delta G$ kJ/mol			$\Delta S$ J/mol.K	$\Delta H$ kJ/mol	$\Delta G$ kJ/mol						
			283	293	303	313	323			283	293	303			313	323	283	293	303	313	323
25	89	18	-7	-8	-9	-10	-11	27	5	-3	-3	-3	-4	-4	32	6	-3	-3	-3	-4	-4
50	72	17	-3	-4	-5	-6	-6	27	5	-3	-3	-3	-4	-4	32	6	-3	-3	-3	-4	-4
75	59	15	-1	-2	-2	-3	-4	26	5	-2	-3	-3	-3	-3	30	6	-2	-3	-3	-3	-3
100	52	14	-1	-1	-	-2	-3	23	5	-2	-3	-2	-2	-3	27	6	-2	-2	-2	-2	-3
150	44	13	1	0	0	-1	-1	22	5	-1	-1	-2	-2	-2	24	6	-1	-1	-1	-1	-2
200	35	12	3	2	2	2	1	19	5	0	-1	-1	-1	-1	21	6	0	-1	-1	-1	-1
250	36	12	2	1	1	1	0	18	5	0	0	0	0	-1	18	5	0	0	0	0	0
350	33	12	2	2	2	1	1	16	5	1	0	0	0	0	16	6	1	1	1	1	1
500	28	11	3	3	3	2	2	14	5	1	1	1	1	1	11	5	2	2	2	2	2
750	24	11	4	4	4	4	3	11	5	2	2	2	2	2	7	5	3	3	3	3	3
1000	18	10	5	5	5	4	4	10	6	3	2	2	2	2	2	4	4	4	4	4	4

The change in  $\Delta H$  values for the adsorption of phenol (in the concentration range of 25 mg/L - 1000 mg/L) on GAC are given as follows GACOZR 1273 (18.2 - 10.1 kJ/mol), GAC 383 (4.85 - 5.45 kJ/mol), and GACO 383 (4.4 - 6.4 kJ/mol), The change in  $\Delta S$  for phenol adsorption on GAC are given as GACOZR 1273 (89.3 - 18.0 J/mol.K), GAC 383 (27.2 - 10.4 J/mol.K), GACO 383 (32.2 - 2.1 J/mol.K).

The obtained values of  $\Delta H$ ,  $\Delta S$  and  $\Delta G$  of adsorption for *p*-nitrophenol uptake on the new carbons are summarized in Table 4.23.

**Table 4.23:** Thermodynamic parameters obtained from plot of  $\ln K_D$  versus  $1/T$  for the adsorption of *p*-nitrophenol

$C_0$ mg/L	GACOZR 1273 - PNP							GAC 383 - PNP					GACO 383 - PNP								
	$\Delta S$ J/mol.K	$\Delta H$ kJ/mol	$\Delta G$ kJ/mol					$\Delta S$ J/mol.K	$\Delta H$ kJ/mol	$\Delta G$ kJ/mol			$\Delta S$ J/mol.K	$\Delta H$ kJ/mol	$\Delta G$ kJ/mol						
			283	293	303	313	323			283	293	303			313	323	283	293	303	313	323
25	92	18	-8	-9	-10	-11	-12	64	9	-9	-9	-10	-11	-11	29	5	-3	-4	-4	-4	-5
50	83	16	-7	-8	-9	-10	-10	63	10	-8	-9	-10	-10	-11	26	5	-3	-3	-3	-3	-4
75	76	15	-6	-7	-8	-9	-9	62	10	-7	-8	-9	-9	-10	23	5	-2	-2	-2	-3	-3
100	71	14	-6	-7	-8	-8	-9	59	10	-7	-8	-8	-9	-9	22	5	-2	-2	-2	-2	-3
150	65	13	-5	-6	-7	-7	-8	55	10	-6	-6	-7	-7	-8	17	5	0	0	-1	-1	-1
200	50	11	-3	-4	-4	-5	-5	49	10	-4	-5	-5	-5	-6	16	5	0	0	-1	-1	-1
250	45	10	-2	-3	-3	-4	-4	47	10	-3	-4	-5	-5	-5	16	5	0	0	0	0	0
350	37	9	-1	-2	-2	-2	-3	40	10	-1	-1	-2	-2	-3	12	4	1	1	1	1	1
500	27	8	0	0	0	-1	-1	35	11	1	0	-1	-1	-1	8	4	2	2	2	2	2
750	20	7	1	1	1	1	1	31	11	2	2	1	1	1	5	4	3	3	3	3	3
1000	16	6	2	2	2	2	1	29	11	3	2	2	2	2	2	4	4	4	4	4	4



The change in  $\Delta H$  values for the adsorption of *p*-nitrophenol (25 mg/L - 1000 mg/L) on GAC varies in the range; GACOZR 1273 (17.8 - 6.5 kJ/mol), GAC 383 (9.38 - 10.78 kJ/mol) and GACO 383 (4.27 - 4.68 kJ/mol). The change in entropy  $\Delta S$  for *p*-nitrophenol adsorption on GAC are given as GACOZR 1273 (91.7 - 15.8 J/mol.K), GAC 383 (64 - 29 J/mol.K) & GACO 383 (29 -2 J/mol.K).

The obtained values of  $\Delta H$ ,  $\Delta S$  and  $\Delta G$  of adsorption for methylene blue uptake on the new carbons are summarized in Table 4.24.

**Table 4.24:** Thermodynamic parameters obtained from plot of  $\ln K_D$  versus  $1/T$  for the adsorption of methylene blue (MB)

$C_0$ mg/L	GACOZR 1273 - MB							GAC 383 - MB							GACO 383 - MB						
	$\Delta S$ J/mol.K	$\Delta H$ kJ/mol	$\Delta G$ kJ/mol					$\Delta S$ J/mol.K	$\Delta H$ kJ/mol	$\Delta G$ kJ/mol					$\Delta S$ J/mol.K	$\Delta H$ kJ/mol	$\Delta G$ kJ/mol				
			283	293	303	313	323			283	293	303	313	323			283	293	303	313	323
25	89	18	-7	-8	-9	-10	-11	106	19	-11	-12	-13	-14	-15	105	19	-11	-12	-13	-14	-15
50	72	17	-3	-4	-5	-6	-6	91	18	-7	-8	-9	-10	-11	91	19	-7	-8	-9	-10	-11
75	59	15	-1	-2	-2	-3	-4	79	18	-4	-5	-6	-7	-7	75	18	-3	-4	-4	-5	-6
100	52	14	-1	-1	-2	-2	-3	61	14	-3	-4	-4	-5	-5	67	18	-1	-2	-3	-3	-4
150	44	13	1	0	0	-1	-1	53	14	-1	-1	-2	-3	-3	57	17	0	0	-1	-1	-2
200	35	12	3	2	2	2	1	44	13	0	0	-1	-1	-2	44	14	1	1	0	0	-1
250	36	12	2	1	1	1	0	35	11	1	0	0	0	-1	36	12	2	1	1	1	0
350	33	12	2	2	2	1	1	31	10	2	1	1	1	0	28	11	3	2	2	2	1
500	28	11	3	3	3	2	2	26	10	3	2	2	2	2	25	11	4	3	3	3	3
750	24	11	4	4	4	4	3	21	10	4	3	3	3	3	21	10	4	4	4	4	4
1000	18	10	5	5	5	4	4	18	9	4	4	4	4	4	18	10	5	5	5	5	4

The change in  $\Delta H$  for the adsorption of methylene blue (25 mg/L - 1000 mg/L) on GAC varies in the range; GACOZR 1273 (18.3 -10.1 kJ/mol), GAC 383 (19.3- 9.34 kJ/mol), and GACO 383 (19.3 - 10.1 kJ/mol). The change in entropy  $\Delta S$  for methylene blue adsorption on GAC are given as GACOZR 1273 (89.3 -18 J/mol.K), GAC 383 (105.6 -18 J/mol.K), GACO 383 (105.3 - 17.6 J/mol.K).

$\Delta H$  demonstrates that the sorption process is by endothermic nature in all cases. This behaviour indicates that higher temperatures are more preferred for higher adsorption. The calculated negative standard Gibbs energy changes in high

temperature depict that the adsorption reactions are largely driven towards the methylene blue but it becomes positive with increase of concentration of solutions. A positive value of  $\Delta S$  theoretically means that more disorder is associated with the adsorption process. It decreases with an increase in the solution concentration. It reveals that the adsorption capacity is varied with respect to the concentration of solute and the solution temperature.

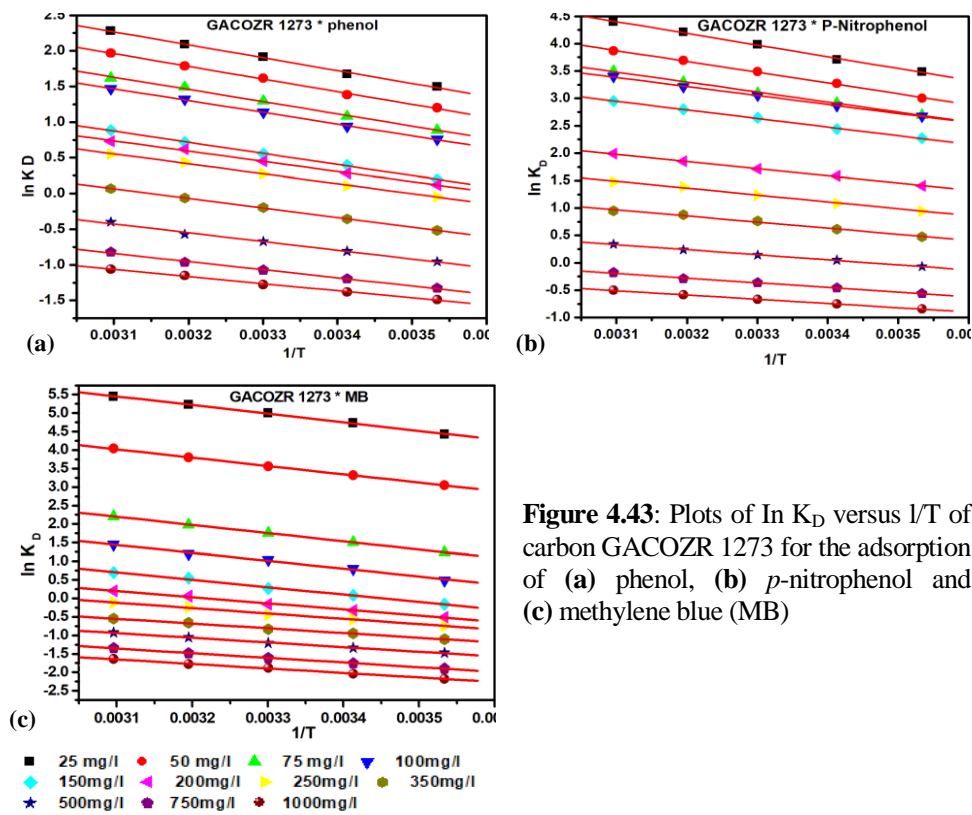


**Figure 4.43:** Plots of  $\ln K_D$  versus  $1/T$  of carbon GACOZR 1273 for the adsorption of (a) phenol, (b) *p*-nitrophenol and (c) methylene blue (MB)

## 4.9 Diffusion Coefficient

Diffusion coefficient for the adsorption of phenol, *p*-nitrophenol and MB on GAC 383, GACO 383 and GACOZR 1273 are calculated and discussed in the following sections.

### 4.9.1 Determination of Diffusivity for Phenol on GACOZR 1273, GAC 383 and GACO 383

The diffusion coefficient of adsorption of phenol on GAC 383, GACO 383 and GACOZR 1273 is determined from the linear plot of  $\ln [1/1-F^2(t)]$  versus  $t$  which is given in the Figure 4.44(a)-(c) and values are listed in the Table 4.25. Straight line plot for different temperature indicate the validity of the equation.

$$\ln \left[ \frac{1}{1-F^2(t)} \right] = \frac{\pi^2 D_e t}{R_a^2} \quad (4.24)$$

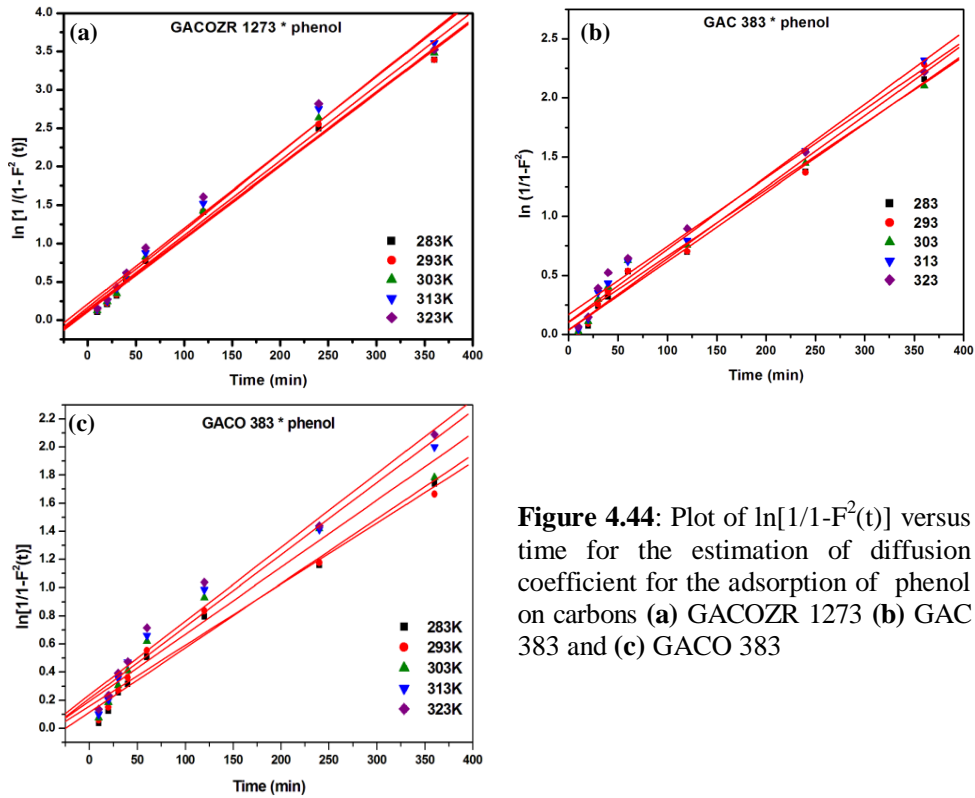


**Figure 4.44:** Plot of  $\ln[1/1-F^2(t)]$  versus time for the estimation of diffusion coefficient for the adsorption of phenol on carbons (a) GACOZR 1273 (b) GAC 383 and (c) GACO 383

Effective diffusion coefficient describes the transport of a phenol molecule into the GAC through a unit section area of GAC per unit of time. It is expressed in unit of  $m^2/s$ . As shown in the Table 4.25 the effective diffusion coefficient of phenol on GAC is given as follows GACOZR 1273 ( $2.65 \times 10^{-10} - 2.81 \times 10^{-10} m^2/s$ ), GAC 383 ( $1.63 \times 10^{-10} - 1.71 \times 10^{-10}$ ), GACO 383 ( $1.21 \times 10^{-10} - 1.47 \times 10^{-10} m^2/s$ ). The

diffusion coefficient increases with the rise of the solution temperatures. It means that, the rate of diffusion of the adsorbate molecules across the external boundary layer and in the internal pores of the adsorbent particle increased with increase in temperature [38].

#### 4.9.2 Determination of Diffusivity for *p*-Nitrophenol on GACOZR 1273, GAC 383 and GACO 383

The diffusion coefficient of adsorption of *p*-nitrophenol on GAC 383, GACO 383 and GACOZR 1273 are determined from the linear plot of  $\ln [1/(1-F^2(t))]$  versus  $t$  which is given in the Figure 4.45(a)-(c) and values are listed in the Table 4.25. Straight line plot for different temperature indicate the validity of the equation.

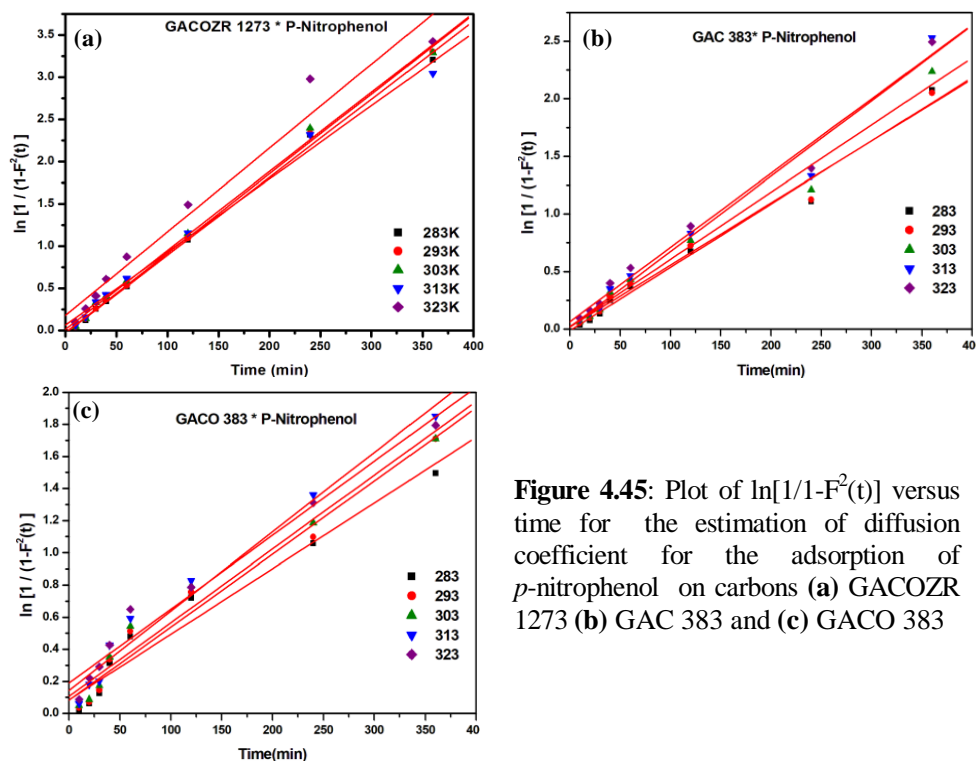


**Figure 4.45:** Plot of  $\ln[1/(1-F^2(t))]$  versus time for the estimation of diffusion coefficient for the adsorption of *p*-nitrophenol on carbons (a) GACOZR 1273 (b) GAC 383 and (c) GACO 383

In order to compare the uptake of *p*-nitrophenol from solution by GACOZR 1273, GAC 383 and GACO 383, effective diffusion coefficient is calculated. It varies for carbons as; GACOZR 1273 ( $2.42 - 2.77 \times 10^{-10} \text{ m}^2/\text{s}$ ), GAC 383 ( $1.5-1.83 \times$

$10^{-10}$  m<sup>2</sup>/s) and GACO 383( $1.14 - 1.38 \times 10^{-10}$  m<sup>2</sup>/s) respectively. The higher diffusion rate of *p*-nitrophenol on GACOZR 1273 indicates that, interaction between the *p*-nitrophenol and GACOZR 1273 is higher. Therefore, more molecules of *p*-nitrophenol get diffused into the pores of zirconium impregnated GACO than that of GAC 383 and GACO 383. Spontaneous movement of *p*-nitrophenol from solution (higher concentration region of *p*-nitro phenol) to GACOZR 1273 (lower concentration region of *p*-nitro phenol) is higher [39]. Increasing order of effective diffusion coefficient calculated for carbons is GACOZR 1273 > GAC 383 > GACO 383.

#### 4.9.3 Determination of Diffusivity for Methylene Blue (MB) on GACOZR 1273, GAC 383 and GACO 383

The diffusion coefficient of adsorption of methylene blue on GAC 383, GACO 383 and GACOZR 1273 are determined from the linear plot of  $\ln [1/(1-F^2(t))]$  versus  $t$  is given in the Figure 4.46 (a)-(c) and values are listed in the Table 4.25. Straight line plot for adsorption at different temperature indicate the validity of the equation.

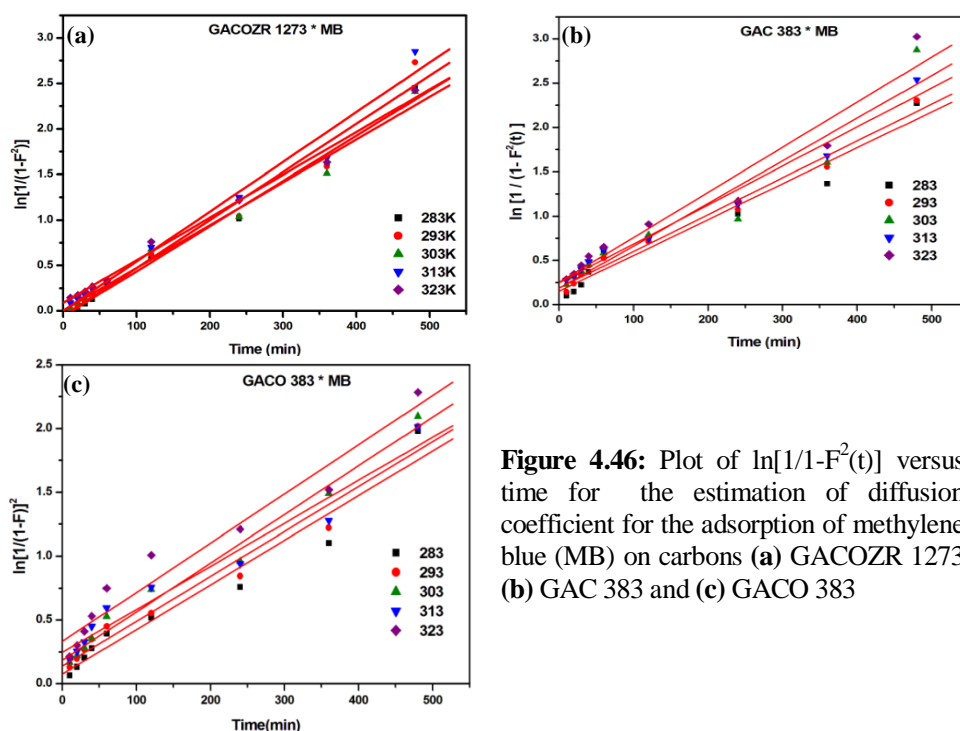


**Figure 4.46:** Plot of  $\ln[1/(1-F^2(t))]$  versus time for the estimation of diffusion coefficient for the adsorption of methylene blue (MB) on carbons (a) GACOZR 1273 (b) GAC 383 and (c) GACO 383

The effective diffusion coefficient obtained for GAC is given as follows; GACOZR 1273 ( $1.31 \times 10^{-10} - 1.53 \times 10^{-10} \text{ m}^2/\text{s}$ ), GAC 383 ( $1.13 \times 10^{-10} - 1.34 \times 10^{-10} \text{ m}^2/\text{s}$ ) and GACO 383 ( $0.94 \times 10^{-10} - 1.08 \times 10^{-10} \text{ m}^2/\text{s}$ ). The diffusion coefficient value obtained for methylene blue adsorption is lower than that of the value obtained for phenol and *p*-nitrophenol adsorption. It means that larger molecular weight species have lower diffusion coefficients.

**Table 4.25:** Effective diffusion coefficient of carbon for phenol, *p*-nitrophenol and methylene blue (MB)

Carbons	T (K)	phenol		<i>p</i> -nitrophenol		methylene blue	
		De x 10 <sup>10</sup> (m <sup>2</sup> /S)	R <sup>2</sup>	De x 10 <sup>10</sup> (m <sup>2</sup> /S)	R <sup>2</sup>	De x 10 <sup>10</sup> (m <sup>2</sup> /S)	R <sup>2</sup>
GACOZR 1273	283	2.65	0.990	2.58	0.996	1.39	0.990
	293	2.65	0.990	2.63	0.998	1.48	0.974
	303	2.72	0.990	2.62	0.996	1.31	0.984
	313	2.81	0.988	2.42	0.992	1.53	0.978
	323	2.76	0.978	2.77	0.968	1.31	0.992
GAC 383	283	1.63	0.988	1.53	0.984	1.13	0.984
	293	1.69	0.986	1.5	0.984	1.16	0.984
	303	1.57	0.980	1.63	0.982	1.34	0.982
	313	1.71	0.986	1.83	0.978	1.23	0.978
	323	1.62	0.978	1.8	0.984	0.25	0.984
GACO 383	283	1.28	0.976	1.14	0.958	0.978	0.958
	293	1.21	0.964	1.27	0.968	0.984	0.968
	303	1.33	0.958	1.28	0.966	1.07	0.966
	313	1.43	0.970	1.38	0.974	0.94	0.974
	323	1.47	0.970	1.29	0.972	1.08	0.972

#### 4.10 Activation Energy

The linear plot of  $\ln K_2$  versus  $1/T$  for the adsorption of phenol on GACOZR 1273, GAC 383 and GACO 383 are given in the Figure 4.47 (a). The activation energy  $E_a$  and pre-exponential factors  $A$ , obtained is given in Table 4.26.

$$\ln K_2 = \ln A - \frac{E_a}{RT} \quad (4.25)$$

The result obtained for activation energy for the adsorption of phenol on the GAC is; GAC 383 (9.95 kJ/mol), GACO 383 (7.59 kJ/mol) and GACOZR

1273 (2.03 kJ/mol) respectively. Low activation energy means that physical adsorption controls the removal of phenol from aqueous solution by GAC 383, GACO 383 and GACOZR 1273. The lower activation energy of GACOZR 1273 shows that very small energy is required to interact between GACOZR 1273 and phenol molecules therefore adsorption rate of phenol on GACOZR 1273 is fast as compared to that of GAC 383 and GACO 383.

$\ln K_2$  versus  $1/T$  plot of *p* - nitro phenol on GACOZR 1273, GAC 383, GACO 383 are given in the Figure 4.47(b) and activation energy obtained is given in Table 4.26. The result obtained for activation energy for the adsorption of *p*-nitrophenol on the GAC is; GAC 383 (7.71 kJ/mol), GACO 383 (10.32 kJ/mol) and GACOZR 1273 (9.44 kJ/mol). The lower magnitude of activation energy indicates that adsorption of *p*-nitrophenol on all the GAC studied follows the physical type of adsorption.

$\ln K_2$  versus  $1/T$  plot of methylene blue (MB) on GACOZR 1273, GAC 383, GACO 383 are given in the Figure 4.47(c) and activation energy obtained is given in Table 4.26

**Table 4.26** : Activation energy obtained from Arrhenius equation

Carbons	phenol		<i>p</i> -nitrophenol		methylene blue	
	$E_a$ kJ/mol	$A \times 10^4$	$E_a$ kJ/mol	A	$E_a$ kJ/mol	$A \times 10^4$
GAC 383	9.95	84.00	7.71	0.001995	2.14	5.95
GACO 383	7.59	46.30	10.33	9.84E-07	7.59	46.22
GACOZR 1273	2.04	5.71	9.44	0.006001	11.24	115

The result obtained for activation energy for the adsorption of methylene blue on GAC follows GAC 383 (2.14 kJ/mol), GACO 383 (7.59 kJ/mol) and GACOZR 1273 (11.24 kJ/mol). Lower magnitude of activation energy indicates that adsorption of methylene blue (MB) on all the GAC studied follows the physical type of adsorption.

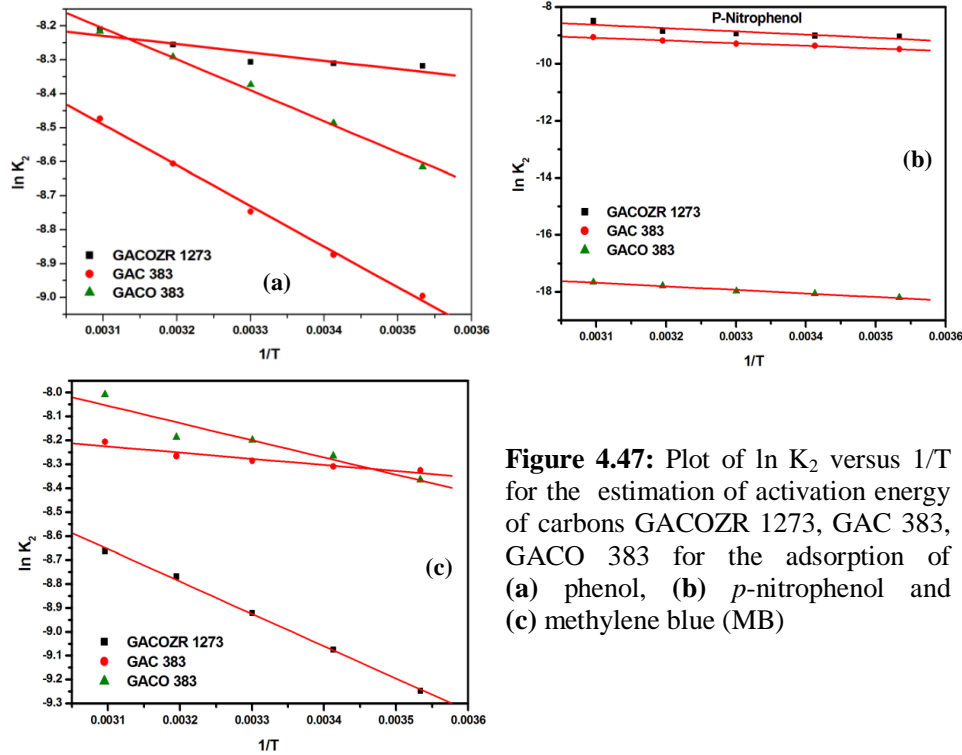


**Figure 4.47:** Plot of  $\ln K_2$  versus  $1/T$  for the estimation of activation energy of carbons GACOZR 1273, GAC 383, GACO 383 for the adsorption of (a) phenol, (b) *p*-nitrophenol and (c) methylene blue (MB)

#### 4.11 Design of Batch Adsorption from Isotherm Data

Adsorption isotherms can be used to predict the design of single-stage batch adsorption systems [40]. The mass balance equation used for calculating the amount of adsorbent required to treat phenol, *p*-nitrophenol and methylene blue is given in equation (4.26)

$$\frac{M}{V} = \frac{C_0 - C_e}{q_e} = \frac{C_0 - C_e}{\frac{q_0 K_L C_e}{1 + K_L C_e}} \quad (4.26)$$

Figure 4.48(a) shows the weight of adsorbents required for the 99 % removal of different concentration phenol from one litre aqueous solution. It shows that nitric acid modification on GAC decreases the efficiency towards phenolic compounds. Therefore, weight of adsorbent required for the removal of phenol from aqueous solution is higher than that of untreated native carbon.



For achieving the same efficiency towards phenol GACO 383 requires the weight of carbon 48 - 50 % more compared to GAC 383 whereas GACOZR 1273 requires only 5 - 7 % more carbon. It indicates that the presence of zirconium in nitric acid modified carbon enhances the efficiency towards phenol molecule. For the 99 % removal of 3000 mg/L phenol from one litre aqueous solution GACOZR 1273 requires 12.54 g carbon, whereas GACO 383 requires 17.5 g of carbon and GAC 383 requires 11.7 g of carbons.

Figure 4.48(b) shows the weight of carbon required for the 99 % removal of different concentration *p*-nitrophenol from one litre aqueous solution. Here, we can see that presence of zirconium in nitric acid modified carbon (GACOZR 1273) shows far better efficiency compared to GACO 383 and also shows little bit higher efficiency compared to GAC 383.

GACO 383 requires more than 2 times weight of carbon compared to GACOZR 1273 for achieving the same efficiency towards *p*-nitro phenol. For the 99 % removal of 3000 mg/L *p*-nitrophenol from one litre aqueous solution, GACOZR 1273 requires 7.5 g carbon, whereas GACO 383 requires 17.3 g of carbon and GAC 383 requires 8.13 g of carbons.

Figure 4.48(c) shows the weight of carbon required for the 99 % removal of different concentration of methylene blue from one litre aqueous solution. Nitric acid modified carbons GACO 383 and GACOZR 1273 requires more amounts compared to basic carbon GAC 383 for the same efficient removal of methylene blue from aqueous solution. Compared to GAC 383, nitric acid modified carbons GACO 383 requires 10 – 11% and GACOZR 1273 requires 8 – 9 % more carbons for attaining the same efficiency. For the 99 % removal of 1500 mg/L methylene blue from one litre aqueous solution GACOZR 1273 requires 10.4 g carbon whereas GACO 383 requires 10.6 g of carbon and GAC 383 requires 9.53 g of carbons.

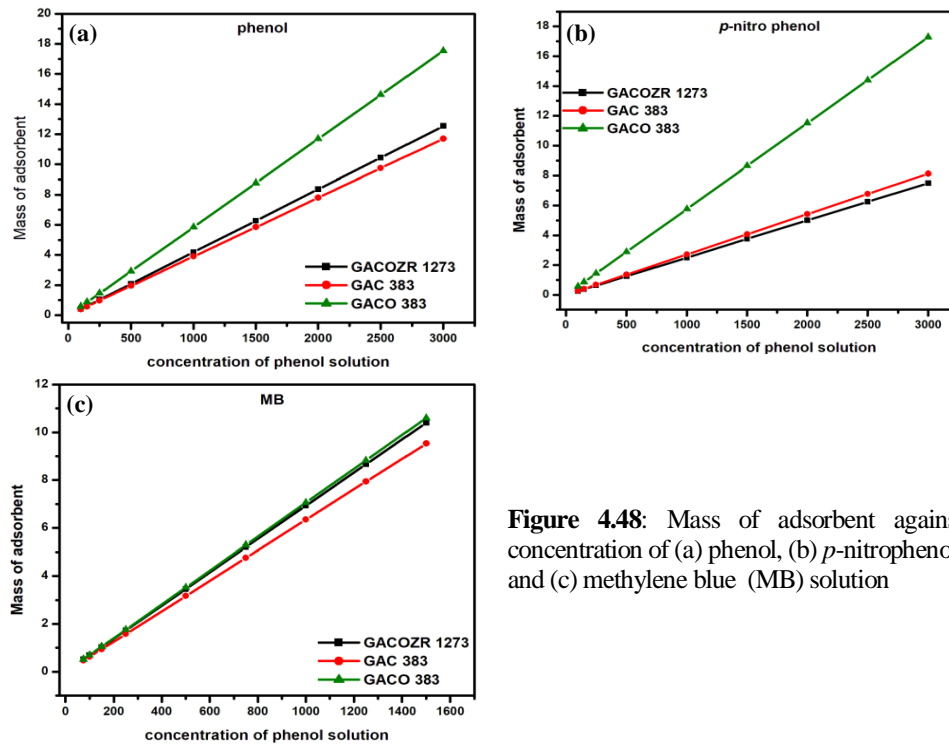


**Figure 4.48:** Mass of adsorbent against concentration of (a) phenol, (b) *p*-nitrophenol, and (c) methylene blue (MB) solution

#### 4.12 Adsorption of Trace Metal Ions by GACOZR Using Contaminated Groundwater

Trace element analysis of water samples is important for the potential application of carbon adsorbents in filtration system. Ground water collected from a contaminated area, whose initial parameters are known is used to study adsorption efficiency of carbons towards trace metal ions. Concentration in the treated water samples was measured by inductively coupled plasma-mass spectroscopy. The percentage adsorption is calculated and presented in Table 4.27.

**Table 4.27:** Efficiency of carbons GAC 383, GACO 383 and GACOZR 1273 for removing trace metals in groundwater.

Trace metals	Initial concentration (ppb)	Initial concentration (ppb)		
		GACOZR 1273	GAC 383	GACO 383
<sup>7</sup> Li	4.5 (% Removal)	4.4 (2.2)	4.29 (4.7)	3.83 (14.9)
<sup>9</sup> Be	0.22 (% Removal)	0.01 (95.5)	0.01 (95.5)	ND (100.0)
<sup>24</sup> Mg	2905.63 (% Removal)	2211.08 (23.9)	2802.3 (3.6)	2395.43 (17.6)
<sup>27</sup> Al	257.22 (% Removal)	6.73 (97.4)	2.84 (98.9)	2.18 (99.2)
<sup>52</sup> Cr	1.5 (% Removal)	0.55 (63.3)	0.92 (38.7)	1.05 (30.0)
<sup>55</sup> Mn	85.73 (% Removal)	1.31 (98.5)	7.34 (91.4)	10.05 (88.3)
<sup>56</sup> Fe	48.78 (% Removal)	22.79 (53.3)	33.15 (32.0)	27.34 (44.0)
<sup>58</sup> Ni	5.46 (% Removal)	1.37 (74.9)	1.82 (66.7)	4.51 (17.4)
<sup>59</sup> Co	2.81 (% Removal)	0.02 (99.3)	0.13 (95.4)	0.23 (91.8)
<sup>63</sup> Cu	21.9 (% Removal)	2.67 (87.8)	3.17 (85.5)	4.46 (79.6)
<sup>64</sup> Zn	40.77 (% Removal)	8.11 (80.1)	17 (58.3)	28.46 (30.2)
<sup>75</sup> As	1.89 (% Removal)	0.34 (82.0)	0.34 (82.0)	0.27 (85.7)
<sup>114</sup> Cd	0.62 (% Removal)	0.18 (71.0)	0.16 (74.2)	0.57 (8.1)
<sup>138</sup> Ba	89.02 (% Removal)	33.49 (62.4)	42.77 (52.0)	21.25 (76.1)
<sup>205</sup> Tl	0.08 (% Removal)	0.02 (75.0)	0.04 (50.0)	0.04 (50.0)
<sup>208</sup> Pb	6.18 (% Removal)	0.12 (98.1)	0.24 (96.1)	0.23 (96.3)

GACOZR 1273, GAC 383 and GACO 383 shows more than 95 % efficiency towards Be, Al, Mn, Co and Pb. GACOZR 1273 give more than 80%

efficiency towards Cu, Zn and As and 75 % efficiency towards Ni, Tl. Whereas, basic carbon GAC 383 (Mg -3.6 %, Cr – 38.7 %, Zn- 58.3 %, Ni – 66.7 %) and GACO 383 (Mg – 17.6 %, Cr – 30 %, Zn - 30.2 %, Ni – 17.4 %) shows only lower efficiency towards Mg, Cr, Zn and Ni compared to GACOZR 1273 (Mg - 23.9 %, Cr – 63.3 %, Zn - 80.1 %, Ni – 74.9 %).

### 4.13 Statistical Analysis of the Data

The statistical significance of the ratio of the mean square variation due to the regression and mean square residual error is tested using analysis of variance (ANOVA) and significance of correlation is tested by Pearson Correlation Coefficient.

**Hypothesis 1:** Whether there is any significant difference in pore volume and surface area of carbons obtained from BET and *I*-plot method

To test the **Hypothesis 1**, pore volume and surface area obtained from BET and *I* plot for GAC 383, GACO 383, GACOZR 1073 and GACOZR 1273 is given in Table 4.4 are analysed statistically using two way ANOVA test

Based on the statistical parameters given in Table 4.28 i.e. sum of squares (SS), degree of freedom (df), mean square (ms), variance ratio (F) and level of significance (P value) observations are summarised below.

**Table 4.28:** Two way ANOVA analysis of pore volume and surface area obtained from BET and *I*-plot method

Source	SS	df	ms	F	P-value
Total	2332178.195	11			
carbons	10299.1280	3	3433.0427	3.504	P > 0.05
SA and $V_m$	2316000.199	2	1158000.099	1181.860	P < 0.001
Residual	5878.867	6	979.8112		

P greater than 0.05 indicates that there is no significant difference in between the pore volume of carbons whereas significant difference ( P < 0.001) exist between pore volume and surface area, which is obtained from BET and *I* plot method.

**Hypothesis 2:** Whether there is any significant difference between the pore volume of carbons obtained from Langmuir, Dubinin-Radushkevich, Alpha S and John isotherm.

To test the **Hypothesis 2**, pore volume obtained from Lanmuir, Dubinin-Radushkevich, Alpha S and John isotherm for GAC 383 GACO 383, GACOZR 1073 and GACOZR 1273 given in the Table 4.8 are chosen.

The sum of squares (SS), degree of freedom (df), mean square (ms), variance ratio (F) and level of significance (P value) are givens in Table 4.29. Based on this result, observations are summerised below.

**Table 4.29** : Statistical analysis of pore volume obtained from from Langmuir, Dubinin-Radushkevich, Alpha S and John isotherm by three way ANOVA

Source	SS	df	ms	F	P-value
Total	4893.314	15			
Langmuir, D-R, Alpha S and John carbons	794.7434	3	264.9145	29.21996	P < 0.01
Residual	4016.975	3	1338.992	147.6902	P < 0.001
	81.59596	9	9.066217		

The result presents that the F value calculated for four isotherm models and carbons are higher than table value. This suggests that there is a 99.9 % probability of difference in pore volume between carbons ( $P < 0.001$ ). And also four isotherm methods differ significantly among themselves ( $P < 0.01$ ) i.e. 99 % probability. Alpha S and Dubinin-Radushkevich method showed significantly higher values than John and Langmuir isotherm.

**Hypothesis 3:** Whether there is any significant difference in quantity adsorbed between the samples for the adsorption of phenol, *p*-nitrophenol and methylene blue.

To test the **Hypothesis 3**, adsorption rate of carbons GACOZR 1273, GAC 383 and GACO 383 with respect to solid – liquid equilibria using phenol, *p*-nitrophenol and methylene blue obtained from Langmuir, Dubinin-Radushkevich

and John-Sivanandan Achari isotherm given in Table 4.13 is subjected to three way ANOVA method.

Based on the statistical parameters given in Table 4.30, observations are summarised below.

**Table 4.30:** Statistical analysis of adsorption system in solid-liquid equilibria with respect to quantity of phenol, *p*-nitrophenol and methylene blue adsorbed on GACNZR 1073, GAC 383 and GACO 383 by three way ANOVA

Source	SS	df	ms	F	P-value
Total	353286.7045	26			
carbons	22604.1747	2	11302.0874	4.201	P < 0.05
methods	214232.0684	2	107116.0342	39.811	P < 0.001
Phenol, PNP,MB	62638.3373	2	31319.1687	11.640	P < 0.001
Residual	53812.1241	20	2690.6060		

The results indicate that there is a significant difference between the carbons ( $P < 0.05$ ). Among the carbon studied GAC 383 and GACOZR 1273 are significantly higher than GACO 383. Between GAC 383 and GACOZR 1273, the difference is not significant.

The amount of rate obtained from three isotherm showed a very high significant difference ( $P < 0.001$ ). Among the three isotherm methods studied John - Sivanandan Achari and Langmuir methods shared significantly high adsorption compared to Dubinin - Radushkevich. Between John - Sivanandan and Langmuir isotherm models, the difference of quantity adsorbed is not significant.

There is a significant difference between methylene blue, phenol and *p*-nitrophenol ( $P < 0.001$ ) with respect to their adsorption rate. Among the three adsorbate, *p*-nitrophenol shared significantly higher adsorption and methylene blue shared significantly lower adsorption.

**Hypothesis 4:** whether there is any correlation between temperature and adsorption of phenol, temperature and adsorption of *p*- nitro phenol & temperature and adsorption of methylene blue.

To test the **Hypothesis 4**, Langmuir adsorption capacity of carbons GACOZR 1273 for phenol (Table 4.10), *p*-nitrophenol (Table 4.11) and methylene blue

(Table 4.12) at five solution temperature (283 K, 293 K, 303 K, 313 K and 323 K) are selected.

There is a significant positive correlation between temperature and adsorption of phenol on GACOZR 1273 ( $r = 0.9961$ ,  $t = 19.428$ ,  $df = 3$ ,  $P < 0.01$ ). This indicates that as temperature increases adsorption of phenol also increases.

There is significant positive correlation between temperature and adsorption of *p*-nitrophenol on GACOZR 1273 ( $r = 0.9978$ ,  $t = 26.2013$ ,  $df = 3$ ,  $P < 0.01$ ). This indicates that as temperature increases adsorption of *p*-nitrophenol also increases.

There is a significant positive correlation between temperature and adsorption of methylene blue on GACOZR 1273 ( $r = 0.99341$ ,  $t = 47.689$ ,  $df = 3$ ,  $P < 0.01$ ). This indicates that as temperature increases adsorption of methylene blue also increases.

#### 4.14 Conclusions

Basic carbon oxidised with  $\text{HNO}_3$  (GACO 383) and its zirconyl chloride impregnated series of carbons (GACOZR) has more surface functional groups as evidenced by FTIR, Boehm and XPS analysis. Low burn off of GACOZR series of carbons even at high activation temperature (1273 K) indicates that high thermal decomposition prevented by the presence of  $\text{Zr}^{4+}$  in GAC. The elemental carbon percentage in GACOZR series increases with activation temperature and lies in the range of 65.8 - 89.7 %. XRD analysis shows that carbon GACOZR 1073 and GACOZR 1273 gives a new peak around at  $2\theta = 30^\circ$  due to diffraction from (101) plane of tetragonal  $\text{ZrO}_2$ . It indicates the generation of  $\text{ZrO}_2$  from  $\text{ZrOCl}_2$  into the porous structure of the GAC at higher activation temperature. SEM images show that nitric acid oxidation/modification, causes the widening of existing pores and the formation of large pores by burnout of the walls between the adjacent pores.

Adsorption isotherm studies ( $\text{N}_2$  at 77 K) of this carbon series following Type I isotherm character. It gives strong evidence for microporosity due to the effective incorporation of activating agent. Surface modification with nitric acid decreases the surface area and porosity of GAC. On comparing with GAC 383, carbon GACOZR 1073 has 13 % and GACOZR 1273 has 6.6 % less specific surface area. This might be due to the partial destruction of meso and macropore network of thinner pore

walls. GACOZR 1073 (920.15 m<sup>2</sup>/g) and GACOZR 1273 (976.25 m<sup>2</sup>/g) clearly shows that surface area and pore volume of GACOZR series is enhanced with activation temperature. By rising the activation temperature up to 1273K, carbon GACOZR 1273 (327.76 cm<sup>3</sup>/g) shows 7.6 % enhancement in micropore volume compared to that of GACOZR 1073. However, it is comparatively lower than that of GAC 383. It indicates that oxidation of GAC with HNO<sub>3</sub> and activation of GACO with Zr<sup>4+</sup> could not achieve higher micropore volume compared to basic carbon GAC 383. The *t*-plot method shows that surface modification of GAC with HNO<sub>3</sub> enhances 6.27 % external surface area compared to that of GAC 383, indicates enlargement of microporosity. However on comparing with GAC 383, carbon GACOZR has 27.2 % and GACOZR 1073 has 19.8 % less external surface area.

Adsorption of phenol, *p*-nitrophenol and methylene blue on carbons indicates that GACOZR 1273 has high adsorption (≈ 32 % more phenol adsorption, 86 % increment in *p*-nitrophenol adsorption and 1.45 % increment in methylene blue adsorption) rate compared to that of GACO 383. But for all solution temperature studied the monolayer adsorption capacity of GACOZR 1273 is found to be comparatively lower than that of basic carbon GAC 383. The successive filling of phenol, *p*-nitrophenol and MB can be represented by different phase changes in John-Sivanandan Achari isotherms (J-SA) and total adsorption capacity obtained from J-SA is more comparable to Langmuir isotherm. According to the nature of pores distributed over the carbon surface different phase changes will occur on plotting *loglog P* or *loglog C<sub>e</sub>* against *log V* or *log qe* ( John isotherm and John-Sivanandan Achari isotherm). Adsorption system studied belongs to a second order kinetics and intra particle diffusion is the rate limiting step. Enhancement of adsorption capacity with rise of solution temperature indicates that adsorption is endothermic in nature. The low activation energy obtained from the Arrhenius equation indicates that adsorption is physical in nature. Trace elemental analysis using carbons shows that GACOZR 1273 have more efficiency compared to basic carbons towards many elements such as Cu, Zn ,As, Ni, and Tl.

Statistical analysis reveals that there was a significant difference exists between carbon samples (P < 0.001). In solid –gas equilibria, isotherm methods differ significantly among themselves, Langmuir and Dubinin-Radushkevich



isotherm pore volume values were significantly higher than the rest ( $P < 0.001$ ). A significant difference exists between carbon samples with respect to the adsorption rate of phenol, *p*-nitrophenol and methylene blue. Among the carbon studied, GAC 383 and GACOZR 1273 are significantly higher than GACO 383. Between GAC 383 and GACOZR 1273, the difference is not significant. John and John-Sivanandan Achari isotherms are agreeing well with Langmuir for the adsorption system studied. A significant positive correlation exists between temperature and adsorption rate in solid-liquid equilibria indicate that adsorption rate increases with increase in solution temperature.

## Reference

- [1] Faulconer, E. K. Effects of Activated Carbon Surface Chemistry Modification on The Adsorption of Mercury from Aqueous Solution. *PhD Thesis* **2012**. University of Florida, America.
- [2] Aspromonte, S. G.; Miró, E. E.; Boix, A. V. FTIR Studies of Butane, Toluene and Nitric Oxide Adsorption on Ag Exchanged NaMordenite. *Adsorption* **2011**, *18* (1), 1–12.
- [3] Caturla, F.; Molina-Sabio, M.; Rodríguez-Reinoso, F. Preparation of activated carbon by chemical activation with  $ZnCl_2$ . *Carbon* **1991**, *29* (7), 999–1007.
- [4] Bouchelta, C.; Medjram, M. S.; Zoubida, M.; Chekkat, F. A.; Ramdane, N.; Bellat, J. P. Effects of Pyrolysis Conditions on the Porous Structure Development of Date Pits Activated Carbon. *J. Anal. Appl. Pyrolysis* **2012**, *94*, 215–222.
- [5] Ganguly, A.; Sharma, S.; Papakonstantinou, P.; Hamilton, J. Probing the Thermal Deoxygenation of Graphene Oxide Using High-Resolution In Situ X-Ray-Based Spectroscopies. *J. Phys. Chem.* **2011**, *115* (34), 17009–17019.
- [6] Shen, W.; Li, Z.; Liu, Y. Surface Chemical Functional Groups Modification of Porous Carbon. *Recent Patents Chem. Eng.* **2008**, *1* (1), 27–40.
- [7] Lee, P.; Ho, C.; Hwang, C.; Ding, S. Surface & Coatings Technology Improved Physicochemical Properties and Biocompatibility of Stainless Steel Implants by PVA /  $ZrO_2$  -Based Composite Coatings. *Surf. Coat. Technol.* **2014**, *258*, 374–380.
- [8] Ma, W.; Herbert, F. W.; Senanayake, S. D.; Yildiz, B. Non-Equilibrium Oxidation States of Zirconium during Early Stages of Metal Oxidation. *Appl. Phys. Lett.* **2015**, *106* (10), 1–6.

- [9] Das, D.; Samal, D. P.; Bc, M. Preparation of Activated Carbon from Green Coconut Shell and Its Characterization. *Chem. Eng. Process Technol.* **2015**, *6* (5), 1415–1420.
- [10] Xu, J.; Wang, L.; Zhu, Y. Decontamination of Bisphenol A from Aqueous Solution by Graphene Adsorption. *Langmuir* **2012**, *28*, 8418–8425.
- [11] Sandoval, R.; Cooper, A. M.; Aymar, K.; Jain, A.; Hristovski, K. Removal of Arsenic and Methylene Blue from Water by Granular Activated Carbon Media Impregnated with Zirconium Dioxide Nanoparticles. *J. Hazard. Mater.* **2011**, *193*, 296–303.
- [12] Moreno-Castilla, C.; Ferro-Garcia, M. A.; Joly, J. P.; Bautista-Toledo, I.; Carrasco-Marín, F.; & Rivera-Utrilla, J. Activated carbon surface modifications by nitric acid, hydrogen peroxide, and ammonium peroxydisulfate treatments. *Langmuir* **1995**, *11*(19), 4386–4392.
- [13] Bindia Ravindran. Adsorption Isotherm Studies on Activated Carbon Prepared by Activation with Cerium Compounds. *Ph.D Thesis* **2016**. School of Environmental Studies, Cochin University of Science and Technology, Cochin, Kerala, India.
- [14] Achari, V.S.; Rajalakshmi, A.S.; Jayasree, S. Surface Area and Porosity Development on Granular Activated Carbon by Zirconium: Adsorption Isotherm Studies. *Journal of Applied Research and Technology*, **2017** (Accepted November 2017).
- [15] Deryło-Marczewska, A.; Marczewski, A. W. Nonhomogeneity Effects in Adsorption from Gas and Liquid Phases on Activated Carbons. *Langmuir* **1999**, *15* (11), 3981–3986.
- [16] John, P. T.; Achari, V.S. Characterisation of Structural Parameters of Finely Divided and Porous Materials by a New Adsorption Isotherm. *Journal of Materials Science* **2002**, *37*, 885-893
- [17] Gunasekar, V.; Ponnusami, V. Kinetics, Equilibrium, and Thermodynamic Studies on Adsorption of Methylene Blue by Carbonized Plant Leaf Powder. *J. Chem.* **2013**, 1-6.
- [18] Rajalakshmi, A. S.; Sivananda Achari, V. Phenol adsorption of zirconium impregnated activated carbon. Extended Abstract, *28<sup>th</sup> Kerala Science congress* **2016**, Calicut University, Malappuram, India, 2644 -2649.
- [19] Achari, V.S.; Jayasree, S. Rajalakshmi, A.S. Adsorption of *p* – nitrophenol on Coconut Shell Granular Activated Carbon: Isotherms, Kinetics and Thermodynamics. *Indian Journal of Chemical Technology.* **2017**, *24*,471-478.

- [20] Achari, V.S.; Rajalakshmi, A.S. Adsorption of phenol using  $Zr^{4+}$  impregnated activated carbon. *Swadeshi Science Congress* **2014**, Thunchath Ezhuthachan Malayalam University, ISBN 978-81-928129-2-2.314-319.
- [21] He, J.; Hong, S.; Zhang, L.; Gan, F.; Ho, Y. Equilibrium and Thermodynamic Parameters of Adsorption of Methylene blue onto Rectorite. *Fresenius Environ. Bull.* **2010**, *19* (11), 2651–2656.
- [22] Singh, B. K.; Pragya, N. Adsorptive Removal of Phenols from aqueous solution by Flyash- Kinetics and Equilibrium Study. *International Research Journal of Environment Sciences* **2015**, *4*(8), 60-73.
- [23] Li, B. Z. F.; Sun, T. W. D.; Li, Y. Adsorption of p-nitrophenol from aqueous solutions using nanographite oxide. *Colloids and Surfaces A: Physicochemical and Engineering Aspects* **2015**, *464*, 78–88.
- [24] Hamdaoui, O.; Naffrechoux, E. Modeling of Adsorption Isotherms of Phenol and Chlorophenols onto Granular Activated carbon Part I. Two-Parameter Models and Equations Allowing Determination of Thermodynamic Parameters. *J. Hazard. Mater.* **2007**, *147* (1–2), 381–394.
- [25] Lyubchik, S.; Lyubchik, A.; Lygina, O.; Lyubchik, S.; Fonseca, I. Comparison of the Thermodynamic Parameters Estimation for the Adsorption Process of the Metals from Liquid Phase on Activated Carbons. *Thermodynamic studies - Interaction Studies - Solids, Liquid and Gases* **2011**, 95–122.
- [26] Mahmoodi, N. M.; Hayati, B.; Arami, M.; Lan, C. Adsorption of Textile Dyes on Pine Cone from Colored Wastewater: Kinetic, Equilibrium and Thermodynamic Studies. *Desalination* **2011**, *268* (1–3), 117–125.
- [27] Alothman, Z.A.; Habila, M.A.; Ali, R. Kinetics and Thermodynamic studies for methylene blue adsorption using Activated Carbon Prepared from Agricultural and Municipal Solid Wastes. *Asian Journal of Chemistry* **2013**, *25* (15), 8301-8306.
- [28] Bao, Y.; Zhang, G. Study of Adsorption Characteristics of Methylene Blue onto Activated Carbon Made by Salix Psammophila. *Energy Procedia* **2012**, *16*, 1141–1146.
- [29] Pathania, D.; Sharma, S.; Singh, P. Removal of methylene blue by adsorption onto activated carbon developed from Ficus carica bast, *Arabian Journal of Chemistry* **2017**, *10*, S1445-S1451.
- [30] Achari, V.S. John Isotherm for Liquid Phase Adsorption: Comparison with Langmuir and Freundlich Models. *International Carbon Conference, Carbon* **2006**, Robert Gordon University, Aberdeen, Scotland, UK. Extended Abstract, 16-21. ISBN 0- 9553365-1-1, 3P 107.

- [31] Mercy T.; Achari. V. S. Characterisation of Porous Materials using John Isotherm model. *23<sup>rd</sup> Swadeshi Science Congress 2013*, Organized by Swadeshi Science Movement – Kerala and Mahatma Gandhi University, ISBN 978-81-928129-1-5, 831-835.
- [32] Abdel-Ghani, N.T.; El-Chaghaby, G. A.; Zahran, E.M. Pentachlorophenol (PCP) adsorption from aqueous solution by activated carbons prepared from corn wastes. *Int. J. Environ. Sci. Tech.* **2015**, *12*, 211–222.
- [33] Abdel-Ghani, N.T.; Rawash, E. S. A. ; El-Chaghaby, G. A. Equilibrium and Kinetic Study for the Adsorption of P-Nitrophenol from Wastewater Using Olive Cake Based Activated Carbon. *Global J. Environ. Sci. Manage.* **2016**, *2* (1), 11–18.
- [34] Arshadi, M.; Amiri, M. J.; Mousavi, S. Kinetic, equilibrium and thermodynamic investigations of Ni(II), Cd(II), Cu(II) and Co(II) adsorption on barley straw ash. *Water Resources and Industry.* **2014**, *6*, 1–17.
- [35] Ma, J.; Zhuang Y.; Yu, F. Equilibrium, kinetic and thermodynamic adsorption studies of organic pollutants from aqueous solution onto CNT/C@Fe/chitosan composites. *New Journal of Chemistry* **2015**, *39*, 9299.
- [36] Achari, V. S. Modified Carbons and Wood Dust: Evaluation of Adsorption Properties. *Ph.D. Thesis 1998*. Department of Chemistry, University of Kerala, Kariavattom, Thiruvananthapuram, Kerala, India.
- [37] Şeker, A.; Shahwan, T.; Eroğlu, A. E.; Yilmaz, S.; Demirel, Z.; Dalay, M. C. Equilibrium, Thermodynamic and Kinetic Studies for the Biosorption of Aqueous lead(II), cadmium(II) and nickel(II) Ions on *Spirulina Platensis*. *J. Hazard. Mater.* **2008**, *154* (1–3), 973–980.
- [38] Ertugay, N.; Malkoc, E. Adsorption Isotherm, Kinetic, and Thermodynamic Studies for Methylene Blue from Aqueous Solution by Needles of *Pinus Sylvestris* L. *Pol. J. Environ. Stud.* **2014**, *23*( 6),1995-2006.
- [39] Streat, M.; Patrick, J.W.; Perez, M. J. C. Sorption of Phenol and Para-Chlorophenol from Water using Conventional and Novel Activated Carbons. *Wat. Res.* **1995**, *29* (2), 467-472.
- [40] Ayhan, I. S. Equilibrium Data and Process Design for Adsorption of Disperse Dyes onto Alunite. *Environmental Geology* **2004**, *45*, 762–768.

.....✂.....

**GRANULAR ACTIVATED CARBON PREPARED BY  
ACTIVATION WITH ZIRCONIUM OXIDE (GACNZR):  
PREPARATION, CHARACTERIZATION AND  
ADSORPTION ISOTHERM STUDIES**

---

**5.1 Introduction**

The porous nature of the activated carbons is well suited to many applications, including molecular sieving, adsorption and catalytic reactions of small molecules. Metal-loaded carbons have been also investigated as efficient adsorbents for organic and inorganic molecules. They have high pore volume as well as having specific interactions with the supported metals. Considerable interest in the synthesis of carbons with high surface areas and pore structures is prevalent in these days.

In the previous chapters were discussing about how  $ZrOCl_2$  affect the surface complexes, porosity and pore size distribution of activated carbon. It is observed that  $ZrOCl_2$  promotes ideal porosity and surface area development to granular activated carbon.

This chapter discusses about the porosity and surface area developments of a series of coconut shell based GAC, prepared under different activation conditions of temperature and  $ZrO_2$ /GAC incorporation ratio are evaluated. Adsorption efficiency and structural parameters were determined by standard isotherm models. Compared with other metal oxide porosity development on GAC by zirconium oxide and its adsorption enhancement towards organic pollutant are less reported. Zirconium dioxide is commonly known as zirconia is a

white powdered inorganic material has excellent resistance and strength. It is chemically stable, non toxic and insoluble in water. They are existing in both amorphous and crystalline nature. Properties of this material include high fracture toughness, high density, high hardness, good frictional behavior and high temperature capability up to 2400<sup>0</sup>C [1].

## 5.2 Granular Activated Carbons – GACNZR Series

There are eight carbons GAC 383, GACO 383, GACNZR 383, GACNZR 473, GACNZR 673, GACNZR 873, GACNZR 1073, and GACNZR 1273 are used in this study. GAC 383 is the native carbon based on coconut shell, GACO 383 is acid oxidised and others are ZrO<sub>2</sub> activated carbons of GAC 383. The methods of preparation and experimental setup for furnace based thermal activation were already discussed in Chapter 2. ZrO<sub>2</sub> is prepared in the laboratory following a standard procedure.

## 5.3 Characterization of Nano Zirconia (ZrO<sub>2</sub>)

Zirconium oxide nano particles were prepared by a simple hydrothermal process is characterised by using XRD, EDS and TEM.

Crystalline nature of nano particles is characterised by XRD analysis. Broad, low-angle peak occurred in the XRD a pattern of synthesized zirconia is shown in Figure 5.1, which indicates very poor crystallization. One broad peak appeared at  $2\theta \approx 31.5^{\circ}$  is due to diffraction from (1 0 1) plane of tetragonal ZrO<sub>2</sub> phase. The largely broad peak and weak peak signal strongly suggest that zirconia (ZrO<sub>2</sub>) is an amorphous material and the particles might be ultrafine [2, 3].

Energy dispersive *x*-ray spectroscopy (EDS) is used for the elemental analysis of metal oxides. Elemental composition of zirconium and oxygen are seen in Figure 5.2. The tabulated results provide a semi-quantitative view of the elemental composition in units of both weight percent and atomic percent. The results reveal that Zr and O are the main elements present within the inspection field, with Zr being the most abundant. The atomic percentage of Zr (78.59 %) and O (21.41%) in synthesised zirconia is comparable to atomic percentage of Zr (74%) and O (25.96 %) in pure ZrO<sub>2</sub>.

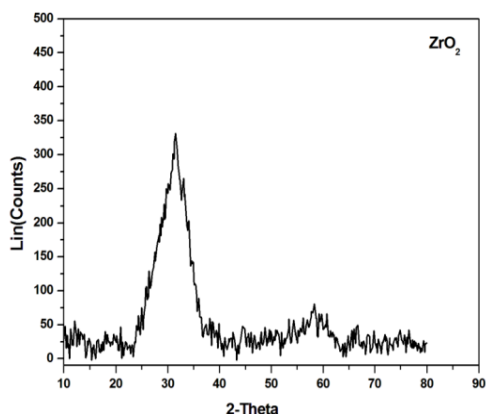


Figure 5.1: XRD spectra of Nano ZrO<sub>2</sub> prepared

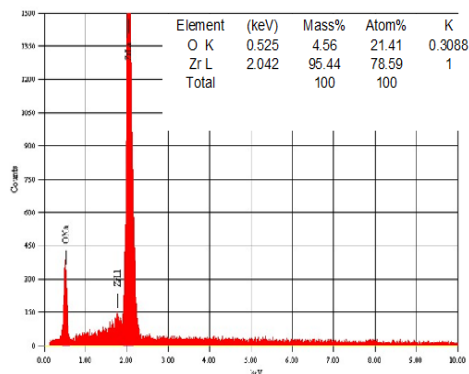


Figure 5.2: EDS analysis of ZrO<sub>2</sub> prepared

Morphology of nano particles is determined by TEM images. TEM samples were made by dispersing a thin film of ZrO<sub>2</sub> powder on Cu grid pre-coated with thin and flat carbon film.

Figure 5.3 indicates a HRTEM image of ZrO<sub>2</sub> nanoparticles. It shows that, nano particles have mostly consisted of spheres in shape and the size is found to be within the range of 1-5nm. It is clear that agglomeration takes place as a result of nanoparticle interaction. The broad ring pattern in the selected area electron diffraction pattern (SAED) indicates the short range order confirm that ZrO<sub>2</sub> is amorphous in nature and the crystalline structure could be observed only on few particles [4].

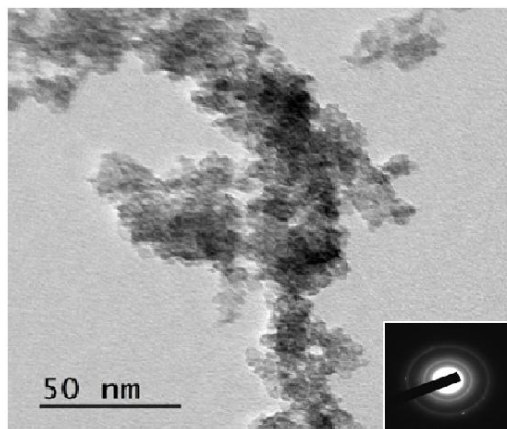
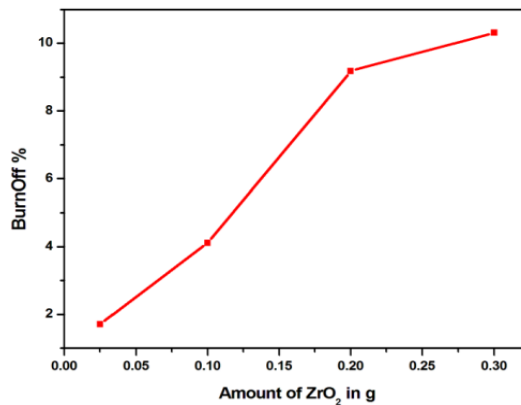


Figure 5.3: TEM images of prepared nano ZrO<sub>2</sub> and its scattered area electron diffraction pattern

### 5.3.1 Effect of $Zr^{4+}$ / GAC Impregnation Ratio

The yield and burn off are studied in relation to the different ratio of zirconia used in the chemical activation process. Figure 5.4 shows visually the burn off obtained for samples by applying different zirconium/carbon ratio. A significant amount of micro porosity is formed in the activated carbons as the degree of burn off increases. Variation of burn off and carbon yield with a different impregnation ratio are given in Table 5.1. The yield of activated carbon produced is also an important factor to be considered. This would set a limit on burn-off that has to be achieved [5].



**Figure 5.4:** Variation of burn off with impregnation ratio

From the series of impregnated carbon samples, 2% of zirconia impregnated (0.2g  $ZrO_2$  in 10g carbon) carbons is used for activation with steam at different temperature. For this ratio burn off value less than 10% and yield is within the limit of 90%. Further impregnation of zirconium in carbon will not make much more effective on burn off and carbon yield.

**Table 5.1:** Effect of  $ZrO_2$  on carbon yield and burn off at 873K as a function of incorporation ratio  $X_{ZrO_2}$  or  $X_{Zr}$

Amount of nano $ZrO_2$	% of nano $ZrO_2$	% of Zr	$X_{ZrO_2}$	$X_{Zr}$	Carbon yield %	Burn off %
0.025	0.2	0.185	0.00025	0.0018	98.3	1.71
0.1	1	0.740	0.001	0.0074	95.9	4.11
0.2	2	1.481	0.002	0.0148	90.8	9.18
0.3	3	2.221	0.003	0.0222	89.7	10.30



## **5.4 Characterization Studies**

### **5.4.1 Carbon Yield and Burn Off**

The pore development in coconut shell based activated carbon depends strongly on the activation temperature. Zirconium impregnated carbon, activated with steam at activation temperatures ranging from 383 K to 1273 K is given in the Table 5.2. It shows that the yield continues to decrease from 95.5 % to 86.9 %, whereas burn off increase from 4.5 % to 13.1 % with a rise of activation temperature from 473 K to 1273 K. Burn off, percentage of GACNZR series of carbon samples was found to be less than 15 %. The mesopore volume is rather insignificant, when burn off is less than 20 %.

### **5.4.2 Elemental Analysis**

CHNS analysis shows that C % increases with activation temperature, whereas the percentage of O and H are decreased. High carbon content is found to be in GACNZR 1273 (92.4 %), whereas other ZrO<sub>2</sub> impregnated carbons show carbon content is given as follows; GACNZR 383 (63.62 %), GACNZR 473 (71.75 %), GACNZR 673 (82.13 %), GACNZR 873 (83.15 %), and GACNZR 1073 (88.84 %). Percentages of oxygen in all carbons were found to be decreased with a rise of activation temperatures; it varies as GACNZR 383 (36.12 %), GACNZR 473 (26.55 %), GACNZR 673 (15.3 %), GACNZR 873 (16.5 %), GACNZR 1073 (10.8 %), GACNZR 1273 (6.96 %). Other elements such as hydrogen and nitrogen were also present in trace quantities.

### **5.4.3 Boehm Surface Analysis**

Table 5.2 showed the acid/base properties of the adsorbents determined by the Boehm titration method. It can be observed that the amount of acidic groups is significantly higher than the total amount of basic groups. These results suggest that all carbon materials have an acidic character.

Surface oxygen complexes on GACNZR series carbon materials are found to be decreased by heating at higher temperature. In carbons of GACNZR series, the carboxylic groups vary from 0.40 to 0.27 meq/g, lactonic group varies from 0.21 to 0.11 meq/g, and phenolic group varies from 0.46 to 0.36 meq/g. Surface oxygen

complexes on carbon materials decompose upon heating by releasing CO and CO<sub>2</sub> at different characteristic temperatures. Large reduction in the carboxylic group from 0.40 to 0.310 meq/g is observed in the temperature range of 383 – 873 K. This is clearly indicated as the decomposition of carboxylic acid into CO<sub>2</sub>, which is occurring mainly in the temperature range of 373 – 673 K. Decomposition of lactonic group is initiated at the temperature range of 463 - 923K which is further confirmed by the reduction of lactonic group from 0.21 to 0.11 meq/g at the activation temperature of 873 K (GACNZR 873). Decomposition of phenol will take place only at higher activation temperatures and it gives CO at 973 - 1253K [6].

**Table 5.2:** Burn off, carbon yield, elemental composition & Boehm titration analysis of GACNZR series at different temperature 383-1273K, GAC 383 and GACO 383

Carbons	Activation T in K	Burn off %	Carbon yield %	% C	% H	% N	% O	Carboxylic/ meq/g	Phenolic/ meq/g	lactones/ meq/g	Base/ meq/g
GACNZR	383	NA	NA	63.6	0.28	ND	36.1	0.40	0.46	0.21	0.5
	473	4.5	95.5	71.8	0.18	ND	26.6	0.35	0.36	0.21	0.5
	673	7.3	92.7	82.1	0.16	ND	15.3	0.35	0.46	0.21	0.6
	873	9.2	90.8	83.2	0.20	ND	16.5	0.31	0.59	0.11	0.6
	1073	12.2	87.8	88.8	0.26	ND	10.8	0.27	0.41	0.11	0.7
	1273	13.1	86.9	92.4	0.13	0.27	7.0	0.27	0.41	0.11	0.7
GAC 383	383	NA	NA	89.4	0.60	0.36	9.6	0.40	0.45	0.18	0.5
GACO 383	383	NA	NA	65.1	2.61	0.58	31.7	1.38	2.10	1.34	0.2

#### 5.4.4 X-ray Diffraction (XRD) Analysis

The XRD patterns of the GAC 383, GACO 383 and GACNZR series of samples are shown in Figure 5.5. All samples showed broad peaks at around  $2\theta \approx 26^\circ$  and  $42^\circ$ . It is typically observed in amorphous materials with micrographitic structure and pyrolytic carbon corresponding (0 0 2) and (1 0 0) diffraction peak.

Diffraction lines due to Zr<sup>4+</sup> or ZrO<sub>2</sub> is not detectable at lower activation temperature for GACNZR series. When activation temperature exceeds 873K,

new diffraction peaks appear in the region  $2\theta$  value of  $31^\circ$  corresponds to (101) plane of  $ZrO_2$ . A small percentage of  $Zr^{4+}$  used for impregnation of GAC may be dispersed as clusters of  $ZrO_2$  which are not detectable by XRD. But as the activation temperature increases, zirconia crystallizes progressively and it will give the diffraction line at  $31^\circ$ .

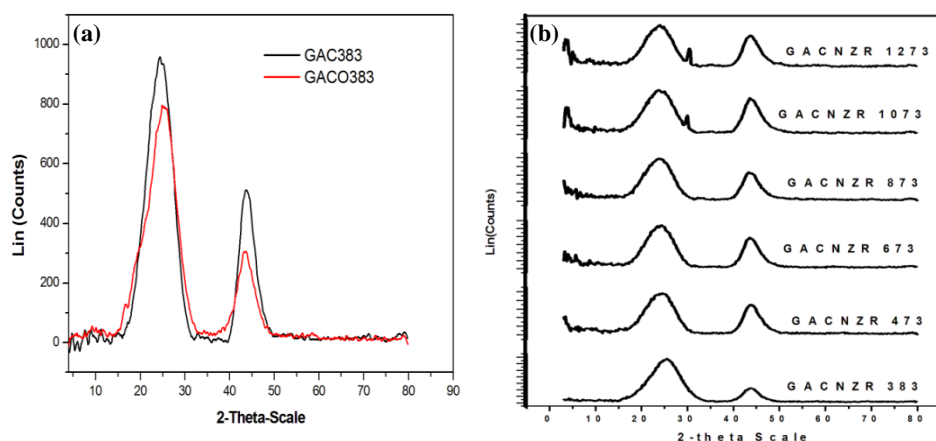


**Figure 5.5:** XRD spectra of (a) GAC 383 & GACO 383 (b) GACNZR series of carbons activated at 383-1273K

The lattice parameters of activated carbon at different temperature are calculated through XRD patterns. GACNZR series of carbons lattice parameters are distorted slightly as compared with that of GAC 383. With increasing temperature,  $L_c$  and  $L_a$  increases for GACNZR series of carbons, c-axis correlation length ( $L_c$ ) varies from 1.02 to 1.35 nm; a-axis correlation length ( $L_a$ ) varies from 2.08 to 2.77 nm. It corresponds to the transition from near-graphitization region to graphitization region at higher activation temperature. The interlayer spacing  $d_{002}$  (0.350 – 0.378 nm) in this structure is larger than the spacing in a graphite single crystal (0.335nm). The differences in the XRD patterns are caused by the lowering of crystallites of the activated carbon during the activation process [7].

**Table 5.3:** XRD crystalline parameters of carbons GAC 383, GACO 383 and GACNZR series at different temperature 383-1273K

Carbons	$L_c$ (0.9) nm	$L_a$ (1.84) nm	$d_{002}$ nm
GAC 383	1.14	2.28	0.364
GACO 383	0.97	1.94	0.356
GACNZR 383	1.02	2.08	0.350
GACNZR 473	1.04	2.13	0.369
GACNZR 673	1.13	2.31	0.378
GACNZR 873	1.16	2.37	0.374
GACNZR 1073	1.35	2.77	0.374
GACNZR 1273	1.35	2.77	0.372

#### 5.4.5 Fourier Transform Infrared Spectroscopy (FTIR) Analysis

FTIR spectra of all the samples have a strong hydroxyl stretching ( $3425 - 3435 \text{ cm}^{-1}$ ) vibrations of physically adsorbed water. The band at  $2892 \text{ cm}^{-1}$  present in the GAC 383 is shifted to higher frequency  $2924 \text{ cm}^{-1}$  in GACO 383. For  $\text{ZrO}_2$  impregnated GAC it is found to be at  $2886 \text{ cm}^{-1}$  which is attributed to the C-H interaction with the surface of the carbon [8].

The presence of peak at  $2347 \text{ cm}^{-1}$  in GAC 383 is shifted to  $2358 \text{ cm}^{-1}$  for nitric acid modified GAC. For  $\text{ZrO}_2$  impregnated GAC samples at higher temperature, it shifted to the region of  $2367 - 2398 \text{ cm}^{-1}$ . This peak corresponds to the absorption of atmospheric  $\text{CO}_2$ . A narrow band of big intensity at  $1615 - 1635 \text{ cm}^{-1}$  indicated the presence of C=O groups. Peaks of weaker intensity at  $1164 - 968 \text{ cm}^{-1}$  indicate the vibration of C=O, C-O and -OH from carbonyl, lactones and phenolic groups. A peak at  $1307-1308 \text{ cm}^{-1}$  is given by GACNZR 1073 and GACNZR 1273 denoted a combination of Zr-O vibration bonds. A weak vibration band in  $1067-1069 \text{ cm}^{-1}$  is given by GACNZR series of carbons except GACNZR 1073 and GACNZR 1273 which was related to Zr - O from  $\text{ZrO}_2$  [9]. The band at  $1067 \text{ cm}^{-1}$  shifted to  $1105 \text{ cm}^{-1}$  for GACNZR 1073. For GACNZR 1273 it is shifted to  $1077 \text{ cm}^{-1}$ , which is attributed to the bending vibrations of hydroxyl groups on metal oxides.

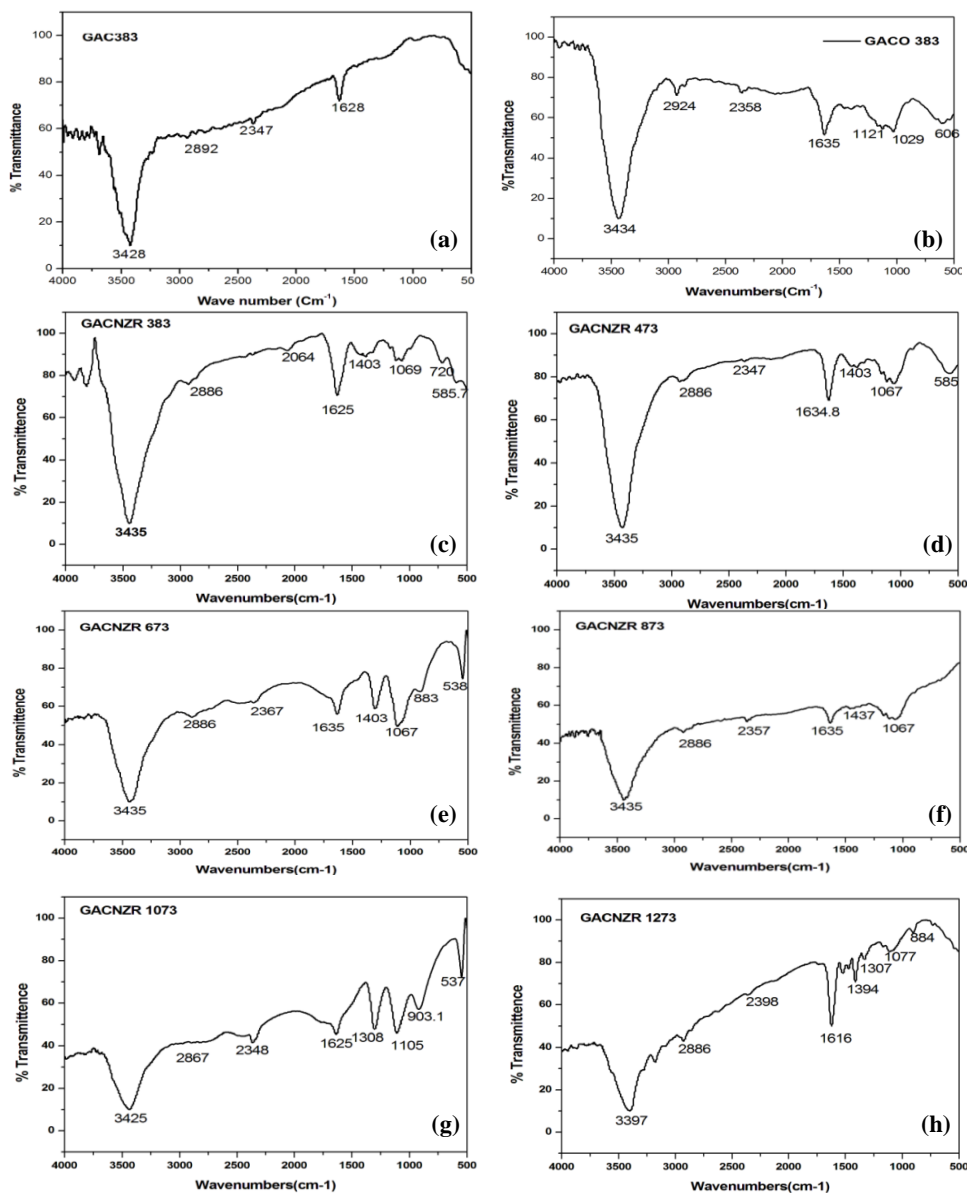


**Figure 5.6:** FTIR spectra of (a) GAC 383 (b) GACO 383 (c)-(h) GACNZR series of carbons activated at 383-1273 K for the evaluation of functional groups

A new peak at 883 cm<sup>-1</sup>, 903 cm<sup>-1</sup>, 884 cm<sup>-1</sup> present at GACNZR series of carbons at higher activation temperatures indicating the presence of Zr-O-H groups in the hydrous zirconium oxide [10].

The region  $450\text{--}750\text{ cm}^{-1}$  are associated with the in plane and out-of-plane aromatic ring deformation vibrations. Peaks at  $598$  and  $680\text{ cm}^{-1}$  are assigned to the out-of-plane C - H bending mode.

#### 5.4.6 X-ray Photoelectron Spectroscopy (XPS) Analysis

Chemical composition and surface chemical states of the samples were examined by *x*-ray photoelectron spectroscopy. The specific binding energy of each electron corresponds to a Gaussian peak, representing a type of functional group. The distribution of C and O structures can be derived from C 1s and O 1s spectra (Figure 5.7(a)–(b)). The C=C peak at  $284.4\text{ eV}$  corresponded to  $\text{sp}^2$  carbon bonding. It is in good agreement with C 1s level at  $284.34\text{ eV}$  for GACNZR 1273 and  $284.66\text{ eV}$  for GAC 383 and GACO 383.

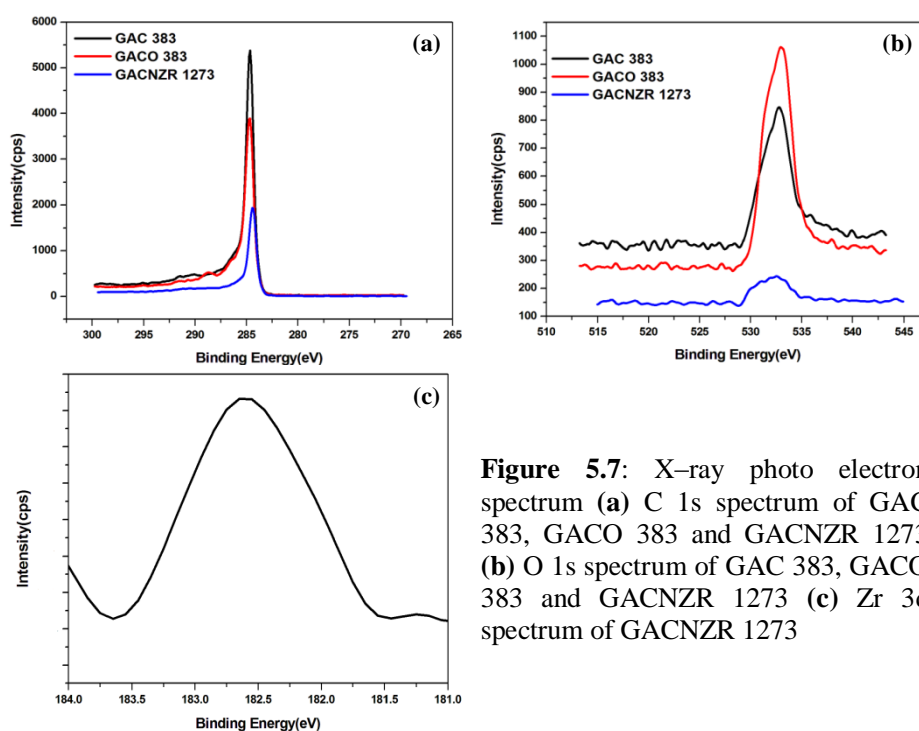


**Figure 5.7:** X-ray photo electron spectrum (a) C 1s spectrum of GAC 383, GACO 383 and GACNZR 1273 (b) O 1s spectrum of GAC 383, GACO 383 and GACNZR 1273 (c) Zr 3d spectrum of GACNZR 1273

The binding energy of O 1s showed peak in the region of  $532\text{ eV}$ . XPS analysis showed the decrease in the intensity of the O 1s signal for GACNZR 1273 with a binding energy between  $532$  and  $533\text{ eV}$  which corresponds to

oxygen complexes such as C-O, C=O, and -COO-. However, GACO 383 showed a considerable increase in oxygen surface complexes which can be explained by nitric acid modification of granular activated carbon.

XPS spectrum of GACNZR 1273 in the Zr 3d level is given in the Figure 5.7(c) It can be seen that the binding energy of Zr 3d<sub>5/2</sub> region corresponding to 182.6 eV which is in good agreement with 182.3 eV of Zr<sup>4+</sup> in ZrO<sub>2</sub>.

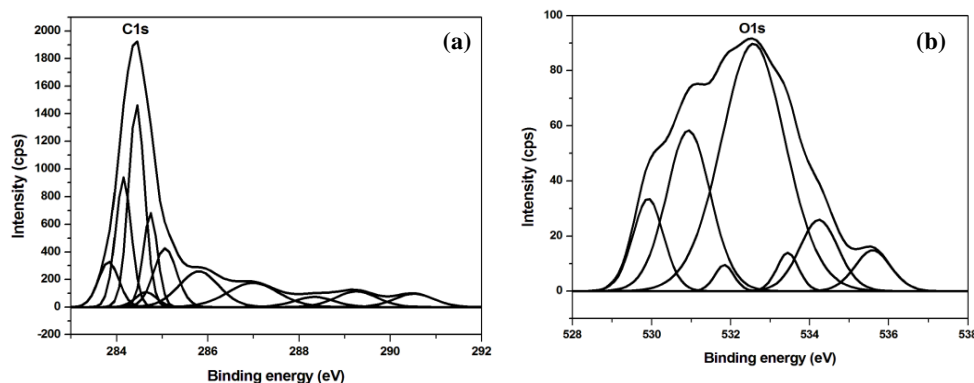


**Figure 5.8:** X-ray photoelectron spectrum (XPS) of GACNZR 1273. Deconvoluted peaks (a) C 1s and (b) O 1s

C 1s signal of GACNZR 1273 consists of different chemically shifted components. sp<sup>2</sup> peak of the C 1s envelope centered at 284.5 eV. Deconvoluted peak at 284.6 eV indicate C=C /C-C in aromatic rings. The component at 285.86 eV is assigned to C atoms directly bonded to oxygen in hydroxyl (C-OH) configurations, 287 eV is characteristic of slightly oxidized carbon atoms in compounds such as alcohol or ethers. The binding energy at the region of 288.1 - 289.3 eV attributed to C(=O) - (OH). The band at 290.6 eV indicates the delocalized  $\pi$  conjugation.

For curve fitting of the O1s peak, the functions as shown in Figure 5.8(b) were considered, namely C=O groups at 530  $\pm$  0.1 eV, carbonyl oxygen atoms in esters, amides, anhydrides. Oxygen atoms in hydroxyls or ethers (C-O-C) are at 532.3  $\pm$  0.3 eV, the ether oxygen atoms in esters and anhydrides (COOCO) at 533.4 eV and the oxygen atoms in carboxyl groups (COOH) at 534.2 eV [11].

### 5.4.7 Scanning Electron Microscopy (SEM) Analysis

The surface morphology of the prepared activated carbons is examined by scanning electron microscope (SEM), and the images are shown in Figure 5.9. It gives the external surface of activated carbon with full of open cavities, voids and many small pores. Highly developed porosities of these samples may increase the internal pore diffusion to the adsorption sites. Large pores were developed on the surface of the activated carbon due to some of the volatiles being evolved at higher activation temperature.

The GAC appeared to have an effect on the morphology of the zirconium nanoparticles in the GACNZR 1273. The  $ZrO_2$  gets distributed around the pore edges, and it is almost irregular in shape. They appeared as white points of different sizes and it will be confirmed by FTIR spectra in the same study. Acidic functional group on the surface of carbon exhibits negative charge in neutral or slightly acidic pH environments providing for lower isoelectric points. The positively charged Zr precursor ions are attracted by these negative surface charges which results distribution of the zirconium precursor material on the surface [12].

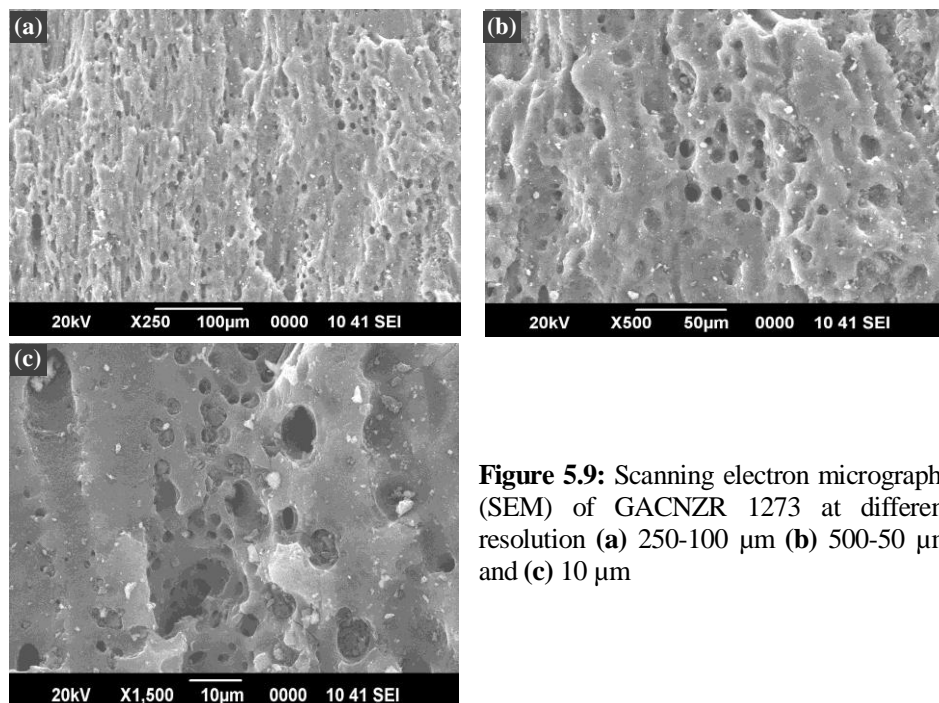


**Figure 5.9:** Scanning electron micrographs (SEM) of GACNZR 1273 at different resolution (a) 250-100  $\mu\text{m}$  (b) 500-50  $\mu\text{m}$  and (c) 10  $\mu\text{m}$



### 5.4.8 Transmission Electron Microscopy (TEM) Analysis

TEM micrograph analysis of GAC impregnated with  $ZrO_2$  nano particles are shown in the Figure 5.10 (a) & (b)

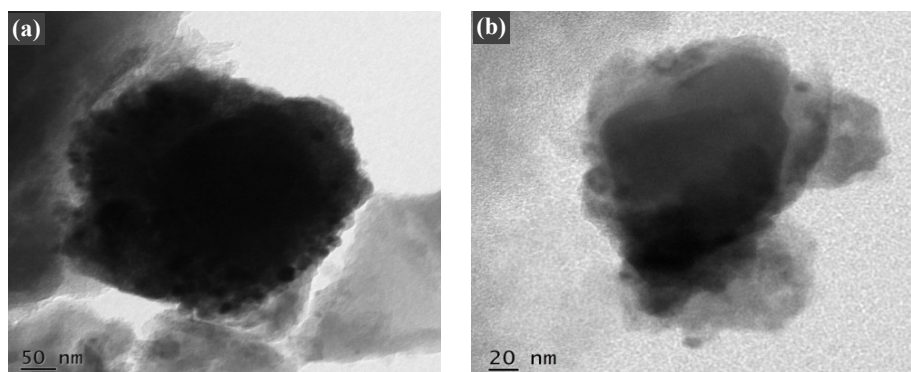


**Figure 5.10:** High resolution transmission electron microscopy (HRTEM) of GACNZR 1273 at different resolutions (a) 50 nm and (b) 20 nm

Transmission electron microscopy of GACNZR 1273 shows that nano zirconia was dispersed onto the inner surface of the porous granular activated carbon and deposited at various positions throughout the surface. The presence of zirconium is indicated by the bright spot. Higher atomic number elements appear as bright relative to low atomic number element carbon. It shows that nano  $ZrO_2$  is well distributed in impregnated GAC. Due to their distinct crystal lattice fringes,  $ZrO_2$  particles are easily differentiated from the highly disordered (amorphous) phase of GAC material as a background [13].

## 5.5 Solid-Gas Adsorption Equilibria

### 5.5.1 Adsorption Isotherm Analysis

The nitrogen adsorption–desorption isotherms for the four selected activated carbons GACNZR 1073, GACNZR 1273, GAC 383 and GACO 383 are presented in the Figure 5.11. The shape of  $N_2$  adsorption–desorption isotherms are similar for all the four carbon studied. As it is clear from the Figure 5.11, the amount of  $N_2$  uptake increases with an increase in the relative pressure, and adsorption approaches to a limit gradually when the adsorbent monolayer is saturated. This isotherm belongs to *Type I* behaviour as per the IUPAC classification [14].

On comparing with different activated carbons, it is suggested that the relative affinity for  $N_2$  adsorption for each activated carbon is different. It indicates the differences in pore volume or accessibility among the activated carbon surfaces. The Figure 5.11 shows that the adsorption of nitrogen on GACNZR 1073 is higher than that of GACNZR 1273, i.e. adsorption decreases with increasing the activation temperature from 1073 K to 1273 K in GACNZR series. This may be due to the destruction of the walls between adjacent pores by activating sample above 1073 K.

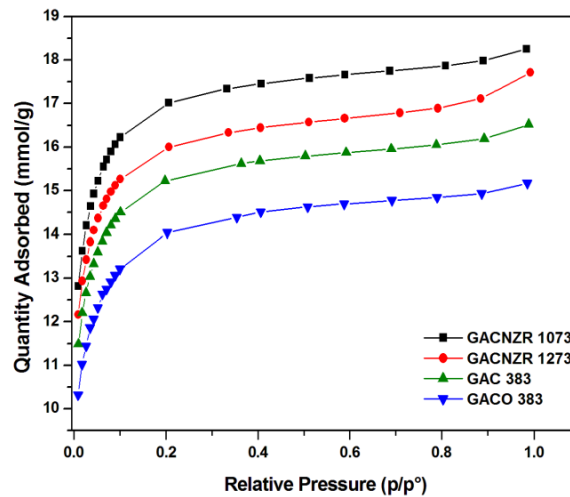


**Figure 5.11:**  $N_2$  adsorption isotherm for GAC 383, GACO 383 and GACNZR series carbonized at temperature 1073 K and 1273 K

### 5. 5.1.1 Brunauer-Emmett-Teller (BET) Isotherm Analysis

The surface area ( $SA_{BET}$ ) of  $ZrO_2$  impregnated activated carbon was estimated by BET (Brunauer–Emmett–Teller) method by applying  $N_2$  adsorption data in the classical BET equation.

$$\frac{1}{V(p_0/p - 1)} = \frac{1}{V_m C} + \frac{C - 1}{V_m C} \left(\frac{p}{p_0}\right) \quad (5.1)$$

The surface areas and pore volumes of each carbons prepared under different activation conditions are given in the Table 5.4.

From Table 5.4 it can be seen that standard  $N_2$  adsorption isotherm data  $p/p_0$  up to 0.1 has large  $C_{BET}$  value. It may be concluded that the BET monolayer volume  $V_m$  (BET) seems to be more reliable at the relative pressure range  $p/p_0$  up to 0.1.

The chemical activation of GAC with zirconia ( $ZrO_2$ ) has a significant influence on surface area and porosity of granular activated carbons. On comparing with basic carbon GAC 383 (1298.48  $m^2/g$ ),  $ZrO_2$  impregnated granular activated carbons shows 12 % (GACNZR 1073) and 5.24 % (GACNZR 1273) increment in surface area ( $SA_{BET}$ ) and monolayer volume ( $V_m$  BET). Whereas for comparing with GACO 383, these  $Zr^{4+}$  modified carbon shows 22.58 % (GACNZR 1073) and 15.17 % (GACNZR 1273) increment in  $SA_{BET}$  and  $V_m$  (BET).

The BET surface area ( $p/p_0$  up to 0.1) and the total pore volumes of the  $ZrO_2$  activated carbons are decreased from 1454.35  $m^2/g$  ( $V_T$  409.4  $cm^3/g$ ) to 1300.47  $m^2/g$  ( $V_T$  397.2  $cm^3/g$ ) by rising the activation temperature from 1073 K to 1273 K.

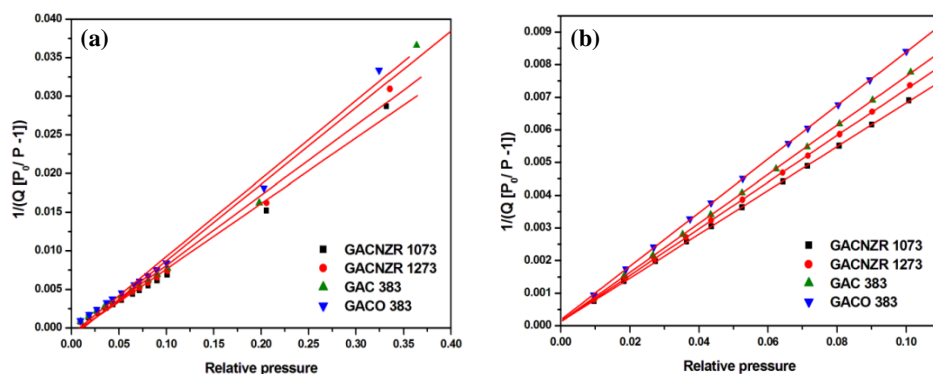


**Figure 5.12:** BET isotherm plot for GAC 383, GACO 383, GACNZR 1073 & GACNZR 1273 (a)  $p/p_0$  up to 0.3 and (b)  $p/p_0$  up to 0.1 using  $N_2/77K$

The high monolayer volume and surface area of GACNZR 1073 compared to GACNZR 1273 indicates that carbonization temperature up to 1073 K accelerates thermal degradation and the volatilization process of the  $ZrO_2$  impregnated carbon. This process leads to increases in the surface area and pore development. A further rise in activation temperature may have induced shrinkage in the carbon structure, resulting in narrowing and closing up to some of the

pores, causes the reduction in surface area and a pore volume [16]. Average pore size obtained from the pore volume is found to be in the range of 1.74 - 1.80 nm which indicates that pores are typically micropores.

### 5.5.1.2 The BET–Scatchard (B–S) Plots (*I* Point Analysis)

The  $N_2$  adsorption isotherm data subjected to modified BET equations (*I* point analysis) for the calculation of specific surface area of carbons. This novel method employs plots of  $[V(1 - P)]/P$  versus  $[V(1 - P)]$  which provides inclined  $V$  type ( $\curvearrowright$ ) curve with an inversion point termed *I* point [17]. This *I* point corresponds exactly to  $V(1 - P) = V_m$ , i.e., the volume of nitrogen necessary for the formation of a monolayer.

$$\frac{[V(1 - P)]}{P} = CV_m - (C - 1)[V(1 - P)] \quad (5.2)$$

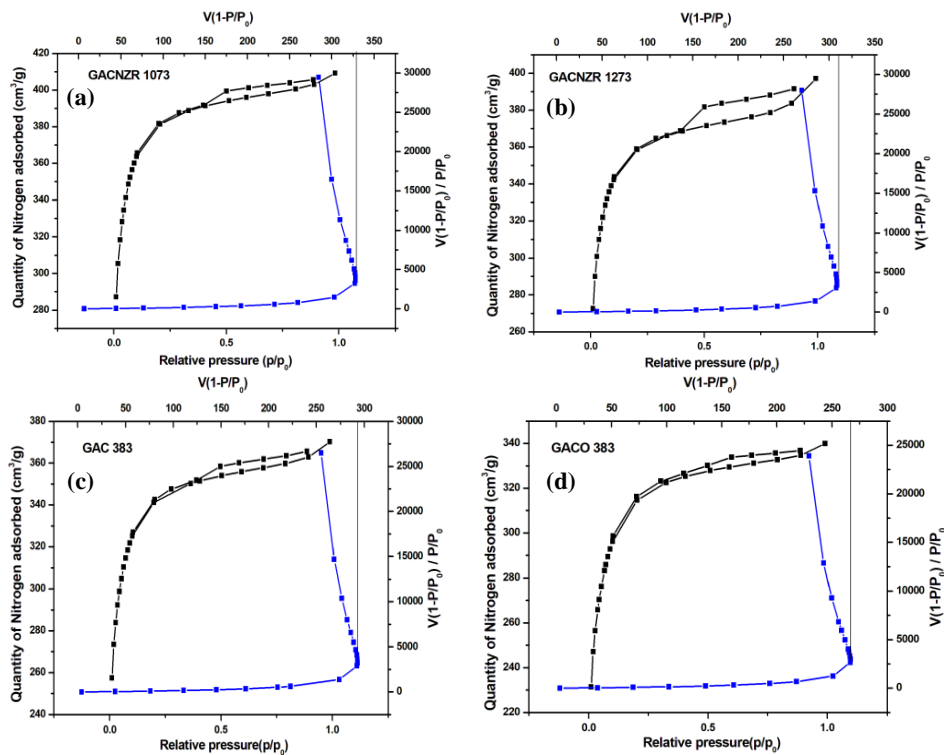


**Figure 5.13 :** Nitrogen adsorption-desorption isotherms and the corresponding *I* plots (a) GACNZR 1073 (b) GACNZR 1273 (c) GAC 383 & (d) GACO 383

The plots are shown in Figure 5.13, and the results are given in Table 5.4, the values of the monolayer capacity ( $V_l$ ) and surface area ( $SA_l$ ) obtained for the modified carbons were GACNZR 1073 ( $SA_l$  1424.89  $m^2/g$  &  $V_l$  327.32  $cm^3/g$ ) and GACNZR 1273 ( $SA_l$  1340.25  $m^2/g$  &  $V_l$  307.88  $cm^3/g$ ).

The monolayer volume and the corresponding specific surface area obtained from BET (up to  $p/p_0 \approx 0.1$ ) and  $I$  plot method is comparable. It shows only 1 – 2 % error difference between values obtained from these two methods. This indicate that  $I$  plot method provide an alternative method for determining the surface area and monolayer volume.

**Table 5.4:** BET and  $I$  plot isotherm parameters for GAC 383, GACO 383, GACNZR 1073 & GACNZR 1273 using  $N_2/77K$

Carbons	Total pore volume $V_T$ $cm^3/g$ .STP	BET $p/p_0$ upto 0.3			$I$ plot method		BET $p/p_0$ upto 0.1			
		$SA_{BET}$ $m^2/g$	$V_m$ $cm^3/g$ .STP	$C_{BET}$	$SA_l$ $m^2/g$	$V_l$ $cm^3/g$ .STP	$SA_{BET}$ $m^2/g$	$V_m$ $cm^3/g$ .STP	$C_{BET}$	Pore width(nm)
GAC 383	370.4	996.8	229.0	-816	1275.4	293.0	1298.5	298.3	524	1.76
GACO 383	340.1	974.3	223.8	-119	1164.7	267.5	1186.5	272.6	439	1.77
GACNZR1073	409.4	1161.5	266.8	-100	1424.9	327.3	1454.3	334.1	514	1.74
GACNZR1273	397.2	1087.6	249.9	-96	1340.3	307.9	1366.5	313.9	572	1.80

### 5.5.1.3 Langmuir Isotherm Analysis

The maximum amount of  $N_2$  adsorbed per gram of adsorbent for the formation of monolayer is determined by using the Langmuir equation. This equation describes microporous material exhibiting *Type I* isotherms.

$$\frac{P}{V} = \frac{1}{bV_m} + \frac{P}{V_m} \tag{5.3}$$

Slope and intercept of the linear fit of the plot were used for the calculation of monolayer capacity.

As shown in the Figure 5.14(a) the Langmuir model gives a good fit to the experimental data for all the four activated carbons studied. This indicates large surface coverage and high interactions between the  $N_2$  molecules for the entire range of pressure studied [18]. The monolayer capacity and corresponding surface area are given in Table 5.5. The monolayer capacity  $V_m$  (L) and surface area  $SA_L$  obtained for the modified carbons are GACNZR 1073 ( $V_m = 376.83 \text{ cm}^3/\text{g}$  &  $SA_L = 1640.43 \text{ m}^2/\text{g}$ ) and GACNZR 1273 ( $V_m = 354.04 \text{ cm}^3/\text{g}$  &  $SA_L = 1541.19 \text{ m}^2/\text{g}$ ) respectively. Impregnation and activation at high temperature increases the pore volume and surface area of about 11.95 % for GACNZR 1073 and 5.18 % for GACNZR 1273 compared to basic carbon GAC 383. On comparing with nitric acid modified GACO 383 impregnated carbons shows 23.76 % (GACNZR 1073) and 16.27 % (GACNZR 1273) enhancement in monolayer volume and surface area.

The calculated Langmuir surface area is more than 11.72–12.79 % compared to  $SA_{BET}$  ( $p/p_0 = 0.1$ ) for all prepared carbons. Surface area based on Langmuir model that considers a surface coverage with a monomolecular layer while  $SA_{BET}$  is based on a model that considers the multilayer coverage.

#### 5.5.1.4 Freundlich Isotherm Analysis

Isothermal variation of a quantity of gas adsorbed by unit mass of solid adsorbent with pressure can be expressed by Freundlich equation. According to this equation extent of gas adsorption varies directly with pressure raised to the power  $1/n$  until saturation pressure is reached.

$$\log V = \log K_F + \frac{1}{n} \log P \quad (5.4)$$

The plots are shown in the Figure 5.14 (b), it indicates that it is generally valid in a limited range of pressure ( $p/p_0=0.3$ ). The empirical constants  $K_F$  and  $n$  for the modified carbons are given in Table 5.5. The constants varies for carbons are, GACNZR 1073 ( $K_F = 233.86 \text{ L/g}$  &  $n = 9.79$ ), and GACNZR 1273 ( $K_F = 223.91 \text{ L/g}$  &  $n = 10.19$ ) respectively.

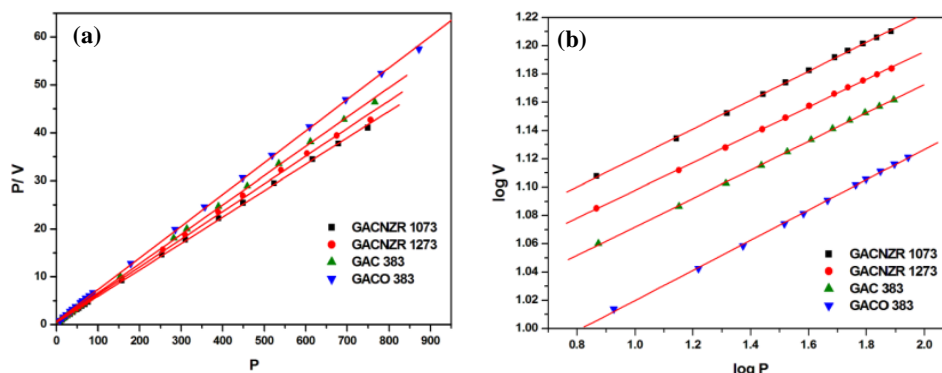


**Figure 5.14:** Adsorption isotherm plots (a) Langmuir (b) Freundlich for GAC 383, GACO 383, GACNZR 1073 & GACNZR 1273 using  $N_2/77K$

Freundlich constant  $K_F$  is a measure of adsorption capacity, which shows 11.46 % increment in GACNZR 1073 and 6.72 % increment in GACNZR 1273 compared to basic carbon GAC 383. On comparing with GACO 383 it shows 27.44 % (GACNZR 1073) and 22.02 % (GACNZR 1273) increment in  $K_F$  value. The measure of heterogeneity can be expressed in value of  $n$ , it is increased from 9.79 to 10.19 for GACNZR series on changing the activation temperature from 1073 K to 1273 K. The correlation coefficient of determination ( $R^2$ ) is greater than 0.99 which indicate that nitrogen adsorption data at 77K is suitably fit to this isotherm model for the relative pressure range up to 0.3.

**Table 5.5:** Langmuir and Freundlich isotherm parameters for GAC 383, GACO 383, GACNZR 1073 and GACNZR 1273 using  $N_2/77K$

Carbons	Langmuir				Freundlich		
	$V_m$ (L) $cm^3/g.STP$	$SA_L(m^2/g)$	$bx10^3$	$R^2$	$n$	$K_F$ L/g	$R^2$
GAC 383	336.6	1465.3	278	0.999	9.9	209.8	0.999
GACO 383	304.5	1325.5	246	0.999	9.4	183.5	0.999
GACNZR 1073	376.8	1640.4	282	0.999	9.8	233.9	0.999
GACNZR 1273	354.0	1541.2	294	0.999	10.2	223.9	0.999

### 5.5.1.5 Dubinin-Radushkevich (D-R) Isotherm Analysis

Dubinin - Radushkevich equation is applied to nitrogen adsorption data of GACNZR 1073, GACNZR 1273, GAC 383 and GACO 383, for the determination of the process of micro pore filling. The D-R equation is based on a plot of  $\log V$

versus  $\log^2 p_0/p$  that leads to a straight line at very low relative pressure, in which the micropores are completely filled at the relative pressure of  $p/p_0 \approx 0.01 - 0.3$

$$\log V = \log V_0 - D \log^2 (p_0/p) \quad (5.5)$$

From the linear plot D-R isotherm, micropore volume  $V_{mi}$  (D-R)  $\text{cm}^3/\text{g}$  (or  $V_0$ ) and characteristic adsorption energy  $E_0$  is obtained. From the  $E_0$  (or  $E$ ) value we can calculate the pore width ( $L$ ) from the empirical correlation between  $E_0$  and  $L$ .

$$L = 6.6 - 1.79 \ln E_0 \text{ nm} \quad (5.6)$$

From  $V_{mi}$  and  $L$  value,  $SA_{D-R}$  can calculate using equation [19]

$$SA = \frac{2 \times 10^3 V_{mi} (\text{cm}^3/\text{g})}{L(\text{nm})} \quad (5.7)$$

The plots are shown in the Figure 5.15 (a), and the results are given in Table 5.6.

Analysis of the data using the Dubinin- Radushkevich models gives micropore ( $< 2$  nm) volumes  $V_{mi}$  (D-R) and  $SA_{D-R}$  of carbons as; GACNZR 1073 ( $V_{mi} = 392.8 \text{ cm}^3/\text{g}$  &  $SA_{D-R} = 723.0 \text{ m}^2/\text{g}$ ) and GACNZR 1273 ( $V_{mi} = 368.9 \text{ cm}^3/\text{g}$  &  $SA_{D-R} = 691.3 \text{ m}^2/\text{g}$ ). These are comparatively higher than basic carbons GAC 383 ( $V_{mi} = 351.3 \text{ cm}^3/\text{g}$  &  $SA_{D-R} = 646.5 \text{ m}^2/\text{g}$ ) and GACO 383 ( $V_{mi} = 322.8 \text{ cm}^3/\text{g}$  &  $SA_{D-R} = 570.2 \text{ m}^2/\text{g}$ ).

This characteristic energy  $E$  depends only on the nature of adsorbent, its value for GACNZR 1073 (15.63 kJ/mol) and GACNZR 1273 (15.88 kJ/mol) is comparatively higher than basic carbons GAC 383 (15.61 kJ/mol) and GACO 383 (15.02 kJ/mol). The pore width ( $L$ ) determined for all new carbons lies in the range of 1.65 - 1.75 nm, which indicates that carbons are microporous in nature.

#### 5.5.1.6 Alpha S ( $\alpha_s$ ) Method

It is used for the determination of micropore volumes and the external surface area (from the slopes of linear portions of Alpha S curves) of carbon materials.

$$\alpha_s = \frac{V_{ads}}{V_{ads}(\frac{p}{p_0}=0.4)} \quad (5.8)$$



The  $\alpha_s$  isotherm analysis of GACNZR 1073 and GACNZR 1273 carbons is shown in the Figure 5.15(b) and the results are tabulated in Table 5.6.

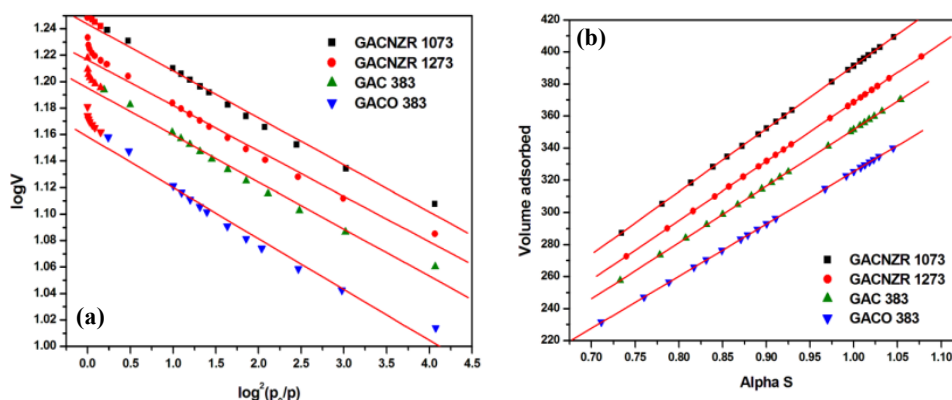


**Figure 5.15:** Adsorption isotherm plots (a) Dubinin - Radushkevich (b) Alpha S ( $\alpha_s$ ) for GAC 383, GACO 383, GACNZR 1073 & GACNZR 1273 using  $N_2/77K$

This method is a highly sensitive analytical method because it covers all the range of pressure, thus their values are more reliable. For the carbon samples, micropore volume  $V_{mi}(\alpha_s)$  varies as; GACNZR 1073 ( $391.30 \text{ cm}^3/\text{g}$ ) and GACNZR 1273 is ( $368.59 \text{ cm}^3/\text{g}$ ). The micropore volume  $V_{mi}(\alpha_s)$  obtained from the  $\alpha_s$  method is more comparable to the value that obtained from Dubinin-Radushkevich method  $V_{mi}(D-R)$  (Table 5.6).

Chemical activation of GAC with  $ZrO_2$  enhances the external surface area  $SA_{ext}$  of about 11.32 % in GACNZR 1073 ( $1119.13 \text{ m}^2/\text{g}$ ) and 5 % in GACNZR 1273 ( $1054.17 \text{ m}^2/\text{g}$ ) compared to basic raw material GAC 383 ( $1005.3 \text{ m}^2/\text{g}$ ).

**Table 5.6:** Dubinin-Radushkevich (D-R) & Alpha S ( $\alpha_s$ ) isotherm parameters of GAC 383, GACO 383, GACNZR 1073 and GACNZR 1273 using  $N_2/77K$

Carbons	Dubinin-Radushkevich (D-R)					Alpha S ( $\alpha_s$ )	
	$SA_{D-R}$ $\text{m}^2/\text{g}$	$V_{mi}$ (D-R) $\text{cm}^3/\text{g.STP}$	L nm	E kJ/mol	$R^2$	$V_{mi}(\alpha_s)$ $\text{cm}^3/\text{g.STP}$	$SA_{ext}$ $\text{m}^2/\text{g}$
GAC 383	646.5	351.3	1.68	15.61	0.986	351.5	1005.3
GACO 383	570.2	322.8	1.75	15.02	0.979	325.3	930.3
GACNZR1073	723.0	392.8	1.68	15.63	0.990	391.3	1119.1
GACNZR1273	691.3	368.9	1.65	15.88	0.989	368.6	1054.2

### 5.5.1.7 John Isotherm Analysis

John isotherm plots for the adsorption of  $N_2$  at 77 K on GACNZR 1073 and GACNZR 1273 are given in the Figure 5.16. It shows three distinct phase changes such as molecular sieve effect, monolayer filling and wider pore filling. Monolayer completion has been observed as distinct phases for adsorption on microporous carbons [20-22]. The general form of John isotherm equation applied to the  $N_2$  adsorption data to study the pore filling mechanism

$$\log \log P = C + n \log V \quad (5.9)$$

Where  $P = p/p_0 \times 10^N$

$N$  is taken conveniently to make  $\log P$  positive, thereby  $\log \log P$  could be found, and  $n$  is adsorbability constant.

The equation (5.9) is further extended to study the adsorption potential of porous materials, from solid - liquid adsorption system known as the John - Sivanandan Achari isotherm given by

$$\log \log C_e = C + n \log q_e \quad (5.9 a)$$

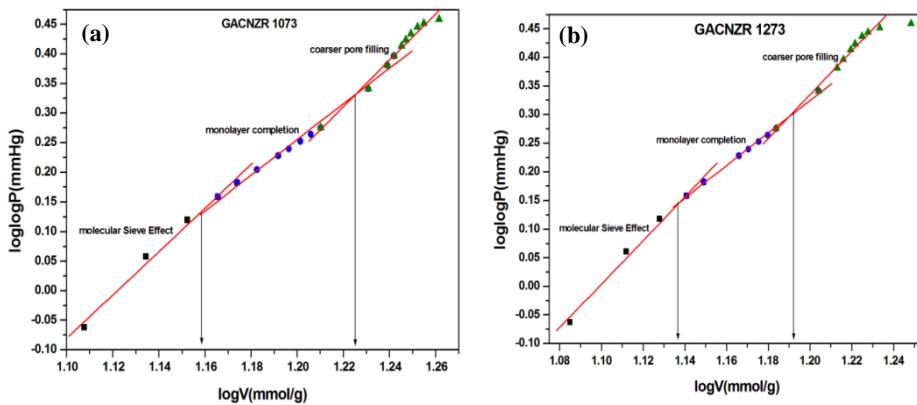


**Figure 5. 16:** John Isotherm plot for carbons (a) GACNZR 1073 (b) GACNZR 1273

Molecular sieve effects (mse), causes an adsorption to take place in pores having a width less than 0.8 nm. It is represented by the *phase I* of the isotherm, the amount of  $N_2$  adsorbed in first phase for carbon samples are given as follows;

GACNZR 1073 (323.31 cm<sup>3</sup>/g) and GACNZR 1273 (304.03 cm<sup>3</sup>/g). These indicate that the contribution of finer pores is 79 % for total microporosity of the material.

**Table 5.7:** John adsorption isotherm parameters of GAC 383, GACO 383, GACNZR 1073 and GACONZR 1273

Carbons	Adsorption Capacity (cm <sup>3</sup> /g)			
	V <sub>mse</sub> cm <sup>3</sup> /g.STP	V <sub>m(J)</sub> cm <sup>3</sup> /g.STP	V <sub>c(J)</sub> cm <sup>3</sup> /g.STP	V <sub>T(J)</sub> cm <sup>3</sup> /g.STP
GAC 383	289.95 n = 3.76	43.61 n = 2.85	32.05 n = 3.60	365.61
GACO 383	264.10 n = 3.43	52.06 n = 2.42	21.55 n = 3.78	337.72
GACNZR 1073	323.31 n = 3.68	54.34 n = 2.88	31.51 n = 3.94	409.16
GACNZR 1273	304.03 n = 3.81	50.36 n = 3.07	28.45 n = 3.82	382.84

Monolayer completion is represented by *phase II* in which molecules fill in the pores having width 0.8-2 nm. The amount of N<sub>2</sub> adsorbed in this phase for carbon samples are given as follows; GACNZR 1073 (54.34 cm<sup>3</sup>/g) and GACNZR 1273 (50.36 cm<sup>3</sup>/g). This indicates the prominence of molecular sieve effects and more accessibility of N<sub>2</sub> into the porous structure of ZrO<sub>2</sub> impregnated carbons. *Phase III* indicates wider pore filling this phase change will give comparatively lower values such as 31.51 cm<sup>3</sup>/g (GACNZR 1073) and 28.45 cm<sup>3</sup>/g (GACNZR 1273). After wider pore filling saturation will occur, this is the characteristic of most *Type I* porous materials.

Pore volume obtained from John, D-R, Alpha S and Langmuir isotherms shows comparable values as shown in the Figure 5.17.

### 5.5.1.8 *t*-Plot Method

The *t*-plot isotherm analysis is used for the determination of micropore volume, micropore surface area and external surface area of carbons GAC 383, GACO 383, GACNZR 1073 and GACNZR 1273.

$$t = \left[ \frac{13.99}{(0.034 - \log(p/p_0))} \right]^{0.5} \quad (5.10)$$

The plots are shown in the Figure 5.18, and the results are given in Table 5.8.

The prepared activated carbon is mainly microporous, but it also contains mesopores that are crucial in facilitating the access of the adsorbate molecules to the interior of the carbon particles. External surface area of the microporous materials can be determined by using the Equation (5.11)

$$SA_{ext} = \frac{slope \times (10^{10} A^0/m) \times D}{F \times 10^6} \quad (5.11)$$

Micropore volume  $V_{mi}(t)$  and micropore surface area  $SA_{mi}(t)$  obtained for carbons are given as follows; GACNZR 1073 ( $V_{mi} = 262.66 \text{ cm}^3/\text{g}$  &  $SA_{mi} = 743.01 \text{ m}^2/\text{g}$ ) and GACNZR 1273 ( $V_{mi} = 248.93 \text{ cm}^3/\text{g}$  &  $SA_{mi} = 701.05 \text{ m}^2/\text{g}$ ). The external surface area  $SA_{ext(t)}$  calculated for carbons are GACNZR 1073 ( $418.47 \text{ m}^2/\text{g}$ ) and GACNZR 1273 ( $386.60 \text{ m}^2/\text{g}$ ) respectively.

There is not a sufficient increment in the external surface area of GACNZR 1073 compared to GAC 383, whereas micropore surface area increases from  $588.65 \text{ m}^2/\text{g}$  to  $743.01 \text{ m}^2/\text{g}$ . This indicates that chemical activation of GAC with  $\text{ZrO}_2$  at 1073 K generates additional micropores without the widening of existing micropores in GAC 383.

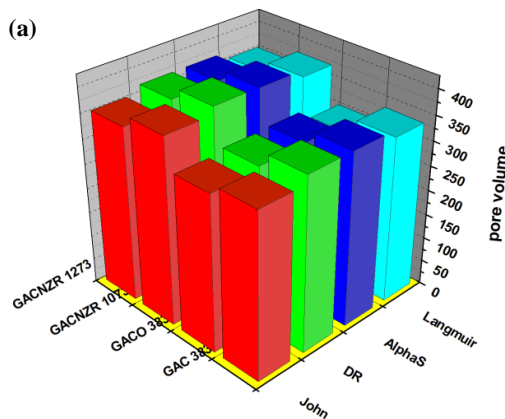


**Figure 5.17:** Comparison of Pore volumes obtained from John (J), D-R, Alpha S and Langmuir models for the adsorption of  $\text{N}_2$  at 77K for microporous carbons

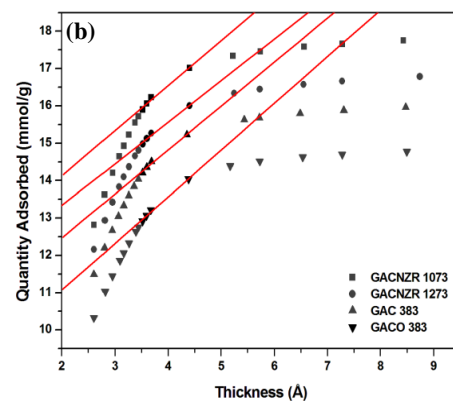


**Figure 5.18:**  $t$ -plot analysis of GAC 383, GACO 383 and GACNZR series carbonized at temperature 1073- 1273 K

Micropore surface area decreases from 743.01 m<sup>2</sup>/g to 701.05 m<sup>2</sup>/g and external surface area decreases from 418.5 m<sup>2</sup>/g to 386.60 m<sup>2</sup>/g by rising activation temperature from 1073 K to 1273 K for GACNZR series of carbons. It may be due to the activation temperature 1273 K may have induced shrinkage in the carbon structure, resulting in a reduction in surface area and a pore volume.

### 5.5.1.9 Barrett-Joyner-Halenda (BJH) Method

The pore size distribution of the prepared activated carbon was determined by BJH (Barrett–Joyner–Halenda) model using N<sub>2</sub> adsorption-desorption isotherms.

The nitrogen adsorption–desorption isotherms of pore width distribution are shown in Figure 5.19 - 5.21. It is seen that maxima pore size distribution centers occur approximately at 3.48 nm (GACNZR 1073), and 3.42 nm (GACNZR 1273) respectively.

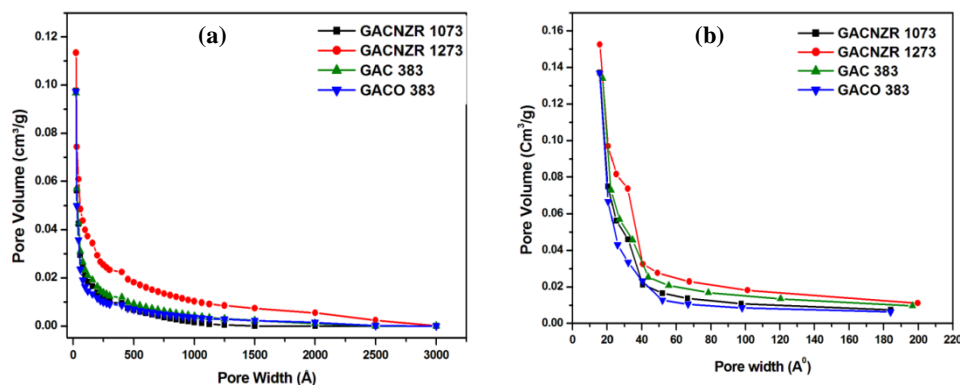


**Figure 5.19:** BJH isotherm analysis (a) Adsorption cumulative pore volume (b) Desorption cumulative pore volume for GAC 383, GACO 383, GACNZR 1073 & GACNZR 1273

For GACNZR 1073 the adsorption cumulative surface area (*ADCSA*) of the respective pore is 237.3 m<sup>2</sup>/g for a cumulative pore volume (*ACPV*) of 0.1416 cm<sup>3</sup>/g (91.58 cm<sup>3</sup>/g.STP). Desorption cumulative surface area (*DCSA*) found to be 229.8 m<sup>2</sup>/g for a cumulative pore volume (*DCPV*) of 0.137 cm<sup>3</sup>/g (88.61 cm<sup>3</sup>/g.STP). The respective adsorption pore width and desorption pore width are 2.387 nm and 2.388 nm.

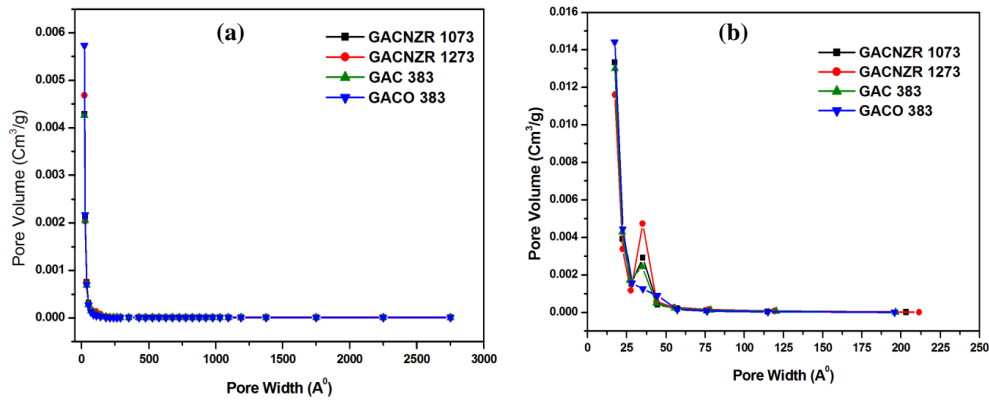


**Figure 5.20:** BJH isotherm analysis (a) Adsorption  $dV/dw$  pore volume (b) Desorption  $dV/dw$  pore volume for GAC 383, GACO 383, GACNZR 1073 & GACNZR 1273

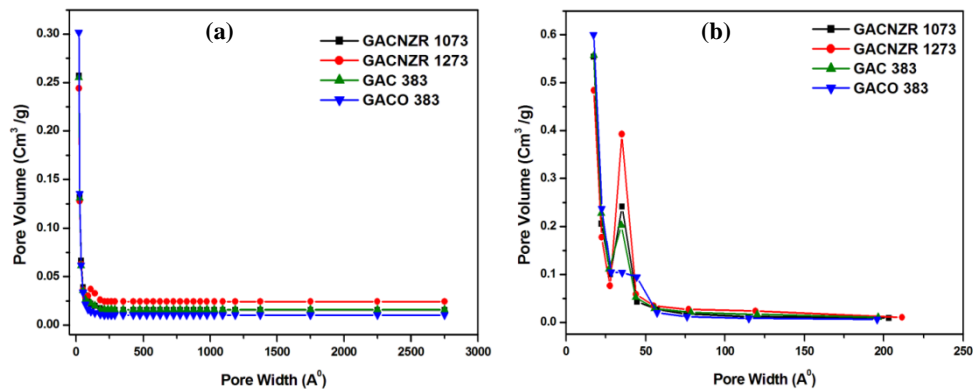


**Figure 5.21:** BJH isotherm analysis (a) Adsorption  $dV/d\log w$  pore volume and (b) Desorption  $dV/d\log w$  pore volume for the carbons, GAC 383, GACO 383, GACNZR 1073 & GACNZR 1273

For GACNZR 1273 the adsorption cumulative surface area ( $ADCSA$ ) of the respective pore are  $224.281 \text{ m}^2/\text{g}$  for a cumulative pore volume ( $ACPV$ ) of  $0.1524 \text{ cm}^3/\text{g}$  ( $98.69 \text{ cm}^3/\text{g.STP}$ ) and desorption cumulative surface area ( $DCSA$ ) of the respective pore found to be  $228.30 \text{ m}^2/\text{g}$  for a cumulative pore volume ( $DCPV$ ) of  $0.15244 \text{ cm}^3/\text{g}$  ( $98.96 \text{ cm}^3/\text{g.STP}$ ). The respective adsorption pore width and desorption pore width are  $2.719 \text{ nm}$  and  $2.673 \text{ nm}$ .

**Table 5.8:** *t*-plot and BJH isotherm parameters of GAC 383, GACO 383, GACNZR 1073 and GACNZR 1273

Carbons	t-plot			Barrett-Joyner-Halenda (BJH)					
	$V_{mi}$ (t) cm <sup>3</sup> /g.STP	$SA_{mi}$ (t) m <sup>2</sup> /g	$SA_{ext}$ (t) m <sup>2</sup> /g	ADCSA m <sup>2</sup> /g	DCSA m <sup>2</sup> /g	*ACPV cm <sup>3</sup> /g	*DCPV cm <sup>3</sup> /g	Pore width	Pore width
GAC 383	226.7	588.7	408.1	226.2	220.5	0.138	0.134	2.44	2.43
GACO 383	192.0	540.3	433.7	250.0	242.8	0.142	0.137	2.28	2.26
GACNZR 1073	262.7	743.0	418.5	237.3	229.8	0.142	0.137	2.39	2.39
GACNZR 1273	248.9	701.1	386.6	224.3	228.3	0.152	0.153	2.72	2.67

$$* V_m (cm^3/g) = \frac{V_m (cm^3/g).STP \times 28}{22414 \times 0.808}$$

### 5.6 Solid-Liquid Equilibria: Adsorption Studies

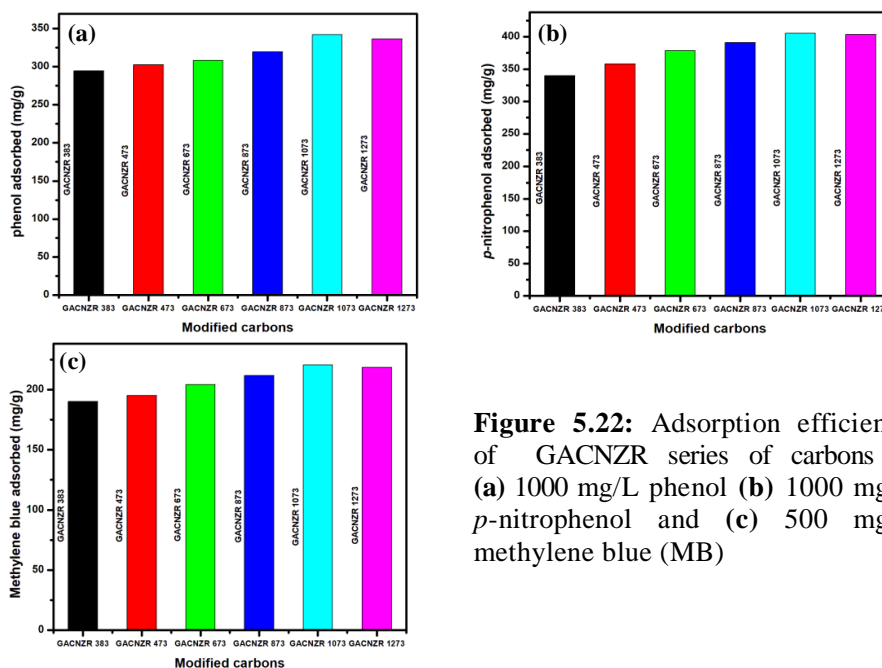


**Figure 5.22:** Adsorption efficiency of GACNZR series of carbons in (a) 1000 mg/L phenol (b) 1000 mg/L *p*-nitrophenol and (c) 500 mg/L methylene blue (MB)

Maximum efficiency of GACNZR series of carbons towards phenol, *p*-nitrophenol and MB is determined by batch tests. Here 0.05 g carbon in 50 ml solution of phenol ( $C_o$  1000 mg/L, equilibrium time 8 hour), *p*-nitrophenol ( $C_o$  1000 mg/L, equilibrium time 8 hour) and MB ( $C_o$  500 mg/L, equilibrium time

10 hour) and placed on a water bath shaker for a required equilibrium time at 30<sup>0</sup>C. Finally the filtered solution is analysed by uv-visible spectrophotometer at the appropriate wavelength. Among the series of GACNZR studied, GACNZR 1073 shows maximum efficiency towards phenol, *p*-nitrophenol and methylene blue (MB) and which also having a high BET surface area and pore volume. This selected GACNZR 1073 is further used for studying solid –liquid equilibria along with GAC 383 and GACO 383.

### 5.6.1 Adsorption Studies of Phenol, *P*-Nitrophenol and Methylene Blue

Figure 5.23(a)-(c) depicts the equilibrium adsorption isotherm of phenol, *p*-nitrophenol and methylene blue onto GAC 383, GACO 383, and GACNZR 1073 at 30<sup>0</sup>C. The entire isotherm might be classified of Langmurian type. Among the carbon studied GACNZR 1073 shows high affinity towards phenol, *p*-nitrophenol and MB compared to GAC 383 and GACO 383. This behaviour indicates that GACNZR 1073 surface may have more readily accessible sites for adsorbate than that of other two activated carbons.

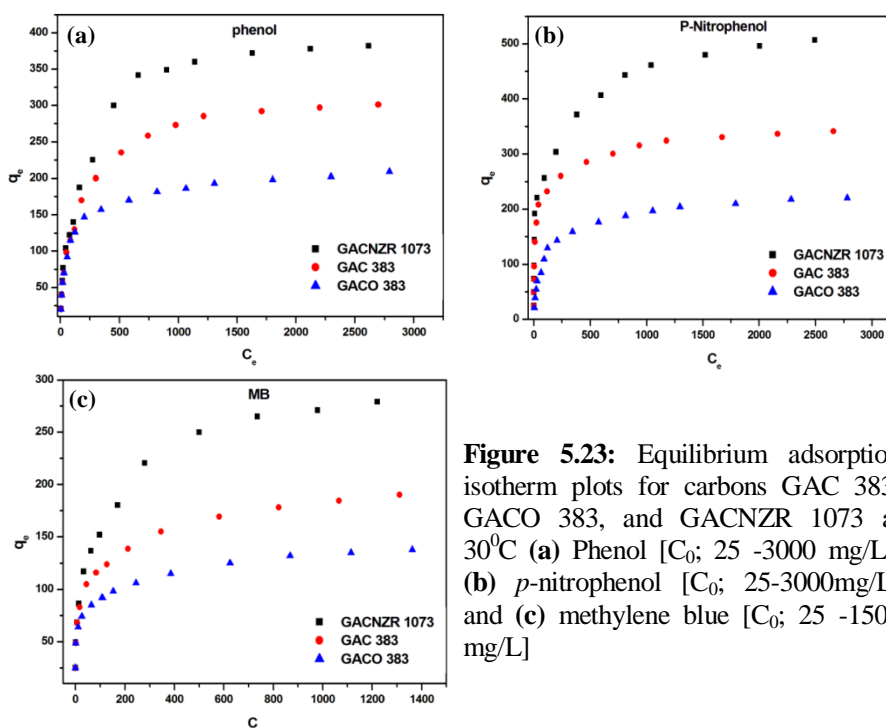


**Figure 5.23:** Equilibrium adsorption isotherm plots for carbons GAC 383, GACO 383, and GACNZR 1073 at 30<sup>0</sup>C (a) Phenol [ $C_0$ ; 25 -3000 mg/L], (b) *p*-nitrophenol [ $C_0$ ; 25-3000mg/L] and (c) methylene blue [ $C_0$ ; 25 -1500 mg/L]



Figure 5.23(a) shows the plot between the amount of phenol adsorbed ( $q_e$ ) against equilibrium concentration ( $C_e$ ) at 303 K. The amount of phenol adsorbed ( $q_e$ ) on GAC given as follows; GACNZR 1073 (382 mg/g), GAC 383 (301 mg/g) and GACO 383 (209 mg/g). The amount of *p*-nitrophenol adsorbed on GAC follows as GACNZR 1073 (507 mg/g), GAC 383 (341 mg/g) and GACO 383 (220 mg/g). The amount of methylene blue adsorbed on GAC follows as; GACNZR 1073 (279 mg/g), GAC 383 (190 mg/g) and GACO 383 (138 mg/g). Increasing order of the adsorption capacity of GAC studied towards phenol, *p*-nitrophenol and MB follows GACO 383 < GAC 383 < GACNZR 1073. The adsorption capacity of GAC increased by impregnating and activating with  $ZrO_2$ . Compared to GAC 383, carbon GACNZR 1073 shows 26.9 % more adsorption efficiency for phenol, 49 % more adsorption efficiency for *p*-nitrophenol and 47 % more efficiency for MB.

### **5.6.2 Adsorption of Phenol on GACNZR 1073, GAC 383 and GACO 383 at Temperatures**

There were three isotherm models were applied to describe the experimental data. They are, Langmuir, Freundlich and Dubinin-Radushkevich isotherm models.

The Langmuir isotherm plot ( $C_e$  against  $C_e/q_e$ ) for phenol adsorption on GAC 383, GACO 383 and GACNZR 1073 with respect to five temperatures are given in Figures 5.24(a)–(c)

Change in monolayer adsorption capacity for GACNZR 1073, GAC 383 and GACO 383 at five different temperatures is given in the Table 5.9. For carbon GACNZR 1073 these values are; 283 K (344.8 mg/g), 293 K (380.2 mg/g), 303 K (401.6 mg/g), 313 K (469.5 mg/g), and 323 K (502.5 mg/g). It can be seen that the enhancement of monolayer capacity compared to basic carbon is more prominent at higher temperature. Percentage of enhancement in monolayer capacity of GACNZR 1073 compared to basic carbon at different solution temperature is given as follows; 283 K (29.3 %), 293 K (33.5 %), 303 K (28.5 %), 313 K (39.4 %), and 323 K (42.7 %). The Langmuir constant  $K_L$  also influenced by solution temperature and varies as; 283 K ( $1.81 \text{ Lg}^{-1}$ ), 293 K ( $2.21 \text{ Lg}^{-1}$ ), 303 K ( $2.90 \text{ Lg}^{-1}$ ), 313 K ( $3.27 \text{ Lg}^{-1}$ ), and 323 K ( $4.14 \text{ Lg}^{-1}$ ).

$$\frac{C_e}{q_e} = \frac{1}{K_L} + \frac{a_L}{K_L} C_e \quad (5.12)$$

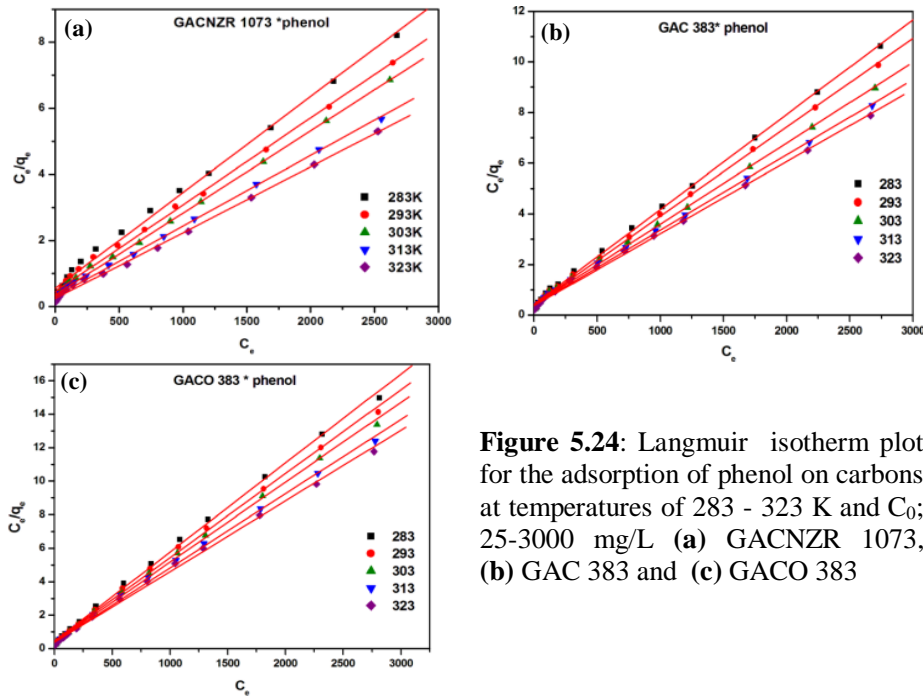


**Figure 5.24:** Langmuir isotherm plot for the adsorption of phenol on carbons at temperatures of 283 - 323 K and  $C_0$ ; 25-3000 mg/L (a) GACNZR 1073, (b) GAC 383 and (c) GACO 383

As the temperature of phenol solution increases, the surface activity and kinetic energy of phenol also increased. This caused the interaction forces between the solute and adsorbent to become stronger than solute and solvent [23]. Linear fits of the equilibrium data in the Langmuir model indicate that the adsorption sites of the GACNZR 1073, GAC 383 and GACO 383 surface are homogeneous and accessed equally by the phenol molecule.

The Freundlich isotherm plots for phenol adsorption on GACNZR 1073, GAC 383, and GACO 383 are given in Figures 5.25(a)–(c).

$$\log q_e = \log K_F + \frac{1}{n} \log C_e \quad (5.13)$$

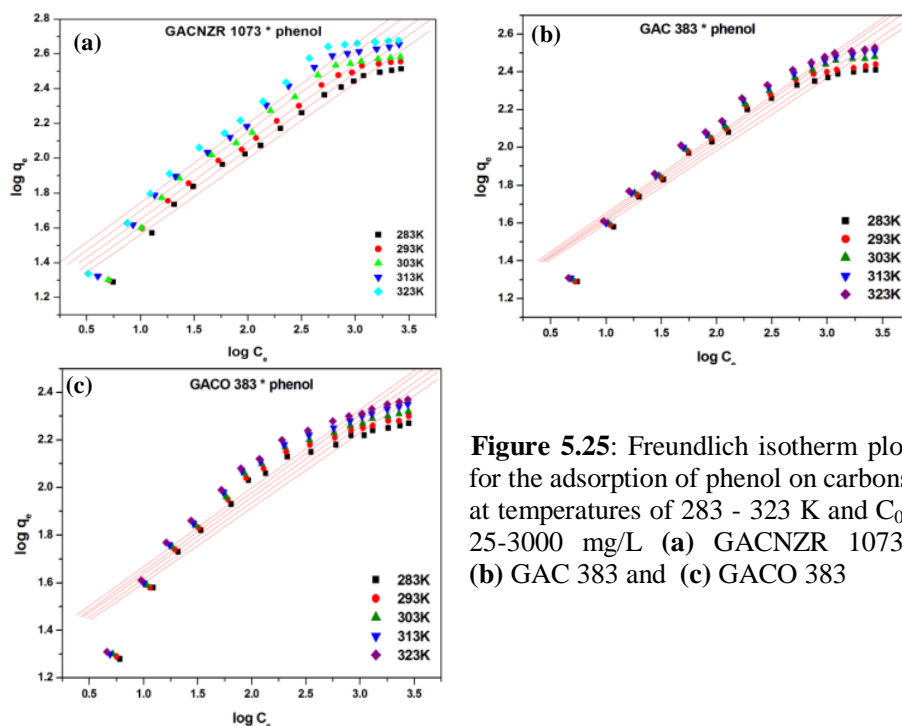


**Figure 5.25:** Freundlich isotherm plot for the adsorption of phenol on carbons at temperatures of 283 - 323 K and  $C_0$ ; 25-3000 mg/L (a) GACNZR 1073, (b) GAC 383 and (c) GACO 383

Freundlich parameter  $K_F$  for GACNZR 1073 is increased with solution temperatures. Its values are given as follows; 283 K ( $13.45 \text{ Lg}^{-1}$ ), 293 K ( $14.69 \text{ Lg}^{-1}$ ), 303 K ( $16.15 \text{ Lg}^{-1}$ ), 313 K ( $17.58 \text{ Lg}^{-1}$ ) and 323 K ( $19.44 \text{ Lg}^{-1}$ ). The higher magnitude of  $K_F$  with temperature indicates the endothermic nature of adsorption. Freundlich constant  $n$  (2.20 - 2.30) indicates favourable adsorption for all temperatures studied. Suggests a high affinity of phenol molecule on the surface of granular activated carbon. Lower correlation coefficient ( $R^2$ ) compared to Langmuir isotherm indicates adsorption data are not well fitted to Freundlich isotherm.

The Dubinin-Radushkevich plot  $\ln q_e$  against  $[RT \ln (1+1/C_e)]^2$  for phenol adsorption on GAC 383, GACO 383 and GACNZR 1073 at five solution temperatures are given in Figures 5.26(a)–(c).

$$\ln q_e = \ln q_{mi} - \beta \varepsilon^2 \quad (5.14)$$

The constant such as  $q_{mi}$  (D-R),  $\beta$  and the mean free energy,  $E$  were determined from the appropriate plot and are given in Table 5.9. The micropore adsorption capacities obtained from D-R isotherm plot for GACNZR 1073 at different temperatures are given as; 283 K (52.7 mg/g), 293 K (56.94 mg/g), 303 K (59.06 mg/g), 313 K (61.9 mg/g) and 323 K (61.24 mg/g).

$$E = \frac{1}{\sqrt{2\beta}} \quad (5.15)$$

The mean free energy is defined as the free energy to transfer one mole of solute from infinity (in solution) to the surface of the adsorbent [24]. It varies between 0.272- 0.491 kJ/mol for GACNZR 1073 at the temperature range of 283 – 323 K.

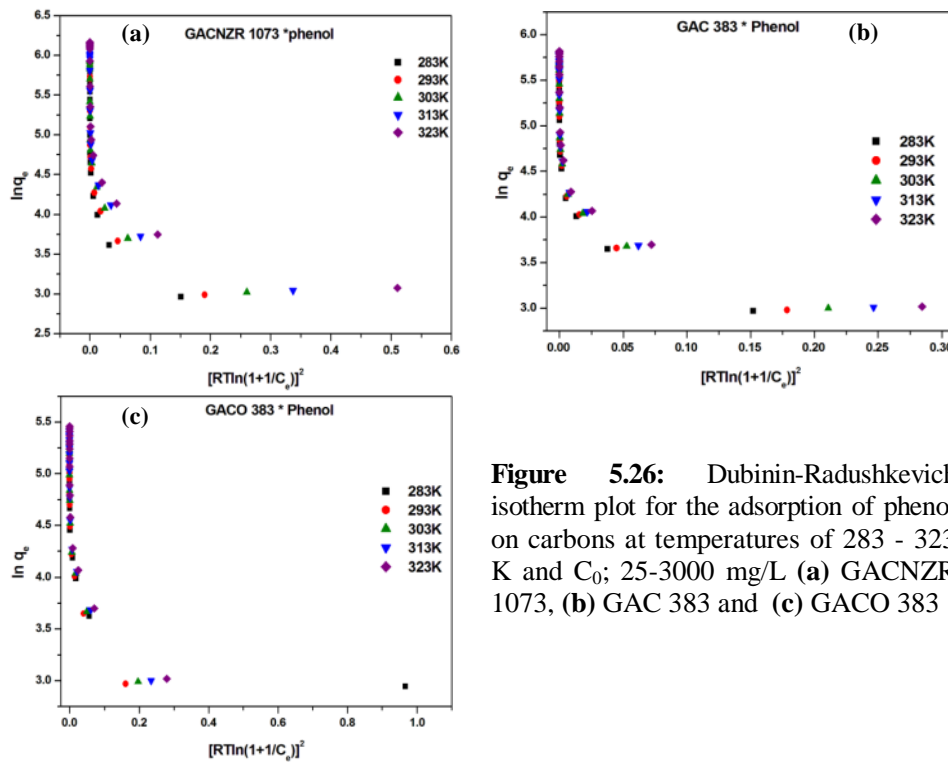


**Figure 5.26:** Dubinin-Radushkevich isotherm plot for the adsorption of phenol on carbons at temperatures of 283 - 323 K and  $C_0$ ; 25-3000 mg/L (a) GACNZR 1073, (b) GAC 383 and (c) GACO 383

Among the three isotherm models studied Langmuir isotherm give better fit of the data, which indicate higher correlation coefficient ( $R^2$ ) compared to other

isotherm models. This suggests that Langmuir isotherm model correlate the adsorption equilibria of the adsorbate as well.

**Table 5.9:** Langmuir, Freundlich and Dubinin-Radushkevich (D-R) isotherm parameters for the adsorption of phenol on carbons GACNZR 1073, GAC 383 and GACO 383 at 283 – 323 K

Carbons	T (Kelvin)	Langmuir isotherm				Freundlich			Dubinin-Radushkevich			
		$K_L/a_L$ (mg/g)	$K_L$ (L.g <sup>-1</sup> )	$a_L \times 10^4$ (L.g <sup>-1</sup> )	R <sup>2</sup>	n	$K_F$ (L.g <sup>-1</sup> )	R <sup>2</sup>	$q_{mi}$ (D-R) (mg/g)	$\beta$ mol <sup>2</sup> /kJ <sup>2</sup>	R <sup>2</sup>	E (kJ/mol)
GACNZR 1073	283	344.8	1.81	53	0.994	2.30	13.5	0.968	52.7	6.7	0.941	0.272
	293	380.2	2.21	58	0.996	2.27	14.7	0.966	56.9	5.6	0.958	0.298
	303	401.6	2.90	71	0.998	2.25	16.2	0.947	59.1	4.1	0.956	0.348
	313	469.5	3.27	70	0.998	2.20	17.6	0.956	61.9	3.8	0.955	0.391
	323	502.5	4.14	82	0.998	2.20	19.4	0.953	61.2	2.1	0.945	0.491
GAC 383	283	266.7	2.33	87	0.998	2.60	16.4	0.935	55.5	7.0	0.966	0.267
	293	284.9	2.46	87	0.998	2.56	16.7	0.935	56.6	6.0	0.966	0.288
	303	312.5	2.48	79	0.998	2.49	16.7	0.945	57.4	5.1	0.966	0.293
	313	336.7	2.53	75	0.998	2.44	17.0	0.951	58.4	4.4	0.966	0.338
	323	352.1	2.68	76	0.998	2.42	17.4	0.951	59.2	3.8	0.966	0.362
GACO 383	283	188.3	2.17	115	0.998	3.17	19.2	0.885	46.9	7.5	0.906	0.258
	293	199.6	2.34	117	0.998	3.13	19.9	0.889	56.1	6.7	0.966	0.273
	303	209.6	2.48	119	0.998	3.12	20.7	0.895	57.4	5.5	0.970	0.302
	313	225.7	2.52	112	0.998	3.05	21.1	0.903	58.8	4.7	0.968	0.328
	323	237.0	2.59	109	0.998	3.02	21.7	0.904	59.3	3.9	0.966	0.359

### 5.6.3 Adsorption of P-Nitrophenol on GACNZR 1073, GAC 383 and GACO 383 at Temperatures

Adsorption efficiency ( $q_e$  mg/g) of granular activated carbons towards *p*-nitrophenol from aqueous solutions as a function of temperature is studied by using different isotherm models

The Langmuir isotherm plot  $C_e$  against  $C_e/q_e$  of *p*-nitrophenol adsorption on GAC 383, GACO 383 and GACNZR 1073 with respect to five temperatures are given in Figures 5.27 (a)–(c).

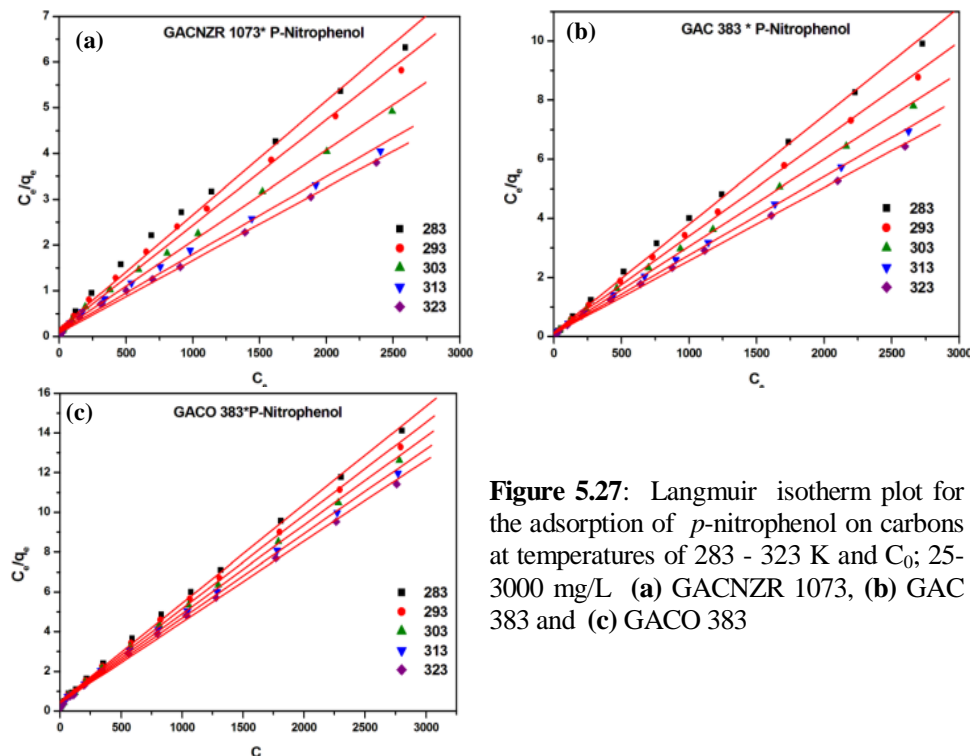


**Figure 5.27:** Langmuir isotherm plot for the adsorption of *p*-nitrophenol on carbons at temperatures of 283 - 323 K and  $C_0$ ; 25-3000 mg/L (a) GACNZR 1073, (b) GAC 383 and (c) GACO 383

The monolayer capacity of GACNZR 1073 at different temperatures are given as 283 K (344.8 mg/g), 293 K (380.2 mg/g), 303 K (401.6 mg/g), 313 K (469.5 mg/g), and 323 K (502.5 mg/g). Considerably high value of  $q_m$  at 323 K indicates that temperatures had a major effect on *p*-nitrophenol adsorption. The modified carbon GACNZR 1073 shows 40 – 47 % enhancement in monolayer volume compared to basic GAC 383. Langmuir constant  $K_L$  also varies with temperature of solution and it ranges 5.84 – 14.3  $Lg^{-1}$  at 283 – 323K.

A plot of  $\log C_e$  versus  $\log q_e$  (Figure 5.28) gave straight line with less fit indicating that the adsorption process did not follow the Freundlich model. Constant  $K_F$  and  $n$  were generated from slope and intercept of plot. It is given in the Table 5.10.  $K_F$  varies from 59.2 to 73.6  $Lg^{-1}$  by rising the solution temperature from 283 to 323 K. Freundlich constant  $n$  is lies within the range of 3.8 - 3.4  $Lg^{-1}$ . High  $K_F$  and  $n$  value for GACNZR 1073 compared to GAC 383 reveals the higher adsorption capacity of GACNZR 1073 towards *p*-nitrophenol.

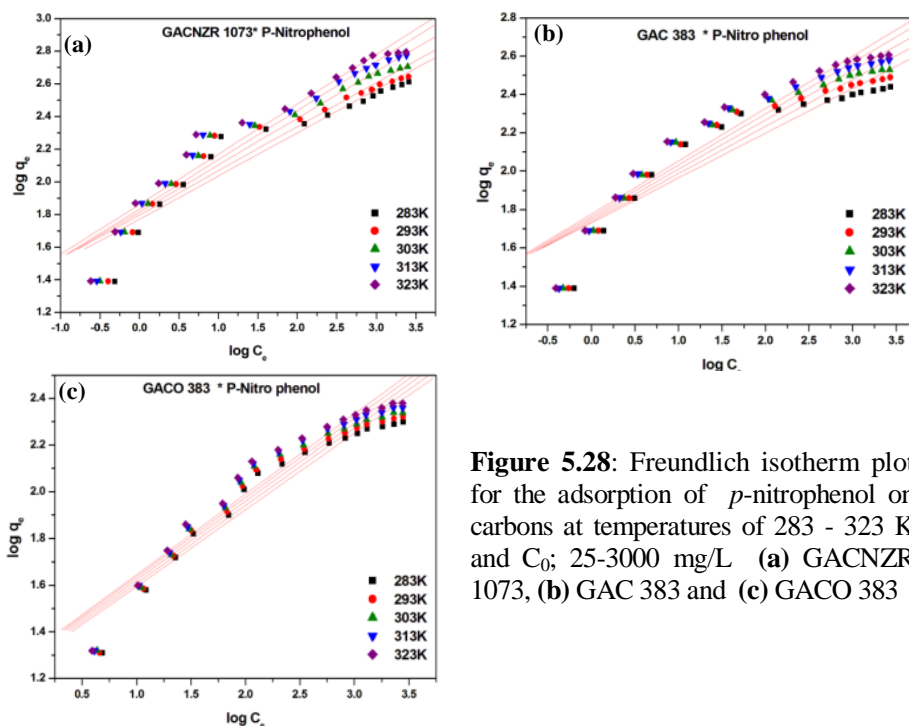


**Figure 5.28:** Freundlich isotherm plot for the adsorption of *p*-nitrophenol on carbons at temperatures of 283 - 323 K and  $C_0$ ; 25-3000 mg/L (a) GACNZR 1073, (b) GAC 383 and (c) GACO 383

The Dubinin-Radushkevich plot of  $\ln q_e$  against  $[RT \ln (1+1/C_e)]^2$  for *p*-nitrophenol adsorption on GAC 383, GACO 383 and GACNZR 1073 with respect to five temperatures are given in Figures 5.29(a)–(c). The constant such as  $q_{mi}$  (D-R),  $\beta$  and the mean free energy,  $E$  were determined from the appropriate plot and are given in Table 5.10.

The mean free energy of adsorption from D-R gave 4.54 to 4.64 kJ/mol. It specifies the physisorption of *p*-nitrophenol on GAC. The micropore adsorption ( $q_{mi}$ ) obtained from the intercept of D-R plot enhances from 94.12 mg/g to 103.99 mg/g with the increasing of solution temperature (283 K – 323 K). The  $q_{mi}$  (D-R) for the uptake of *p*-nitrophenol onto GACNZR 1073 shows more than 23 – 28 % enhancement compared to basic GAC 383.

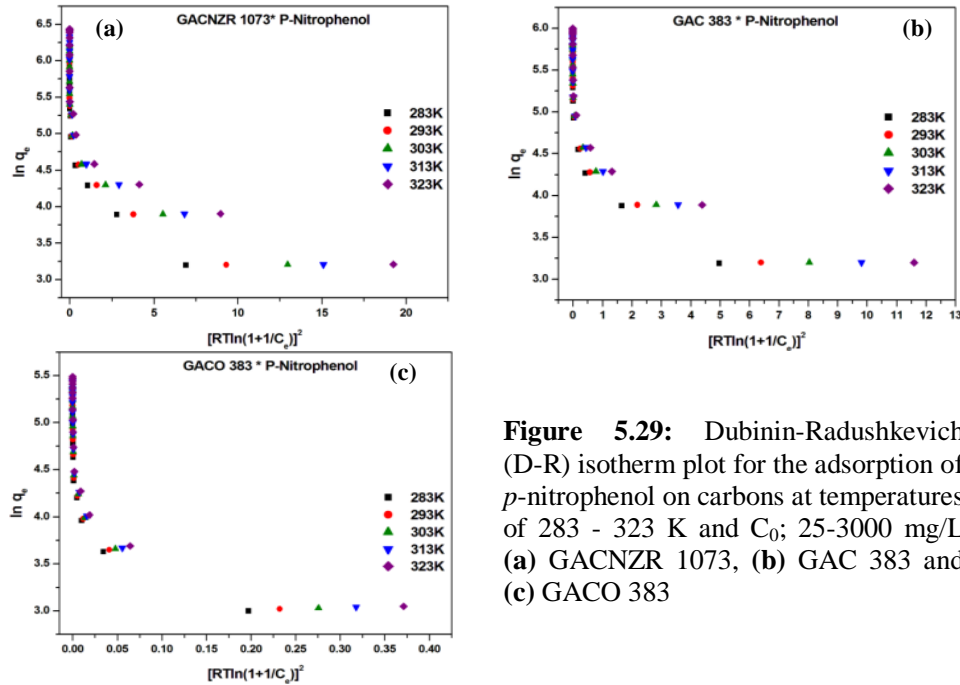


**Figure 5.29:** Dubinin-Radushkevich (D-R) isotherm plot for the adsorption of *p*-nitrophenol on carbons at temperatures of 283 - 323 K and  $C_0$ ; 25-3000 mg/L (a) GACNZR 1073, (b) GAC 383 and (c) GACO 383

**Table 5.10:** Langmuir, Freundlich and Dubinin-Radushkevich (D-R) isotherm parameters for the adsorption of *p*-nitrophenol on carbons on GACNZR 1073, GAC 383, and GACO 383 at 283 – 323 K

Carbons	T (Kelvin)	Langmuir isotherm				Freundlich			Dubinin-Radushkevich			
		$K_L/a_L$ (mg/g)	$K_L$ ( $Lg^{-1}$ )	$a_L \times 10^4$ ( $Lg^{-1}$ )	$R^2$	n	$K_F$ ( $Lg^{-1}$ )	$R^2$	$q_{mi}$ (D-R) mg/g	$\beta$ mol <sup>2</sup> /kJ <sup>2</sup>	$R^2$	E (kJ/mol)
GACNZR 1073	283	401.6	5.84	145	0.990	3.89	59.2	0.901	94.1	0.20	0.980	4.5
	293	434.8	7.31	168	0.994	3.71	62.9	0.901	96.3	0.15	0.980	4.6
	303	505.1	8.95	177	0.996	3.49	65.6	0.927	96.8	0.11	0.980	4.6
	313	529.1	12.9	244	0.998	3.42	69.2	0.925	100.9	0.10	0.980	4.6
	323	581.4	14.3	245	0.998	3.36	73.6	0.931	104.0	0.08	0.980	4.6
GAC 383	283	272.5	7.61	279	0.998	4.26	53.5	0.861	75.8	0.23	0.966	1.6
	293	304.9	8.36	274	0.998	4.06	55.0	0.880	77.0	0.18	0.966	1.8
	303	340.1	9.03	265	0.998	3.88	56.6	0.893	78.2	0.15	0.966	1.9
	313	377.4	9.40	249	0.998	3.73	58.1	0.906	79.5	0.12	0.966	2.1
	323	403.2	10.7	265	0.998	3.64	59.9	0.914	81.2	0.10	0.966	2.2
GACO383	283	201.6	2.06	102	0.998	3.05	18.5	0.925	49.6	4.63	0.951	0.33
	293	213.2	2.14	101	0.998	3.01	18.9	0.927	50.6	3.97	0.953	0.36
	303	224.2	2.24	100	0.998	2.97	19.3	0.929	51.3	3.35	0.951	0.39
	313	235.3	2.31	98	0.998	2.94	19.7	0.931	52.1	2.92	0.951	0.41
	323	245.7	2.41	98	0.998	2.91	20.0	0.933	52.7	2.51	0.949	0.45



### 5.6.4 Adsorption of Methylene Blue on GACNZR 1073, GAC 383 and GACO 383 at Temperatures

The effective removal of methylene blue (MB) from aqueous solution by GACNR 1073, GAC 383 and GACO 383 at different temperature are expressed by different isotherm methods.

The Langmuir isotherm plot  $C_e$  against  $C_e/q_e$  of MB adsorption on GAC 383, GACO 383 and GACNZR 1073 with respect to five temperatures are given in Figures 5.30 (a) – (c). The constants are evaluated from slope and intercept of the linear plot are given in Table 5.11.

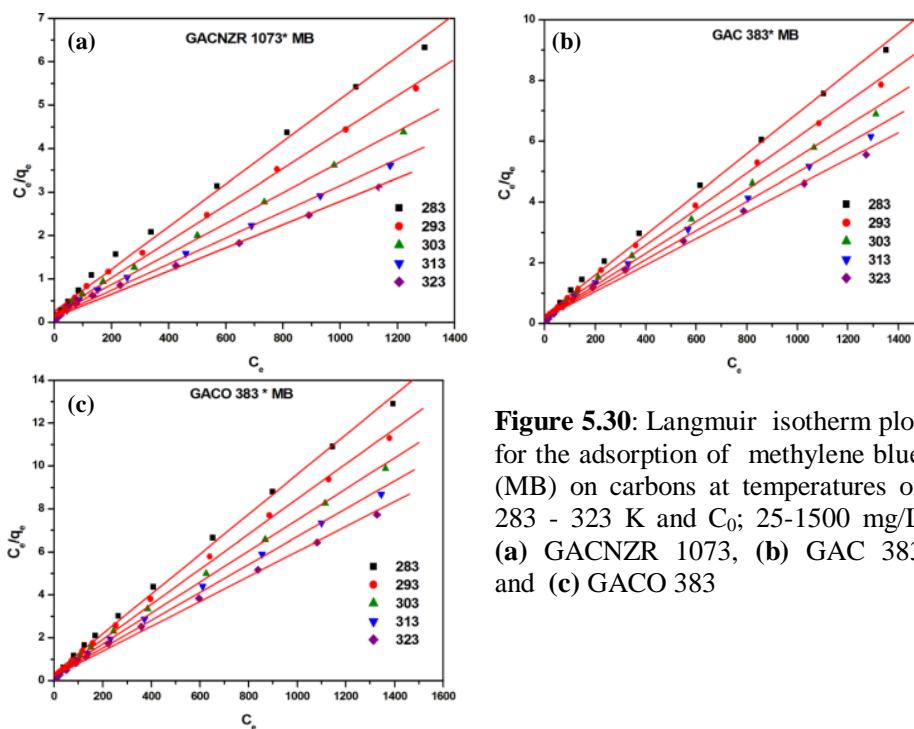


**Figure 5.30:** Langmuir isotherm plot for the adsorption of methylene blue (MB) on carbons at temperatures of 283 - 323 K and  $C_0$ ; 25-1500 mg/L (a) GACNZR 1073, (b) GAC 383 and (c) GACO 383

The Langmuir adsorption maxima ( $K_L/a_L$ ) for MB adsorption on GACNZR 1073 at different solution temperature are given as follows; 283K (204.5 mg/g), 293K (238.7 mg/g), 303K (283.3 mg/g), 313K (332.2 mg/g), and 323K (374.5 mg/g). As the solution temperature rises the percentage of monolayer volume increases from

35.8 % to 63.3 % compared to GAC 383. Langmuir equilibrium constant  $K_L$  varies with temperature are given as; 283 K ( $3.94 \text{ Lg}^{-1}$ ), 293 K ( $5.24 \text{ Lg}^{-1}$ ), 303 K ( $6.00 \text{ Lg}^{-1}$ ), 313 K ( $6.91 \text{ Lg}^{-1}$ ), 323 K ( $8.18 \text{ Lg}^{-1}$ ). The high correlation coefficient shows that Langmuir equation gives excellent fit to the adsorption isotherm data.

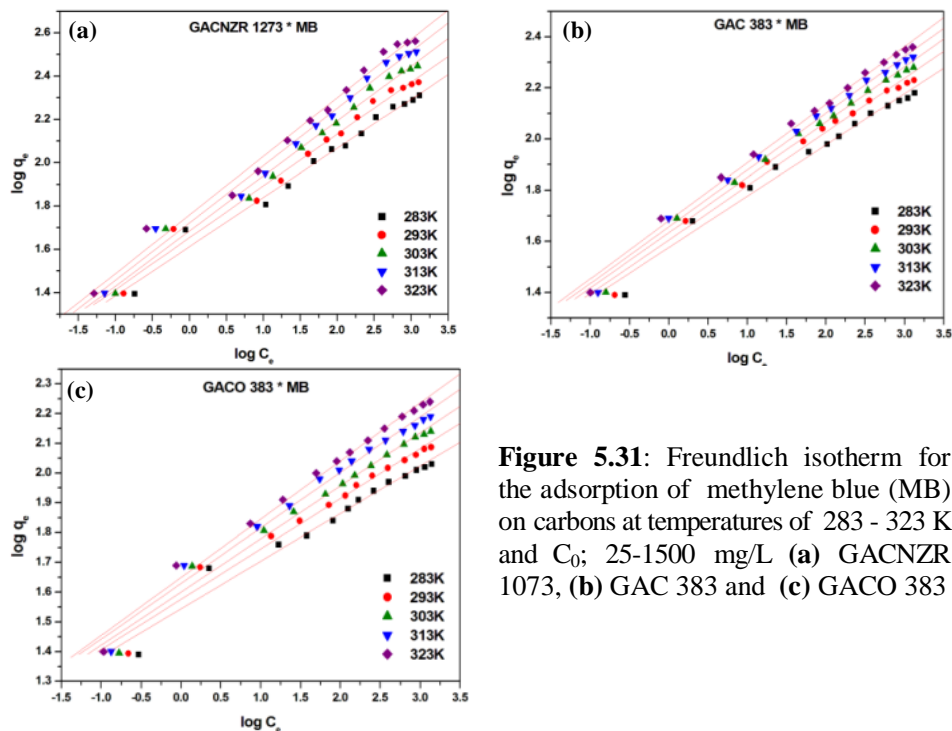


**Figure 5.31:** Freundlich isotherm for the adsorption of methylene blue (MB) on carbons at temperatures of 283 - 323 K and  $C_0$ ; 25-1500 mg/L (a) GACNZR 1073, (b) GAC 383 and (c) GACO 383

The Freundlich plots for methylene blue adsorption on GACNZR 1073, GAC 383, and GACO 383 are given in Figures 5.31(a)–(c).  $K_F$  values for GACNZR 1073 increased with temperatures and given as 283 K ( $40.95 \text{ Lg}^{-1}$ ), 293 K ( $44.99 \text{ Lg}^{-1}$ ), 303 K ( $48.38 \text{ Lg}^{-1}$ ), 313 K ( $52.68 \text{ Lg}^{-1}$ ) and 323K ( $57.37 \text{ Lg}^{-1}$ ). Table 5.11 reveals that for all the temperature conditions,  $K_F$  of GACNZR 1073 is higher than that of GAC 383 and GACO 383 i.e. carbon GACNZR 1073 perform better than other two carbons. Freundlich constant  $n$  values are found to be within range (4.40 - 3.70) of favourable adsorption.

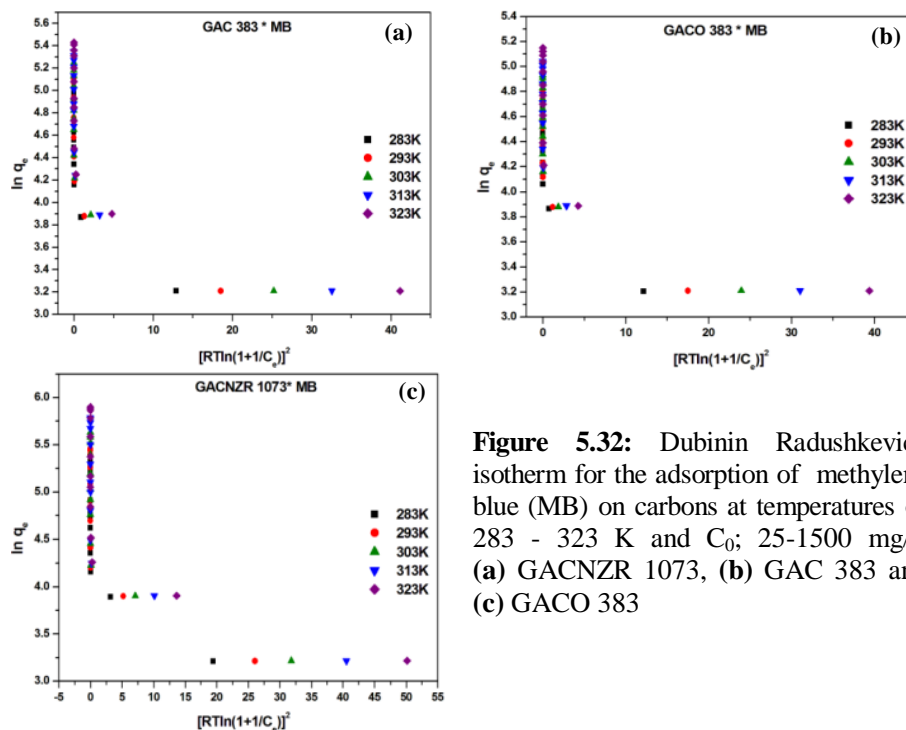


**Figure 5.32:** Dubinin Radushkevich isotherm for the adsorption of methylene blue (MB) on carbons at temperatures of 283 - 323 K and  $C_0$ ; 25-1500 mg/L (a) GACNZR 1073, (b) GAC 383 and (c) GACO 383

The Dubinin–Radushkevich (D-R) plots for methylene blue adsorption on GACNZR 1073, GAC 383, and GACO 383 are given in Figures 5.32 (a)–(c). The Adsorption energy ( $E$ ) obtained from D-R isotherm at different temperatures are given as 283 K (3.27 kJ/mol), 293 K (3.83 kJ/mol), 303 K (4.31 kJ/mol), 313 K (4.96 kJ/mol) and 323 K (5.63 kJ/mol). Lower  $E$  suggests that the uptake of MB on to GACNZR 1073 is physisorption. The adsorption capacity obtained from the D-R isotherm equation for GACNZR 1073 at different solution temperatures are given as follows; 283 K (60.78 mg/g), 293 K (63.61 mg/g), 303 K (65.52 mg/g), 313 K (67.42 mg/g) and 323 K (68.90 mg/g). On comparing with GAC 383, percentage enhancement of  $q_{mi}$  (D-R) for the uptake of MB onto GACNZR 1073 is given as, 283 K (5.83 %), 293 K (8.12 %), 303 K (8.66 %), 313 K (9.48 %) and 323 K (9.75 %).

**Table 5.11:** Langmuir, Freundlich and Dubinin-Radushkevich isotherm parameters of methylene blue on carbons GACNZR 1073, GAC 383, and GACO 383 at 283 – 323 K

Carbons	T (Kelvin)	Langmuir isotherm				Freundlich			D-R Isotherm			
		$K_L/a_L$ (mg/g)	$K_L$ ( $Lg^{-1}$ )	$a_L \times 10^4$ ( $Lg^{-1}$ )	$R^2$	n	$K_F$ ( $Lg^{-1}$ )	$R^2$	$q_{mi}$ (D-R) mg/g	$\beta$ mol <sup>2</sup> /kJ <sup>2</sup>	$R^2$	E (kJ/mol)
GACNZR 1073	283	204.5	3.94	193	0.994	4.40	41.0	0.984	60.8	0.047	0.984	3.3
	293	238.7	5.24	219	0.996	4.17	45.0	0.984	63.6	0.034	0.986	3.8
	303	283.3	6.00	212	0.994	3.94	48.4	0.986	65.5	0.027	0.988	4.3
	313	332.2	6.91	208	0.994	3.78	52.7	0.988	67.4	0.020	0.992	5.0
	323	374.5	8.18	218	0.992	3.70	57.4	0.988	68.9	0.016	0.994	5.6
GAC 383	283	150.6	3.74	248	0.996	1.58	37.7	0.982	57.4	0.066	0.943	2.8
	293	169.5	4.54	268	0.996	1.61	40.7	0.984	58.8	0.047	0.935	3.3
	303	190.1	4.80	252	0.996	1.63	42.9	0.990	60.3	0.036	0.935	3.8
	313	209.6	5.13	245	0.994	1.66	45.3	0.992	61.6	0.028	0.937	4.2
	323	229.4	5.51	240	0.994	1.68	47.8	0.994	62.8	0.023	0.941	4.7
GACO 383	283	108.0	2.89	268	0.998	6.27	35.1	0.968	54.2	0.065	0.972	2.8
	293	122.4	3.37	275	0.996	5.92	37.7	0.976	56.3	0.047	0.960	3.3
	303	138.7	3.60	259	0.996	5.61	39.8	0.982	58.0	0.036	0.955	3.7
	313	154.3	4.31	279	0.996	5.33	42.3	0.984	59.5	0.028	0.951	4.2
	323	172.4	4.59	266	0.996	5.12	44.6	0.988	61.0	0.023	0.953	4.7

### 5.6.5 John-Sivanandan Achari (J-SA) Isotherm Plots for Solid- Liquid Equilibria

Systematic evaluation of different solid-liquid adsorption systems are analysed and evaluated using John – Sivanandan Achari isotherm models [22, 25]

$$\log \log C_e = C + n \log q_e \quad (5.16)$$

The adsorption system selected for applying the *J-SA* isotherms are given as (i) *MB* adsorption of surface treated microporous carbon GACNZR 1073, GAC 383 and GACO 383 (ii) Phenol adsorption on GACNZR 1073, GAC 383 and GACO 383 (iii) *p*-nitrophenol adsorption on GACNZR 1073, GAC 383 and GACO 383.

It shows that surface treatment of porous materials through physico-chemical activation leads to changes in porosity and pore dimensions. Therefore,

adsorption of different adsorbate on these carbons occurs through a series of phase change phenomena.

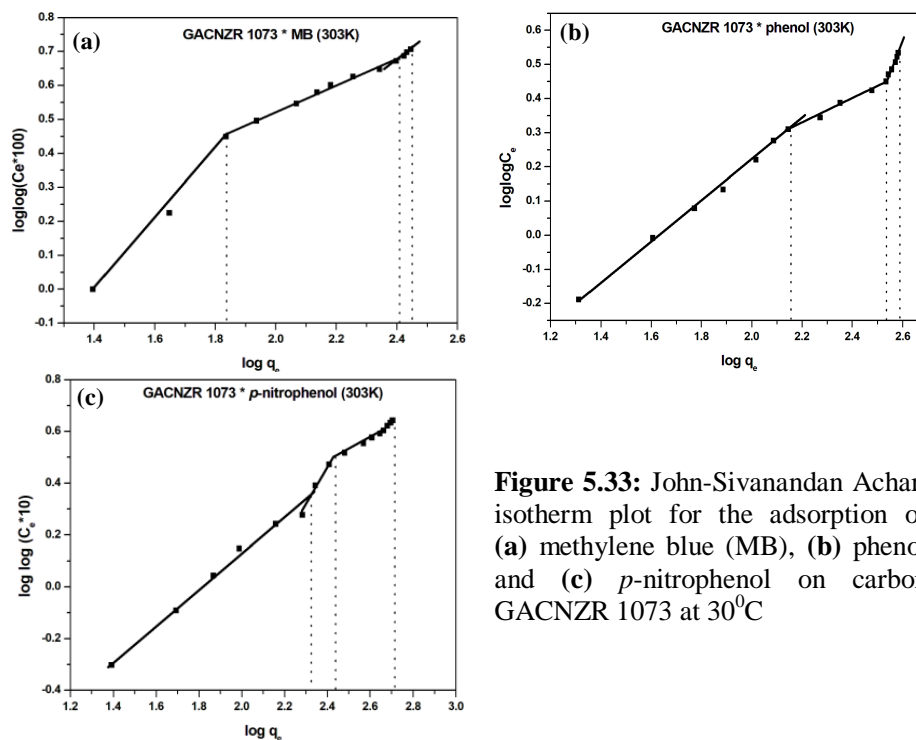


**Figure 5.33:** John-Sivanandan Achari isotherm plot for the adsorption of (a) methylene blue (MB), (b) phenol and (c) *p*-nitrophenol on carbon GACNZR 1073 at 30°C

Figure 5.33(a) indicates the *J-SA* isotherm plot of carbon for MB adsorption. Isotherm has three distinct phases marked by kinks or distinct lines for phase change. Adsorption of MB in *phase I* for GACNZR 1073 is 68.52 mg/g. A sharp kink obtained at the end of *phase I* indicate the change in adsorption mechanism into *phase II*, in which quantity of MB adsorbed for GACNZR 1073 is 186.67 mg/g. Here adsorption occurs at the edges of graphene layers. Surface functional groups present on the edges of graphene layers are ionised and exist as negatively charged. It shows strong electrostatic attraction towards cationic dye like MB. Therefore, considerable increase in the adsorption occurs in this phase. The adsorption capacity during *phase III* is found to be 25.86 mg/g. It indicates the wider pores accessible for adsorption of MB in micro porous carbon.

The *J-SA* plots of phenol and *p*-nitrophenol adsorption exhibited three distinct phases of adsorption as shown in the Figure 5.33(b)&(c). In *J-SA*

isotherm, molecular sieve effect indicated by *phase I* will adsorb 142.56 mg/g of phenol and 210.62 mg/g of *p*-nitrophenol for GACNZR 1073. Electron donor acceptor interaction between surface of carbon and aromatic rings of phenol constitute *phase I* of J–SA isotherm plot.

**Table 5.12:** John-Sivanandan Achari (J-SA), Langmuir, Dubinin-Radushkevich (D-R) and Freundlich isotherm models: comparison of adsorption capacity (mg/g) and surface area (m<sup>2</sup>/g) for the adsorption of phenol, *p*-nitrophenol and MB on carbon GACNZR 1073, GAC 383 and GACO 383 (T = 303K)

Carbons	Adsorbate (cross sectional area nm <sup>2</sup> )	J-SA adsorption capacity mg/g				Langmuir q <sub>m</sub> (L) mg/g (*SA m <sup>2</sup> /g)	q <sub>m</sub> (D-R) mg/g (*SA m <sup>2</sup> /g)	Freundlich q <sub>f</sub> (mg/g) (*SA m <sup>2</sup> /g)
		q <sub>I</sub> (J-SA) mg/g (*SA m <sup>2</sup> /g)	q <sub>II</sub> (J-SA) mg/g (*SA m <sup>2</sup> /g)	q <sub>III</sub> (J-SA) mg/g (*SA m <sup>2</sup> /g)	q <sub>T</sub> (J-SA) mg/g (*SA m <sup>2</sup> /g)			
GACNZR 1073	*MB (1.2)	68.52 (154.8)	186.67 (421.8)	25.86 (58.4)	281.05 (635.1)	283.29 (640.2)	65.52 (148.1)	48.38 (109.3)
	*P (0.522)	142.56 (476.2)	200.88 (671.1)	42.47 (141.8)	385.91 (1289.2)	401.61 (1341.7)	59.06 (197.3)	16.15 (54.0)
	*PNP (0.525)	210.6 (478.8)	56.82 (129.1)	250.63 (569.7)	518.07 (1177.6)	505.05 (1148.0)	96.75 (219.9)	65.62 (149.2)
GAC 383	MB	67.5 (152.5)	124.4 (281.1)	*ND	191.9 (433.6)	190.1 (429.6)	60.3 (136.3)	42.9 (96.9)
	P	72.9 (243.4)	209.8 (700.9)	19.2 (64.3)	301.9 (1008.7)	312.5 (1044.0)	57.4 (191.7)	16.7 (55.9)
	PNP	*ND	210.15 (477.7)	134.07 (304.8)	345.22 (784.7)	334.5 (760.2)	78.2 (177.7)	60.7 (138.1)
GACO 383	MB	66.6 (150.5)	71.8 (162.2)	*ND	138.4 (312.7)	138.7 (313.4)	58.0 (131.0)	39.8 (90.0)
	PNP	56.4 (188.4)	93.1 (311.1)	62.7 (209.4)	212.2 (708.8)	209.6 (700.2)	57.4 (191.8)	20.7 (69.2)
	P	52.3 (118.8)	85.6 (194.6)	84.2 (191.5)	222.1 (504.9)	224.2 (509.7)	51.3 (116.6)	19.3 (43.9)

\*MB - Methylene blue \*P - phenol, \*PNP - *p*-nitrophenol, \*ND – not detected

$$*SA(m^2/g) = \frac{q \text{ (mg/g)} \times 6.022 \times 10^{23} \times \text{cross sectional area of adsorbate}}{\text{Molecular weight of adsorbate}}$$

Higher adsorption of *p*-nitrophenol attributed to the electron withdrawal group in para position. Finer micropores accessible for adsorption are indicated by *phase II*; for GACNZR 1073, this phase will adsorb 200.88 mg/g of phenol and 56.82mg/g of *p*-nitrophenol respectively. The *phase III* in *J*-SA isotherm is probably due to wider pores, in which 42.47 mg/g of phenol and 250.63 mg/g of *p*-nitrophenol will get adsorbed and ultimately saturation occur at the final stage. The percentage contribution of each phase for the adsorption of phenol is given as follows; *phases I* (37%), *phase II* (52%), *phase III* (11%). Whereas for *p*-nitrophenol, *phase I* (41%), *phase II* (11%), *phase III* (48%). Adsorption capacity evaluated from Langmuir isotherm shows agreeable results with that of John-Sivanandan Achari isotherm. The results are presented in Table 5.12.

#### 5.6.5.1 John – Sivanandan Achari Isotherm for Phenol, *P*-Nitrophenol and Methylene Blue Adsorption on GACNZR 1073 at Temperatures

Systematic enhancements of adsorption for phenol, *p*-nitrophenol and methylene blue in three distinct phases by rising the temperature from 283 K to 323 K are represented by John-Sivanandan Achari isotherm.

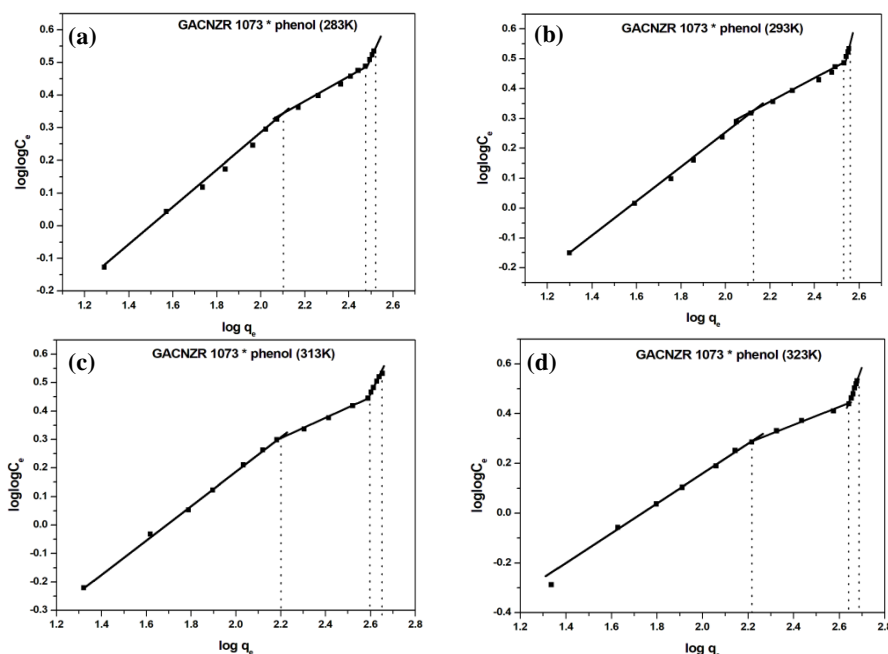


**Figure 5.34:** John-Sivanandan Achari isotherm for phenol adsorption on GACNZR 1073 at temperatures (a) 283 K (b) 293 K (c) 313 K & (d) 323 K

Different phase changes for the adsorption of phenol at different temperature are given in the Figure 5.34. Quantity of phenol adsorbed in each phase will increase with a rise of solution temperature from 283 K to 323 K. Phenol adsorbed in *phase I* increases from 127.1 mg/g to 164mg/g, In *phase II* adsorption increases from 170.3 mg/g to 267.5 mg/g and in *phase III* adsorption increases from 33.3 mg/g to 51.5 mg/g.

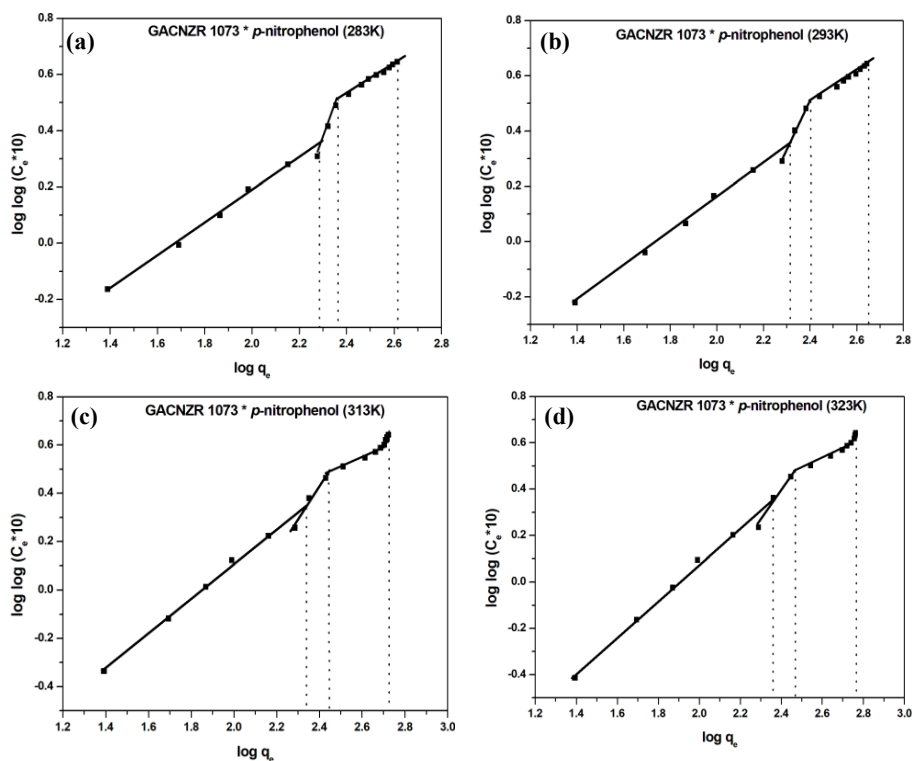


**Figure 5.35** : John-Sivanandan Achari isotherm for *p*-nitrophenol adsorption on GACNZR 1073 at temperatures (a) 283 K (b) 293 K (c) 313 K (d) 323 K

Figure 5.35 indicates John – Sivanandan Achari isotherm for *p*-nitrophenol adsorption on GACNZR 1073 at different temperature. Compared to phenol, adsorption of *p*-nitrophenol in the first phase is high and it varies from 192.9 mg/g to 227.6 mg/g in the temperature range of 283-323K. Second phase of adsorption changes from 38.4 mg/g to 65.6 mg/g and third phase changes from 182.4 mg/g to 290.6 mg/g.



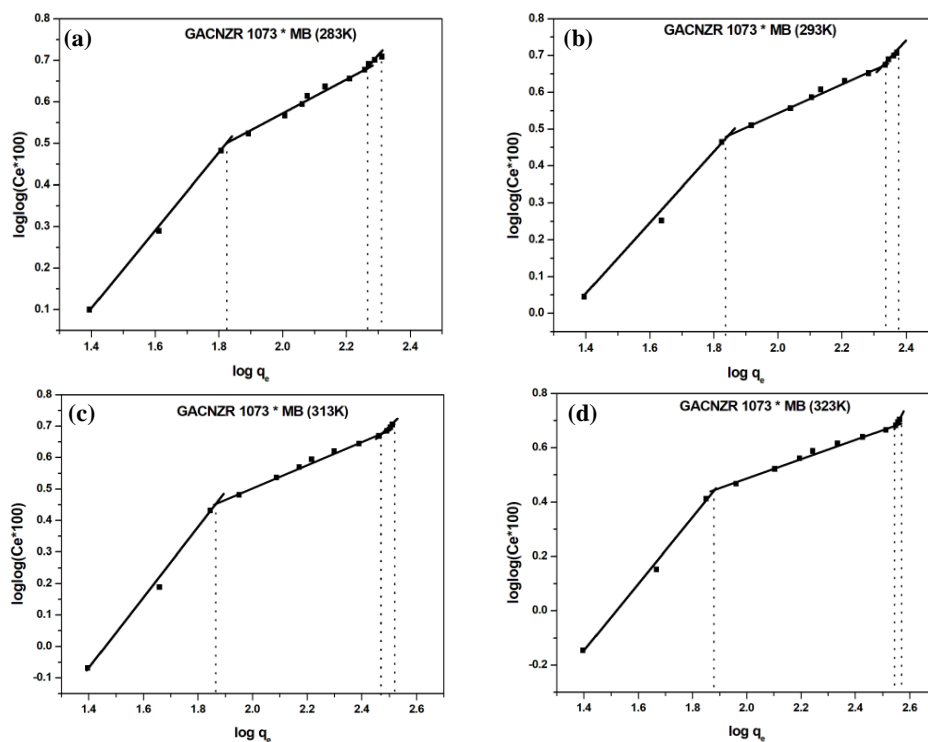


Figure 5.36: John-Sivanandan Achari isotherm for methylene blue adsorption on GACNZR 1073 at temperatures (a) 283 K (b) 293 K (c) 313 K and (d) 323 K

Table 5.13: John - Sivanandan Achari (J-SA) isotherm parameter for the adsorption of phenol, *p*-nitrophenol and methylene blue on carbon GACNZR 1073 at 283 - 323K

Carbons	T (K)	Phenol			<i>p</i> -nitrophenol			Methylene blue		
		q <sub>I</sub> (J-SA) mg/g (SA m <sup>2</sup> /g)	q <sub>II</sub> (J-SA) mg/g (SA m <sup>2</sup> /g)	q <sub>III</sub> (J-SA) mg/g (SA m <sup>2</sup> /g)	q <sub>I</sub> (J-SA) mg/g (SA m <sup>2</sup> /g)	q <sub>II</sub> (J-SA) mg/g (SA m <sup>2</sup> /g)	q <sub>III</sub> (J-SA) mg/g (SA m <sup>2</sup> /g)	q <sub>I</sub> (J-SA) mg/g (SA m <sup>2</sup> /g)	q <sub>II</sub> (J-SA) mg/g (SA m <sup>2</sup> /g)	q <sub>III</sub> (J-SA) mg/g (SA m <sup>2</sup> /g)
GACNZR 1073	283	127.1 (426.6)	170.3 (568.9)	33.3 (111.3)	192.9 (438.5)	38.4 (87.3)	182.4 (414.6)	66.8 (150.9)	117.9 (266.4)	18.2 (41.1)
	293	132.8 (443.7)	190.8 (637.4)	39.5 (132.0)	205.4 (466.9)	48.8 (110.9)	194.3 (441.7)	68.5 (154.8)	147.3 (332.9)	21.2 (47.9)
	303	142.6 (476.4)	200.9 (671.2)	42.5 (142.0)	210.6 (478.7)	56.8 (129.1)	250.6 (569.6)	68.5 (154.8)	186.7 (332.9)	25.9 (47.9)
	313	159.0 (531.2)	239.1 (798.8)	48.6 (162.4)	218.1 (495.8)	62.8 (142.8)	251.7 (572.1)	73.3 (165.6)	220.5 (498.3)	37.4 (84.5)
	323	164.0 (547.9)	267.5 (893.7)	51.5 (172.1)	227.6 (517.4)	65.6 (149.1)	290.6 (660.6)	164.0 (370.6)	270.8 (611.9)	51.8 (117)

J-SA isotherms for MB adsorption on GACNZR 1073 at different temperature are given in the Figure 5.36. As given in the Table 5.13, first phase change increases from 66.8 mg/g to 164.0mg/g. Second phase change increases from 118.0 mg/g to 270.8 mg/g and third phase changes from 18.2 mg/g to 51.77mg/g.

### 5.7 Comparison of Adsorption Isotherms for the Adsorption of Phenol, *p*-Nitrophenol and Methylene Blue on GACNZR 1073

In order to predict the design of single-stage batch adsorption systems we need to know the best fitted isotherm model. Figure 5.37 shows Langmuir, Freundlich, Dubinin-Radushkevich and John–Sivanandan Achari adsorption isotherms for the adsorption of phenol, *p*-nitrophenol and methylene blue on GACNZR 1073 by nonlinear analysis and corresponding equations for Freundlich, Langmuir, Dubinin-Radushkevich, and John–Sivanandan Achari isotherm is given in Table 5.14.

**Table 5.14:** The predicted non linear form of Freundlich, Langmuir, Dubinin-Radushkevich and John –Sivanandan Achari isotherm equations for GACNZR 1073

Isotherms	Phenol	<i>p</i> -nitrophenol	MB
Langmuir	$q_e = \frac{C_e \times 4.14}{1 + 0.0082 C_e}$	$q_e = \frac{C_e \times 12.45}{1 + 0.0214 C_e}$	$q_e = \frac{C_e \times 8.18}{1 + 0.0218 C_e}$
Freundlich	$q_e = 19.4 \times C_e^{0.456}$	$q_e = 72.98 \times C_e^{0.2910.306}$	$q_e = 57.37 \times C_e^{0.23290.271}$
*D-R	$q_e = 70.10 \times e^{-2.38 \varepsilon^2}$	$q_e = 103.9 \times e^{-0.0761 \varepsilon^2}$	$q_e = 77.27 \times e^{-0.0178 \varepsilon^2}$
*J-SA	$q_e = e^{\frac{\log \log C_e + 0.955}{0.5456}}$	$q_e = e^{\frac{\log \log C_e + 3.17}{1.33}}$	$q_e = e^{\frac{\log \log C_e + 1.79}{0.894}}$

\*D-R : Dubinin-Radushkevich    \*J-SA: John-Sivanandan Achari

Compared to all other isotherms Langmuir isotherm gives the best fit to experimental data for all the studied solid- liquid adsorption systems. Therefore, by comparison, order of the best fits isotherm for three sets of experimental data in this study is given as Langmuir > John –Sivanandan Achari > Freundlich > Dubinin –Radushkevich isotherms.

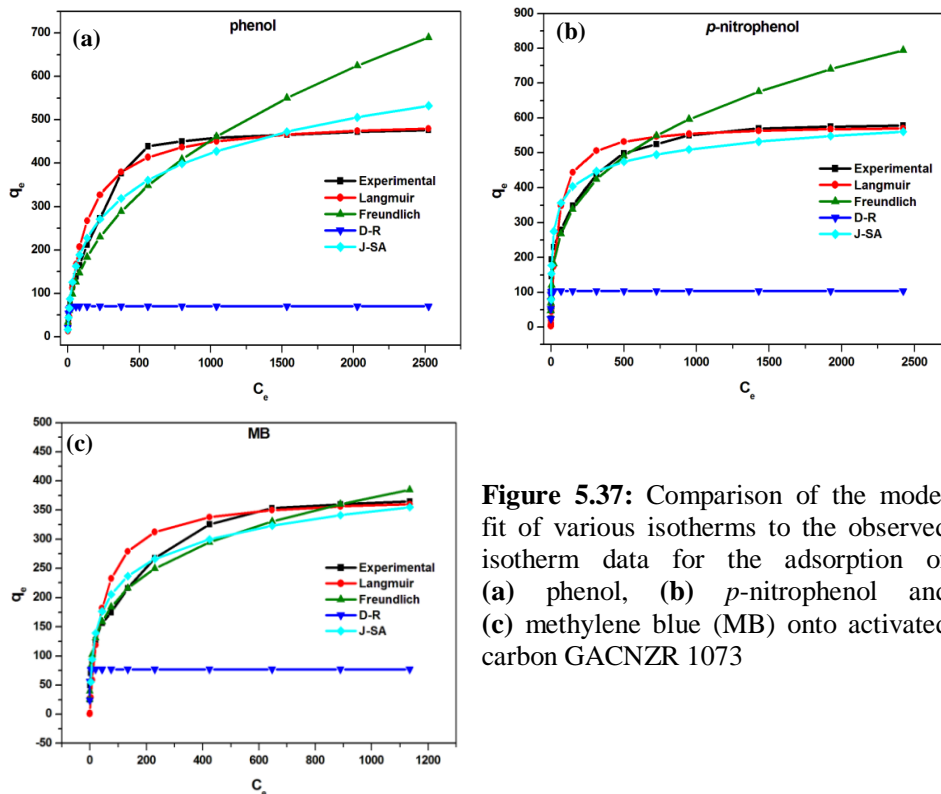


**Figure 5.37:** Comparison of the model fit of various isotherms to the observed isotherm data for the adsorption of (a) phenol, (b) *p*-nitrophenol and (c) methylene blue (MB) onto activated carbon GACNZR 1073

## 5.8 Adsorption Kinetic Studies

The adsorption kinetics data obtained from particular time interval for the initial concentration of  $C_0$  is 250 mg/L is applied in various kinetic models. The pseudo-first order and pseudo-second order equations are applied to investigate the controlling mechanism of adsorption processes such as mass transfer and chemical reaction. Intraparticle diffusion model is applied to predict the rate-limiting step in an adsorption process.

### 5.8.1 Kinetic Study of Phenol at Temperatures

The first order kinetic plots  $\log(q_e - q_t)$  versus  $t$  for phenol adsorption onto three adsorbents( GAC 383, GACO 383 and GACNZR 1073) at 283, 293, 303, 313 and 323 K temperatures are given in Figure 5.38 (a)–(c). Kinetic parameter

along with correlation co-efficient for pseudo -first order kinetic model is listed in the Table 5.15.

$$\log(q_e - q_t) = \log q_e - \frac{k_1 t}{2.303} \quad (5.17)$$

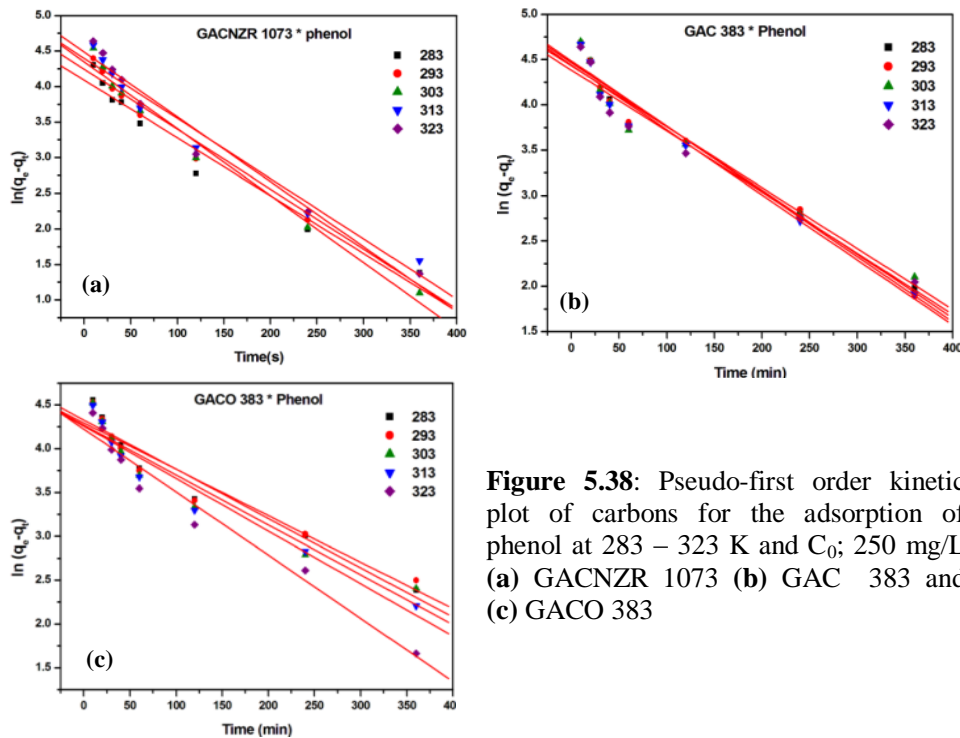


**Figure 5.38:** Pseudo-first order kinetic plot of carbons for the adsorption of phenol at 283 – 323 K and  $C_0$ ; 250 mg/L (a) GACNZR 1073 (b) GAC 383 and (c) GACO 383

It shows that data does not fit well with the whole range of contact time and is generally applicable over the initial stage of the adsorption processes.

Percentages of error calculated between the experimental  $q_e$  and calculated  $q_e$  for GACNZR 1073 at different solution temperature are given as; 283 K (47.6 %), 293 K (45.9 %), 303 K (43.5 %), 313 K (45 %), and 323 K (44.2 %). The high percentage error between the  $q_e$  value and lower correlation coefficient suggested that adsorption of phenol on this carbons is not following the pseudo-first order kinetics.

The second order kinetic plots of phenol adsorption onto three adsorbents GACNZR 1073, GAC 383, and GACO 383 at five different temperatures are given in Figure 5.39(a)-(c). Correlation co-efficient  $R^2$  and experimental equilibrium uptake,  $q_e$  obtained from pseudo second order kinetics is listed in the Table 5.15.

$$\frac{t}{q_t} = \frac{1}{k_2 q_e^2} + \frac{1}{q_e} t \quad (5.18)$$

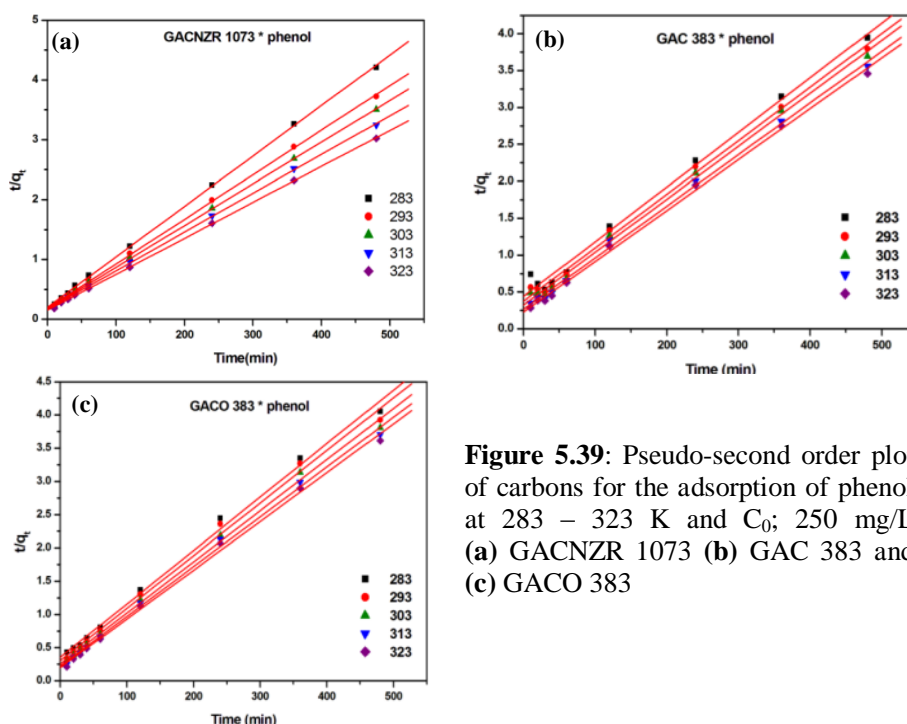


**Figure 5.39:** Pseudo-second order plot of carbons for the adsorption of phenol at 283 – 323 K and  $C_0$ ; 250 mg/L (a) GACNZR 1073 (b) GAC 383 and (c) GACO 383

Percentages of error calculated between the experimental  $q_e$  and calculated  $q_e$  value of GACNZR 1073 at different solution temperature are given as; 283 K (4.1 %), 293 K (3.3 %), 303 K (3.2 %), 313 K (2.4 %), and 323 K (2.3 %). Lower percentage error between the two  $q_e$  indicates that, experimental value and theoretical value are very close to each other and also the difference between these two values decreasing at high solution temperature. The  $R^2$  value close to unity suggests that kinetic data fitted well into pseudo second order kinetics equation. This confirms that adsorption of phenol on all these carbons following the pseudo second order kinetics [26, 27].

Intra particle diffusion plots of ( $q_t$  versus  $t^{1/2}$ ) phenol at five different temperatures are given in the Figure 5.40(a)-(c). From the slope and intercept of the plot, intra particle diffusion parameters  $K_{id1}$ ,  $K_{id2}$  and  $C$  are obtained, which is given in the Table 5.15.

$$q_t = k_{id} t^{1/2} + C \quad (5.19)$$

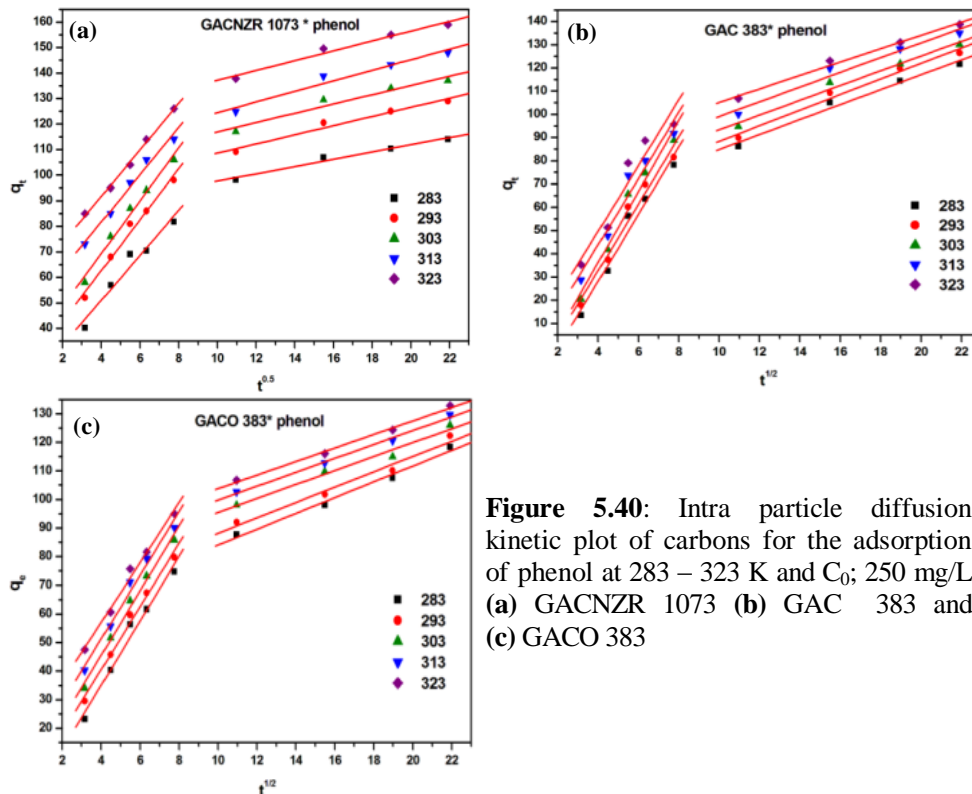


**Figure 5.40:** Intra particle diffusion kinetic plot of carbons for the adsorption of phenol at 283 – 323 K and  $C_0$ ; 250 mg/L (a) GACNZR 1073 (b) GAC 383 and (c) GACO 383

The adsorption data exhibit double linear plots, i.e. two steps influence the adsorption process. High concentration of phenol on the surface pushes the adsorbed particle from the surface through the pores (intraparticle diffusion) to the internal sites of the adsorbent [28].

The first linear portion is due to external resistance to mass transfer, which is significant only in the early stages of adsorption. The second linear portion is the gradual adsorption stage, which controlling intra-particle diffusion.

External mass transfer coefficients  $K_{id1}$  for GACNZR 1073 at different temperatures are given as; 283 K (8.84 mg/g min<sup>1/2</sup>), 293 K (9.99), 303 K (10.4), 313 K (9.28) and 323 K (9.13 mg/g min<sup>1/2</sup>). Whereas intraparticle diffusion coefficient  $K_{id2}$  at different solution temperatures are; 283 K (1.42 mg/g min<sup>1/2</sup>), 293 K (1.79), 303 K (1.81), 313 K (2.07), and 323 K (1.93 mg/g min<sup>1/2</sup>). Higher  $K_{id1}$  value compared to  $K_{id2}$  indicates that external mass transfer is more predominating than intra particle diffusion for the adsorption of phenol on GACNZR 1073. Smaller values of second linear portion compared to first (external mass transfer coefficient) indicate that there was very little intra-particle diffusion resistance because of the rigid pore structures of the GAC.

**Table 5.15:** Kinetic parameters of carbons GACNZR 1073, GAC 383, GACO 383 for the adsorption of phenol at temperatures ranging from 283 – 323 K [ $C_0 = 250$  mg/L]

Carbons	T (Kelvin)	$q_e$ (exp) mg/g	Pseudo first order kinetics			Pseudo second order kinetics			Intra particle diffusion					
			$q_e$ (cal) mg/g	$K_1 \times 10^4$ min <sup>-1</sup>	$R^2$	$q_e$ (cal) mg/g	$K_2 \times 10^5$ g mg <sup>-1</sup> min <sup>-1</sup>	$R^2$	$K_{id1}$ mg/g min <sup>1/2</sup>	$C_1$	$R^2$	$K_{id2}$ mg/g min <sup>1/2</sup>	$C_2$	$R^2$
GACNZR 1073	283	114	60	81	0.96	119	35	0.99	9	16	0.95	1.4	84	0.98
	293	129	70	84	0.98	133	36	0.99	10	23	0.98	1.8	91	0.97
	303	137	77	94	0.98	141	37	0.99	10	28	0.98	1.8	99	0.95
	313	148	81	85	0.97	152	37	0.99	9	45	0.98	2.1	104	0.96
	323	159	89	91	0.97	163	38	0.99	9	55	0.99	1.9	118	0.97
GAC383	283	122	87	71	0.96	135	12	0.99	14	-30	0.97	3.2	53	0.98
	293	126	89	72	0.97	138	14	0.99	14	-25	0.97	3.4	55	0.98
	303	130	84	67	0.95	140	16	0.99	15	-25	0.97	3.2	62	0.98
	313	135	85	72	0.96	143	18	0.99	14	-13	0.95	3.2	67	0.97
	323	139	80	67	0.95	145	21	0.99	14	-7	0.93	2.9	76	0.99
GACO383	283	118	76	56	0.94	125	18	0.99	11	-10	0.98	2.8	56	0.99
	293	122	73	53	0.93	126	21	0.99	11	-4	0.99	2.7	61	0.97
	303	126	71	57	0.93	130	23	0.99	11	0	0.99	2.4	71	0.98
	313	130	71	60	0.94	134	25	0.99	11	7	0.98	2.4	76	0.99
	323	133	69	61	0.95	136	27	0.99	10	15	0.99	2.4	80	0.99

### 5.8.2 Kinetic Study of *P*-Nitrophenol at Temperatures

The plot of the  $\log (q_e - q_t)$  as a function of  $t$  is given in the Figure 5.41(a)–(c), which provides  $K_1$  and  $q_e$  from slope and intercept. The kinetic parameters at various temperatures are given in Table 5.16.

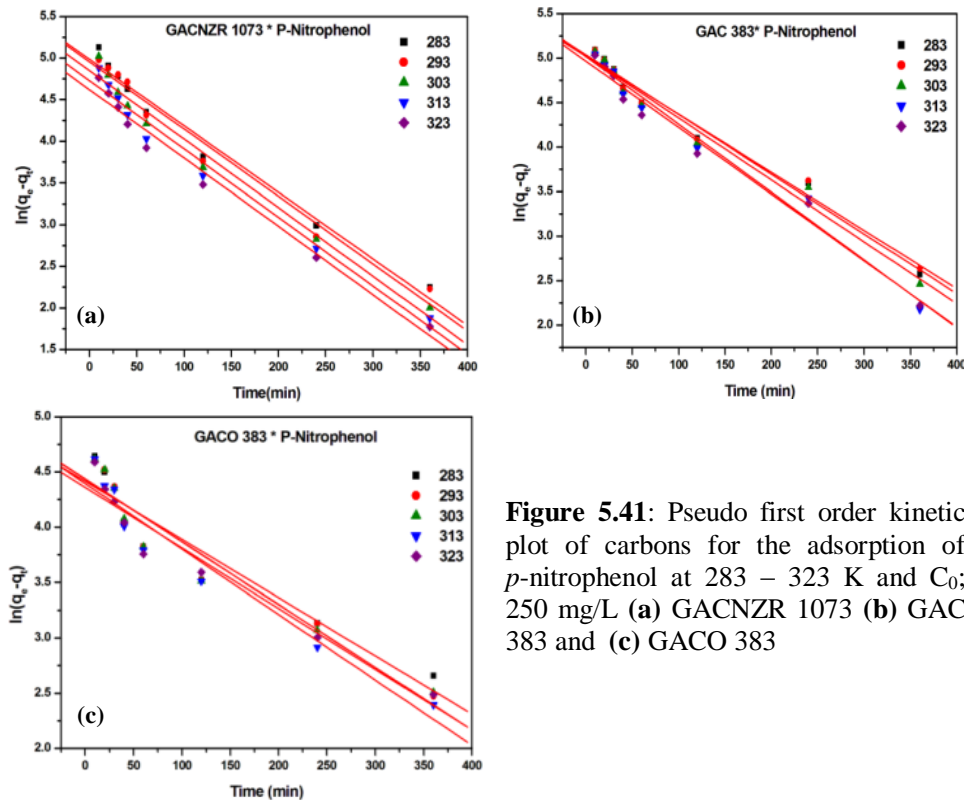


**Figure 5.41:** Pseudo first order kinetic plot of carbons for the adsorption of *p*-nitrophenol at 283 – 323 K and  $C_0$ ; 250 mg/L (a) GACNZR 1073 (b) GAC 383 and (c) GACO 383

Large deviation noticed between the experimental  $q_e$  (*exp*) and calculated  $q_e$  (*cal*) and the percentages of error between these two values for GACNZR 1073 is given as; at 283 K (29.7 %), 293 K (33.7 %), 303 K (42.05 %), 313 K (50.58 %), and 323 K (56.67 %). The high percentage error between the two values suggested poor fit of the data with the pseudo first order kinetic model.



The pseudo second order plots at various temperatures are given in Figure 5.42(a)-(c) and results are listed in the Table 5.16. The plots  $t/q_t$  versus  $t$  provided excellent linearity, which gives  $R^2 > 0.99$ .

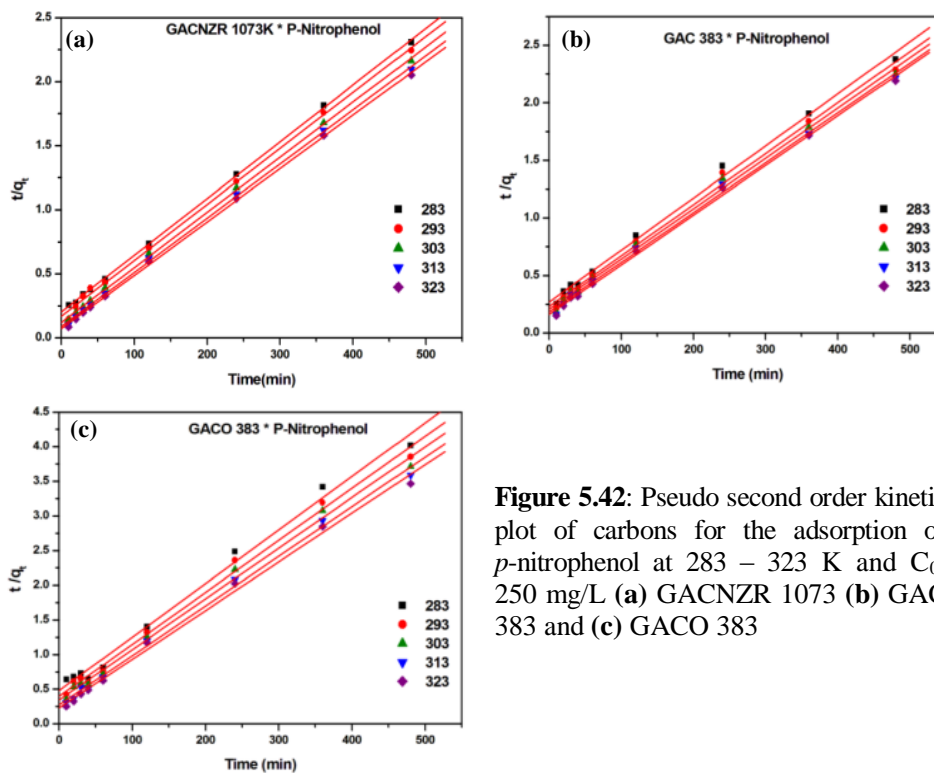


**Figure 5.42:** Pseudo second order kinetic plot of carbons for the adsorption of *p*-nitrophenol at 283 – 323 K and  $C_0$ ; 250 mg/L (a) GACNZR 1073 (b) GAC 383 and (c) GACO 383

The experimental  $q_e$  (*exp*) and calculated  $q_e$  (*cal*) values are comparable. Percentages of error calculated for GACNZR 1073 at a different solution temperature are: 283 K (8.75 %), 293 K (6.92 %), 303 K (5.73 %), 313 K (3.49 %) and 323 K (2.48 %). It indicates that the adsorption of *p*-nitrophenol by GACNZR 1073 is explained well by pseudo second order kinetics.

Intraparticle diffusion plot of  $q_t$  against  $t^{1/2}$  for the adsorption of *p*-nitrophenol on carbons are given in the Figure 5.43(a)-(c).

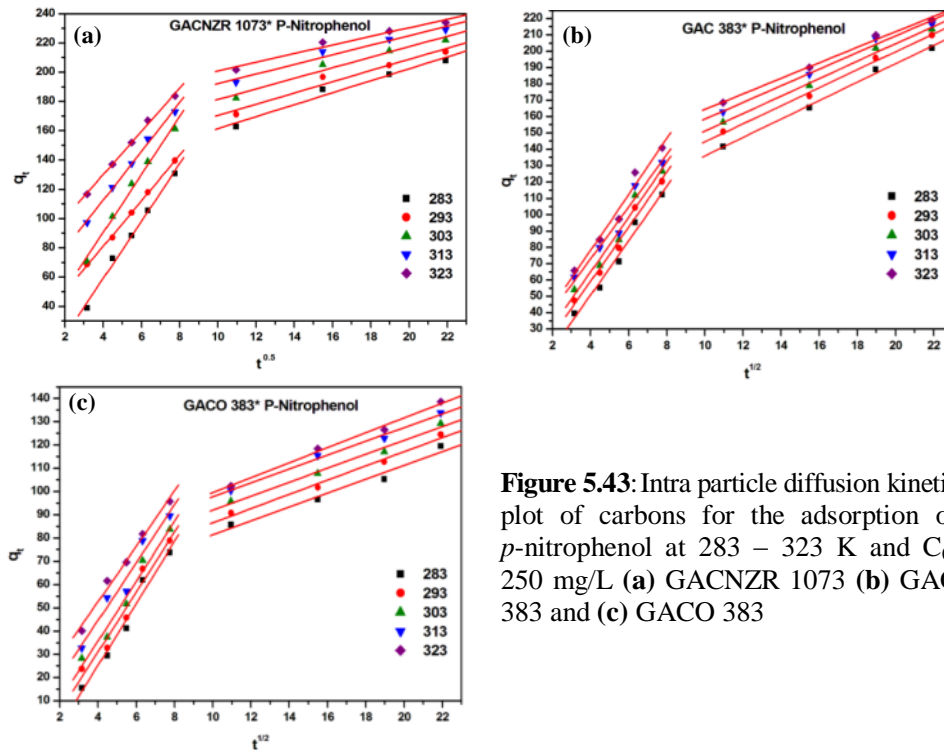


**Figure 5.43:** Intra particle diffusion kinetic plot of carbons for the adsorption of *p*-nitrophenol at 283 – 323 K and  $C_0$ ; 250 mg/L (a) GACNZR 1073 (b) GAC 383 and (c) GACO 383

The linear portion of the plot does not pass through the origin. This is due to the variation of mass transfer in the initial and final stage adsorption. Two linear portions are occurring in the plot. The first sharper portion due to external surface adsorption or instantaneous adsorption stage gives high  $K_{idl}$  for GACNZR 1073, which is given as 283 K (19.6 mg/g min<sup>1/2</sup>), 293 K (15.6), 303 K (15.6), 313 K (16.7) and 323 K (14.8 mg/g min<sup>1/2</sup>). The second portion is the gradual adsorption stage where the intra particle diffusion is rate-controlled and for GACNZR 1073 it is given as; at 283 K (4.09 mg/g min<sup>1/2</sup>), 293 K (3.83), 303 K (3.61), 313 K (3.27), and at 323 K (2.97 mg/g min<sup>1/2</sup>). High value of  $K_{idl}$  indicates that external mass transfer is more predominating than intra particle diffusion for the adsorption of *p*-nitrophenol on GACNZR 1073 [29].

**Table 5.16:** Kinetic parameters of carbons GACNZR 1073, GAC 383, GACO 383 for the adsorption of *p*-nitrophenol at temperatures ranging from 283 – 323 K. [C<sub>0</sub> = 250 mg/L]

Carbons	T ( Kelvin)	q <sub>e</sub> (exp) mg/g	Pseudo first order			Pseudo second order			Intra particle diffusion					
			q <sub>e</sub> (cal) (mg/g)	K <sub>1</sub> × 10 <sup>4</sup> min <sup>-1</sup>	R <sup>2</sup>	q <sub>e</sub> (cal) (mg/g)	K <sub>2</sub> × 10 <sup>5</sup> g mg <sup>-1</sup> min <sup>-1</sup>	R <sup>2</sup>	K <sub>ia1</sub> mg/g min <sup>1/2</sup>	C <sub>1</sub>	R <sup>2</sup>	K <sub>ia2</sub> mg/g min <sup>1/2</sup>	C <sub>2</sub>	R <sup>2</sup>
GACNZR 1073	283	208	146	80	0.98	226	10	0.99	20	-19	0.99	4.1	121	0.97
	293	214	142	98	0.98	229	11	0.99	16	19	0.99	3.8	132	0.96
	303	220	127	82	0.98	233	15	0.99	20	11	0.99	3.6	145	0.96
	313	229	113	82	0.98	237	20	0.99	17	46	0.99	3.3	160	0.96
	323	234	101	82	0.98	240	24	0.99	15	71	0.99	2.9	172	0.96
GAC 383	283	202	154	67	0.98	221	8	0.99	17	-16	0.98	5.6	80	0.99
	293	210	152	65	0.98	226	9	0.99	17	-8	0.98	5.1	89	0.99
	303	213	151	69	0.98	229	9	0.99	17	-2	0.97	5.3	98	0.99
	313	217	151	76	0.98	232	10	0.99	16	9	0.96	5.1	108	0.99
	323	219	143	75	0.98	232	12	0.99	17	10	0.97	4.8	117	0.99
GACO 383	283	120	83	53	0.91	130	12	0.99	13	-28	0.98	3.0	52	0.97
	293	125	85	57	0.93	133	14	0.99	13	-21	0.96	3.1	56	0.99
	303	129	84	57	0.93	137	16	0.99	13	-16	0.97	3.0	62	0.99
	313	134	81	59	0.94	140	19	0.99	12	-5	0.96	3.0	68	0.99
	323	139	78	55	0.94	143	21	0.99	12	5	0.99	3.2	67	0.99

### 5.8.3 Kinetic study of Methylene Blue (MB) at Temperatures

Pseudo first order equation by Lagergren is used for the adsorption of methylene blue ( $C_0 = 250$  mg/L) on new GAC.  $\log (q_e - q_t)$  versus  $t$  at 283, 293, 303, 313, and 323 K are shown in the Figure 5.44(a)-(c).

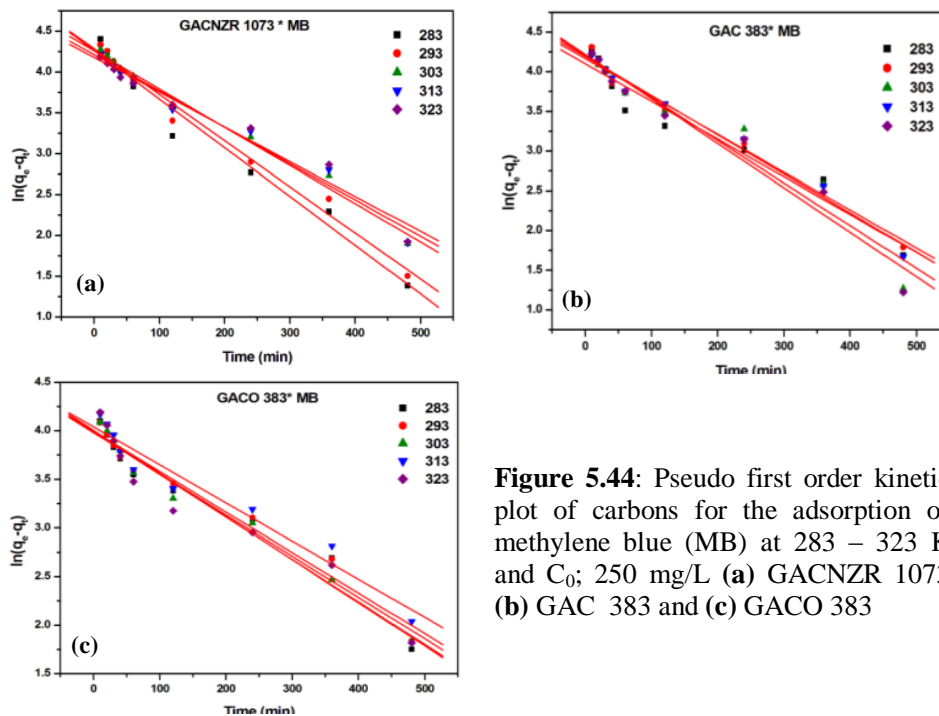


**Figure 5.44:** Pseudo first order kinetic plot of carbons for the adsorption of methylene blue (MB) at 283 – 323 K and  $C_0$ ; 250 mg/L (a) GACNZR 1073 (b) GAC 383 and (c) GACO 383

Intercept of the straight line plot should be equal to  $\log q_e$ . Percentages of error calculated between the experimental  $q_e$  and calculated  $q_e$  of GACNZR 1073 shows 36.63 – 58.29 % at 283 – 323 K. It indicates that reaction is not likely to be first order even the plot has high correlation co-efficient with experimental data.

The straight line plots of  $t/q_t$  versus  $t$  at five different temperatures are schematically represented in the Figure 5.45(a)-(c). Kinetic parameters are listed in the Table 5.17.

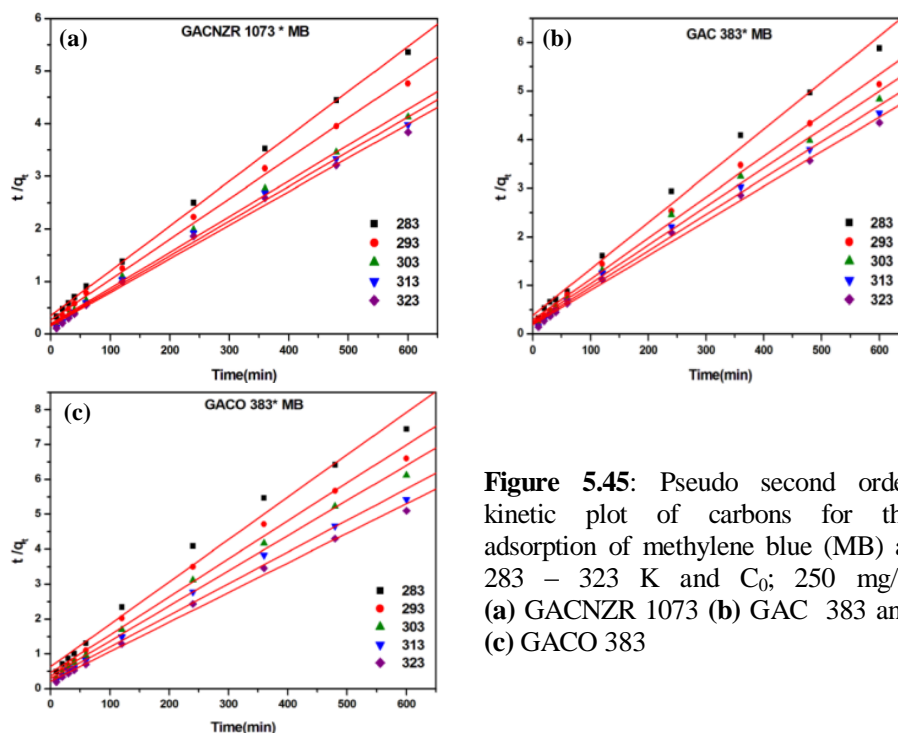


**Figure 5.45:** Pseudo second order kinetic plot of carbons for the adsorption of methylene blue (MB) at 283 – 323 K and  $C_0$ ; 250 mg/L (a) GACNZR 1073 (b) GAC 383 and (c) GACO 383

Percentages of error calculated between the experimental  $q_e$  and calculated  $q_e$  of GACNZR 1073 at 283 – 323K are given as; 283 K (4.64 %), 293 K (3.1 %), 303 K (1.03%), 313 K (0.3%), and 323 K (0 %). The equilibrium adsorbed capacities obtained from the slope of this plot are equal to the experimentally obtained equilibrium capacity, suggesting that system following pseudo second order kinetics. Variation of rate constant ( $K_2$ ) with solution temperature for GACNZR 1073 is given as; ( $20.8 \times 10^{-5}$  -  $27.1 \times 10^{-5}$  g/mg min<sup>-1</sup>), GAC 383 ( $24.2 \times 10^{-5}$  -  $27.3 \times 10^{-5}$  g/mg min<sup>-1</sup>) and GACO 383 ( $23.3 \times 10^{-5}$  -  $33.2 \times 10^{-5}$  g/mg min<sup>-1</sup>). Enhancement of  $K_2$  with the solution temperature indicates that the increment of temperature leads to a decrease of system viscosity thereby increasing the adsorption rate [30].

As seen from the Figure 5.46(a)–(c), the intra particle diffusion plot were not linear over the whole time range. It implies that more than one process affected the adsorption of methylene blue (MB) on GAC.

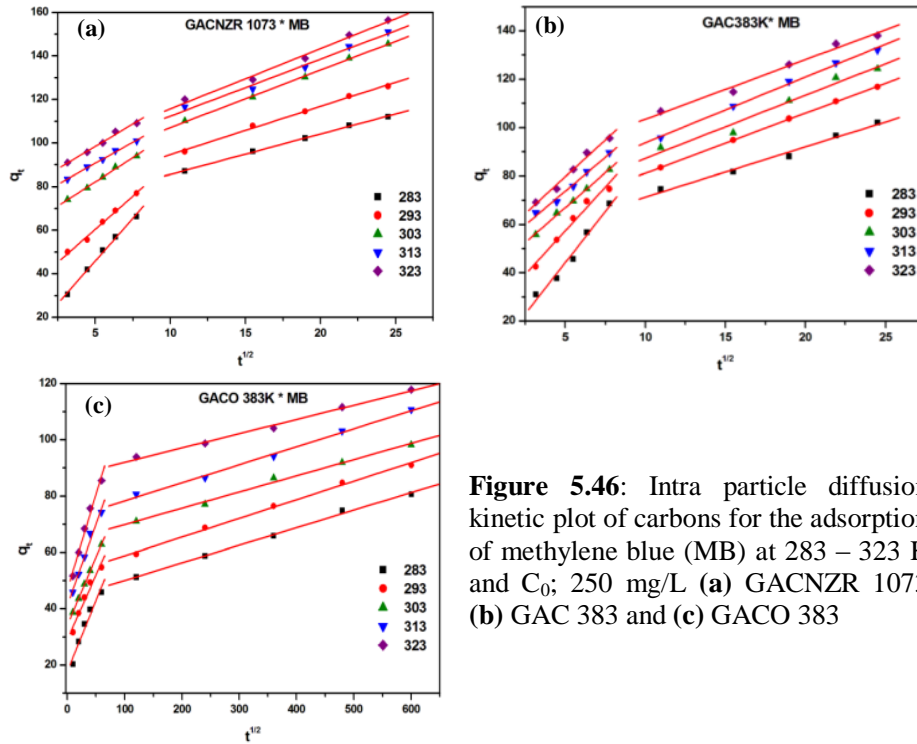


**Figure 5.46:** Intra particle diffusion kinetic plot of carbons for the adsorption of methylene blue (MB) at 283 – 323 K and  $C_0$ ; 250 mg/L (a) GACNZR 1073 (b) GAC 383 and (c) GACO 383

The double linear natures of these plots explain boundary layer diffusion and intra particle diffusion. On comparing the slope of two linear portions, shows that the first linear portion is generally greater than second linear portion. External mass transfer coefficient  $K_{id1}$  for GACNZR 1073 at various temperature is; 283 K (7.85 mg/g min<sup>1/2</sup>), 293 K (6.09), 303 K (4.44), 313 K (3.85) and 323K (4.13 mg/g min<sup>1/2</sup>). Intra particle diffusion coefficient  $K_{id2}$  is given as; 283K (1.85 mg/g min<sup>1/2</sup>), 293K (2.21), 303K (2.64), 313K (2.62), and 323K (2.76 mg/g min<sup>1/2</sup>). It corresponds to an enhanced diffusion of dye molecule from the exterior surface of adsorbent. It indicates that external mass transfer is more predominating than intra particle diffusion for the adsorption of methylene blue on GACNZR 1073.

**Table 5.17:** Kinetic parameters of carbons GACNZR 1073, GAC 383, GACO 383 for the adsorption of methylene blue at temperatures ranging from 283 – 323 K. [C<sub>0</sub> = 250 mg/L]

Carbons	Temperature (K)	q <sub>e</sub> (exp) mg/g	Pseudo first order			Pseudo second order			Intra particle diffusion					
			q <sub>e</sub> (cal) mg/g	K <sub>1</sub> × 10 <sup>4</sup> min <sup>-1</sup>	R <sup>2</sup>	q <sub>e</sub> (cal) mg/g	K <sub>2</sub> × 10 <sup>5</sup> g mg <sup>-1</sup> min <sup>-1</sup>	R <sup>2</sup>	K <sub>id1</sub> mg/g min <sup>1/2</sup>	C <sub>1</sub>	R <sup>2</sup>	K <sub>id2</sub> mg/g min <sup>1/2</sup>	C <sub>2</sub>	R <sup>2</sup>
GACNZR 1073	283	112	71	60	0.98	117	21	0.99	7.9	7	0.99	1.90	67	0.99
	293	126	73	56	0.99	130	23	0.99	6.1	30	0.99	2.20	73	0.99
	303	146	71	47	0.99	147	24	0.99	4.4	60	0.99	2.60	81	0.99
	313	151	67	45	0.98	152	26	0.99	3.9	71	0.99	2.60	86	0.99
	323	156	65	43	0.97	156	27	0.99	4.1	78	0.99	2.80	88	0.99
GAC 383	283	102	60	48	0.94	104	24	0.99	8.5	2	0.98	2.10	51	0.97
	293	117	64	48	0.98	119	25	0.99	7.2	21	0.97	2.50	56	0.99
	303	124	67	54	0.94	126	25	0.99	5.8	38	0.99	2.60	61	0.97
	313	132	66	49	0.98	134	26	0.99	5.6	46	0.99	2.70	67	0.99
	323	138	68	56	0.96	140	27	0.99	6.1	49	0.98	2.50	79	0.98
GACO 383	283	81	54	42	0.96	82	23	0.99	0.5	18	0.96	0.06	44	0.99
	293	91	54	42	0.97	92	26	0.99	0.5	29	0.96	0.07	52	0.99
	303	98	55	44	0.98	100	28	0.99	0.5	34	0.99	0.06	64	0.99
	313	111	57	39	0.95	110	28	0.99	0.6	41	0.98	0.06	72	0.99
	323	118	54	44	0.94	118	33	0.99	0.7	47	0.98	0.05	87	0.99

## 5.9 Thermodynamic Parameters

Thermodynamics analysis provides an insight into the energy changes that are associated with the process of adsorption.

$$\ln K_L = \frac{\Delta S}{R} - \frac{\Delta H}{RT} \quad (5.20)$$

Figure 5.47(a) indicates thermodynamic study for the adsorption of phenol on GACNZR 1073, GAC 383 and GACO 383. The thermodynamic parameters of

Gibbs free energy change  $\Delta G$ , enthalpy change  $\Delta H$ , and entropy change  $\Delta S$ , for the adsorption processes are calculated and are given in Table 5.18

**Table 5.18:** Thermodynamic parameters for adsorption of phenol onto carbons GAC 383, GACO 383 and GACNZR 1073

Carbon	$(\Delta H)$ kJ/mol	$(\Delta S)$ J/mol.K	$\Delta G$ (kJ/mol)				
			283K	293K	303K	313K	323K
GAC 383	2.33	15.32	-2.01	-2.16	-2.31	-2.47	-2.62
GACO 383	3.28	18.20	-1.87	-2.05	-2.23	-2.42	-2.60
GACNZR 1073	15.56	59.87	-1.38	-1.98	-2.58	-3.18	-3.78

Enthalpy change for GAC - phenol system is given as follows; GACNZR 1073 (15.56 kJ/mol), GAC 383 (2.33 kJ/mol) and GACO 383 (3.28 kJ/mol). Positive value of  $\Delta H$  indicates endothermic nature of adsorption and it is less than 40 kJ/mol, indicates physical adsorption for GAC-phenol systems. This enthalpy represents the interaction energy for the amount adsorbed on the adsorbent-adsorbate interface. The free energy change  $\Delta G$  obtained were negative, suggesting spontaneity of adsorption process. The high temperatures increase the entropy factor  $T\Delta S$  to a large extent hence  $\Delta G$  become more negative. The entropy change  $\Delta S$  for GAC is given as follows; GACNZR 1073 (59.87 J/mol. K), GAC 383 (15.32 J/mol. K) and GACO 383 (18.20 J/mol. K). Positive values of  $\Delta S$  suggest that the arrangement of the adsorbate in the solid-solution interface becomes more random. Higher  $\Delta S$  for surface modified carbons such as GACNZR 1073 and GACO 383 is inferred that more water molecules are displaced by phenol molecule with higher substitution degrees on the surface of these carbons [31].

Figure 5.47(b) indicates thermodynamic study for the adsorption of *p*-nitrophenol on GACNZR 1073, GAC 383 and GACO 383. The thermodynamic parameters of Gibbs free energy change  $\Delta G$ , enthalpy change  $\Delta H$ , and entropy change  $\Delta S$ , for the adsorption processes are calculated and given in Table 5.19.



**Table 5.19:** Thermodynamic parameters for adsorption of *p*-nitrophenol onto GAC 383, GACO 383 and GACNZR 1073

Carbons	$(\Delta H)$ kJ/mol	$(\Delta S)$ J/mol. K	$\Delta G$ (kJ/mol)				
			283K	293K	303K	313K	323K
GAC 383	6.04	38.22	-4.78	-5.16	-5.54	-5.92	-6.31
GACO 383	2.94	16.38	-1.70	-1.86	-2.02	-2.19	-2.35
GACNZR 1073	17.90	77.75	-4.10	-4.88	-5.66	-6.44	-7.21

Enthalpy change for GAC- *p*-nitrophenol system is given as follows; GACNZR 1073 (17.90 kJ/mol), GAC 383 (6.04 kJ/mol) and GACO 383 (2.94 kJ/mol). Enthalpy reflects the interaction between the *p*-nitrophenol with the granular activated carbons. Smaller value  $\Delta H$  for GAC modified with  $HNO_3$  corresponds to lower interaction between GACO 383 and *p*-nitrophenol.  $\Delta H$  for  $ZrO_2$  impregnated GAC (GACNZR 1073) is high related with high adsorptive capacity and extra physicochemical properties of GACNZR 1073 due to incorporated  $ZrO_2$ . Hence nano  $ZrO_2$  incorporated carbons have better material properties.

The free energy value ( $-\Delta G$ ) of GAC follows in the order of GACNZR 1073 > GAC 383 > GACO 383. This indicates that thermodynamic results are well agreement with adsorption capacity obtained from well known isotherm models. The high free energy change ( $-\Delta G$ ) obtained for *p*-nitrophenol adsorption indicates, there is more interaction between PNP and GAC and therefore more *p*-nitrophenol get adsorbed on GAC.

**Table 5.20:** Thermodynamic parameters for adsorption of methylene blue (MB) onto GAC 383, GACO 383 and GACNZR 1073

Carbon	$(\Delta H)$ kJ/mol	$(\Delta S)$ J/mol.K	$\Delta G$ (kJ/mol)				
			283K	293K	303K	313K	323K
GAC 383	6.87	35.60	-3.20	-3.56	-3.92	-4.27	-4.63
GACO 383	8.91	40.35	-2.51	-2.91	-3.32	-3.72	-4.12
GACNZR 1073	13.25	58.56	-3.32	-3.91	-4.49	-5.08	-5.66

Figure 5.47(c) indicates thermodynamic study for adsorption of methylene blue on GACNZR 1073, GAC 383 and GACO 383. The thermodynamic parameters

of Gibbs free energy change  $\Delta G$ , enthalpy change  $\Delta H$ , and entropy change  $\Delta S$ , for the adsorption processes are calculated and given in Table 5.20.

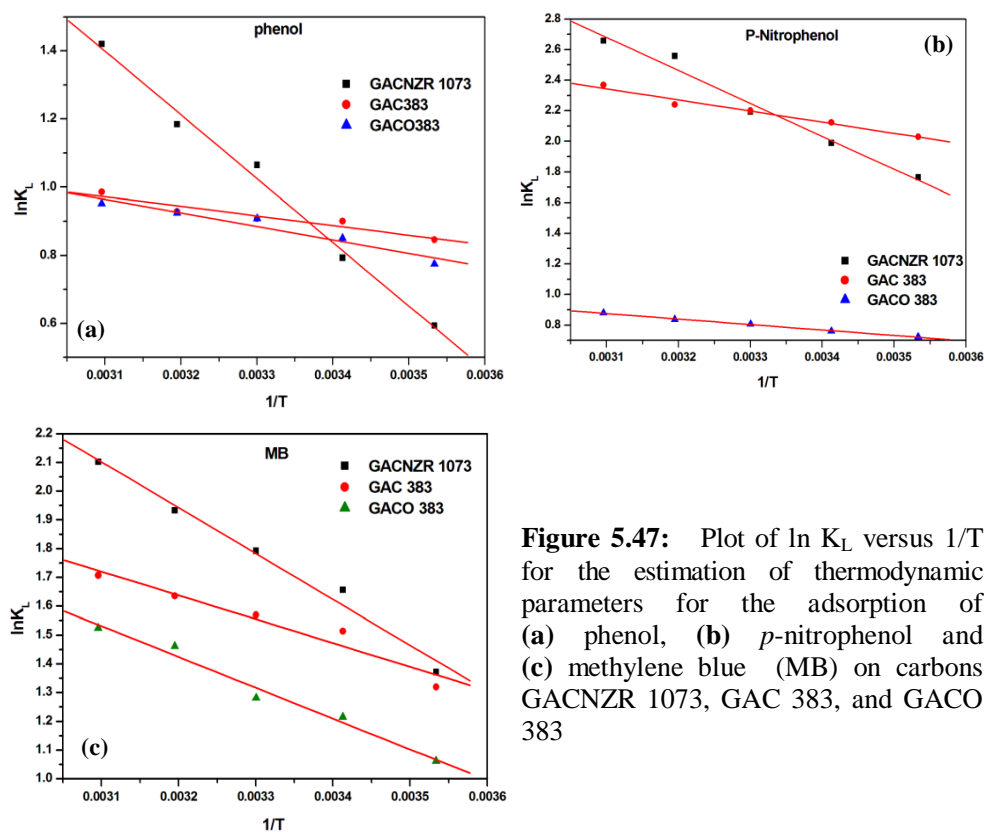


**Figure 5.47:** Plot of  $\ln K_L$  versus  $1/T$  for the estimation of thermodynamic parameters for the adsorption of (a) phenol, (b) *p*-nitrophenol and (c) methylene blue (MB) on carbons GACNZR 1073, GAC 383, and GACO 383

Enthalpy change for GAC - methylene blue system is given as follows; GACNZR 1073 (13.25 kJ/mol), GAC 383 (6.87 kJ/mol) and GACO 383 (8.91 kJ/mol). Positive value of  $\Delta H$  indicates endothermic nature of adsorption and further indicates physical adsorption for GAC- MB systems.  $\Delta G$  value is consistently negative at all temperatures measured, which revealed the adsorption process was feasible and spontaneous in nature.

The entropy change  $\Delta S$  corresponds to the movement of  $H_2O$  molecule adsorbed by adsorbate. High positive value of  $\Delta S$  for GACNZR 1073 (58.56

J/mol.K) indicate that more water molecule is displaced by methylene blue molecule from the surface of carbon.

### 5.9.1 Thermodynamic Parameters from Distribution Coefficient

Relation between distribution coefficients  $K_D$  and solution temperatures are given by the equation

$$\ln K_D = \frac{\Delta S}{R} - \frac{\Delta H}{RT} \quad (5.21)$$

$$\text{where } K_D = \frac{C_o - C_e}{C_e} \quad (5.22)$$

Equation indicates that distribution coefficient not only depends on adsorbed concentration, but also depends on temperature of solution. Distribution coefficient is decreased with increasing the concentration of adsorbate in aqueous solution, whereas increases with rise of the solution temperature.

**Table 5.21:** Thermodynamic parameters obtained from plot of  $\ln K_D$  versus  $1/T$  for the adsorption of phenol on GACNZR 1073

$C_0$ mg/L	$\Delta S$ J/mol.K	$\Delta H$ kJ/mol	$\Delta G$ kJ/mol				
			283K	293K	303K	313K	323K
25	52.3	11.9	-2.9	-3.4	-3.9	-4.4	-4.9
50	52.7	12.4	-2.6	-3.1	-3.6	-4.1	-4.7
75	53.2	12.8	-2.3	-2.8	-3.4	-3.9	-4.4
100	53.1	13.2	-1.9	-2.4	-2.9	-3.5	-4.0
150	51.4	13.5	-1.0	-1.5	-2.1	-2.6	-3.1
200	50.4	14.1	-0.2	-0.7	-1.2	-1.7	-2.2
250	49.6	14.3	0.3	-0.2	-0.7	-1.2	-1.7
350	48.8	14.5	0.7	0.2	-0.3	-0.7	-1.2
500	47.9	14.9	1.4	0.9	0.4	-0.1	-0.5
750	47.3	15.3	2.0	1.5	1.0	0.5	0.1
1000	45.6	15.4	2.5	2.1	1.6	1.2	0.7

Thermodynamic parameters obtained from the distribution co-efficient for the adsorption of phenol is given in Table 5.21. Negative values of  $\Delta G$  shows that the adsorption of phenol on GACNZR 1073 is spontaneous. The  $\Delta H$  calculated was positive, indicates that the adsorption of phenol is favoured at higher

temperatures. The  $\Delta H$  increased with an increase in the initial concentration of phenol solution. The variation of  $\Delta H$  in a range of concentration 25 – 1000 mg/L for phenol is given as; GACNZR 1073 (11.9 – 15.4 kJ/mol). Smaller values of  $\Delta H$  indicate the loose bonding between the adsorbate molecules (phenol) and the adsorbent (GACNZR 1073) surface [32]. The entropy change ( $\Delta S$ ) is also calculated for phenol adsorption on new carbons. For GACNZR 1073 the entropy change is found to be in the range of 45.57 - 52.28 J/mol. K. These are most likely to be due to structural changes occurred to the adsorbate as well as to the adsorbent [33].

**Table 5.22:** Thermodynamic parameters obtained from plot of  $\ln K_D$  versus  $1/T$  for the adsorption of *p*-nitrophenol on GACNZR 1073

C <sub>0</sub> mg/L	$\Delta S$ J/mol.K	$\Delta H$ kJ/mol	$\Delta G$ kJ/mol				
			283K	293K	303K	313K	323K
25	79.5	13.2	-9.3	-10.1	-10.9	-11.6	-12.4
50	79.5	13.3	-9.2	-10.0	-10.8	-11.6	-12.4
75	78.2	13.4	-8.7	-9.5	-10.3	-11.1	-11.8
100	75.5	13.6	-7.7	-8.5	-9.3	-10.0	-10.8
150	73.1	13.9	-6.8	-7.5	-8.2	-9.0	-9.7
200	73.6	14.1	-6.7	-7.4	-8.2	-8.9	-9.6
250	65.0	14.5	-3.9	-4.5	-5.2	-5.8	-6.5
350	57.9	15.0	-1.4	-2.0	-2.6	-3.1	-3.7
500	53.6	15.1	0.0	-0.6	-1.1	-1.7	-2.2
750	51.0	15.5	1.1	0.6	0.1	-0.4	-1.0
1000	48.2	15.6	1.9	1.4	1.0	0.5	0.0

Thermodynamic parameters obtained from the distribution co-efficient for the adsorption of *p*-nitrophenol is given in Table 5.22. The variation of  $\Delta H$  in the range of concentrations 25 – 1000 mg/L for *p*- nitrophenol adsorption on GACNZR 1073 is 13.2 – 15.6 kJ/mol, positive value suggests an endothermic reaction mechanism.  $\Delta H$  increases with solute concentration in solution. For GACNZR 1073 the  $\Delta H$  shows highest value compared with GAC 383 (9 - 11 kJ/mol) and GACO 383 (4 - 5 kJ/mol). The entropy change  $\Delta S$  decreases with increase of concentration of *p*-nitrophenol. The change in entropy for *p*-nitrophenol adsorption on GACNZR 1073 is 79.5 – 48.2 J/mol.K. It reflects an increase in randomness at the solid/solution interface during the *p*- nitrophenol adsorption.

The change in free energy for *p*-nitrophenol adsorption is more negative at lower concentrations and at high solution temperature, it suggests an endothermic reaction.

**Table 5.23:** Thermodynamic parameters obtained from plot of  $\ln K_D$  versus  $1/T$  for the adsorption of methylene blue (MB) on GACNZR 1073

$C_0$ mg/L	$\Delta S$ J/mol.K	$\Delta H$ kJ/mol	$\Delta G$ kJ/mol				
			283	293	303	313	323
25	124.0	23.6	-11.5	-12.8	-14.0	-15.3	-16.5
50	114.9	23.0	-9.5	-10.6	-11.8	-12.9	-14.1
75	90.8	21.5	-4.2	-5.1	-6.0	-6.9	-7.8
100	84.4	20.9	-3.0	-3.8	-4.7	-5.5	-6.4
150	76.1	19.8	-1.7	-2.5	-3.2	-4.0	-4.7
200	67.9	18.5	-0.7	-1.4	-2.1	-2.7	-3.4
250	62.3	17.8	0.2	-0.4	-1.1	-1.7	-2.3
350	58.1	17.5	1.0	0.4	-0.1	-0.7	-1.3
500	53.7	16.9	1.7	1.2	0.6	0.1	-0.4
750	49.6	16.7	2.7	2.2	1.7	1.2	0.7
1000	46.7	16.7	3.5	3.0	2.6	2.1	1.6

Thermodynamic parameters obtained from the distribution co-efficient for the adsorption of methylene blue is given in Table 5.23. The positive value of  $\Delta H$  shows that the adsorption of methylene blue on GACNZR 1073 is an endothermic process. The variation of  $\Delta H$  for GACNZR 1073 at range of concentration 25 – 1000 mg/L for MB is given as 23.6 – 16.7 kJ/mol. The  $\Delta H$  decreases with increase in the concentration of solute. The values of  $\Delta H$  are high enough to ensure strong interaction between the MB and the GACNZR 1073. The  $\Delta S$  shows the same behaviour as that of  $\Delta H$ , it also decreases with increasing concentration of MB and shows high value for GACNZR 1073 (23.56-16.70 J/ mol. K). High value of  $\Delta S$  compared to basic carbon GAC 383 and GACO 383 indicate higher affinity of GACNZR 1073 towards methylene blue. Positive value of  $\Delta S$  clearly states that the randomness increased at the solid–solution interface during the MB adsorption onto the GACNZR 1073. The change in free energy ( $\Delta G$ ) for MB adsorption at lower concentrations was negative and shows an endothermic reaction. The increase in adsorption capacity of GACNZR 1073 at higher temperatures may be caused by the enlargement of pore size and/or activation of the adsorbent surface.

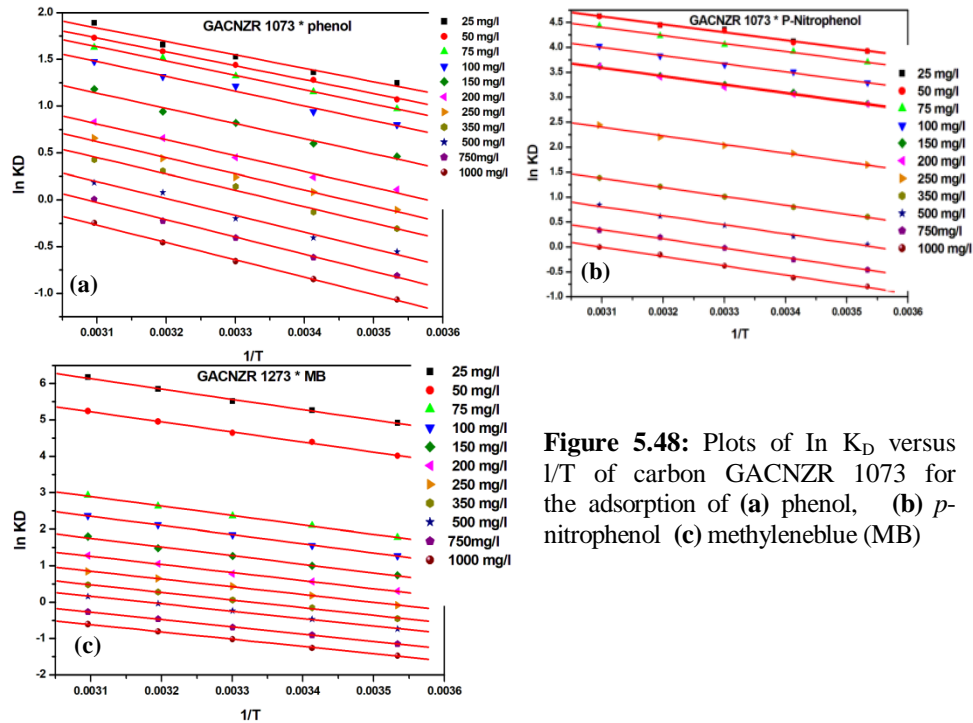


**Figure 5.48:** Plots of  $\ln K_D$  versus  $1/T$  of carbon GACNZR 1073 for the adsorption of (a) phenol, (b) *p*-nitrophenol (c) methyleneblue (MB)

## 5.10 Diffusion Coefficient

Diffusion coefficient for the adsorption of phenol, *p*-nitrophenol and methylene blue (MB) on GAC 383, GACO 383 and GACNZR 1073 are calculated and discussed in the following sections.

### 5.10.1 Determination of Diffusivity for Phenol on GACNZR 1073, GAC 383 and GACO 383

The diffusion coefficient for the adsorption of phenol on GACNZR 1073, GAC 383 and GACO 383 are determined from the linear plot of  $\ln [1/(1-F^2)]$  versus  $t$  which is given in the Figure 5.49 (a)-(c) and values are listed in the Table 5.24.

The effective diffusivity was found to be rather low; usually it is in the order of  $10^{-10}$   $\text{m}^2/\text{s}$ . The low value was explained on the basis of restriction of pore accessibility associated with small pores.

$$\ln \left[ \frac{1}{1 - F^2(t)} \right] = \frac{\pi^2 D_e t}{R_a^2} \quad (5.23)$$

Adsorbent-adsorbate interactions and competition change the diffusivity of each component and alter its sorption energy, leading to changes in adsorption capacities.

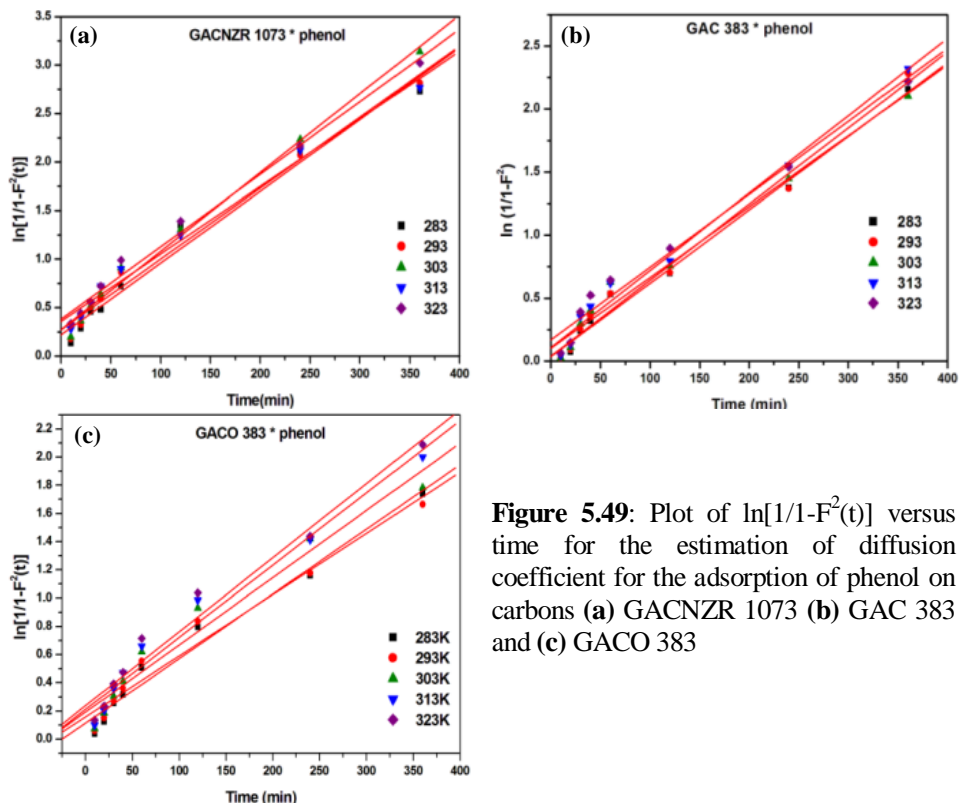
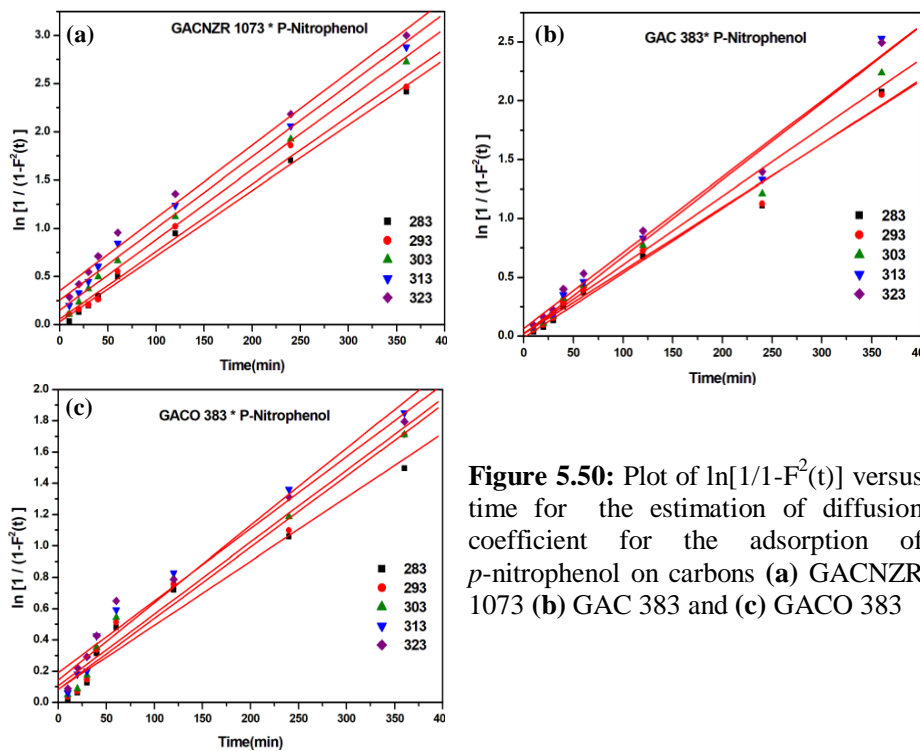


Figure 5.49: Plot of  $\ln[1/(1-F^2(t))]$  versus time for the estimation of diffusion coefficient for the adsorption of phenol on carbons (a) GACNZR 1073 (b) GAC 383 and (c) GACO 383

Diffusion coefficient ( $D_e$ ) of GACNZR 1073 for the adsorption of phenol at different solution temperature are given as; at 283 K ( $2.07 \times 10^{-10} \text{ m}^2/\text{s}$ ), 293 K ( $2.04 \times 10^{-10}$ ), 303 K ( $2.27 \times 10^{-10}$ ), 313 K ( $1.95 \times 10^{-10}$ ) and at 323 K ( $2.09 \times 10^{-10}$ ). The effective diffusion coefficient of GACNZR 1073 is found to be greater than the GAC 383 and GACO 383. This indicates that diffusion of phenol within the pores of wider width and the electrostatic interaction on the surface of GAC increases with  $\text{ZrO}_2$  impregnation and activation at 1073K.

### 5.10.2 Determination of Diffusivity for *p*-Nitrophenol on GACNZR 1073, GAC 383 and GACO 383

The diffusion coefficient for the adsorption of *p*-nitrophenol on GACNZR 1073, GAC 383 and GACO 383 are determined from the linear plot of  $\ln [1/(1-F^2(t))]$  versus  $t$  which is given in the Figure 5.50(a)-(c) and values are listed in the Table 5.24.



**Figure 5.50:** Plot of  $\ln[1/(1-F^2(t))]$  versus time for the estimation of diffusion coefficient for the adsorption of *p*-nitrophenol on carbons (a) GACNZR 1073 (b) GAC 383 and (c) GACO 383

Diffusion coefficient ( $D_e$ ) value of GACNZR 1073 for the adsorption of *p*-nitrophenol at different solution temperature are given as; at 283 K ( $1.90 \times 10^{-10}$ ), 293 K ( $1.96 \times 10^{-10}$ ), 303 K ( $2.04 \times 10^{-10}$ ), 313 K ( $2.08 \times 10^{-10}$ ) and 323 K ( $2.11 \times 10^{-10}$ ). Higher  $D_e$  value of GACNZR 1073 compared to GAC 383 and GACO 383 indicate that it experience lower film and intraparticle resistance. Thus *p*-nitrophenol molecule can diffuse much faster inside the pores of granular activated carbon. Diffusion rate of *p*-nitrophenol within the pores of GAC is enhanced by increasing the solution temperature. Therefore the mobility of



*p*-nitrophenol from solution to solid surface is fast, hence more molecule get diffused into the pores [34].

### 5.10.3 Determination of Diffusivity for Methylene Blue on GACNZR 1073, GAC 383 and GACO 383

The diffusion coefficient for the adsorption of methylene blue on GACNZR 1073, GAC 383 and GACO 383 are determined from the linear plot of  $\ln [1/(1-F^2(t))]$  versus  $t$  which is given in the Figure 5.51 (a)-(c) and values are listed in the Table 5.24.

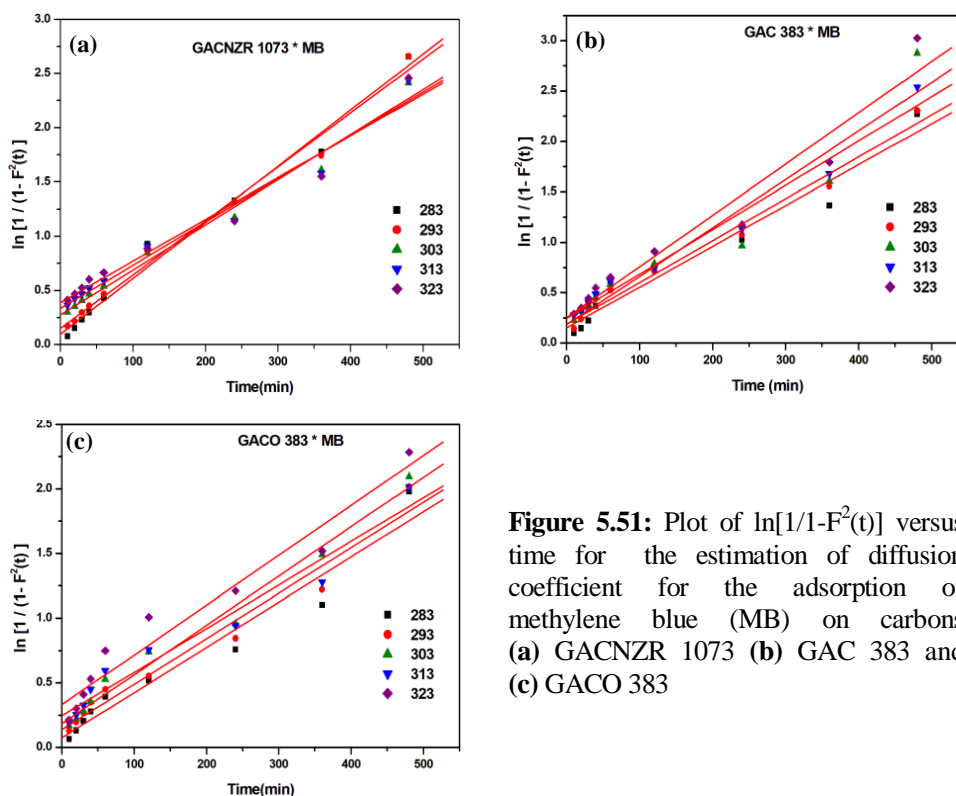


**Figure 5.51:** Plot of  $\ln[1/(1-F^2(t))]$  versus time for the estimation of diffusion coefficient for the adsorption of methylene blue (MB) on carbons (a) GACNZR 1073 (b) GAC 383 and (c) GACO 383

Effective diffusion coefficient is decreased as the molecular size of the adsorbate is large and it exerts large resistivity to enter into the small pores.  $D_e$  value for GACNZR 1073 ranged from  $1.44 \times 10^{-10}$  to  $1.07 \times 10^{-10}$  which shows that  $D_e$  only varied in a limited extent with increasing the solution temperature from 283 – 323 K. The internal pores play a significant role in the high adsorption

capacity, but this result cannot be used to explain the diffusion of organic macromolecules (such as methylene blue) onto pores. Methylene blue cations cannot enter the small micropores of GAC and the major adsorption occurs on the mesopores or external surface.

**Table 5.24:** Effective diffusion coefficient of carbon samples on phenol, *p*-nitrophenol and methylene blue (MB)

Carbons	T (K)	Phenol		<i>p</i> -nitrophenol		Methylene blue	
		$D_e \times 10^{10}$ m <sup>2</sup> /s	R <sup>2</sup>	$D_e \times 10^{10}$ m <sup>2</sup> /s	R	$D_e \times 10^{10}$ m <sup>2</sup> /s	R
GACNZR 1073	283	2.07	0.978	1.90	0.996	1.44	0.994
	293	2.04	0.986	1.96	0.990	1.39	0.993
	303	2.27	0.992	2.04	0.994	1.16	0.998
	313	1.95	0.986	2.09	0.990	1.12	0.999
	323	2.09	0.990	2.11	0.990	1.07	0.995
GAC 383	283	1.63	0.988	1.53	0.984	1.13	0.992
	293	1.69	0.986	1.50	0.984	1.16	0.992
	303	1.57	0.980	1.63	0.982	1.34	0.991
	313	1.71	0.986	1.83	0.980	1.23	0.990
	323	1.62	0.978	1.80	0.984	0.25	0.992
GACO 383	283	1.28	0.976	1.14	0.958	0.98	0.979
	293	1.21	0.964	1.27	0.968	0.98	0.984
	303	1.33	0.958	1.28	0.968	1.07	0.984
	313	1.43	0.970	1.38	0.974	0.94	0.987
	323	1.47	0.970	1.29	0.972	1.08	0.986

### 5.11 Activation Energy

Arrhenius plot of rate constant ( $\ln K_2$ ) versus reciprocal of temperature ( $1/T$ ) for the adsorption of phenol on GACNZR 1073, GAC 383, GACO 383 are given in the Figure 5.52(a). The activation energy  $E_a$  and pre-exponential factors,  $A$ , obtained is given in Table 5.25. Activation energy parameters for the adsorption of the phenol, *p*-nitrophenol and MB on GAC can be obtained from the following relation.

$$\ln K_2 = \ln A - \frac{E_a}{RT} \quad (5.24)$$

For all the three carbons, a plot of  $\ln K_2$  against the reciprocal of absolute temperature  $1/T$ , gives straight lines and the corresponding  $E_a$ , were determined from the slope of each linear plot.

The result obtained for activation energy for the adsorption of phenol on GAC follows as: GAC 383 - 9.95 kJ/mol, GACO 383 - 7.59 kJ/mol and GACNZR 1073 - 1.30 kJ/mol. The obtained value of activation energy confirms the nature of physisorption processes of phenol onto these carbons.

Activation energy of GAC 383, GACO 383 and GACNZR 1073 for the adsorption of *p*-nitrophenol is obtained from the slope of linear relationship between  $\ln K_2$  and  $1/T$  (Figure 5.52(b)). The minimum energy required to initiate the adsorption of *p*-nitrophenol on GACNZR 1073 is higher than that of GAC 383 and GACO 383. The activation energy for the adsorption of *p*-nitrophenol on GAC is given as; GAC 383 (7.71 kJ/mol), GACO 383 (10.33 kJ/mol) and GACNZR 1073 (18.37 kJ/mol) respectively.

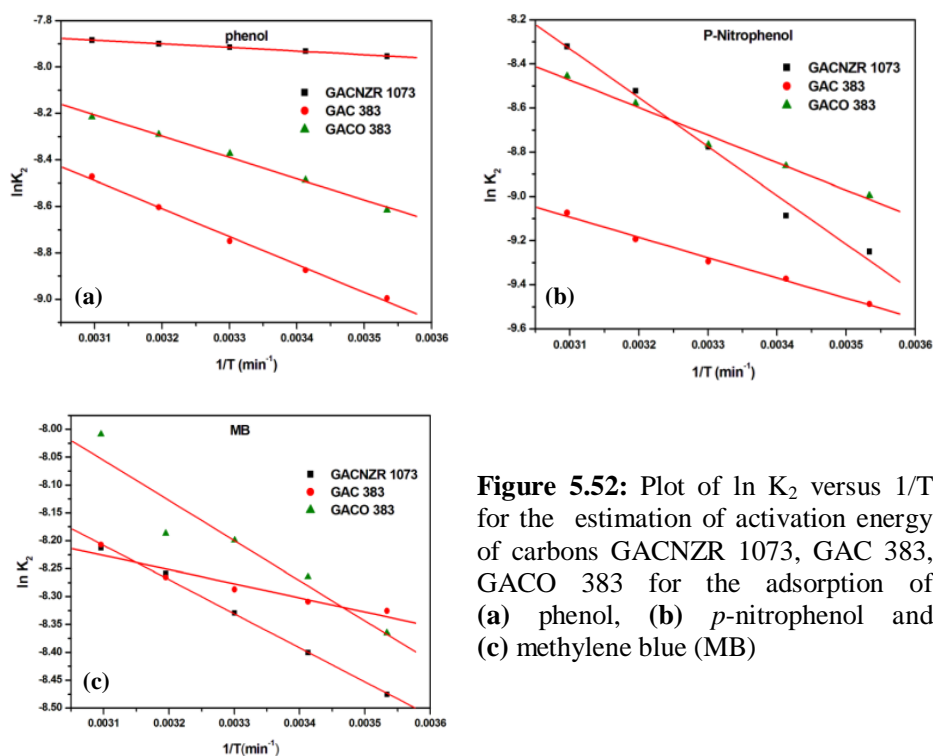


**Figure 5.52:** Plot of  $\ln K_2$  versus  $1/T$  for the estimation of activation energy of carbons GACNZR 1073, GAC 383, GACO 383 for the adsorption of (a) phenol, (b) *p*-nitrophenol and (c) methylene blue (MB)

The activation energy for the adsorption of MB on GAC is given as; GAC 383 (2.14 kJ/mol), GACO 383 (7.59 kJ/mol) and GACNZR 1073 (5.08 kJ/mol). Small activation energy indicates that, the rate is controlled by film diffusion mechanism and more MB molecule can adsorb on the surface of carbon.

**Table 5.25:** Activation energy obtained from Arrhenius equation

Carbon	phenol		<i>p</i> -nitrophenol		methylene blue	
	$E_a$ kJ/mol	$A \times 10^4$	$E_a$ kJ/mol	A	$E_a$ kJ/mol	$A \times 10^4$
GAC 383	9.95	84.0	7.71	0.001995	2.14	5.95
GACO 383	7.59	46.3	10.33	9.84E-07	7.59	46.22
GACNZR 1073	1.30	6.1	18.37	0.2272	5.08	18.12

## 5.12 Design of Batch Adsorption from Isotherm Data

Best fitted isotherm model can be used to predict the design of single stage batch adsorption system. From this design we can calculate the amount of carbon required to treat different concentration of phenol, *p*-nitrophenol and methylene blue in one litre of solutions.

$$\frac{M}{V} = \frac{C_0 - C_e}{q_e} = \frac{C_0 - C_e}{\frac{q_0 K_L C_e}{1 + K_L C_e}} \quad (5.25)$$

The required amount of GAC to reduce 99 % of the phenol content (various concentrations) in one litre of solution is well represented in the Figure 5.53(a). For treating one litre of solution containing 3000 mg/L phenol, the required masses of GAC is given as; GACNZR 1073 - 7.4 g, GAC 383 – 11.7 g and GACO 383 – 17.5 g. Similarly, for treating different concentration of phenol in aqueous solution phase different weight of carbon is required. On comparing the efficiency of GACNZR 1073 for treating phenol we can see that, 57.6 – 59.2 % more weight of GAC 383 and 2 times more weight of GACO 383 is needed.

The required amount of GAC to reduce 99 % of the *p*-nitrophenol content (various concentrations) in one litre of solution is well represented in the Figure 5.53(b). It shows that amount of weight required for treating the same concentrations of adsorbate solution vary for different carbon. For treating one litre of solution

containing 3000 mg/L *p*-nitrophenol, the required masses of GAC is given as; GACNZR 1073 (5.57 g), GAC 383 (8.13 g) and GACO 383 (17.3g). Compared to GACNZR 1073, carbon GAC 383 requires 45.6 – 46.9 % more weight and GACO 383 requires more than 3 times weight are needed.

The required amount of GAC to reduce 99% of methylene blue (various concentrations) in one litre of solution is well represented in the Figure 5.53(c). For the MB treatment the amount of GAC 383 and GACO 383 needs more than two times of weight compared to GACNZR 1073.

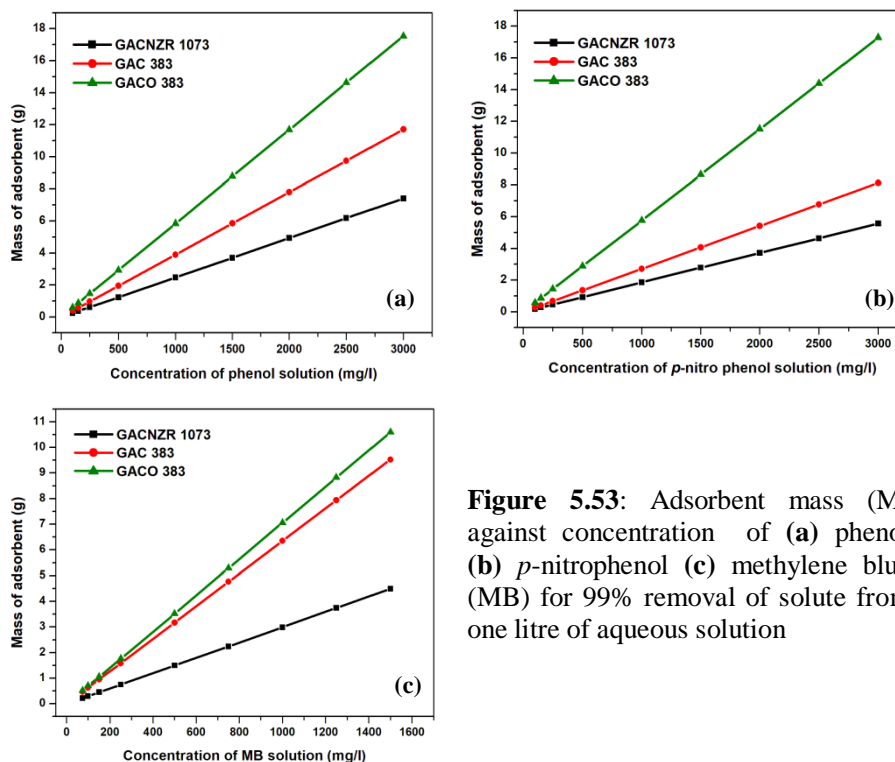


**Figure 5.53:** Adsorbent mass (M) against concentration of (a) phenol (b) *p*-nitrophenol (c) methylene blue (MB) for 99% removal of solute from one litre of aqueous solution

### 5.13 Adsorption of Trace Metal Ions by GACNZR Using Contaminated Groundwater

Groundwater collected from a contaminated area, whose initial parameters are known is used to study adsorption efficiency of carbons towards trace metal ions. Adsorption experiments were performed by batch experiments using field groundwater with 8 hours of contact time

Percentage recoveries of elements from solution with respect to their initial concentrations are listed in the Table 5.26.

**Table 5.26:** Efficiency of carbons GAC 383, GACO 383 and GACNZR 1073 for removing trace elements in ground water

Trace metals	Initial concentration (ppb)	Concentration after adsorption (ppb)		
		GACNZR 1073	GAC 383	GACO 383
<sup>7</sup> Li	4.5 (% Removal)	3.45 (21.6)	4.29 (4.7)	3.83 (14.9)
<sup>9</sup> Be	0.22 (% Removal)	ND (100.0)	0.01 (95.5)	ND (100.0)
<sup>24</sup> Mg	2905.63 (% Removal)	2453.54 (15.6)	2802.3 (3.6)	2395.43 (17.6)
<sup>27</sup> Al	257.22 (% Removal)	6.2 (97.6)	2.84 (98.9)	2.18 (99.2)
<sup>52</sup> Cr	1.5 (% Removal)	0.2 (46.7)	0.92 (38.7)	1.05 (30.0)
<sup>55</sup> Mn	85.73 (% Removal)	2.32 (97.3)	7.34 (91.4)	10.05 (88.3)
<sup>56</sup> Fe	48.78 (% Removal)	24.04 (50.7)	33.15 (32.0)	27.34 (44.0)
<sup>58</sup> Ni	5.46 (% Removal)	2.16 (60.4)	1.82 (66.7)	4.51 (17.4)
<sup>59</sup> Co	2.81 (% Removal)	0.02 (99.3)	0.13 (95.4)	0.23 (91.8)
<sup>63</sup> Cu	21.90 (% Removal)	4.02 (81.6)	3.17 (85.5)	4.46 (79.6)
<sup>64</sup> Zn	40.77 (% Removal)	13.21 (67.6)	17 (58.3)	28.46 (30.2)
<sup>75</sup> As	1.89 (% Removal)	0.41 (78.3)	0.34 (82.0)	0.27 (85.7)
<sup>114</sup> Cd	0.62 (% Removal)	0.045 (75.0)	0.16 (74.2)	0.57 (8.1)
<sup>138</sup> Ba	89.02 (% Removal)	40.75 (54.2)	42.77 (52.0)	21.25 (76.1)
<sup>205</sup> Tl	0.08 (% Removal)	0.02 (75.0)	0.04 (50.0)	0.04 (50.0)
<sup>208</sup> Pb	6.18 (% Removal)	0.53 (91.4)	0.24 (96.1)	0.23 (96.3)

All the newly prepared activated carbons show more than 95 % efficiency towards Be, Al, Mn, Co, Pb. Percentage removal of Fe, Ni, Zn and Tl by GACNZR 1073 (Fe – 50.7%, Ni -60.4% , Zn- 67.6% Tl - 75%) is comparatively higher than basic carbons GAC 383 (Fe – 32.0 % , Ni -66.7 % , Zn- 58.3 % Tl – 50 %) and GACO 383 (Fe – 44.0 % , Ni - 17.4% , Zn- 30.2 % Tl - 50%).

### 5.14 Statistical Analysis of the Data

Data obtained from different isotherm methods (solid- gas/ solid –liquid) were compiled and analysed statistically using ANOVA techniques and Karl Pearson’s coefficient of correlation/ t-test

**Hypothesis 1:** Whether there is any significant difference in pore volume and surface area of carbons obtained from BET and *I*-plot method

To test the **Hypothesis 1**, pore volume and surface area obtained from BET and *I* plot for GAC 383, GACO 383, GACNZR 1073 and GACNZR 1273 given in Table 5.4 are analysed statistically using two way ANOVA test. The results are interpreted based on the constants in Table 5.27 & 5.28

**Table 5.27:** Statistical analysis of pore volume obtained from BET and *I* plot using two way ANOVA

Source	SS	df	ms	F	P-value
Total	3995.9750	7			
carbons	3927.8050	3	1309.2683	4412.768	P < 0.001
Methods	67.2800	1	67.2800	226.7610	P < 0.001
Residual	0.8900	3	0.2967		

There is a significant difference in pore volume of carbons (P < 0.001). GACNZR 1073 significantly higher volume than the rest

**Table 5.28:** Statistical analysis of surface area obtained from BET and *I* plot using two way ANOVA

Source	SS	df	ms	F	P-value
Total	75707.6888	7			
carbons	74427.8638	3	24809.2879	4303.7310	P < 0.001
Methods	1262.5313	1	1262.5313	219.015	P < 0.001
Residual	17.2937	3	5.7646		

The surface area between carbons is highly significant ( $P < 0.001$ ), carbon GACNZR 1073 shared significantly higher surface area than others.

There is a significant difference between *I* point method and BET ( $P < 0.001$ ). BET surface area is significantly higher than that of *I* point method ( $P < 0.001$ ).

**Hypothesis 2:** Whether there is any significant difference between the pore volume of carbons obtained from Langmuir, D-R, Alpha S ( $\alpha_s$ ) and John isotherm

To test the **Hypothesis 2**, pore volume obtained from Langmuir, Dubinin-Radushkevich, Alpha S and John isotherm for GAC 383 GACO 383, GACNZR 1073 and GACNZR 1273 are statistically analysed by ANOVA test. The results are interpreted based on the constants in Table 5.29.

**Table 5.29:** Statistical analysis of pore volume obtained from Langmuir, Dubinin-Radushkevich (D-R), Alpha S ( $\alpha_s$ ) and John isotherm by two way ANOVA

Source	SS	df	ms	F	P-value
Total	10733.4394	15			
carbons	9771.5719	3	3257.1906	426.947	$P < 0.001$
Methods	893.2069	3	297.7356	39.027	$P < 0.001$
Residual	68.6606	9	7.6290		

There exists significant different between carbons with respect to pore volume ( $P < 0.001$ ). The pore volume in GACNZR 1073 is significantly higher and that in GACO 383 is significantly lower ( $P < 0.001$ ).

Methods also exhibited a significant difference between pore volumes ( $P < 0.001$ ). Dubinin-Radushkevich and Alpha S ( $\alpha_s$ ) method showed a significantly higher pore volume compared to John and Langmuir ( $P < 0.001$ ). Between Dubinin-Radushkevich and Alpha S ( $\alpha_s$ ) method the difference is not significant. Between John and Langmuir isotherm methods, the difference is not significant.



**Hypothesis 3:** Whether there is any significant difference in quantity adsorbed and surface area between the samples for the adsorption of phenol, *p*-nitrophenol and methylene blue.

To test the **Hypothesis 3**, adsorption rate and surface area of carbons GACNZR 1073, GAC 383 and GACO 383 with respect to solid –liquid equilibria using phenol, *p*-nitrophenol and MB obtained from Langmuir, D-R and John-Sivanandan Achari isotherms (Table 5.12) are analysed statistically using two way ANOVA test. The results are interpreted based on the constants in Table 5.30.

**Table 5.30:** Three way ANOVA statistical analysis of adsorption system in solid-liquid equilibria with respect to quantity of phenol, *p*-nitrophenol and methylene blue (MB) adsorbed on GACNZR 1073, GAC 383 and GACO 383

Source	SS	df	ms	F	P-value
Total	514743.1546	26			
carbons	92149.2140	2	46074.607	13.325	P < 0.001
methods	300528.0214	2	150264.0107	43.456	P < 0.001
Phenol, PNP,MB	52908.8044	2	26454.4022	7.651	P < 0.001
Residual	69156.1148	20	3457.8057		

Adsorption capacity varies significantly among carbons (P < 0.001). GACNZR 1073 is having significantly higher adsorption capacity than the rest.

Methods also shared a very high significant difference (P < 0.001). John-Sivanandan Achari and Langmuir isotherm model showed significantly higher values than D-R (P < 0.001). Between John –Sivanandan Achari and Langmuir the difference is not significant (P > 0.05)

Phenol, *p*-nitrophenol and methylene blue also exhibited a significant difference in the amount adsorbed (P < 0.001). Adsorption capacity significantly varies high in *p*-nitrophenol (P < 0.001) and significantly low in methylene blue.

**Hypothesis 4:** whether there is any correlation between temperature and adsorption of phenol, temperature and adsorption of *p*-nitrophenol & temperature and adsorption of methylene blue

To test the **Hypothesis 4**, Langmuir adsorption capacity of carbon GACONZR 1273 for phenol (Table 5.9), *p*-nitrophenol (Table 5.10) and methylene blue (Table 5.11) at five solution temperature (283 K, 293 K, 303 K, 313 K and 323 K) are selected.

There is significant positive correlation between temperature and adsorption of phenol on GACNZR 1073 ( $r = 0.98637$ ,  $t = 10.3856$ ,  $df = 3$ ,  $P < 0.01$ ). This indicates that as temperature increases adsorption of phenol also increases.

There is significant positive correlation between temperature and adsorption of *p*-nitrophenol on GACNZR 1073 ( $r = 0.9912$ ,  $t = 12.9412$ ,  $df = 3$ ,  $P < 0.01$ ). This indicates that as temperature increases adsorption of *p*-nitrophenol also increases.

There is significant positive correlation between temperature and adsorption of MB on GACNZR 1073 ( $r = 0.99843$ ,  $t = 30.847$ ,  $df = 3$ ,  $P < 0.01$ ). This indicates that as temperature increases adsorption of methylene blue also increases.

## 5.15 Conclusions

Zirconium oxide nano particles prepared in the laboratory by a simple hydrothermal process is amorphous in nature and the size lies within the range of 1-5nm. The porosity and surface area developments of a series of GAC, based on coconut shell were prepared under different activation conditions of temperature and ZrO<sub>2</sub>/GAC incorporation ratios are evaluated. It shows that during activation the carbon yield continues to decrease from 98.3 % to 94.1 % whereas burn off increase from 1.7 % to 5.9 % as the activation temperature increases from 473K to 1273K. CHNS analysis shows that C% increases with increase in activation temperature where as percentage of O and H is decreases. High carbon content is found to be in GACNZR 1273 (94.14%). Acid/base properties of the adsorbents determined by Boehm titration method suggest that all carbon materials had a acidic character. XRD analysis of samples showed broad peaks at around  $2\theta = 26^{\circ}$  and  $42^{\circ}$ . It is typically observed for amorphous materials with micro graphitic

structure and pyrolytic carbon corresponding (0 0 2) and (1 0 0) diffraction peak. FTIR peak at 1307-1308  $\text{cm}^{-1}$  is given by GACNZR 1073 and GACNZR 1273 denoted a combination of Zr-O vibration bonds. Transmission electron microscopy of GACNZR 1273 shows that nano zirconia was dispersed onto the inner surface of the porous granular activated carbon.

Surface area and monolayer volume of  $\text{ZrO}_2$  impregnated granular activated carbons GACNZR 1073 ( $V_m = 334.1 \text{ cm}^3/\text{g}$ ,  $SA = 1454.3 \text{ m}^2/\text{g}$ ) and GACNZR 1273 ( $V_m = 313.9 \text{ cm}^3/\text{g}$ ,  $SA = 1366.5 \text{ m}^2/\text{g}$ ) shows enhancement compared to basic carbon GAC 383 ( $V_m = 298.3 \text{ mg/g}$ ,  $SA = 1298.5 \text{ m}^2/\text{g}$ ) and GACO 383 ( $V_m = 272.6 \text{ cm}^3/\text{g}$ ,  $SA = 1186.5 \text{ m}^2/\text{g}$ ). Analysis of the data using the Dubinin-Radushkevich models shows that micro pore ( $< 2 \text{ nm}$ ) volumes ( $V_{mi}$ ) of GACNZR 1073 is  $392.8 \text{ cm}^3/\text{g}$  ( $SA = 722.980 \text{ m}^2/\text{g}$ ) and GACNZR 1273 is  $368.9 \text{ cm}^3/\text{g}$  ( $SA = 691.322 \text{ m}^2/\text{g}$ ). These values are comparatively higher than basic carbons GAC 383 ( $V_{mi} = 351.3 \text{ cm}^3/\text{g}$ ,  $SA = 646.51 \text{ m}^2/\text{g}$ ) and GACO 383 ( $V_{mi} = 322.8 \text{ cm}^3/\text{g}$ ,  $SA = 570.21 \text{ m}^2/\text{g}$ ). External surface area obtained from Alpha S method shows that thermal activation of GAC with  $\text{ZrO}_2$  enhances the external surface area of about 11.32% (GACNZR 1073 -  $1119.13 \text{ m}^2/\text{g}$ ) and 5% (GACNZR 1273 -  $1054.17 \text{ m}^2/\text{g}$ ) compared to basic raw material GAC 383 ( $1005.30 \text{ m}^2/\text{g}$ ). John isotherm studies shows that monolayer completion has been observed as distinct phases for adsorption on micro porous carbons. Results obtained from  $t$ -plot analysis shows that impregnation and activation with steam at 1073K generate additional micro pores without widening existing micro pores of GAC.

Increasing order of adsorption capacity of GAC studied towards phenol,  $p$ -nitrophenol and methylene blue follows as GACO 383 < GAC 383 < GACNZR 1073. Among the isotherm model studied Langmuir isotherm give better fit to data related to the higher correlation coefficient compared to other isotherm models. This indicates that Langmuir isotherm model can be confidently employed to accurately correlate the adsorption equilibria of the adsorbate as well. Kinetic studies show that adsorption of phenol,  $p$ -nitrophenol and methylene blue on all these carbons following the pseudo second order kinetics. Intraparticle diffusion study shows that external mass transfer is more predominating than intra particle diffusion for the adsorption of phenol,  $p$ -nitrophenol and methylene blue.

Higher negative value of  $\Delta G$  suggesting that adsorption process is spontaneous. Positive value of  $\Delta H$  and  $\Delta S$  indicate endothermic nature and the organization of the adsorbate in the solid-solution interface becomes more random during the process of adsorption. The effective diffusivity of phenol, *p*-nitrophenol and methylene blue was found to be rather low, of the order of  $10^{-10}$  m<sup>2</sup>/s. The low value was explained on the basis of restrictively effect associated with small pores. The obtained value of activation energy confirms the nature of physisorption processes. Design of batch sorption from isotherm data indicate that ZrO<sub>2</sub> impregnated carbon GACNZR 1073 needs comparatively lower weight than GAC 383 and GACO 383 for treating the solution of phenol, *p*- nitro phenol and MB. Trace elemental analysis by activated carbon shows that carbon GACNZR 1073 has comparatively higher adsorption efficiency towards Fe, Ni, Zn and Tl than basic carbons GAC 383 and GACO 383

Statistical analysis reveals that there is a significant difference in pore volume between carbons determined by BET, *I* plot, Langmuir, Dubinin-Radushkevich, John isotherm method ( $P < 0.001$ ). GACNZR 1073 has significantly higher pore volume than the rest. Isotherm methods in solid –liquid equilibria also show very high significant difference ( $P < 0.001$ ) in adsorption capacity. Among the carbon studied, adsorption rate of GACNZR 1073 is significantly higher than other carbons. John- Sivanandan Achari and Langmuir isotherm showed significantly higher values than Dubinin-Radushkevich ( $P < 0.001$ ) isotherm. Between John –Sivanandan Achari isotherm and Langmuir isotherm the difference is not significant ( $P > 0.05$ ). There is a significant positive correlation exists between temperature and adsorption rate in solid-liquid equilibria.

## Reference

- [1] Zhu, X.; Jyo, A. Removal of Arsenic ( V ) By Zirconium ( IV ) -Loaded Phosphoric Acid Chelating Resin. *Separation Science And Technology* **2001**, 36(14), 3175–3189.
- [2] Mahanta, N.; Chen, J. P. A Novel Route to the Engineering of Zirconium Immobilized Nano-Scale Carbon for Arsenate Removal from Water. *J. Mater. Chem. A*. **2013**, 1 (30), 8636.

- [3] Liu, X.; Lu, G.; Yan, Z. Preliminary Synthesis and Characterization of Mesoporous Nanocrystalline Zirconia. *J. Nat. Gas Chem.* **2003**, *12*, 161–166.
- [4] Cui, H.; Li, Q.; Gao, S.; Ku, J. Strong Adsorption of Arsenic Species by Amorphous Zirconium Oxide Nanoparticles. *Journal of Industrial Engineering Chemistry* **2012**, *18*, 1418–1427.
- [5] Daud, W. M. A. W.; Ali, W. S. W.; Sulaiman, M. Z. The Effects of Carbonization Temperature on Pore Development in Palm-Shell-Based Activated Carbon. *Carbon* **2000**, *38* (14), 1925–1932.
- [6] Chiang, H.L.; Huang, C. P.; Chiang, P. C. The Surface Characteristics of Activated Carbon as Affected by Ozone and Alkaline Treatment. *Chemosphere* **2002**, *47* (3), 257–265.
- [7] Lemraski, E. G.; Sharafinia, S. Kinetics, Equilibrium and Thermodynamics Studies of  $Pb^{2+}$  Adsorption onto New Activated Carbon Prepared from Persian Mesquite Grain. *J. Mol. Liq.* **2016**, *219*, 482–492.
- [8] Al-Qodah, Z.; Shawabkha, R. Production and Characterization of Granular Activated Carbon from Activated Sludge. *Brazilian J. Chem. Eng.* **2009**, *26* (1), 127–136
- [9] Velazquez-Jimenez, L. H.; Hurt, R. H.; Matos, J.; Rangel-Mendez, J. R. Zirconium-Carbon Hybrid Sorbent for Removal of Fluoride from Water: Oxalic Acid Mediated Zr(IV) Assembly and Adsorption Mechanism. *Environ. Sci. Technol.* **2014**, *48* (2), 1166–1174.
- [10] Mishra, S. P.; Singh, V. K.; Tiwari, D. Radiotracer Technique in Adsorption Study: Part XIV. Efficient Removal of Mercury from Aqueous Solutions by Hydrous Zirconium Oxide. *Appl. Radiat. Isot.* **1996**, *47* (1), 15–21.
- [11] Zielke, U.; Huttinger, K. J.; Hoffman, W. P. Surface-Oxidized Carbon Fibers : I. Surface Structure And Chemistry. *Carbon* **1996**, *34* (8), 983–998.
- [12] Sandoval, R.; Cooper, A. M.; Aymar, K.; Jain, A.; Hristovski, K. Removal of Arsenic and Methylene Blue from Water by Granular Activated Carbon Media Impregnated with Zirconium Dioxide Nanoparticles. *J. Hazard. Mater.* **2011**, *193*, 296–303.
- [13] Zhang, Q.; Jiang, P.; Pan, B.; Zhang, W.; Lv, L. Impregnating Zirconium Phosphate onto Porous Polymers for Lead Removal from Waters: Effect of Nanosized Particles and Polymer Chemistry. *Ind. Eng. Chem. Res.* **2009**, *48* (9), 4495–4499.

- [14] Thommes, M.; Kaneko, K.; Neimark, A. V.; Olivier, J. P.; Rodriguez-Reinoso, F.; Rouquerol, J.; Sing, K. S. W. Physisorption of Gases, with Special Reference to the Evaluation of Surface Area and Pore Size Distribution ( IUPAC Technical Report ). *Pure Applied Chemistry* **2015**, 87 (9-10), 1051 -1061.
- [15] Bindia Ravindran. Adsorption Isotherm Studies on Activated Carbon Prepared by Activation with Cerium Compounds. *Ph.D Thesis* **2016**. School of Environmental Studies, Cochin University of Science and Technology, Cochin, Kerala, India.
- [16] Kumar, A.; Jena, H. M. Preparation and Characterization of High Surface Area Activated Carbon from Fox Nut (*Euryale Ferox*) Shell by Chemical Activation with  $H_3PO_4$ . *Results Phys.* **2016**, 6, 651–658.
- [17] Achari, V.S.; Rajalakshmi, A.S.; Jayasree, S. Surface Area and Porosity Development on Granular Activated Carbon by Zirconium: Adsorption Isotherm Studies. *Journal of Applied Research and Technology* **2017** (Accepted November 2017).
- [18] Yu, F. D.; Luo, L. A.; Grevillot, G. Adsorption Isotherms of VOCs onto an Activated Carbon Monolith: Experimental Measurement and Correlation with Different Models. *J. Chem. Eng. Data* **2002**, 47 (3), 467–473.
- [19] Achari, V. S. Modified Carbons and Wood Dust: Evaluation of Adsorption Properties. *Ph.D. Thesis* **1998**. Department of Chemistry, University of Kerala, Kariavattom, Thiruvananthapuram, Kerala, India.
- [20] John, P.T.; Suri, D. K.; Nagpal, K. C. Characterization of structural parameters of porous materials by a new adsorption isotherm. *Journal of material science*, **1985**, 20 (6), 2071–2086.
- [21] John, P. T.; Achari, V. S. Characterisation of Structural Parameters of Finely Divided and Porous Materials by a New Adsorption Isotherm. *Journal of Materials Science* **2002**, 37 (4), 885–893.
- [22] Mercy Thomas. Adsorption Isotherm Characterization of Porous Materials Using John Isotherm. *Ph.D Thesis* **2016**, School of Environmental Studies, Cochin University of Science and Technology, Cochin, India.
- [23] Ahmed, M. J.; Theydan, S. K.; Mohammed, A. A. K. Adsorption of Phenol and P-Nitrophenol onto Date Stones: Equilibrium Isotherms, Kinetics and Thermodynamics Studies. *Journal of Engineering* **2012**, 18 (6), 743-761.
- [24] Basu, T.; Gupta, K.; Ghosh, U. C. Equilibrium and Thermodynamics on arsenic(III) Sorption Reaction in the Presence of Background Ions Occurring in Groundwater with Nanoparticle Agglomerates of Hydrous iron(III) + chromium(III) Mixed Oxide. *J. Chem. Eng. Data* **2010**, 55 (5), 2039–2047.

- [25] Achari, V.S. John Isotherm for Liquid Phase Adsorption: Comparison with Langmuir and Freundlich Models. *International Carbon Conference, Carbon 2006*, Robert Gordon University, Aberdeen, Scotland, UK. Extended Abstract, ISBN 0- 9553365-1-1, 3P 107.
- [26] Achari, V.S.; Jayasree, S.; Rajalakshmi, A.S. Adsorption of *p* – nitrophenol on Coconut Shell Granular Activated Carbon: Isotherms, Kinetics and Thermodynamics. *Indian Journal of Chemical Technology*. **2017**, *24*,471-478.
- [27] Jayasree, S.; Achari, V. S. Adsorption of *p* - Nitrophenol on ZnO Incorporated Activated Carbons: Isotherms, Kinetics & Surface area. *International Conference on Material Science, MATCON 2016*, Department of Applied Chemistry, Cochin University of Science And Technology, **2016**, 541-544.
- [28] Fierro, V.; Torné-Fernández, V.; Montané, D.; Celzard, A. Adsorption of Phenol onto Activated Carbons Having Different Textural and Surface Properties. *Microporous Mesoporous Mater.* **2008**, *111* (1–3), 276–284.
- [29] Rajalakshmi, A. S.; Achari, V. S. Adsorption of Methylene Blue From Aqueous Solution by Zirconium Impregnated Activated Carbon. *International Confernece on material for the millennium MatCon2016*, Department of Applied chemistry, Cochin University of Science And Technology, **2016**, 362-365.
- [30] Shuchuan, P.; Shisheng, W.; Tianhu, C.; Shaotong, J.; Chuanhu, H. Adsorption Kinetics of Methylene Blue from Aqueous Solutions onto Palygorskite. *Acta Geologica Sinica* **2006**, *80* (2), 236–242.
- [31] Rincón-Silva, N. G.; Moreno-Piraján, J. C.; Giraldo, L. G. Thermodynamic Study of Adsorption of Phenol, 4-Chlorophenol, and 4-Nitrophenol on Activated Carbon Obtained from Eucalyptus Seed. *J. Chem.* **2015**, 1-12.
- [32] Lin, K.; Pan, J.; Chen, Y.; Cheng, R.; Xu, X. Study the Adsorption of Phenol from Aqueous Solution on Hydroxyapatite Nanopowders. *Journal of Hazardous Materials* **2009**, *161*, 231–240
- [33] Wang, S. B.; Boyjoo, Y.; Choueib, A. Zeolitisation of fly ash for sorption of dyes in aqueous solutions. *Studies in surface science and catalysis* **2005**, *158*, 161-168.
- [34] Carmona, M.; Garcia,M. T.; Carnicer, A.; Madrid, M.; Rodriguez, J. F. Adsorption of phenol and chlorophenol onto Granular activated carbon and their desorption by supercritical CO<sub>2</sub>. *J Chem Technol Biotechnol* **2014**, *89*, 1660–1667.







## GRANULAR ACTIVATED CARBON OXIDISED AND ACTIVATED WITH ZIRCONIUM OXIDE (GACONZR): PREPARATION, CHARACTERISATION AND ADSORPTION ISOTHERM STUDIES

### 6.1 Introduction

Adsorption capacity of the activated carbon depends on the porosity as well as the reactivity of its surface functional groups. The adsorptive properties of the carbons are significantly improved in the presence of such surface complexes. Oxygen surface groups which are mainly developed during the activation process are the most important. They influence chemical natures of the carbon surface and adsorptive behaviour. The oxidation of porous carbon with air, nitric acids, hydrogen peroxide, etc may introduce a dramatic increase in the content of lactone, quinone, carboxyl and ether groups. These surface functional groups can make a noticeable change in the chemical nature of carbon. So the studies of oxidised activated carbons are very important to evaluate the effect of oxygen surface groups on the adsorption of molecules with different polarity.

In this chapter the preparation, characterization, and adsorption isotherm studies of zirconium as zirconium dioxide ( $ZrO_2$ ) impregnated nitric acid oxidised granular activated carbon are discussed. The carbon, whose textural analysis was done, is further subjected to adsorption isotherm studies, to test their efficiency to remove phenol, *p*-nitrophenol and methylene blue from the liquid phase.

### 6.2 Granular Activated Carbons – GACONZR Series

There are eight carbons GAC 383, GACO 383, GACONZR 383, GACONZR 473, GACONZR 673, GACONZR 873, GACONZR 1073 and GACONZR 1273

are prepared and used in this study. GAC 383 is the native carbon based on coconut shell, GACO 383 is acid oxidized and others are  $Zr^{4+}$  activated carbons of GACO 383. The methods of preparation and experimental setup for furnace based thermal activation were discussed in Chapter 2.

### 6.3 Characterization Studies

#### 6.3.1 Carbon Yield and Burn Off

The rise of activation temperature decreases the yield of activated carbon continuously. The lower yield and the higher burn off (Table 6.1) with steam activation can be related to the effect of the water to go inside of the material, causing an efficient removal of volatile material and helping desorption.

A mass loss of about 14 % (burn off) is obtained by activating the carbon (GACONZR series) from 473 K to 673 K is due to carboxylic groups decomposition as  $CO_2$  [1]. Mass loss of nearly 2 % in the range 673-973 K is due to carbonyl groups decomposition as CO complexes and above 973 K, a mass loss of nearly 3 % occurred probably due to the disintegration of neutral groups [2].

#### 6.3.2 Elemental Analysis

The interaction of a molecule on the surface of activated carbon will depend upon the presence of hetero atoms like hydrogen, oxygen, nitrogen and sulfur present in the form of functional groups. The elemental analyses of carbons are given in Table 6.1. It can be seen that on oxidation of GAC with  $HNO_3$  acid enhances the oxygen content considerably.

The elemental composition of GACONZR series of carbon, activated at different temperatures are given as; C (61.40 - 91.71 %), O (7.89 % - 36.1 %), H (0.32 % - 2.57%), N (0.49 % - 0.77 %).

Elemental analysis shows that the percentage of fixed carbon is highest in GACONZR 1073 (87 %), and GACONZR 1273 (91.7 %). High carbon content of GACONZR series at a higher activation temperature (1073 and 1273 K) indicates that the aromatic structure becomes more dominant after steam activation in the presence of  $Zr^{4+}$ . Because at higher activation temperature, the organic substances

have decompose into volatile gases and liquid, where the solid carbonaceous residue left behind with high carbon content [3].

### 6.3.3 Boehm Analysis

The determination of acidic and basic surface functional groups on the activated carbon has been done according to the procedure established by Boehm. Table 6.1 indicates the results of surface functional groups of various activated carbon determined by the Boehm method.

The total oxygen containing acidic functional group is 4.352 meq/g with a breakdown of 0.917 meq/g carboxylic (21 %), 1.345 meq/g lactonic (31 %), and 2.09 meq/g phenolic (48 %) groups for GACONZR 383. When activating with steam at 1073 K (GACONZR 1073) the total oxygen acid functional group decreases to 0.832 meq/g, it indicates the decay of 81 % acid functional group compared to the GACONZR 383. The carboxylic group decreases to 0.092 meq/g, the lactone group decreases to 0.06 meq/g and the phenolic group decreases to 0.70 meq/g during higher activation treatment. It is interesting to note that the composition among these three oxygen containing functional groups remains relatively unchanged even when the activation temperature increases from 1073 K to 1273 K.

**Table 6.1:** Burn off, carbon yield ,elemental composition & Boehm titration analysis of GACONZR series at different temperature 383-1273K , GAC 383 and GACO 383

Carbons	Activation T (K)	Burn off %	Carbon yield %	Carbon yield %				Carboxylic/ meq/g	Phenolic/ meq/g	lactones/ meq/g	Base/ meq/g
				C%	H%	N%	O%				
GACONZR	383	NA	NA	61.4	2.48	0.49	36.1	0.92	2.1	1.35	0.05
	473	7.2	92.8	77.6	1.70	0.62	27.3	0.87	2.0	1.11	0.10
	673	13.7	86.3	72.5	2.57	0.66	25.5	0.64	1.5	0.76	0.14
	873	15.6	84.4	74.3	0.34	0.57	22.0	0.51	1.5	0.64	0.24
	1073	18.7	81.3	86.8	0.32	0.67	13.0	0.09	0.7	0.06	0.34
	1273	19.5	80.5	91.7	0.60	0.77	7.9	0.09	0.7	0.06	0.33
GAC 383	383	NA	NA	89.4	0.60	0.36	9.6	0.40	0.5	0.18	0.50
GACO 383	383	NA	NA	65.1	2.61	0.58	31.7	1.38	2.1	1.34	0.20

### 6.3.4 Fourier Transform Infrared Spectroscopy (FTIR) Analysis

Broad band observed in the spectra are expected from the functional group which exist in the wide range of different electronic environment.

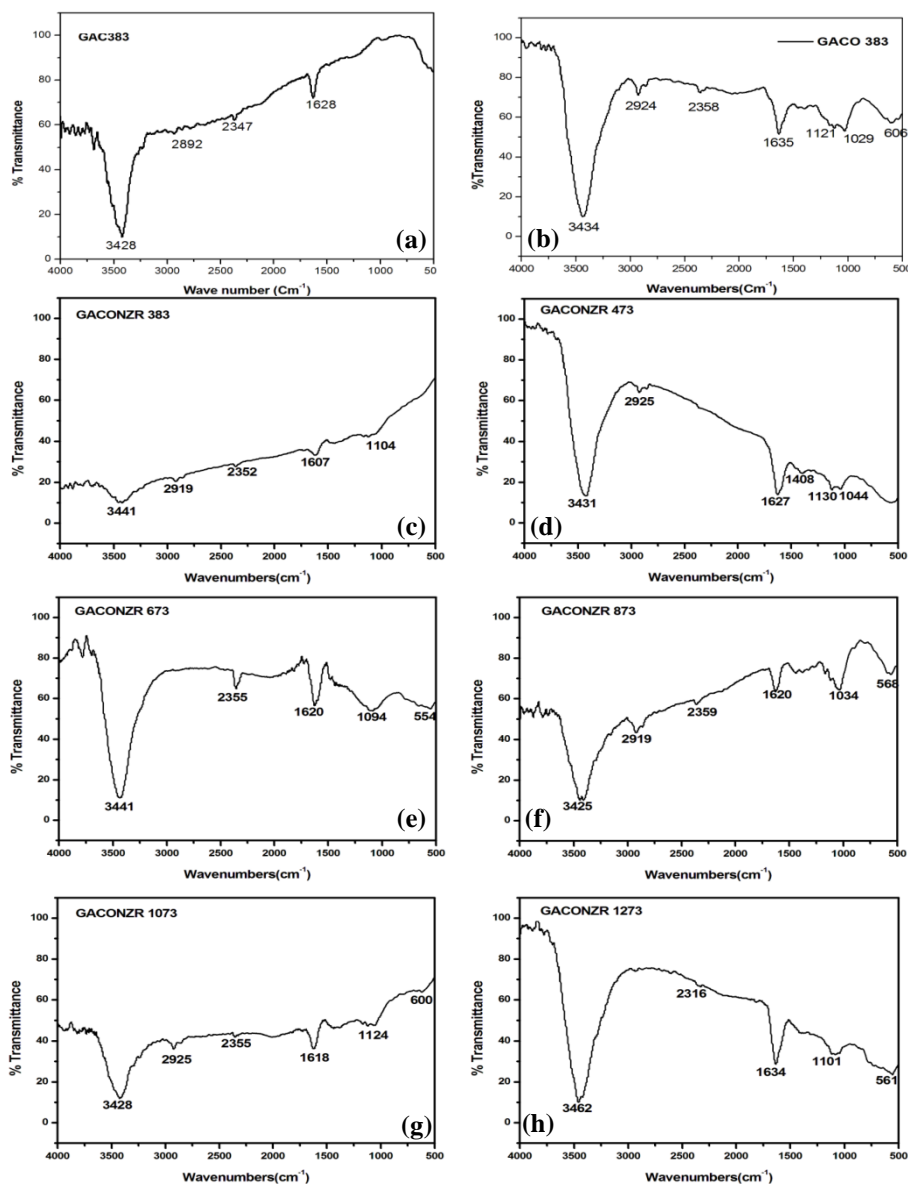


**Figure 6.1:** FTIR spectra of (a) GAC 383 (b) GACO 383 and (c)-(h) GACONZR series of carbons activated at 383-1273 K for the evaluation of functional groups

FTIR spectra of all carbons present a band around at  $3420 - 3450 \text{ cm}^{-1}$  which is assigned to OH stretching vibration of the hydroxyl group. The increased intensity of the peak in this region after acid treatment indicates the formation of the hydroxyl groups ( $-\text{OH}$ ) on the surface of prepared activated carbon. The band at  $2892, 2919$  and  $2925 \text{ cm}^{-1}$  is due to the asymmetric and symmetric C-H stretching vibration in aliphatic  $-\text{CH}$ ,  $-\text{CH}_2$  and  $-\text{CH}_3$ . Physically adsorbed  $\text{CO}_2$  will show a characteristic peak at  $2345 \text{ cm}^{-1}$  [4]. The carboxylate ion ( $\text{CO}_2^-$ ) will show its characteristic asymmetric stretching absorption around  $1600 \text{ cm}^{-1}$  [5].

The peak around at  $1046 \text{ cm}^{-1}$  represents the C-O-C functional group. The small peaks located at  $400 - 700 \text{ cm}^{-1}$  could be the C-H out-of-plane bending in benzene derivatives that is quite common for activated carbon [6, 7].

### 6.3.5 X-ray Photoelectron Spectroscopy (XPS) Analysis

The XPS C 1s, O 1s and Zr 3d spectra of GACONZR 1273 is shown in the Figure 6.2.

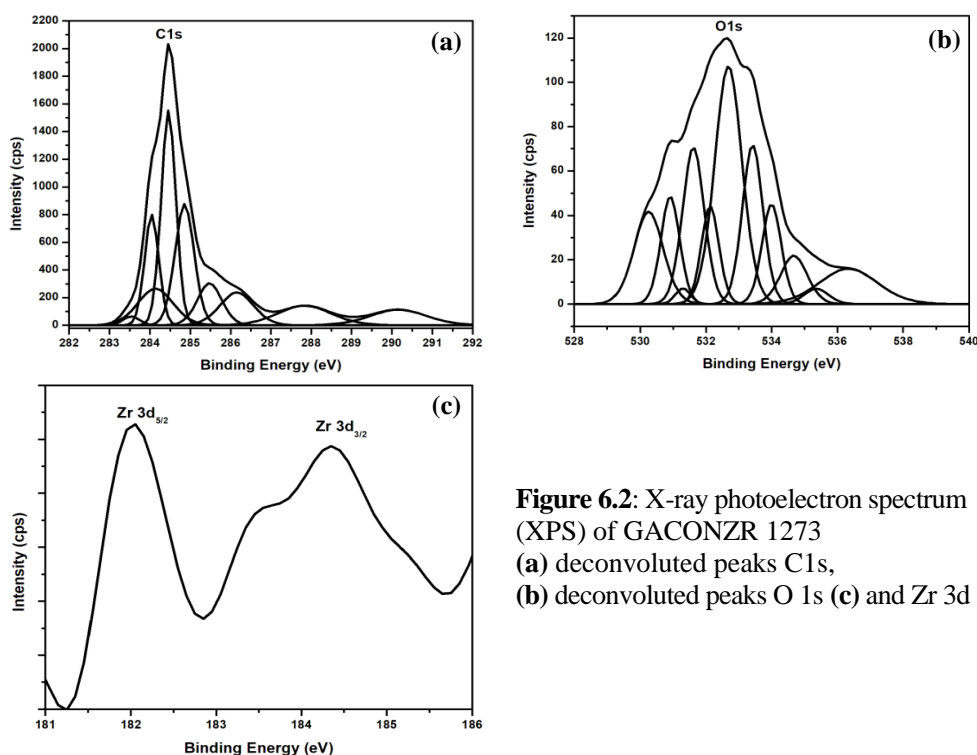


**Figure 6.2:** X-ray photoelectron spectrum (XPS) of GACONZR 1273  
(a) deconvoluted peaks C 1s,  
(b) deconvoluted peaks O 1s (c) and Zr 3d

Deconvoluted peaks of C1s spectra shows  $sp^2$  peak of the graphite component envelope centered at 284.5 eV and peak at  $\sim 285.5$  eV to hydroxyl / phenolic group, and its neighbouring peak at  $\sim 286.5$  eV due to epoxy group should have a larger BE compared to hydroxyl groups. 287.54 eV related to carbonyl and carboxyl groups, 290.21 eV indicates the delocalized  $\pi$  conjugation, a characteristic of the aromatic carbon structure. O 1s peaks are corresponding to quinones (530.27 eV), C=O (carbonyl and carboxyl, 531.6 eV), C-O (epoxy and hydroxyl, 532.14 eV) and O-H (carboxyl, 533.5 eV). XPS spectra of Zr 3d reveals that it consists of two peaks with the binding energy of 182 eV and 184.5 eV for Zr  $3d_{5/2}$  and Zr  $3d_{3/2}$  respectively. This clearly indicates the presence of oxidized zirconium in its  $Zr^{4+}$  state [8].

### 6.3.6 X-ray Diffraction (XRD) Analysis

X-ray diffractograms of activated carbon GAC 383, GACO 383 and GACONZR series are shown in Figures 6.3(a)&(b). The crystalline sizes  $L_a$ ,  $L_c$  and inter planar distance  $d_{002}$  for each carbons are tabulated in Table 6.2.

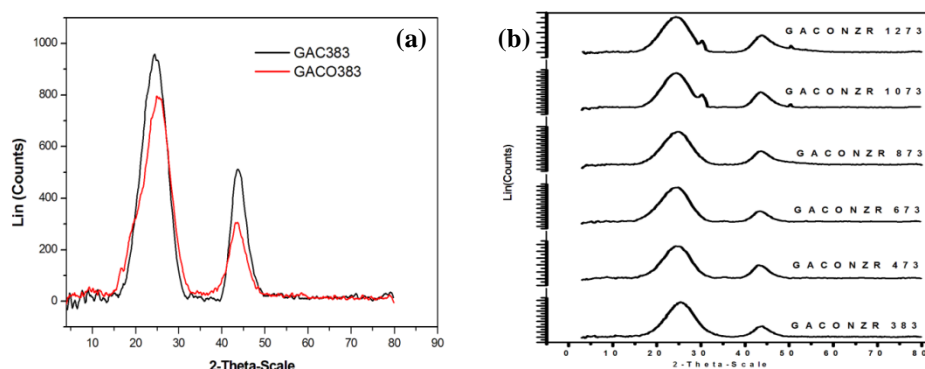


**Figure 6.3:** XRD spectra of (a) GAC 383 & GACO 383 (b) GACONZR series of carbons activated at 383-1273K

X-ray diffraction profile of activated carbons shows broad diffraction peak corresponding to  $2\theta \approx 25^\circ$  and  $43.6^\circ$  these are assigned to the disordered graphitic (002) and (100) plane respectively.

**Table 6.2:** XRD crystalline parameters of GACONZR series activated at different temperature 383-1273K, GAC 383 and GACO 383

Carbons	$L_c$ (0.9) nm	$L_a$ (1.84) nm	$d_{002}$ nm
GAC 383	1.14	2.28	0.364
GACO 383	0.97	1.94	0.356
GACONZR 383	1.29	2.64	0.358
GACONZR 473	1.18	2.42	0.360
GACONZR 673	1.11	2.26	0.365
GACONZR 873	1.18	2.41	0.351
GACONZR 1073	1.18	2.41	0.351
GACONZR 1273	1.22	2.50	0.362

Crystalline thickness and crystalline width of GAC 383, GACO 383 and GACONZR series shows a slight variation as seen in the Table 6.2. For GACONZR series  $L_a$  varies as (2.64 -2.26 nm),  $L_c$  varies (1.29 – 1.11 nm) and  $d_{002}$  varies (0.3578 – 0.3618 nm). Compared to GAC 383, the nitric acid modified GACONZR series shows large  $L_c$  and  $L_a$ . It indicates that oxidation of granular activated carbon increases the crystalline width and thickness. The interplanar distance also increases with oxidation. The value of  $L_c$  and  $L_a$  of GACONZR series diminishes whereas the interplanar distance increases upto activation temperature of 673 K. But in none of the above samples the interplanar distance reaches a value close to the  $d_{002}$  of graphite (0.335 nm) it indicate highly disordered turbostratic structure [5].

### 6.3.7 Scanning Electron Microscopy (SEM) Analysis

The porous properties of the prepared activated carbon samples are analyzed by observing the SEM images. Surface images of granular activated carbon GACONZR 1273 at different magnification are given in the Figure 6.4.

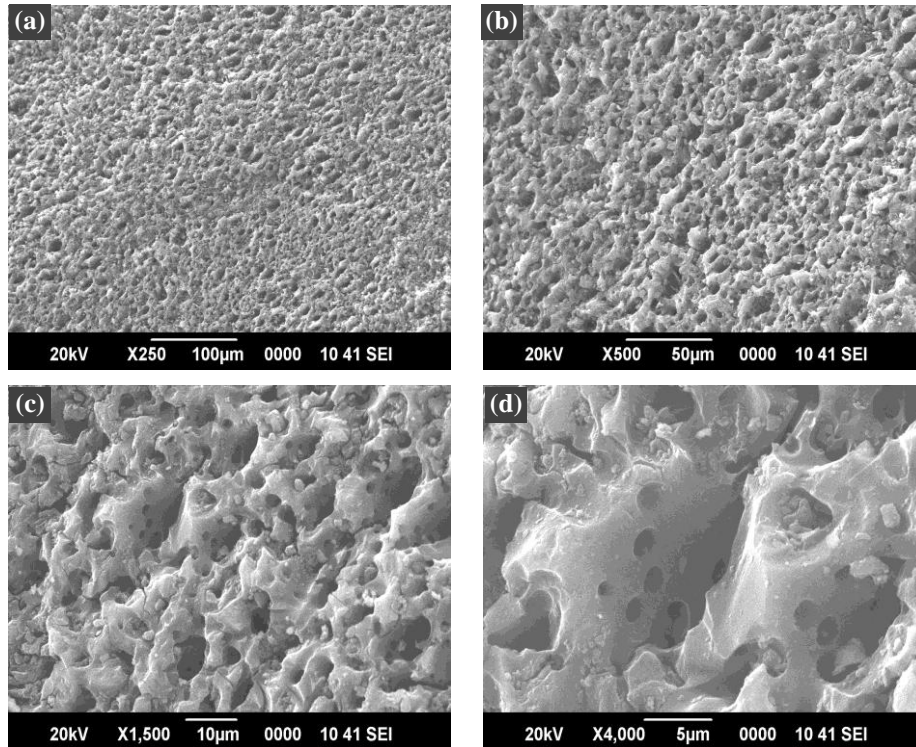


**Figure 6.4:** Scanning electron micrographs (SEM) of GACONZR 1273 at different resolution (a) 250-100  $\mu\text{m}$  (b) 500-50  $\mu\text{m}$  (c) 10  $\mu\text{m}$  and (d) 5  $\mu\text{m}$

SEM image revealed that, it is highly porous in nature. Different pores were observed in activated carbon sample. Due to activation, volatiles are removed producing a fixed carbon mass with widening of pore networks that are present in activated carbon sample.

Figure 6.4 (a) & (b) indicates that surface is smooth and distributed with small pores. Some particles are scattered on the surface of GAC due to metal compounds on the GAC. Figure 6.4 (c) & (d) indicates that large pores are developed during activation at higher temperature and it will enable the rapid diffusion of solute [9].

### 6.3.8 Transmission Electron Microscopy (TEM) Analysis

The TEM images of the impregnated carbons are shown in Figure 6.5. The carbon particle aggregate structure was observed from TEM observation. No



features indicative of crystalline phases were detected in the impregnated carbon by TEM. In the case of heavier elements stronger contrasts observed. It indicates the presence of Zr in impregnated carbon samples [10].

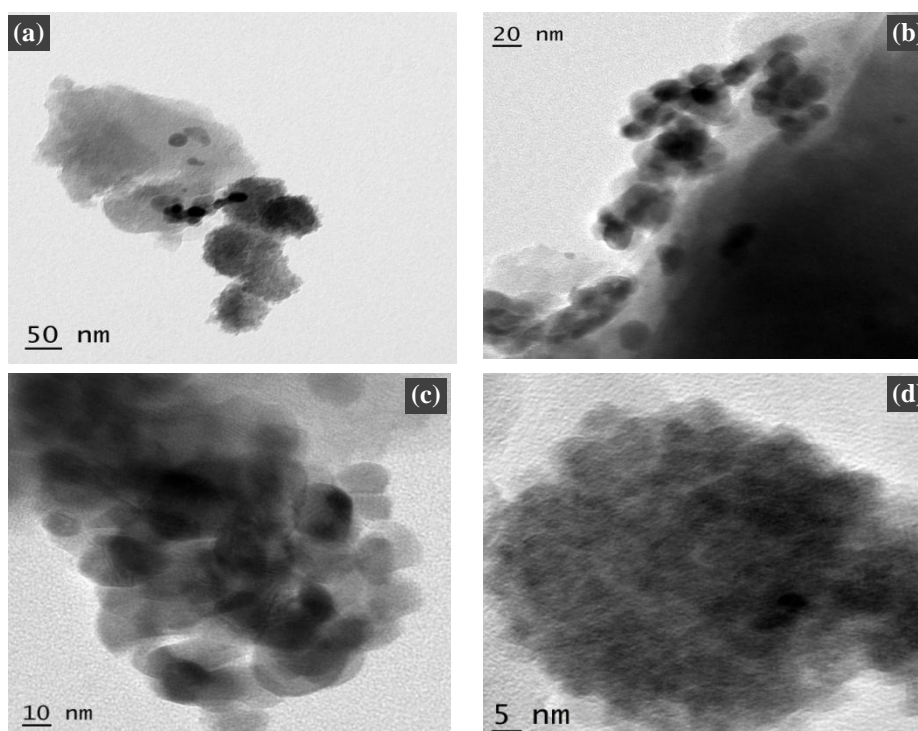


**Figure 6.5:** High resolution transmission electron microscopy (HRTEM) of GACONZR 1273 at different resolutions (a) 50 nm (b) 20 nm (c) 10 nm and (d) 5 nm

## 6.4 Solid-Gas Adsorption Equilibria

Surface area, pore size, and pore volume of the carbons is assessed by nitrogen adsorption analysis.

### 6.4.1 Adsorption Isotherm Analysis

The adsorption isotherm of  $N_2$  gas adsorbed on GAC 383, GACO 383, GACONZR 1073 and GACONZR 1273 are given in Figure 6.6. It has a sharp initial rise at the lower relative pressures indicate the presence of micropores in

the activated carbons. As the relative pressure is increased, the amount of nitrogen adsorbed by the sample becomes more. At higher  $p/p_0$ , it moves slightly upward with deviation which can be attributed to the capillary condensation in mesopores.

These materials are strictly microporous as they have a typical *Type I* isotherm. As we can see in the Figure 6.6 the oxidation of activated carbon (GACO 383) leads to the downward shift of the isotherm.

The nitrogen adsorption-desorption data is further processed by using various isotherm models such as Brunauer-Emmett-Teller (BET), Langmuir, Freundlich, Dubinin-Radushkevich (D-R), Alpha S ( $\alpha_s$ ), John isotherm,  $t$ -plot and BJH models to obtain the porosity and surface area.

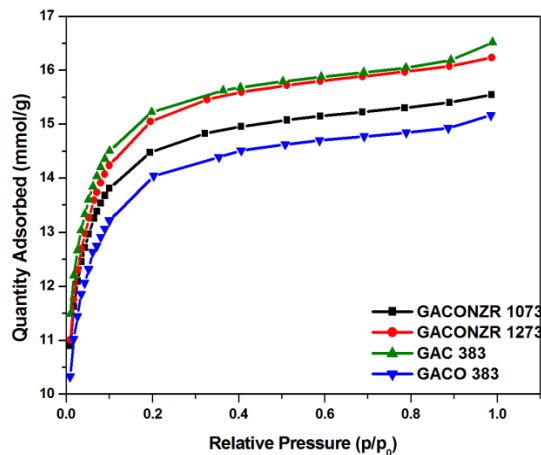


**Figure 6.6:** N<sub>2</sub> adsorption isotherm for carbons GAC 383, GACO 383, GACONZR 1073 and GACONZR 1273 at 77K

#### 6.4.1.1 Brunauer-Emmett-Teller (BET) Isotherm Analysis

BET isotherm is applied for the determination of specific surface area of GACONZR 1073, GACONZR 1273, GAC 383 and GACO 383.

$$\frac{1}{v(p^0/p-1)} = \frac{1}{v_m c} + \frac{c-1}{v_m c} \left( \frac{p}{p_0} \right) \quad (6.1)$$

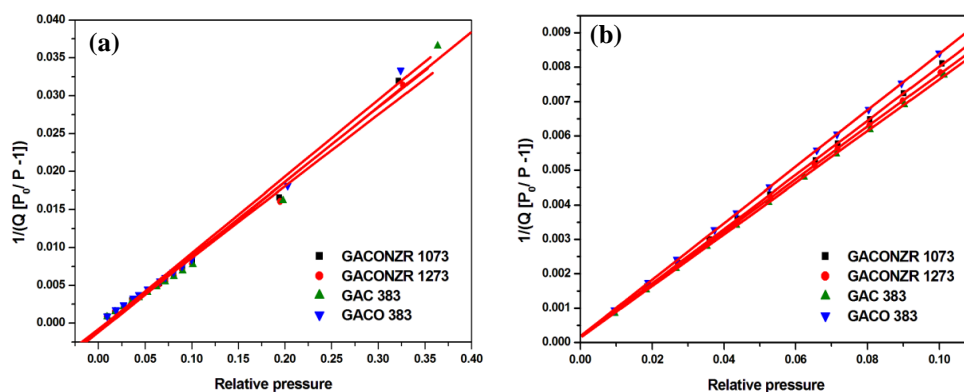


**Figure 6.7 :** BET isotherm plot for GACONZR 1073, GACONZR 1273, GAC 383 and GACO 383 (a)  $p/p_0$  up to 0.3 and (b)  $p/p_0$  up to 0.1 using  $N_2/77K$

BET analysis is done in the range of  $p/p_0$  0.01- 0.35 modified carbon samples are depicted in the Figure 6.7 (a). Surface area of activated carbon obtained from BET ( $p/p_0=0.3$ ) along with corresponding monolayer volume  $V_m$  (and surface area  $SA_{BET}$ ) of carbons is given as follows; GAC 383 ( $V_m = 228.97 \text{ cm}^3/\text{g}$  &  $SA_{BET} = 997 \text{ m}^2/\text{g}$ ), GACO 383 ( $V_m = 223.81 \text{ cm}^3/\text{g}$  &  $SA_{BET} = 974 \text{ m}^2/\text{g}$ ), GACONZR 1073 ( $V_m = 231.24 \text{ cm}^3/\text{g}$  &  $SA_{BET} = 1006 \text{ m}^2/\text{g}$ ), and GACONZR 1273 ( $V_m = 239.61 \text{ cm}^3/\text{g}$  &  $SA_{BET} = 1043 \text{ m}^2/\text{g}$ ). Impregnation of nano zirconia and steam activation at higher temperature enhances the surface area of nitric acid modified GAC.

The deviation of BET plot from linearity becomes clearly remarkable from the relative pressure ( $p/p_0$ ) of 0.1. A negative 'C' arises from a negative intercept on the BET plot is due to data point at too high  $P/P_0$  values. The stronger adsorption in microporous materials will make the monolayer formation very fast so the data point range selected for analysis has to be in the range below  $p/p_0 < 0.3$ . By shifting the  $p/p_0$  range from  $p/p_0$  0.3 to 0.1, C becomes positive on evaluation.

BET surface area obtained from  $N_2$  adsorption isotherm measuring in the relative pressure range up to 0.1 is found to be higher than the BET surface area obtained in the relative pressure range of 0.3. Specific surface area obtained by plotting relative pressure  $p/p_0$  up to 0.1 is followed as; GAC 383 ( $SA_{BET} 1298.5 \text{ m}^2/\text{g}$ ), GACO 383 ( $SA_{BET} 1186.5 \text{ m}^2/\text{g}$ ), GACONZR 1073 ( $SA_{BET} 1238.046 \text{ m}^2/\text{g}$ ), and GACONZR 1273 ( $SA_{BET} 1279.256 \text{ m}^2/\text{g}$ ). Percentage of enhancement observed in specific surface area by shifting the relative pressure from 0.3 to 0.1 for new

carbons is given as; GAC 383 (30 %), GACO 383 (22 %), GACONZR 1073 (23 %), GACONZR 1273 (23 %). The relatively large values of the  $C_{BET}$  parameters are summarized in Table 6.3.

#### 6.4.1.2 The BET–Scatchard (B–S) Plots (I Point Method Analysis)

The rearrangement of the BET equation for calculating the specific surface area is given by the equation (6.2) [11, 12].

$$\frac{[V(1 - P)]}{P} = CV_m - (C - 1)[V(1 - P)] \quad \text{where } p = \frac{p}{p_0} \quad (6.2)$$

The specific surface area is calculated from the relationship as given in equation (6.3).

$$\text{Specific surface area, } SSA \text{ (m}^2\text{g}^{-1}\text{)} = 4.356 V_m \quad (6.3)$$

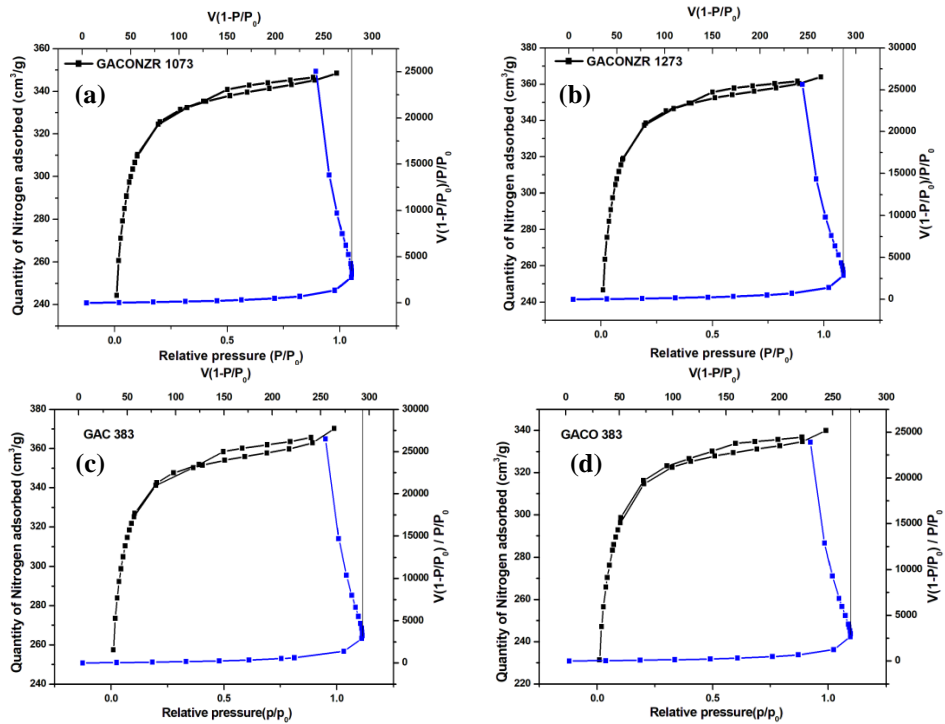


**Figure 6.8 :** Nitrogen adsorption-desorption isotherms and the corresponding  $I$  plots for (a) GACONZR1073 (b) GACONZR 1273 (c) GAC 383 & (d) GACO 383

Specific surface area obtained from *I* plot method is given as follows; GACONZR 1073 ( $SA_I$  1213.21 m<sup>2</sup>/g), GACONZR 1273 ( $SA_I$  1248.55 m<sup>2</sup>/g) GAC 383 ( $SA_I$  1275.39 m<sup>2</sup>/g) and GACO 383 ( $SA_I$  1164.66 m<sup>2</sup>/g). These results are similar to the surface area obtained from BET upto relative pressure 0.1.

**Table 6.3:** BET and *I* plot isotherm parameters for GAC 383, GACO 383, GACONZR 1073 & GACONZR 1273 using N<sub>2</sub> at 77K

Carbons	Total pore volume $V_T$ cm <sup>3</sup> /g,STP	BET p/p <sub>0</sub> upto 0.3			I plot method		BET p/p <sub>0</sub> upto 0.1			
		$SA_{BET}$ m <sup>2</sup> /g	$V_m$ cm <sup>3</sup> /g,STP	$C_{BET}$	$SA_I$ m <sup>2</sup> /g	$V_m=V_I$ cm <sup>3</sup> /g,STP	$SA_{BET}$ m <sup>2</sup> /g	$V_m$ cm <sup>3</sup> /g. STP	$C_{BET}$	Pore Width (nm)
GAC 383	370.4	996.8	229.0	-816	1275.4	293.0	1298.5	298.3	524	1.76
GACO 383	340.2	974.3	223.8	-119	1164.7	267.5	1186.5	272.6	439	1.77
GACONZR 1073	348.7	1006.7	231.2	-109	1213.2	278.7	1238.0	284.4	519	1.73
GACONZR1273	364.1	1043.1	239.6	-114	1248.6	286.8	1279.3	293.9	417	1.75

### 6.4.1.3 Langmuir Isotherm Analysis

The Langmuir adsorption model is one of the most common one used to quantify the amount of adsorbate adsorbed on an adsorbent as a function of the partial pressure at a given temperature. The linear form of the equation is

$$\frac{P}{V} = \frac{1}{bV_m} + \frac{P}{V_m} \tag{6.4}$$

Langmuir adsorption isotherms for the adsorption of N<sub>2</sub> gases on GAC 383, GACO 383, GACONZR 1073 and GACONZR 1273 are shown in Figure 6.9(a).

The linear form of the Langmuir plot for GACONZR 1073, GACONZR 1273, GAC 383 and GACO 383 shows good correlation coefficient. The monolayer volume  $V_m$  (L) and surface area  $SA_L$  obtained for the modified carbons are GACONZR 1073 ( $V_m$  320.75 cm<sup>3</sup>/g &  $SA_L$  1396.288 m<sup>2</sup>/g), GACONZR 1273 ( $V_m$  331.52 cm<sup>3</sup>/g &  $SA_L$  1443.17 m<sup>2</sup>/g), GAC 383 ( $V_m$  336 cm<sup>3</sup>/g &  $SA_L$  1465.27 m<sup>2</sup>/g) and GACO 383 ( $V_m$  304.5 cm<sup>3</sup>/g &  $SA_L$  1325.54 m<sup>2</sup>/g).

On comparing with GACO 383, zirconium impregnated GACO series have 5.3% (GACONZR 1073) and 8.9% (GACONZR 1273) increment in the Langmuir surface area.

#### 6.4.1.4 Freundlich Isotherm Analysis

Variation of the extent of adsorption with pressure of gas is also expressed using Freundlich isotherm by linear relationship given as

$$\log V = \log K_F + \frac{1}{n} \log P \quad (6.5)$$

Figure 6.9(b) shows that the extent of adsorption varies directly with pressure raised to power  $1/n$  until the saturation pressure is reached. The plot of  $\log P$  versus  $\log V$  gives straight line with slope  $1/n$  and intercept  $\log K_F$ .

$K_F$  and  $n$  obtained from intercept and slope of the linear plot are given in Table 6.4. The  $K_F$  and  $n$  obtained for carbons are GAC 383 ( $K_F = 209.82 \text{ Lg}^{-1}$  &  $n = 9.94$ ), GACO 383 ( $K_F = 183.51 \text{ Lg}^{-1}$  &  $n = 9.36$ ), GACONZR 1073 ( $K_F = 199.29 \text{ Lg}^{-1}$  &  $n = 9.80$ ) and GACONZR 1273 ( $K_F = 197.61 \text{ Lg}^{-1}$  &  $n = 9.04$ ) respectively.

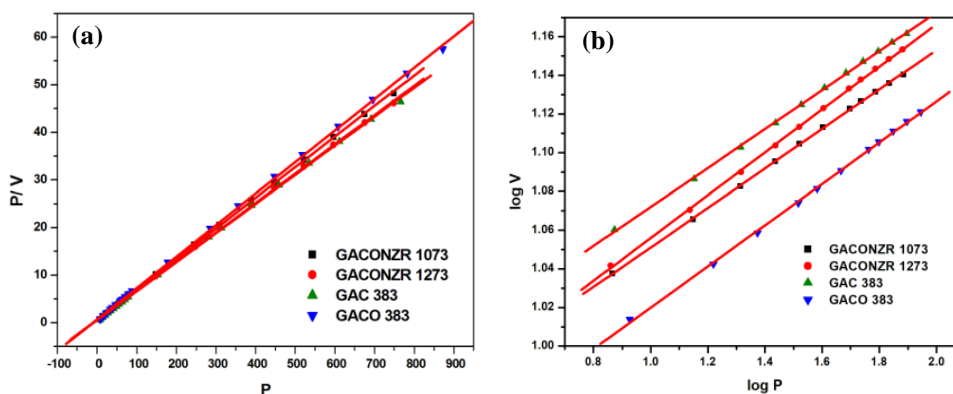


**Figure 6.9:** Adsorption isotherm plots (a) Langmuir (b) Freundlich for GAC 383, GACO 383, GACONZR 1073 & GACONZR 1273 using  $\text{N}_2$  at 77K

The high  $K_F$  and  $n$  for GAC 383 suggests that more nitrogen get adsorbed on this carbon compared to all other nitric acid modified carbons.

**Table 6.4:** Langmuir and Freundlich isotherm parameters for GAC 383, GACO 383, GACONZR 1073 and GACONZR 1273 using N<sub>2</sub> at 77K

Carbons	Langmuir				Freundlich		
	V <sub>m</sub> (L) cm <sup>3</sup> /g.STP	S <sub>A,L</sub> m <sup>2</sup> /g	b	R <sup>2</sup>	n	K <sub>F</sub> L/g	R <sup>2</sup>
GAC 383	336.6	1465.3	0.278	0.999	9.94	209.8	0.999
GACO 383	304.5	1325.5	0.246	0.999	9.36	183.5	0.999
GACONZR 1073	320.7	1396.3	0.284	0.999	9.80	199.3	0.999
GACONZR 1273	331.5	1443.2	0.257	0.999	9.04	197.6	0.999

#### 6.4.1.5 Dubinin-Radushkevich Isotherm (D-R) Analysis

The empirical equation proposed by Dubinin and Radushkevich is used to describe the adsorption of N<sub>2</sub> gas on the modified carbons. The equation is given below [13]

$$\log V = \log V_0 - D \log^2 (P_0/p) \quad (6.6)$$

$$D = 2.303 \left( \frac{RT}{\beta E_0} \right)^2 \quad (6.7)$$

$$L = 6.6 - 1.79 \ln E_0 \text{ nm} \quad (6.8)$$

Relationship between  $L$  and  $V_{mi}$  (or  $V_0$ ) gives micropore surface area  $SA_{D-R}$  as per the equation.

$$SA_{D-R} = \frac{2 \times 10^3 V_{mi} (\text{cm}^3/\text{g})}{L(\text{nm})} \quad (6.9)$$

Where  $SA_{D-R}$  is the micropore surface area in m<sup>2</sup>/g.  $V_{mi}$  (D-R) is the micropore volume in cm<sup>3</sup>/g and  $L$  is the accessible pore width in nanometres. The volume of the micro pores is obtained by extrapolating the line from the low-pressure region ( $P/P_0 < 0.1$ ) to the y-intercept (Figure 6.10 (a)).

The micropore volume  $V_{mi}$  (D-R) cm<sup>3</sup>/g and micropore surface area  $SA_{D-R}$  obtained for the modified carbons are GACONZR 1073 ( $V_{mi} = 335.08$  cm<sup>3</sup>/g &  $SA_{D-R} = 613.79$  m<sup>2</sup>/g), GACONZR 1273 ( $V_{mi} = 347.99$  cm<sup>3</sup>/g &  $SA_{D-R} = 607.98$  m<sup>2</sup>/g),

GAC 383 ( $V_{mi} = 351.28 \text{ cm}^3/\text{g}$  &  $SA_{D-R} = 646.51 \text{ m}^2/\text{g}$ ) and GACO 383 ( $V_{mi} = 322.75 \text{ cm}^3/\text{g}$  &  $SA_{D-R} = 570.21 \text{ m}^2/\text{g}$ ).

GACONZR series shows that the maximum micropore volume is obtained at the activation temperature of 1073 K (GACONZR 1073). Further rise of temperature at 1273K causes the widening of existing pores this will cause the lowering of micropore volume and micropore surface area. This can be attributed to the increases of  $L$  value from 1.69 nm to 1.78 nm during activation at 1273 K. Compared to GACO 383, modified carbons shows 6.7 % (GACONZR 1073) and 6.6 % (GACONZR 1273) enhancement in micropore surface area, during the  $\text{ZrO}_2$  activation.

#### 6. 4.1.6 Alpha S ( $\alpha_s$ ) Method

In order to construct the Alpha S ( $\alpha_s$ ) plot for a given adsorbent, the amount adsorbed is plotted as a function of the reduced standard isotherm,  $\alpha_s$ . It is used for the determination of micropore volumes by extrapolation of curves to  $\alpha_s = 0$ . The external surface area is determined from the slopes of linear portions of Alpha S ( $\alpha_s$ ) curves.

The  $\alpha_s$  plots of the carbon samples GACONZR 1073, GACONZR 1273, GAC 383 and GACO 383 are shown in Figure 6.10(b) and the results are given Table 6.5.

$$\frac{V_{ads}}{V_{ads} \left( \frac{p}{p_0} = 0.4 \right)} = \alpha_s \quad (6.10)$$

The shape of  $\alpha_s$  plot gives useful indication of the type of pore structure. It shows perfect linearity for all the relative pressure range.

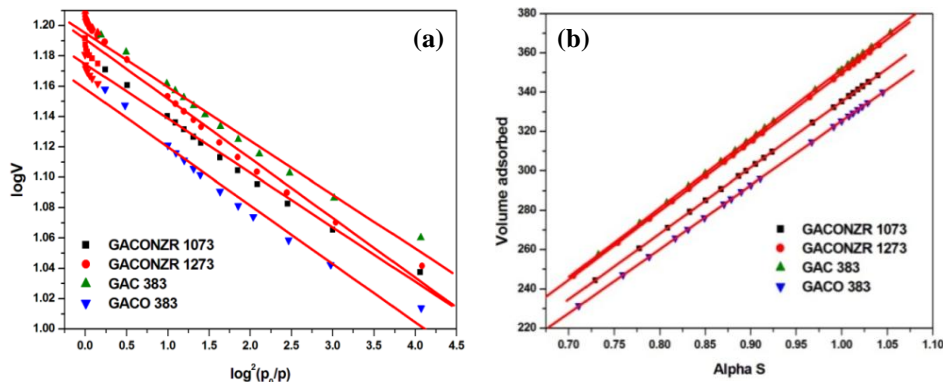


**Figure 6.10:** Adsorption isotherm (a) Dubinin-Radushkevich (D-R) (b) Alpha S ( $\alpha_s$ ) plot of GAC 383, GACO 383, GACONZR 1073 and GACONZR 1273



The micropore volume  $V_{mi} (\alpha_s)$  and external surface area  $SA_{ext}$  obtained for the modified carbons are GACONZR 1073 ( $V_{mi}$  335.27 cm<sup>3</sup>/g &  $SA_{ext}$  958.88 m<sup>2</sup>/g), GACONZR 1273 ( $V_{mi}$  349.56 cm<sup>3</sup>/g &  $SA_{ext}$  999.73 m<sup>2</sup>/g), GAC 383 ( $V_{mi}$  351.49 cm<sup>3</sup>/g &  $SA_{ext}$  1005.3 m<sup>2</sup>/g), GACO 383 ( $V_{mi}$  325.28 cm<sup>3</sup>/g &  $SA_{ext}$  930.30 m<sup>2</sup>/g). The carbon samples GACONZR 1273 gives 4.3 % enhancement of external surface area and pore volume compared to that of GACONZR 1073.

**Table 6.5:** Dubinin-Radushkevich (D-R) & Alpha S ( $\alpha_s$ ) isotherm parameters of GAC 383, GACO 383, GACONZR 1073 and GACONZR 1273 using N<sub>2</sub> at 77K

Carbons	Dubinin – Radushkevich (D-R)					Alpha S ( $\alpha_s$ )	
	$SA_{D-R}$ m <sup>2</sup> /g	$V_{mi}$ (D-R) cm <sup>3</sup> /g.STP	L nm	E kJ/mol	$R^2$	$V_{mi} (\alpha_s)$ cm <sup>3</sup> /g	$SA_{ext}$ m <sup>2</sup> /g
GAC 383	646.5	351.3	1.68	15.6	0.986	351.5	1005.3
GACO 383	570.2	322.8	1.75	15.0	0.979	325.3	930.3
GACONZR 1073	613.8	335.1	1.69	15.6	0.989	335.3	958.9
GACONZR 1273	608.0	348.0	1.77	14.9	0.984	349.6	999.7

#### 6.4.1.7 John Isotherm Analysis

The general form of John isotherm equation applied to the N<sub>2</sub> adsorption data is given in equation (6.11) [14 , 15].

$$\log \log P = C + n \log V \quad (6.11)$$

Where  $P = p/p_0 \times 10^N$  to make  $p/p_0$  as a positive integer

Equation (6.11) is further modified as John – Sivanandan Achari isotherm for solid – liquid equilibria

$$\log \log C_e = C + n \log q_e \quad (6.11 a)$$

The John isotherm plots, based upon N<sub>2</sub> uptake data provide three distinct phases for GAC 383, GACO 383, GACONZR 1073, and GACONZR 1273, which are presented in a Figure 6.11.

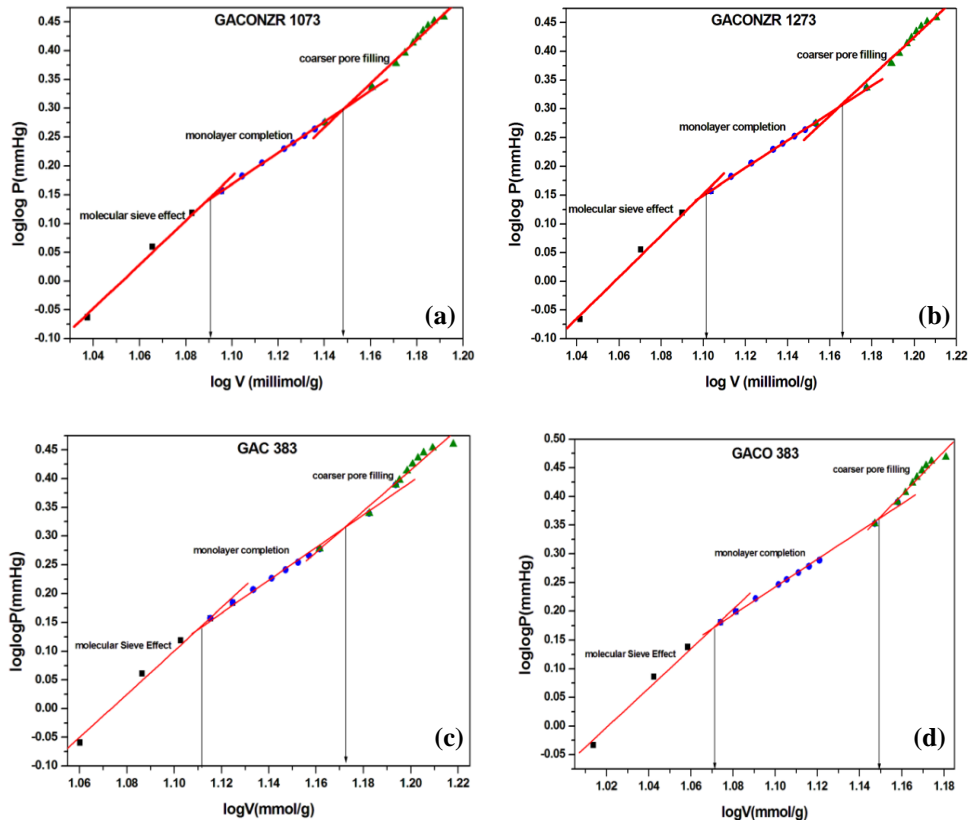


**Figure 6.11:** John Isotherm plot of GAC 383, GACO383, GACONZR 1073 and GACONZR 1273 using  $N_2$  adsorption data at 77 K

Molecular sieve effects (*mse*), cause higher adsorption to take place in *phase I*. Adsorption of  $N_2$  in *phase I* for new carbons are given as; GAC 383 ( $289.95 \text{ cm}^3/\text{g}$ ), GACO 383 ( $264.10 \text{ cm}^3/\text{g}$ ), GACONZR 1073 ( $275.32 \text{ cm}^3/\text{g}$ ) and GACONZR 1273 ( $282.33 \text{ cm}^3/\text{g}$ ). This indicates that the contribution of finer pores (pore width less than 0.8 nm) is higher for total microporosity of the material. The presence of micropores having width 0.8 - 2 nm is indicated by *Phase II* of John isotherm and it is given as GAC 383 ( $43.61 \text{ cm}^3/\text{g}$ ), GACO 383 ( $52.06 \text{ cm}^3/\text{g}$ ) GACONZR 1073 ( $39.85 \text{ cm}^3/\text{g}$ ) and GACONZR 1273 ( $45.49 \text{ cm}^3/\text{g}$ ).

**Table 6.6:** John isotherm parameters of GAC 383, GACO 383 GACONZR 1073 & GACONZR 1273 using N<sub>2</sub> /77K

Carbons	Adsorption Capacity (cm <sup>3</sup> /g)			
	V <sub>mse</sub> cm <sup>3</sup> /g.STP	V <sub>m</sub> (J) cm <sup>3</sup> /g.STP	V <sub>c</sub> (J) cm <sup>3</sup> /g.STP	V <sub>T</sub> (J) cm <sup>3</sup> /g.STP
GAC 383	289.95 n = 3.76	43.61 n = 2.85	32.05 n = 3.60	365.61
GACO 383	264.10 n = 3.43	52.06 n = 2.42	21.55 n = 3.78	337.72
GACONZR 1073	275.32 n = 3.96	39.85 n = 3.27	33.20 n = 4.21	348.37
GACONZR 1273	282.33 n = 3.61	45.49 n = 2.93	36.34 n = 3.67	364.16

Contribution of wider micropore ( $V_c(J)$ ) in GAC 383 is 32.05 cm<sup>3</sup>/g, GACO 383 is 21.55 cm<sup>3</sup>/g, GACONZR 1073 is 33.20 cm<sup>3</sup>/g and GACONZR 1273 is 36.34 cm<sup>3</sup>/g. Compared to basic carbons zirconia impregnated GACO series shows more wider pore filling, it again confirms the possibility of widening of existing pores by rising the activation temperature.

**Table 6.7:** John, Dubinin-Radushkevich (D-R), Alpha S ( $\alpha_s$ ) and Langmuir isotherm: comparison of pore volume obtained from Isotherm models

Carbons	Pore volume			
	John (V <sub>mse</sub> + V <sub>m</sub> ) cm <sup>3</sup> /g STP	D-R V <sub>mi</sub> (D-R) cm <sup>3</sup> /g STP	Alpha S V <sub>mi</sub> ( $\alpha_s$ ) cm <sup>3</sup> /g STP	Langmuir V <sub>m</sub> (L) cm <sup>3</sup> /g STP
GAC 383	333.6	351.3	351.5	336.6
GACO 383	316.2	322.8	325.3	304.5
GACONZR 1073	315.2	335.1	335.3	320.7
GACONZR 1273	327.8	348.0	349.6	331.5

Comparison of pore volumes obtained from John (J), Dubinin-Radushkevich (D-R), Alpha S ( $\alpha_s$ ), and Langmuir isotherm models are schematically represented in the Figure 6.12. It shows that all isotherms are having the approximately same value and error percentages between these values lies within the limit of 10%.

### 6.4.1.8 *t* – Plot Method

The *t*-plot isotherm analysis is used for the determination of micropore volume, micropore surface area and mesopore surface area of carbon samples.

The thickness of the pores is calculated using the equation (6.12)

$$t = \left[ \frac{13.99}{(0.034 - \log(p/p_0))} \right]^{0.5} \quad (6.12)$$

The plots are shown in the Figure 6.13, and the results are given in Table 6.8. The intercept on the y-axis indicates the volume of the micropores which have been filled with nitrogen molecules. This method is widely used to evaluate the micropore volume of a porous materials.

The micropore volume  $V_{mi}(t)$  and micropore surface area  $SA_{mi}(t)$  obtained for the modified carbons are GACONZR 1073 ( $V_{mi} = 215.9 \text{ cm}^3/\text{g}$  &  $SA_{mi} = 617.4 \text{ m}^2/\text{g}$ ), GACONZR 1273 ( $V_{mi} = 206.3 \text{ cm}^3/\text{g}$  &  $SA_{mi} = 574.0 \text{ m}^2/\text{g}$ ), GAC 383 ( $V_{mi} = 226.7 \text{ cm}^3/\text{g}$  &  $SA_{mi} = 588.7 \text{ m}^2/\text{g}$ ), GACO 383 ( $V_{mi} = 192.0 \text{ cm}^3/\text{g}$  &  $SA_{mi} = 540.3 \text{ m}^2/\text{g}$ ).

External surface area ( $SA_{ext}(t)$ ) increases from  $389.2 \text{ m}^2/\text{g}$  (GACONZR 1073) to  $469.1 \text{ m}^2/\text{g}$  (GACONZR 1273) by increasing the activation temperature from 1073 K to 1273 K for GACONZR series i.e. 20.5 % enhancement in the external surface area.

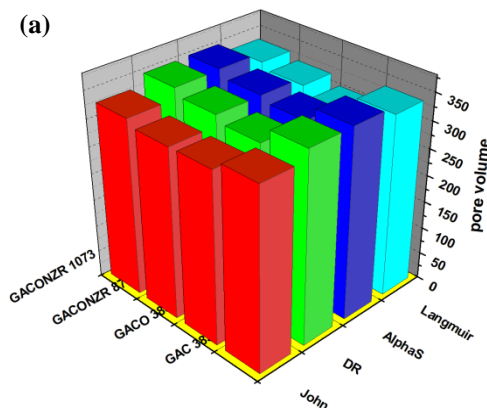


**Figure 6.12:** Comparison of pore volumes obtained for John (J) /D-R/ Alpha S ( $\alpha_s$ )/ Langmuir isotherm models

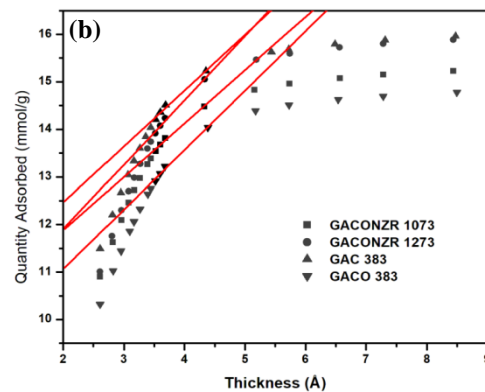


**Figure 6.13:** *t*-plot analysis of GAC 383, GACO383 and GACONZR series carbonized at temperature 1073 and 1273 K.

All the carbon studied exhibit relatively high microporosity. On comparing, the surface area obtained from the Dubinin – Radushkevich (D-R) equation are consistently larger than those obtained from the  $t$ -plot methods. Extrapolating the  $V_{mi}$  (D-R) from the low-pressure region ( $P/P_0 < 0.1$ ) does not completely reduce the effect of mesopores present in the system, causing the value obtained for  $V_{mi}$  (D-R) is larger than the real micropore volume of materials[16].

#### 6.4.1.9 Barrett-Joyner-Halenda (BJH) Method

The pore size distributions (PSDs) of activated carbons are calculated by applying nitrogen adsorption-desorption isotherms data by Barrett-Joyner-Halenda (BJH) method.

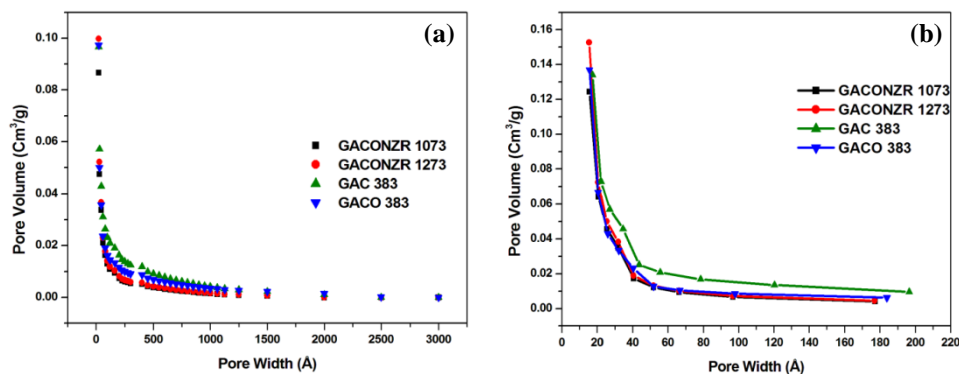


**Figure 6.14:** BJH isotherm analysis (a) Adsorption cumulative pore volume (b) Desorption cumulative pore volume for GAC 383, GACO 383, GACONZR 1073 & GACONZR 1273

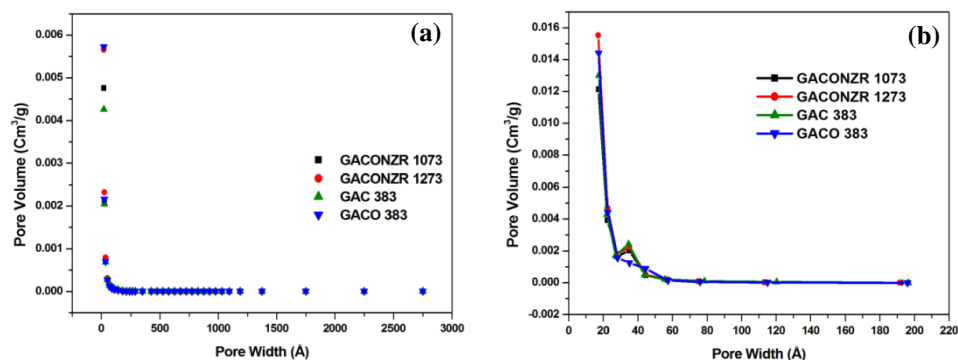


**Figure 6.15 :** BJH isotherm analysis (a) Adsorption dV/dw pore volume (b) Desorption dV/dw pore volume for GAC 383, GACO 383, GACONZR 1073 & GACONZR 1273

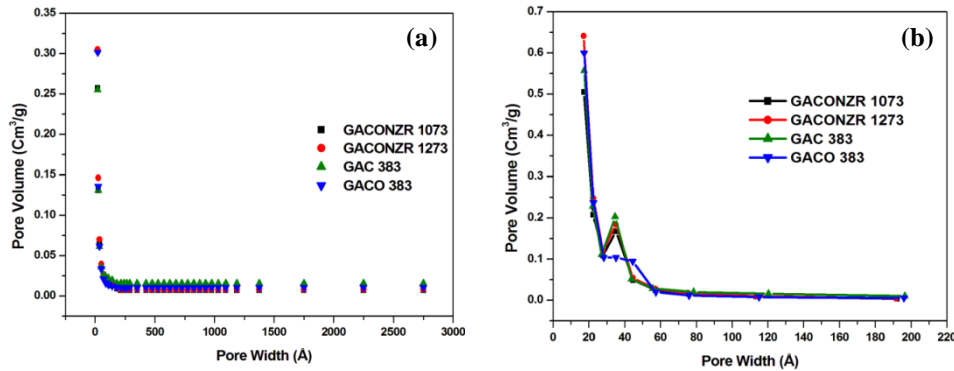


**Figure 6.16:** BJH isotherm analysis (a) Adsorption  $dV/d\log w$  pore volume and (b) Desorption  $dV/d\log w$  pore volume for the carbons, GAC 383, GACO 383, GACONZR 1073 & GACONZR 1273

For GACONZR 1073 the adsorption cumulative surface area ( $ADCSA$ ) of the respective pore is  $216.19 \text{ m}^2/\text{g}$  for a cumulative pore volume ( $ACPV$ ) of  $0.125 \text{ cm}^3/\text{g}$  ( $80.85 \text{ cm}^3/\text{g.STP}$ ) and their desorption cumulative surface area ( $DCSA$ ) found to be  $216.99 \text{ m}^2/\text{g}$  for a cumulative pore volume ( $DCPV$ ) of  $0.124 \text{ cm}^3/\text{g}$  ( $80.20 \text{ cm}^3/\text{g.STP}$ ). The respective adsorption pore width and desorption pore width are  $2.31 \text{ nm}$  and  $2.29 \text{ nm}$ .

**Table 6.8:**  $t$ -plot and BJH isotherm parameters of GAC 383, GACO 383, GACONZR 1073 and GACONZR 1273 using  $\text{N}_2/77\text{K}$

Carbons	$t$ -plot			Barrett-Joyner-Halenda (BJH)					
	$V_{mi}(t) \text{ cm}^3/\text{g.STP}$	$SA_{mi}(t) \text{ m}^2/\text{g}$	$SA_{ext}(t) \text{ m}^2/\text{g}$	$ADCSA \text{ m}^2/\text{g}$	$DCSA \text{ m}^2/\text{g}$	* $ACPV \text{ cm}^3/\text{g}$	* $DCPV \text{ cm}^3/\text{g}$	Pore width (ads) nm	Pore width (des) nm
GAC 383	226.7	588.7	408.1	226.2	220.5	0.138	0.134	2.44	2.43
GACO 383	192.0	540.3	433.7	250.0	242.8	0.142	0.137	2.28	2.25
GACONZR 1073	215.9	617.4	389.2	216.2	217.0	0.125	0.124	2.31	2.29
GACONZR 1273	206.3	574.0	469.1	260.0	276.9	0.147	0.153	2.26	2.21

$$* V_m (\text{cm}^3/\text{g}) = \frac{V_m (\text{cm}^3/\text{g}).\text{STP} \times 28}{22414 \times 0.808}$$

For GACONZR 1273 the adsorption cumulative surface area (ADCSA) of the respective pore is 259.96 m<sup>2</sup>/g for a cumulative pore volume (ACPV) of 0.147 cm<sup>3</sup>/g (95.08 cm<sup>3</sup>/g.STP) and their desorption cumulative surface area (DCSA) found to be 276.85 m<sup>2</sup>/g for a cumulative pore volume (DCPV) of 0.153 cm<sup>3</sup>/g (98.96 cm<sup>3</sup>/g.STP). The respective adsorption pore width and desorption pore width are 2.26 nm and 2.21 nm.

### 6.5 Solid – Liquid Equilibria: Adsorption Studies

Maximum efficiency of GACONZR series of carbons in solid-liquid adsorption is determined by contacting 0.05 g of selected carbons in 100 ml Erlenmeyer flask with 50 ml solutions of phenol (C<sub>0</sub> = 1000 mg/L, equilibrium time 8 hours), p-nitrophenol (C<sub>0</sub> = 1000 mg/L, equilibrium time 8 hours) and methylene blue (C<sub>0</sub> = 500 mg/L, equilibrium time 10 hours). It placed on a water bath shaker for a required equilibrium time at 30<sup>0</sup>C.

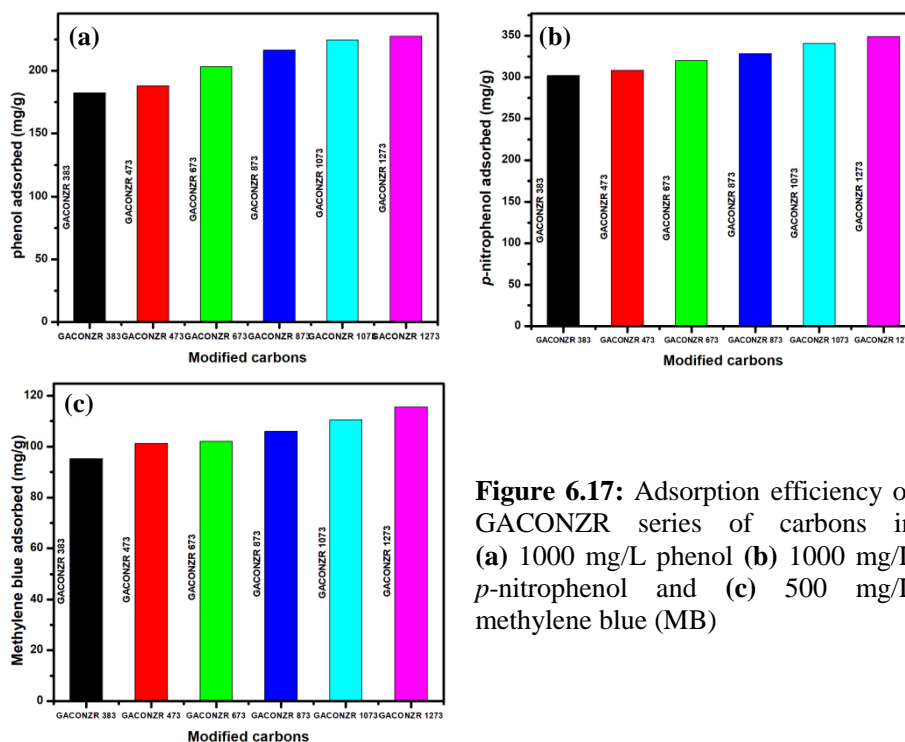
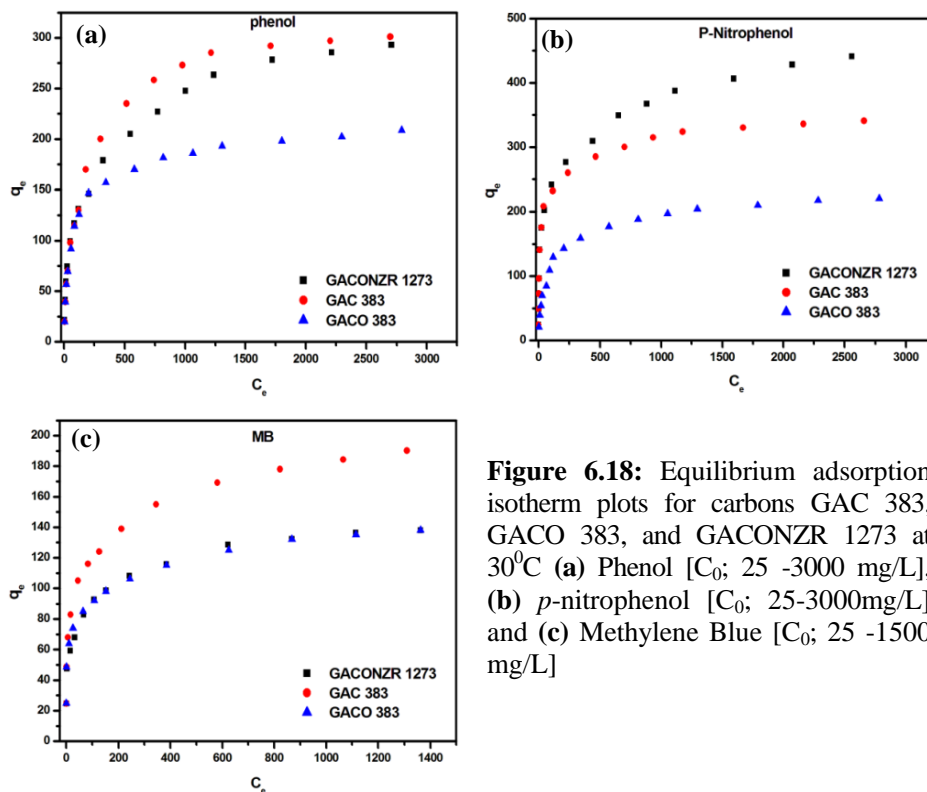


Figure 6.17: Adsorption efficiency of GACONZR series of carbons in (a) 1000 mg/L phenol (b) 1000 mg/L p-nitrophenol and (c) 500 mg/L methylene blue (MB)

Finally the filtered solution is analysed by uv-visible spectrophotometer at appropriate wavelength. Among the series of GACONZR studied, GACONZR 1273 shows maximum efficiency towards phenol, *p*-nitrophenol and methylene blue. This selected GACONZR 1273 is further used for studying solid –liquid equilibria along with basic carbons GAC 383 and GACO 383.

### 6.5.1 Adsorption Studies of Phenol, *P*-Nitrophenol and Methylene Blue

To evaluate the performance of adsorbents and to interpret the experimental data in adsorption processes common adsorption isotherms like Langmuir, Freundlich and Dubinin – Radushkevich (D-R) isotherms are used in this study. Figure 6.18(a)-(c) shows adsorption isotherm of phenol, *p*-nitrophenol and methylene blue (MB) on GAC 383, GACO 383, and GACONZR 1273 at 303 K.



**Figure 6.18:** Equilibrium adsorption isotherm plots for carbons GAC 383, GACO 383, and GACONZR 1273 at 30°C (a) Phenol [ $C_0$ ; 25 -3000 mg/L], (b) *p*-nitrophenol [ $C_0$ ; 25-3000mg/L] and (c) Methylene Blue [ $C_0$ ; 25 -1500 mg/L]



Figure 6.18(a) shows the plot between the amount of phenol adsorbed ( $q_e$ ) against equilibrium concentration ( $C_e$ ). The amount of phenol adsorbed on GACONZR 1273 shows maximum of 293 mg/g. Whereas GAC 383 shows 301 mg/g and GACO 383 shows 209 mg/g. The carbon GACONZR 1273 has more than 40 % efficiency towards phenol compared to GACO 383.

The maximum amount of *p*-nitrophenol adsorbed at equilibrium time of 8 hour on activated carbon samples follows GACONZR 1273 (441 mg/g), GAC 383 (341 mg/g) and GACO 383 (220 mg/g). GACONZR 1273 has twice the efficiency compared to GACO 383 and 29 % efficiency compared to GAC 383 towards *p*-nitrophenol.

Adsorption isotherm plot of new carbons for the adsorption of methylene blue is given in the Figure 6.18(c). The amount of methylene blue adsorbed on GACONZR 1273 has a maximum of 137 mg/g, whereas GAC 383 has value of 190 mg/g and GACO 383 has 138 mg/g.

### **6.5.2 Adsorption of Phenol on GACONZR 1273, GAC 383 and GACO 383 at Temperatures**

Adsorption of phenol on GACONZR 1273, GAC 383 and GACO 383 at five temperatures from 283 to 323K is plotted in the form of different isotherm models. The parameters obtained from Langmuir, Freundlich and Dubinin - Radushkevich isotherm equations along with the coefficient of determination ( $R^2$ ) are given in Table 6.9.

The Langmuir isotherm, which represents monolayer coverage of the adsorbate on the adsorbent surface, is expressed as

$$\frac{C_e}{q_e} = \frac{1}{K_L} + \frac{a_L}{K_L} C_e \quad (6.13)$$

The Langmuir plots of phenol adsorption on GAC 383, GACO 383 and GACONZR 1273 with respect to five temperatures are given in Figure 6.19 (a)–(c). The monolayer capacity  $K_L/a_L$  (or  $q_m$ ) and  $K_L$  are given in Table 6.9. Isotherms constants obtained from GACONZR 1273 are compared with the values obtained from GAC 383 and GACO 383.

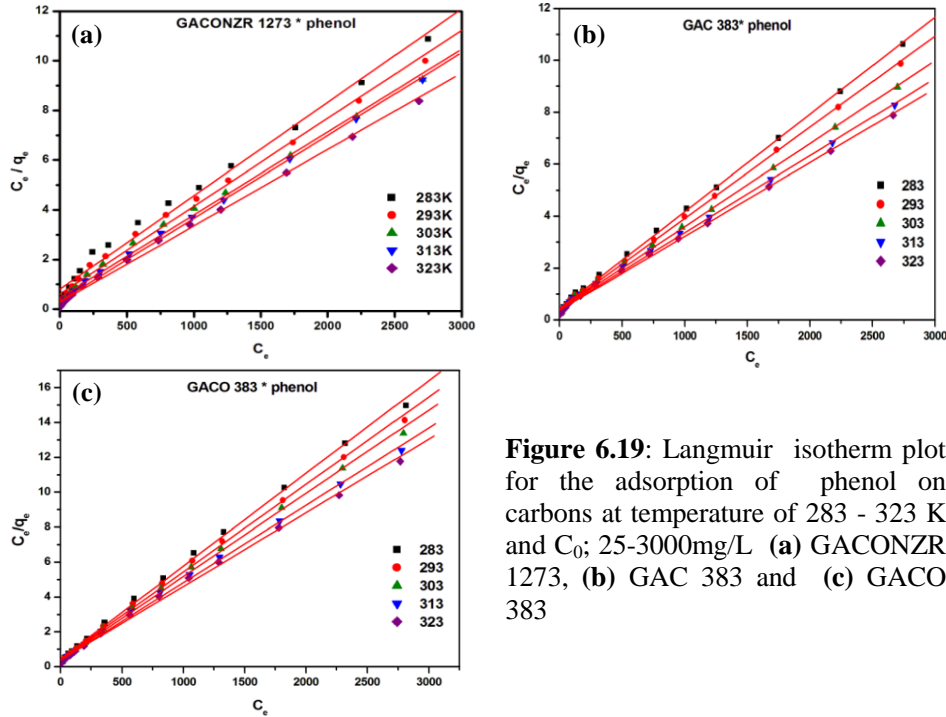


**Figure 6.19:** Langmuir isotherm plot for the adsorption of phenol on carbons at temperature of 283 - 323 K and  $C_0$ ; 25-3000mg/L (a) GACONZR 1273, (b) GAC 383 and (c) GACO 383

The monolayer capacity  $K_L/a_L$  (or  $q_m$ ) increases with temperature, indicates that adsorption is favoured at high temperatures. As seen from Table 6.9, Langmuir isotherm fits well with the experimental data ( $R^2 = 0.99$ ). This may be due to homogenous distribution of active sites on GAC. The maximum monolayer adsorption capacity for GACONZR 1273 at different solution temperature are given as follows 283 K ( $q_m = 265.25$  mg/g &  $K_L = 1.26$  Lg $^{-1}$ ), at 293 K ( $q_m = 282.49$  mg/g &  $K_L = 1.65$  Lg $^{-1}$ ), at 303 K ( $q_m = 295.8$  mg/g &  $K_L = 2.14$  Lg $^{-1}$ ), at 313 K ( $q_m = 301.0$  mg/g &  $K_L = 3.08$  Lg $^{-1}$ ) and at 323 K ( $q_m = 324.68$  mg/g &  $K_L = 3.63$  Lg $^{-1}$ ). It is clearly suggesting the endothermic nature of adsorption i.e. the adsorption rate of phenol on GACONZR 1273 favouring at higher temperature. There is 22 % enhancement in monolayer capacity by rising the temperature from 283 K to 323 K. Percentage of enhancement in monolayer adsorption capacity at each temperature by comparing with GACO 383 are given as follows at 283 K (41 %), at 293 K (42 %), at 303 K (41 %), at 313 K (33 %) and 323K (37 %). For all the temperature studied the percentage of enhancement in monolayer adsorption capacity for GACONZR 1273 is more than 30 % compared to GACO 383.

The linearized form of Freundlich isotherm equation applied is given by the following equation

$$\log q_e = \log K_F + \frac{1}{n} \log C_e \quad (6.14)$$

Plots are given in the Figure 6.20(a)-(c). The calculated Freundlich constant and correlation coefficient are given in the Table 6.9.

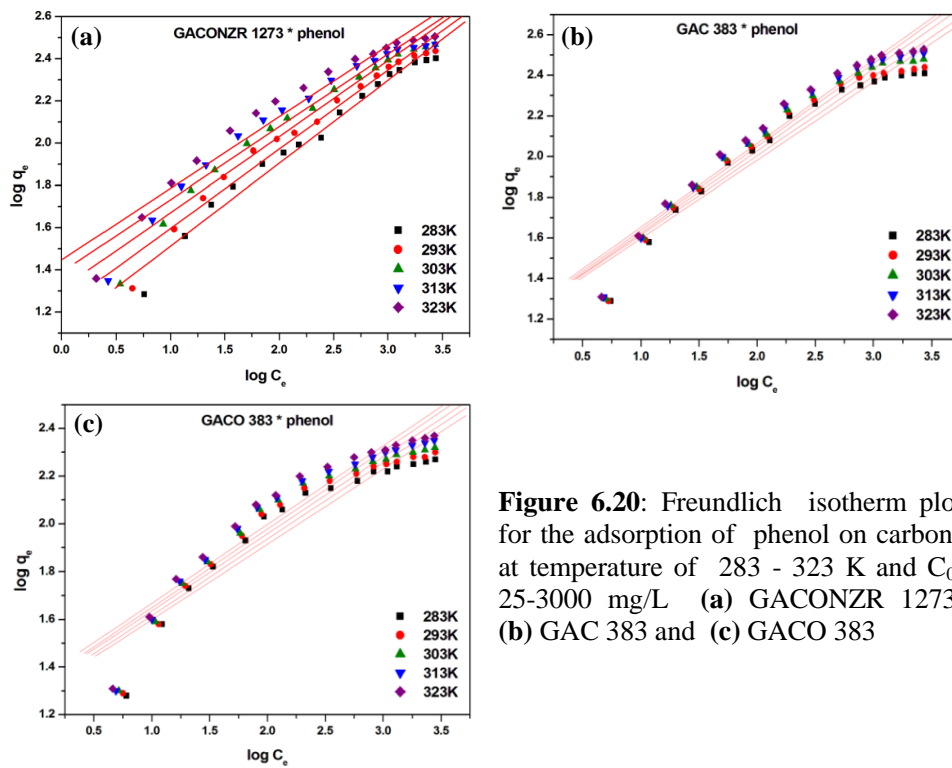


**Figure 6.20:** Freundlich isotherm plot for the adsorption of phenol on carbons at temperature of 283 - 323 K and  $C_0$ ; 25-3000 mg/L (a) GACONZR 1273, (b) GAC 383 and (c) GACO 383

Higher the value of  $n$ , the more favourable the adsorption and stronger the adsorption intensity.  $K_F$  can serve as a measure of the relative adsorptive capacity.

Heterogeneity factor  $n$  and Freundlich constant  $K_F$  ( $\text{Lg}^{-1}$ ) for GACONZR 1273 at different solution temperature are varies as 283K ( $K_F = 13.19 \text{ Lg}^{-1}$  &  $n = 2.55$ ), 293K ( $K_F = 16.64 \text{ Lg}^{-1}$  &  $n = 2.67$ ), 303 K ( $K_F = 20.4 \text{ Lg}^{-1}$  &  $n = 2.77$ ), 313K ( $K_F = 24.99 \text{ Lg}^{-1}$  &  $n = 2.9$ ) and 323K ( $K_F = 27.99 \text{ Lg}^{-1}$  &  $n = 2.95$ ),

whereas for GAC 383,  $K_F$  are found to be within the range of 16.38 – 17.38  $\text{Lg}^{-1}$  and for GACO 383 it is 19.16 – 21.66  $\text{Lg}^{-1}$ . As the values of  $1/n$  are less than unity, the isotherms are characterized by a concave Freundlich isotherm, indicate that significant adsorption takes place at low concentrations, and adsorption becomes less significant at higher concentration [17].

The linear form of the Dubinin-Radushkevich isotherm model applied to the data is

$$\ln q_e = \ln q_{mi} - \beta \varepsilon^2 \quad (6.15)$$

The Dubinin-Radushkevich plot of  $\ln q_e$  against  $[RT \ln(1+1/C_e)]^2$  of phenol adsorption on GAC 383, GACO 383 and GACONZR 1273 with respect to five temperatures are given in Figures 6.21(a)–(c). The parameters such as  $q_{mi}$  (D-R),  $\beta$  and the mean free energy,  $E$  determined from the appropriate plot are given in Table 6.9.

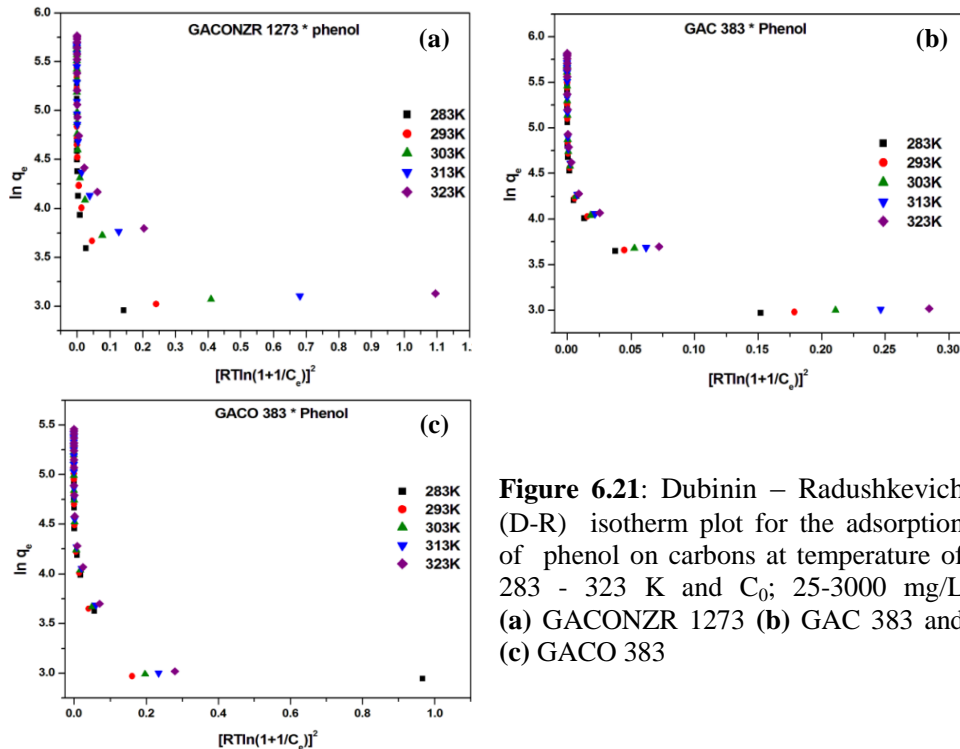


**Figure 6.21:** Dubinin – Radushkevich (D-R) isotherm plot for the adsorption of phenol on carbons at temperature of 283 - 323 K and  $C_0$ ; 25-3000 mg/L (a) GACONZR 1273 (b) GAC 383 and (c) GACO 383

Micropore adsorption capacity  $q_{mi}$  (D-R), and characteristic energy  $E$  obtained from the Dubinin – Radushkevich (D-R) isotherm model for GACONZR 1273 at different temperature are given as; 283K ( $q_{mi} = 49.25$  mg/g &  $E = 0.2728$  kJ/mol), 293K ( $q_{mi} = 52.78$  mg/g &  $E = 0.3544$  kJ/mol), 303K ( $q_{mi} = 56.66$  mg/g &  $E = 0.4564$  kJ/mol), 313K ( $q_{mi} = 59.05$  mg/g &  $E = 0.5872$  kJ/mol), and 323K ( $q_{mi} = 61.26$  mg/g &  $E = 0.7393$  kJ/mol). Whereas, for GAC 383  $q_{mi}$ (D-R) ranges from 55.52 – 59.22 mg/g and  $E$  ranges from 0.267 – 0.362 kJ/mol. For GACO 383  $q_{mi}$  (D-R) range from 46.9- 59.3 mg/g and adsorption energy  $E$  is low and it ranges from 0.273 kJ/mol to 0.359 kJ/mol.

**Table 6.9:** Adsorption isotherm parameter of phenol on GACONZR 1273, GAC 383 and GACO 383 at temperatures ranging from 283-323K

Carbon	Temperature (K)	Langmuir isotherm				Freundlich			D-R Isotherm			E (kJ/mol)
		$K_L/a_L$ (mg/g)	$K_L$ (Lg <sup>-1</sup> )	$a_L \times 10^4$ (Lg <sup>-1</sup> )	$R^2$	n	$K_F$ (Lg <sup>-1</sup> )	$R^2$	$q_{mi}$ (D-R) (mg/g)	$\beta$ mol <sup>2</sup> /kJ <sup>2</sup>	$R^2$	
GACONZR 1273	283	265.3	1.26	47	0.988	2.55	13.2	0.978	49.3	6.7	0.951	0.273
	293	282.5	1.65	58	0.992	2.67	16.6	0.970	52.8	4.0	0.955	0.354
	303	295.8	2.14	71	0.994	2.77	20.4	0.964	56.7	2.4	0.945	0.456
	313	301.0	3.08	103	0.998	2.90	24.5	0.951	59.1	1.5	0.945	0.587
	323	324.7	3.63	112	0.998	2.95	28.0	0.947	61.3	0.9	0.945	0.739
GAC 383	283	266.7	2.33	87	0.998	2.60	16.4	0.935	55.5	7.0	0.966	0.267
	293	284.9	2.46	87	0.998	2.56	16.7	0.935	56.6	6.0	0.966	0.288
	303	312.5	2.48	79	0.998	2.49	16.7	0.945	57.4	5.0	0.966	0.293
	313	336.7	2.53	75	0.998	2.44	17.0	0.951	58.4	4.4	0.966	0.338
	323	352.1	2.68	76	0.998	2.42	17.4	0.951	59.2	3.8	0.966	0.362
GACO 383	283	188.3	2.17	115	0.998	3.17	19.2	0.885	46.9	0.9	0.906	0.729
	293	199.6	2.34	117	0.998	3.13	19.9	0.889	56.1	6.7	0.966	0.273
	303	209.6	2.48	119	0.998	3.12	20.7	0.895	57.4	5.5	0.970	0.302
	313	225.7	2.52	112	0.998	3.05	21.1	0.903	58.8	4.7	0.968	0.328
	323	237.0	2.59	109	0.998	3.02	21.7	0.904	59.3	3.9	0.966	0.359

Experimental data obtained for the adsorption of phenol, *p*-nitrophenol and methylene blue on all the carbon studied are well agreeing with the Langmuir model with the high correlation coefficient values being close to one, as compared with Freundlich model and Dubinin- Radushkevich model. It represents a homogeneous surface of the activated carbon in terms of functional groups and bonding energy [7].

### 6.5.3 Adsorption of *P*-Nitrophenol on GACONZR 1273, GAC 383 and GACO 383 at Temperatures

Distribution of *p*-nitrophenol in the solid -liquid phase adsorption equilibrium state can be expressed by Langmuir, Freundlich and Dubinin-Radushkevich isotherm models.

The Langmuir plots of *p*-nitrophenol adsorption on GAC 383, GACO 383 and GACONZR 1273 with respect to five temperatures are given in Figures 6.22(a)–(c).

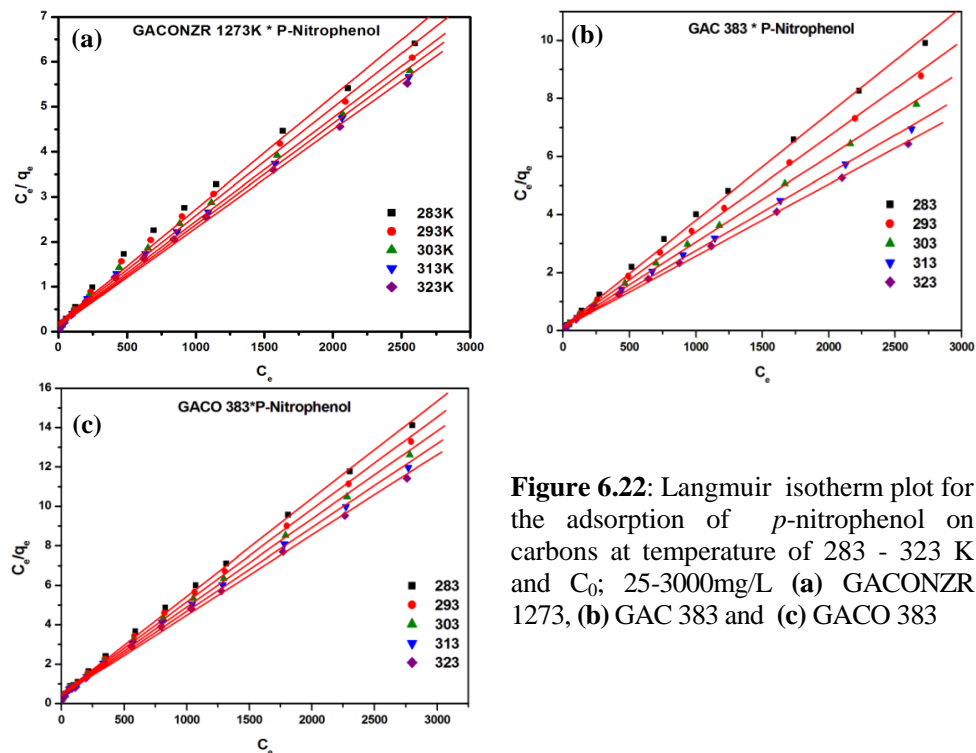


**Figure 6.22:** Langmuir isotherm plot for the adsorption of *p*-nitrophenol on carbons at temperature of 283 - 323 K and  $C_0$ ; 25-3000mg/L (a) GACONZR 1273, (b) GAC 383 and (c) GACO 383

The maximum monolayer adsorption capacity of GACONZR 1273 for the adsorption of *p*-nitrophenol at different temperature are given as follows; at 283K ( $q_m = 396.83 \text{ mg/g}$  &  $K_L = 4.98 \text{ Lg}^{-1}$ ) at 293K ( $q_m = 416.07 \text{ mg/g}$  &  $K_L = 5.62 \text{ Lg}^{-1}$ ), at 303K ( $q_m = 434.78 \text{ mg/g}$  &  $K_L = 6.26 \text{ Lg}^{-1}$ ), at 313K ( $q_m = 444.44 \text{ mg/g}$  &  $K_L = 7.45 \text{ Lg}^{-1}$ ) and at 323K ( $q_m = 458.72 \text{ mg/g}$  &  $K_L = 8.36 \text{ Lg}^{-1}$ ). Large values of the Langmuir constant ( $K_L$ ) implies a strong bonding on a finite number of binding sites. Langmuir constants (Table 6.10) slightly increased with temperature indicate an endothermic process for the *p*-nitrophenol adsorption on studied activated carbons.

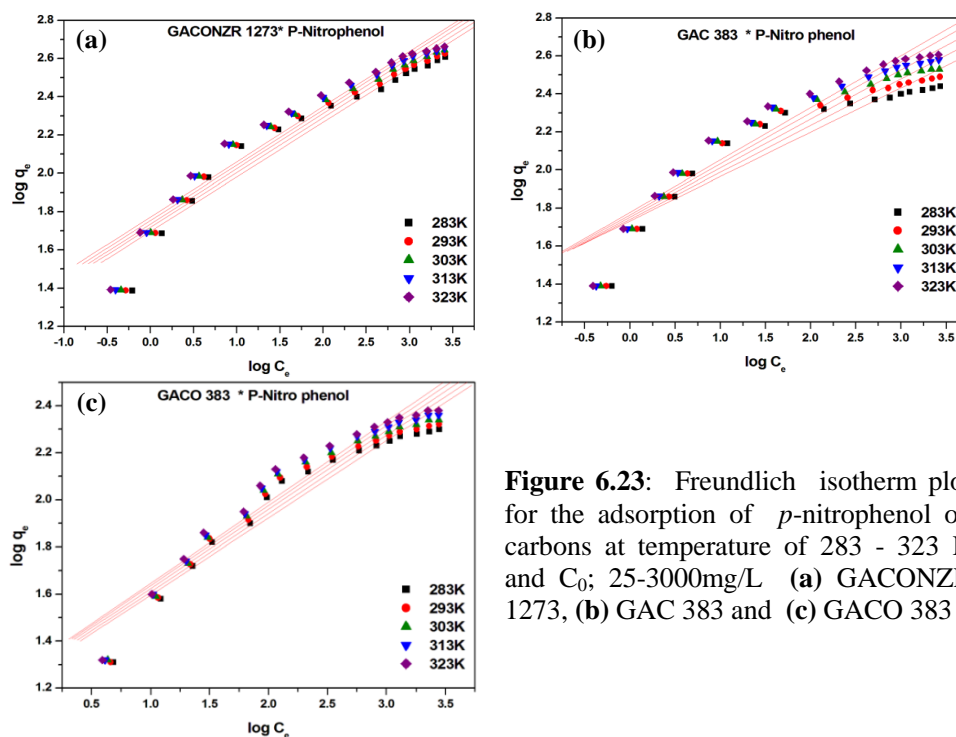


**Figure 6.23:** Freundlich isotherm plot for the adsorption of *p*-nitrophenol on carbons at temperature of 283 - 323 K and  $C_0$ ; 25-3000mg/L (a) GACONZR 1273, (b) GAC 383 and (c) GACO 383

Percentage of enhancement in monolayer capacity of GACONZR 1273 for the adsorption of *p*-nitrophenol compared to GAC 383 at temperatures are given as; 283K (46 %), 293K (37 %), 303K (28 %), 313K (18 %) and for 323K (14 %). On comparing with GACO 383, percentage enhancement at temperatures are 283K (97 %), 293K (95 %), 303K (94 %), 313K (89 %) and at 323K (87 %). It shows that removal was increased with the solution temperature. At higher

temperatures more molecules have sufficient energy to interact with the active sites of adsorbent.

The isotherm data for *p*-nitrophenol adsorption on GAC 383, GACO 383 and GACONZR 1273 were fitted into the Freundlich equation is given in Figures 6.23(a)–(c). Parameters are listed in Table 6.10.

$K_F$  and  $n$  values of GACONZR 1273 at temperatures are given as follows; 283K ( $K_F = 49.69 \text{ Lg}^{-1}$  &  $n = 3.51$ ), 293K ( $K_F = 52.23 \text{ Lg}^{-1}$  &  $n = 3.49$ ), 303K ( $K_F = 54.39 \text{ Lg}^{-1}$  &  $n = 3.47$ ), 313K ( $K_F = 56.73 \text{ Lg}^{-1}$  &  $n = 3.46$ ), and at 323K ( $K_F = 59.16 \text{ Lg}^{-1}$  &  $n = 3.47$ ) whereas for GAC 383,  $K_F$  values are found to be within the range of 53.49 – 59.9  $\text{Lg}^{-1}$  and for GACO 383 it is 18.48 – 20.04  $\text{Lg}^{-1}$ .

The value of  $n$  indicates favourable adsorption when  $1 < n < 10$ . It varies for carbons are given as; GACONZR 1273 (3.46–3.51), GAC 383 (4.26–3.64), and for GACO 383 (3.90–3.97). Therefore, the adsorption of phenol on GACONZR 1273, GAC 383 and GACO 383 are appears to be favourable.

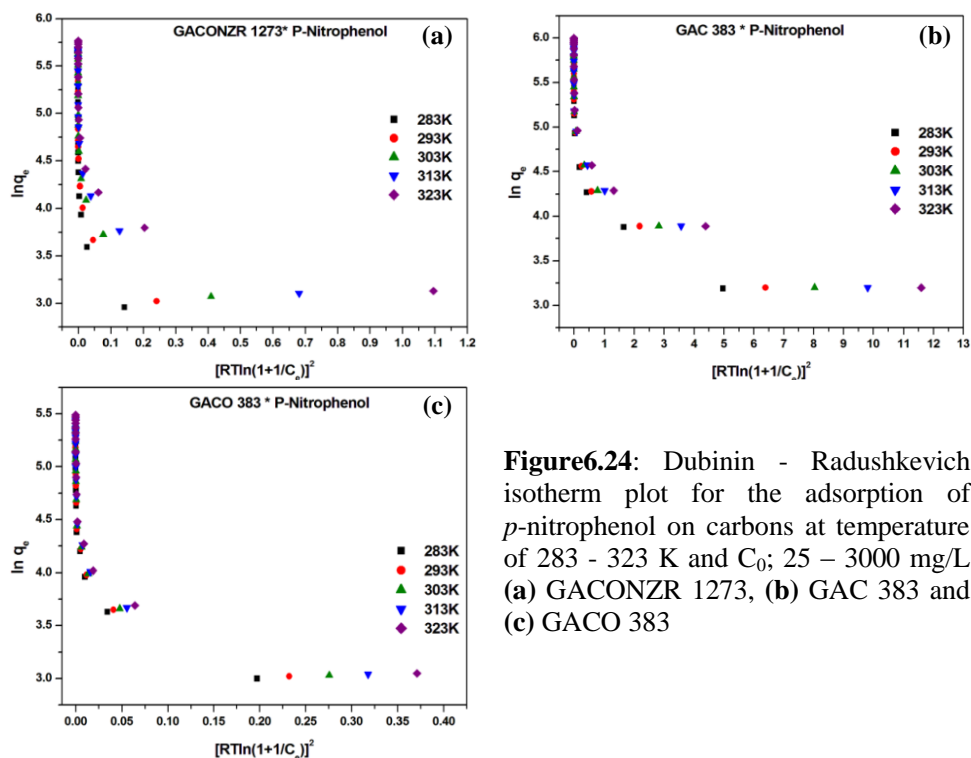


**Figure 6.24:** Dubinin - Radushkevich isotherm plot for the adsorption of *p*-nitrophenol on carbons at temperature of 283 - 323 K and  $C_0$ ; 25 – 3000 mg/L (a) GACONZR 1273, (b) GAC 383 and (c) GACO 383



The Dubinin-Radushkevich (D-R) plot of  $\ln q_e$  against  $[RT \ln (1+1/C_e)]^2$  of *p*-nitrophenol adsorption on GAC 383, GACO 383 and GACONZR 1273 with respect to five temperatures are given in Figures 6.24(a)–(c). Parameters were determined from the appropriate plot and are given in Table 6.10.

Micropore volume  $q_{mi}(D-R)$ , and characteristic energy  $E$  obtained from Dubinin – Radushkevich (D-R) isotherm model for GACONZR 1273 at different temperature are given as; 283 K ( $q_{mi} = 85.81$  mg/g &  $E = 1.40$  kJ/mol), 293K ( $q_{mi} = 86.88$  mg/g &  $E = 1.62$  kJ/mol), 303K ( $q_{mi} = 88.14$  mg/g &  $E = 1.80$  kJ/mol), 313K ( $q_{mi} = 88.69$  mg/g &  $E = 2.01$  kJ/mol), and at 323K ( $q_{mi} = 90.48$  mg/g &  $E = 2.23$  kJ/mol). Whereas for GAC 383  $q_{mi}(D-R)$  varies 75.77 – 81.24 mg/g and  $E$  value ranges 1.6 – 2.21 kJ/mol. For GACO 383  $q_{mi}(D-R)$  value varies from 49.61 – 52.74 mg/g and  $E$  value ranges from 0.329 kJ/mol to 0.446 kJ/mol.

**Table 6.10:** Adsorption isotherm parameter of *p*-nitrophenol on GACONZR 1273, GAC 383 and GACO 383 at temperatures ranging from 283-323K

Carbon	Temperature (K)	Langmuir isotherm				Freundlich			D-R Isotherm			E (kJ/mol)
		$K_L/a_L$ (mg/g) ( $q_m$ )	$K_L$ (Lg <sup>-1</sup> )	$a_L * 10^4$ (Lg <sup>-1</sup> )	R <sup>2</sup>	n	$K_F$ (Lg <sup>-1</sup> )	R <sup>2</sup>	$q_{mi}$ (D-R) (mg/g)	$\beta$ mol <sup>2</sup> /kJ <sup>2</sup>	R <sup>2</sup>	
GACONZR 1273	283	396.8	4.98	125	0.990	3.51	49.7	0.933	85.8	0.26	0.953	1.40
	293	416.7	5.62	135	0.992	3.49	52.2	0.937	86.9	0.19	0.956	1.62
	303	434.8	6.26	144	0.994	3.47	54.4	0.918	88.1	0.16	0.960	1.80
	313	444.4	7.45	168	0.996	3.46	56.7	0.933	88.7	0.12	0.958	2.01
	323	458.7	8.36	182	0.996	3.47	59.2	0.937	90.5	0.10	0.966	2.23
GAC 383	283	272.5	7.61	279	0.998	4.26	53.5	0.861	75.8	0.23	0.966	1.60
	293	304.9	8.36	274	0.998	4.06	55.0	0.880	77.0	0.18	0.966	1.75
	303	340.1	9.03	265	0.998	3.88	56.6	0.893	78.2	0.15	0.966	1.90
	313	377.4	9.40	249	0.998	3.73	58.1	0.906	79.5	0.12	0.966	2.07
	323	403.2	10.7	265	0.998	3.64	59.9	0.914	81.2	0.10	0.966	2.21
GACO 383	283	201.6	2.06	102	0.998	3.05	18.5	0.925	49.6	4.63	0.951	0.33
	293	213.2	2.14	101	0.998	3.01	18.9	0.927	50.6	3.97	0.953	0.36
	303	224.2	2.24	100	0.998	2.97	19.3	0.929	51.3	3.35	0.951	0.37
	313	235.3	2.31	98	0.998	2.94	19.7	0.931	52.1	2.92	0.951	0.41
	323	245.7	2.41	98	0.998	2.91	20.0	0.933	52.7	2.51	0.949	0.45

### 6.5.4 Adsorption of Methylene Blue (MB) on GAONZR 1273, GAC 383 and GACO 383 at Temperatures

Equilibrium adsorption isotherm for the removal of methylene blue from aqueous solution using activated carbons GAC 383, GACO 383 and GAONZR 1273 has been investigated at different temperature 283, 293, 303, 313 and 323 K.

The Langmuir plots of methylene blue adsorption on GAC 383, GACO 383 and GAONZR 1273 with respect to five temperatures are given in Figures 6.25(a)–(c).

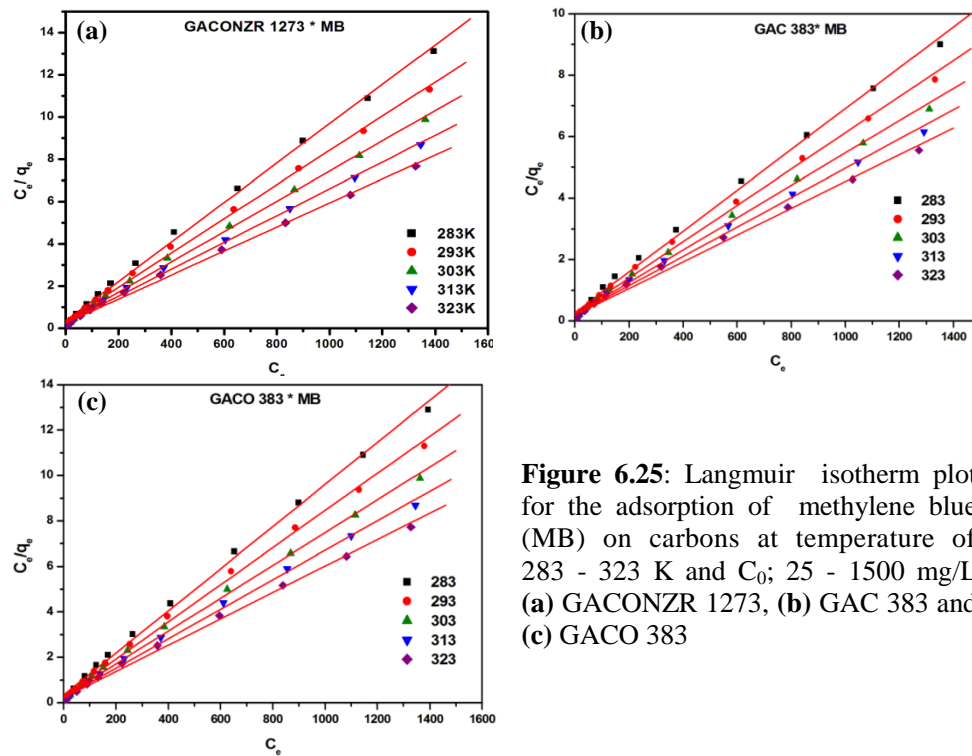


**Figure 6.25:** Langmuir isotherm plot for the adsorption of methylene blue (MB) on carbons at temperature of 283 - 323 K and  $C_0$ ; 25 - 1500 mg/L (a) GAONZR 1273, (b) GAC 383 and (c) GACO 383

The maximum monolayer adsorption capacity of GAONZR 1273 for the adsorption of methylene blue at different temperature are given as; 283 K ( $q_m = 107.30$  mg/g &  $K_L = 2.77$  Lg<sup>-1</sup>), 293 K ( $q_m = 123.61$  mg/g &  $K_L = 3.07$  Lg<sup>-1</sup>), 303 K ( $q_m = 139.86$  mg/g &  $K_L = 3.46$  Lg<sup>-1</sup>), 313 K ( $q_m = 157.73$  mg/g &  $K_L = 3.78$  Lg<sup>-1</sup>), 323K ( $q_m = 176.06$  mg/g &  $K_L = 4.01$  Lg<sup>-1</sup>). For GAC 383

monolayer adsorption capacity increases from 150.6 mg/g to 229.36 mg/g and for GACO 383 increases from 107.99 mg/g to 172.41 mg/g.

The monolayer adsorption capacity of GACONZR 1273 increases 15.8 %, GAC 383 increases 48 % and GACO 383 increases 22 % by rising the temperature from 283 K to 323 K. This indicates that adsorption uptake increases with temperature. This phenomenon may be caused by the fact that the adsorption reaction is an endothermic process. Higher temperature promotes the methylene blue to penetrate inside the carbon pores, and otherwise chemical interaction occurred between adsorbate and surface functional group of adsorbent. As a result, the adsorption capacity increased along with the solution temperature [18].

The Freundlich plots of phenol adsorption on GAC 383, GACO 383 and GACONZR 1273 with respect to five temperatures are given in Figures 6.26(a)–(c).  $K_F$  and  $n$  value are given in the Table 6.11.

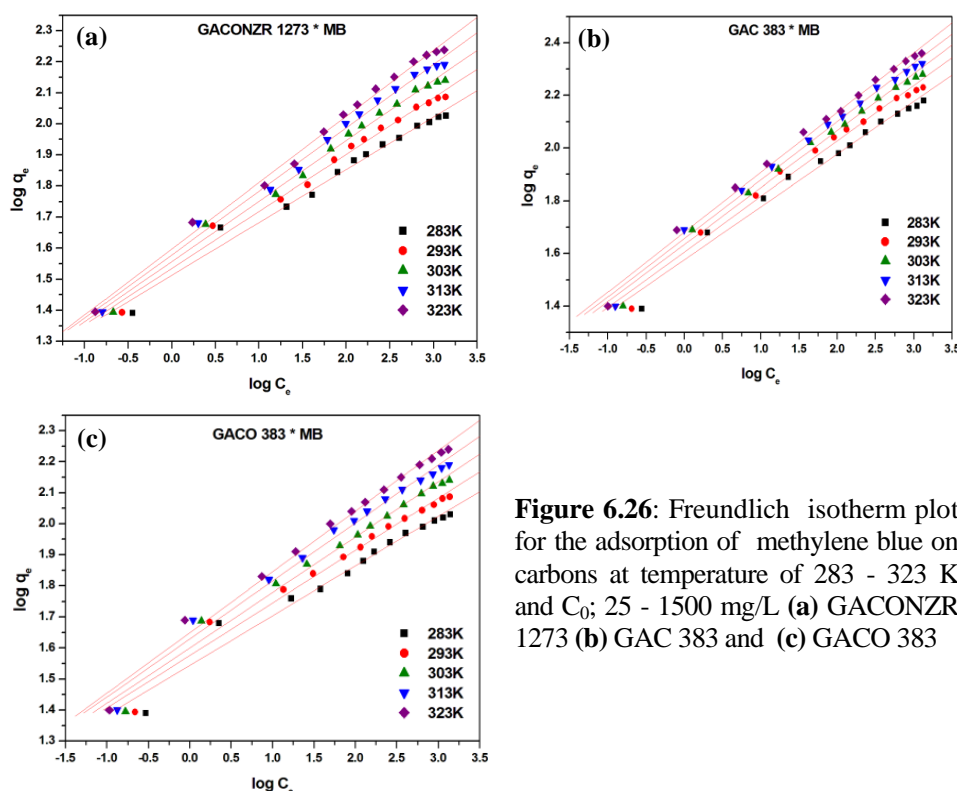


**Figure 6.26:** Freundlich isotherm plot for the adsorption of methylene blue on carbons at temperature of 283 - 323 K and  $C_0$ ; 25 - 1500 mg/L (a) GACONZR 1273 (b) GAC 383 and (c) GACO 383

$K_F$  and  $n$  values of GACONZR 1273 at different temperature are given as follows; 283 K ( $K_F = 32.57 \text{ Lg}^{-1}$  &  $n = 5.89$ ), 293 K ( $K_F = 34.29 \text{ Lg}^{-1}$  &  $n = 5.47$ ), 303 K ( $K_F = 36.03 \text{ Lg}^{-1}$  &  $n = 5.15$ ), 313 K ( $K_F = 37.89 \text{ Lg}^{-1}$  &  $n = 4.9$ ), 323 K ( $K_F = 39.59 \text{ Lg}^{-1}$  &  $n = 4.69$ ) whereas for GAC 383,  $K_F$  values are found to be within the range of  $37.67 - 47.80 \text{ Lg}^{-1}$  and for GACO 383 it is  $35.09 - 44.58 \text{ Lg}^{-1}$ .

These  $n$  values are found to be in the range of  $4.69 - 5.89$  for GACONZR 1273,  $1.58 - 1.68$  for GAC 383 and  $6.27 - 5.12$  for GACO 383. Therefore, the adsorption of methylene blue (MB) on GACONZR 1273, GAC 383 and GACO 383 are appearing to be favourable.

The Dubinin-Radushkevich (D-R) plot for methylene blue (MB) adsorption on GAC 383, GACO 383 and GACONZR 1273 with respect to five temperatures are given in Figure 6.27 (a) – (c).

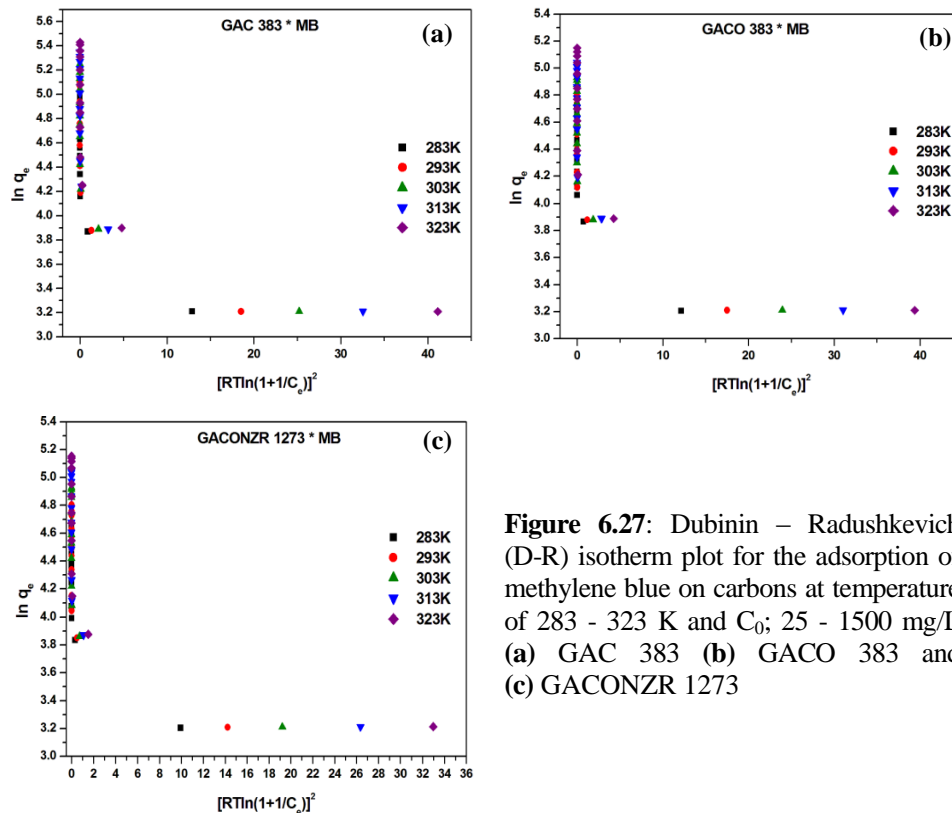


**Figure 6.27:** Dubinin – Radushkevich (D-R) isotherm plot for the adsorption of methylene blue on carbons at temperature of 283 - 323 K and  $C_0$ ; 25 - 1500 mg/L (a) GAC 383 (b) GACO 383 and (c) GACONZR 1273

Micro pore volume  $q_{mi}$  (D-R) and characteristic energy  $E$  obtained from Dubinin – Radushkevich (D-R) isotherm model for GACONZR 1273 at different temperature are given as; at 283K ( $q_{mi} = 50.78$  mg/g &  $E = 2.62$  kJ/mol), 293K ( $q_{mi} = 52.67$  &  $E = 3.06$  kJ/mol), 303K ( $q_{mi} = 54.07$  mg/g &  $E = 3.50$  kJ/mol), 313K ( $q_{mi} = 55.35$ mg/g &  $E = 4.04$  kJ/mol), 323K ( $q_{mi} = 56.54$  mg/g &  $E = 4.46$  kJ/mol). Whereas for GAC 383  $q_{mi}$  (D-R) ranges from 57.43– 62.78 mg/g and  $E$  ranges from 2.75 – 4.68 kJ/mol. For GACO 383  $q_{mi}$  (D-R) range from 54.15 – 60.98 mg/g and  $E$  ranges from 2.78 kJ/mol to 4.66 kJ/mol.

**Table 6.11:** Adsorption isotherm parameter of methylene blue (MB) on GACONZR 1273, GAC 383 and GACO 383 at temperatures ranging from 283-323K

Carbon	Temperature (K)	Langmuir isotherm				Freundlich			D-R Isotherm			
		$K_L/a_L$ (mg/g)	$K_L$ (Lg <sup>-1</sup> )	$a_L \times 10^{-4}$ (Lg <sup>-1</sup> )	$R^2$	$n$	$K_F$ (Lg <sup>-1</sup> )	$R^2$	$q_{mi}$ (D-R) mg/g	$\beta$ mol <sup>2</sup> /kJ <sup>2</sup>	$R^2$	$E$ (kJ/mol)
GACONZR 1273	283	107.3	2.77	260	0.998	5.89	32.6	0.982	50.8	0.073	0.974	2.62
	293	123.6	3.07	250	0.998	5.47	34.3	0.988	52.7	0.053	0.962	3.06
	303	139.9	3.46	250	0.998	5.15	36.0	0.990	54.1	0.041	0.955	3.50
	313	157.7	3.78	240	0.996	4.90	37.9	0.992	55.4	0.031	0.949	4.04
	323	176.1	4.01	230	0.996	4.69	39.6	0.994	56.5	0.025	0.941	4.46
GAC 383	283	150.6	3.74	248	0.996	1.58	37.7	0.982	57.4	0.066	0.943	2.75
	293	169.5	4.54	268	0.996	1.61	40.7	0.984	58.8	0.047	0.935	3.26
	303	190.1	4.8	252	0.996	1.63	42.9	0.990	60.3	0.036	0.935	3.75
	313	209.6	5.13	245	0.994	1.66	45.3	0.992	61.6	0.028	0.937	4.21
	323	229.4	5.51	240	0.994	1.68	47.8	0.994	62.8	0.023	0.941	4.68
GACO 383	283	108.0	2.89	268	0.998	6.27	35.1	0.968	54.2	0.065	0.972	2.77
	293	122.4	3.37	275	0.996	5.92	37.7	0.976	56.3	0.047	0.960	3.26
	303	138.7	3.60	259	0.996	5.61	39.8	0.982	58.0	0.036	0.955	3.74
	313	154.3	4.31	279	0.996	5.33	42.3	0.984	59.5	0.028	0.951	4.19
	323	172.4	4.59	266	0.996	5.12	44.6	0.988	61.0	0.023	0.953	4.66

### 6.5.5 John-Sivanandan Achari (J-SA) Isotherm for Solid-Liquid Equilibria

Systematic evaluation of different solid-liquid adsorption systems are analysed and evaluated using John – Sivanandan Achari (J-SA) isotherm models [19- 21]

$$\log \log C_e = C + n \log q_e$$

Where  $C_e = C_e \times 10^N$  to make  $\log \log C_e$  positive.

The adsorption efficiency of the newly developed carbons GACONZR 1273 towards methylene blue (MB), phenol (P) and *p*-nitrophenol (PNP) are evaluated using John-Sivanandan Achari isotherm models. The adsorption efficiency obtained from John-Sivanandan Achari isotherm model is compared to Langmuir (L), Dubinin-Radushkevich (D-R) and Freundlich (F) isotherm models.

The John-Sivanandan Achari isotherm plot for methylene blue (MB) adsorption shows three distinct phases in the graph. The quantity of methylene blue adsorbed in each phase is given as *phase I*  $q_I(J)$  (60.66mg/g), *phase II*  $q_{II}(J)$  (73.36 mg/g), *phase III*,  $q_{III}(J)$  (5.03 mg/g) and the total adsorption capacity  $q_T(J)$  determined from  $\log q_T(J)$  corresponding to the highest  $\log \log C_e$  is 139.05 mg/g.

This means 43.6 % of the total adsorption takes place during the *phase I* with specific adsorption mechanism while 52.8 % coverage occurs during the second phase and 3.6 % of the total adsorption takes place during the *phase III* with a different adsorption mechanism.

According to John-Sivanandan Achari (J-SA) isotherm model, adsorption of phenol on GACONZR 1273 follows three distinct phase change mechanism. For adsorption in *Phase I*  $q_I(J)$  is 144.51mg/g, *phase II* is 130.28 mg/g, *Phase III* is 22.17 mg/g. These three phase changes indicate that higher adsorption of phenol is favoured by the large proportion of micropores in GACONZR 1273.

*p*-nitrophenol is less soluble in water due to the presence of a hydrophobic group  $NO_2$  in it and therefore adsorbed strongly than phenol and methylene blue, which indicate the high values of  $q_T(J)$  equal to 444.73 mg/g.

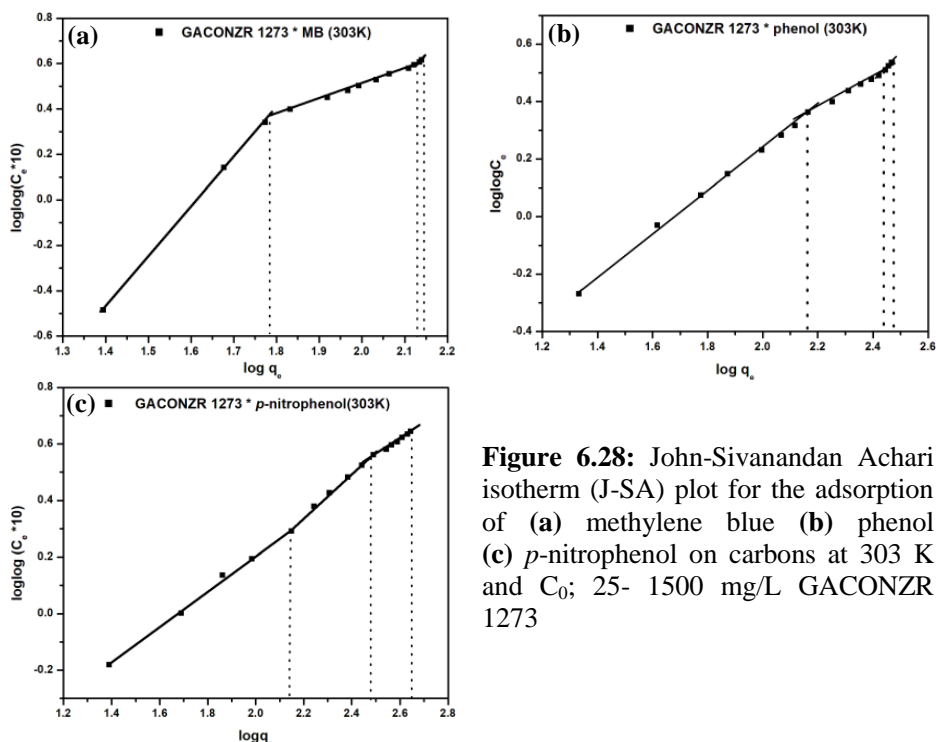


**Figure 6.28:** John-Sivanandan Achari isotherm (J-SA) plot for the adsorption of (a) methylene blue (b) phenol (c) *p*-nitrophenol on carbons at 303 K and  $C_0$ ; 25- 1500 mg/L GACONZR 1273

Comparison of adsorption capacity (mg/g) obtained for the adsorption of methylene blue, phenol and *p*-nitrophenol using John-Sivanandan Achari (*J-SA*) isotherm, Langmuir (*L*) isotherm, Freundlich (*F*) isotherm and Dubinin – Radushkevich (*D-R*) isotherm models are given in Table 6.12.

Adsorption capacity of carbon obtained from Langmuir and John-Sivanandan Achari (*J-SA*) isotherm models are more comparable.

**Table 6.12:** John-Sivanandan Achari (J-SA), Langmuir, Dubinin-Radushkevich (D-R) and Freundlich isotherm models: comparison of adsorption capacity (mg/g) and surface area (m<sup>2</sup>/g) for the adsorption of phenol, *p*-nitrophenol and methylene blue on carbon GACONZR 1273, GAC 383 and GACO 383 (T = 303K)

Carbons	Adsorbate (cross sectional area nm <sup>2</sup> )	J-SA adsorption capacity mg/g				Langmuir q <sub>m</sub> (L) mg/g (*SA m <sup>2</sup> /g)	q <sub>m</sub> (D-R) mg/g (*SA m <sup>2</sup> /g)	Freundlich q <sub>r</sub> (mg/g) (*SA m <sup>2</sup> /g)
		q <sub>I</sub> (J-SA) mg/g (*SA m <sup>2</sup> /g)	q <sub>II</sub> (J-SA) mg/g (*SA m <sup>2</sup> /g)	q <sub>III</sub> (J-SA) mg/g (*SA m <sup>2</sup> /g)	q <sub>r</sub> (J-SA) mg/g (*SA m <sup>2</sup> /g)			
GACONZR 1273	*MB (1.2)	60.7 (137.1)	73.4 (165.8)	5.0 (11.3)	139.1 (314.2)	139.9 (316.1)	54.1 (122.2)	36.0 (81.3)
	*P (0.522)	144.5 (482.8)	130.3 (435.2)	22.2 (74.1)	297.0 (992.1)	299.4 (1000.2)	20.4 (68.2)	56.7 (189.4)
	*PNP (0.525)	141.5 (321.5)	159.9 (363.4)	143.4 (326.0)	444.7 (1010.9)	434.8 (988.3)	88.1 (200.3)	54.4 (123.7)
GAC 383	MB	67.5 (152.5)	124.4 (281.1)	*ND	191.9 (433.6)	190.1 (429.6)	60.3 (136.3)	42.9 (96.9)
	P	72.9 (243.4)	209.8 (700.9)	19.2 (64.3)	301.9 (1008.7)	312.5 (1044.0)	57.4 (191.7)	16.7 (55.9)
	PNP	*ND	210.15 (477.7)	134.07 (304.8)	345.22 (784.7)	334.5 (760.2)	78.2 (177.7)	60.7 (138.1)
GACO 383	MB	66.6 (150.5)	71.8 (162.2)	*ND	138.4 (312.7)	138.7 (313.4)	58.0 (131.0)	39.8 (90.0)
	PNP	56.4 (188.4)	93.1 (311.1)	62.7 (209.4)	212.2 (708.8)	209.6 (700.2)	57.4 (191.8)	20.7 (69.2)
	P	52.3 (118.8)	85.6 (194.6)	84.2 (191.5)	222.1 (504.9)	224.2 (509.7)	51.3 (116.6)	19.3 (43.9)

\*MB - Methylene blue \*P - phenol, \*PNP - *p*-nitrophenol, \*ND – not detected

$$*SA(m^2/g) = \frac{q \text{ (mg/g)} \times 6.022 \times 10^{23} \times \text{cross sectional area of adsorbate}}{\text{Molecular weight of adsorbate}}$$



### 6.5.5.1 John - Sivanandan Achari Isotherm for Phenol, *p*-Nitrophenol and Methylene Blue (MB) Adsorption on GACONZR 1273 at Temperatures

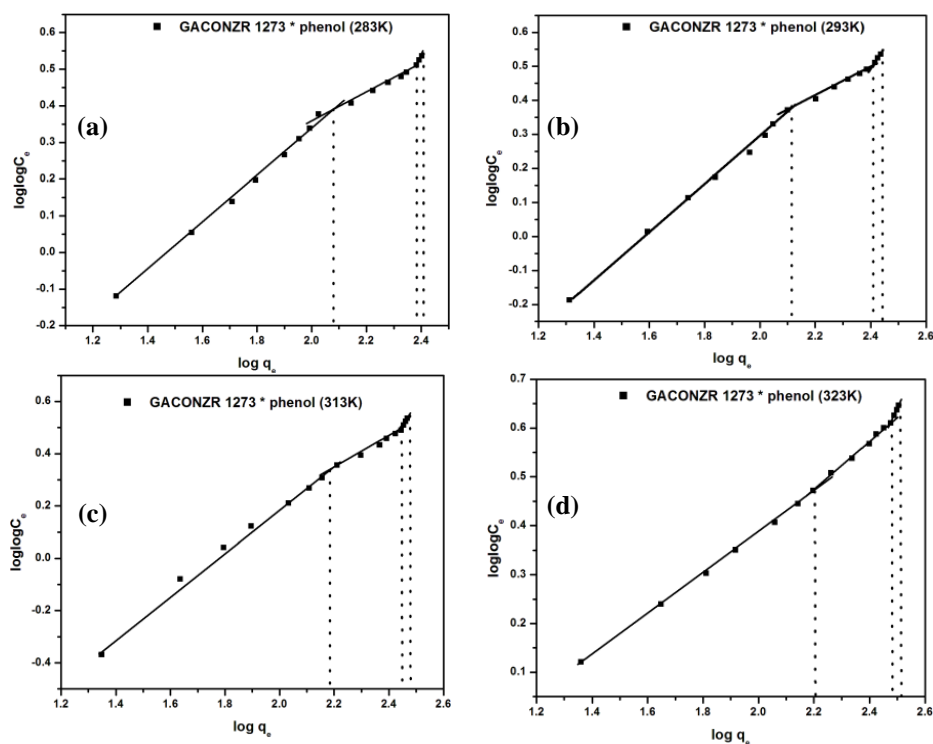


**Figure 6.29:** John-Sivanandan Achari (J-SA) isotherm plots for phenol adsorption on GACONZR 1273 at temperatures (a) 283 K (b) 293 K (c) 313 K and (d) 323 K

Adsorption of phenol, *p*-nitrophenol and methylene blue on GACONZR 1273 in each phase increases with increase in temperature. Regarding the adsorption of phenol, enhancement of adsorption in each phase is given as;  $q_I$  J-SA (from 115.56 mg/g to 160.25 mg/g),  $q_{II}$  J-SA (from 120.34 to 140.58 mg/g) and  $q_{III}$  J-SA (from 18.80 to 30.32 mg/g).

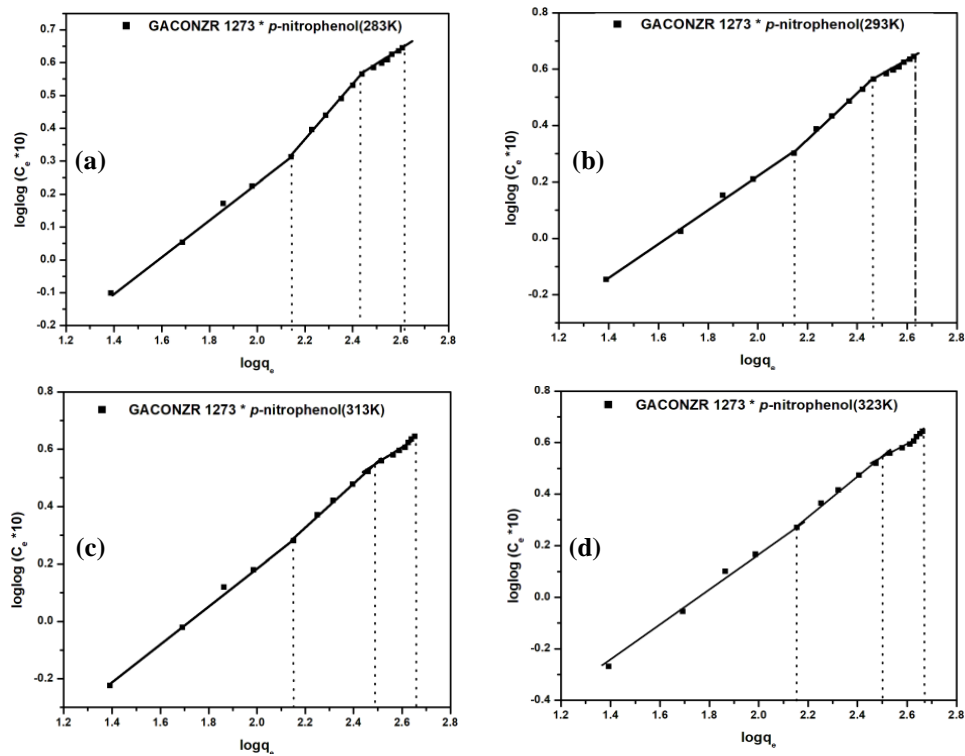


**Figure 6.30:** John-Sivanandan Achari (J-SA) isotherm plots for *p*-nitrophenol adsorption on GACONZR 1273 at temperatures (a) 283 K (b) 293K (c) 313K and (d) 323 K

For *p*-nitrophenol adsorption, phase change occurs with rise of temperature is given as;  $q_I J-SA$  (139.38 mg/g - 142.50 mg/g),  $q_{II} J-SA$  (134.53 -165.86 mg//g) and  $q_{III} J-SA$  (139.27– 156.53 mg/g).

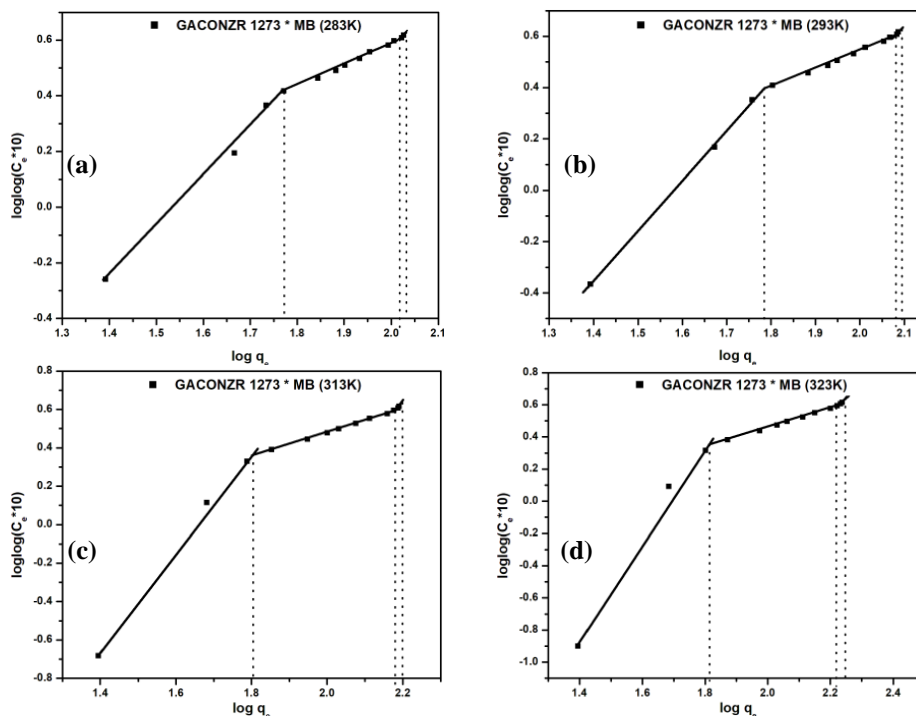


Figure 6.31: John-Sivanandan Achari (J-SA) isotherm plot for methylene blue adsorption on GACONZR 1273 at temperatures (a) 283 K (b) 293K (c) 313K and (d) 323 K

Table 6.13: John - Sivanandan Achari (J-SA) isotherm parameter for the adsorption of phenol, *p*-nitrophenol and methylene blue (MB) on carbon GACONZR 1273 at 283 - 323K

Carbon	T temperature (K)	Phenol			<i>p</i> -nitrophenol			Methylene blue		
		q <sub>I</sub> (J-SA) mg/g (SA m <sup>2</sup> /g)	q <sub>II</sub> (J-SA) mg/g (SA m <sup>2</sup> /g)	q <sub>III</sub> (J-SA) mg/g (SA m <sup>2</sup> /g)	q <sub>I</sub> (J-SA) mg/g (SA m <sup>2</sup> /g)	q <sub>II</sub> (J-SA) mg/g (SA m <sup>2</sup> /g)	q <sub>III</sub> (J-SA) mg/g (SA m <sup>2</sup> /g)	q <sub>I</sub> (J-SA) mg/g (SA m <sup>2</sup> /g)	q <sub>II</sub> (J-SA) mg/g (SA m <sup>2</sup> /g)	q <sub>III</sub> (J-SA) mg/g (SA m <sup>2</sup> /g)
GACONZR 1273	283	115.6 (386.0)	120.3 (402.0)	18.8 (62.8)	139.4 (316.8)	134.5 (305.8)	139.3 (316.6)	59.0 (133.2)	44.8 (101.3)	3.9 (8.8)
	293	129.6 (433.1)	126.6 (422.9)	20.4 (68.2)	140.4 (319.2)	150.1 (341.3)	141.3 (321.2)	60.7 (137.1)	59.4 (134.3)	3.8 (8.5)
	303	144.5 (482.8)	130.3 (435.2)	22.2 (74.1)	141.5 (321.5)	159.9 (363.4)	143.4 (326.0)	60.7 (137.1)	73.4 (165.8)	5.0 (11.3)
	313	153.1 (511.5)	134.4 (449.1)	28.7 (95.8)	142.5 (323.9)	165.5 (376.3)	150.1 (341.1)	63.4 (143.3)	86.9 (196.4)	7.1 (16.0)
	323	160.3 (752.4)	140.6 (252.6)	30.3 (101.3)	142.5 (323.9)	165.9 (377.0)	156.5 (355.8)	64.9 (146.6)	100.6 (227.2)	10.4 (23.4)

Effective adsorption of methylene blue with rise of temperature in each phase is given as;  $q_I$ J-SA (58.95mg/g - 64.88mg/g),  $q_{II}$ J-SA (44.82-100.55 mg/g),  $q_{III}$ J-SA (3.90 – 10.37 mg/g).

## 6.6 Comparison of Adsorption Isotherms for the Adsorption of Phenol, *P*-Nitrophenol and Methylene Blue (MB) on GACONZR 1273

Isotherm data were fitted to various isotherm models to establish the most appropriate correlation for the adsorption system. In this study nonlinear form of Langmuir, Freundlich, Dubinin – Radushkevich (D-R) and John-Sivanandan Achari (J-SA) isotherms models were used. Non linear form of isotherm equation is listed in Table 6.14.

**Table 6.14:** The predicted non linear form of Freundlich, Langmuir, Dubinin – Radushkevich, John-Sivanandan Achari isotherm equations for carbon GACONZR 1273

Isotherms	Phenol	<i>p</i> -nitrophenol	Methylene Blue
Langmuir	$q_e = \frac{C_e \times 3.63}{1 + 0.0112 C_e}$	$q_e = \frac{C_e \times 8.36}{1 + 0.0182 C_e}$	$q_e = \frac{C_e \times 4.01}{1 + 0.02278 C_e}$
Freundlich	$q_e = 27.99 \times C_e^{0.3387}$	$q_e = 59.16 \times C_e^{0.2882}$	$q_e = 39.59 \times C_e^{0.2132}$
*D-R	$q_e = 69.5 \times e^{-1.05 \varepsilon^2}$	$q_e = 90.48 \times e^{-0.1006 \varepsilon^2}$	$q_e = 62.14 \times e^{-0.0281 \varepsilon^2}$
*J-SA	$q_e = e^{\frac{\log \log C_e + 0.5159}{0.455}}$	$q_e = e^{\frac{\log \log C_e + 0.4739}{0.447}}$	$q_e = e^{\frac{\log \log C_e + 2.576}{1.47}}$

\*D-R: Dubinin-Radushkevich \*J-SA: John-Sivanandan Achari isotherms

Equilibrium data was getting valid for Langmuir isotherm model while John-Sivanandan Achari isotherm, Freundlich, and Dubinin – Radushkevich isotherm do not much well represent the experimental data.

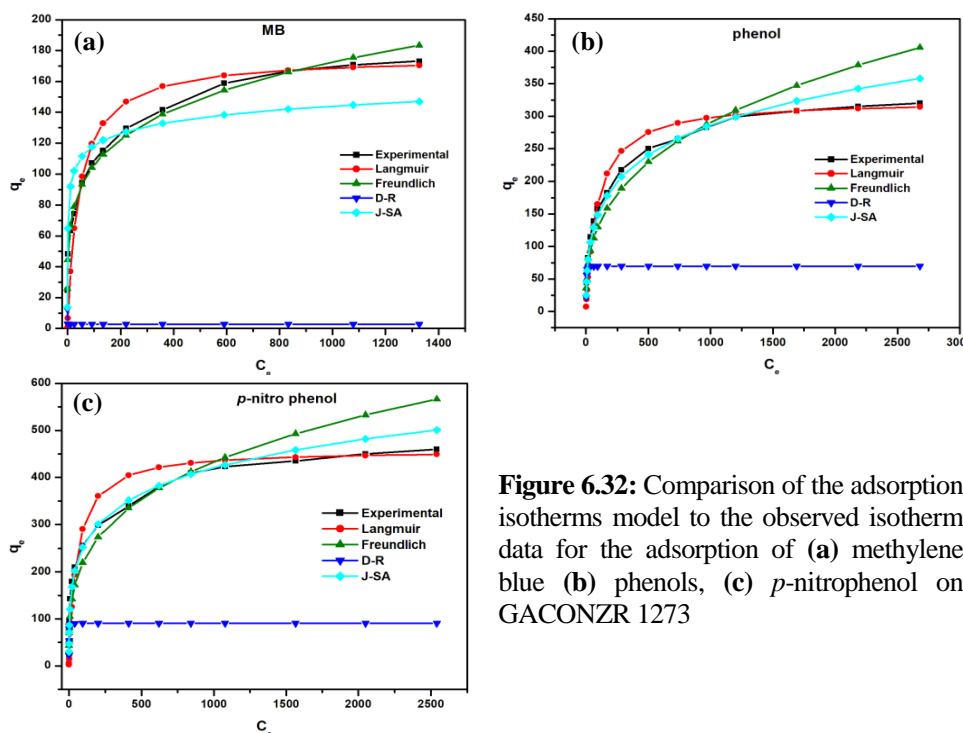


**Figure 6.32:** Comparison of the adsorption isotherms model to the observed isotherm data for the adsorption of (a) methylene blue (b) phenols, (c) *p*-nitrophenol on GACONZR 1273

## 6.7 Adsorption Kinetic Study

In order to evaluate the kinetic mechanism that controls the adsorption process, the pseudo-first order, pseudo-second order models and intraparticle diffusion models were tested to interpret the experimental data. The pseudo first order plots of phenol, *p*-nitrophenol and methylene blue adsorption on GAC 383, GACO 383 and GACONZR 1273 samples at 283-323K are given in the following section.

### 6.7.1 Kinetic Studies of Phenol on GACONZR 1273, GAC 383 and GACO 383 at Temperatures

The first order kinetic plots of phenol adsorption onto three adsorbents GAC 383, GACO 383 and GACONZR 1273 at 283, 293, 303, 313 and 323 K temperature are given in Figure 6.33 (a)–(c). Kinetic parameters along with correlation co-efficient for pseudo first order kinetic models are listed in the Table 6.15.

$$\ln(q_e - q_t) = \ln q_e - K_1 t \quad (6.16)$$

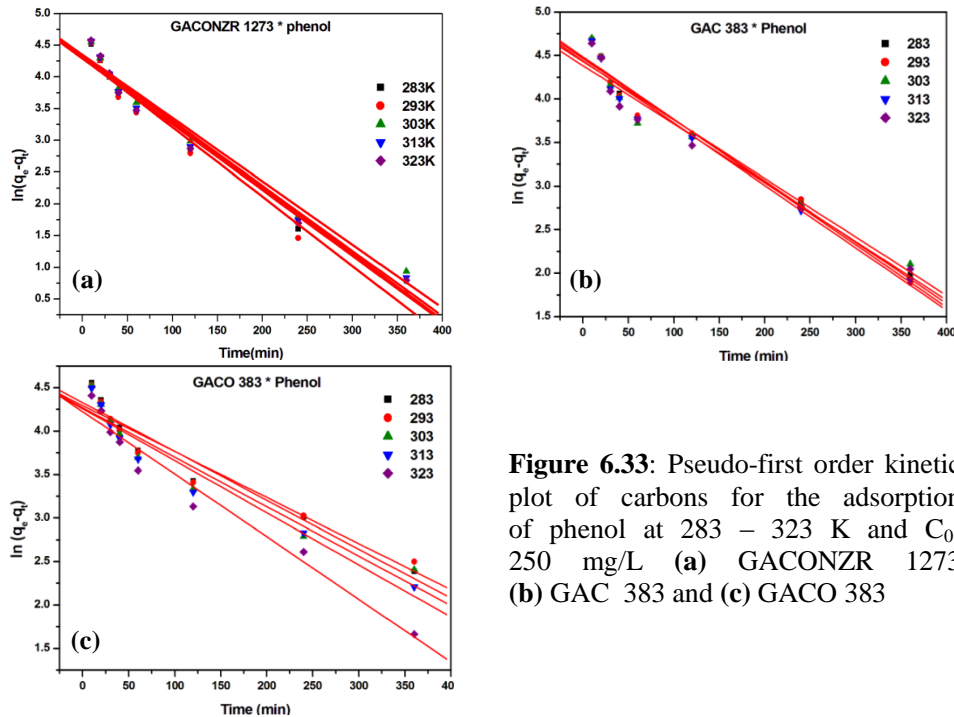


**Figure 6.33:** Pseudo-first order kinetic plot of carbons for the adsorption of phenol at 283 – 323 K and  $C_0$ ; 250 mg/L (a) GACONZR 1273 (b) GAC 383 and (c) GACO 383

The Table 6.15 shows that the experimental data deviated considerably from the theoretical data obtained from pseudo first order model. Percentages of error calculated between the experimental  $q_e$  and calculated  $q_e$  are found to be greater than 40 % for all the carbon studied. Correlation coefficient obtained at all temperatures was found to be low. The adsorption equilibrium  $q_e$  obtained for GACONZR 1273 for the adsorption of phenol at different temperature are given as; 283K (73.203 mg/g), 293K (73.74 mg/g), 303K (77.76 mg/g), 313K (76.47 mg/g), and 323K (76.70 mg/g). The error percentage varies as; GACONZR 1273 (41.6% - 45.9%), GAC 383 (28.46 % - 42.25%) and GACO 383 (35.95% - 47.81%) by rising the temperature from 283K to 323K. The relatively high percentage error between the  $q_e$  experimental with  $q_e$  calculated and lower correlation coefficient suggested adsorption of phenol on all these carbons do not follow the pseudo first order kinetics.

The second order kinetic plots of phenol adsorption onto three adsorbents GACONZR 1273, GAC 383, and GACO 383 at five different temperatures are given in Figure 6.34(a)-(c). Kinetic parameters along with correlation co-efficient for pseudo second order kinetic model are listed in the Table 6.15.

$$\frac{t}{q_t} = \frac{1}{k_2 q_e^2} + \frac{1}{q_e} t \quad (6.17)$$

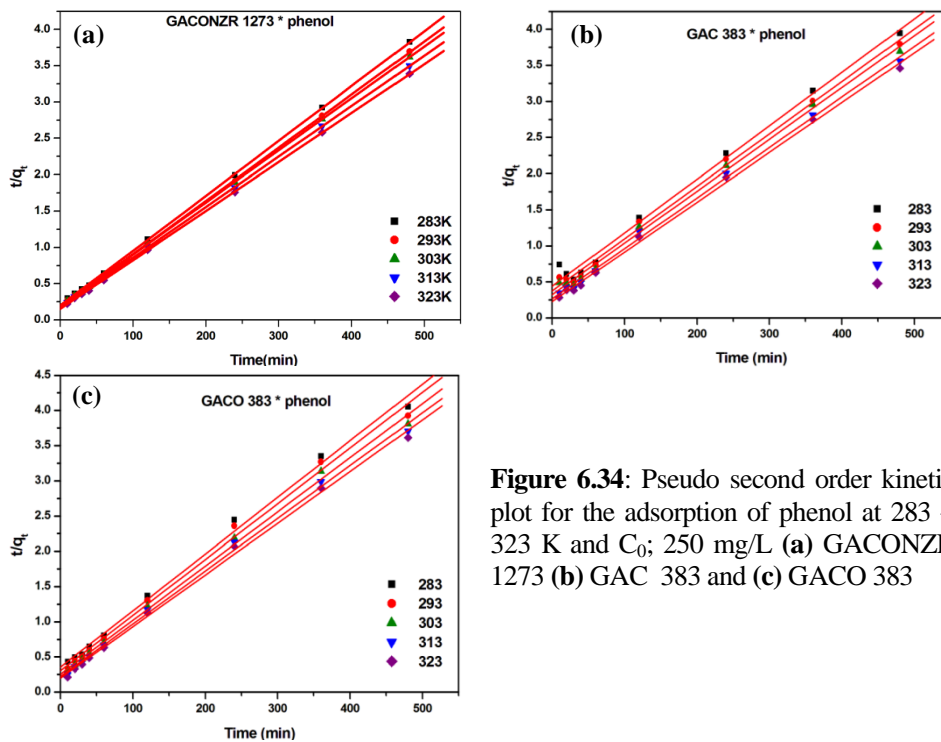


**Figure 6.34:** Pseudo second order kinetic plot for the adsorption of phenol at 283 – 323 K and  $C_0$ ; 250 mg/L (a) GACONZR 1273 (b) GAC 383 and (c) GACO 383

Percentages of error calculated between the experimental  $q_e$  and calculated  $q_e$  value of GACONZR 1273 at different temperatures are 283 K (6.6 %), 293 K (6.3 %), 303 K (5.4 %), 313 K (5 %), 323 K (4.7 %).

The  $q_e$  obtained from pseudo second order kinetics is found to be very close to  $q_e$  (exp). The correlation coefficient ( $R^2$ ) is closer to one for pseudo second order kinetics compared with that of pseudo first order kinetics. It is assumed that the adsorption capacity is proportional to the number of active sites occupied on the adsorbent surface [22].

Intra particle diffusion plot of ( $q_t$  versus  $t^{1/2}$ ) phenol at five different temperatures is given in the Figure 6.35(a)-(c). From the slope and intercept intra particle diffusion parameters  $K_{id1}$ ,  $K_{id2}$  and  $C$  are obtained, which are given in the Table 6.15

$$q_t = k_{id}t^{1/2} + C \quad (6.18)$$

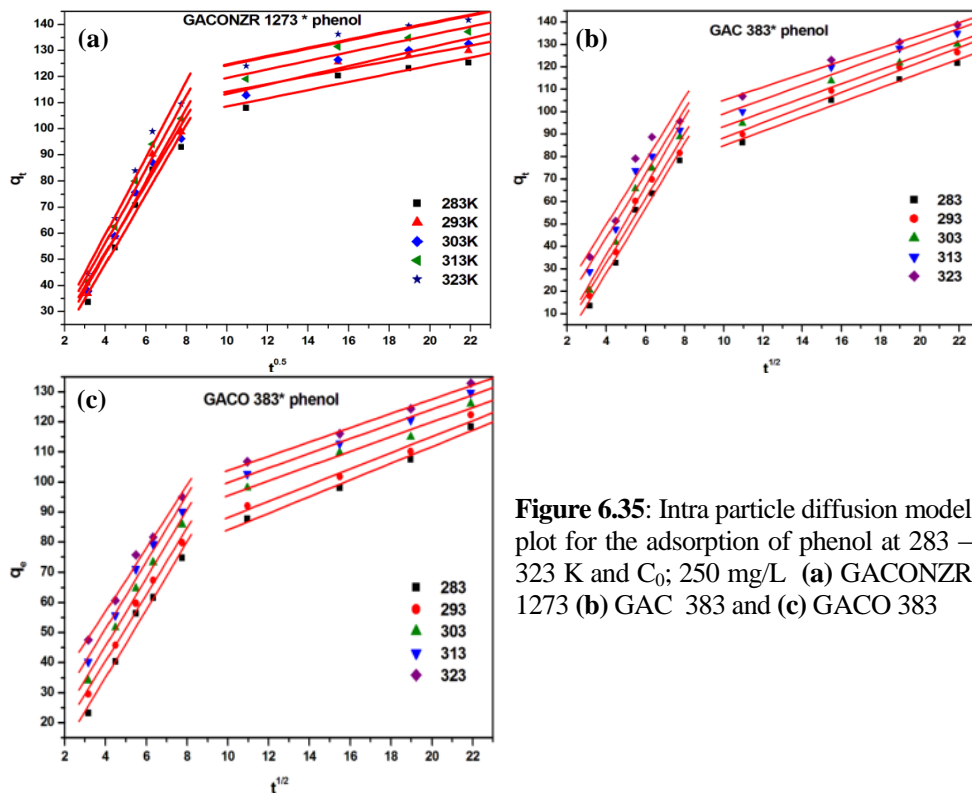


**Figure 6.35:** Intra particle diffusion model plot for the adsorption of phenol at 283 – 323 K and  $C_0$ ; 250 mg/L (a) GACONZR 1273 (b) GAC 383 and (c) GACO 383

The plot of  $q_t$  versus  $t^{0.5}$  shows two stages of adsorption with deviation of a straight line from the origin. The first line from 10 min to one hour is attributed to the fast diffusion of the adsorbate molecules from the aqueous phase to the adsorbent surface. The second line from one hour to eight hours is due to the intraparticle diffusion.



External mass transfer coefficient  $K_{id1}$  given by GACONZR 1273 at different temperature are 283 K (13.78), 293 K (14.60), 303 K (13.06), 313 K (14.10) and 323 K (14.71  $\text{mg/g min}^{-1}$ ) whereas intraparticle diffusion coefficient  $K_{id2}$  is 283 K (1.56), 293 K (1.47), 303 K (1.78), 313 K (1.64), and 323 K (1.59  $\text{mg/g min}^{-1}$ ). The higher  $K_{id1}$  value compared to  $K_{id2}$  indicates that external mass transfer is more predominating than intra particle diffusion for the adsorption of phenol on GACONZR 1273 and it is increasing with temperature. This indicates that the intra particle diffusion was the only rate-controlling step.

**Table 6.15:** Kinetic parameters of carbons GACONZR 1273, GAC 383, and GACO 383 for the adsorption of phenol at temperatures 283 - 323K. [ $C_0 = 250 \text{ mg/L}$ ]

Carbon	Temperature (K)	$q_e$ (exp) mg/g	Pseudo first order kinetics			Pseudo second order kinetics			Intra particle diffusion					
			$q_e$ (cal) mg/g	$K_1 \times 10^4 \text{ min}^{-1}$	$R^2$	$q_e$ (cal) mg/g	$K_2 \times 10^5 \text{ g mg}^{-1} \text{ min}^{-1}$	$R^2$	$K_{id1} \text{ mg/g min}^{1/2}$	$C_1$	$R^2$	$K_{id2} \text{ mg/g min}^{1/2}$	$C_2$	$R^2$
GACONZR 1273	283	125	73	104	0.97	134	25	0.99	14	-11	0.98	1.6	93	0.90
	293	130	74	109	0.97	138	26	0.99	15	-11	0.98	1.5	100	0.88
	303	133	78	100	0.98	140	27	0.99	13	0.2	0.97	1.8	96	0.91
	313	137	77	103	0.97	144	29	0.99	14	-0.3	0.97	1.6	103	0.91
	323	142	77	104	0.97	148	30	0.99	15	0.5	0.97	1.6	109	0.91
GAC383	283	122	87	71	0.96	135	12	0.99	15	-30	0.97	3.2	53	0.98
	293	126	89	72	0.97	138	14	0.99	14	-25	0.97	3.4	55	0.98
	303	130	84	67	0.95	140	16	0.99	15	-25	0.97	3.2	62	0.98
	313	135	85	72	0.96	143	18	0.99	14	-13	0.95	3.2	67	0.97
	323	139	80	67	0.95	145	21	0.99	14	-7	0.93	2.9	76	0.99
GACO383	283	118	76	56	0.94	125	18	0.99	11	-10	0.98	2.8	56	0.99
	293	122	73	53	0.93	126	21	0.99	11	-4	0.99	2.7	61	0.97
	303	126	71	57	0.93	130	23	0.99	11	0.3	0.99	2.4	71	0.98
	313	130	71	60	0.94	134	25	0.99	11	7	0.98	2.4	76	0.99
	323	133	69	61	0.95	136	27	0.99	11	15	0.99	2.4	80	0.99

### 6.7.2 Kinetic Study of *p*-Nitrophenol on GACONZR 1273, GAC 383 and GACO 383 at Temperatures

In order to analyze the adsorption kinetics of *p*-nitrophenol, kinetic data obtained from different time interval is tested using mathematical expressions corresponding to various models, namely: Lagergren's first order equation, pseudo – second order reaction and intra particle diffusion.

The first order kinetic plots of *p*-nitrophenol adsorption onto three adsorbents GAC 383, GACO 383 and GACONZR 1273 at 283, 293, 303, 313 and 323 K are given in Figure 6.36(a)–(c). Kinetic parameter along with correlation co-efficient for pseudo first order kinetic model listed in the Table 6.16.

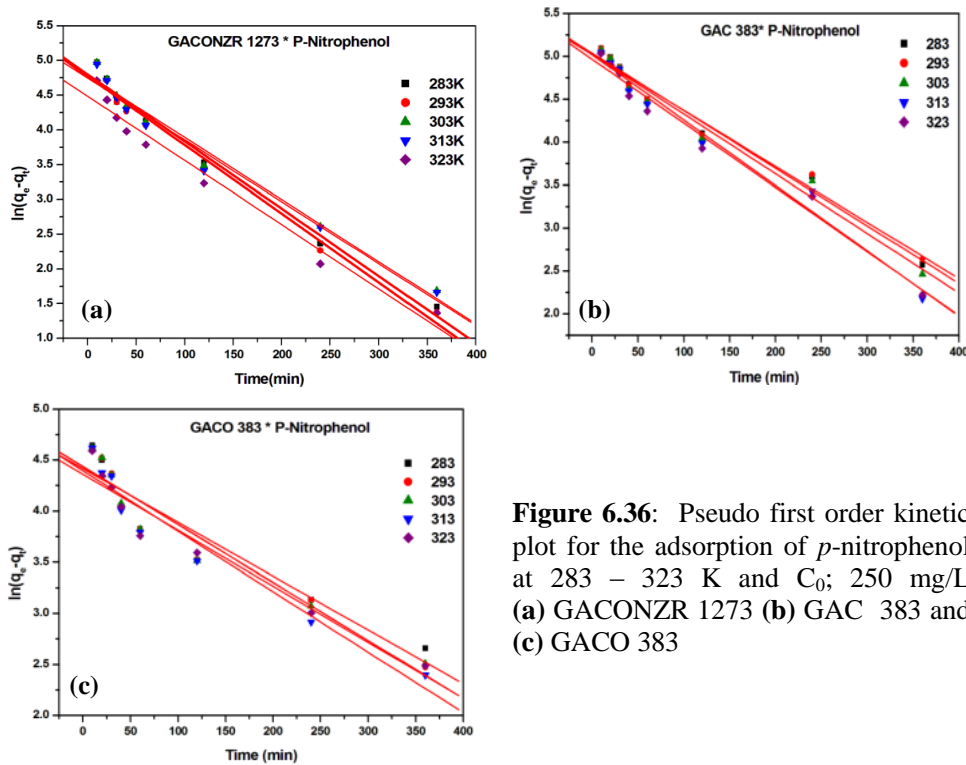


**Figure 6.36:** Pseudo first order kinetic plot for the adsorption of *p*-nitrophenol at 283 – 323 K and  $C_0$ ; 250 mg/L (a) GACONZR 1273 (b) GAC 383 and (c) GACO 383

Error percentage between  $q_e$  experimental and  $q_e$  calculated from pseudo first order is increased with temperature and it varies for carbons as GACONZR 1273 (35.62 % to 58.27 %), GAC 383 (23.80 % to 34.63 %), and GACO 383 (30.79 % to 43.58 %) by rising the temperature from 283K to 323K. On the basis of the

correlation coefficient ( $R^2$ ) and the difference between the experimental and theoretical adsorption capacities suggested that kinetic data obtained from the adsorption of *p*-nitrophenol on GAC is not following the pseudo first order kinetics.

The second order kinetic plots of *p*-nitrophenol adsorption onto three adsorbents GACONZR 1273, GAC 383, and GACO 383 at five different temperatures are given in Figure 6.37(a-c). Kinetic parameter along with correlation co-efficient for pseudo second order kinetic model is listed in the Table 6.16.

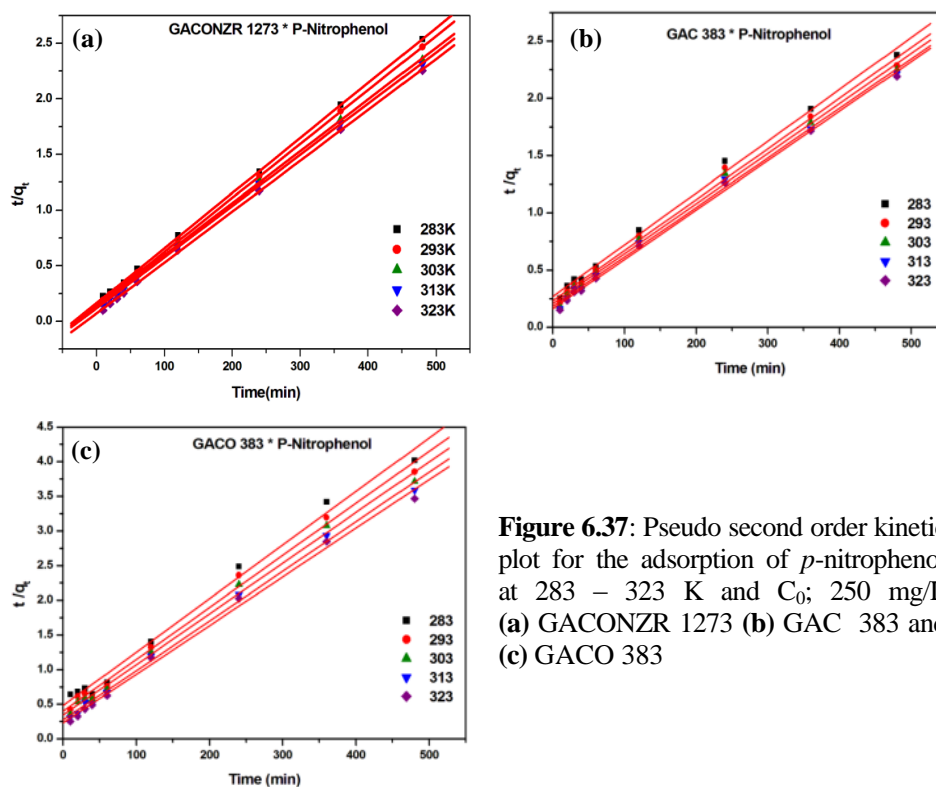


**Figure 6.37:** Pseudo second order kinetic plot for the adsorption of *p*-nitrophenol at 283 – 323 K and  $C_0$ ; 250 mg/L (a) GACONZR 1273 (b) GAC 383 and (c) GACO 383

Percentages of error calculated between the experimental  $q_e$  and calculated  $q_e$  of GACONZR 1273 at different temperature are given as; 283 K (6.77 %), 293 K (5.96 %), 303 K (5.22%), 313 K (4.64%), and 323 K (2.59 %) respectively. This shows that error percentage between  $q_e$  experimental and  $q_e$  calculated from pseudo second order is less than 10 % for all three carbons i.e. calculated  $q_e$  is more close to experimental  $q_e$ .

The lower percentage of error at higher temperature indicates that adsorption systems follows the pseudo second order kinetics is more favourable at higher temperatures. Conformity between the experimental  $q_e$  and calculated  $q_e$  is also given by a straight line plot with the high correlation coefficient ( $R^2 \approx 0.99$ ).

Intra particle diffusion plot of ( $q_t$  versus  $t^{1/2}$ )  $p$ -nitrophenol at five temperatures are given in the Figure 6.38. From the slope and intercept intra particle diffusion parameters  $K_{id1}$ ,  $K_{id2}$  and  $C$  obtained are given in the Table 6.16.

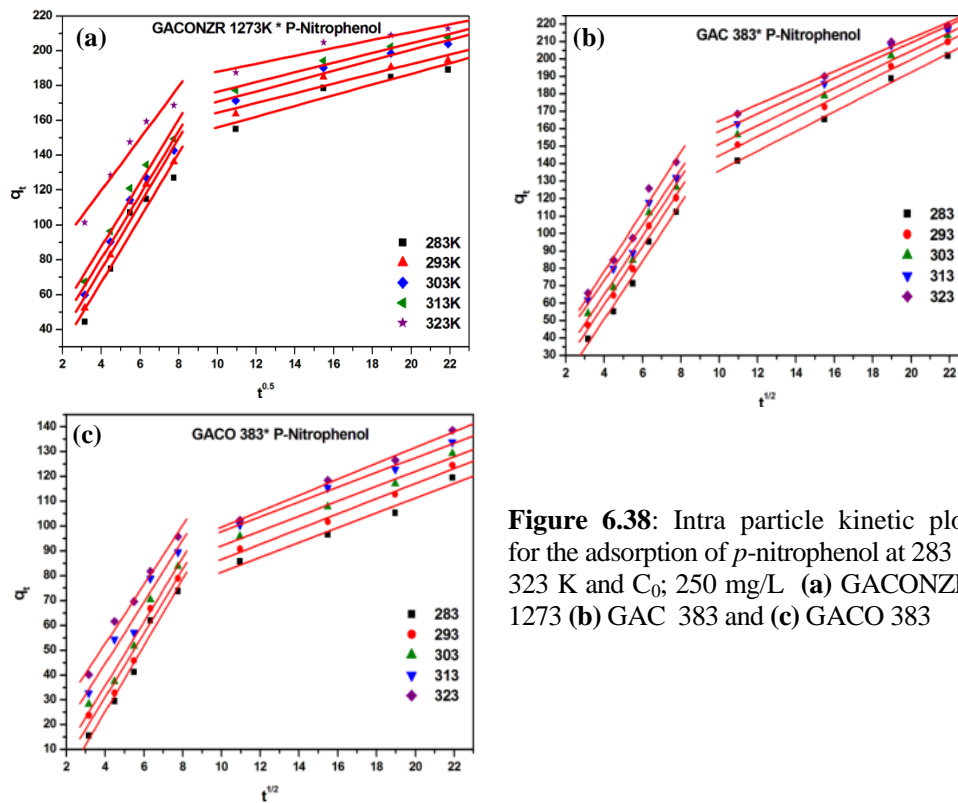


**Figure 6.38:** Intra particle kinetic plot for the adsorption of  $p$ -nitrophenol at 283 – 323 K and  $C_0$ ; 250 mg/L (a) GACONZR 1273 (b) GAC 383 and (c) GACO 383

Two linear plots suggest that the adsorption process proceeds by surface adsorption and intraparticle diffusion. The  $K_{id}$  is the intraparticle diffusion coefficient and  $C$  is the boundary layer effect. Higher the intercept, greater the contribution of surface adsorption in the rate limiting step.

The plot of  $q_t$  versus  $t^{0.5}$  shows two stages of adsorption with deviation of a straight line from the origin because of the difference in the rate of mass transfer between initial and final stages of adsorption. The initial linear portion refers to the external mass transfer effect or boundary layer effect and the later portion due to the intra particle diffusion. External mass transfer coefficient and intraparticle diffusion coefficient of GACONZR 1273 at each temperature *is* given as; 283 K ( $K_{id1} = 18.53$  &  $K_{id2} = 3.08$ ), 293 K ( $K_{id1} = 18.77$  &  $K_{id2} = 2.79$ ), 303 K ( $K_{id1} = 18.30$  &  $K_{id2} = 2.98$ ), 313K ( $K_{id1} = 18.23$  &  $K_{id2} = 2.77$ ) and 323 K ( $K_{id1} = 14.93$  mg/g min<sup>1/2</sup> &  $K_{id2} = 2.27$  mg/g min<sup>1/2</sup>).

**Table 6.16 :** Kinetic parameters of carbons GACONZR 1273, GAC 383, and GACO 383 for the adsorption of *p*-nitrophenol at temperatures 283 - 323K [ $C_0 = 250$  mg/L]

Carbons	T (Kelvin)	$q_e$ (exp) mg/g	Pseudo first order			Pseudo second order			Intra particle diffusion					
			$q_e$ (cal) mg/g	$K_1 \times 10^4$ min <sup>-1</sup>	R <sup>2</sup>	$q_e$ (cal) mg/g	$K_2 \times 10^5$ g mg <sup>-1</sup> min <sup>-1</sup>	R <sup>2</sup>	$K_{id1}$ mg/g min <sup>1/2</sup>	C <sub>1</sub>	R <sup>2</sup>	$K_{id2}$ mg/g min <sup>1/2</sup>	C <sub>2</sub>	R <sup>2</sup>
GACONZR 1273	283	189	122	97	0.98	202	15	0.99	19	-7	0.93	3.1	125	0.91
	293	195	118	99	0.98	206	17	0.99	19	-1	0.94	2.8	137	0.91
	303	204	120	89	0.98	215	17	0.99	18	7	0.97	3.0	141	0.96
	313	208	115	89	0.98	217	18	0.99	18	15	0.97	2.8	149	0.97
	323	213	89	92	0.98	218	30	0.99	15	60	0.95	2.3	165	0.92
GAC 383	283	202	154	67	0.98	221	8	0.99	17	-16	0.98	5.6	80	1.00
	293	210	152	65	0.98	226	9	0.99	17	-8	0.98	5.1	89	0.99
	303	213	151	69	0.98	229	9	0.99	17	-2	0.97	5.3	98	0.99
	313	217	151	76	0.98	232	10	0.99	16	9	0.96	5.1	108	0.99
	323	219	143	75	0.98	232	12	0.99	17	10	0.97	4.8	117	0.99
GACO 383	283	120	83	53	0.91	130	12	0.99	13	-28	0.98	3.0	52	0.97
	293	125	85	57	0.93	133	14	0.99	13	-21	0.96	3.1	56	0.99
	303	129	84	57	0.93	137	16	0.99	13	-16	0.97	3.0	62	0.99
	313	134	81	59	0.94	140	19	0.99	12	-5	0.96	3.0	68	0.99
	323	139	78	55	0.94	143	21	0.99	12	5	0.99	3.2	67	0.99

### 6.7.3 Kinetic Studies of Methylene Blue (MB) on GACONZR 1273, GAC 383 and GACO 383 at Temperatures

To identify the overall removal rate in the adsorption process pseudo first order, pseudo-second order and intra particle kinetic models were tested to fit the experimental data.

Pseudo first order plot  $\log (q_e - q_t)$  versus  $t$  of methylene blue at five different temperatures on GACONZR 1273, GAC 383 and GACO 383 is given by the Figure 6.39(a)-(c).

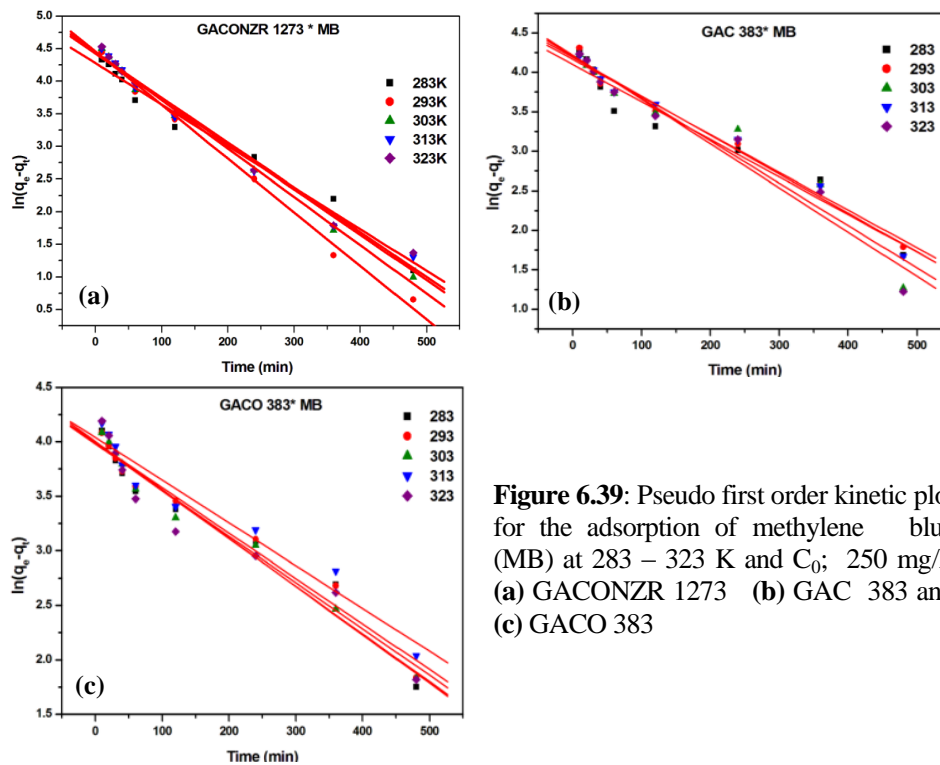


**Figure 6.39:** Pseudo first order kinetic plot for the adsorption of methylene blue (MB) at 283 – 323 K and  $C_0$ ; 250 mg/L (a) GACONZR 1273 (b) GAC 383 and (c) GACO 383

The straight line relationship was not valid in the whole range of contact time, i.e. the adsorption of methylene blue by the carbons GACONZR 1273, GAC 383 and GACO 383 investigated is not an ideal first order reaction. Percentages of error calculated between the experimental  $q_e$  and calculated  $q_e$  value of GACONZR 1273 at different solution temperature are; 283 K (15.01 %), 293 K

(9.39 %), 303 K (14.79 %), 313 K (25.74 %) and 323 K (29.15 %). The percentage of error between  $q_e$  experimental and  $q_e$  calculated from pseudo first order is increased with temperature. For GACONZR 1273 error percentage increased from 12.87 % to 22.09 %, for GAC 383 it varies 40.86 % to 50.88 % , and for GACO 383 it is 33.60 % to 54.27 % by rising the solution temperature from 283 K to 323 K.

Figure 6.40 represents the plot of  $t/q_t$  versus  $t$  for the adsorption of methylene blue onto GACONZR 1273, GAC 383 and GACO 383 at 283, 293, 303, 313 and 323 K. Second order rate constant  $K_2$  and equilibrium capacity  $q_e$  were obtained from slope and intercept of the above plot are listed in Table 6.17.

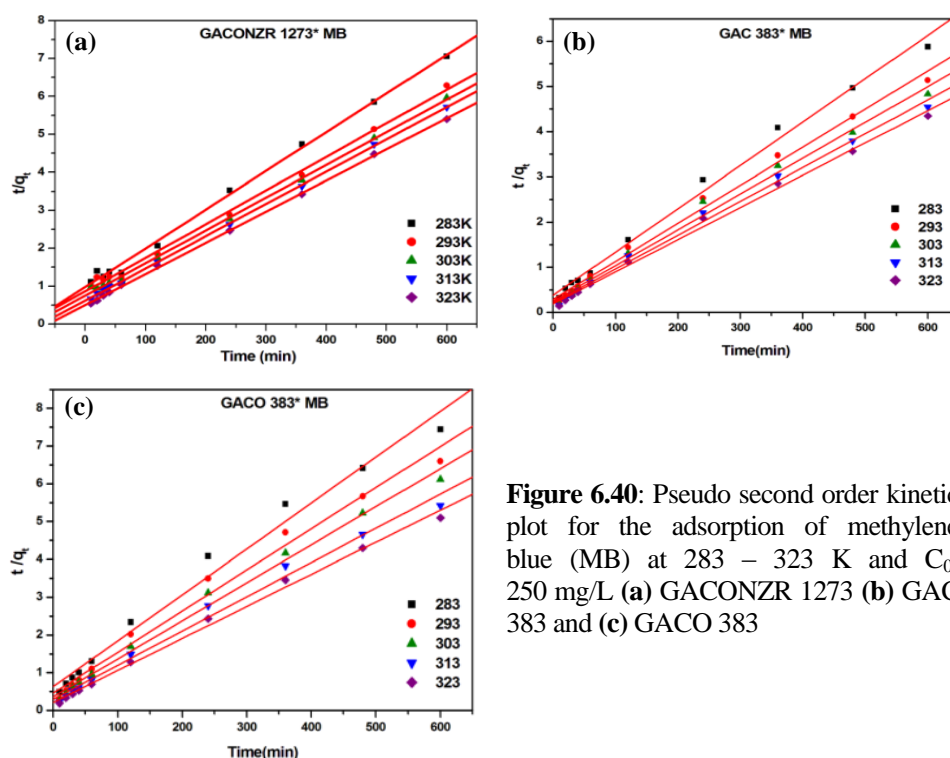


**Figure 6.40:** Pseudo second order kinetic plot for the adsorption of methylene blue (MB) at 283 – 323 K and  $C_0$ ; 250 mg/L (a) GACONZR 1273 (b) GAC 383 and (c) GACO 383

Percentages of error calculated between the experimental  $q_e$  and calculated  $q_e$  value of GACONZR 1273 at different temperature are; 283 K (12.15 %), 293 K (8.85 %), 303 K (7.15 %), 313 K (7.5 %), and 323 K (6.13 %) respectively. The

lower percentage of error indicates that the pseudo-second order kinetic model explains the adsorption in a better way.

The  $q_t$  versus  $t^{1/2}$  for the intraparticle diffusion model (Figure 6.41) of methylene blue adsorption onto GAC 383, GACO 383 and GAONZR 1273 has been tested to obtain the rate parameters at different temperature. Double linear plot, indicate the two stages of adsorption.

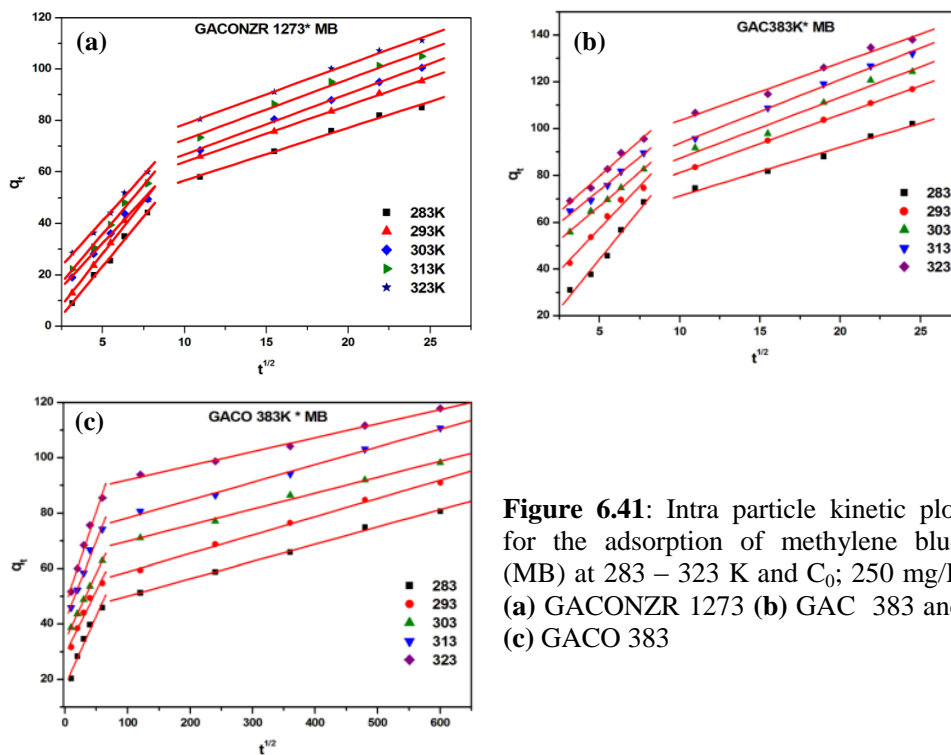


**Figure 6.41:** Intra particle kinetic plot for the adsorption of methylene blue (MB) at 283 – 323 K and  $C_0$ ; 250 mg/L (a) GAONZR 1273 (b) GAC 383 and (c) GACO 383

The first sharper linear portion is assumed to be the instantaneous adsorption or external surface adsorption. It is significant in the early stages of adsorption after that followed controlled intra particle diffusion indicated by the second linear portion.

External mass transfer coefficient  $K_{id1}$  for GAC varies as; GAONZR 1273 (6.92 – 8.13 mg/g min<sup>1/2</sup>), GAC 383 (5.59 – 8.49 mg/g min<sup>1/2</sup>) and GACO 383 (0.460 - 0.678 mg/g min<sup>1/2</sup>). Whereas intraparticle diffusion coefficient  $K_{id2}$  of



GACONZR 1273 (2.05-2.36 mg/g min<sup>1/2</sup>), GAC 383 (2.07-2.72 mg/g min<sup>1/2</sup>), and GACO 383 (0.051-0.066 mg/g min<sup>1/2</sup>). Intra particle diffusion transport is considered as a rate limiting step in case of adsorption on porous solid adsorbent from aqueous solution.

**Table 6.17:** Kinetic parameters of carbons GACONZR 1273, GAC 383, and GACO 383 for the adsorption of methylene blue (MB) at temperatures 283 - 323K [C<sub>0</sub> = 250 mg/L]

Carbons	T (K)	q <sub>e</sub> (exp) mg/g	Pseudo first order			Pseudo second order			Intra particle diffusion					
			q <sub>e</sub> (cal) mg/g	K <sub>1</sub> × 10 <sup>4</sup> min <sup>-1</sup>	R	q <sub>e</sub> (cal) mg/g	K <sub>2</sub> × 10 <sup>5</sup> g mg <sup>-1</sup> min <sup>-1</sup>	R	K <sub>id1</sub> mg/g min <sup>1/2</sup>	C <sub>1</sub>	R <sup>2</sup>	K <sub>id2</sub> mg/g min <sup>1/2</sup>	C <sub>2</sub>	R <sup>2</sup>
GACONZR 1273	283	85	72	64	0.98	95	13	0.99	7.7	-15	0.99	2.1	36	0.99
	293	95	86	82	0.99	104	14	0.99	8.1	-12	0.99	2.2	42	0.98
	303	101	86	74	0.99	108	15	0.99	6.9	-2	0.98	2.4	43	0.99
	313	105	78	62	0.99	113	16	0.99	7.6	-2	0.99	2.4	49	0.99
	323	111	79	60	0.99	118	17	0.99	7.1	6	0.99	2.3	55	0.99
GAC 383	283	102	60	48	0.94	104	24	0.99	8.5	2	0.98	2.1	51	0.97
	293	117	65	48	0.98	119	25	0.99	7.2	21	0.97	2.5	56	0.98
	303	124	67	54	0.94	126	25	0.99	5.8	38	0.99	2.6	61	0.97
	313	132	66	49	0.98	134	26	0.99	5.6	46	0.99	2.7	67	0.99
	323	138	68	56	0.96	140	27	0.99	6.1	49	0.98	2.5	79	0.98
GACO 383	283	81	54	42	0.96	82	23	0.99	0.51	18	0.96	0.06	44	0.99
	293	91	54	42	0.97	92	26	0.99	0.46	29	0.96	0.07	52	0.99
	303	98	55	44	0.98	100	28	0.99	0.48	34	0.98	0.06	64	0.99
	313	111	57	39	0.95	110	28	0.99	0.58	41	0.98	0.06	72	0.99
	323	118	54	44	0.94	118	33	0.99	0.68	47	0.98	0.05	87	0.99

## 6.8 Thermodynamic Parameters

The  $\Delta H$  and  $\Delta S$  are obtained from the linear plot of  $\ln K_L$  versus  $1/T$ . The  $\Delta G$  obtained from the relationship between  $\Delta H$ ,  $\Delta S$  and  $T$  (reaction temperature).

$$\ln K_L = \frac{\Delta S}{R} - \frac{\Delta H}{RT} \quad (6.19)$$

The linearized form of the van't Hoff equation is depicted in Figure 6.42(a). The thermodynamic parameters of Gibbs free energy change  $\Delta G$ , enthalpy change  $\Delta H$ , and entropy change  $\Delta S$ , for the adsorption processes are calculated and are given in Table 6.18.

**Table 6.18:** Thermodynamic parameters for the adsorption of phenol onto GAC 383, GACO 383 and GACONZR 1273

Sample	$(\Delta H)$ kJ/mol	$(\Delta S)$ J/mol.K	$\Delta G$ (kJ/mol)				
			283K	293K	303K	313K	323K
GAC 383	2.3	15.3	-2.0	-2.2	-2.3	-2.5	-2.6
GACO 383	3.3	18.2	-1.9	-2.1	-2.2	-2.4	-2.6
GACONZR 1273	20.8	75.4	-0.5	-1.3	-2.0	-2.8	-3.5

The  $\Delta H$  calculated for phenol adsorption on carbon gives; GAC 383 (2.3 kJ/mol), GACO 383 (3.3 kJ/mol) and GACONZR 1273 (20.8 kJ/mol). These enthalpies represent the interaction energy of the amount adsorbed on the absorbent-adsorbate interface. The positive value  $\Delta H$  of all adsorbents indicates the endothermic nature of adsorption. In endothermic processes where the reaction is not favoured energetically, a favourable change in entropy may provide the necessary driving force.

The spontaneity of the process appears to be associated with a highly ordered system going to a less ordered. The positive  $\Delta S$  suggests the randomness of the adsorption process, indicated also greater stability of an adsorption process with no structural changes at the solid-liquid interface. The magnitude of  $\Delta S$  for new carbon is given as GAC 383 (15.32 J/mol.K), GACO 383 (18.20 J/mol.K) and GACONZR 1273 (75.40 J/mol.K). Positive  $\Delta S$  for the adsorption of phenol on GAC shows affinity of the adsorbent toward phenol molecule.

Smaller values of  $\Delta H$  and  $\Delta S$  indicate the existence of the repulsive force between the charged carbon surfaces and the phenolate ions which have the same charge as the carbon surface. Such electrostatic repulsion causes the weakening of the adsorption forces and increases the degree of freedom of the phenol molecules

on the carbon surface. To overcome such repulsive forces, the system must take some energy from the environment to adsorb the phenolate ions on the activated carbon surface. The electrostatic repulsion, which acts against the adsorption force, leads to an endothermic process with small values of enthalpy and entropy changes [23].

The obtained values for Gibbs free energy change ( $\Delta G$ ) for carbons at temperature of 283 K to 323 K are given as; GAC 383 (- 2.0 to - 2.6 kJ/mol ), GACO 383 (- 1.9 to -2.6 kJ/mol ) and for GACONZR 1273 (-0.51 to -3.5 kJ/mol). It was also observed that with the increase of temperature the value of  $\Delta G$  becomes more negative, which indicated that adsorption of phenol on GAC leads to a decrease in Gibbs energy and confirms the spontaneous nature of the adsorption process.

Figure 6.42(b) indicates thermodynamic study of adsorption process of *p*-nitrophenol on GACONZR 1273, GAC 383 and GACO 383. The thermodynamic parameters of Gibbs free energy change  $\Delta G$ , enthalpy change  $\Delta H$ , and entropy change  $\Delta S$  for the adsorption processes are calculated and are given in Table 6.19.

**Table 6.19:** Thermodynamic parameters for *p*-nitrophenol adsorption on GAC 383, GACO 383 and GACONZR 1273

carbons	$(\Delta H)$ kJ/mol	$(\Delta S)$ J/mol.K	$\Delta G$ (kJ/mol)				
			283 K	293 K	303 K	313K	323 K
GAC 383	6.0	38.2	-4.8	-5.2	-5.5	-5.9	-6.3
GACO383	2.9	16.4	-1.7	-1.9	-2.0	-2.2	-2.4
GACONZR 1273	10.0	48.5	-3.7	-4.2	-4.7	-5.2	-5.7

The  $\Delta H$  calculated for *p*-nitrophenol adsorption on GAC follows GAC 383 (6.0 kJ/mol), GACO 383 (2.9 kJ/mol) and GACONZR 1273 (10.0 kJ/mol) respectively. The positive  $\Delta H$  of all adsorbents indicates the endothermic nature of adsorption. Lower adsorption energy indicates the physical nature of adsorption. The high degree of disorder of an adsorption system gives a positive value of  $\Delta S$  for new carbons as GAC 383 (38.2 J/mol.K), GACO 383 (16.4 J/mol.K) and GACONZR 1273 (48.5 J/mol.K). Positive values of  $\Delta S$  show the increased randomness at the solid/solution interface during the adsorption process. The

adsorbed water molecules, which are displaced by the adsorbate species, gain more translational energy than is lost by the adsorbate ions, thus allowing the prevalence of randomness in the system [24].

The negative values of  $\Delta G$  confirm the feasibility of the process and the spontaneous nature of adsorption with a high preference of *p*-nitrophenol by GACONZR 1273, GAC 383 and GACO 383. The obtained values for Gibbs free energy change ( $\Delta G$ ) at temperature from 283 K to 323 K for new carbons are given as; GAC 383 (-4.8 to -6.3 kJ/mol), GACO 383 (-1.7 to -2.4 kJ/mol) and GACONZR 1273 (-3.7 to -5.7 kJ/mol). The negative value of  $\Delta G$  increased with temperature, indicating that the spontaneous nature of adsorption is directly proportional to the temperature.

Figure 6.42(c) indicates thermodynamic study of adsorption process of methylene blue on GACONZR 1273, GAC 383 and GACO 383. The thermodynamic parameters of Gibbs free energy change  $\Delta G$ , enthalpy change  $\Delta H$  and entropy change  $\Delta S$  for the adsorption processes are calculated and are given in Table 6.20.

**Table 6.20:** Evaluation of Thermodynamic parameters for methylene blue (MB) adsorption on GACONZR 1273, GAC 383 and GACO 383

Sample	$(\Delta H)$ kJ/mol	$(\Delta S)$ J/mol.K	$\Delta G$ (kJ/mol)				
			283K	293K	303K	313K	323K
GAC 383	6.9	35.6	-3.2	-3.6	-3.9	-4.3	-4.6
GACO383	8.9	40.4	-2.5	-2.9	-3.3	-3.7	-4.1
GACONZR 1273	7.2	34.1	-2.4	-2.8	-3.1	-3.4	-3.8

As seen in Table 6.20 positive values of  $\Delta H$  indicate the endothermic nature of adsorption, GAC 383 (6.87 kJ/mol) GACO 383 (8.91 kJ/mol), GACONZR 1273 (7.23 kJ/mol). The negative values of  $\Delta G$  indicate the spontaneous nature of adsorption of methylene blue. It varies for new carbons as GAC 383 (- 3.20 to - 4.63 kJ/mol), GACO 383 (- 2.51 to - 4.12 kJ/mol) and for GACONZR 1273 (- 2.41 to - 3.77 kJ/mol) at 283 to 323 K. The high negative value of  $\Delta G$  at higher temperatures means higher adsorption capability at higher temperature. At higher temperatures, organic molecule overcome space hindrances while diffusing into GACs. The positive  $\Delta S$ , given by the new carbons

suggest, the increased randomness at the solid/solution interface during the adsorption of methylene blue on GAC 383 (35.60 J/mol. K), GACO 383 (40.35 J/mol. K) and GACONZR 1273 (34.05 J/mol. K).

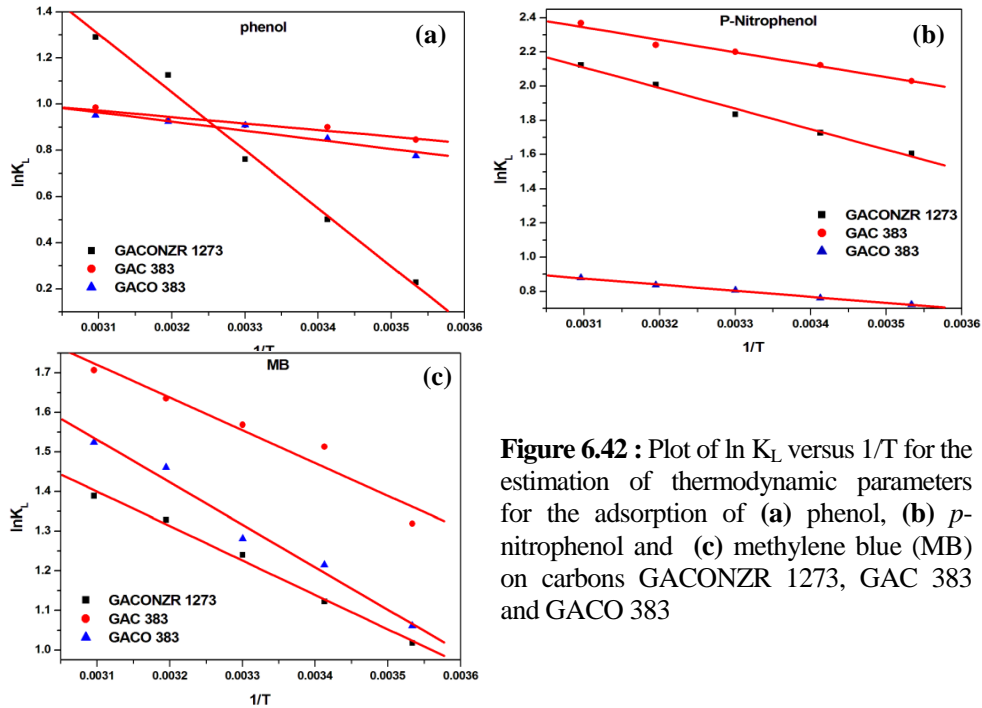


**Figure 6.42 :** Plot of  $\ln K_L$  versus  $1/T$  for the estimation of thermodynamic parameters for the adsorption of (a) phenol, (b) *p*-nitrophenol and (c) methylene blue (MB) on carbons GACONZR 1273, GAC 383 and GACO 383

### 6.8.1 Thermodynamic Parameters from Distribution Coefficient

Thermodynamic parameters are obtained from distribution coefficient by using the equations

$$\ln K_D = \frac{\Delta S}{R} - \frac{\Delta H}{RT} \quad (6.20)$$

Distribution coefficient ( $K_D$ ) is defined as the ratio of the quantity of the adsorbate adsorbed per mass of solid to the amount of the adsorbate remaining in solution. Usually it is expressed in terms of L/g.

The  $\Delta G$ ,  $\Delta H$  and  $\Delta S$  were computed from the slopes and intercepts of linear variations of  $\ln K_D$  with the reciprocal of temperature ( $1/T$ ) as shown in the Figure 6.43(a)–(c).

**Table 6.21:** Thermodynamic parameters obtained from plot of  $\ln K_D$  versus  $1/T$  for the adsorption of phenol on GACONZR 1273

$C_0$ mg/L	$\Delta S$ J/mol.K	$\Delta H$ kJ/mol	$\Delta G$ kJ/mol				
			283 K	293K	303K	313K	323K
25	89.6	22.5	-2.8	-3.7	-4.6	-5.5	-6.4
50	83.3	21.3	-2.3	-3.1	-4.0	-4.8	-5.6
75	80.2	20.9	-1.8	-2.6	-3.4	-4.2	-5.0
100	74.6	19.5	-1.6	-2.4	-3.1	-3.8	-4.6
150	70.8	19.7	-0.3	-1.0	-1.8	-2.5	-3.2
200	66.6	19.3	0.5	-0.2	-0.9	-1.5	-2.2
250	62.0	18.6	1.1	0.4	-0.2	-0.8	-1.4
350	54.2	17.3	2.0	1.4	0.9	0.3	-0.2
500	38.3	13.1	2.2	1.9	1.5	1.1	0.7
750	27.6	10.8	3.0	2.7	2.4	2.1	1.9
1000	16.9	8.2	3.4	3.3	3.1	2.9	2.7

The change in enthalpy for the phenol adsorption on GACONZR 1273 is in the range 22.52 to 8.19 kJ/mol, and entropy of phenol adsorption varied between 89.56 to 16.88 J/mol. K. The decrease in free energy change with the increase of temperature indicates that adsorption of phenol onto activated carbon GACONZR 1273, GAC 383 and GACO 383 favourable at higher temperature. Entropy change during the adsorption of phenol on activated carbon studied decreases with increase in concentration of phenol.

**Table 6.22:** Thermodynamic parameters obtained from plot of  $\ln K_D$  versus  $1/T$  for the adsorption of *p*-nitrophenol on GACONZR 1273

$C_0$ mg/L	$\Delta S$ J/mol.K	$\Delta H$ kJ/mol	$\Delta G$ kJ/mol				
			283 K	293 K	303 K	313 K	323 K
25	69.8	11.1	-8.7	-9.4	-10.1	-10.8	-11.5
50	68.1	10.8	-8.4	-9.1	-9.8	-10.5	-11.2
75	61.6	10.0	-7.4	-8.1	-8.7	-9.3	-9.9
100	58.8	9.6	-7.1	-7.6	-8.2	-8.8	-9.4
150	52.5	9.0	-5.9	-6.4	-6.9	-7.5	-8.0
200	44.6	8.6	-4.0	-4.5	-4.9	-5.4	-5.8
250	38.5	8.0	-2.9	-3.3	-3.7	-4.1	-4.4
350	31.8	7.6	-1.4	-1.7	-2.0	-2.3	-2.7
500	25.6	7.2	0.0	-0.3	-0.5	-0.8	-1.1
750	19.8	6.9	1.3	1.1	0.9	0.7	0.5
1000	15.2	6.2	1.9	1.8	1.6	1.4	1.3

The change in  $\Delta H$  for the *p*-nitrophenol adsorption on GACONZR 1273 was in the range 11.1 to 6.2 kJ/mol, The change in  $\Delta S$  for *p*-nitrophenol adsorption on GACONZR 1273 is in the range 69.8 to 15.2 J/mol. K. The spontaneity of the reaction can be explained by the value of  $\Delta G$ . Higher negative value of  $\Delta G$  at higher temperature indicate the feasibility of reaction at higher temperature.

**Table 6.23:** Thermodynamic parameters obtained from plot of  $\ln K_D$  versus  $1/T$  for the adsorption of methylene blue (MB) on GACONZR 1273

$C_0$ mg/L	$\Delta S$ J/mol.K	$\Delta H$ kJ/mol	$\Delta G$ kJ/mol				
			283 K	293 K	303 K	313 K	323 K
25	102.2	19.0	-10.0	-11.0	-12.0	-13.0	-14.1
50	74.5	15.1	-6.0	-6.7	-7.5	-8.2	-9.0
75	56.7	13.8	-2.3	-2.8	-3.4	-4.0	-4.5
100	49.9	13.3	-0.9	-1.4	-1.9	-2.4	-2.9
150	43.5	12.6	0.3	-0.1	-0.5	-1.0	-1.4
200	38.0	11.9	1.1	0.8	0.4	0.0	-0.4
250	34.3	11.5	1.8	1.4	1.1	0.8	0.4
350	30.6	11.3	2.6	2.3	2.0	1.7	1.4
500	27.1	11.2	3.6	3.3	3.0	2.8	2.5
750	23.1	11.0	4.4	4.2	4.0	3.8	3.5
1000	20.4	10.9	5.1	4.9	4.7	4.5	4.3

The change in enthalpy for the methylene blue adsorption on GACONZR 1273 is in the range 19.0 to 10.9 kJ/mol, entropy of methylene blue adsorption varies 102.2 to 20.4 J/mol. K (GACONZR 1273). Entropy change during the adsorption of methylene blue on activated carbon studied decreases with increase in concentration of methylene blue in aqueous solution.

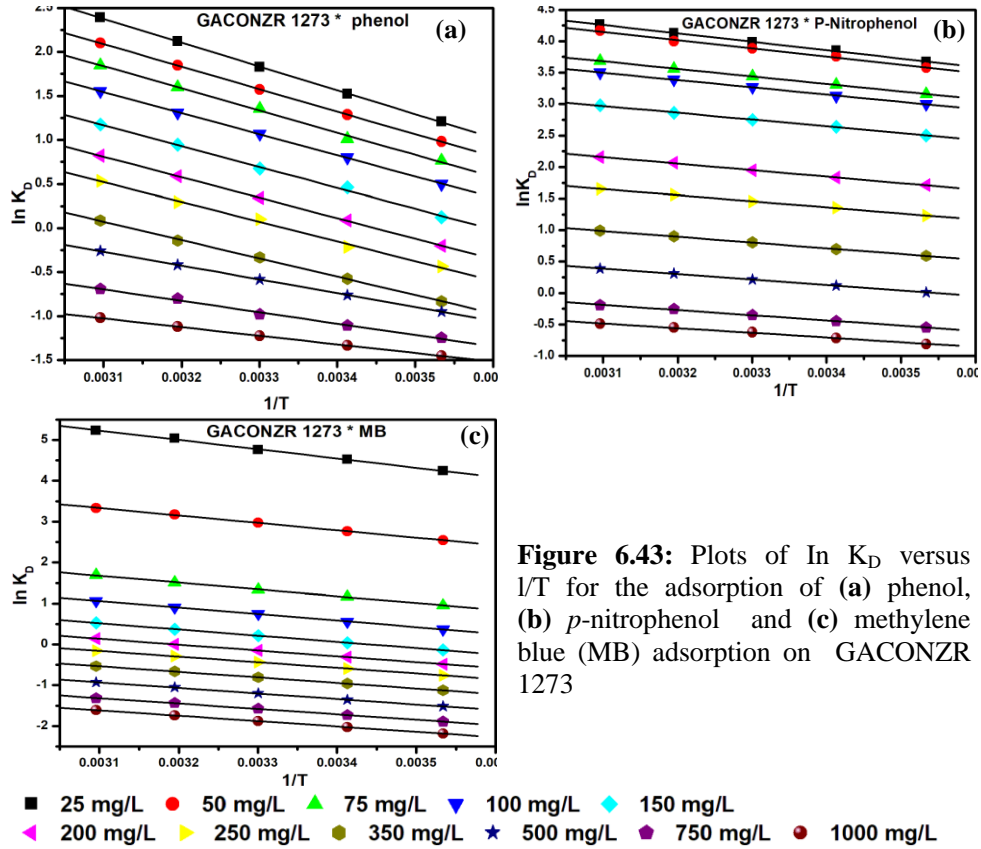


**Figure 6.43:** Plots of  $\ln K_D$  versus  $1/T$  for the adsorption of (a) phenol, (b) *p*-nitrophenol and (c) methylene blue (MB) adsorption on GACONZR 1273

## 6.9 Diffusion Coefficient

Diffusion coefficient for the adsorption of phenol, *p*-nitrophenol and methylene blue on GACONZR 1273, GAC 383 and GACO 383 are elaborately studied

### 6.9.1 Determination of Diffusivity for Phenol on GACONZR 1273, GAC 383 and GACO 383

The diffusion coefficient for the adsorption of phenol on GAC 383, GACO 383 and GACONZR 1273 are determined from the linear plot of  $\ln [1/1-F^2(t)]$  versus  $t$  is given in the Figure 6.44(a)-(c) and values are listed in the Table 6.24. Straight line plot for different temperature indicate the validity of the equation.

$$\ln \left[ \frac{1}{1 - F^2(t)} \right] = \frac{\pi^2 D_e t}{R_a^2} \quad (6.21)$$



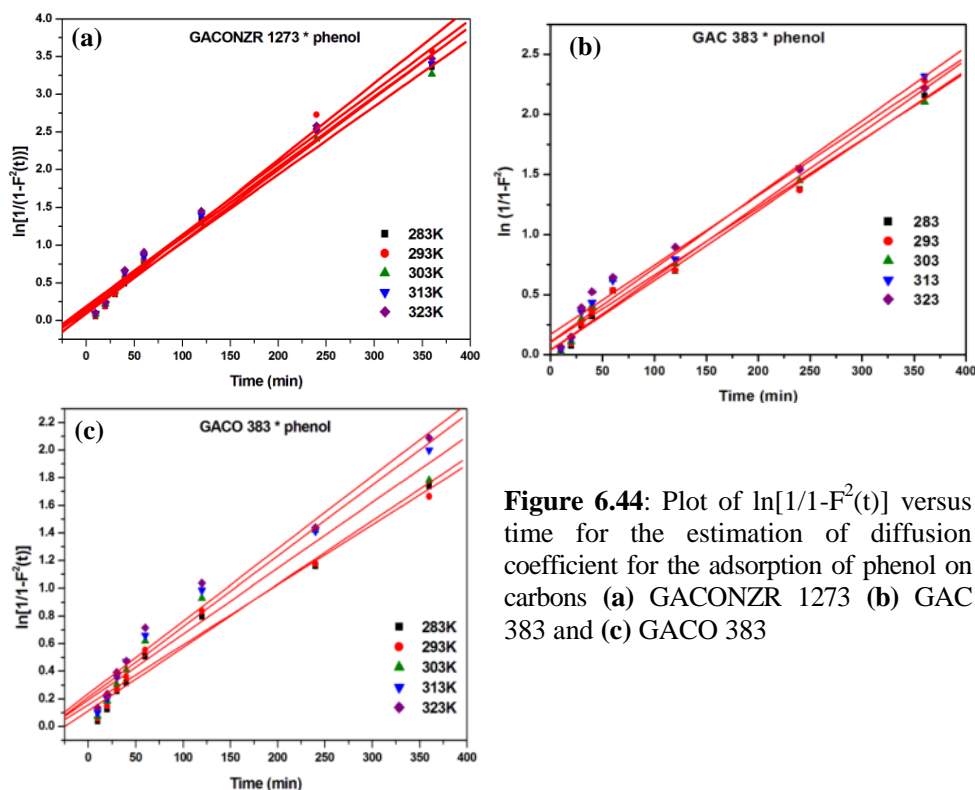


**Figure 6.44:** Plot of  $\ln[1/(1-F^2(t))]$  versus time for the estimation of diffusion coefficient for the adsorption of phenol on carbons (a) GACONZR 1273 (b) GAC 383 and (c) GACO 383

The diffusivity values of phenol into activated carbon for the range of concentration studied is found to be between  $2.79 \times 10^{-10}$  to  $3.12 \times 10^{-10} \text{ m}^2/\text{s}$ .

Effective diffusion coefficient describes the transport of a phenol molecule into GAC through a unit section area of GAC per unit of time. It is expressed in unit of  $\text{m}^2/\text{s}$ . As shown in the Table 6.24 the effective diffusion coefficient of phenol on carbons varies as GACONZR 1273 ( $2.79 \times 10^{-10} - 3.12 \times 10^{-10} \text{ m}^2/\text{s}$ ), for GAC 383 ( $1.57 \times 10^{-10} - 1.71 \times 10^{-10}$ ) and for GACO 383 ( $1.21 \times 10^{-10} - 1.47 \times 10^{-10} \text{ m}^2/\text{s}$ ) respectively.

### 6.9.2 Determination of Diffusivity for *P*-Nitrophenol on GACONZR 1273, GAC 383 and GACO 383

The diffusion coefficient of adsorption of *p*-nitrophenol on GAC 383, GACO 383 and GACONZR 1273 are determined from the linear plot of  $\ln [1/(1-F^2(t))]$  versus  $t$  which is given in the Figure 6.45(a)-(c) and values are listed in the

Table 6.24. Straight line plot at different temperature indicate the validity of the equation.

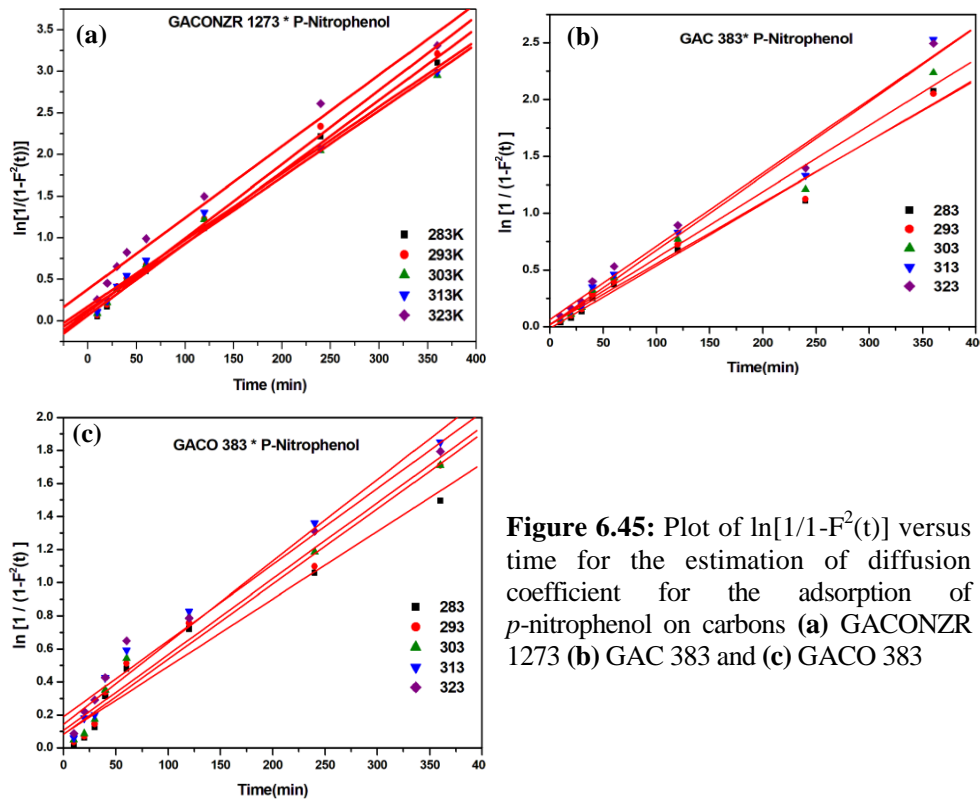


**Figure 6.45:** Plot of  $\ln[1/(1-F^2(t))]$  versus time for the estimation of diffusion coefficient for the adsorption of *p*-nitrophenol on carbons (a) GACONZR 1273 (b) GAC 383 and (c) GACO 383

In order to compare the uptake of *p*-nitrophenol from solution by GACONZR 1273, GAC 383, GACO 383, the effective diffusion coefficient is calculated. The effective diffusion coefficient is found to be in the range of new carbons as GACONZR 1273 ( $1.85 \times 10^{-10}$  to  $2.12 \times 10^{-10}$  m<sup>2</sup>/s), GAC 383 ( $1.5 \times 10^{-10}$  to  $1.83 \times 10^{-10}$  m<sup>2</sup>/s) and GACO 383 ( $1.14 \times 10^{-10}$  to  $1.38 \times 10^{-10}$  m<sup>2</sup>/s). It shows that diffusion is faster at higher temperature and the increasing order of the effective diffusion coefficient of GAC is GACONZR 1273 > GAC 383 > GACO 383.

### 6.9.3 Determination of Diffusivity for Methylene Blue on GACONZR 1273, GAC 383 and GACO 383

The diffusion coefficient of adsorption of methylene blue on GAC 383, GACO 383 and GACONZR 1273 are determined from the linear plot of  $\ln [1/1-F^2(t)]$  versus  $t$  which is given in the Figure 6.46(a)-(c) and values are listed in the Table 6.24. Straight line plot for different temperature indicate the validity of the equation.

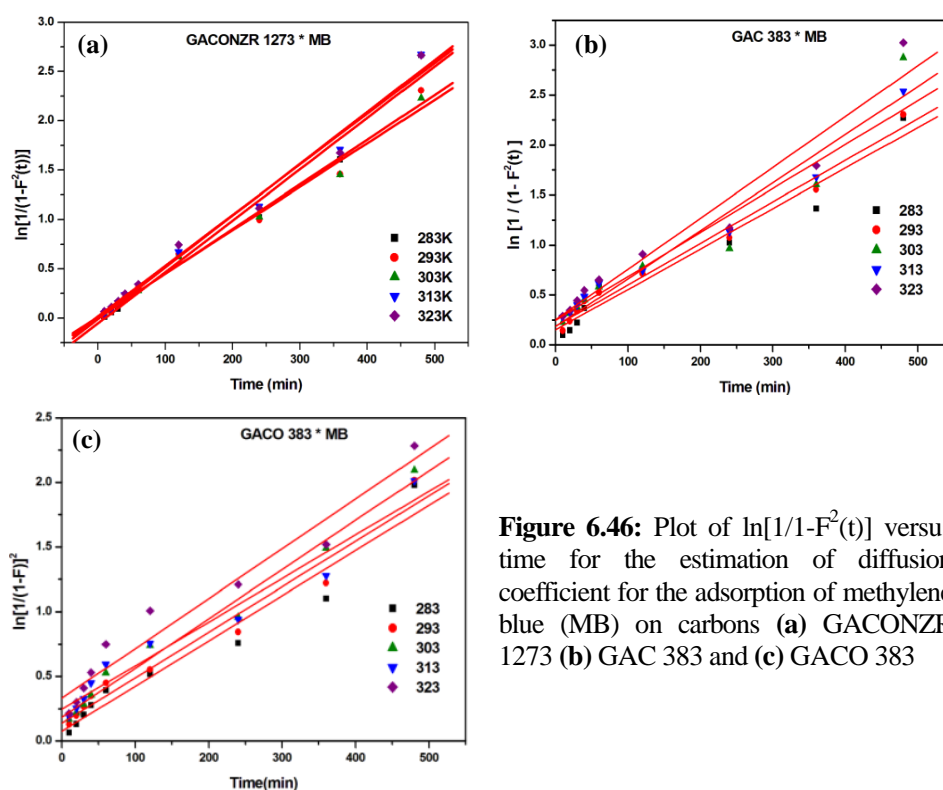


**Figure 6.46:** Plot of  $\ln[1/1-F^2(t)]$  versus time for the estimation of diffusion coefficient for the adsorption of methylene blue (MB) on carbons (a) GACONZR 1273 (b) GAC 383 and (c) GACO 383

The effective diffusion coefficient calculated from the adsorption of methylene blue on new carbons is given as follows; GACONZR 1273 ( $1.2 \times 10^{-10}$  -  $1.5 \times 10^{-10}$  m<sup>2</sup>/s), GAC 383 ( $1.13 \times 10^{-10}$  -  $1.34 \times 10^{-10}$  m<sup>2</sup>/s) and GACO 383 ( $0.94 \times 10^{-10}$  -  $1.08 \times 10^{-10}$  m<sup>2</sup>/s).

The high diffusion coefficient for GACONZR 1273 compared to GAC 83 and GACO 383 indicates higher diffusion rates of methylene blue within the pores of GACONZR 1273.

**Table 6.24:** Effective diffusion coefficient of carbon on phenol, *p*-nitrophenol and methylene blue (MB)

Carbon	T (Kelvin)	phenol		<i>p</i> -nitrophenol		methylene blue	
		De x 10 <sup>10</sup> (m <sup>2</sup> /S)	R <sup>2</sup>	De x 10 <sup>10</sup> (m <sup>2</sup> /S)	R <sup>2</sup>	De x 10 <sup>10</sup> (m <sup>2</sup> /S)	R <sup>2</sup>
GACONZR 1273	283	2.96	0.990	1.85	0.996	1.46	0.980
	293	3.12	0.988	1.92	0.994	1.27	0.986
	303	2.79	0.992	2.00	0.994	1.23	0.990
	313	2.87	0.990	2.08	0.990	1.47	0.988
	323	2.91	0.986	2.12	0.984	1.44	0.984
GAC 383	283	1.63	0.988	1.53	0.984	1.13	0.984
	293	1.69	0.986	1.50	0.984	1.16	0.984
	303	1.57	0.980	1.63	0.982	1.34	0.982
	313	1.71	0.986	1.83	0.980	1.230	0.980
	323	1.62	0.978	1.80	0.984	0.250	0.984
GACO 383	283	1.28	0.976	1.14	0.958	0.978	0.958
	293	1.21	0.964	1.27	0.968	0.984	0.968
	303	1.33	0.958	1.28	0.968	1.070	0.968
	313	1.43	0.970	1.38	0.974	0.940	0.974
	323	1.47	0.970	1.29	0.972	1.080	0.972

## 6.10 Activation Energy

The linear plot of  $\ln K_2$  versus  $1/T$  for the adsorption of phenol on GACONZR 1273, GAC 383, and GACO 383 are given in the Figure 6.47(a). The activation energy  $E_a$  and pre-exponential factors,  $A$ , obtained is given in Table 6.25.

$$\ln K_2 = \ln A - \frac{E_a}{RT} \quad (6.22)$$

The result obtained for activation energy for the adsorption of phenol on GAC follows GAC 383 (9.95 kJ/mol), GACO 383 (7.59 kJ/mol) and GACONZR 1273 (0.233 kJ/mol) respectively. Low activation energy means that physical

adsorption controls the removal of phenol from aqueous solution by GAC 383, GACO 383 and GACONZR 1273. The lower activation energy of GACONZR 1273 shows that very small energy is required to interact between GACONZR 1273 and phenol molecules, therefore the adsorption rate of phenol on GACONZR 1273 is fast as compared to that of GAC 383 and GACO 383.

$\ln K_2$  versus  $1/T$  plot of *p*-nitrophenol on GACONZR 1273, GAC 383, GACO 383 are given in the Figure 6.47(b) and activation energy obtained is given in Table 6.25.

The result obtained for activation energy for the adsorption of *p*-nitrophenol on GAC follows as; GAC 383 (7.71 kJ/mol), GACO 383 (10.32 kJ/mol) and GACONZR 1273 (10.88 kJ/mol). Lower magnitude of activation energy indicates that adsorption of *p*-nitrophenol on all the GAC studied follows the physical type of adsorption.

$\ln K_2$  versus  $1/T$  plot of methylene blue on GACONZR 1273, GAC 383 and GACO 383 are given in the Figure 6.47(c) and activation energy obtained is given in Table 6.25

**Table 6.25:** Activation energy obtained from Arrhenius equation

sample	phenol		<i>p</i> -nitrophenol		methylene blue	
	$E_a$ kJ/mol	A x 10 <sup>4</sup>	$E_a$ kJ/mol	A	$E_a$ kJ/mol	A x 10 <sup>4</sup>
GAC 383	9.95	84.00	7.71	0.001995	2.14	5.95
GACO 383	7.59	46.30	10.33	9.84E-07	7.59	46.22
GACONZR 1273	0.2331	3.164	10.877	0.014197	4.70	9.44

The activation energy for the adsorption of methylene blue (MB) on GAC is given as follows GAC 383 (2.14 kJ/mol), GACO 383 (7.59 kJ/mol) and GACONZR 1273 (4.67 kJ/mol). Lower magnitude of activation energy indicates that adsorption of MB on all the GAC studied follows the physical type of adsorption.

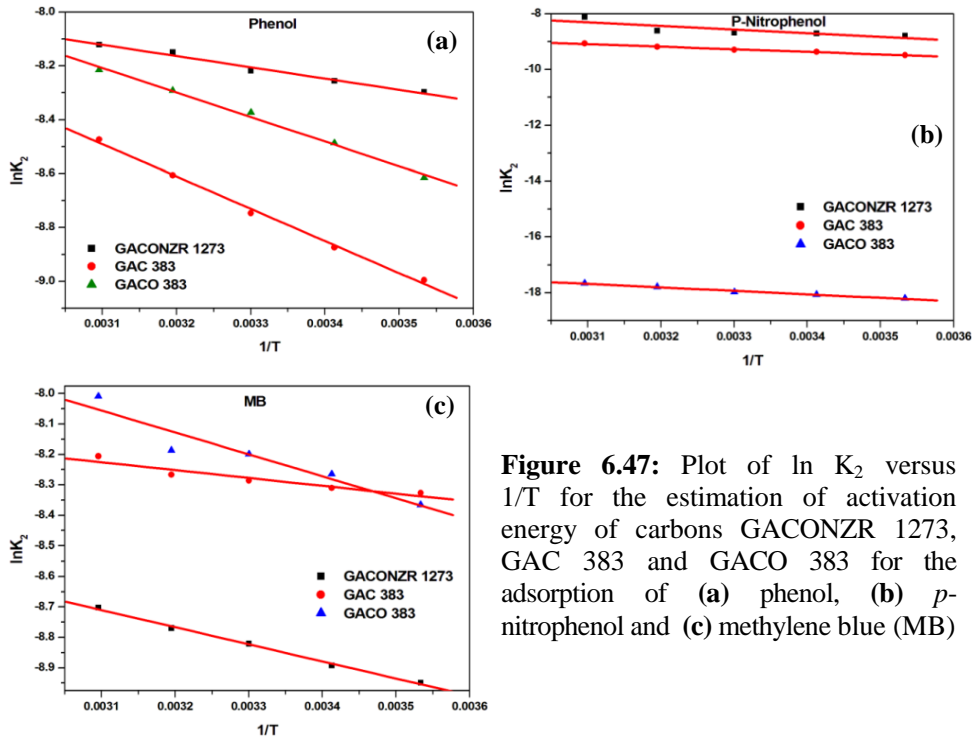


**Figure 6.47:** Plot of  $\ln K_2$  versus  $1/T$  for the estimation of activation energy of carbons GACONZR 1273, GAC 383 and GACO 383 for the adsorption of (a) phenol, (b) *p*-nitrophenol and (c) methylene blue (MB)

## 6.11 Design of Batch Adsorption from Isotherm Data

Mass balance equation used for calculating the amount of adsorbent required to treat phenol, *p*-nitrophenol and methylene blue is given in equation (6.23)

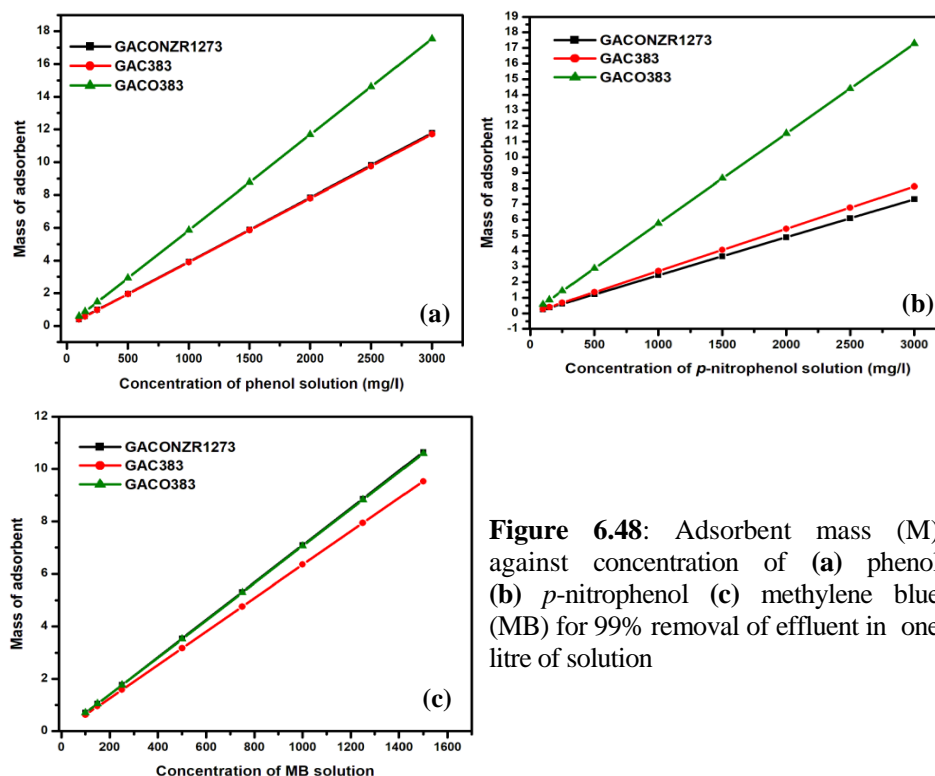
$$\frac{M}{V} = \frac{C_0 - C_e}{q_e} = \frac{C_0 - C_e}{\frac{q_0 K_L C_e}{1 + K_L C_e}} \quad (6.23)$$

Figure 6.48 shows that weight of carbons required for treating the solution of phenol, *p*-nitrophenol and methylene blue having different concentration. For treating one litre of solution containing 3000 mg/L phenol, the required masses of GAC is given as; GACONZR 1273 (11.78 g), GAC 383 (11.7 g) and GACO 383 (17.5 g). Similarly for treating different concentration of phenol in aqueous solution different weight of carbon is required. By comparing the efficiency of material with their weight required for treating the water having phenol, we can

see that GAC 383 and GACONZR 1273 requires approximately equal weight, whereas GACO 383 requires 48.9 % more weight compared to GACONZR 1273.

For treating one litre of solution containing 3000 mg/L *p*-nitrophenol, the required masses of GAC is given as; GACONZR 1273 (7.32 g), GAC 383 (8.13 g) and GACO 383 (17.3 g). The oxidised carbon (GACO 383) having low adsorption efficiency towards phenolic compounds. The impregnation of  $ZrO_2$  in GACO (GACONZR 1273) can enhance its efficiency and therefore reduces the weight into its half for treating the sample. GAC 383 requires 11% more weight compared to GACONZR 1273.

The amount of carbons required for treating the methylene blue solution having concentration of 1500mg/L is given as; GAC 383 (9.53 g), GACO 383 (10.59 g) and GACONZR 1273 (10.64 g). It indicates that approximately equal weight is required for both nitric acid modified carbon GACO 383 and GACONZR 1273. Efficiency of both of these carbons is lower than that of GAC 383.



**Figure 6.48:** Adsorbent mass (M) against concentration of (a) phenol (b) *p*-nitrophenol (c) methylene blue (MB) for 99% removal of effluent in one litre of solution

## 6.12 Adsorption of Trace Metal Ions by GACONZR Using Contaminated Groundwater

The newly prepared carbons are applied to trace metal analysis.

**Table 6.26:** Efficiency of GACONZR 1273 for removing trace metals in contaminated groundwater

Trace metals	Initial concentration (PPb)	Concentration after adsorption (PPb)		
		GACONZR 1273	GAC 383	GACO 383
<sup>7</sup> Li	4.5 (% Removal)	3.88 (13.8)	4.29 (4.7)	3.83 (14.9)
<sup>9</sup> Be	0.22 (% Removal)	0 (100.0)	0.01 (95.5)	ND (100.0)
<sup>24</sup> Mg	2905.63 (% Removal)	2421.23 (16.7)	2802.3 (3.6)	2395.43 (17.6)
<sup>27</sup> Al	257.22 (% Removal)	37.04 (85.6)	2.84 (98.9)	2.18 (99.2)
<sup>52</sup> Cr	1.5 (% Removal)	0.76 (49.3)	0.92 (38.7)	1.05 (30.0)
<sup>55</sup> Mn	85.73 (% Removal)	3.76 (95.6)	7.34 (91.4)	10.05 (88.3)
<sup>56</sup> Fe	48.78 (% Removal)	83.58 (31.2)	33.15 (32.0)	27.34 (44.0)
<sup>58</sup> Ni	5.46 (% Removal)	3.54 (35.2)	1.82 (66.7)	4.51 (17.4)
<sup>59</sup> Co	2.81 (% Removal)	0.13 (95.4)	0.13 (95.4)	0.23 (91.8)
<sup>63</sup> Cu	21.90 (% Removal)	2.47 (88.7)	3.17 (85.5)	4.46 (79.6)
<sup>64</sup> Zn	40.77 (% Removal)	16.76 (58.9)	17 (58.3)	28.46 (30.2)
<sup>75</sup> As	1.89 (% Removal)	0.36 (81.0)	0.34 (82.0)	0.27 (85.7)
<sup>114</sup> Cd	0.62 (% Removal)	0.45 (27.4)	0.16 (74.2)	0.57 (8.1)
<sup>138</sup> Ba	89.02 (% Removal)	37.69 (57.7)	42.77 (52.0)	21.25 (76.1)
<sup>205</sup> Tl	0.08 (% Removal)	0.02 (75.0)	0.04 (50.0)	0.04 (50.0)
<sup>208</sup> Pb	6.18 (% Removal)	0.2 (96.8)	0.24 (96.1)	0.23 (96.3)



The contaminated groundwater from fireworks accident area is collected and subjected to batch experiments for 8 hours with carbons by keeping the concentration of adsorbent at 1g/L. Concentration in the treated water samples was measured by inductively coupled plasma-mass spectroscopy. The percentage adsorption is calculated and presented in Table 6.26.

The adsorption capacity of GAC 383, GACO 383 and GACONZR 1273 shows more than 95 % efficiency towards Be, Mn, Co and Pb. Removal efficiency of GACONZR 1273 shows slightly higher for some trace elements like Cr (49.3 %), Cu (88.7 %), Zn (58.9 %), Tl (75.0 %) than basic carbons GAC 383 (Cr – 38.7 %, Cu - 85.5 %, Zn - 58.3 % Tl – 50 %) and GACO 383 (Cr – 30 % Cu – 79.6 % Zn – 30.2 % Tl – 50 %). Quantity of Li and Mg get adsorbed on GACO 383 (Li – 14.9 %, Mg – 17.6 %) and GACONZR 1273 (Li – 13.8 %, Mg – 16.7 %) is comparatively higher than GAC 383 whereas Cd and Ni more adsorbed on GAC 383 (Cd – 74.2 % Ni – 66.7 %) than oxidised carbons.

### **6.13 Statistical Analysis of the Data**

**Hypothesis 1:** Whether there is any significant difference in pore volume and surface area of carbons obtained from BET and *I* plot method.

To test the **Hypothesis 1**, pore volume and surface area obtained from BET and *I* plot for GAC 383, GACO 383, GACONZR 1073 and GACONZR 1273 is given in Table 6.3 are analysed statistically using **two way ANOVA** test

Based on the statistical parameters given in Table 6.27 and Table 6.28 i.e. sum of squares (SS), degree of freedom (df), mean square (ms), variance ratio (F) and level of significance (P value) observations are summarised below.

Pore volume and surface area of carbons (GAC 383, GACO 383, GACONZR 1073 and GACONZR 1273) calculated from *BET* and *I* plot are used for proving the Hypothesis 1.

**Table 6.27:** Two way ANOVA analysis of pore volume obtained from BET and *I*-plot method

Source	SS	df	ms	F	P-value
Total	819.4526	7			
carbons	751.4076	3	250.4692	584.253	P < 0.001
Methods	66.7590	1	66.7590	155.724	P < 0.001
Residual	1.2860	3	0.4287		

There is a significant difference in volume between carbons ( $P < 0.001$ ). Pore volume is significantly higher in GAC 383 and significantly low in GACO 383 ( $P < 0.001$ ).

Methods also showed a significant difference in pore volume between them ( $P < 0.001$ ). The volume by BET method is significantly higher than that *I* point method ( $P < 0.001$ ).

**Table 6.28:** Two way ANOVA analysis of surface area obtained from BET and *I*-plot method

Source	SS	df	ms	F	P-value
Total	15521.9970	7			
carbons	14238.6017	3	4746.2006	615.7420	P < 0.001
Methods	1260.2710	1	1260.2710	163.4996	P < 0.001
Residual	23.1243	3	7.7081		

It shows that there is a significant difference in surface area between carbons ( $P < 0.001$ ). Among the carbon studied GAC 383 is having significantly higher surface area compared to others.

There is a significant difference between *BET* and *I* plot as far as surface area is considered ( $P < 0.001$ ). Surface area is significantly higher in *BET* than that in the *I* plot ( $P < 0.001$ ).

**Hypothesis 2:** Whether there is any significant difference between the pore volume of carbons obtained from Langmuir, Dubinin – Radushkevich (D-R), Alpha S ( $\alpha_s$ ) and John isotherm

To test the **Hypothesis 2**, pore volume obtained from Lanmuir, Dubinin-Radushkevich, Alpha S ( $\alpha_s$ ) and John isotherm for GAC 383 GACO 383,

GACONZR 1073 and GACONZR 1273 are statistically analysed by two way ANOVA test. The results are interpreted based on the constants in Table 6.29

**Table 6.29:** Two way Anova analysis of pore volume obtained from Langmuir, Dubinin-Radushkevich (D-R), Alpha S ( $\alpha_s$ ) and John Isotherm

Source	SS	df	ms	F	P-value
Total	2913.9300	15			
carbons	1701.3700	3	567.1233	45.944	P < 0.001
Methods	1101.4650	3	367.1550	29.744	P < 0.001
Residual	1110950	9	12.3439		

Pore volume of carbons (GAC 383, GACO 383, GACONZR 1073 and GACONZR 1273) obtained from four isotherm models i.e. Langmuir, Dubinin – Radushkevich, Alpha S ( $\alpha_s$ ) and John isotherm are used to prove the Hypothesis 2.

The result shows that there is a significant difference between carbons with respect to pore volumes (P < 0.001), Pore volume is significantly higher in GAC 383 and significantly low in GACO 383.

Methods also showed a significant difference in pore volume (P < 0.001). Pore volume is significantly higher in Alpha S ( $\alpha_s$ ) followed by Dubinin – Radushkevich (P < 0.001).

**Hypothesis 3:** Whether there is any significant difference in quantity adsorbed and surface area between the carbons for the adsorption of phenol, *p*-nitrophenol and methylene blue.

To test the **Hypothesis 3**, adsorption rate and surface area of carbons GACONZR 1273, GAC 383 and GACO 383 with respect to solid – liquid equilibria using phenol, *p*-nitrophenol and MB obtained from Langmuir, Dubinin-Radushkevich and John–Sivanandan Achari isotherms given in Table 6.12 are analysed statistically using three way ANOVA test. The results are interpreted based on the constants given in Table 6.30

**Table 6.30:** Three way ANOVA statistical analysis of adsorption system in solid-liquid equilibria with respect to quantity of phenol, *p*-nitrophenol and methylene blue adsorbed on GACONZR 1273, GAC 383 and GACO 383

Source	SS	df	ms	F	P-value
Total	405567.1354	26			
carbons	32538.6523	2	16269.3262	7.674	P < 0.01
methods	237315.8540	2	118757.9270	56.013	P < 0.001
Phenol, PNP,MB	93309.0262	2	46654.5131	22.006	P < 0.001
Residual	42403.6029	20	2120.1801		

There is a significant difference between carbons in the aspects of amount adsorbed ( $P < 0.01$ ) is considered. Methods also showed a significant difference between them ( $P < 0.01$ ). John - Sivanandan Achari and Langmuir methods showed a significantly higher amount of adsorption than Dubinin – Radushkevich. Between Langmuir and John – Sivanandan Achari isotherm, the difference is not significant.

Between methylene blue, phenol and *p*-nitrophenol the adsorption rate differs significantly ( $P < 0.001$ ). Adsorption rate is significantly higher in *p*-nitrophenol and significantly low in methylene blue ( $P < 0.001$ ).

**Hypothesis 4:** whether there is any correlation between temperature and adsorption of phenol, temperature and adsorption of *p*-nitrophenol & temperature and adsorption of methylene blue.

To test the **Hypothesis 4**, Langmuir adsorption capacity of GACONZR 1273 for phenol (Table 6.9), *p*-nitrophenol (Table 6.10) and methylene blue (Table 6.11) at five solution temperature (283 K, 293 K, 303 K, 313 K and 323 K) are correlated by Karl Pearson's Coefficient.

Coefficient of correlation between temperature and adsorption of phenol on GACONZR 1273 ( $r = 0.970174$ ,  $t = 6.93205$ ,  $df = 3$ ,  $P < 0.01$ ) is significant. This indicates that as temperature increases adsorption of phenol also increases.

There is a significant positive correlation between temperature and adsorption of *p*-nitrophenol on GACONZR 1273 ( $r = 0.99191$ ,  $t = 13.532$ ,  $df = 3$ ,

P < 0.01). This indicates that as temperature increases adsorption of *p*-nitrophenol also increases.

There is a significant positive correlation between temperature and adsorption of methylene blue on GACONZR 1273 ( $r = 0.99959$ ,  $t = 60.2178$ ,  $df = 3$ ,  $P < 0.01$ ). This indicates that as temperature increases adsorption of methylene blue also increases.

## 6.14 Conclusions

Nano zirconium can be incorporated into porous structure of oxidised carbon GACO to prepare a new series of carbon designated as GACONZR. Carbon series GACONZR have shown a burn off vary from 7.2 % to 19.5 % and carbon yield vary from 92.8 % to 80.5 % with rise of activation temperature from 383 to 1273 K. Elemental analysis shows that the percentage of fixed carbon is highest in GACONZR 1073 (87 %), and GACONZR 1273 (91.7 %). Percentage of oxygen was found to be decreasing with an increase of activation temperature. High carbon content of GACONZR series at a higher activation temperature (1073 and 1273 K) indicates that the aromatic structure becomes more dominant after steam activation in the presence of  $Zr^{4+}$ . Compared to GAC 383, the nitric acid modified GACO 383 and GACONZR series shows large  $L_c$  and  $L_a$  value. It indicates that oxidation of granular activated carbon increases the crystalline width and thickness.

On comparing with GACO 383, zirconia ( $ZrO_2$ ) impregnated GACO series shows 5.3 % (GACONZR 1073) and 8.9 % (GACONZR 1273) increment in Langmuir surface area. The *t*-plot method shows that there is a 20.5 % enhancement in external surface area by increasing the activation temperature from 1073 K to 1273 K for GACONZR carbons. The average pore width calculated for GACONZR 1073 and GACONZR 1273 are found to be in the micropore range (< 2.0 nm). But the BJH analysis give adsorptive and desorptive cumulative pore volume of 2.25 - 2.44 nm in range. This may be due to the presence of a small proportion of super micropores (wider micropores) that are formed during carbonization. Comparison of pore volumes obtained from John, Dubinin -Radushkevich, Alpha S ( $\alpha_s$ ), and Langmuir isotherm models are having the approximately same value.

On comparing with GACO 383, carbon GACONZR 1273 has 40 % more efficiency towards phenol, and 29 % more efficiency towards *p*-nitrophenol. Intraparticle diffusion shows that external mass transfer is more predominating than intra particle diffusion for the adsorption of phenol, *p*-nitrophenol and methylene blue. Activation energy obtained from the Arrhenius equation shows that physical adsorption control the adsorption of phenol, *p*-nitrophenol and methylene blue. The positive  $\Delta H$  of all adsorbents indicates the endothermic nature of adsorption. The positive  $\Delta S$  suggests an increase in the randomness at adsorbate-solution interface during the adsorption process. The increase in negative  $\Delta G$  values with increasing temperature indicates the feasibility of adsorption at higher temperatures. Trace metal ion analysis using carbon GACONZR 1273 shows higher adsorption efficiency for some trace elements like Cr, Cu, Zn, and Tl than basic carbons GAC 383 and GACO 383.

Statistical analysis shows that among the carbon studied GAC 383 is having significantly higher surface area and pore volume compared to GACONZR 1273. John and John-Sivanandan Achari isotherm agree well with Langmuir for the adsorption system studied. A significant positive correlation exists between temperature and adsorption rate for phenol, *p*-nitrophenol and methylene blue on GACONZR 1273.

## Reference

- [1] Otake, Y.; Jenkins, R. G. Characterization of Oxygen-Containing Surface Complexes Created on a Microporous Carbon by Air and Nitric Acid Treatment. *Carbon* **1993**, *31* (1), 109–121.
- [2] Perez-Aguilar, N. V.; Muñoz-Sandoval, E.; Diaz-Flores, P. E.; Rangel-Mendez, J. R. Adsorption of Cadmium and Lead onto Oxidized Nitrogen-Doped Multiwall Carbon Nanotubes in Aqueous Solution: Equilibrium and Kinetics. *J. Nanoparticle Res.* **2010**, *12* (2), 467–480.
- [3] Bedmohata, M.A.; Chaudhari, A.R.; Singh, S.P.; Choudhary, M. D. Adsorption Capacity of Activated Carbon Prepared by Chemical Activation of Lignin for the Removal of Methylene Blue Dye. *International Journal of Advanced Research in Chemical Science* **2016**, *2* (8), 1-13.

- [4] Ishizaki, C.; Martí, I. Surface Oxide Structures on a Commercial Activated Carbon. *Carbon* **1981**, *19* (6), 409–412.
- [5] Bhabendra, K.; Pradhan, B. K.; Sandle, N. K. Effect of Different Oxidizing Agent Treatments on the Surface Properties of Activated Carbons. *Carbon* **1999**, *37* (8), 1323–1332.
- [6] Chiang, H.L.; Huang, C. P.; Chiang, P. C. The Surface Characteristics of Activated Carbon as Affected by Ozone and Alkaline Treatment. *Chemosphere* **2002**, *47* (3), 257–265.
- [7] Mohammadi, M.; Hassani, A. J.; Mohamed, A. R.; Najafpour, G. D. Removal of Rhodamine B from Aqueous Solution Using Palm Shell-Based Activated Carbon: Adsorption and Kinetic Studies. *J. Chem. Eng. Data* **2010**, *55* (12), 5777–5785.
- [8] Lee, P.; Ho, C.; Hwang, C.; Ding, S. Improved Physicochemical Properties and Biocompatibility of Stainless Steel Implants by PVA / ZrO<sub>2</sub> -Based Composite Coatings. *Surf. Coat. Technol.* **2014**, *258*, 374–380.
- [9] Anisuzzaman, S. M.; Joseph, C. G.; Krishnaiah, D.; Tay, V. V. Modification of Commercial Activated Carbon for the Removal of 2, 4-Dichlorophenol from Simulated Wastewater. *J. King Saud Univ. - Sci.* **2015**, *27*, 318–330.
- [10] Schwickardi, M.; Johann, T.; Schmidt, W.; Schüth, F. High-Surface-Area Oxides Obtained by an Activated Carbon Route. *Chem. Mater.* **2002**, *14* (9), 3913–3919.
- [11] Bindia Ravindran. Adsorption Isotherm Studies on Activated Carbon Prepared by Activation with Cerium Compounds. *Ph.D Thesis* **2016**. School of Environmental Studies, Cochin University of Science and Technology, Cochin, Kerala, India.
- [12] Achari, V.S.; Rajalakshmi, A.S.; Jayasree, S. Surface Area and Porosity Development on Granular Activated Carbon by Zirconium: Adsorption Isotherm Studies. *Journal of Applied Research and Technology* **2017** (Accepted November 2017).
- [13] Achari, V. S. Modified Carbons and Wood Dust: Evaluation of Adsorption Properties. *Ph.D. Thesis* **1998**. Department of Chemistry, University of Kerala, Kariavattom, Thiruvananthapuram, Kerala, India.
- [14] John, P.T.; Suri, D. K.; Nagpal, K. C. Characterization of structural parameters of porous materials by a new adsorption isotherm. *Journal of material science* **1985**, *20* (6), 2071–2086.

- [15] John, P. T.; Achari, V. S. Characterisation of Structural Parameters of Finely Divided and Porous Materials by a New Adsorption Isotherm. *Journal of Materials Science* **2002**, *37* (4), 885–893.
- [16] Parent, M. A.; Moffat, J. B. A Comparison of Methods for the Analysis of Adsorption-Desorption Isotherms of Microporous Solids. *Langmuir* **1995**, *11*, 4474–4479.
- [17] Teng, H.; Hsieh, C.T. Influence of Surface Characteristics on Liquid-Phase Adsorption of Phenol by Activated Carbons Prepared from Bituminous Coal. *Ind. Eng. Chem. Res.* **1998**, *37* (9), 3618–3624.
- [18] Yan, D. L. J.; Liu, Z. L. Z. Adsorption Kinetic Studies for Removal of Methylene Blue Using Activated Carbon Prepared from Sugar Beet Pulp. *Int. J. Environ. Sci. Technol.* **2016**, *13*(7), 1815–1822
- [19] Achari, V.S. John Isotherm for Liquid Phase Adsorption: Comparison with Langmuir and Freundlich Models. *International Carbon Conference, Carbon 2006*, Robert Gordon University, Aberdeen, Scotland, UK. Extended Abstract, 16-21. ISBN 0- 9553365-1-1, 3P 107.
- [20] Mercy Thomas. Adsorption Isotherm Characterization of Porous Materials Using John Isotherm. *Ph.D Thesis 2016*. School of Environmental Studies, Cochin University of Science and Technology, Cochin, India.
- [21] Achari, V.S.; Jayasree, S. Rajalakshmi, A.S. Adsorption of *p* – nitrophenol on Coconut Shell Granular Activated Carbon: Isotherms, Kinetics and Thermodynamics. *Indian Journal of Chemical Technology.* **2017**, *24*, 471-478.
- [22] Tofighy, M A.; Mohammadi, T. Methylene blue Adsorption onto Granular Activated Carbon Prepared from Harmal Seeds Residue. *Desalination and Water Treatment.* **2014**, *52*, 2643–2653.
- [23] Rodriguez, A.; Garcia, J.; Ovejero, G.; Mestanza, M. Adsorption of Anionic and Cationic Dyes on Activated Carbon from Aqueous Solutions: Equilibrium and Kinetics. *J. Hazard. Mater.* **2009**, *172*, 1311–1320.
- [24] Bulut, Y.; Tez, Z. Removal of heavy metals from aqueous solution by sawdust adsorption. *Journal of Environmental Science* **2007**, *19* (2), 160–166.

.....❧.....



## SUMMARY AND CONCLUSION

Preparation, material characterization, Isotherm features, adsorption efficiency with respect to porosity and surface area of four prominent series of  $Zr^{4+}/ZrO_2$  based carbon (such as GACZR, GACOZR, GACNZR and GACONZR) is elaborately presented in this bound thesis. This chapter summarizes the major findings and inferences with the support of statistical tools. Detailed examinations of thermodynamic properties are also systematically evaluated.

Major results and conclusions are summarized as

- Activation of coconut shell based granular activated carbon materials using  $HNO_3$ ,  $ZrOCl_2$  and  $ZrO_2$  as porosity promoting agents results new series of carbons (GACZR, GACOZR, GACNZR and GACONZR series). Chemical activation under steam – heat treatment produced carbon with good yield and fixed carbon. This activation causes changes in the structure, porosity, surface area, pore size distribution and adsorption efficiency of the modified carbons.
- XRD pattern of activated carbons reveals the amorphous structure due to rupture of C-C bond in aromatic rings. The interlayer spacing ( $d_{002}$ ) vary from 0.352 – 0.382 nm for GACZR series, 0.352 – 0.362 nm for GACOZR series, 0.350 – 0.378 nm for GACNZR series, 0.351 – 0.365 nm for GACOZR series. It is larger than the spacing in typical graphitic single crystal (0.335 nm). This observation indicates that obtained carbons are composed of turbostratic (fully disordered) structures. During activation at higher temperature, slight difference in the diffraction pattern is observed, caused by the lowering of

crystallites,  $L_c$  (height) and  $L_a$  (width). It reveals that the degree of ordered graphitization of activated carbon decreases at higher activation temperatures. The two broad peak around  $2\theta$  at  $25^\circ$  and  $43.6^\circ$  is ascribed to (002) and (100) diffraction peak of turbostratic carbon structure. During activation at a higher temperature  $Zr^{4+}$  crystallizes and gives additional peaks at  $30^\circ$  for  $Zr^{4+}/ZrO_2$  impregnated carbons distinct for M-C (C –  $ZrO_2$ ) bond.

- Elemental analysis of new carbons indicates that activated carbons having appreciable amounts of oxygen and hydrogen in addition to carbon. All the four series of activated carbons (activated at 1073 – 1273 K) shows the percentage of carbon content more than 85 %. But the nitric acid modified carbon GACO 383 has only low carbon content as 65 %. During activation at high temperature, most of the non carbon elements are eliminated as volatile compounds as revealed by low carbon yield and high burn off value. The carbon yield is given as; for GACZR series: 94.5 % to 82.22 %, GACOZR series: 85.5 to 76.4 %, GACNZR series: 98.3 % to 94.1 %, GACONZR series: 92.8 to 80.5%. Reduction of carbon yield at the temperature range 383 – 673 K is due to decomposition of carboxylic acid into  $CO_2$ . Decomposition of lactonic group is initiated at the temperature range of 473 – 873 K. Decomposition of phenol will take at higher activation temperatures and it gives CO at 1073 – 1273 K.
- The surface functional groups analyzed by FTIR, XPS and Boehm titration method suggests the existence of functional groups as carbonyls, carboxyls, lactones, quinones, and phenols on the surface of activated carbons. On comparing with GAC 383, nitric acid modified carbon GACO 383 has peaks around at  $1121-992\text{ cm}^{-1}$  due to C-OH stretching in carboxylic acid. This indicates, the generation of more oxygen complexes by the surface oxidation of active sites on graphene edges. This is further confirmed by the presence of peak around at  $1029\text{ cm}^{-1}$  (C-O-C) in GACO 383. The band appears at near  $589\text{ cm}^{-1}$  for GACZR series and  $1067 - 1077\text{ cm}^{-1}$  in GACNZR series

is attributed to the Zr - O from  $ZrO_2$ . In XPS spectra presence of surface oxygen groups and chemisorbed species on a carbon surface can be identified by the chemical shift of the C 1s peak and O 1s peaks. Uniform dispersion of  $Zr^{4+}$  in GAC for GACZR series, GACOZR series, GACNZR series and GACONZR series is revealed by Zr 3d peaks. XPS spectra of GACZR 1073 and GACOZR 1273 gives strong spin orbit doublet of  $3d_{5/2}$  (182.6 eV) and  $3d_{3/2}$  (185.3 eV) in the Zr 3d spectrum corresponding to  $Zr^{4+}$  in  $ZrO_2$ .

- Microscopic analysis of activated carbons by SEM and TEM at higher magnification shows well-developed porous structures on the surface of carbons GACZR 1273, GACOZR 1273, GACNZR 1273 and GACONZR 1273. Particles of  $Zr^{4+}$  get distributed around the pore edges as they appeared as white points of different sizes. On Comparison with GAC 383, the nitric acid oxidation/modified carbons GACO 383, GACOZR 1273 and GACONZR 1273 indicates large diameters of the pores on the surface. The nitric acid oxidation/modification causes the widening of existing pores and the formation of large pores by burn out of the walls between the adjacent pores.
- Surface area and pore volume analysis using  $N_2$  adsorption isotherm at 77 K indicates that activation temperature has a significant effect on porosity and surface area development of  $ZrOCl_2/ZrO_2$  based carbons. For GACZR series as the activation temperature increases from 873 K to 1273 K the pore volume  $V_m$  (BET  $P/P_0$  upto 0.1) increases from 327.4 to 387.6  $cm^3/g$ . Whereas, for GACOZR carbons pore volume increases from 259.7 to 278.5  $cm^3/g$ . For GACONZR series, it increases from 320.7 to 331.5  $cm^3/g$  by rising the activation temperature from 1073 to 1273 K. But differently, for carbon GACNZR pore volume decreases from 376.8 to 354.0  $cm^3/g$  with increasing the activation temperature from 1073 to 1273 K.
- Zirconyl chloride ( $ZrOCl_2$ ) impregnated carbon, GACZR 1273 ( $V_m = 344 \text{ cm}^3/g$  &  $SA_{BET} = 1497.3 \text{ m}^2/g$ ) has 16 % and  $ZrO_2$  impregnated carbon, GACNZR 1073 ( $V_m = 334 \text{ cm}^3/g$  &  $SA_{BET} = 1454.3 \text{ m}^2/g$ ) has a

12 % enhancement in BET surface area ( $SA_{BET}$ ) and pore volume ( $V_m$ ) compared to GAC 383 ( $V_m = 298.3 \text{ cm}^3/\text{g}$  &  $SA_{BET} = 1298.5 \text{ m}^2/\text{g}$ ). It indicates that,  $\text{Zr}^{4+}$  impregnation on GAC and the steam activation at higher temperature enhances the specific surface area and pore volume. Compared to basic GAC 383, treatment with nitric acid causes, the reduction in monolayer volume and surface area of 8.68 % in GACO 383 ( $V_m = 272.6 \text{ cm}^3/\text{g}$  &  $SA_{BET} = 1186.5 \text{ m}^2/\text{g}$ ). The pore volume and surface area obtained from BET  $p/p_0 \approx 0.1$  is in close agreement with  $I$  point method.

- The monolayer volume  $V_m(L)$  and surface area  $SA_L$  obtained from Langmuir adsorption isotherm of carbon are GAC 383 ( $V_m = 336.6 \text{ cm}^3/\text{g}$  &  $SA_L = 1465.27 \text{ m}^2/\text{g}$ ), GACO 383 ( $V_m = 304.5 \text{ cm}^3/\text{g}$  &  $SA_L = 1325.54 \text{ m}^2/\text{g}$ ), GACZR 1273 ( $V_m = 387.58 \text{ cm}^3/\text{g}$  &  $SA_L = 1687.23 \text{ m}^2/\text{g}$ ) and GACNZR 1073 ( $V_m = 376.83 \text{ cm}^3/\text{g}$  &  $SA_L = 1640.43 \text{ m}^2/\text{g}$ ). Monolayer volume and surface area of GACZR 1273 and GACNZR 1073 made from basic GAC 383 indicate that the impregnation of zirconium and successive activation with steam enhances the monolayer adsorption capacity.
- Dubinin – Radushkevich (D-R) isotherm analysis using  $\text{N}_2$  adsorption data at 77 K shows that granular activated carbon incorporated with  $\text{Zr}^{4+}/\text{ZrO}_2$  series (GACZR and GACNZR) has a relatively high proportion of micropore surface area. Uniform pore generation occurs throughout the activation temperature range of 1073-1273 K with respect to GACNZR 1073 and GACZR 1273. GACZR 1273 has 26 % ( $SA_{D-R} = 814.3 \text{ m}^2/\text{g}$ ) and GACNZR 1073 has 12 % ( $SA_{D-R} = 722.980 \text{ cm}^3/\text{g}$ ) enhancement in micropore surface area compared to basic carbon GAC 383 ( $SA_{D-R} = 646.5 \text{ m}^2/\text{g}$ ). The micropore volumes provided by Dubinin-Radushkevich analysis i.e.  $V_{mi}$  (D-R) and Alpha S  $V_{mi}$  ( $\alpha_S$ ) methods are in excellent agreement for all carbons.
- The average pore width calculated from Dubinin-Radushkevich (D-R) isotherm for GACZR 1073 ( $L = 1.50$ ) and GACZR 1273 ( $L = 1.53$ ) gives values less than 2 nm. This value is comparatively smaller than

the average pore width of GAC 383 ( $L = 1.68$ ). It indicates that pore having a width less than 2 nm are more generated by chemical activation by incorporating with  $Zr^{4+}$  on coconut shell based precursor.

- The  $t$ -plot method shows that zirconyl chloride impregnated GAC i.e carbon GACZR 1073 has 763.9  $m^2/g$  micropore surface area (total surface area 1085.0  $m^2/g$ ) and GACZR 1273 has 863.8  $m^2/g$  micropore surface area (total surface area 1217  $m^2/g$ ). For  $ZrO_2$  impregnated GAC i.e. GACNZR 1073, has 743.3  $m^2/g$  micropore surface area (total surface area 1161.8  $m^2/g$ ) and GACNZR 1273 has 701.1  $m^2/g$  micropore surface area (total surface area of 1087.7  $m^2/g$ ). It suggests that 70% total surface area of GACZR 1073 and GACZR 1273 has contributed by micropore surface area ( $< 2$  nm) and the remaining 30 % contributed by external surface area ( $> 2$  nm). Whereas, for GACNZR 1073 and GACNZR 1273, 64 % of total surface area is contributed by micropore surface. It means that  $Zr^{4+}$  activation leads to the acceleration of micropores on the activated carbon matrix of GAC 383 ( $SA_{mi} = 588.7$   $m^2/g$  &  $SA_{ext} = 408.1$   $m^2/g$ ). Pore size distribution studies (PSD) using BJH analysis showed that adsorption and desorption pore width ranges 2.3 - 2.5 nm for zirconium activated carbon series, which indicate the presence of wider micropores on the carbon surface.
- The precise information about the phase changes during adsorption process are revealed by John isotherm. It suggests the three different pore filling mechanisms of  $N_2$  molecule in GAC. Each phase on the plots are represented as a molecular sieve effect, monolayer coverage and mesopore filling. Among the three phases of adsorption, molecular sieve effect (adsorption in pores having a width less than 0.8 nm) is found to be prominent for  $N_2$  atoms for all the carbon studied. The percentage contribution of  $V_{mse}$  ( $J$ ) in total adsorption ( $V_T$ ) for series of carbon is given as GAC 383 (80.9 %), GACO 383 (82.9 %), GACZR 1073 (79.30 %), GACZR 1273 (78.20 %), GACOZR 1073 (80.9%), GACOZR 1273 (78.9%), GACNZR 1073 (79.01%), GACNZR 1273 (79.41%), GACONZR 1073 (79.03%) and GACONZR 1273 (77.52%).

- The experimental data with respect to solid –liquid (GAC – phenol/ *p*-nitrophenol/ methylene blue) equilibria obtained from batch experiments were subjected to linear and nonlinear equations of Langmuir, Freundlich, Dubinin-Radushkevich, John-Sivanandan Achari isotherm models. Adsorption capacity estimated from the linear equations of isotherm models suggests that the presence of the nitro group on para position make the phenol ring more positive (electron acceptor) and therefore increasing electron donor acceptor interaction between adsorbent and adsorbate. This results more adsorption of *p*-nitrophenol on the carbon surface compared to phenol molecule. The adsorption rate of methylene blue is comparatively less than phenolic compounds. It was suggested that some of the micropores in active carbons were not accessible to MB dye molecules due to large molecular size.
- Linear and Nonlinear form of equation suggest that John – Sivanandan Achari and Langmuir isotherm models are best fitted to isotherm data than, Freundlich and Dubinin- Radushkevich isotherm for the adsorption of phenols, *p*-nitrophenol and methylene blue onto activated carbon.
- John-Sivanandan Achari isotherm exhibits different phases for the adsorption of phenol, *p*-nitrophenol and methylene blue. The rise of solution temperature is showing systematic quantitative enhancement of adsorption in each phase. Total adsorption capacity obtained from John-Sivanandan Achari and Langmuir isotherms have no significant differences.
- Nitric acid oxidised carbon (GACO 383) showed comparatively less adsorption towards phenol, *p*-nitrophenol and methylene blue. GAC 383 shows 48.6 % more adsorption towards phenol, 64.1 % more adsorption towards *p*-nitrophenol and 33.1% more adsorption towards methylene blue compared to GACO 383.
- Impregnation of  $Zr^{4+}$  on GAC enhances the adsorption towards phenol, *p*-nitrophenol and methylene blue. On comparing with GAC

383,  $Zr^{4+}$  impregnated GAC such as GACZR 1273 has 32.7 % more efficiency towards phenol, 40.1% more efficiency towards *p*-nitrophenol and 37.6 % more efficiency towards methylene blue. And also GACNZR shows 42.7 % more efficiency towards phenol, 44 % more efficiency towards *p*-nitrophenol and 63 % more efficiency towards methylene blue.

- On comparing with carbon GACO 383,  $Zr^{4+}$  impregnated GACO such as GACOZR 1273 has 33.1 % more efficiency towards phenol, 82 % more efficiency towards *p*-nitrophenol and 0.98 % more efficiency towards methylene blue. And also GACONZR 1273 has 37 % more efficiency towards phenol, 86 % more efficiency towards *p*-nitrophenol and 2.15% more efficiency towards methylene blue.
- The kinetic study shows that the new carbon adsorption system based on  $Zr^{4+}/ZrO_2$  studied follows the second order kinetic model. Two distinct phases in the intra particle diffusion plot suggest that the adsorption process proceeds by surface adsorption and intra particle diffusion. The second phase of adsorption shows a steady increase result of intraparticle diffusion effects, i.e. the transfer of the adsorbed molecule from the surface to the intra-particle active sites, which determine the rate limiting step.
- Activation energy obtained from the Arrhenius' equation shows that physical adsorption controls the adsorption of phenol, *p*-nitrophenol and methylene blue on new carbons. It suggests that adsorbate molecules studied are bound to the surface of the GAC by relatively weak van der Waals forces.
- The positive  $\Delta H$  of all the carbon studied indicates the endothermic nature of adsorption i.e the adsorption is favoured at higher temperatures. Enthalpy reflects the interaction of adsorbate molecules with the granular activated carbons. The high  $\Delta H$  obtained for  $Zr^{4+}/ZrO_2$  impregnated carbons (GACZR 1273, GACOZR 1273, GACNZR 1073, GACONZR 1273) are related with high adsorptive capacity and extra physicochemical properties of these carbons due to incorporated

zirconium. Hence nano  $Zr^{4+}/ZrO_2$  incorporated carbons have better material properties than basic carbons GAC 383 and GACO 383.

- The high positive  $\Delta S$  for GACZR 1273, GACOZR 1273, GACNZR 1073, GACONZR 1273 suggests, high randomness at adsorbate-solution interface during the adsorption process due to replacement of water molecules on the surface of these carbons by adsorbate. The increase in negative  $\Delta G$  values with the solution temperature indicates the feasibility of adsorption at higher temperatures due to the increase in number of adsorption sites generated as a result of breaking of some internal bonds near edge of active surface sites of carbons.
- Design of batch adsorption system shows that, on comparing the weight of carbon for treating phenol, 35 % less weight is required for GACZR 1273 than the weight of GAC 383. Similarly for treating *p*-nitrophenol, GACZR 1273 requires 30 % less weight than that required for GAC 383. And also for treating methylene blue, modified carbon GACZR 1273 requires weight of 43 % less than that needed for GAC 383.
- On comparing with basic carbon, for treating phenol, 37 % less weight is used by GACNZR 1273 than the amount used by GAC 383. Similarly for treating *p*-nitrophenol, GACNZR 1273 requires 31% less weight than that required for GAC 383. And also for treating methylene blue, modified carbon required for adsorption treatment is half than that needed for GAC 383.
- The percentage adsorption of each trace element present in a natural ground water with respect to their initial concentration by carbons shows that all granular activated carbons have more than 95 % adsorption efficiency towards Be, Al, Co and Pb elements with respect to their initial concentration.

GACZR 1273 has more than 80 % adsorption efficiency towards Cu (88.9 %) and Zn (81.4 %), more than 75 % efficiency towards As (78.8 %) and Tl (75 %) whereas GAC 383 and GACO 383 shows only 58.3 % and 30.2 % efficiency towards Zn and 50 % removal efficiency towards Tl.



GACOZR 1273 give more than 80% adsorption efficiency towards Cu, Zn and As and 75% efficiency towards Ni and Tl. Basic carbons GAC 383 and GACO 383 shows only less efficiency towards Mg, Cr, Zn and Ni compared to GACOZR 1273 (Mg -23.9%, Cr – 63.3%, Zn- 80.1%, Ni – 74.9 %).

The adsorption of Fe, Ni, Zn and Tl by GACNZR 1073 (Fe – 50.7%, Ni -60.4%, Zn- 67.6% Tl - 75%) is comparatively higher than basic carbons GAC 383 (Fe – 32.0 %, Ni -66.7 %, Zn- 58.3 % Tl – 50 %) and GACO 383 (Fe – 44.0 %, Ni - 17.4%, Zn- 30.2 % Tl - 50%).

The adsorption efficiency of GACONZR 1273 shows slightly higher for some trace elements like Cr (49.3%), Cu (88.7%), Zn (58.9%), Tl (75.0%) than basic carbons GAC 383 (Cr – 38.7%, Cu - 85.5%, Zn - 58.3% Tl – 50%) and GACO 383 (Cr – 30% Cu – 79.6% Zn – 30.2% Tl – 50%).

### Statistical Analysis

The pore volume obtained from both BET and *I* plot method for the new carbon series were statistically analyzed by using ANOVA method. It suggests on comparing with GAC 383 and GACO 383, the new carbons in GACZR series ( $P < 0.05$ ), GACNZR series ( $P < 0.001$ ) and GACONZR series ( $P < 0.001$ ) has significant differences in pore volume.

Statistical analysis (ANOVA) of pore volume obtained from Langmuir, Dubinin-Radushkevich (D-R), Alpha S ( $\alpha_s$ ) and John isotherm shows that highly significant differences exist between the carbons ( $P < 0.001$ ) for GACZR series, GACOZR series, GACNZR series and GACONZR series.

The correlation between pore volume and activation temperatures are statistically analyzed by Karl Pearson's co-efficient of correlation using GACZR series of carbons activated at different temperatures (873K, 1073K and 1273K). It gives a significant positive correlation between activation temperature and micro pore volume ( $r = 0.99674$ ,  $t = 12.35$ ,  $P < 0.01$ ). This indicates that with rise of activation temperature micropore volume also increases.

The adsorption rate of phenol, *p*-nitrophenol and methylene blue varies significantly ( $P < 0.001$ ) and also shows significant differences between carbons with respect to adsorption rate. There is no significant difference exists between the Langmuir and John-Sivanandan Achari isotherms. Application of John-Sivanandan Achari isotherm model is useful for the adsorption characterization of porous materials.

There is a significant positive correlation between temperature and adsorption of phenol ( $r = 0.9941$ ,  $t = 15.82$ ,  $df = 3$ ,  $P < 0.01$ ), *p*-nitrophenol ( $r = 0.9957$ ,  $t = 18.51$ ,  $df = 3$ ,  $P < 0.01$ ) and methylene blue ( $r = 0.9980$ ,  $t = 27.5$ ,  $df = 3$ ,  $P < 0.01$ ) on GACZR 1273.

There is a significant positive correlation between temperature and adsorption of phenol ( $r = 0.9961$ ,  $t = 19.428$ ,  $df = 3$ ,  $P < 0.01$ ), *p*-nitrophenol ( $r = 0.9978$ ,  $t = 26.2013$ ,  $df = 3$ ,  $P < 0.01$ ) and methylene blue ( $r = 0.99341$ ,  $t = 47.689$ ,  $df = 3$ ,  $P < 0.01$ ) on GACZR 1273.

There is a significant positive correlation between temperature and adsorption of phenol ( $r = 0.98637$ ,  $t = 10.3856$ ,  $df = 3$ ,  $P < 0.01$ ), *p*-nitrophenol ( $r = 0.9912$ ,  $t = 12.9412$ ,  $df = 3$ ,  $P < 0.01$ ) and methylene blue ( $r = 0.99843$ ,  $t = 30.847$ ,  $df = 3$ ,  $P < 0.01$ ) on GACZR 1073.

There is a significant positive correlation between temperature and adsorption of phenol ( $r = 0.970174$ ,  $t = 6.93205$ ,  $df = 3$ ,  $P < 0.01$ ), *p*-nitrophenol ( $r = 0.99191$ ,  $t = 13.532$ ,  $df = 3$ ,  $P < 0.01$ ) and methylene blue ( $r = 0.99959$ ,  $t = 60.2178$ ,  $df = 3$ ,  $P < 0.01$ ) on GACZR 1273.

### **Future Scope of The Study**

Design and fabrication of an adsorption reactor system for the purpose of treating drinking water and industrial wastewater. The study of further application of  $Zr^{4+}/ZrO_2$  loaded carbon materials for catalytic performance and applications, as electrochemical hydrogen storage material, energy storage purpose and fuel cell applications.

.....✂.....

## LIST OF PUBLICATIONS

---

- [1] Achari, V.S.; Rajalakshmi, A.S.; Jayasree, S. Surface Area and Porosity Development on Granular Activated Carbon by Zirconium: Adsorption Isotherm Studies. *Journal of Applied Research and Technology* **2017** (Accepted November 2017)
- [2] Achari, V.S.; Jayasree, S.; Rajalakshmi, A.S. Adsorption of *p* – nitrophenol on Coconut Shell Granular Activated Carbon: Isotherms, Kinetics and Thermodynamics. *Indian Journal of Chemical Technology* **2017**, 24, 471-478.
- [3] Achari, V.S.; Rajalakshmi, A.S. Adsorption of Methylene Blue From Aqueous Solution by Zirconium Impregnated Activated Carbon Proceedings of the International Conference *MATCON* **2016**, Department of Applied Chemistry, Cochin University of Science and Technology, January 14-16, 2016, 362- 365.

### View Letter

Close

**Date:** Nov 16, 2017  
**To:** "Sivanandan V.Sivanandan Achari Achari" vsachari@gmail.com,vsachary@yahoo.co.uk  
**cc:** jart.dgrafico@gmail.com;jart@ccadet.unam.mx  
**From:** "Journal of Applied Research and Technology " eesserver@eesmail.elsevier.com  
**Reply To:** "Journal of Applied Research and Technology " jart@elsevier.com  
**Subject:** Your Submission

---

Ms. Ref. No.: JART-D-17-00173R1  
Title: Surface Area and Porosity Development on Granular Activated Carbon by Zirconium: Adsorption Isotherm Studies  
Journal of Applied Research and Technology

Dear Dr. Achari,

I am pleased to inform you that your paper "Surface Area and Porosity Development on Granular Activated Carbon by Zirconium: Adsorption Isotherm Studies" has been accepted for publication in Journal of Applied Research and Technology.

Below are comments from the editor and reviewers.

Thank you for submitting your work to Journal of Applied Research and Technology.

Yours sincerely,

Alejandro Barragán  
Journal Manager  
Journal of Applied Research and Technology

Comments from the editors and reviewers:

The manuscript can be accepted.

\*\*\*\*\*

For further assistance, please visit our customer support site at <http://help.elsevier.com/app/answers/list/p/7923>. Here you can search for solutions on a range of topics, find answers to frequently asked questions and learn more about EES via interactive tutorials. You will also find our 24/7 support contact details should you need any further assistance from one of our customer support representatives.

---

Close

## Surface Area and Porosity Development on Granular Activated Carbon by Zirconium: Adsorption Isotherm Studies

V. Sivanandan Achari\*, A.S. Rajalakshmi, S Jayasree, Raichel Mary Lopez

*School of Environmental Studies, Cochin University of Science and Technology, Kochi-682022, Kerala, India.*

### Abstract

In this study, a new series of coconut shell based granular activated carbons (GAC) are prepared by impregnating with zirconium ions as zirconyl chloride and activated under superheated steam. These carbons are designated with activation temperature/ conditions as GAC 383 (activated at 383K), GACO 383 (HNO<sub>3</sub> oxidised), GACZR 1273 (ZrOCl<sub>2</sub> activated at 1273K) and GACOZR 1273 (HNO<sub>3</sub> oxidised, ZrOCl<sub>2</sub> activated at 1273K). Surface characteristics of these carbons are evaluated using Boehm titration methods, Fourier-transform infrared spectroscopy (FTIR), X-ray diffraction techniques (XRD), Scanning electron microscopy (SEM) and Transmission electron microscopy (TEM). The pore volume and the respective specific surface area of each carbon are determined by BET, I plot, Langmuir, Freundlich, and Dubinin-Radushkevich isotherms using N<sub>2</sub> adsorption data at 77K. Analysis shows that zirconium ion enhances the surface area and porosity of granular activated carbon. The adsorption characteristics of newly prepared GAC are tested by solid-liquid equilibria using phenol as adsorbate. Equilibrium phenol adsorption data fitted to standard isotherm models of Langmuir, Freundlich, and Dubinin-Radushkevich (D-R) equations. Adsorption constants and parameters indicate that zirconium impregnated granular activated carbons are relatively more efficient for the removal of phenol than the native carbon used.

*Key words:* Adsorption, Granular activated carbon, Phenol, Pore volume, Surface area.

### 1. Introduction

Activated carbons are regarded as one of the most important commercial materials, with many unique properties with large specific surface areas, high porosity, and adequate pore size distributions. Also, they mostly have high mechanical strength to be used for separation, purification and catalysis (Hameed et al., 2007). Activated carbons are produced from many carbonaceous materials of lignocellulosic in origin; this includes coal, wood, peat and agricultural materials (Rodriguez-Reinoso et al., 1992).

Granular activated carbons (GAC) in various forms are quite widely employed in water and wastewater treatment processes for removing organic compounds including phenol and its derivatives (Tan et al., 2008). Most carbonaceous materials available in nature can be converted into active carbons, differ by their porosity and specific surface area. Depending upon the nature of raw material used and the condition of the activation process chosen, properties of the final carbon product vary. Also, surface modifications of many carbon materials leads to generate more active sites on their solid surface, can be suitably utilized for effective adsorption removal and separation purposes. Such carbons are used as a substitute for other more expensive ion exchange resins, adsorbents and catalyst support (Mohd Din et al., 2009; Liu et al., 2010). Literature on carbon science discuss a multitude of activating agents extensively known employed for the production of activated carbon materials with desired pore structure. The purpose of physical/chemical activation is to create and develop porosity in the carbon material and thereby increase their adsorption efficiency. This enhanced porous surface quality has been exploited for the removal of many organic compounds from solutions particularly using coconut shell based carbons (Shen et al., 2008).

All the known carbon activation procedure belongs into two types, namely, physical activation or chemical activation depending on whether a gaseous or the chemical activating agent is used. Chemical activation is a single step process for the preparation of activated carbon where carbonization of precursor in the

<sup>1</sup> \*Corresponding Author.

E-mail address: vsachari@gmail.com / vsachari@cusat.ac.in

presence of chemical agents is done under controlled conditions in a furnace. For this, a solid activating agent like alkali and alkaline earth metal containing substances or some acids are used (e.g. KOH, NaOH,  $\text{Li}_2\text{CO}_3$ ,  $\text{Na}_2\text{CO}_3$ ,  $\text{K}_2\text{CO}_3$ ,  $\text{Rb}_2\text{CO}_3$ ,  $\text{Cs}_2\text{CO}_3$ ,  $\text{ZnCl}_2$ , and  $\text{H}_3\text{PO}_4$ ). Physical activation involves two steps, namely (i) carbonization of the precursor in an inert atmosphere (ii) subsequent activation of the resulting char in the presence of carbon gasification agents such as carbon dioxide, steam, air or a suitable combination of these (Namasivayam & Kadirvelu, 1997). However, the impregnation of metal ion/salts onto char matrix modifies the porous structure of resulting activated carbon. An increase in the adsorption efficiency was given by metal ions impregnated carbon for the removal of mercury, lead, arsenic, chromium, Nickel etc. (Sreedhar, Madhukumar & Anirudhan, 1999). Innovative approach regarding activation of carbon with new catalysts is an area of active research in adsorption science.

Zirconium and its salts are reported to be relatively safe and acceptable inorganic substance, has low biotoxicity and are relatively inexpensive. The most important characteristics of this material is their catalytic potential, high reactivity, large specific surface area, ease of separation, and the presence of a large number of active sites for interaction with different contaminants (Holmes et al., 1972). Adsorption performances of various activated carbons with respect to phenol removal have been reported in many earlier studies (Stoeckli et al., 2001; Achari & Anirudhan, 1995). An active carbon granule with remarkable porous structure has many advantages over the native carbon form, with respect to porosity and adsorption capacity. In this study, we report the adsorption efficiency of coconut shell based granular activated carbon (GAC) incorporated with zirconium (as  $\text{ZrOCl}_2$ ) that resulted extra porosity during thermal activation. Adsorption efficiency of the new activated carbon has been tested with phenol in aqueous phase as regards to study of solid-liquid equilibria.

Phenol is a common organic pollutant and its maximum concentration level in the industrial effluents for safe discharge into surface water bodies is 1.0 mg/L (EPA, 2002). WHO recommends a permissible phenol concentration of 0.001mg/L in potable waters (WHO 1963). The main sources of phenol in aquatic environments are the wastewater discharges from industries; mainly coke ovens in steel plants, petroleum refineries, resin, petrochemical, fertilizer, pharmaceutical, chemical and dye industries (Girish & Murty, 2012).

The current study is done with a purpose to correlate the effect of  $\text{Zr}^{4+}$  ions onto native carbon (GAC 383) to generate extra porosity, how it effect the surface complexes, porosity and pore size distribution of activated carbon. The study also discusses the adsorption behaviour of zirconium impregnated carbon for the removal of phenol from aqueous solution.

## 2. Methodology

The activated carbon purchased from Indo German Carbon Limited, Binanipuram, Cochin, Kerala, India [particle size (US mesh) 12 x 40, iodine No. 1100 mg/g, apparent density 0.50 g/cc, moisture 5%, ash 4 %] was used throughout the study as the starting material. It was washed with 0.5M NaOH solution and repeated with 0.5M HCl. Finally, more than 1L bed volume of distilled water is passed through a glass column until a neutral pH was noted. Washed carbon was then dried in a hot air oven at  $110^\circ\text{C}$ ; it is designated as GAC 383. A portion of this carbon was then nitric acid treated for surface oxidation.

The oxidation of GAC was done in a reaction mixture consisting of 100 g acid washed activated carbon, 130ml of con. $\text{HNO}_3$  and 540ml of distilled water, it is refluxed for 3 hours. After filtration, the procedure was repeated by adding a fresh solution of  $\text{HNO}_3$  and distilled water in the same ratio as the previous. After oxidation, carbon filtered and thoroughly washed with distilled water and dried in a hot air oven at  $110^\circ\text{C}$ . This nitric acid oxidised granular activated carbon is designated as GACO 383.

### 2.1 Impregnation ratio of zirconium

Different weights of zirconyl chloride ( $\text{ZrOCl}_2 \cdot 8\text{H}_2\text{O}$ ) noted as the impregnation ratio ( $I_{\text{Zr}}$  = weight of salt to carbon weight for every 10g carbon) 0.0065, 0.026, 0.052 and 0.078 were used for surface loading. This

*Journal of Applied Research and Technology (Accepted November 2017)*

was done by mixing the raw carbon and activating agent zirconyl chloride at 85<sup>0</sup>C for 2 hours using magnetic stirrer. After stirring samples were placed in a water bath for about 5-6 hours and finally dried in a hot air oven at 110<sup>0</sup>C.

All these impregnated carbons were activated under steam at 873K for choosing the best impregnation ratio for better efficiency in a temperature programmed furnace designed/maintained in the laboratory. The samples with best impregnation ratio, were further activated under steam at a higher temperature of 1273K. This granular activated carbon impregnated with Zr<sup>4+</sup> is designated as GACZR 1273. Similarly, carbon GACOZR 1273 (carbon oxidized zirconyl chloride impregnated and activated at 1273K) was also prepared.

#### *Granular activated carbons*

Four carbon samples used for characterization and adsorption studies are designated as GACZR 1273, GACOZR 1273, GAC 383 and GACO 383, being ZR for zirconium and the last figures are for activation temperatures.

The granular activated carbon (GAC) prepared were assigned by the degree of burn off, which was calculated as follows (Ngah & Fatinathan, 2006).

$$\text{Burn off (\%)} = \frac{W_{\text{initial}} - W_{\text{final}}}{W_{\text{initial}}} \times 100 \quad (1)$$

W<sub>initial</sub> is the initial weight of GAC; W<sub>final</sub> is the weight of GAC after activation.

#### *2.2 Carbon characterization and Analytical methods*

Surface characterization of newly prepared carbons was performed using FTIR (Thermo Nicolet, Avatar 370) spectroscopy for analyzing the surface functional groups. Boehm's titration method was used for their quantitative determination. In this method, the number of acidic sites, namely carboxylic, lactonic, and phenolic groups on the carbon surface were distinguished by neutralization with bases (NaHCO<sub>3</sub>, Na<sub>2</sub>CO<sub>3</sub>, NaOH). Their basic character was determined by neutralization with HCl. XRD analyzer (Bruker AXS D8 Advance) was used to measure powder X-ray diffraction patterns of the new GAC series. Scanning Electron Microscope (JOEL Model JSM - 6390LV) and High-Resolution Transmission Electron Microscopy (JOEL/JEM 2100) were used for the study of surface morphological features of carbon material.

#### *2.3 Solid-Gas Equilibria studies*

The pore structure characteristic of the new activated carbon series was determined by N<sub>2</sub> adsorption-desorption isotherm at 77K volumetrically using Micromeritics TriStar 3000 V6.07 BET analyzer. Isotherm data were subjected to BET, I point, Langmuir, Dubinin-Radushkevich (D-R), *t* plot and BJH isotherm methods for the determination of pore volume and specific surface area.

#### *2.4 Batch Equilibrium Adsorption Study.*

Batch test reactors are used for the adsorption studies. 25 ml aqueous solutions of known concentrations of phenol [25, 50, 75, 100, 150, 200, 250, 35, 500, 750, 1000, 1250, 1500, 2000, 2500 & 3000 mg/L] were prepared and added to 0.025g of GAC in a 100 ml Erlenmeyer flask and placed in a temperature-controlled water bath shaker (model LABLINE). The solution was withdrawn from the shaker at the predetermined time interval, filtered through Whatmann No.1 filter paper prior to analysis. The concentration of the phenol in aqueous solution is determined using uv-visible spectrophotometer (CARY 50 Probe) at wavelength 260 nm. The amount of phenol adsorbed at a time *t*, represented as *q<sub>t</sub>* (mg/g) and adsorbed at equilibrium condition, *q<sub>e</sub>* (mg/g) was calculated according to the following Eq.(2) and Eq.(3) (Srivastava et al., 2006; Kyzas et al., 2016., Gebresemati., 2017).

$$q_t = \frac{V(C_0 - C_t)}{W} \quad (2)$$

$$q_e = \frac{V(C_0 - C_e)}{W} \quad (3)$$

Where  $C_0$  and  $C_e$  are initial and equilibrium phenol concentrations (mg/L) respectively.  $C_t$  is phenol concentration at time  $t$  (mg/L).  $V$  is the volume of solution (L) and  $W$  is the mass of carbon. An adsorption isotherm profile describes the interaction between adsorbate and adsorbent and is critical for the design of adsorption process. The Langmuir, Freundlich and Dubinin-Radushkevich (D-R) isotherms models were used to describe the equilibrium adsorption isotherm data.

### 3. Results and Discussion

#### 3.1 Impregnation ratio and Burn off

Burn off value of a carbon impregnated with a metal catalyst is the weight loss occurred during the process of activation. **Figure 1** shows that burn off found to increase with the amount of zirconium (as zirconyl chloride) loaded. An incorporation of 0.2 % zirconium results 13.1% burn off. Active carbon formed by low burn off are usually undesirable as they lead to a low surface area carbon product, which in turn may reduce adsorption capacity for the target molecule. In the present study burn off is in the range 13-17 % given in **Table 1**. Development of microporosity occurs in carbon char without a noticeable increase in the micropore width when the burn off value is in between 10- 25% (**Molina-Sabio et al., 2006**).

**Table 1:**  
Effect of zirconyl chloride on carbon yield and burn off

Amount of (ZrOCl <sub>2</sub> .8H <sub>2</sub> O)	% of zirconium in carbon	Carbon yield%	Burn off%
0.065	0.2	86.89	13.11
0.26	0.7	85.68	14.32
0.52	1.5	84.72	15.28
0.78	2.2	82.72	17.28

The optimum carbon yield 84.72 % with a burn off of 15.28 % is given by an impregnation of 1.5% zirconium, indicate a stage of progressive carbonization [Fig .1]. Further incorporation of  $Zr^{4+}$  (2.2%) exhibited marked enhancement in burn off (17.28 %) leads to results a lower carbon yield (82.72 %). It is presumed that the impregnation of 1.5 % attributes to a better carbon yield due to uniform distribution and large dispersion of  $Zr^{4+}$  ions throughout the accessible interior of the carbon granules.

Based on this observation, 1.5 % of  $Zr^{4+}$  impregnated carbon char are used for activation at temperature 1273K for better yield and burn off to obtain GACZR 1273 and GACOZR 1273. More impregnation of zirconium may cause the widening of the existing pores as well as the formation of large pores by additional burning of the walls between the adjacent pores during the later stages of activation.

#### 3.2 Surface chemistry of $Zr^{4+}$ impregnated carbon

Nitric acid treatment of carbons generate larger amounts of oxygen functional groups on the carbon surface. These extra surface oxygen groups on the resulted carbons are having acidic character, due to carboxylic, phenolic, and lactonic groups are determined by neutralization with a base of NaHCO<sub>3</sub>, NaOH, and Na<sub>2</sub>CO<sub>3</sub> respectively in aqueous phase. Whereas, basic groups (pyrones) are determined by neutralization with HCl. The results shown in **Table 2** indicate surface modified carbon GACO has more C-O acid functional groups. It indicates that, the number of acidic sites increases when carbon is reacted with the oxidizing agent. On the other hand, the numbers of basic sites are decreased during acid oxidation modification (**Pradhan & Sandle, 1999**).



**Figure 2(a)** and **Figure 2(b)** shows the FTIR spectra of new activated carbon series. Relatively high intensity-peak is observed at 3460 cm<sup>-1</sup>, 1640 cm<sup>-1</sup>, 2919 cm<sup>-1</sup> and 1100 cm<sup>-1</sup> for HNO<sub>3</sub> modified carbons compared to the native form GAC 383.

The peak at 3460 cm<sup>-1</sup> attributed to O-H stretching vibration of the hydroxyl group and 2919 cm<sup>-1</sup> is due to symmetric and asymmetric stretching vibration of C-H bond. The peak at 1640 cm<sup>-1</sup> is a characteristic of most carbon materials, is ascribed to the carbonyl group which is highly conjugated in the graphene layers having quinone structure C=O. The band at 1100 cm<sup>-1</sup> is ascribed as C-O stretching and O-H bending modes of alcoholic, phenolic, and carboxylic groups (Belhamdi et al., 2016; Jia & Thomas, 2000; Liao et al., 2016; Liu et al., 2012).

XRD spectrum for GAC 383 and GACZR 1273 is given in **Figure 3(a)** and GACO 383 and GACOZR 1273 given in **Figure 3(b)**. From the XRD spectrum, the interlayer spacing  $d_{002}$  is determined using the Bragg Eq.(4)

$$d = \lambda / 2 \sin \theta \quad (4)$$

Where  $\lambda$  is the x-ray wavelength and  $\theta$  is the scattering angle for the peak position. The crystallite size along c- axis  $L_c$ , and the size of the layer planes  $L_a$ , are determined from the half-width of the respective diffraction peak using the Scherrer Eq.(5)

$$L = K \lambda / B \cos \theta \quad (5)$$

Where  $L$  is  $L_c$  or  $L_a$ ,  $B$  is the half-width of the peak in radians, and  $K$  is the shape factor. The quantities  $L_c$  and  $L_a$  are named as stack height and stack width of carbon crystallites for the new carbon respectively. The shape factor  $K = 0.9$  and  $K = 1.84$  are used for calculation of  $L_c$  and  $L_a$ , respectively (Zhao et al., 2009; Kercher & Nagle, 2003). The diffraction pattern had broad peaks at around 24 and 42° for the new carbon are assigned to the reflection from (002) and (100) planes, respectively. The (002) peaks are used to calculate  $L_c$  and  $L_a$ . The occurrence of broad peaks at  $2\theta$  indicated a well-defined crystal structure that resulted in better layer alignment. The interlayer spacing ( $d_{002}$ ), summarized in **Table 2** are in the range of 0.36 to 0.37 nm. This indicates that the granular activated carbons obtained are nongraphitized carbons.

**Table 2**  
Surface oxygen functional groups by Boehm titration and Crystalline parameters by XRD

Sample name	Surface functional group				XRD parameters		
	Carboxylic meq/g	Phenolic meq/g	Lactonic meq/g	Base meq/g	$L_c$ (0.9)	$L_a$ (1.84)	$d_{002}$
GAC 383	0.40	0.45	0.18	0.50	1.14	2.28	0.36
GACO 383	1.38	2.10	1.34	0.20	0.97	1.94	0.36
GACZR 1273	0.39	0.44	0.20	0.62	0.98	2.00	0.37
GACOZR 1273	0.62	1.52	0.90	0.38	1.31	2.68	0.36

It is known that nongraphitized carbon shows well developed microporous structure, that is preserved even during the high temperature treatment. Most activated carbons exhibit a more open structure, characteristic of highly defective carbon plates. Subsequently, smaller regions of orientational order (microscale order) are more prevalent (Thomson & Gubbins, 2000).

Morphological observation by SEM shows that, the wide ranges of pores are present on new granular activated carbon. Pores present in GACOZR 1273 are appearing more open compared to GACZR 1273 as seen in the **Figure 4(a) & (b)**. It reveals nitric acid modification caused the widening of pores on GACOZR 1273. This carbon has relatively less N<sub>2</sub> adsorption; measured BET pore volume and surface area are lower than that of starting carbon GAC 383 as seen in **Table 3**. This is because an increase in the degree of activation makes the pore walls thin. These are more easily destroyed during the HNO<sub>3</sub> treatment, results in widening of the microporosity (Fierro et al., 2008).

TEM images illustrate (**Fig. 5**) the variation of the surface features due to the loading of the zirconium ions onto the GAC. In the TEM image, the presence of dark area on carbon suggests successful impregnation of zirconyl chloride onto GAC granules and the particles are randomly oriented inside the pore structure.

### 3.3 Solid-Gas Adsorption Isotherms ( $N_2$ Isotherm at 77 K)

The  $N_2$  adsorption isotherms of the activated carbons show Type 1 isotherm as per the IUPAC classification. It is seen in the **Figure 6** that all isotherms have a steep rise in the initial stage of adsorption at lower  $p/p_0$  range. Thereafter adsorption progressed well to attain saturation at high pressure range. Micropores are preferably filled at  $p/p_0 < 0.2$  as evidenced by a distinct steep adsorption front, assigned to very high adsorption efficiency of the material within the narrow micropore range (**Simões et al., 2016**).

The pore volume and the respective specific surface area of each carbon have been determined for predicting the efficiency of the material. In this regard, a series of isotherm analysis applied. BET, I plot, Langmuir, Freundlich, and Dubinin- Radushkevich (D-R) methods were followed using  $N_2$  adsorption data at 77K.

#### 3.3.1 Brunauer Emmett Teller (BET) Isotherm Analysis

The BET isotherm method based on a theory of multilayer adsorption was applied for the carbons and the respective BET surface area was calculated from the isotherm using Eq. (6)

$$\frac{1}{V\left(\frac{p_0}{p}-1\right)} = \frac{1}{V_m C} + \frac{C-1}{V_m C} \left(\frac{p}{p_0}\right) \quad (6)$$

A plot of  $\frac{1}{V\left(\frac{p_0}{p}-1\right)}$  versus  $\left(\frac{p}{p_0}\right)$  for each carbon gives a straight line with slope  $\frac{C-1}{V_m C}$  and intercept  $\frac{1}{V_m C}$ . Accordingly, the monolayer volume  $V_m$  and the constant  $C$  are calculated. The linear plot, is extended in the range  $0.05 < P < 0.3$  for the respective BET analysis. From the isotherm constant  $V_m$  calculated the specific surface area using Eq. (7)

$$SA_{BET} = \frac{V_m (Cm^3/g) \times 6.023 \times 10^{23} \times 0.162 \times 10^{-18} (m^2/N_2 \text{ molecule})}{22414 (cm^3/mol)} \quad (7)$$

**Table 3** shows the results of BET analysis for the new carbons. Here some discrepancy due to lack of a positive  $C$  character is observed for the BET equation in the region  $0.05 < P < 0.3$ . The negative value of  $C$  has no significant meaning. For ideal microporous materials,  $C_{BET}$  is usually positive and it has to be greater than 150. This shows the multilayer adsorption on the new carbons is not fully following the BET model. BET analysis of the adsorption data for the relative pressure range  $p/p_0$  up to 0.1 make  $C_{BET}$  become positive. Here, the condition for  $C_{BET}$  value greater than 150 is satisfied in all cases (**Fig.7**).

Furthermore, it is known that  $C$  in Eq. (6) is not actually a constant but a parameter, is given by the relation  $C = \exp(q_1 - q_L)/RT$ . The determination of  $C$  parameter in the whole range of adsorption is unattainable. Also, the linear part of the traditional BET plot ( $0.05 < P < 0.3$ ) is not well defined. So there are many ambiguities in the determination of  $V_m$  and specific surface area (SA) by BET method, particularly with respect to microporous materials (**Sing, 2001**).

#### 3.3.2 I-Point method Analysis

The rearrangement of the BET equation in Scatchard-type form, provide the isotherm line with slope equal to  $(C-1)$  at any  $p/p_0$  and  $V$ . This plot is known as BET-Scatchard (B-S) plot (**Pomonis et al., 2005**) given by Eq. (8)

$$\left[V\left(1 - \frac{p}{p_0}\right)\right] / \frac{p}{p_0} = CV_m - (C - 1)\left[V\left(1 - \frac{p}{p_0}\right)\right] \quad (8)$$

The graphs (**Fig. 8**) give an inclined V shape curve ( $\blacktriangleright$ ) with an inversion point termed I point. The extrapolation of this point towards x-axis is marked and taken as  $V_m$  i.e.

*Journal of Applied Research and Technology (Accepted November 2017)*

$[V(1-P)]_{I\text{ point}} = V_m$  (monolayer volume of I plot method).  $V_m$  can be used for the determination of surface area. Specific surface area is calculated using Eq. (9)

$$SA = 4.356V_m \quad (9)$$

Hence the I point method provides an alternate way to determine the surface area of new carbons without any ambiguities. Mostly, these carbons have a C parameter (BET) positive for further plotting of  $N_2$  data at  $p/p_0 < 0.1$  and simultaneously fitting the BET model for confirmation. The surface area was calculated from the monolayer volume  $[V_m = V_I(1 - \frac{p}{p_0})]$ .

On BET analysis of isotherm data up to  $p/p_0 = 0.1$  has resulted comparable surface area similar to that obtained from I plot. The critical evaluation of isotherm constants by the BET and I-plot method revealed that the materials are convincingly microporous with pore width ranges 1.71 - 1.77 nm. The average pore width of carbon calculated using the Eq. (10)

$$d = 4V_T/SA_{BET} \quad (10)$$

The major factors governing the selectivity of active carbons is the pore characteristics, i.e. pore size distribution and pore volume (Branton & Bradley, 2011). In this regard, pore volume, pore width and surface area of new carbons are shown in Table 3.

**Table 3**

Porosity parameters calculated from nitrogen adsorption isotherms ( $N_2/77K$ ) using BET and I plot methods

Sample	Total Pore volume $cm^3/g$	BET Analysis ( $p/p_0$ upto 0.3)			I plot		BET Analysis ( $p/p_0$ upto 0.1)			Pore width (nm)
		$SA_{BET}$ $m^2/g$	$V_m$ $cm^3/g$ STP	$C_{BET}$	$S_I$ $m^2/g$	$V_m = V_I$ $cm^3/g$ STP	$SA_{BET}$ $m^2/g$	$V_m$ $cm^3/g$ STP	$C_{BET}$	
GAC 383	0.573	996.8	229	-81.6	1275.4	293	1298.5	298.3	524	1.76
GACO 383	0.526	974.3	224	-119	1164.6	267.5	1186.5	272.5	439	1.77
GACZR 1273	0.640	1217.2	280	-104	1482.1	340.5	1497.3	343.9	873	1.71
GACOZR1273	0.531	976.2	224	-103	1193.2	274.1	1212.2	278.5	563	1.75

BET surface area of the carbon activated and impregnated with  $Zr^{4+}$  has been 1497.3  $m^2/g$  for the pore volume of 0.640  $cm^3/g$  while, that for GAC 383 was 1298.5  $m^2/g$  for the pore volume 0.573  $cm^3/g$ . The significance of this study is that  $Zr^{4+}$  activation enhanced the total pore volume, micropore volume and specific surface area of GAC.

The monolayer-multilayer adsorption appears to happen as a cooperative micropore filling at high  $p/p_0$  prior to capillary condensation. This allows to apply a series of isotherm models for the evaluation of monolayer volume valid for a Type I (Langmuir type) isotherm.

### 3.3.3 Langmuir Isotherm Analysis

Langmuir equation (Langmuir, 1918) is applied to the new carbons to study monolayer adsorption behaviour. The general form used to plot  $N_2$  isotherm at 77K is given by Eq. (11)

$$\frac{P}{V} = \frac{1}{bV_m} + \frac{P}{V_m} \quad (11)$$

$P = \frac{p}{p_0}$ , where,  $p$  is equilibrium vapour pressure,  $p_0$  is the saturation vapour pressure and  $V_m$  is monolayer adsorption capacity (mmol/g). From the graph of  $P/V$  versus  $P$ , a straight line is obtained and from the slope and intercept,  $V_m$  (monolayer volume) and constant  $b$  are calculated. As per the IUPAC (2015), most Type 1 isotherms corresponds to the so-called Langmuirian isotherms. In the case of physical adsorption, the Type 1 isotherm represents the presence of micropores, where molecules are adsorbed by micropore filling (Kaneko, 1994). The resulting Langmuir isotherms have perfect linearity (0.999) for all GACs as

shown in the **Figure 9(a)**. The  $Zr^{4+}$  impregnated carbon GACZR 1273 has relatively high monolayer capacity ( $V_m = 388 \text{ cm}^3/\text{g}$ ) and hence specific surface area ( $1687 \text{ m}^2/\text{g}$ ). This indicates that the monolayer coverage of the carbon was associated with so-called micropore filling. Surface area obtained from Langmuir and BET methods shown difference of 12-13%. This reveals that the monolayer capacity and the corresponding surface area does not reflect exact surface area, rather than an equivalent or characteristic surface area (**Lowell & Shields, 1991**). The nature of the physical interaction of  $N_2$  if any exists in the new carbon materials have to be revealed on applying Freundlich isotherm model.

3.3.4 Freundlich Isotherm Analysis

Physisorption of  $N_2$  gas on the carbons was evaluated using the Freundlich isotherm equation by the relationship as per Eq. (12) (**Achari, 1998; Kumar et al., 2010**).

$$\log V = \log K_F + \frac{1}{n} \log P \tag{12}$$

A plot of  $\log V$  versus  $\log P$  gives a straight line with intercept  $\log K_F$  and slope  $1/n$  as given in **Figure 9(b)**. All the carbons have straight line graphs with the correlation coefficient  $R^2 = 0.999$  revealed a strong interaction between the carbon and nitrogen gas at 77K. It is known that Freundlich “ $n$ ” value is a measure of adsorption intensity for physisorption mechanism to occur and it ranges from 9.4 -11.5 for the carbon studied. The modified carbon GACZR 1273 shows the highest ‘ $n$ ’ (11.5) and  $K_F$  (259) compared to others (Table 4).

The isotherm behaviour and porosity development of the new carbon have been further evaluated, applying the Dubinin-Radushkevich (D-R) isotherm model.

3.3.5 Dubinin-Radushkevich (D-R) Isotherm Analysis

Dubinin-Radushkevich (D-R) equation (**Dubinin & Kadlec, 1975; Dubinin, 1960**) is used to determine micropore volume of the new carbons from the  $N_2$  adsorption isotherm at 77K. A plot of  $\log W$  versus  $\log^2 (\frac{p}{p_0})$  gives linearity in the low pressure region, ( $p/p_0 < 0.1$ ) i.e. where the narrow micropores are filled as shown in the **Figure 9(c)**.

$$\log W = \log W_0 - D \log^2 (\frac{p}{p_0}) \tag{13}$$

$W$  is the amount (mmol) of  $N_2$  gas gets filled in micropore of carbons. The parameters, characterization energy ( $E_0$ ), pore width ( $L$ ), and micropore surface area ( $SA_{D-R}$ ) are calculated and given in **Table 4**.  $E_0$  is related to pore width  $L$  as per the Eq. (14)

$$L = \frac{10.8}{(E_0 - 11.4)} \text{ nm} \tag{14}$$

$$SA_{D-R} = \frac{2 \times 10^3 \times W_0 (\text{cm}^3/\text{g})}{L} \tag{15}$$

The carbon obtained by incorporating  $Zr^{4+}$  has an  $L$  value between 1.92 - 2.48 nm i.e the micropore surface area was contributed mainly by pores less than 2.0 nm that are very much generated by  $Zr^{4+}$  ions during chemical activation.

**Table 4**  
Porosity parameters calculated from nitrogen adsorption  $N_2/77K$  using Langmuir, Freundlich, & Dubinin-Radushkevich isotherms

Sample	Langmuir			Freundlich			D-R				
	$SA_L$ $m^2/g$	$V_m$ $cm^3/g$	$R^2$	$n$	$K_F$	$R^2$	$SA_{D-R}$ $m^2/g$	$W_0$ $cm^3/g$	$L$ $nm$	$E$ kJ/ $mol$	$R^2$
GAC 383	1465	337	0.99	9.4	210	0.99	424.7	351.3	2.56	15.6	0.98
GACO 383	1326	304	0.99	9.4	184	0.99	334.1	322.8	2.99	15.0	0.98
GACZR 1273	1687	388	0.99	11.5	259	0.99	647.9	401.7	1.92	17.0	0.99
GACOZR1273	1367	314	0.99	10.1	196	0.99	409.4	327.8	2.48	15.8	0.99

*Journal of Applied Research and Technology (Accepted November 2017)*

Dubinin-Radushkevich (D-R) isotherm analysis shows that GACZR 1273 has much higher micropore volume ( $401.7 \text{ cm}^3/\text{g}$ ) and micropore surface area ( $648 \text{ m}^2/\text{g}$ ) as compared to that of basic carbon GAC 383 (micropore volume of  $351.3 \text{ cm}^3/\text{g}$  and surface area,  $425 \text{ m}^2/\text{g}$ ). This indicates that carbon has extra porosity due to  $\text{Zr}^{4+}$  activation and the energy of adsorption ( $E_0$ ) is 15-17 KJ/mol, common for the physical nature of adsorption in pores having width  $< 2.0 \text{ nm}$ .

### 3.3.6 *t*-plot method

Lippens and de Boer (Lippens et al., 1964 a; Lippens et al., 1964 b) proposed '*t*' plot method for the determination of micropore volume and external surface area by plotting the thickness of adsorbed layer *t* against the amount adsorbed as shown in the Figure 9 (d). This isotherm is specific to determine micropore and mesopore filling. The external surface area ( $SA_{ext}$ ), micro pore surface area ( $SA_{mic}$ ), and micropore volume ( $V_{mi}$ ) are given in Table 5. The GAC has the distinct steep rise with respect to quantity adsorbed (mmol/g) in '*t*' plot in the initial range of adsorbed thickness, to attain maximum with a round knee. Finally become oriented slightly parallel to x-axis at the higher ranges of adsorbed thickness. A straight line is drawn in the linear region of the *t* plot. From the slope and intercept the external surface area ( $SA_{EXT}$ ) and micropore volume ( $V_{mi}$ ) are calculated.

$$t = [13.99 / (0.034 - \log(p/p_0))] \quad (16)$$

Where *t* is the thickness of the pores and  $p/p_0$  is the relative pressure

External surface area,

$$SA_{EXT} = \frac{\text{slope} \times (10^{10} A^0 / m) \times D}{F \times 10^6} \quad (17)$$

Where *D* is the density conversion factor = 0.0015468. *F* = surface area correction factor, for most samples it is taken as 1.0.

Micropore volume,  $V_{mi}$  ( $\text{cm}^3/\text{g}$ ), can be calculated by multiplying *intercept* obtained from the *t* plot with density conversion factor *D*, given in Eq. (18).

$$V_{mi} = \text{intercept} (\text{cm}^3/\text{g STP}) \times D \quad (18)$$

$$\text{Micropore surface area } SA_{mi} (\text{m}^2/\text{g}) = SA_{BET} - SA_{EXT} \quad (19)$$

Where  $SA_{BET}$  is the BET surface area and  $SA_{EXT}$  is the external surface area

High external surface area of GACO 383 indicates that nitric acid modified carbon possesses a significant amount of larger pores. This is evidenced by the external surface area up to 6.28 % more compared to basic carbon GAC 383. This is caused by the reduction of micropore volume up to 15.32 % due to the widening of existing micropores. Activation of carbon GAC 383 with  $\text{Zr}^{4+}$  (GACZR 1273) enhances the micropore volume up to 28.40 %, indicate that the activated carbon GACZR 1273 produced is predominantly consists of micropores. In fact, of the total surface area of this carbon ( $S_T$ ), micropore surface area contributes 70.0 % and only the remaining 30.0 % contribute external surface area. Means,  $\text{Zr}^{4+}$  activation leads to the acceleration of porosity development on the activated carbon matrix of GAC 383. It is seen that  $\text{Zr}^{4+}$  activated nitric acid modified carbon GACOZR 1273 has a less proportion of micropores. This is evidenced by a 24.56 % decrease in micropore volume compared to GACZR 1273. Simultaneously, there is no increase in the external surface area, because the extent of pore widening in GACOZR 1273 is relatively less.

### 3.3.7 BJH (Barrett Joyner Halenda) method

Pore size distribution of GAC series has been done based on  $SA_{BET}$ ,  $V_{mi}$ ,  $V_{ext}$  and adsorption average pore width from the  $N_2$  adsorption data at 77 K. The pore size distribution is a measure of physical characteristics of carbon (porous) materials to predict the extent of pore accessibility of an adsorbate molecule. The pore size distribution was determined by the BJH (Barrett Joyner Halenda) method.

Distribution curves of pore volume and specific surface area are described as a function of pore width ( $A^0$ ) drawn from the  $N_2$  adsorption-desorption data. The adsorption cumulative surface area (ADSCA), desorption cumulative surface area (DCSA), respective pore volumes (ACPV and DCPV) and pore width (ads and des) are computed, given in **Table 5**.

**Table 5**

Porosity parameters calculated from nitrogen adsorption isotherms at 77K using t-plot & BJH method

Sample	t-plot			BJH					
	$V_{mi}$ $cm^3/g$	$SA_{mi}$ $m^2/g$	$SA_{ext}$ $m^2/g$	$ADSCA$ $m^2/g$	$DCSA$ $m^2/g$	$ACPV$ $cm^3/g$	$DCPV$ $cm^3/g$	Pore width (ads) $A^0$	Pore width (des) $A^0$
GAC 383	226.70	588.65	408.10	226.21	220.52	0.138	0.134	24.35	24.30
GACO 383	191.96	540.28	433.72	250.00	242.84	0.142	0.137	22.78	22.55
GACZR 1273	291.07	863.84	353.40	196.07	207.50	0.117	0.121	23.89	23.22
GACOZR 1273	219.58	628.45	347.80	204.04	205.76	0.123	0.123	24.10	23.86

The BJH pore size distribution shows the new carbons are having pore width in the range 2.0-2.24 nm. This supports the evidence for the existence of the fractional mesoporosity (**Bindia, 2016**).

### 3.4 Solid-liquid Adsorption isotherm study: Phenol

Adsorption characteristics of all carbons for the removal of phenol are shown in the **Figure 10**. Equilibrium adsorption isotherm studies show that the adsorption increases with phenol concentration. Adsorption data are fitted to well-known models of Langmuir, Freundlich, and Dubinin-Radushkevich (D-R) isotherms. Adsorptive capacity of  $Zr^{4+}$  impregnated coconut shell based granular carbon is relatively high. Among this group studied, oxidized carbon GACO 383 has less adsorption capacity than others. This is because, a higher proportion of carbon- oxygen surface functional groups (mainly COOH) ionize in water to produce  $H^+$  ions. The resulting  $COO^-$  directed towards liquid phase bear negative charges on the carbon surface hence suppresses the further adsorption of phenol. Langmuir, Freundlich and D-R isotherm parameters were determined and presented in Table 6.

#### 3.4.1 Langmuir isotherm:

The Langmuir isotherm is prominent to describe a homogeneous adsorption system in liquid phase where each molecule adsorbed onto the surface has uniform adsorption energy. Linear form of Langmuir isotherm model is used to evaluate phenol adsorption behaviour of new carbons. (**Achari & Jayasree, 2014; Achari & Rajalakshmi, 2014**)

$$\frac{C_e}{q_e} = \frac{1}{K_L} + \frac{a_L}{K_L} C_e \quad (20)$$

Where  $C_e$  and  $q_e$  are the phenol concentration in the liquid phase and solid phase respectively at equilibrium.  $K_L$  and  $a_L$  are the Langmuir constants,  $K_L/a_L (=q_m)$  is known as monolayer adsorption capacity. The parameter  $q_m$  and  $K_L$  are determined by plotting  $C_e$  versus  $\frac{C_e}{q_e}$ . Langmuir isotherm assumes that, monolayer adsorption takes place onto the solid surface (carbon) containing a finite number of adsorption sites having uniform adsorption energies, without transmigration of the adsorbate (phenol) in the plane of the adsorbent surface. Langmuir isotherm plot for carbons GAC 383, GACO 383, GACZR 1273 and GACOZR 1273 is shown in the **Figure 11**. Isotherms show the Type I features of uniform microporosity for all carbons.

#### 3.4.2 Freundlich isotherm:

Freundlich isotherm model commonly used to describe the adsorption characteristic of heterogeneous surfaces is applied to the new carbon – phenol adsorption system. **Figure 12** represents the Freundlich

isotherm plots of phenol adsorbed by unit mass of carbon. The linear form of the equation applied is given as follows (Ma et al., 2016).

$$\log q_e = \log K_F + \frac{1}{n} \log C_e \quad (21)$$

Where  $C_e$  and  $q_e$  are the liquid phase phenol concentration (mg/L) and solid phase concentration (mg/g) respectively at equilibrium.  $K_F$  is a function of the energy of adsorption as well as a measure of adsorptive capacity.  $1/n$  determines the intensity of adsorption. As regards to new carbon series,  $K_F$  and  $n$  are evaluated and given in Table 6.

### 3.4.3 Dubinin-Radushkevich (D-R) isotherm:

The D-R isotherm generally applied to express the adsorption mechanism with a Gaussian energy distribution onto a heterogeneous surface specifically for gas-solid equilibria. In the case of liquid-phase adsorption Dubinin-Radushkevich (D-R) equation assumes that, the adsorption occurs in micropores and is limited to a monolayer. The linear form of D-R equation is expressed as

$$\ln q_e = \ln q_{mi} - \beta \varepsilon^2 \quad (22)$$

$\beta$  is a constant related to the energy of adsorption,  $\varepsilon$  is the Dubinin-Radushkevich isotherm constant and  $q_{mi}$  is a measure of adsorption capacity.

$$\text{Where } \varepsilon = RT \ln \left[ 1 + \frac{1}{C_e} \right] \quad (23)$$

D-R isotherm is plotted as a function of the logarithm of amount adsorbed ( $\ln q_e$ ) versus  $\varepsilon^2$  (Fig.13).

The mean free energy,  $E$  per molecule of adsorbate (for removing a molecule from its location in the sorption space to the infinity) can be determined by the Eq.(24) (Stoeckli et al., 2001; Dada et al., 2012).

$$E = \frac{1}{\sqrt{2\beta}} \quad (24)$$

Regarding the isotherm analysis, equilibrium data for phenol adsorption were well fitted to the Langmuir model with monolayer adsorption capacity of GACZR 1273 (342.5 mg/g), GAC 383 (312.5 mg/g) for GACOZR 1273 (280.9 mg/g) and GACO 383 (209 mg/g). From the Table 6 it is clear that, the interaction of phenol on the GACZR 1273 is prominent due to chemical activation with zirconium ( $Zr^{4+}$ ) ions. At the same time nitric acid modification of carbon decreased the adsorption efficiency of GACO 383 and GACOZR 1273 towards phenol.

**Table 6**

Adsorption parameters of phenol on GAC obtained from Langmuir, Freundlich and Dubinin- Radushkevich isotherm at 30°C

Sample	Langmuir isotherm parameter			Freundlich isotherm parameter			D-R isotherm parameter			
	$q_m$	$K_L$	$R$	$n$	$K_F$	$R$	$q_{mi}$	$\beta$	$R$	$E$
	(mg/g)	L/mg			L/g		mg/g			KJ/mol
GAC 383K	312.50	2.48	0.999	2.49	16.73	0.972	57.38	5.08	0.983	0.293
GACO383K	209.64	2.48	0.999	3.12	20.71	0.945	57.41	5.50	0.985	0.302
GACZR 1273	342.47	4.83	0.999	3.10	33.85	0.973	69.21	0.622	0.984	0.897
GACOZR 1273	280.90	2.11	0.997	2.87	20.99	0.981	55.51	2.07	0.974	0.492

Adsorption analysis of phenol using Freundlich finds that constant  $K_F$  (adsorption binding constant ) varies in the range of 16.7 - 33.8, and  $n$  (adsorption intensity) is in the range of 2.49 - 3.12, confirms favourable adsorption as it lies between 1-10.

Dubinin-Radushkevich parameters  $q_{mi}$  and  $\beta$  are determined from the intercept and slope of isotherm plot and are given in Table 6. The adsorbed amount ( $q_{mi}$ ) is 69.2 mg/g for  $Zr^{4+}$  modified carbon GACZR 1273. It indicates that micropores are developed on GAC 383 during activation after impregnation with  $Zr^{4+}$  are

accessible in solid-liquid adsorption equilibria. Dubinin-Radushkevich adsorption isotherm analysis of solid-gas equilibria of  $N_2$  at 77K [Table 4] substantiate the formation and contribution of enough micropores (hence evaluation of micropore volume) towards specific surface area. The result reveals that GACZR 1273 has micropore surface area  $SA_{D-R}$  of 647.9  $m^2/g$ , whereas the native carbon GAC 383 has  $SA_{D-R}$  of 424.7  $m^2/g$  only. This means  $Zr^{4+}$  ions promoted an extra microporosity of 223.2  $m^2/g$ . This is further confirmed by the results of  $t$  – plot analysis (Table 5), which reveals  $SA_{mi}$  is 863.8  $m^2/g$  for GACZR 1273, whereas  $SA_{mi}$  is 588.65  $m^2/g$  for GAC 383. Extra porosity due to  $Zr^{4+}$  activation promotes higher phenol adsorption efficiency for the carbons. The mean free energy  $E$  calculated is in the range of 0.292 - 0.896 kJ/mol shows phenol adsorption follows physisorption process, i.e. adsorbate is bound to the surface of the carbons by relatively weak Van der Waals forces.

Nitric acid modified carbon GACO 383, and its zirconium ( $Zr^{4+}$ ) activated form GACZR 1273 has a less adsorption efficiency compared to GAC 383 and GACZR 1273 (Table 6). More acidic groups already occupied on the carbon surface make them unfavourable and inaccessible for the approach of phenol molecule. Because, it reduces the electron density on the basal plane of the carbon. This further reduces the  $\pi - \pi^*$  interaction between the phenol aromatic ring and the basal plane of the carbon. Also, surface acidic functional group COOH ionizes and exist as negative sites (-COO<sup>-</sup>) on the carbon surface. It repels the incoming phenoxide ions reducing the extent of donor-acceptor interaction between the phenolic group and carbon surface (Vinod & Anirudhan, 2002).

#### 4. Conclusion

Chemical activation of GAC with  $ZrOCl_2 \cdot 8H_2O$  brought marked changes in the burn off, pore development, and carbon yield. The nitric acid oxidation of GAC 383 causes changes in the microcrystallinity of the carbon layers as evidenced by distinct changes in  $La$ ,  $Lc$  and  $d_{002}$  values. The nitric acid treatment enhances the proportion of surface oxygen groups on carbon surface. Surface morphological studies using SEM indicate that carbon has a uniform and well developed porous structure.  $HNO_3$  acid treatment destroys the nature of thin pore walls existed on GAC 383 surface that leads to the widening of micropores. Activating agent  $Zr^{4+}$  ions are randomly distributed deep inside the GAC as evidenced by TEM profile. All the four carbons studied shows Type I isotherm character as per IUPAC classification. The critical evaluation of isotherms and constants by BET and  $t$ -plot method revealed that the carbons (GAC 383, GACO 383, GACZR 1273 and GACZR 1273) are convincingly microporous with average pore width ranges 1.71-1.77 nm. Langmuir and Dubinin-Radushkevich isotherm analysis established that pore volume and specific surface area of zirconium impregnated carbon GACZR 1273 is significantly higher than the native carbons GAC 383 and its prodigy GACO 383. The  $t$ -plot Analysis showed that of the total surface area of GACZR 1273 (1217.24  $m^2/g$ ) only 30% (353.40  $m^2/g$ ) is contributed by external surface area. This suggests that 70% (863.84  $m^2/g$ ) of the total surface area is truly contributed by the micropores. Hence  $Zr^{4+}$  activation promotes extra microporosity on the coconut shell based granular activated carbon. Pore size distribution (PSD) showed that the adsorption pore diameter is in ranges 2.28 - 2.43 nm, and desorption pore width ranges 2.25 - 2.43 nm for the group of activated carbons studied.  $HNO_3$  oxidized carbon (GACO 383) has relatively less affinity for the adsorption of phenol. Carbon impregnated and activated with  $Zr^{4+}$  (GACZR 1273) has a higher phenol uptake capacity (342.5 mg/g). From these observations, it is concluded that higher adsorption performance of the new  $Zr^{4+}$  incorporated carbons are due to the formation of more open pore structures with greater proportions of well defined micropores (< 2 nm), developed during chemical activation.

#### Acknowledgement

The first author is thankful to University Grants Commission (UGC), Government of India, New Delhi for the financial support by awarding the project UGC – SAP- DRS Phase II as per the order No: F4 - 14/2015/DRS-II (SAP-II) Dated 19/12/2015 and the second is thankful to UGC-BSR for the financial assistance in the form of Senior Research Fellowship.



## Reference

- Achari, V. S. (1998). *Ph D Thesis: Modified Carbons and Wood dust Evaluation of Adsorption properties*. University of Kerala. Retrieved from Shodhganga a reservoir of Indian Thesis. <http://hdl.handle.net/10603/120409>
- Achari, V.S., & Anirudhan, T.S.(1995). Phenol removal from aqueous systems by sorption on jackwood sawdust. *Indian journal of Chemical Technology*, 2, 137- 141. <http://nopr.niscair.res.in/handle/123456789/31110>
- Achari, V.S., & Jayasree, S. (2014, November 6-8). Adsorption of nitrophenol on Zn<sup>2+</sup> Impregnated Activated Carbons. In *Jayaprakash R (Edr): Learning and Dissemination of Science and Technology through Malayalam*. Paper presented at the Proceedings of the 24<sup>th</sup> Swadeshi Science Congress (India), Malappuram, Kerala (pp. 328-333). Kochi : Swadeshi science movement. ISBN: 978-81-928129-2-2.
- Achari, V.S., & Rajalakshmi, A. S. (2014, November 6-8). Adsorption of Phenol using Zr<sup>4+</sup> Impregnated Activated Carbon: Equilibrium and Kinetic Study. In *Jayaprakash R (Edr): Learning and Dissemination of Science and Technology Through Malayalam*. Paper presented at the Proceedings of the 24<sup>th</sup> Swadeshi Science Congress (India), Malappuram, Kerala (pp. 314-319). Kochi : Swadeshi science movement. ISBN: 978-81-928129-2-2.
- Belhamdia, B., Merzougui, Z., Trarib, M., & Addouna, A. (2016). A Kinetic equilibrium and Thermodynamics study of L-phenylalanine adsorption using activated carbon based on agricultural waste (date stone), *Journal of applied research and Technology*, 14, 354-366. <https://doi.org/10.1016/j.jart.2016.08.004>
- Bindia, R. (2016). *Ph D Thesis: Adsorption Isotherm Studies on Activated Carbon Prepared by Activation with Cerium Compounds* (Unpublished). Cochin University of Science and Technology, Cochin, India.
- Branton, P., & Bradley, R. H. (2011). Effects of active carbon pore size distributions on adsorption of toxic organic compounds. *Adsorption*, 17(2), 293–301. <http://doi.org/10.1007/s10450-010-9284-4>
- Collins, K.E., Collins, C.H., Maroneze, C.M., Cappovila, V., & Custodio, R. (2011). Evaluations of the BET, I-point, and  $\alpha$ -plot procedures for the routine determination of external specific surface areas of highly dispersed and porous silicas. *Langmuir*, 27(1), 187–195. <http://doi.org/10.1021/la103640z>
- Dada, A., Olalekan, A., Olatunya, A., & Dada, O. (2012). Langmuir , Freundlich , Temkin and Dubinin – Radushkevich Isotherms Studies of Equilibrium Sorption of Zn<sup>2+</sup> Unto Phosphoric Acid Modified Rice Husk. *IOSR Journal of Applied Chemistry*, 3(1), 38–45. <http://doi.org/10.9790/5736-0313845>
- Dubinin, M. M. (1960). The Potential Theory of Adsorption of Gases and Vapors for adsorbents with energetically non-uniform surface. *Chemical Reviews*, 60, 35-41.
- Dubinin, M. M., & Kadlec, O. (1975). New Ways in Determination of the Parameters of Porous Structure of Microporous. *Carbon*, 13, 263–265. [https://doi.org/10.1016/0008-6223\(75\)90026-3](https://doi.org/10.1016/0008-6223(75)90026-3)
- EPA. (2002). *Manual Report for List of Chemical Priority*. USA: Environmental Protection Agency.
- Fierro, V., Torné-Fernández, V., Montané, D., & Celzard, A. (2008). Adsorption of phenol onto activated carbons having different textural and surface properties. *Microporous and Mesoporous Materials*, 111(1-3), 276–284. <http://doi.org/10.1016/j.micromeso.2007.08.002>
- Gebresemati, M., Gabbiye, N., & Sahu, O. (2017). Sorption of cyanide from aqueous medium by coffee husk: Response surface methodology, *Journal of applied research and Technology*, 15, 27-35. <https://doi.org/10.1016/j.jart.2016.11.002>
- Girish, C., & Murty, V. (2012). Adsorption of phenol from wastewater using locally available adsorbents. *Journal of Environmental Research and Development*, 6 (3), 763-772. <http://eprints.manipal.edu/id/eprint/137329>
- Hameeda, B.H., Din, A. T. M., & Ahmad, A. L. (2007). Adsorption of methylene blue onto bamboo-based activated carbon: Kinetics and equilibrium studies. *Journal of Hazardous Materials*, 141(3), 819–825. <http://doi.org/10.1016/j.jhazmat.2006.07.049>
- Holmes, H.F., Fuller, E.L., & Gammage, R.B.(1972). Heats of Immersion in the Zirconium Oxid-Water System. *The Journal of Physical Chemistry*, 76 (10), 1497–1502. <http://doi.org/10.1021/j100654a023>
- Jia, Y.F., & Thomas, K. M. (2000). Adsorption of cadmium ions on oxygen surface sites in activated carbon. *Langmuir*, 16 (3), 1114–1122. <http://doi.org/10.1021/la990436w>
- Kaneko, K. (1994). Determination of pore size and pore size distribution I. Adsorbents and catalysts. *Journal of Membrane Science*, 96(4), 59–89. [http://doi.org/10.1016/0376-7388\(94\)00126-x](http://doi.org/10.1016/0376-7388(94)00126-x)
- Kercher, A. K., & Nagle, D.C. (2003). Microstructural evolution during charcoal carbonization by X-ray diffraction analysis. *Carbon*, 41, 15–27. [http://doi.org/10.1016/S0008-6223\(02\)00261-0](http://doi.org/10.1016/S0008-6223(02)00261-0)
- Kumar, K.V., de Castro, M.M., Martinez-Escandell, M., Molina-Sabio, M., & Rodriguez-Reinoso, F. (2010). A Continuous Binding Site Affinity Distribution Function from the Freundlich Isotherm for the Supercritical Adsorption of Hydrogen on Activated Carbon. *The Journal of Physical Chemistry C*, 114(32), 13759–13765. <http://doi.org/10.1021/jp104014f>
- Kyzas, G. Z., Deliyanni, E. A., & Matis, K. A. (2016). Activated carbons produced by pyrolysis of waste potato peels : Cobalt ions removal by adsorption. *Colloids and Surfaces A : Physicochemical and Engineering Aspects*, 490, 74–83. <https://doi.org/10.1016/j.colsurfa.2015.11.038>
- Langmuir, I. (1918). The Adsorption of Gases on Plane Surfaces of Glass, Mica and Platinum. *Journal of the American Chemical Society*, 40 (9), 1361–1403. <http://doi.org/doi:10.1021/ja02242a004>

- Liao, B., Sun, W., Guo, N., Ding, S., & Su, S. (2016). Equilibriums and kinetics studies for adsorption of Ni (II) ion on chitosan and its triethylenetetramine derivative. *Colloids and Surfaces A: Physicochemical and Engineering Aspects*, 501, 32–41. <http://doi.org/10.1016/j.colsurfa.2016.04.043>
- Lippens, B.C., Linsen, B.G., & de Boer, J. H. (1964 a). Studies on Pore Systems in Catalysts. The Adsorption of Nitrogen; Apparatus and Calculation. *Journal of Catalysis*, 3, 32–37. [https://doi.org/10.1016/0021-9517\(64\)90089-2](https://doi.org/10.1016/0021-9517(64)90089-2)
- Lippens, B.C., & de Boer, J. H. (1964 b). Studies on Pore Systems in Catalysts III. Poresize distribution curves in aluminium oxide system. *Journal of Catalysis*, 3, 44–49. [https://doi.org/10.1016/0021-9517\(64\)90091-0](https://doi.org/10.1016/0021-9517(64)90091-0)
- Liu, Q. S., Zheng, T., Wang, P., Jiang, J. P., & Li, N. (2010). Adsorption isotherm, kinetic and mechanism studies of some substituted phenols on activated carbon fibers. *Chemical Engineering Journal*, 157(2-3), 348–356. <http://doi.org/10.1016/j.cej.2009.11.013>
- Liu, T., Li, Y., Du, Q., Sun, J., Jiao, Y., Yang, G., Wang, Z., Xia, Y., Zhang, W., Wang, K., Zhu, H., & Wu, D. (2012). Adsorption of methylene blue from aqueous solution by graphene. *Colloids and Surfaces B: Biointerfaces*, 90, 197–203. <http://doi.org/10.1016/j.colsurfb.2011.10.019>
- Lowell, S., & Shields, J. E. (1991). *Powder Surface Area and Porosity*. (3<sup>rd</sup> ed.). NY: Chapman and Hall
- Ma, L., Zhu, J., Xi, Y., Zhu, R., & He, H. (2016). Adsorption of phenol, phosphate and Cd (II) by inorganic – organic montmorillonites: A comparative study of single and multiple solute. *Colloids and Surfaces A: Physicochemical and Engineering Aspects*, 497, 63–71. <http://doi.org/10.1016/j.colsurfa.2016.02.032>
- Mohd Din, A. T., Hameed, B. H., & Ahmad, A. L. (2009). Batch adsorption of phenol onto physicochemical-activated coconut shell. *Journal of Hazardous Materials*, 161(2-3), 1522–1529. <http://doi.org/10.1016/j.jhazmat.2008.05.009>
- Molina-Sabio, M., Sánchez-Montero, M.J., Juárez-Galan, J.M., Salvador, F., Rodríguez-Reinoso, F., & Salvador, A. (2006). Development of porosity in a char during reaction with steam or supercritical water. *The journal of physical chemistry B*, 110 (25), 12360–4. <http://doi.org/10.1021/jp0614289>
- Namasivayam, C., & Kadirvelu, K. (1997). Activated carbons prepared from coir pith by physical and chemical activation methods. *Bioresource Technology*, 62 (3), 123–127. [http://doi.org/10.1016/S0960-8524\(97\)00074-6](http://doi.org/10.1016/S0960-8524(97)00074-6)
- Ngah, W. S. W., & Fatinathan, S. (2006). Chitosan flakes and chitosan- GLA beads for adsorption of p-nitrophenol in aqueous solution. *Journal of Colloids and Surfaces A: Physicochemical and Engineering Aspects*, 277, 214–222.
- Pomonis, P. J., Petrakis, D.E., Ladavos, A. K., Kolonia, K.M., Pantazis, C.C., Giannakas, A. E., & Leontiou, A. A. (2005). The I-point method for estimating the surface area of solid catalysts and the variation of C-term of the BET equation. *Catalysis Communications*, 6 (1), 93–96. <http://doi.org/10.1016/j.catcom.2004.11.006>
- Pradhan, B. K., & Sandle, N. K. (1999). Effect of different oxidizing agent treatments on the surface properties of activated carbons. *Carbon*, 37(8), 1323–1332. [http://doi.org/10.1016/S0008-6223\(98\)00328-5](http://doi.org/10.1016/S0008-6223(98)00328-5)
- Rodríguez-Reinoso, F., Molina-Sabio, M., & Munecas, M. (1992). Effect of Microporosity and Oxygen Surface Groups of Activated Carbon in the Adsorption of Molecules of Different Polarity. *J. Phys. Chem*, 96, 2707–2713.
- Shen, W., Li, Z., & Liu, Y. (2008). Surface Chemical Functional Groups Modification of Porous Carbon. *Recent Patents on Chemical Engineering*, 1(1), 27–40. <http://doi.org/10.2174/2211334710801010027>
- Simões, G., Hoffmann, C., Claudio, E., & Wilhelm, M. (2016). Preparation of novel adsorbents based on combinations of polysiloxanes and sewage sludge to remove pharmaceuticals from aqueous solutions. *Colloids and Surfaces A: Physicochemical and Engineering Aspects*, 497, 304–315. <https://doi.org/10.1016/j.colsurfa.2016.03.021>
- Sing, K. (2001). The use of nitrogen adsorption for the characterisation of porous materials. *Colloids and Surfaces A: Physicochemical and Engineering Aspects*, 187–188, 3–9. [https://doi.org/10.1016/S0927-7757\(01\)00612-4](https://doi.org/10.1016/S0927-7757(01)00612-4)
- Sreedhar, M.K., Madhukumar, A., & Anirudhan, T.S. (1999). Evaluation of an adsorbent prepared by treating coconut husk with polysulphide for the removal of mercury from wastewater. *Indian Journal of material and Engineering Science*, 6, 279–285. <http://nopr.niscair.res.in/handle/123456789/22330>
- Srivastava, V.C., Swamy, M.M., Mall, I.D., Prasad, B., & Mishra, I.M. (2006). Adsorptive removal of phenol by bagasse fly ash and activated carbon: Equilibrium, kinetics and thermodynamics. *Colloids and Surfaces A: Physicochemical and Engineering Aspects*, 272 (1-2), 89–104. <https://doi.org/10.1016/j.colsurfa.2005.07.016>
- Stoekli, F., López-Ramón, M.V., & Moreno-Castilla, C. (2001). Adsorption of phenolic compounds from aqueous solutions, by activated carbons, described by the dubinin - Astakhov equation. *Langmuir*, 17(11), 3301–3306. <http://doi.org/10.1021/la0014407>
- Tan, I. A. W., Ahmad, A. L., & Hameed, B.H. (2008). Preparation of activated carbon from coconut husk: Optimization study on removal of 2,4,6-trichlorophenol using response surface methodology. *Journal of Hazardous Materials*, 153(1-2), 709–717. <http://doi.org/10.1016/j.jhazmat.2007.09.014>
- Thomson, K.T., & Gubbins, K. E. (2000). Modeling Structural Morphology of Microporous Carbons by Reverse Monte Carlo. *Langmuir*, 16 (13), 5761–5773. <http://doi.org/10.1021/la991581c>
- Vinod, V.P., & Anirudhan, T. S. (2002). Effect of experimental variables on phenol adsorption on activated carbon prepared from coconut husk by single-step steam pyrolysis: Mass transfer process and equilibrium studies. *Journal of Scientific & Industrial Research*, 61(2), 128–138. <http://nopr.niscair.res.in/handle/123456789/17710>
- WHO. (1963). *International standards for drinking water*. Geneva: World Health Organisation.
- Zhao, J., Yang, L., Li, F., Yu, R., & Jin, C. (2009). Structural evolution in the graphitization process of activated

carbon by high-pressure sintering. *Carbon*, 47(3), 744–751. <https://doi.org/10.1016/j.carbon.2008.11.006>

Figures

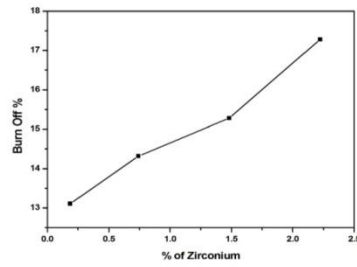


Fig. 1. plot of burnoff vs % of zirconium ion impregnated

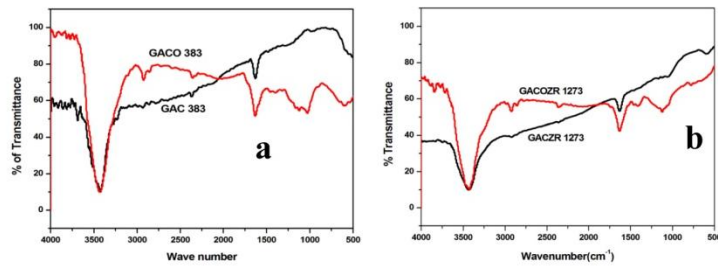


Fig. 2. FTIR spectra of (a) GAC 383, GACO 383 and (b) GACZR1273 and GACQZR 1273

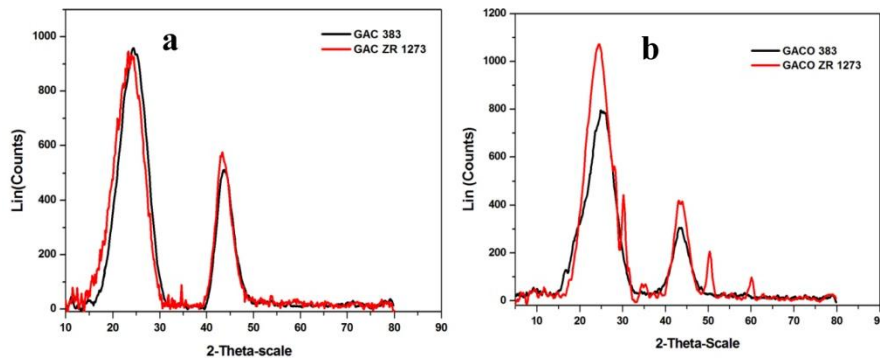


Fig. 3. XRD spectra of (a) GAC 383, GACZR 1273 and (b) XRD spectra of GACO 383, GACQZR 1273

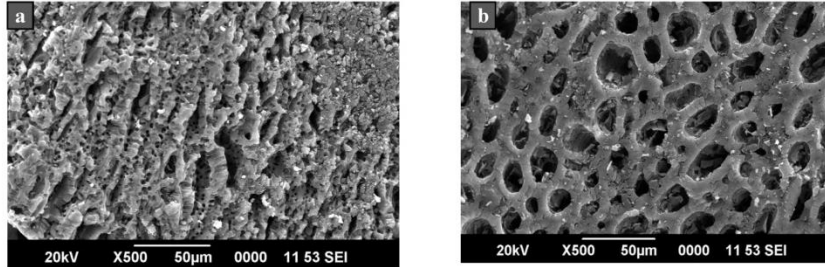


Fig. 4. SEM images of carbon (a) GACZR 1273 and (b) nitric acid modified form of carbon GACZR 1273

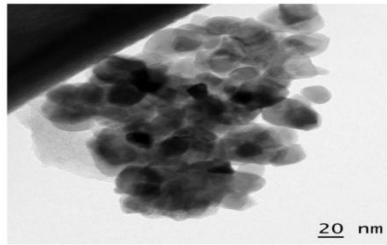


Fig. 5. TEM images of GACZR 1273

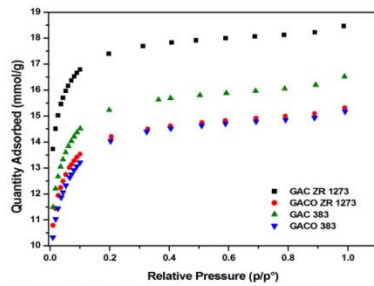


Fig. 6. N<sub>2</sub> adsorption isotherm plot for the new carbons at 77K

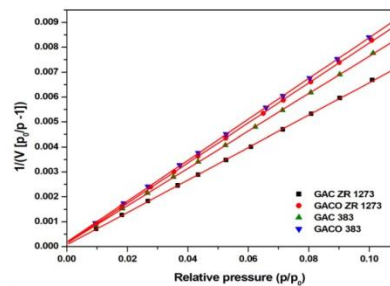


Fig. 7. BET isotherm plot for the new carbons at 77K

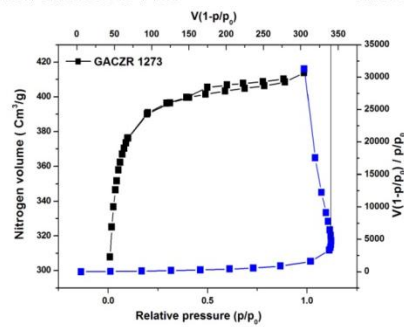


Fig .8. I plot method for the new carbons at 77K

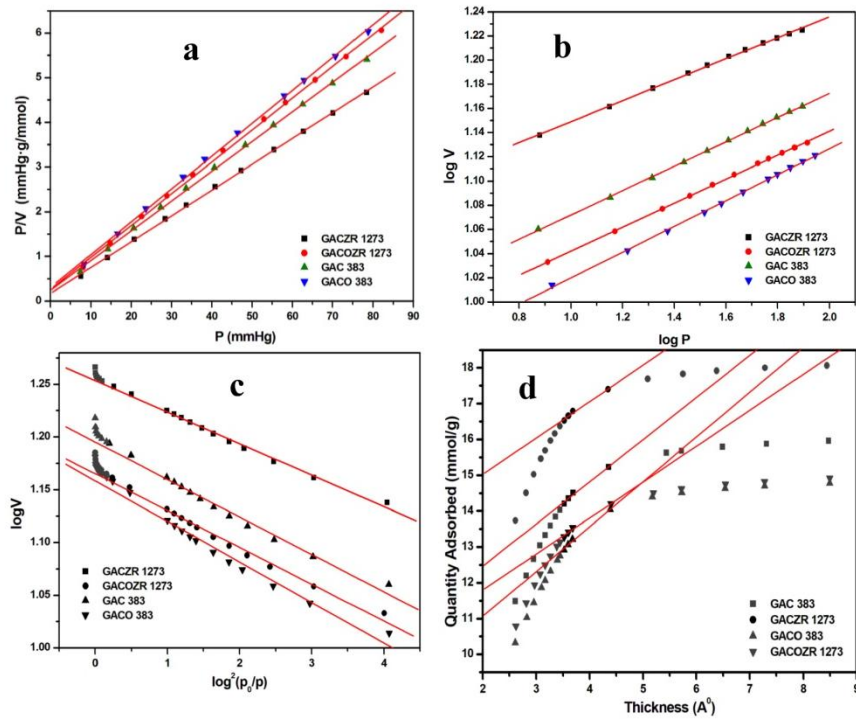


Fig. 9 (a) Langmuir, and (b) Freundlich, (c) Dubinin-Radushkevich (D-R) isotherm and (d)  $t$  plots of GAC 383, GACO 383 and GACZR 1273 and GACOZR 1273 using  $N_2$  adsorption data.

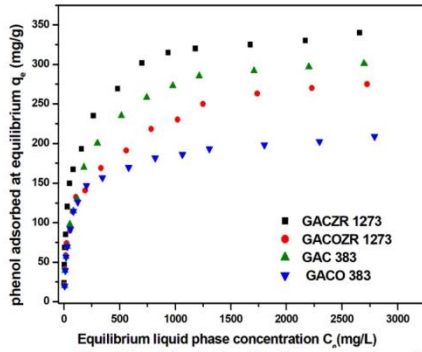


Fig. 10. Adsorption isotherm of phenol on GAC 383, GACO 383, GACZR 1273 and GACOZR 1273

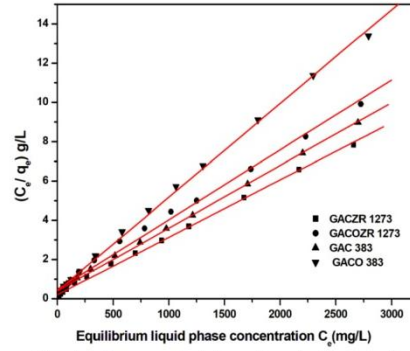


Fig. 11. Langmuir Adsorption isotherm of phenol on GAC 383, GACO 383, GACZR 1273 and GACOZR 1273

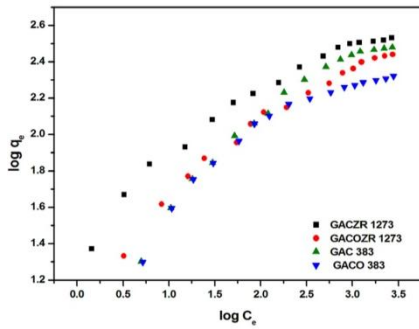


Fig. 12. Freundlich Adsorption isotherm of phenol on GAC 383, GACO 383, GACZR 1273 and GACOZR 1273

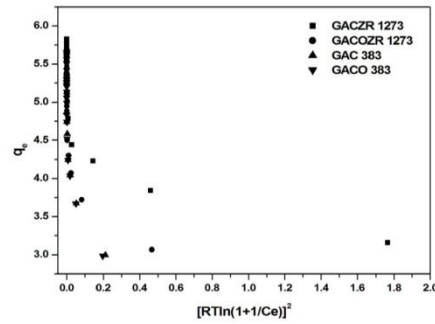


Fig. 13. Dubinin-Radushkevich Adsorption Isotherm of phenol on GAC 383, GACO 383, GACZR 1273 and GACOZR 1273

## Adsorption of *p*-nitrophenol on coconut shell granular activated carbon: Isotherms, kinetics and thermodynamics

V Sivanandan Achari\*, S Jayasree &amp; A S Rajalakshmi

School of Environmental Studies

Cochin University of Science and Technology, Kochi 682 022, Kerala, India

E-mail: vsachari@gmail.com

Received 18 January 2017; accepted 28 April 2017

Adsorption of *p*-nitrophenol by modified granular activated carbons based on coconut shell from aqueous solutions has been studied under laboratory conditions. Four granular activated carbons GAC383 (native form), GACO383 (its nitric acid oxidised form), GACZC1073 (native form incorporated with  $Zn^{2+}$  ions and activated at 1073) and GACOZC1073 (oxidised form impregnated with  $ZnCl_2$ ) have been used. Batch experiments have been carried out with variants being concentration, time, temperature and equilibrium conditions. Pseudo first, second order kinetic models, intraparticle diffusion models and Elovich kinetic model are applied to study the respective kinetics. Pseudo second order rate equations are found to be best suited for the adsorption systems. Equilibrium isotherm for concentration range (25-3000 mg/L) is analysed by Langmuir (L) and John - SivanandanAchari (J-SA) isotherm models. GACZC1073 has higher adsorption capacity (490.2 mg/g) than GACO383 (224.2 mg/g). The temperature on the adsorption of *p*- nitrophenol is studied at different temperatures. The thermodynamic parameters such as Gibbs free energy, enthalpy and entropy are calculated using Van't Hoff equation. It is inferred that, the adsorption of *p*-nitrophenol on new modified carbons is endothermic and occurs through physisorption. This study reveals that  $Zn^{2+}$  ions impregnated activated carbon GACZC1073 has more adsorption efficiency evidenced by a high adsorption of rate  $\alpha$  and surface diffusion  $K_{sd}$  promoted by extra adsorption sites generated during activation.

**Keywords:** Adsorption, Adsorption kinetics, Granular Activated Carbon, John-Sivanandan Achari (J-SA) Isotherm, *p*-nitrophenol

Adsorption kinetics, equilibrium isotherm and thermodynamic studies are very important for the optimization of adsorption process for the design of unit operation<sup>1</sup>. Adsorption kinetics involves the determination of the rate at which pollutants are removed from solution media onto carbon surface. Also it controls the residence time of the solute and hence its uptake at the solid-solution interfaces<sup>2</sup>.

Studies on adsorption isotherms are essential to understand how adsorbate interact with carbon granules and are critical in optimizing the use of adsorbent<sup>3</sup>. To design an adsorption reactor system, heat change of adsorption process is also important. Hence, study of the prominent thermodynamic parameters of the adsorption process such as enthalpy, entropy and free energy change are mostly done in adsorption science<sup>4</sup>. In this regard, adsorption of *p*-nitrophenol by modified granular activated carbons based on coconut shell from aqueous solutions had been studied under laboratory conditions. Four granular activated carbons GAC383 (native form), GACO383 (its nitric acid oxidised form),

GACZC1073 (native form incorporated with  $Zn^{2+}$  ions and activated at 1073) and GACOZC1073 (oxidised form impregnated with  $Zn^{2+}$  ions) were used. Batch experiments were carried out as a function of concentration time, temperature and equilibrium conditions. The main objective of this work is to make an attempt to evaluate the relative adsorption potential of coconut shell based granular activated carbons (GAC383, GACO383, GACZC1073 and GACOZC1073) newly developed under a set of activation conditions using *p*-nitrophenol as adsorbate.

### Experimental Section

Commercially available coconut shell based granular activated carbon (manufactured by Indo German Carbon Industry, Cochin, India) was used as the basic carbon source for the preparation of new carbon series<sup>5</sup>. One kilogram of this carbon washed with NaOH and HCl to remove impurities and neutralize to neutral pH 7.0 and dried at 110°C and marked as GAC383. This was then oxidised by 12.9%  $HNO_3$  washed with distilled water and dried at 110°C

and labelled as GACO383. About 10 g of GAC383 mixed with 50 mL water containing 0.035 g  $ZnCl_2$  ( $Zn^{2+} = 0.017g$ ) and activated under steam at 1073K in a temperature controlled furnace. The carbon was then dried in oven and the product was designated as GACZC1073. The same procedure was followed for GACO383 and the sample was marked as GACOZC1073. These four carbons were further used for the study of adsorption kinetics, isotherm and thermodynamic studies.

Selection of granular activated carbon for the adsorption process is largely dependent due to favourable physico chemical characteristics such as porosity, surface area, surface functional groups, surface morphology, crystallinity etc. The textural properties of the carbon materials are given in Table 1. Evaluation of physical characteristics such as pore volume and surface area were undertaken by using nitrogen adsorption-desorption isotherm at liquid nitrogen 77K using Micromeritics (Tristar 3000 V6. 07A). Surface functional groups were quantitatively measured using Boehm titration method. The elemental composition [C, H, N & O] of the modified granular activated carbons were evaluated by using Elemental Vario EL III. The surface morphology was evaluated by using Scanning Electron Microscope (SEM) Jeol Model JSM-6390LV and High Resolution Transmission Electron Microscope (HRTEM) Jeol /JEM 2100.

The batch experiments of the adsorption kinetics and isotherms were conducted at a temperature of 30°C in a 100 mL screw cap conical flask. 1.0 g/L adsorbent dosage was weighed and placed in the flask containing 50 mL solution of *p*-nitrophenol of a desired concentration ranging from 25-3000 mg/L and temperature ranging from 10 to 50°C. The adsorption kinetics were studied using initial concentration of

*p*-nitrophenol 250 mg/L in a temperature controlled bath shaker. For isotherm study shaking time was fixed as 480 minute based on preliminary studies conducted for the determination of equilibration time. After shaking, the suspension was filtered using Whatmann No.1 filter paper. The concentration of the filtrate was measured using a UV-Visible Spectrophotometer at 317 nm.

Adsorption kinetic studies were undertaken using *p*-nitrophenol and the time dependent data were used to test different kinetic models such as pseudo first, Ho second, intraparticle diffusion and Elovich models<sup>6</sup>. Equilibrium data were applied to different isotherm models such as Langmuir isotherm and John – Sivanandan Achari (J- SA)<sup>7-9</sup> isotherm to calculate the adsorption capacity and other structural constants. The thermodynamic parameters such as enthalpy, entropy and Gibbs free energy ( $\Delta H$ ,  $\Delta S$  and  $\Delta G$ ) were calculated from the Langmuir isotherms parameter ( $K_L$ ) by using the Van't Hoff Equation<sup>10</sup>.

## Results and Discussion

### Characterisation of modified GACs

The physico chemical characteristics of modified granular activated carbons (GAC383, GACO383, GACZC1073 and GACOZC1073) are listed in Table 1. The granular activated carbon impregnated with  $Zn^{2+}$  ions and activated at high temperature shows high basic groups, high carbon content, large micropore volume and surface area compared to other carbons. Granular carbons having very high carbon content is expected to have high surface area. It is known that the  $Zn^{2+}$  ions incorporated into the interior of GAC inhibits the expected contraction during activation temperature, which implies that  $Zn^{2+}$  may act as a template for creation of micro porosity<sup>11</sup>. In this, carbon GACZC1073 has higher micropore volume and micro porous surface area. GACOZC1073 shows higher BET surface area and

Table 1 — Physico – chemical characterization of modified granular activated carbon (GAC) based on coconut shell

Carbon	Carboxylic(meq/g)	Lactones(meq/g)	Phenolic(meq/g)	Basic (meq/g)	C%	H%	N%	O%	$V_{mic}^{(1)}$ ( $Cm^3/g$ )	$V_{me}^{(1)}$ ( $Cm^3/g$ )	$S_{ABET}$ ( $m^2/g$ )	$S_{A_{mi}}$ ( $m^2/g$ )
GAC383	0.40	0.17	0.45	0.50	89.43	0.60	0.36	9.6	0.573	0.351	996.8	588.7
GACO383	1.38	1.34	2.10	0.20	65.10	2.61	0.58	31.7	0.526	0.297	974.3	540.6
GACZC1073	0.39	0.10	0.20	0.90	94.47	0.09	0.31	5.1	0.569	0.378	1083.6	767.0
GACOZC1073	0.23	0.94	0.17	0.43	84.07	0.52	0.59	14.8	0.604	0.221	1101.8	349.4



lower micro pore volume and micro pore surface area that is because oxidation/ activation enlarge the pore structure. Granular activated carbon oxidized with nitric acid (GACO383) shows high oxygen content, less percentage of carbon and enhances the acidic functional groups. The SEM (Fig. 1) and TEM (Fig. 2) images showed that GACZC1073 is highly microporous evidenced by the porosity (0.378 cm<sup>3</sup>/g) and surface area (767 m<sup>2</sup>/g) value determined by N<sub>2</sub> gas adsorption at 77K.

**Adsorption kinetic study**

The adsorption kinetic study of *p*-nitrophenol on four carbons (GAC383, GACO383, GACZC1073 and GACOZC1073) was undertaken using initial concentration (250 mg/L) at a temperature 30°C. Figure 3 shows the *p*-nitrophenol uptake behaviour as a function of time. Among these four carbons Zn<sup>2+</sup>

impregnated granular activated carbon activated at 1073K (GACZC1073) shows maximum adsorption capacity (229.5 mg/g) for an initial concentration of 250 mg/L *p*-nitrophenol used for kinetic study (Table 2). These time dependent data are applied in

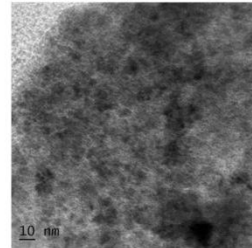


Fig. 2 — Transmission electron microscopy of GACZC1073

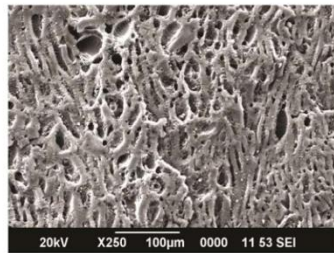


Fig. 1 — Scanning electron micrographs of GACZC1073 at 100µm magnification

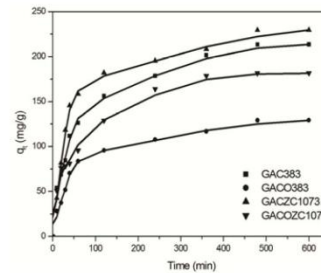


Fig. 3 — Effect of contact time on the adsorption of *p*-nitrophenol on granular activated carbon (GAC) based on coconut shell

Table 2 — Kinetic Parameters for the adsorption of *p*-nitrophenol on granular activated carbon (GAC) based on coconut shell

Kinetic Models	Parameters	Carbon			
		GAC383	GACO383	GACZC1073	GACOZC1073
Experimental value	$q_{exp}$ (mg/g)	213.4	129.3	229.5	181.6
Pseudo first order	$q_{cal}$ (mg/g)	151.3	84.2	129.3	151.5
	$K_1$ (min <sup>-1</sup> )	0.007	0.006	0.006	0.0103
	$R^2$	0.98	0.93	0.87	0.98
Pseudo second order	$q_{cal}$ (mg/g)	228.8	136.8	258.6	199.2
	$K_2 * 10^5$ (gm <sup>2</sup> g <sup>-1</sup> min <sup>-1</sup> )	9.20	15.6	11.30	10.40
	$R^2$	0.99	0.99	0.99	0.99
Intraparticle diffusion Model	$K_{id1}$ (mg <sup>1/2</sup> g <sup>-1/2</sup> min <sup>-1/2</sup> )	16.80	12.89	26.56	8.77
	$C_1$	-2.21	-15.83	-35.02	28.67
	$R^2$	0.97	0.97	0.95	0.89
	$K_{id2}$ (mg <sup>1/2</sup> g <sup>-1/2</sup> min <sup>-1/2</sup> )	5.34	2.99	4.18	4.91
	$C_2$	97.64	62.04	133.47	80.75
	$R^2$	0.99	0.99	0.96	0.95
Elovich Kinetic Model	$\alpha$ (mg <sup>1/2</sup> g <sup>-1/2</sup> min <sup>-1</sup> )	12.76	10.75	18.24	11.64
	$\beta$ (gm <sup>1/2</sup> g <sup>-1/2</sup> )	0.0233	0.0397	0.0226	0.0276
	$R^2$	0.99	0.97	0.94	0.97
	$E_a$ (kcal/mol)	0.2267	0.1792	0.4943	0.1926

different kinetic models such as Pseudo first order, Ho second order, Weber intra particle diffusion model and Elovich model to identify the mechanism of adsorption on modified carbons.

**Pseudo first order model**

Among the common kinetic models known to study adsorption,

Lagergen model is the simplest one followed for solute adsorption. This model is expressed in a linear form<sup>12</sup>,

$$\ln(q_e - q_t) = \ln q_e - K_1 t \quad \dots (1)$$

where  $K_1$  ( $\text{min}^{-1}$ ) is the pseudo-first order rate constant,  $t$  (min) the contact time,  $q_t$  and  $q_e$  are the amount of nitrophenol adsorbed at any time  $t$  and at equilibrium respectively for the granular activated carbon under study. The constants are given in Table 2.

**Ho second order kinetic model**

Ho presented a sorption based pseudo-second order rate law expression for the reaction rate dependence on the adsorption capacity on solid phase but not the concentration of adsorbate. The model is represented in the following form<sup>13</sup>.

$$\frac{t}{q_t} = \frac{1}{K_2 q_e^2} + \frac{t}{q_e} \quad \dots (2)$$

where  $q_e$  is the amount of adsorbate adsorbed at equilibrium (mg/g),  $t$  is the reaction time (min),  $q_t$  is the amount of adsorbate adsorbed at time  $t$  (mg/g),  $K_2$  is the equilibrium rate constant of pseudo second order adsorption ( $\text{g/mgmin}$ ). This model is used to express the kinetics of  $p$ -nitrophenol adsorption on the new carbons and the graph shown in Fig. 4.

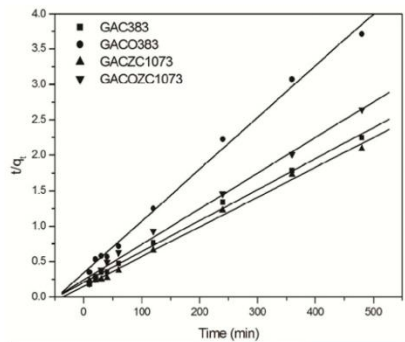


Fig. 4 — Pseudo second order kinetic model for the adsorption of  $p$ -nitrophenol on granular activated carbon (GAC) based on coconut shell

**Intraparticle diffusion model**

Weber and Morris<sup>14</sup> used intraparticle diffusion model to predict the rate controlling step of an adsorption process. When mass transfer is the controlling step, it is important to identify the diffusion mechanism. According to intraparticle diffusion model, the initial rate of diffusion is given by the following Equation:

$$q_t = K_{id} t^{0.5} + C \quad \dots (3)$$

where  $q_t$  (mg/g) is the amount of  $p$ - nitrophenol adsorbed at any time  $t$  (min),  $K_{id}$  ( $\text{mgg}^{-1}\text{min}^{-1/2}$ ) is the intra particle diffusion constant and  $C$  is the boundary layer thickness from the slope and intercept respectively, the plot of  $q_t$  vs. square root of time in min shown in Fig. 5, for the new granular activated carbons.

**Elovich kinetic model**

The simplest form of Elovich model<sup>15</sup> is represented by

$$q_t = \frac{1}{\beta} (\ln \alpha \beta) + \frac{1}{\beta} \ln t \quad \dots (4)$$

The  $\alpha$  ( $\text{mg g}^{-1} \text{min}^{-1}$ ) is the initial rate constant and  $\beta$  ( $\text{g mg}^{-1}$ ) is related to the extent of surface coverage and activation energy of adsorption, can be determined respectively from the intercept and slope of the plot  $q_t$  vs.  $\ln t$ . Activation energy ( $E_a$ ) for the adsorption of  $p$ -nitrophenol on these modified carbons is obtained using Arrhenius equation based on Elovich constant ( $\beta$ ), from a linear plot of  $\log \beta$  against  $1/T$  for the temperature ranges from 283 to 323K.

The kinetic parameters for the adsorption of  $p$ - nitrophenol on modified granular activated

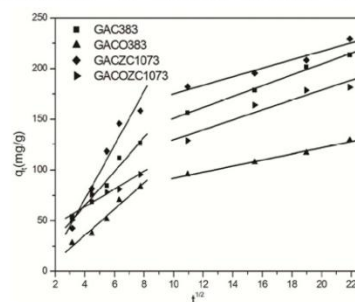


Fig. 5 — Intraparticle diffusion model for the adsorption of  $p$ -nitrophenol on granular activated carbon (GAC) based on coconut shell

carbons are calculated and listed in Table 2. The amount adsorbed ( $q_{exp}$ ) determined from the batch kinetic study is more comparable with  $q_e$  calculated ( $q_{cal}$ ) obtained from the pseudo second order kinetic model whose correlation coefficient ( $R^2=0.99$ ) was found to be high compared to the first order model applied ( $R^2$  ranges 0.87-0.98). This means the adsorption of *p*-nitrophenol on these modified GAC follows Ho second order kinetic model<sup>16</sup> which implies adsorption is controlled by the square of unoccupied sites on granular activated carbons. To determine the adsorption mechanism, the intraparticle diffusion model by Weber is applied on this time dependent adsorption data. Figure 5 shows two straight line portions on plotting the data. The first stage is attributed to surface diffusion and the second stage is due to pore diffusion. The  $K_{id1}$  (ranges 8.77-26.56  $\text{mgg}^{-1}\text{min}^{-1/2}$ ) is higher than the  $K_{id2}$  (ranges 2.99-5.34  $\text{mgg}^{-1}\text{min}^{-1/2}$ ) for all carbons indicating that pore diffusion is a slow step (Table 2). This reveals that the adsorption mechanism of *p*-nitrophenol on the new carbons also follow intraparticle diffusion model. As regards to Elovich model tested, GACZC1073 shows higher initial adsorption rate ( $\alpha$ ) compared to other carbons. The activation energy ( $E_a$ ) calculated ranges 0.17-0.49 kcal/mol (is less than 4.0 kcal/mol) indicate that the surface diffusion<sup>17</sup> has a major role on adsorption.  $\text{Zn}^{2+}$  ions impregnation increases adsorption sites on the surface of granular activated carbon. Hence, enhances the overall adsorption efficiency.

#### Adsorption Isotherm and thermodynamic study

Figure 6 depicts the isotherm plot for *p*-nitrophenol over the new GAC's, in which the

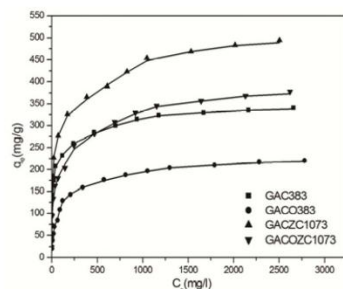


Fig. 6 — General isotherm plot for the adsorption of *p*-nitrophenol on granular activated carbons based on coconut shell

amount of *p*-nitrophenol adsorbed per gram of adsorbent ( $q_e$ ) is plotted against the equilibration concentration ( $C_e$ ). The isotherm has a steep phase in the beginning followed by saturation at higher initial concentration typical for type I microporous materials as per IUPAC (2015) classification<sup>18</sup>. The equilibrium data are further processed to fit the standard adsorption isotherm models of Langmuir and John – Sivanandan Achari (*J-SA*) Isotherm models.

**Langmuir isotherm** is a mathematical construct to evaluate the adsorption efficiency of activated carbon (Fig. 7). The form of the model is<sup>19</sup>

$$\frac{C_e}{q_e} = \frac{1}{q_{max}K_L} + \frac{C_e}{q_{max}} \quad \dots (5)$$

$K_L$  ( $\text{Lmg}^{-1}$ ) is adsorption energy and  $q_{max}$  ( $\text{mg/g}$ ) is monolayer adsorption capacity.

**John – Sivanandan Achari (J-SA) Isotherm** is an empirical isotherm<sup>20-22</sup> and the equation can be expressed as

$$\log \log C_e = C + n \log q_e \quad \dots (6)$$

$C$  and  $n$  are the *J-SA* isotherm constants;  $n$  is referred as adsorbability constants and is a measure of adsorption efficiency.

Monolayer adsorption capacity increases according to the order GACZC1073 (490.2  $\text{mg/g}$ ) > GACOCZC1073 (377.4  $\text{mg/g}$ ) > GAC383 (340.1  $\text{mg/g}$ ) > GACO383 (224.2  $\text{mg/g}$ ), that indicates granular activated carbon incorporated with  $\text{Zn}^{2+}$  ions and activated / carbonized at 1073K has the highest adsorption efficiency among the group selected for isotherm study. The *J-SA* plot Fig. 8 shows a straight line with single phase adsorption and the  $q_m$  (*J-SA*) and monolayer adsorption capacity  $q_{max}(L)$  of

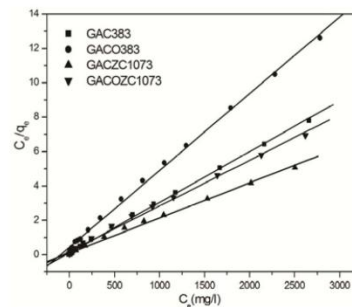


Fig. 7 — Langmuir isotherm for the adsorption of *p*-nitrophenol on granular activated carbons based on coconut shell

Langmuir model (Fig. 7) are comparable for all GAC's as listed in Table 3 indicating that these modified carbon are microporous and belongs to type I category according to classification by John and Achari (2002)<sup>23</sup>.

**Thermodynamic parameters**

The mechanism of adsorption of *p*-nitrophenol on the above carbon is elucidated by different thermodynamic parameters such as Gibbs free energy change ( $\Delta G$ ), enthalpy change ( $\Delta H$ ) and entropy change ( $\Delta S$ ). These parameters were calculated from the Langmuir isotherm constants ( $K_L$ ) adopting the Van't Hoff's Equation (7 and 8). The temperature effect on the adsorption of *p*-nitrophenol was studied at 5 different temperatures (10, 20, 30, 40 and 50°C) as shown in Figs 9 and 10.

$$\Delta G = -RT \ln K_L \quad \dots (7)$$

$$\ln K_L = -\frac{\Delta H}{RT} + \frac{\Delta S}{R} \quad \dots (8)$$

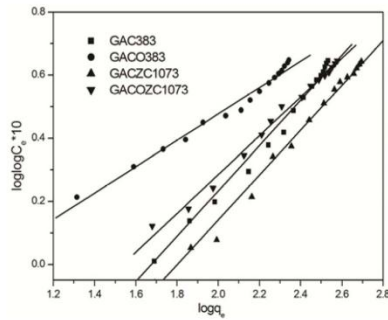


Fig. 8 — John – Sivanandan Achari isotherm for the adsorption of *p*-nitrophenol on granular activated carbons based on coconut shell

The values of  $\Delta S$  and  $\Delta H$  are calculated from the intercept and slope of the plot  $\ln K_L$  versus  $1/T$  for *p*-nitrophenol adsorption on different GAC and are given in Table 4. The positive value of  $\Delta H$  indicates that adsorption of *p*-nitrophenol on GAC were

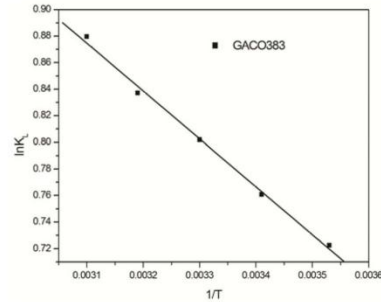


Fig. 9 — Plot of  $\ln K_L$  versus  $1/T$  for the estimation of thermodynamic parameters for the adsorption of *p*-nitrophenol on GACO383 based on coconut shell

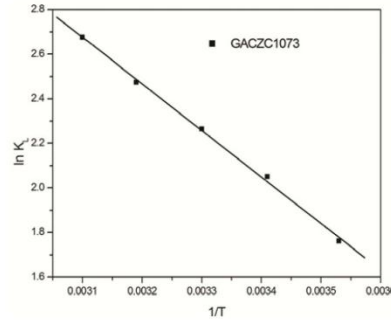


Fig. 10 — Plot of  $\ln K_L$  versus  $1/T$  for the estimation of thermodynamic parameters for the adsorption of *p*-nitrophenol on GACZC1073 based on coconut shell

Table 3 — Equilibrium adsorption isotherm parameters for the adsorption of *p*-nitrophenol on granular activated carbon (GAC) based on coconut shell

Isotherm Models	Parameters	Granular Activated Carbon (GAC)			
		GAC383	GACO383	GACZC1073	GACZC1073
Langmuir Model	$q_{max}(L)$ (mg/g)	340.1	224.2	490.2	377.3
	$K_L$ (L/mg <sup>3</sup> )	9.0	2.2	9.7	5.2
	$a_L$ (L/mg <sup>3</sup> )	0.026	0.010	0.019	0.014
	$R^2$	0.99	0.99	0.99	0.99
John Sivanandan Achari (J-SA) isotherm	$q_m$ (J-SA) (mg/g)	349.95	238.78	509.45	389.13
	C	1.20	0.3580	1.28	0.945
	n	0.718	0.417	0.711	0.615
	$R^2$	0.99	0.98	0.99	0.99

Table 4 — Thermodynamic Parameters for the adsorption of *p*-nitrophenol on granular activated carbon (GAC) based on coconut shell

Carbon	$\Delta G$ (KJmol <sup>-1</sup> )					$\Delta H$ (KJmol <sup>-1</sup> )	$\Delta S$ (Jmol <sup>-1</sup> K <sup>-1</sup> )
	283	293	303	313	323		
GAC383	-4.78	-5.17	-5.54	-5.83	-6.36	6.02	38.18
GACO383	-1.70	-1.85	-2.02	-2.18	-2.36	2.96	16.45
GACZC1073	-4.14	-4.99	-5.71	-6.44	-7.19	17.16	75.44
GACOZC1073	-3.31	-3.72	-4.20	-4.68	-5.52	11.85	53.26

endothermic in nature. The adsorption occurs by endothermic process. Increasing temperature enhances the rate of diffusion of the adsorbate molecule across the external boundary layer and in the internal pores of the adsorbate particle, due to the decrease in the viscosity of the solution<sup>24</sup>. The magnitude of the standard enthalpy change, gives an idea for adsorption is physical or chemical in nature on carbon surfaces. The  $\Delta H$  for all the new GAC is less than 20 KJ/mol which indicates that adsorption of *p*-nitrophenol on new modified GAC follows physisorption mechanism. The positive value of entropy change ( $\Delta S$ ) reflects good affinity towards the GAC and the increasing randomness at the solid-solution interface during the adsorption reaction. The negative  $\Delta G$  confirms the feasibility and spontaneity of the adsorption process. From these data, we ascertain that the adsorption process is more favourable at higher temperature (323K), due to endothermic nature of the adsorption system.

#### Conclusion

Zinc ions impregnated activated carbon (GACZC1073) based on Indian coconut shell shows higher adsorption efficiency to remove *p*-nitrophenol compared to other granular activated carbons. Kinetic studies showed that adsorption of *p*-nitrophenol followed pseudo-second order model. Two phases in the intraparticle diffusion suggest that the adsorption process proceeds by surface adsorption and intraparticle diffusion, the particle diffusion is a slow step. Adsorption of *p*-nitrophenol on GAC shows good agreement between Langmuir and John-Sivanandan Achari isotherm plot and it indicate the development of microporosity during Zn<sup>2+</sup> activation. The adsorption capacity of the carbon studied for the present communication can be arranged in the following order GACZC1073 (490.2 mg/g) > GACOZC1073 (377.4 mg/g) > GAC383 (340.1 mg/g) > GACO383 (224.2 mg/g). Thermodynamic parameters such as enthalpy change, free energy change and entropy change

showed that the adsorption process of *p*-nitrophenol is endothermic and spontaneous.

#### Acknowledgement

The first author is thankful to University Grants Commission (UGC), Government of India, New Delhi for the financial support by awarding the project UGC – SAP- DRS Phase II as per the order No: F4 - 14/2015/DRS-II (SAP-II) Dated 19/12/2015 and the second author is thankful to Cochin University of Science and Technology for the financial assistance in the form of University Senior Research Fellowship.

#### References

- 1 Arabi S, Sohrabi M R & Khosravi M, *Indian J Chem Technol*, 20 (2013) 173.
- 2 Jayasree S & Sivanandan Achari V, (Central Marine Fisheries Research Institute, Cochin), 2016.
- 3 Altenor S, Carene B, Emmanuel E, Lambert J, Ehrhardt J J & Gaspard S, *J Hazard Mater*, 165 (2009) 1029.
- 4 Singh K & Chandra B, *Indian J Chem Technol*, 22 (2015) 11.
- 5 Sivanandan Achari V & Jayasree S, Adsorption of *p*- nitrophenol on Zn<sup>2+</sup> impregnated activated carbons, *Proceedings, 24<sup>th</sup> Swadeshi Science Congress*, (Thunchath Eezhuthachan Malayalam University, Tirur, Malappuram) 2014.
- 6 Jayasree S & Sivanandan Achari V, Adsorption of *p*- nitrophenol on ZnO Incorporated Activated Carbons: Isotherms, Kinetics and Surface Area, *Proceedings, International Conference, MATCON*, Department of Applied Chemistry, CUSAT, 2016.
- 7 Sivanandan Achari V, *Modified Carbons and Wood Dust: Evaluation of Adsorption Properties*, Ph.D. Thesis, University of Kerala, Trivandrum, 1998.
- 8 John P T & Bohra J N, *Indian J Chem Technol*, 1 (1963) 437.
- 9 Mercy T, *Adsorption Isotherm Characterisation of Porous Materials Using John Isotherm*, Ph.D. Thesis, School of Environmental Studies, Cochin University of Science and Technology, Cochin, Kerala, 2016.
- 10 Argun M E, Dursun S, Ozdemir C & Karatas M, *J Hazard Mater*, 141 (2007) 77.
- 11 Gonzalez-Serrano E, Cordero T, Rodriguez-Mirasol J & Rodriguez J J, *Ind Eng Chem Res*, 36 (1997) 4832.
- 12 Lagergren S, *K Sven Vetenskapsakad Handl*, 24 (1898) 6.
- 13 McKay G & Ho Y S, *Process Biochem*, 34 (1999) 451.
- 14 Weber W J & Morris J C J, *Sanit Eng Div Am Soc Civil Eng*, 89 (1963) 31.
- 15 Varank G, Demir A, Yetil Mezsoy K & Top S, *Indian J Chem Technol*, 19 (2012) 7.

- 16 Singh H & Choden S, *Indian J Chem Technol*, 21 (2014) 359.
- 17 Juang R S, Chen M L, *Ind Eng Chem Res*, 36 (1997) 813.
- 18 Thommes M, Kaneko K, Neimark A V, Olivier J P, Rodriguez – reinoso F, Rouquerol J & Sing K S W, *Pure Appl Chem*, 87 (2015) 1051.
- 19 McKay G, Geundi M E L & Nassar M M, *Wat Res*, 21 (1987) 1513.
- 20 Sivanandan Achari V, Isotherm for Liquid Phase adsorption: Comparison with Langmuir and Freundlich models: *Proceedings, International Carbon Conference, Carbon*, (Robert Gordon University, Aberdeen, Scotland, UK), 2006.
- 21 Jayasree S, Rajalakshmi A S & SivanandanAchari V, Determination of Surface Area of Activated Carbons using John- SivanandanAchari Isotherm Plots, *Proceedings, 26<sup>th</sup> Kerala Science Congress*, (Veterinary and animal sciences University, Pookode, Wayanadu), 2014.
- 22 Rakhi, P, *John Isotherm Model – Evaluation of adsorption parameters*, M.Tech Thesis, Department of Civil Engineering, Government Engineering College, Thrissur, Kerala, 2010.
- 23 John P T & Achari V S, *J Mater Sci*, 37 (2002) 885.
- 24 Wang S & Zhu Z H, *Dyes Pigm*, 75 (2007) 306.

## EGM82

## Adsorption of Methylene Blue from Aqueous Solution by Zirconium Impregnated Activated Carbon

Rajalakshmi A. S., Achari V. S.

School of Environmental Studies, Cochin University of Science and Technology.  
srajaleshmi@gmail.com, vsachari@gmail.com

## ABSTRACT

The present study discusses the adsorption efficiency of coconut shell based granular activated carbon (GAC) for the removal of organic dyes. Four carbons viz GAC-383 (native carbon), its nitric acid modified GACO-383K its  $ZrO_2$  impregnated activated form (GACNZR 1073) and zirconyl chloride activated forms (GACZR 1273) are used to study Methylene Blue (MB) adsorption in batch reactors under laboratory condition. The adsorption of MB dye on the new carbon was determined for 25-1500 mg/l concentration range to evaluate, the monolayer coverage, kinetics, porosity and surface area. The equilibrium data for MB adsorption well fitted to the Langmuir, Freundlich and John-SivanandanAchari isotherm. The monolayer coverage has been 283mg/g for Carbon GACNZR 1073, 228mg/g for GACZR 1273, 190mg/g for GAC-383 and 138mg/g for GACO - 383. The surface areas (SA) were determined from this monolayer coverage and it compared with BET results. Reaction kinetic equations of pseudo first order, and pseudo second order were applied to kinetic data for the concentration of 250mg/l. Comparison of the isotherm features and the porosity confirmed that the new carbon are highly micropore with a relative properties of mesopores.

KEYWORDS: activated carbon, adsorption, kinetic study, methylene blue (MB), John isotherm

## INTRODUCTION

Organic dyes and its disposal to aquatic environment cause micro toxicity to aquatic life and slow down self-purification of streams reducing light penetration and aesthetic quality leads. They are highly toxic in natural water, are harmful to fish and other aquatic organisms [1]. Methylene blue (MB) can causes eye burns, leads to permanent injury once in contact with human body. Many toxic yarn, fabric and coir industry effluent have appreciable amount of MB. Ingestion through the mouth by accidental contamination produces burning sensation and may cause conditions of nausea, vomiting, profuse sweating, mental confusion, painful micturition and methemoglobinemia [2]. Activated carbon adsorption is a suitable method proposed for the removal of MB from waste water. However research focussed on improving adsorption efficiency of GAC by enhancing the porosity and surface area are active area of research [3,4]. Surface modification of granular activated carbon by chemical/thermal activation generates more additional adsorption sites on their porous surface[5,6]. In this work use of zirconium impregnated activated carbon to remove Methylene Blue from aqueous solution are discussed with respect to their isotherm behaviour, kinetics and porosity.

## EXPERIMENTAL TECHNIQUES

Granular activated carbon (GAC, coconut shell based) manufactured by Indo-German carbon Ltd, Cochin was procured and further purified according to a known standard method using 0.5N HCl, 0.5N NaOH and water. Modification of carbon was done by conc.  $HNO_3$  it is refluxed for 3hrs and dried in an oven at  $110^\circ C$ . Activated carbon loaded with  $Zr^{4+}$  as  $ZrOCl_2 \cdot 8 H_2O$  and  $ZrO_2$  are prepared and activated with steam at different temperature [7]. From the new GAC series consisting of four carbons viz GAC-383, its nitric acid modified form (GACO-383),  $ZrO_2$  impregnated activated form (GACNZR 1073) and its Zirconyl chloride activated form (GACZR 1273) are made. Adsorption experiment was carried out with different concentrations of MB and 1.0 g/L activated carbons. MB content quantitatively analysed by using UV-Visible spectrophotometer at 540nm. Adsorption equilibration data are used to fit into Langmuir, Freundlich and John-SivanandanAchari isotherms. Kinetic studies has been carried out, and various kinetic models like pseudo first order and pseudo second order kinetic were applied.

RESULTS AND DISCUSSION

Adsorption Isotherm Studies

The adsorption isotherms of MB (Figure 1) show the adsorption isotherm profile of MB and their mass progressive on GAC surfaces. When an adsorption process reaches an equilibrium state at higher equilibrium concentration the isotherm is more convex to the y-axis with a round knee. All the new carbon exhibit type I behaviour as per Brunauer's classification.

Freundlich Isotherm

Freundlich adsorption isotherm [8] is derived by assuming a heterogeneous surface with a non-uniform distribution of the heat of sorption over the surface. It can be linearly expressed as

$$\log q_e = \log K_F + (1/n) \log C_e \quad (1)$$

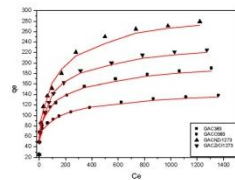


Figure 1 Equilibrium adsorption isotherm for new GAC at 30°C

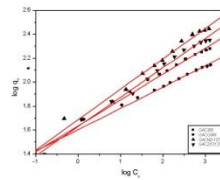


Figure 2 Freundlich adsorption isotherm of MB on new GAC at 30°C

$K_F$  is the Freundlich constants related to the adsorption capacity (mg/g (mg/L)<sup>1/n</sup>),  $n$  is the empirical parameter representing the energy of heterogeneity of the adsorption sites, it also gives an indication of how adsorption is favourable if  $1/n < 1$ ; indicates Langmuir isotherm.

Langmuir Isotherm

The Langmuir isotherm model [9] is based on the assumption that a maximum limiting uptake occurs, corresponding to a saturated monolayer of adsorbate molecule at the adsorbent surface.

$$\frac{C_e}{q_e} = \frac{1}{K_L} + \frac{q_m}{K_L} C_e \quad (2)$$

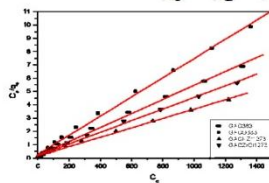


Figure 3 Langmuir adsorption isotherm of MB on new GAC carbons

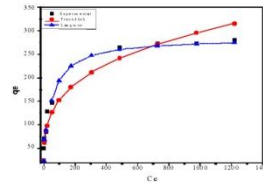


Figure 4 Equilibrium adsorption isotherms for GACZR at 30°C

$C_e$  is the equilibrium concentration of Methylene blue in the solution (mg/l).  $q_e$  is amount adsorbed at equilibrium (mg/g). Parameters are shown in the Table 1. The carbon GACNZr1273 have highest MB uptake efficiency with 283.3 mg/g. Respectively for others have GACZR 1273 (228.3 mg/g), GAC-383 (190.0 mg/g) and GACO-383 (138 mg/g). This corresponds to GACNZr 1073 shows 40% and GACZR 1273 shows 24.5% adsorption efficiency enhancement by  $Zr^{4+}$  activation compared to GAC-383, the basic carbon used. Equilibrium adsorption study of the GACZR -1273 (Figure 4) confirms that Langmuir model fit better than the Freundlich model, as its  $1/n$  value is  $0.24 \leq 1/n < 1$ .



MatCon-2016

Materials for Environmental Applications and Green Materials

Table 1 Isotherm parameter of zirconium based adsorbents for the removal of MB

Sample	Langmuir parameter			Freundlich parameter			SA <sub>F</sub>
	V <sub>m</sub>	K <sub>L</sub>	R	n	K <sub>F</sub>	R	
GACNZR 1073	283.3	6.24	0.994	3.94	48.38	0.986	640.15
GACZR 1273	228.3	5.29	0.996	4.08	42.43	0.990	515.91
GAC-383	190.1	4.80	0.996	1.632	42.90	0.988	429.59
GACO383	138.7	3.60	0.996	5.61	39.84	0.982	313.39

Surface Area Of Porous Material By BET, Langmuir And John-Sivanandanachari isotherm (J-SA) Models

BET surface areas (SA) of the new GACs are found that they are highly porous in nature. They all have a SA of 996 m<sup>2</sup>/g. GACO-383 have the 974.3m<sup>2</sup>/g and GACZR 1273 have 1217 m<sup>2</sup>/g. The activation by ZrOCl<sub>2</sub> enhances the total surface area (1802 m<sup>2</sup>/g). This indicates zirconium ion promotes micro pores this constitute micropore surface area of 863 m<sup>2</sup>/g and others also have micropores measures 588.6 m<sup>2</sup>/g for GAC-383 and 540.3 m<sup>2</sup>/g for GACO-383. The nature of the pores that constitute the additional porosity has to be investigated. Surface area of the materials are then evaluated using the new isotherm model, John-SivanandanAchari isotherm [10,11] equations are given below.

$$\log \log C_e = C + n \log q_e \quad (3)$$

So as we seen in the table 2 for many microporous material BET Surface area is incomparable with Langmuir Surface area and the surface area obtained from liquid phase adsorption is the active surface area of porous material in liquid phase.

$$SA = A \times N \times V_m / M_{wt} \quad (4)$$

A-area of crosssection (for MB, 1.2 nm<sup>2</sup>) N- Avogadro's number M -molecular weight (319.8 g). Surface area obtained from Langmuir and John isotherm using the following equation (4) are comparable indicate the mesoporous nature of material as these effective pores on GAC provide adsorption sites to bind MB molecules.

Table 2 Comparison of Surface area

Sample	Total Surface area(m <sup>2</sup> /g)	BET Surface area(m <sup>2</sup> /g)	Mesopore Surface area(m <sup>2</sup> /g)	Langmuir Surface area(mg/g)	J-SA Surface area(mg/g)
GAC 383	1612.6	996.8	408.10	429.59	424.82
GACO 383	1480.8	974.3	433.72	313.39	309.2
GACZR 1273	1802.60	1217.2	353.40	515.91	505.4

### Adsorption Kinetic Study

Three kinetic models, pseudo first order kinetics, and pseudo second order kinetics were used to investigate the adsorption process and discussed in the following sections.

#### Pseudo first order kinetics

Pseudo first order equation by Lagergren [12] is used for the adsorption of MB on new GAC

$$(q_e - q_t) = \log q_e - k t / 2.303 \quad (4)$$

**Pseudo second order kinetics**

$$\text{Linearised form of equation [13]} \quad \frac{t}{q_t} = \frac{1}{K_2 q_e^2} + \frac{1}{q_e} t \quad (5)$$

$q_e$  obtained from the slope of Eqn (5) is equal to the experimentally obtained equilibrium capacity ( $q_{\text{exp}}$ ) and  $R^2$  is found to be near to unity; therefore the sorption reaction is approximated more favourably by the pseudo second order kinetic model for these GAC-MB adsorption systems

Table 3 Kinetic parameters of GACNZR, GACZR, and GAC

Adsorbent	$q_e$ (Experimental)	Pseudo first order			Pseudo second order		
		$K_1$	$q_e$ (cal)	$R^2$	$K_2$	$q_e$ (Cal)	$R^2$
GACZR 1273	128.47	$5.5 \times 10^{-3}$	80.58	0.990	$2.1 \times 10^{-4}$	133.9	0.998
GACNZR 1073	145.56	$4.7 \times 10^{-3}$	70.66	0.993	$2.4 \times 10^{-4}$	147.1	0.997
GAC-383	124.24	$5.4 \times 10^{-3}$	67.07	0.972	$2.5 \times 10^{-4}$	126.4	0.996
GACO-383	98.13	$4.4 \times 10^{-4}$	54.75	0.989	$2.7 \times 10^{-4}$	99.8	0.996

**CONCLUSION**

The present study summarises that zirconium impregnated activated carbons based on coconut shells are efficient for the removal of Methylene Blue dye from their aqueous solutions. Among the three carbons used GACNZR 1073 shows 40% and GACZR 1273 shows 24% higher adsorption capacity than the native/basic GAC-383. Surface modification of granular activated carbon by chemical/thermal activation generates more additional adsorption sites on their porous surface. The adsorption process could be best described by second order kinetic model i.e molecule get adsorbed on the surface of carbon is directly proportional to the square of the unoccupied vacant site.

**REFERENCE**

1. Ramakrishnana K. R., Viraraghavan T., Dye removal using low cost adsorbents, Water Sci. Technol. 1997, 36, 189-196.
2. Avom J., Noubactep C., Germain P., adsorption of Methylene blue from an aqueous solution onto activated carbon from palm tree cobs, Carbon 1997, 35, 365-369.
3. Bindia R., Sivanandan Achari V., Porosity development on activated carbon using  $\text{Ce}^{2+}$  ions: Proceedings of a 23<sup>rd</sup> Swadeshi Science Congress November 2013, ISBN 978-81-928129-1-5, 2013, 399-404.
4. Jayasree S., and Sivanandan Achari V., Preparation of activated carbon using  $\text{Zn}^{2+}$ : Determination of yield, and surface area: Proceedings of a 23<sup>rd</sup> Swadeshi Science Congress November 2013, ISBN 978-81-928129-1-5, 2013, 440-445.
5. Mohandas A., Rajalakshmi A S., Sivanandan Achari V., and Preparation of Activated carbon using  $\text{Zr}^{4+}$ : Activation and Adsorption study: Proceedings of a 23<sup>rd</sup> Swadeshi Science Congress November 2013, ISBN 978-81-928129-1-5, 2013, 465-470.
6. V. Sivanandan Achari., A.S Rajalakshmi., Adsorption of phenol using Zirconium impregnated activated carbon: Equilibrium and Kinetic study: Proceedings of a 24<sup>th</sup> Swadeshi Science Congress November 2014, ISBN: 978-81-928129-2-2, 2014, pp 314-319.
7. Rajalakshmi A S., Sivanandan Achari V., Removal of p-nitrophenol from aqueous solution by  $\text{Zr}^{4+}$  impregnated activated carbons. ICWA 2015, Mahatma Gandhi University, Kottayam, 2015.
8. Irving Langmuir., The adsorption of gases on plane surface of glass, mica and Platinum. J. Am. Chem. Soc., 1918, 40 (9), pp 1361-1403.
9. Irving Langmuir., The adsorption of gases on plane surface of glass, mica and Platinum. J. Am. Chem. Soc., 1918, 40 (9), pp 1361-1403.
10. John P. T., and Sivanandan Achari V., Characterization of structural parameters of finely divided and porous materials by a new adsorption isotherm, J. Materials Science, 2002, 37, pp 885-893.
11. Jayasree S., Rajalakshmi A.S., Sivanandan Achari V., Determination of Surface area of Activated carbon using John-Sivanandan Achari isotherm plots, 26<sup>th</sup> KSC, Wayanad, 2014, pp 1362-1371.
12. Lagergran S., Kungliga Svenska., Vetenskapsakademiens. Handlingar, Band 24, 1898, 1-39.
13. Ho Y. S., and McKay G., Sorption of Dye from Aqueous Solution by Peat, Chemical Engineering Journal, 1978, 50, pp. 926-939.